INFORMATION TO USERS

This manuscript has been reproduced from the microfilm master. UMI films the text directly from the original or copy submitted. Thus, some thesis and dissertation copies are in typewriter face, while others may be from any type of computer printer.

The quality of this reproduction is dependent upon the quality of the copy submitted. Broken or indistinct print, colored or poor quality illustrations and photographs, print bleedthrough, substandard margins, and improper alignment can adversely affect reproduction.

In the unlikely event that the author did not send UMI a complete manuscript and there are missing pages, these will be noted. Also, if unauthorized copyright material had to be removed, a note will indicate the deletion.

Oversize materials (e.g., maps, drawings, charts) are reproduced by sectioning the original, beginning at the upper left-hand corner and continuing from left to right in equal sections with small overlaps.

Photographs included in the original manuscript have been reproduced xerographically in this copy. Higher quality 6" x 9" black and white photographic prints are available for any photographs or illustrations appearing in this copy for an additional charge. Contact UMI directly to order.

Bell & Howell Information and Learning
300 North Zeeb Road, Ann Arbor, MI 48106-1346 USA
800-521-0600

Université d'Ottawa · University of Ottawa

Cyclic Testing of Concrete-Filled Circular Steel Tube Bridge Columns having Encased Fixed Based Detail

by

Julia Marson

Thesis submitted to the School of Graduate Studies
in partial fulfillment of the requirements for the
Master of Applied Science Degree in Civil Engineering
under the auspices of the Ottawa-Carleton Institute for Civil Engineering

Spring 2000

Department of Civil Engineering, University of Ottawa
Ottawa, Canada, 2000

To my husband, Rob

Abstract

Concrete-filled steel tube columns have been recognized to have many desirable characteristics that can lead to stable hysteretic energy dissipation during earthquakes. They also have many other properties that make them advantageous for bridge applications (i.e. steel tube provides confinement to the concrete and acts as formwork during construction; concrete enhances the local buckling resistance of the steel tube; construction can be accelerated when the tube alone can carry the dead-loads; no need for stain protection on piers when superstructure is of weathering steel; final aesthetic of the product compatible with current practice, etc.)

A literature review was performed to collect data on the behaviour of concrete-filled steel tubes under axial load, combined axial and bending forces, and cyclic forces. Analytical work was performed to ensure that the test columns chosen would be representative of full-scale bridge piers found in North America. The foundation detail was designed to ensure that the full moment capacity of the composite column could be developed at its base without failure of the foundation.

This study involved testing four concrete-filled steel tubes under a constant axial load and subjected to an increasing cyclic horizontal force applied at the top of the column. All four columns sustained drifts of 7% before failure occurred by the steel tube fracturing at the location of the local buckles. Subsequent analytical work lead to two new proposed design equations. These produce axial-flexure interaction equations in much better agreement with the existing data than the equations for circular concrete-filled steel tubes currently used by the Canadian CAN/CSA-S16.1-M94 standard, or American AISC LRFD 1994 Specifications.

Acknowledgments

Thanks are due to the many people who have assisted me during the research of this thesis.

I would like to thank my professors throughout my university studies. Dr. D. Surry and Dr. M. Bartlett from the University of Western for my introduction into research during my undergraduate degree at the University of Western Ontario and instilling a desire to pursue research studies. Dr. M. Bruneau, my thesis supervisor, Dr. M. Saatcioglu and Dr. N. Gardner for their insight and knowledge in structural engineering. The instruction and knowledge imparted by my supervisor, Dr. Bruneau, during my graduate studies has been invaluable. My fellow students have challenged me during my graduate studies, and for this I thank them.

The help during long hours spent in the laboratory constructing and testing the specimens by the technical staff at the University of Ottawa, by my fellow students, and especially by my father and husband was notably welcomed.

The advice and guidance given to me by Peter Wells of CANRON and Mike Gilmour of the Canadian Institute of Steel Construction was greatly appreciated. The financial support provided by the Steel Structures Education Foundation and the National Science and Engineering Research Council has made this research possible.

Finally, I would like to thank my family and my husband for your support and encouragement throughout all my endeavors and especially throughout my university career.

Table of Contents

List of Tables

List of Figures

Notation

A Cross sectional area of a member

AE_{comp} Composite stiffness under axial load

A_a Cross sectional area of the steel tube

A_c Cross sectional area of the concrete core

A_{cv} Shear area of the concrete core which is equivalent to one half of the concrete core area

A_e Effective area of a steel tube using the effective diameter

A_g Gross cross sectional area of the column

A_s Cross sectional area of the steel shell

A_{st} Area of tensile steel in the steel shell

A_t Transformed area of a concrete-filled steel column

A_w Area of web of steel shape

A_1 Area of the stiffeners of a stiffened steel plate

$\overline{A}$ Angle in radians from the centre of the steel tube and sustaining L^*

B Ratio altering the straight line axial thrust interaction curve

b Smallest width of a rectangular steel shell

b_s Width of stiffener

C_c Axial resistance of the concrete core

C_{ec} Euler buckling strength of a concrete-filled steel tube

C_e Euler buckling load

C_f Factored axial load

C_r Factored axial compressive resistance of the steel shell

C_{rcm} Compressive resistance of the concrete core with no slenderness effect taken into account

C_{rco} Compressive resistance of a concrete-filled column with $\lambda=0$

C_r' Factored axial compressive resistance of the concrete core

C_{rc} Factored compressive resistance of the concrete-filled steel column

C_{rhc} Axial force required for the location of the neutral axis to match the center of gravity of a the composite section,

C_s Axial resistance of the steel tube

c_1 coefficient for uncertainty in the concrete contribution to the buckling strength

c_2 coefficient for concrete cylinder strength

D Diameter of the steel shell

D_e Effective diameter of the steel shell

D_i Inner steel tube diameter

D_o Outer steel tube diameter

E Modulus of elasticity

EI_{comp} Composite stiffness under flexural load

E_a Modulus of elasticity for steel tube

E_c Modulus of elasticity of concrete core

E_{cd} Modulus of elasticity of concrete core

E_{co} Initial slope of the stress strain curve

E_{ct} Modulus of elasticity of concrete core

E_i Energy absorption in cycle i of a test

E_m Modified modulus of elasticity of a concrete-filled steel column

E_s Modulus of elasticity of steel shell

E_{st} Modulus of elasticity of steel shell

$\hat{E}$ Normalized energy absorption

e End eccentricity of load

e_i Initial eccentricity

e_{min} Minimum eccentricity

e_x Initial eccentricity about the major axis caused by the applied load.

e_y Initial eccentricity about the minor axis caused by the applied load.

F_{cr} Critical column stress

F_{my} Modified yield stress of a concrete-filled steel column

F_y (f_y) Yield stress of steel tube

f_c Stress in concrete

f_c' Cylinder strength of concrete

f_c'' Compressive strength of concrete in a structural member

f_{ck} characteristic compressive strength of concrete

f_{cu} Ultimate buckling stress of a concrete column
cube strength of concrete (Neogi et al. 1969, Shakir-Khalil and Zeghiche 1989)

f_{cuk} Strength of a 150 mm cube of concrete below which 55% of all possible strength measurements for the specified concrete are expected to fall

f'_o Strength of the concrete core under a compressive load

f_p proportional limit of steel obtained from tensile tests.

f_s Stress in steel

f_{sd} Design strength of the steel tube

f_{sk} Guaranteed minimum value for yield stress as supplied by the steel supplier

f_s' Specified yield strength of steel

f_{su} Ultimate buckling stress of a steel tube

f_1 Axial compressive stress of confined concrete at failure

f'_1 Circumferential stress

f_2 Lateral pressure on concrete

g Slenderness factor to convert maximum compressive strength to buckling strength

HSS Hollow structural section

h unsupported length of the column

h_1 Concrete width perpendicular to the plane of bending

h_2 Concrete thickness in the plane of bending

I Moment of inertia

I_a Second moment of area for steel tube

I_c Second moment of area for concrete core

I_g Moment of inertia of the gross concrete core

I_s Moment of inertia of the steel shell

I_t Transformed moment of inertia of a concrete-filled steel column

K Effective length of the member

k Equivalent length factor

k_3 Factor representing the compressive strength of concrete

L Length of the member

L_e Equivalent effective length of a column

L^* Arc length of the tube in compression measured at mid-thickness of the steel tube

l_c Height of concrete-fill

l_d Distance between interior horizontal diaphragms

l_s Height of longitudinal stiffeners with greater stiffness

M Applied moment

$M_{A,B,C,D}$ Moments on the axial-moment interaction diagram (Eurocode 4 1994)

M_c Moment resistance of the concrete core

M_f Bending moment in a member under factored load

M_{fu} Factored bending moment

M_L Moment resistance "lost" due to slenderness of a concrete-filled steel column

M_n Plastic moment capacity of a concrete-filled steel column

M_o Plastic bending strength of the steel tube

M_r Moment resistance of a concrete-filled column taking into account slenderness

M_{no} Bending moment on a beam column with no axial load present

M_{n1}, Specific bending moments on a thrust-moment interaction diagram corresponding to P_{n1}

M_{n2} Specific bending moments on a thrust-moment interaction diagram corresponding to P_{n2}

M_r Factored moment of resistance

M_{rc} Moment resistance of the composite section

M_{rcm} Moment resistance corresponding to C_{rcm}

M_{rhc} Moment resistance corresponding to C_{rhc}

M_s Moment resistance of the steel tube

M_u Applied bending moment

M_{ux} Ultimate major moment of resistance of the composite section

M_{uy} Ultimate minor moment of resistance of the composite section

M_{u1} Smaller required moment applied at one end of the column

M_{u2} Larger required moment applied at the opposite end of the column

M_2 Larger of the two end moments on a column

M^*_{rcm} Moment resistance at M_{rcm} taking into account slenderness

M^*_{rhm} Moment resistance at M_{rhm} taking into account slenderness

$M_{\delta x}$ Major axis moment at failure at the mid-height of the column

$M_{\delta y}$ Minor axis moment at failure at the mid-height of the column

$N_{A,B,C,D}$ Axial forces on the axial-moment interaction diagram (Eurocode 4 1994)

N_c Buckling strength of centrally loaded column

N_{cr} Concrete-filled steel column at critical state

N_f Applied axial load

N_o Squash load of concentrically loaded short concrete-filled steel column

N_p Plastic compressive resistance of the composite column

N_{pl} Axial load capacity of a concrete-filled steel column

N_s Axial load capacity of the steel shell

N_{sd} Design Axial force (Eurocode 4 1994)

N_u Axial load capacity of a short column

N_y Squash load of a column

n Modular ratio = E_s/E_c

1.34 for Class C hollow structural sections

2.24 for Class H hollow structural sections

P Concrete-filled steel tube axial strength (ACI 318-63)

P_c Concrete core axial strength

P_{cr} Axial strength of a long column

P_{cu} Ultimate buckling load of a concrete column

P_d Permanent axial load

P_e Euler buckling load of a column

P_{exp} Experimental failure mode

$P_{failure}$ Experimental failure load

P_{fu} Factored axial force

P_n Nominal strength of a concrete-filled steel column

P_{no} Axial load on a beam column with no moment applied

P_{n1} Specific axial loads on a thrust-moment interaction diagram corresponding to M_{n1}

P_{n2} Specific axial loads on a thrust-moment interaction diagram corresponding to M_{n2}

P_o Squash load of a column

P_s Steel tube axial strength

P_{su} Ultimate buckling load of a concrete column

P_y Squash load of the composite column (Kawaguchi et al. 1992)

P_u Applied axial force

R_c Radius of the concrete core

R_f Panel slenderness factor for steel plates using flange dimensions

R_p Panel slenderness factor for steel plates

R_w Panel slenderness factor for steel plates using web dimensions

R^* Radius of the centre line of the steel tube

r Radius of the steel shell

Ratio of the lesser to the greater end moment (Eurocode 4 1994)

r_c Radius of gyration of the concrete core

r_m Modified radius of gyration of a concrete-filled steel column

r_s Radius of gyration of the steel shell

S Short tem load on the concrete-filled steel column

T Total load on the concrete-filled steel column

T_{max} Total force if the entire steel tube is in tension

T_r Tensile force in the steel tube

t Thickness of the steel shell

t_s Thickness of stiffener

V_n Nominal shear strength of a concrete-filled steel column

V_s Shear resisted by the steel shell

v_c Nominal concrete shear resistance = $2\sqrt{0.001 f_c'}$

w Density of concrete

y_{sc} Distance from the centre of the column to the neutral axis of the steel tube in compression

y_c Distance from the centre of the column to the neutral axis of the concrete core in compression

y_{st} Distance from the centre of the column to the neutral axis of the steel tube in tension

Z Plastic section modulus of the steel shell

Z_c Plastic section modulus for the concrete core

Z_s Plastic section modulus of the steel shell (Eurocode 4 1994)

α Ratio between the area of the steel shell to the area of the concrete core

	Factor depending on degree of imperfections (Kato 1996)
	Displacement amplitude ratio (Kawaguchi et al. 1992)
β_d	Ratio of the required permanent axial load to the required total axial load, $1.4P_d/P_u$
χ	Reduction coefficient for the relevant buckling mode
δ	Moment magnification
	Steel contribution ratio (Eurocode 4 1994)
δ_x	mid-length displacement at failure perpendicular to the major axis
δ_y	mid-length displacement at failure perpendicular to the minor axis
δ_i	Initial deflection
δ_y	Yield deflection
δ_1	Extensional rigidity of a steel plate
Δ_{cr}	Displacement at first occurrence of local buckling
ϵ	Longitudinal strain
ϵ_o	Longitudinal strain in concrete at a stress of f_c'
ϵ_c	Longitudinal strain in concrete
ϵ_c'	Longitudinal strain in concrete at a stress of f_c'
ϵ_m	Longitudinal strain in concrete corresponding to the peak stress in concrete
γ_c	Importance factor of concrete
γ_{Ma}	Partial safety factor for steel 1.10 (Eurocode 4 1994)
γ_o	Importance factor
γ_s	Importance factor of steel
γ_1	relative flexural stiffness of a longitudinal stiffener to a plate panel
γ_1^*	Optimum rigidity of the stiffeners
λ	Slenderness ratio = 2L/r
	Non-dimensional slenderness factor (Eurocode 4 1994)
$\overline{\lambda}$	Relative Slenderness
λ_c	Non-dimensional slenderness ratio of concrete core
λ_{crit}	Relative slenderness
λ_o	Boundary slenderness ratio

μ Ductility factor for the elasto-plastic model

Degree of lateral and rotational restraints at the ends of the columns (Cai 1992)

μ_m Ductility factor of a structure

ν Stability coefficient for concrete-filled steel columns under axial compressive loading

η_1, η_{10} Amplification factor for concrete core

η_2, η_{20} Reduction factor for steel tube

ϕ Reduction factor

ϕ_b Resistance factor for bending

ϕ_c Resistance factor for compression

ϕ_{con} Resistance factor for concrete

ϕ_e Strength reduction factor due to the eccentricity ratio

ϕ_s Resistance factor for steel

ϕ_l Strength reduction factor due to slenderness ratio

ρ Ratio of area of steel to the gross cross sectional area of the column.

ρ_{comp} Effective radius of gyration

ρ_s Coefficient taking into account the slenderness ratio

π Pi = 3.14159

σ Stress in concrete

σ_{cr} Buckling stress of a steel plate panels

σ_m Peak stress in concrete which is taken equal to 80% of the cube strength of the concrete

Φ Modulus of the composite column

τ Coefficient used to reduce the contribution of the steel when concrete strength increases due to confinement

τ' Coefficient used to increase the contribution of the concrete

θ Confinement index

υ Stability coefficient

ω density of concrete

ω_1 Coefficient used to determine equivalent uniform bending effect in beam-columns

1 INTRODUCTION

1.1 General

Fifty percent of the Canadian population lives in moderate to severe seismic regions. Along with roadways, bridges form a vital link to connect all regions of Canada. Therefore, bridges must be designed with due attention to seismic considerations. Seismic design is not only concerned with the strength of the structure but also the ductility and energy absorption of members during earthquakes. According to the design philosophy prevailing in North America (CSA 1999, ASHTO 1994), bridges are designed to ensure that during an earthquake, their superstructure remains elastic while their substructure yields and behaves in a ductile manner.

Currently in North America, nearly all new highway bridge substructures are constructed of reinforced concrete, even when bridges have a steel superstructure. Undeniably, the reinforced concrete industry has developed an expedient and inexpensive formwork method for those piers that currently gives them an economic advantage. However, in view of the growing worldwide emphasis on ductile detailing and sound earthquake resistance design, steel may be well positioned to regain competitiveness in this market.

In seismic regions where ductile detailing must be provided, a large amount of transverse reinforcement is required in concrete piers. This is achieved by spiral reinforcement which is still relatively inexpensive compared to the cost required for steel piers of the types that have been used in the past. Hence, a new type of steel substructure must be developed to give steel the necessary edge over concrete. This research project focuses on the development and experimental validation of a ductile composite steel bridge pier as an alternative to the reinforced concrete bridge piers currently used in Canada and many regions of North America. The ultimate objective is to provide a design concept that can reposition steel as a competitive substructure alternative to concrete in the moderate to severe seismic regions of North America.

The proposed composite pier consists of a steel tube filled with unreinforced concrete. This sort of construction method is popular in Japan, but direct import of the Japanese practice to

North America is not advantageous because their typical detailing requires many stiffeners, resulting in relatively expensive detailing (Japanese also prefer rectangular pier cross-sections). Furthermore, in Japan, concrete is only added for a few metres to enhance impact resistance of the pier in the event of a vehicle collision, and composite action is not considered. Instead, in the design proposed here, for cost efficiency, only unstiffened circular tubes are considered and true composite action is sought.

Beyond cost considerations alone, concrete-filled steel columns have other advantages over reinforced concrete columns.

- Ductility of a reinforced concrete member increases as the concrete is confined; this confinement is established using spiral ties in circular cross-section. In that perspective, the proposed composite pier effectively confines the concrete as it can exert a constant pressure on the entire surface area of the column. Therefore, the energy dissipation ability of the composite column should exceed that of a reinforced concrete member.
- Because there is no cover concrete in a concrete-filled steel column, all concrete in the member contributes to the strength and ductility of the member avoiding concrete spalling outside of the spiral reinforcement which would normally occur in a typical reinforced concrete column.
- Unlike a reinforced concrete pier that needs formwork during construction, the steel shell acts as the formwork for the concrete in a concrete-filled steel column.
- Construction of the bridge may be accelerated if the steel shell alone can provide resistance to dead-loads.
- Labour during construction can be reduced as the steel components are fabricated off site in a controlled environment.
- Hollow steel sections are susceptible to local buckling, but the concrete core prevents premature local buckling by restricting the inward buckling of the steel tube. By enhancing the buckling resistance of the steel shell, ductility also increases as the column is able to undergo more cycles of loading.

- The addition of concrete also adds to the strength of the steel column, allowing the composite column to carry more load than a hollow steel column.
- The exterior steel provides nearly all the lateral load resistance, while the unreinforced concrete mostly provides the gravity resistance so rebars are unnecessary in the concrete.
- There is no need for stain protection on piers when the superstructure is of weathering steel. Although some protection may be necessary at the base (depending on the particular detailing used), it can be accomplished easier there.
- The final aesthetics of a concrete-filled steel column are compatible with current practice.

The potential economical advantages of concrete-filled steel columns in tall buildings have long been recognized (Tarics 1972). In North America, concrete-filled steel columns have recently been used in some buildings, such as Two Union Square in Seattle (Bauer 1988) as well as five additional tall buildings in Seattle (Engineering News-Record 1989). These columns have also been used in the Casselden Place and in the Market City in Australia (Webb and Peyton 1990). These composite columns have also been used much earlier in non-building applications, as pylons for hydroelectric lines in Switzerland (Preiswerk 1948, Vogeli 1948,1950) and as piles for railway bridges (Committee No. 30, 1954). A four level interchange was built in Almondsbury, UK and supported on concrete-filled steel piers (Kerensky and Dallard 1968) and the first rectangular steel bridge pier partially filled with concrete was built in 1982 by the Hanshin Expressway Public Corporation (Kitada 1998). The results of the above applications and results from previous experimental research, presented in Section 2.5, are very encouraging and suggest that filling a steel tube with concrete is a cost-effective strategy to obtain columns having excellent strength and ductility.

1.2 Statement of Problem

The benefits of a concrete-filled steel tube structural member have previously been stated. However, it appears that no such composite bridge piers have been built in North America. One reason that may have contributed to this situation is the lack of research conducted to fully understand the ultimate behaviour of such bridge piers. The following are some areas of concern

identified by previous researchers working on composite columns for building applications; some of these will be studied throughout this thesis:

- A natural bond exists between the concrete and the steel in the composite design. However, it is still unresolved whether or not this bond remains when load is applied to the column or if additional bond must be provided through mechanical means, in the form of shear studs.
- The response of a steel tube to cyclic loading in the inelastic range has been well researched. However, the inelastic behaviour of the steel tube filled with concrete is not fully defined, and hence, the ductility of these columns needs to be investigated further.
- One of the failure modes of a steel tube is by local buckling. The addition of concrete inside the tube will delay local buckling by preventing inward local buckling. However, the tolerable amount of local buckling under cyclic loading is unknown, especially if inexpensive subsequent repair is desirable.
- Concrete-filled steel tubes with small diameters have been studied, tested, and shown to exhibit additional strength due to concrete confinement by the steel tube, however, it is unknown if composite columns with larger diameters can still achieve this increase in strength.

1.3 Objectives

The main objectives of this research project are as follows:

1. To review the literature for experimental results and existing equations available for the analysis or design of concrete-filled steel tubes and compare this data to the concrete-filled steel columns tested in this study.
2. To design four concrete-filled steel columns with varying cross-sectional dimensions using the analytical results of previous research and a computer program developed by the author to simulate cyclic loading of a composite column.
3. To develop a practical foundation detail that can be used to develop the full composite capacity at the base of these columns, and experimentally verify the adequacy of this detail.

4. To subject the designed concrete-filled steel column to conventional cyclic inelastic tests to determine their maximum strength and ductility and identify the most effective design conditions.

1.4 Outline of Thesis

In Chapter 2, some fundamental concepts of concrete-filled steel columns as well as the review of analytical solutions prepared by other researchers and past experimental results are presented. In Chapter 3, the background to selecting the experimental columns and the set-up required to perform these experiments are presented. In Chapter 4, visual observations as well as information gathered from the instrumentation of the specimens is presented for the four experimental specimens. Chapter 5 presents the analysis of the test data including the behaviour of the specimens and the effect of $P\Delta$ analysis. The calculation of the maximum moments of the specimens and previously tested columns are presented in Chapter 6 with proposed new equations for CAN/CSA-S16.1 also introduced. A summary of the experimental study and theoretical analysis, concluding remarks, and recommendations for further research are presented in Chapter 7.

2.0.0 LITERATURE REVIEW

Although the research project at hand focuses on the study of concrete-filled steel tubes subjected to cyclic loading, to fully understand the advantages of composite construction in seismic design, this literature review on the behaviour of composite columns under static and cyclic loading has been extended to include some relevant experimental results on the behaviour of hollow steel sections and hollow steel sections partially filled with concrete. A summary of some fundamental concepts on the ultimate behaviour of concrete-filled tubes, current code requirements, and a review of analytical solutions presented by other researchers to model the observed behaviour is included. This summary precedes the presentation of experimental results by previous researchers. The chapter concludes with a comparison of the theories introduced and the results obtained from experimental data.

2.1 Behaviour of Concrete-Filled Composite Columns

Filling a steel pipe, tubing or hollow section fabricated from plates with unreinforced concrete can remarkably increase its strength and ductility. This enhancement of ductility and strength is due in large part to the complimentary behaviour of steel and concrete. The steel shell provides confinement for the concrete, which in turn prevents premature local buckling of the steel. The concrete carries the bulk of the axial load in compression, while the steel absorbs the bending and tension forces. Because of these actions, the ultimate load carrying capacity of composite members may become greater than the cumulative load carrying capacity of the individual members.

In the United States, the first code clauses for composite column construction of the type considered in this study was introduced in 1963 by the American Concrete Institute "Building Code Requirements for Reinforced Concrete" (ACI-318-63) and later by the steel industry in 1986 by the 1st edition of the American Institute of Steel Construction "Load and Resistance Factor Design Specifications for Structural Steel Buildings" (AISC 1986). In North America some newer buildings with composite columns have been designed using these procedures (Viest

et al. 1997). When such designs were accomplished prior to the availability of codified rules, the designers followed fundamental engineering principles with a good measure of conservatism.

Although concrete-filled steel columns have not commonly been used as bridge piers in North America to date, the American Association of State Highway and Transportation Officials (AASHTO) LRFD provisions, (AASHTO 1994, Clause 6.9.5) introduced design equations for composite compression members similar to those proposed by AISC (1986), but without mentioning restrictions on material properties or cross-section sizes specified by the AISC. In Canada, composite columns were not addressed by the 1988 edition of the CSA Standard for the Design of Highway Bridges CAN/CSA-S6-88 (CSA 1988), nor by the 1991 edition of the Ontario Highway Bridge Design Code (MTO 1991).

The behaviour of a concrete-filled steel column depends primarily on its effective slenderness ratio, properties of the steel and concrete materials, and the diameter-to-thickness ratio of the steel member, the latter being directly related to the local buckling resistance of the steel shell. A good understanding of the ultimate behaviour of concrete-filled steel columns requires a closer look at some of the mechanisms that develop when these structural elements are subjected to axial loads as well as bending. Such an examination follows.

2.1.1 Behaviour Under Non-Cyclic Loading

2.1.1.1 Axial Strength

The compressive strength of a concrete-filled steel column is at least equal to the strength of the structural steel shell and the strength of the concrete core. The concrete core is in tri-axial confinement when the lateral expansion of concrete is larger than the lateral expansion for steel; this occurs approximately at a longitudinal strain of 0.002. Tri-axial confinement from the steel shell can increase the effective strength of the concrete and the ductility of the composite column. However, the steel shell does not provide confinement to the concrete before concrete reaches the longitudinal strain at which it's lateral expansion is greater than steel. Therefore, without these confining pressures there is no increase in concrete strength. This absence of confinement is

notable in axially loaded columns that fail by global member buckling rather than by compression failure. When instability failure occurs before the steel reaches its yield stress, the concrete will not have reached the strain needed for the development of confinement.

2.1.1.2 Axial and Bending Strength

A column can be subjected to non-cyclic axial and bending forces when subjected to eccentric axial loading. The flexural stiffness of a concrete-filled steel column is dominated by the steel shell. The confined concrete bears against the steel shell under bending forces, thereby continuing to ensure some transfer of shear forces to the interface of the two materials. However, it is still uncertain if full bond is maintained at the contact surface. If not, the neutral axis of the two materials would no longer be in the same location even though curvatures must remain the same (Viest et al. 1997).

If compositeness is preserved, the concrete's neutral axis will migrate toward the tension face as the axial load is increased. This movement delays tension cracking in the concrete by reducing the area of concrete in tension and the lateral confinement of the steel shell assists the compression concrete to resist more lateral stress at higher strains than if the concrete was unconfined.

2.1.1.3 Shear Strength

The shear strength of a concrete-filled steel column is defined as the sum of shear capacities of the concrete and the steel walls. Confined by the steel shell, concrete helps to resist the shear force by developing a series of compression struts pushing against the compression and tension surfaces of the shell while the shell itself acts as a series of tension struts. As the column is loaded to high shears, bond strength may decrease, therefore allowing slippage of the concrete with respect to the steel shell. However, this slippage allows a more effective re-alignment of the compressions struts, and concrete resists more shear force in the process. To this strength must be added the shear force that can be resisted by the steel section alone.

2.1.1.4 Bond Strength

For effective composite action, the concrete must remain bonded to the steel shell to develop the necessary shear transfer by friction. The bond between the steel and concrete would easily be broken if the plain concrete shrank during the curing and drying process. However, it can be argued that concrete in a steel tube will not shrink since moisture loss is prevented by the outer tube.

Bond could also fail in a composite member due to the differential lateral expansion of the two materials. For concrete-filled steel tubes in the early stages of loading, the lateral expansion for concrete is lower than for steel, and thus, the steel tube has no restraining effect on the concrete core. An alternative point of view expressed by some researchers, is that there must remain enough frictional force between the steel and concrete to ensure surface contact. However, the coefficient of sliding between concrete and smooth steel is 0.5. Therefore, a shear stress up to one half the normal stress can be transferred from the concrete to the steel if pressure is applied normal to the interface.

2.1.1.5 Effect of Loading Methods

The behaviour of an axially loaded steel tube filled with concrete also depends on how the load is applied at its ends. Three different methods of applying the loading are possible:

- ***Loading the Steel Tube:***

  The steel shell acts alone since the load is only applied to the steel tube. No contribution from the concrete core is attained because if the steel tube is loaded, it increases in diameter due to Poisson's ratio and the bond with the concrete is broken, severing all shear transfer to the concrete core. Therefore, the axial load capacity of the column is the resistance of the steel shell alone.

- ***Loading the Concrete Core:***

  The steel shell acts as an encasement for the concrete core and is not expected to resist axial loads but only to provide a confining stress to the concrete. Steel used in this manner can be very effective because it will be strained only in its circumference direction. However, the steel will not achieve its full yield strength in the circumference direction because any bond between the steel and the concrete causes some longitudinal strain to develop in the steel. In absence of an effective bond, the load capacity would equal that of a confined concrete column with no additional load resistance from the steel shell.

- ***Loading both the Steel Tube and the Concrete Core:***

  The longitudinal strain is the same in both materials and true composite action is possible. The load capacity will be equal to or greater than the sum of the steel shell and the concrete core strengths. When the concrete core is confined by the steel shell, the concrete can achieve higher strains and resist more stress. Although, as mentioned earlier, the benefits of tri-axial compression may only be significant for a small range of member slenderness.

2.1.1.6 Effect of Slenderness Ratio

The behaviour of any axially loaded column depends on its slenderness ratio, itself a function of the column's flexural stiffness. For composite members, the relative contribution of the steel and concrete to the flexural stiffness, EI/L, does not remain constant during loading. Therefore, to efficiently represent the slenderness of a composite column, both the concrete slenderness ratio, kL/r_c, and the steel slenderness ratio, kL/r_s, have been commonly used by researchers and found to be useful parameters for concrete-filled steel tubes.

Short composite columns axially loaded in compression exhibit a failure mechanism characterized by yielding of steel and crushing of concrete. Composite columns of intermediate slenderness fail by inelastic buckling, a mechanism that develops with partial yielding of the steel, crushing of the concrete in compression, and cracking of the concrete in tension, as the column

deforms laterally due to the bending moment resulting from the axial loads acting on the initial imperfections and ensuring flexural deformations. Very long columns behave elastically until they buckle. This behaviour also affects columns subjected to both axial force and bending.

2.1.2 Behaviour under Cyclic Loading

The behaviour of concrete-filled steel tubes subjected to repeated cycles of large inelastic deformations is less understood. Yet this knowledge is essential to ensure satisfactory performance during earthquakes. A concrete-filled steel column must be able to dissipate large amounts of energy in a ductile manner to effectively withstand seismic forces. The design strength of a structure can be substantially reduced if the structure is able to provide this ductility beyond the elastic limit, without significant loss of strength, up to displacements 4 to 6 times larger than the yield displacement.

The failure mechanisms of concrete-filled tubes under non-cyclic loading suggest favourable behaviour under cyclic loading. However, when the side of a tube yields in tension, it plastically returns to a longer length in absence of external loads. When that side of the tube is subsequently subjected to compression, it is more susceptible to buckling, even if just to return to the position needed to close cracks in the concrete core opened in the previous half-cycle. Therefore, the propensity of the steel tube to buckle increases with the magnitude of the inelastic lateral displacement of the column.

Nonetheless, compared to an equivalent non-composite column, the steel tube provides an effective containment for concrete, resulting in a ductile structural response to large flexural deformations. The lateral force versus displacement curve obtained under monotonic loading for a concrete-filled steel column provides an envelope for the behaviour expected under cyclic loading. The composite member may suffer some stiffness degradation when subjected to repeated load reversals but little strength degradation up to a high ductility. Concrete-filled steel columns have been reported to provide damping in the order of 1.5% to 2% in response to dynamic loads. (Viest et al. 1997)

2.2 Design of a Composite Column

It is more difficult to analyze concrete-filled steel columns than either steel or reinforced concrete columns, owing largely to the interaction and load sharing between the steel and concrete. A number of assumptions are made when designing a concrete-filled steel column, namely:

- Plane sections remain plane.
- Shear deformations can be ignored.
- The stress-strain relationship for steel is taken as the bilinear model shown in Figure 2.1a), instead of the more exact one illustrated in Figure 2.1b).
- The stress-strain relationship taken for unconfined concrete is a model proposed by Hognestad (1951) as shown in Figure 2.1c) in which ϵ_o is the strain in concrete at a stress of f_c'.
- Many models have been proposed for confined concrete. Some of these models are shown in Figure 2.1d). These models differ from unconfined concrete in that they all consider a slower strength degradation beyond ϵ_o.

Analysis can be further complicated by the anticipated construction sequence and methods. To calculate the long term deflections, the time of load application to the structure and the duration of those loads must be known. The total deflection is the sum of all short term and long term deflections. For example, the steel shell may carry some dead load before the concrete has achieved its full compressive strength. Concrete is also subject to creep and shrinkage which will lead to time dependent column shortening and possible stress redistribution.

2.3 Code Design Rules

2.3.1 ACI 318-63

The American Concrete Institute Building Code, ACI 318-63, was the first code in North America to include concrete-filled steel tubes and introduced a working stress design equation for concrete-filled pipe columns that treated the steel shell, P_s and the concrete core, P_c as individual members to achieve the column strength, P:

$$P = P_c + P_s$$

$$\text{where} \quad P_c = 0.25 f_c' \left[1 - 0.000025 \left(\frac{h}{r_c}\right)^2\right] A_c \qquad (2.2)$$

$$\text{and} \quad P_s = \left[17{,}000 - 0.485 \left(\frac{h}{r_s}\right)^2\right] A_s$$

where all units are either in pounds or inches and h is the unsupported length of the column, r_c and r_s are the radius of gyration of the concrete core and hollow steel tube respectively, A_c and A_s are the areas of the concrete core and the hollow steel tube, respectively, and f_c' is the strength of the concrete core. The ACI 318-63 required yield stress of at least 33,000 psi (228 MPa) for the steel pipe and limited the column slenderness ratio, $h/r_s \leq 120$. Knowles (1967) showed that the calculations of both P_c and P_s in Equation 2.2 was based on approximations for the tangent moduli assuming a parabolic variation of tangent modulus load with slenderness ratio.

Knowles and Park (1970) argued that the drawback to this ACI code equation was in the low values of ultimate concrete and steel strengths used. They discovered this discrepancy when their test results produced values 2.83 to 5.73 times larger than those predicted by the ACI working load equations above.

2.3.2 AISC LRFD (1986)

The first provisions for the design of composite columns to be introduced into the American Institute of Steel Construction's Manual of Steel Construction were published in the 1986 "Load and Resistance Factor Design Specification for Structural Steel Buildings". Furlong (1976) demonstrated the adequancy of this equation based on data available at the time, and these revisions have remained unchanged to date (AISC 1994). The AISC (1986) defines a composite column as "a steel column fabricated from rolled or built-up steel shapes and encased in structural concrete or fabricated from steel pipe or tubing and filled with structural concrete." Only the latter case of concrete-filled pipes or tubes is considered here. For a concrete-filled tube to

qualify as a composite column, according to clause I2.1 of the AISC code, the following limits must be satisfied:

- The steel pipe cross-section must be at least 4% of the gross total column cross-sectional area.
- The specified concrete strength must be between 20 MPa and 55 MPa - the lower limit to ensure a minimum degree of quality control, the upper limit because AISC believes that an insufficient number of tests have been performed on composite columns built with high strength concrete.
- The specified minimum yield stress of the steel must not exceed 379 MPa, although the commentary to Clause I2.1 indicates that this limit is implicitly intended only for concrete-encased columns to prevent spalling of the concrete that provides stability to the encased steel, a condition that develops when longitudinal strains of 0.18% are reached, corresponding to a steel stress of 379 MPa.
- The minimum wall thickness of the steel member, to prevent local buckling before yielding, shall be:

$$D\sqrt{\frac{F_y}{8E_s}} \quad \text{for circular cross sections}$$

$$b\sqrt{\frac{F_y}{3E_s}} \quad \text{for rectangular cross sections}$$

where D is the diameter of the circular steel shell, b is the smallest width of the rectangular steel shell, E_s is the modulus of elasticity of steel, and F_y is the steel yield stress.

2.3.2.1 Axial Compression

Compressive strength calculations for concrete-filled steel columns are the same as for bare steel structural members in AISC (1986) with the exception that the modified properties F_{my}, E_m, and r_m are used. The axial design strength, P_n is calculated as:

$$\phi_c P_n = 0.85 A_s F_{cr} \tag{2.3}$$

where 0.85 is the value of the resistance factor for compression, ϕ_c, and the critical column stress, F_{cr} is:

$$\begin{aligned} F_{cr} &= \left(0.658^{\lambda_c^2}\right) F_{my} \qquad \text{for } \lambda_c^2 \le 2.25 \\ F_{cr} &= \frac{0.877}{\lambda_c^2} F_{my} \qquad \text{for } \lambda_c^2 > 2.25 \\ \lambda_c^2 &= \left(\frac{KL}{\pi r_m}\right)^2 \frac{F_{my}}{E_m} \end{aligned} \tag{2.4}$$

where r_m is the modified radius of gyration about the axis of buckling. The modified yield stress, F_{my}, and the modified modulus of elasticity, E_m are defined as:

$$\begin{aligned} F_{my} &= F_y + \frac{c_2 f_c' A_c}{A_s} \\ E_m &= E_s + \frac{c_3 E_c A_c}{A_s} \end{aligned} \tag{2.5}$$

where c_2 is a coefficient equal to 0.85 because the confined concrete inside a tube can reach stresses as high as $0.85 * f_c'$, and c_3 is a coefficient equal to 0.4 that accounts for uncertainty in the concrete contribution to the buckling strength of a composite concrete-filled tube. The value of E_c used by the AISC Specifications is $\omega^{1.5}\sqrt{f_c'}$ in kips/in^2, where ω is the density of concrete in lb/ft^3 and f_c' is in kips/in^2. (Corresponds to $0.041\,\omega^{1.5}\sqrt{f_c'}$ in S.I. units, with f_c' and E_c in MPa and ω in kg/m^3). Note that for $\lambda = 0$, the strength equation becomes:

$$\phi P_n = 0.85\left[A_s F_y + 0.85 A_c f_c'\right] \tag{2.6}$$

which means that the capacity of a concrete filled steel column is taken as the sum of the strengths of its parts.

The conventional calculation of the radius of gyration cannot be used in a concrete-filled steel column because, although both the steel and the concrete contribute to the flexural deformation of the cross-section, either steel or concrete may dominate flexural stiffness, depending on cross-section width and thickness. There is no single equation that can reliably be used to account for the composite flexural stiffness. Therefore, the AISC indicates that if the steel predominates, the radius of gyration of steel is adequate for the entire section, however if the flexural deformation is resisted primarily by the concrete, the radius of gyration of concrete is adequate for the section. Consequently, AISC specifies that r_m should be taken as the radius of gyration of the steel tube alone, but no less than 30% of the thickness of gross composite section in the plane of buckling.

2.3.2.2 Bending and Axial Load

For symmetrical composite columns about the plane of bending, the interaction of compression and flexure should be limited by:

$$\begin{aligned} &\frac{P_u}{\phi_c P_n} + \frac{8M_u}{9\phi_b M_n} \le 1.0 \qquad \text{for } P_u \ge 0.2\phi_c P_n \\ &\frac{P_u}{2\phi_c P_n} + \frac{M_u}{\phi_b M_n} \le 1.0 \qquad \text{for } P_u < 0.2\phi_c P_n \end{aligned} \tag{2.7}$$

where P_u is the factored axial force, and M_u is the factored moment increased for member and global slenderness effects. The axial design strength, $\phi_c P_n$, is given by Equation 2.3, and ϕ_b is the resistance factor for bending, taken equal to 0.85. The AISC specifications states that the specified flexural design strength be computed using the plastic strength distribution on the cross-section, and requires an empirical reduction of that value in absence of shear connectors when $\frac{P_u}{\phi P_n}$ is less than 0.3.

Alternately, an approximate and slightly conservative equation for the plastic moment capacity of the composite section, M_n, proposed by Galambos and Chapuis (1980), presented in the commentary to the AISC Specifications, gives:

$$M_n = ZF_y + \left(\frac{h_2}{2} - \frac{A_w F_y}{1.7 f_c' h_1} \right) A_w F_y \tag{2.8}$$

in which Z is the plastic section modulus of the steel shape alone, h_1 is the concrete width perpendicular to the plane of bending, h_2 is the concrete thickness in the plane of bending, and A_w is the web area of the steel shape. This equation is said to be applicable to concrete-filled pipe and tubes.

2.3.3 ACI Building Code (1995)

The American Concrete Institute Building Code 318-95 (ACI 1995) defines a composite column as "reinforced longitudinally with structural shapes, pipe or tubing with or without longitudinal bars." The design procedures in this code are similar to the procedures for standard reinforced concrete columns. For concrete-filled steel tubes to be designed as a beam-column, a moment magnification factor (δ) must first be calculated to account for the effects of column slenderness:

$$\delta = \frac{0.6 - 0.4 \frac{M_{u1}}{M_{u2}}}{1 - \frac{P_u}{\phi P_e}} \tag{2.9}$$

where M_{u1} and M_{u2} are the smaller and larger required moments applied at each end of the column, respectively, ϕ is the capacity-reduction factor taken as 0.7 for concrete-filled tubes, and P_u is the factored axial force acting on the column. P_e is the Euler buckling strength given as:

$$P_e = \frac{\pi^2 EI}{(kL)^2} \tag{2.10}$$

in which k is the effective length factor.

The calculation of EI for the elastic Euler buckling strength can be calculated in one of two ways, the second equation usually giving larger EI values for concrete-filled steel tubes:

$$EI = \frac{0.40E_cI_g}{1+\beta_d}$$
$$EI = \frac{0.20E_cI_g}{1+\beta_d} + E_sI_s \qquad (2.11)$$

where β_d is the ratio of the factored permanent axial load to the factored total axial load, usually taken as $1.4\frac{P_d}{P_u}$, I_g is the moment of inertia of the gross concrete core section, and all other terms are as defined previously. A minimum eccentricity, e, of the axial force is specified by the ACI 1995 specifications as:

$$e_{min}=0.6+0.03h \qquad (2.12)$$

where h is the column depth in inches.

For the design of concrete-filled steel tubes, ACI 1995 limits the longitudinal strain in concrete to 0.3%, and the axial resistance of columns is restricted to 85% of the value calculated in Equation 2.6 using a reduction factor, ϕ, equal to 0.75. Therefore,

$$P_u \leq 0.85\phi P_o = 0.85\ (0.75P_o) = 0.63P_o \qquad (2.13)$$

2.3.4 CAN/CSA-S16.1-M94

According to the Canadian Standard CAN/CSA-S16.1-M94 "Limit States Design of Steel Structures", hollow structural sections (HSS) classified as Class 1, 2, 3, and completely filled with concrete may be used as composite columns to carry axial loads. Class 4 sections completely filled with concrete may also be designed as composite columns if the width-to-thickness ratio of walls of rectangular HSS is less than $\frac{1350}{\sqrt{F_y}}$, and the outside diameter-to-thickness ratios of circular HSS is less than $\frac{28\,000}{F_y}$.

2.3.4.1 Axial Compression

The clauses of the CAN/CSA-S16.1-M94 for HSS composite sections indicate that the steel shell carries the same axial load, C_r, as if it were hollow, and C_r' is the additional strength provided by the presence of a concrete core. Therefore, the factored compressive resistance, C_{rc} shall be taken as:

$$C_{rc} = \tau C_r + \tau' C_r' \tag{2.14a}$$

$$C_r' = 0.85\phi_c f_c' A_c \lambda_c^{-2} \left[\sqrt{1+0.25\lambda_c^{-4}} - 0.5\lambda_c^{-2} \right] \tag{2.14b}$$

$$\lambda_c = \frac{kL}{r_c}\sqrt{\frac{f_c'}{\pi^2 E_c}} \tag{2.14c}$$

$$C_r = \phi A_s F_y (1+\lambda_s^{2n})^{\left(-\frac{1}{n}\right)} \tag{2.14d}$$

$$\lambda_s = \frac{kL}{r_s}\sqrt{\frac{F_y}{\pi^2 E_s}} \tag{2.14e}$$

where τ is a coefficient used to reduce the contribution of the steel when concrete strength increases due to confinement, and τ' is a coefficient that increases the contribution of the concrete for the same reason. E_c is specified to be $(1+S/T)\ 2500\sqrt{f_c'}$ in MPa for normal-weight concrete where S is the short-term load and T is the total load on the column, as it is assumed that the effects of long-term loading and creep reduce the contribution of the concrete core to resist the applied axial loads by decreasing the value of λ_c.

For all rectangular hollow structural sections and for circular hollow structural sections with a height-to-diameter ratio of 25 or greater, CAN/CSA-S16.1-M94 specifies, $\tau=\tau'=1.0$ (which implies no effective confinement). Otherwise:

$$\tau = \frac{1}{\sqrt{1+\rho_s+\rho_s^2}}$$

$$\tau' = 1+\left(\frac{25\rho_s^2\tau}{(D/t)}\right)\left(\frac{F_y}{0.85f_c'}\right) \qquad (2.15)$$

$$\rho_s = 0.02\left(25-\frac{L}{D}\right)$$

2.3.4.2 Combined Bending and Axial Load

In CAN/CSA-S16.1-M94, the steel section is assumed to resist all bending forces. Therefore, the steel shell must be designed as a beam-column to resist all flexure, plus the axial compression load equal to the difference between the total axial compression load applied, C_f, and the portion that is resisted by the concrete core, $\tau' C_r'$. Therefore, when $M_f \le \tau M_r$ and $C_f > \tau' C_r'$:

$$\frac{C_f-\tau' C_r'}{\tau C_r}+\frac{\omega_1 M_f}{\tau M_r\left(1-\dfrac{C_f-\tau' C_r'}{C_e}\right)} \le 1.0 \qquad (2.16)$$

where M_f is the factored applied moment, C_e is the Euler buckling strength of the steel tube alone, and ω_1 is the equivalent uniform bending effect in beam-columns (Clause 13.8.4). M_r is the factored moment resistance equal to $\phi_s Z F_y$ for Class 1 and 2 sections, and $\phi_s S F_y$ for Class 3 sections. The resistance factor for steel, ϕ_s, is equal to 0.9, and for concrete, ϕ_c, equals 0.6.

2.3.5 CAN3-A23.3-M94

The Canadian Concrete Design Handbook CAN3-A23.3-M94 (1994) states that "composite compression members shall include all such members reinforced longitudinally with bars and structural steel shapes, pipe or tubing." The design equations are the same as the ACI 1995 code. However, CAN3-A23.3-M94 adds that the total cross-section area of the steel shell

shall not exceed 20% of the gross area of the composite column, and that the specified minimum yield strength of the steel shall not exceed 350 MPa.

2.3.6 Chinese Design Specifications (Interpreted by Cai (1992))

The design approach of the "Chinese Specification for the Design and Construction of Concrete-Filled Steel Tubular Structures," CECS 28:90 (1991) has been reported by Cai (1992). The design equations are based on limit states design principles. There are a few limitations proposed on a concrete filled steel column by the CECS 28:90 (1991). The cross-section property, should be limited by $0.3 \le \theta \le 3$, as described in Equation 2.17. The D/t ratio of the steel tube, must be between 20 and $85\sqrt{(235/F_y)}$, where F_y is the yield strength of the steel. The slenderness ratio, L/d should not exceed 50.

The ultimate load-carrying capacity of the concrete filled steel columns, N_u is defined as,

$$\begin{aligned} N_u &= \phi_1 \phi_e N_o \\ \text{where} \quad N_o &= A_c f_c (1 + \sqrt{\theta} + \theta) \\ \theta &= \frac{A_s f_s}{A_c f_c} \end{aligned} \tag{2.17}$$

where N_o is the squash load of a concentrically-loaded short column, and θ is the confinement index. The strength reduction factor due to the eccentricity ratio, φ_e is estimated as:

$$\begin{aligned} \varphi_e &= 1/(1+1.85e_o/r_c) && \text{for } e_o/r_c \le 1.55 \\ \varphi_e &= 0.4/(e_o/r_c) && \text{for } e_o/r_c > 1.55 \end{aligned} \tag{2.18}$$

where e_o is equal to the initial eccentricity (taken as M_2/N) where M_2 is the larger of the end moments of column, N is the applied axial load and r is the radius of concrete core.

The strength reduction factor due to the slenderness ratio, φ_1 is estimated:

$$\begin{aligned} \varphi_1 &= 1 && \text{for } L_e/d \le 4 \\ \varphi_1 &= 1 - 0.115\sqrt{(L_e/d - 4)} && \text{for } L_e/d > 4 \end{aligned} \tag{2.19}$$

where d is the diameter of the column and L_e is the equivalent-effective length of the column computed by $L_e = \mu kL$. The effective length factor, μ, is dependent on the degree of lateral and rotational restraints at the ends of columns and the equivalent length factor, k is dependent on the gradient of moment distribution and can be determined as:

$$k = 0.5 + 0.3\beta + 0.2\beta^2 \qquad \text{for braced frame columns} \qquad (2.20)$$

$$k = 1 - 0.625e_0/r_c \text{ but } k \geq 0.5 \qquad \text{for unbraced frame columns}$$

in which β is the ratio of the smaller to the larger end moment on column, taking single curvature as positive and double curvature bending as negative. The condition, $\varphi_1\varphi_e \leq \varphi_0$ should be satisfied and φ_0 equals φ_1 when $L_e = \mu L$.

The stiffness of the composite column is taken as if both materials act independently,

$$EI = E_cI_c + E_sI_s \qquad \text{for flexural load,} \qquad (2.21)$$

$$EA = E_cA_c + E_sA_s \qquad \text{for axial load.}$$

The bearing capacity of a concrete-filled steel column, N_{ub} loaded over a local bearing area of concrete, A_1 can be calculated as:

$$N_{ub} = N_o\sqrt{(A_1/A_c)} \qquad (2.22)$$

2.3.7 Japanese Code (Interpreted by Prion and Boehme (1994))

The Japanese Code has an ultimate strength provision for earthquake design for concrete-filled steel columns based on the superposition method (Figure 2.2). The premise behind the method is that bond does not exist between the steel shell and the concrete core. Therefore, no strain compatibility is assumed, and the steel and concrete contribution to total flexure and axial resistance is calculated separately. The designer has control over the allotment of loads that are carried by each material. If the concrete is deemed to resist all of the axial load, the entire steel tube can be used for moment resistance which gives the largest composite column strength per the Japanese design procedure. The equations from this code are:

$$
\begin{aligned}
C_c &= 0.25(0.85f_c')D^2(\alpha - \sin\alpha\cos\alpha) \\
M_c &= \frac{1}{12}(0.85f_c')D^3(\sin^2\alpha) \\
M_s &= F_yZ \qquad\qquad \text{if } C_s \le 0.2A_sF_y \\
M_s &= 1.25\left(1-\frac{C_s}{A_sF_y}\right)F_yZ \qquad \text{if } 0.2A_sF_y \ge A_sF_y
\end{aligned}
\tag{2.23}
$$

where C_c and C_s are the axial resistance of the concrete core and steel tube, respectively, M_c and M_s are the moment resistance for the concrete core and steel tube, respectively, and α is the angle as shown in Figure 2.2. Prion and Boehme (1994) commented that the Japanese code can be unconservative for large D/t ratios, based on their test results for concrete-filled steel tubes having a D/t of 92.

2.3.8 Eurocode 4 (1994)

Eurocode 4 (1994) - "Design of Composite Steel and Concrete Structures" limits its scope to concrete-filled steel tubes that are isolated non-sway columns either as part of a non-sway frame or as an independent member. Two methods of design are included in this code; a general method and a simplified method, but only the latter will be discussed here. To use the simplified method, the following conditions must be met:

1. The column must have a uniform cross-section and be doubly symmetric over the entire column length.
2. The steel members must be rolled or welded, and the steel contribution ratio, δ, must be between 0.2 and 0.9, where

$$
\delta = \frac{(A_a f_y)/\gamma_{Ma}}{N_p} \tag{2.24}
$$

and A_a is the cross-sectional area of the steel tube, γ_a is the partial safety factor for steel taken equal to 1.10, and N_p is the plastic compressive resistance of the composite column.

3. The non-dimensional slenderness factor, λ, must not exceed 2.0:
where N_{cr} is defined in Equation 2.34.

$$\lambda = \sqrt{\frac{N_p}{N_{cr}}} \tag{2.25}$$

4. The 28 day concrete strength must be greater than 20 MPa.

Furthermore, local buckling of the steel tube must be taken into account, unless the following conditions are met:

$$\begin{aligned} \frac{d}{t} &\le 90\left(\frac{235}{f_y}\right) && \text{circular sections} \\ \frac{h}{t} &\le 52\sqrt{\frac{235}{f_y}} && \text{rectangular sections} \end{aligned} \tag{2.26}$$

2.3.8.1 Axial Compression

The axial resistance, N_p for a concrete-filled steel section is calculated using the characteristic compressive strength of concrete, f_{ck}, instead of the value $0.85f_{ck}$ used for encased sections or reinforced concrete sections. The equation for N_p is:

$$N_p = \frac{A_a f_y}{\gamma_{Ma}} + \frac{A_c f_{ck}}{\gamma_c} \tag{2.27}$$

where A_c is the cross-sectional area of the concrete core, and γ_{Ma} and γ_c are the partial safety factors for steel and concrete. For circular sections, an increased concrete strength due to confinement is used, if the following conditions are met:

- λ as calculated by Equation 2.25 is not greater than 0.5, and

- M_f is not greater than $N_f \frac{d}{10}$, where d is the diameter of the column, M_f and N_f are the applied moment and axial load, respectively.

Likewise, a reduced steel strength due to biaxial stresses is considered if the same conditions are met.

Therefore, the plastic axial resistance, N_p of a circular concrete-filled steel column becomes:

$$N_p = \frac{A_a \eta_2 f_y}{\gamma_{Ma}} + \frac{A_c f_{ck}}{\gamma_c} * \left(1 + \eta_1 \left(\frac{t}{d}\right)\left(\frac{f_y}{f_{ck}}\right)\right) \tag{2.28}$$

Values of η_1 and η_2 are defined depending on the eccentricity of the axial load. If $e = \frac{M_f}{N_f} = 0$ then

$$\begin{aligned} \eta_{10} &= 4.9 - 18.5\lambda + 17.0\lambda^2 \quad (\text{but } \eta_{10} \geq 0) \\ \eta_{20} &= 0.25 * (3 + 2\lambda) \quad (\text{but } \eta_{20} \leq 1.0) \end{aligned} \tag{2.29}$$

If $0 < e \leq \frac{d}{10}$ then:

$$\begin{aligned} \eta_1 &= \eta_{10}\left(1 - 10\frac{e}{d}\right) \\ \eta_2 &= \eta_{20} + (1 + \eta_{20})\left(10\frac{e}{d}\right) \end{aligned} \tag{2.30}$$

If $e > \frac{d}{10}$ then:

$$\eta_1 = 0.0 \quad \text{and} \quad \eta_2 = 1.0 \tag{2.31}$$

The member has sufficient resistance if, for both axes:

$$N_f \leq \chi N_p \tag{2.32}$$

where χ is the reduction coefficient for the relevant buckling mode, and calculated as:

$$\chi = f_k - \sqrt{(f_k^2 - \lambda^{-2})} \leq 1.0$$
$$\text{where} \quad f_k = 0.5\lambda^{-2}(1 + 0.21(\lambda - 0.2) + \lambda^2) \tag{2.33}$$

N_{cr} is the elastic critical load used to calculate the slenderness factor, and is given by:

$$N_{cr} = \frac{\pi^2 (EI)_e}{L^2} \tag{2.34}$$

where L is the buckling length, and $(EI)_e$ is the equivalent elastic modulus of the composite column calculated as the sum of the individual components:

$$(EI)_e = E_a I_a + 0.8 E_{cd} I_c \tag{2.35}$$

where I_a and I_c are the second moments of area for the steel and uncracked concrete core, respectively, E_a is the elastic modulus for the structural steel taken as 210000 MPa and E_{cd} is the secant modulus of elasticity for short term loading of concrete.

2.3.8.2 Bending and Axial Load

The bending moment on the column is determined by assuming the axial load acts through the centroid. Second order effects must be checked unless the column:

- Is an isolated non-sway column,
- $\frac{N_f}{N_{cr}} \leq 0.1$,
- Has end moments, and then the relative slenderness, λ_{crit}, does not exceed $\lambda_{crit} \leq 0.2(2-r)$, where r is the ratio of the end moments, if any transverse loading exists, $r = 1.0$.

Using the above criteria, M_f is the maximum design bending moment within the column length.

A separate check is required for each axis of symmetry taking into account slenderness, bending moments and resistance in bending. The code uses a simplified force versus moment

interaction diagram to calculate the resistance of a section in combined bending and axial loading. Plastic analysis and a rectangular stress block for the steel tube and concrete core are used to derive the equations.

Figure 2.3 shows a typical interaction diagram. Point A (N_A and M_A) represents the case of zero moment and full plastic axial load. This load was described previously in Equation 2.28 as N_p. The second point on the graph, point C (N_C and M_C), corresponds to the compressive resistance of the concrete core. The third point on the graph, point D (N_D and M_D) is calculated as half of the axial resistance at point C. The final point, point B (N_B and M_B), corresponds to the plastic moment in absence of axial force applied, therefore, N_B is equal to zero. The representative axial load resistance for each of the points are defined by Eurocode as:

$$
\begin{aligned}
N_A &= \frac{A_a \eta^2 f_y}{\gamma_{Ma}} + \frac{A_c f_{ck}}{\gamma_c} * \left(1 + \eta_1 \left(\frac{t}{d}\right)\left(\frac{f_y}{f_{ck}}\right)\right) \quad \text{.....circular section} \\
N_A &= \frac{A_a f_y}{\gamma_{Ma}} + \frac{A_c f_{ck}}{\gamma_c} \quad \text{.....rectangular section} \\
N_C &= \frac{f_{ck} * A_c}{\gamma_c} \\
N_D &= 0.5 * \frac{f_{ck} * A_c}{\gamma_c}
\end{aligned}
\tag{2.36}
$$

The representative bending moment resistance for each of the points are defined as:

$$
\begin{aligned}
M_A &= 0 \\
M_D &= Z_s \frac{f_y}{\gamma_{Ma}} + 0.5 * Z_c \frac{f_{ck}}{\gamma_c} \\
M_B &= M_C = M_D - 2\left(t * h_n^2\right)\frac{f_y}{\gamma_{Ma}} - 0.5\left((D-2t) * h_n^2\right)\frac{f_{ck}}{\gamma_c}
\end{aligned}
\tag{2.37}
$$

$$
\text{where} \quad h_n = \frac{N_C}{\left(2Df_{ck} + 4t(2f_y - f_{ck})\right)}
$$

where Z_s and Z_c are the plastic section moduli of the steel tube and concrete core, respectively, D and t are the outside diameter and thickness of the steel tube, respectively. M_B is also considered the plastic moment resistance, M_p. The parameters η_1 and η_2 are defined in Equations 2.29, 2.30, or 2.31.

The code also stipulates that member resistance to bending and compression must account for slenderness and imperfections. The value of χ as found in Equation 2.33 is used to calculate χN_p. Figure 2.4 shows a graphical representation of all forces and Equation 2.38 defines χ_n and χ_d.

$$\chi_d = \frac{N_f}{N_p}$$
$$\chi_n = \chi * 0.25 * (1 - r) \quad \text{but } \chi_n \leq \chi_d \tag{2.38}$$

where r is the ratio of the lesser to the greater end moment. The corresponding bending moment resistance, μ_k and μ_d are determined from the graph and the respective axial resistance factor, χ and χ_d. The length of μ as seen in Figure 2.4, is calculated as:

$$\mu = \mu_d - \mu_k * \frac{\chi_d - \chi_n}{\chi - \chi_n} \tag{2.39}$$

The value of μ must not be greater than unity unless the bending moment and axial load are dependent as is the case with an eccentric axial load. When $N_f < N_C$, as in Figure 2.4, the increase in bending resistance due to the axial force may be overestimated if the axial force, N_f, and the applied bending moment, M_f are independent. The code recommends reducing the partial safety factors, γ_{Ma} and γ_c, by 20% when calculating the applied loads, N_f.

Therefore, the member flexural resistance is given by the following equation:

$$M_f \leq 0.9 \mu M_p \tag{2.40}$$

2.3.9 Shear Strength

None of the above codes provide guidance to calculate the shear strength of concrete-filled tubes. Engineers may elect to rely solely on the steel tube for that purpose; in that case, the shear strength can be calculated from basic principles, for a round tube by:

$$V_s = A_{eq}\tau_y = 0.6A_{eq}Fy = 0.3A_sF_y \tag{2.41}$$

where A_{eg} is the equivalent shear areas, equal to half of the steel gross area for a round tube (Computers & Structures Inc. 1992)

Alternatively, composite action may be estimated by assuming that part of the steel shell can act as steel stirrups, by analogy with reinforced concrete design. The strength of circular concrete-filled tubes is therefore the sum of the concrete shear strength, V_c, and the shear strength, V_s, of the remaining steel after deducting the portions of the steel shell needed to complete the concrete compression-tension strut analysis. Therefore,

$$\begin{aligned} V_n &= V_c + V_s \\ V_n &= 5v_cA_{cv} + \left[0.6\left(\frac{1}{2}A_sF_y - 5v_cA_{cv}\right)\right] \\ V_n &= 2v_cA_{cv} + 3A_sF_y \end{aligned} \tag{2.42}$$

where v_c, in ksi, is the nominal concrete shear resistance, in ksi equal to $2\sqrt{0.001\ f_c'}$. A_{cv} is the shear area of the concrete in in^2, assumed to be equal to one half of the concrete area, with f_c' and F_y in ksi.

2.4 Other Design Equations Proposed by Researchers

Design equations have been proposed by many researchers based on results from experimental work. Since this study focuses on circular concrete-filled columns, the analytical work and design equations related to this type of composite section is reported in more detail. Some of the design equations strictly developed for rectangular concrete-filled steel tubes are also

briefly explained here, but the reader is left to consult the presented references for a more in-depth explanation.

2.4.1 Rectangular Columns

2.4.1.1 Non-Cyclic Analysis

Bradford (1996) reported on the calculation of an axial load and bending moment interaction curve. The cross-sectional strength was calculated by simple plastic theory, using an elastic-perfectly plastic steel model and a concrete model that reaches an ultimate stress of 0.85 f_c' at a strain of 0.003. The neutral axis is found for the balanced condition, when the outermost concrete strain has a value of 0.003 and bottom steel flange has a strain of 0.002. The resulting force and moment are obtained to produce one point on the axial load and bending moment curve. By adjusting the neutral axis, other points can be calculated producing a complete interaction curve.

Wang and Moore (1997) investigated the design methods of the British Standards 5400 and Eurocode 4 for rectangular concrete-filled steel tubes, and proposed an alternative approach which is simpler to use and reduces design time but is as accurate as the two code methods. The proposed method uses the analysis from the British Standards 5950 for the design of bare steel members and replaces the properties with applicable equations for composite structures. Their method uses a capacity check as well as an overall buckling check. The equations were not checked for use with circular concrete-filled columns.

2.4.1.2 Cyclic Analysis

Usami et al. (1992) use descriptive parameters to analyze the ductility and energy-absorption capacity of columns under cyclic loading. Ohno and Nishioka (1984) noted that the inelastic behaviour of a structure is dependent on its displacement history. Therefore, Usami et al. proposed normalized energy absorption as a more objective measure of the inelastic performance of a specimen taking into account its load displacement history.

Hajjar and Gourley (1997) developed a finite-element "macro" model to investigate the beam-column behaviour of concrete-filled rectangular steel tubes subjected to cyclic loading. Full bond was assumed (even in the absence of shear connectors). The stiffness model took into account the reduction of the elastic modulus of concrete as a function of member rotation and curvature. Non-linear modeling was used to account for strength degradation, stiffness degradation, Bauschinger effect, steel local buckling, or concrete crushing.

An iterative method to calculate the cyclic moment curvature relationship of rectangular concrete-filled columns was used by Kawaguchi et al. (1997). The cyclic constitutive steel model proposed by Morino et al. (1992) was used together with the concrete model proposed by Popovics (1973). A trial and error method was used to find the strains and stresses that satisfy equilibrium for a given curvature. The length of the plastic hinge was taken equal to the width of the column. Results from the analysis procedure were compared with results from cyclic tests on columns. Kawaguchi et al. (1997) noted that the hysteresis curve resembled a series of parallelograms and attributed it to poor modelling of Baushinger's effect.

2.4.2 Circular Columns

2.4.2.1 Design Equations by Furlong (1967, 1968)

Furlong (1968) proposed design equations for both long and short composite columns. The ultimate load of a short concrete-filled steel tube is calculated by assuming that the steel tube has reached its yield stress, the maximum strain in the concrete is equal to the yield strain of the steel, and the stress at any point in the concrete is calculated directly from the concrete stress-strain curve given by:

$$f_c = f_c' \sqrt{\frac{\epsilon_c}{\epsilon_o}} \qquad \frac{\epsilon_c}{\epsilon_o} \leq 1.0 \tag{2.43}$$

in which f_c and ϵ_c are the stress and strain in the concrete, f_c' is the ultimate compression strength of a concrete cylinder, ϵ_o is the maximum strain in the concrete, taken as equal to 0.0018. For mild steels having a yield strain, ϵ_s no greater than 0.0018, this gives the following ultimate load P_o for short columns as:

$$P_o = A_s f_y + A_c f_c' \sqrt{\frac{f_y}{0.0018\ E_s}}$$

$$\text{or} \quad P_o = A_g \left[\rho f_y + (1-\rho) f_c' \sqrt{\frac{f_y}{0.0018\ E_s}} \right] \tag{2.44}$$

where A_g is the gross cross-sectional area of the column, $\rho = \frac{A_s}{A_g}$, and all other terms are as previously defined. The plastic bending strength of the circular steel alone, M_o, is given by:

$$M_o = \left(\frac{f_y}{6}\right)(D_o^3 - D_i^3) = \left(\frac{f_y}{6}\right) D_o^3 \left(1-(1-\rho)^{\frac{3}{2}}\right) \tag{2.45}$$

where D_o and D_i are the outer and inner steel tube diameters, respectively. Based on test results available at the time on concrete-filled tubes and pipes of up to 150 mm diameter, Furlong proposed the following as a lower bound strength interaction formula suitable for hand calculation:

$$\left(\frac{P}{P_o}\right)^2 + \left(\frac{M}{M_o}\right)^2 \le 1.0 \tag{2.46}$$

in which P and M are the axial load and bending moment applied to the concrete-filled steel column. Furlong (1968) recognized the large conservatism of this equation as shown in Figure 2.5. However, the more precise interaction is tedious to obtain without a computer. Furlong found better agreement with test results when considering the composite column simply as a reinforced concrete column using ACI design equations but with a maximum concrete stress of $1.0 f_c'$ instead of $0.85 f_c'$, at a maximum concrete strain of 0.003, as shown in Figure 2.6.

Furlong (1968) also investigated the bond between the steel shell and the concrete core. Having observed nearly identical axial force versus axial strain curves and moment curvature results for specimens greased to prevent bond between the steel and concrete and ungreased specimens, Furlong concluded that the bond between the steel shell and the concrete core was insignificant during testing. Therefore, stiffness of the composite column was stated to be the algebraic sum of each component's stiffness as if they were acting independently. This relationship can be expressed as,

$$AE_{comp} = A_c E_c + A_s E_s \tag{2.47a}$$

$$EI_{comp} = E_c I_c + E_s I_s \tag{2.47b}$$

where AE_{comp} and EI_{comp} are the composite stiffness under axial load and under flexural load, respectively, and $E_c = w^{1.5}\sqrt{f_c'}$ where w is in lb/ft^3 and f_c' is in ksi. Experimental data available at the time agreed with this expression. Furlong (1968) defined the effective radius of gyration, r, as,

$$r = \sqrt{\frac{E_c I_c + E_s I_s}{A_c E_c + A_s E_s}} \tag{2.48}$$

With only limited experimental data available on the behaviour of axially loaded long-composite columns, Furlong proposed a Euler buckling load to calculate the axial strength of long concrete-filled steel columns, P_{cr}:

$$P_{cr} = \frac{\pi^2}{h^2} EI_{comp} \tag{2.49}$$

where h is the effective unsupported height of the column. Substituting the following equation,

$$EI_{comp} = I_g[E_s + (1-\rho)^2(E_c - E_s)] \tag{2.50}$$

where I_g is the moment of inertia of the gross section, gives an equation for P_{cr},

$$P_{cr} = \left(\frac{\pi}{kL}\right)^2 I_g[E_s+(1-\rho)^2\ (E_c-E_s)] \tag{2.51}$$

Furlong judged the above to be valid only for $P_{cr} \leq 0.5P_o$ with P_o defined in Equation (2.44) and recommended reducing the expression for EI_{comp} for axial load in excess of 0.5 P_o to account for observed reduction in EI under large axial forces. This is achieved as follows:

$$EI_{comp} = I_g[E_s+(1-\rho)^2(E_c-E_s)]\frac{4P_{cr}}{P_o}\left(1-\frac{P_{cr}}{P_o}\right)$$

and $$P_{cr} = P_o\left(1 - \frac{(kL)^2}{I_g}\left(\frac{P_o}{4\pi^2}\right)\left(\frac{1}{E_s + (1-\rho)^2\,(E_c-E_s)}\right)\right) \tag{2.52}$$

2.4.2.2 Design Equations by Neogi et al. (1969)

Neogi et al. (1969) proposed design equations for concrete-filled steel columns under eccentric loads. These were analytically derived using the uniaxial stress-strain curves for steel and concrete, neglecting the tensile strength of concrete. Other assumptions include:

- Complete interaction takes place between the steel tube and the concrete core.
- Plane sections remain plane after bending.
- Failure due to local buckling or due to shear stress does not occur.
- Elasto-plastic stress-strain curve for steel with a parabolic transition between the elastic and plastic regions. Some calculations take into account the strain hardening in steel.
- The concrete stress-strain curve is given as:

$$\frac{f_c}{f_c'} = \frac{2\left(\frac{\epsilon}{\epsilon_m}\right)}{1+\left(\frac{\epsilon}{\epsilon_m}\right)^2} \tag{2.53}$$

where f_c is the concrete stress, ϵ is the concrete strain, f_c' is the peak stress in concrete taken equal to $0.8f_{cu}$ where f_{cu} is the cube strength of concrete, and ϵ_m is the strain corresponding to f_c'. The

initial slope of that stress-strain curve, E_{co} equal to $2\frac{f_c'}{\epsilon_m}$ is related to the maximum stress f_c by the linear equation given by Hognestad (1951):

$$E_{co}=1800000 + 415f_c \tag{2.54}$$

where E_{co} and f_c are in psi.

For concentrically loaded concrete-filled steel columns, the tangent modulus load approach along with the stresses in each material was used to find the ultimate buckling load, P_{tan}. Equating the tangent Euler Buckling expression to the axial load expression for the composite column gives:

$$\begin{aligned} & P_{\tan} = \frac{\pi^2}{L^2}(E_{ts}I_s + E_{tc}I_c) \\ \text{and} \quad & P_{\tan} = A_s\sigma_s + A_c\sigma_c \\ \text{therefore} \quad & \frac{\pi^2}{L^2}(E_{ts}I_s + E_{tc}I_c) = (A_s\sigma_s + A_c\sigma_c) \end{aligned} \tag{2.55}$$

This equation is solved iteratively by a computer program that finds a satisfactory strain distribution.

For eccentrically loaded columns, Neogi et al. used the well known differential equation of equilibrium in the deformed configuration:

$$M + Py = 0 \tag{2.56a}$$

$$EI \cdot \frac{d^2y}{dz^2} + Py = 0 \tag{2.56b}$$

where EI is the flexural stiffness, and y is the lateral deflection of the column. Stresses and strains in both materials are considered. The procedure is otherwise identical to what is customarily done for the development of beam-column interaction curves.

The linear strain distribution at any section can be completely specified by the curvature ρ and the distance Y of the neutral axis from the central axis, as shown in Figure 2.7 for two different neutral axis positions. A layer model of the cross-section was used to calculate the corresponding stresses acting on the cross-section, and the resulting axial force and moment. An iterative procedure was used to find the curvatures and neutral axis position corresponding to the desired forces acting on the cross-section. The deflected shape was calculated using finite difference at a number of different sections along the column length. Nearly identical results were also found using the simplified deflected shape,

$$y = y_o \cos\frac{\pi z}{L} \tag{2.57}$$

in which y_o is the lateral deflection of the member at mid-height, and z is defined as (0,0) at the mid-height of the column. Good correlation with experimental results suggested that full composite behaviour develops in concrete-filled tubes.

2.4.2.3 Design Equations by Knowles and Park (1969)

Knowles and Park (1969) tested concrete cylinders in special steel moulds stacked vertically to simulate concrete-filled tubes subjected to axial load. Transverse and longitudinal strains were measured for each cylinder in a uniaxial testing machine to obtain stress-strain data. Then, the power law,

$$f_c = C_1\epsilon_c + C_2\epsilon_c^n \tag{2.58}$$

in which C_1, C_2, and n are constants, was used to fit a stress-strain curve. Considering both a least squares approach (n=1.5), and a parabolic curve (n=2) to find the best fit, the following two equations were derived to describe the stress-strain relationship of the concrete at mid-height of the concrete-filled tube. (i.e. This height corresponds to the location of the largest stresses and strains would occur in an eccentrically-loaded pin-pin column):

$$f_c = (6.22\epsilon_c - 76.0\epsilon_c^{1.5}) \cdot 10^6 \quad \text{(least squares approach)}$$
$$f_c = (4.925\epsilon_c - 1061.5\epsilon_c^2) \cdot 10^6 \quad \text{(parabolic curve)} \tag{2.59}$$

where stresses are expressed in psi. Knowles and Park (1969) experimentally found that when concrete increases in volume at a greater rate than the steel, occurring at a longitudinal strain of 0.002, it will exert a pressure on the steel which will provide a confining force to the concrete. Knowles and Park reasoned that slender columns that buckle before concrete strains reached values of 0.002 would not benefit from this confinement. To identify the range of slenderness ratios over which confinement is possible, the Euler buckling equation for the concrete core alone was used:

$$f_{cu} = \frac{\pi^2 E_{tc}}{\left(\frac{kL}{r_c}\right)^2} \tag{2.60}$$

where $\frac{kL}{r_c}$ is the slenderness ratio of the concrete core alone, and the tangent modulus of the concrete is obtained directly by the derivative of Equation 2.58:

$$E_{tc} = \frac{df_c}{d\epsilon} = C_1 + nC_2\epsilon_c^{n-1} \tag{2.61}$$

Substituting the stress-strain relationships of Equation 2.59 into Equation 2.60 the slenderness ratio of the concrete core, kL/r_c can be determined at a value of ϵ_c equal to 0.002. Using the least squares approach, and the parabolic relationships, this slenderness ratio of the concrete core can be calculated as 44.3 and 34.8 respectively. Knowles and Park noted that only small differences exist between the two stress-strain curves at a strain of 0.002. Therefore the steel tube could be assumed to confine the concrete core when kL/r_c is less than 34.8.

The interaction between axial force and bending moment was also analyzed by Knowles and Park (1969). The following straight line interaction curve based on limited data from tests on eccentrically loaded concrete-filled tube columns was proposed:

$$\left(\frac{P_u}{P_o}\right)+\left(\frac{M_u}{M_o}\right)=1.0 \tag{2.62}$$

where P_o was taken as the experimental result for a concentrically loaded column, M_o was taken as Sf_y of the steel tube, and M_u was the experimentally obtained ultimate bending moment calculated by multiplying P_u by the measured eccentricity at the ultimate axial load. Knowles and Park (1969) found the comparison of test results to the interaction formula to be conservative except for columns subjected to axial loads applied with large eccentricities, and warned that the straight line interaction formula is likely unsafe for slender columns (although this was beyond the scope of their study).

2.4.2.4 Design Equations by Knowles and Park (1970)

Knowles and Park (1970) developed design equations to determine the ultimate strength of axially loaded concrete-filled steel columns by following a tangent modulus approach and by assuming this strength to be equal to the sum of the strengths of the hollow steel tube and concrete core taken as acting independently. This approach was deemed appropriate for long columns because it does not take into account the increase in concrete strength caused by confinement due to the steel shell. However, for short composite columns where this confinement is possible, the proposed design equation was expected to give conservative result.

The ultimate buckling stress, f_{cu} of the concrete core taken alone was calculated using the following tangent modulus equation:

$$f_{cu} = \frac{\pi^2 E_{tc}}{\left(\frac{kL}{r_c}\right)^2} \tag{2.63}$$

in which E_{tc} is the tangent modulus of concrete and $\frac{kL}{r_c}$ is the slenderness ratio of the concrete core. By differentiating the stress strain curve for concrete proposed by Hognestad (1951):

$$f_c = f_c'' \left[2\frac{\epsilon_c}{\epsilon_o} - \left(\frac{\epsilon_c}{\epsilon_o} \right)^2 \right] \tag{2.64}$$

where $f_c'' = k_3 f_c'$, k_3 is a factor the represents the compressive strength of concrete in a member and f_c' is the concrete cylinder compressive strength. The following tangent modulus of concrete is obtained:

$$E_{tc} = E_c \sqrt{1 - \frac{f_c}{f_c'}} \tag{2.65}$$

where the initial modulus of elasticity of concrete, E_c can be taken as $2f_c'/\epsilon_o$. Therefore, the ultimate buckling load, P_{cu} of a concrete column can be calculated as:

$$\begin{aligned} P_{cu} &= f_c'' A_c 2q \left(\sqrt{q^2+1} - q \right) = 0.85 f_c' A_c 2q (\sqrt{q_1+1} - q) \\ q &= \frac{\pi^2}{\epsilon_o \left(\frac{KL}{r_c} \right)^2} = \frac{\pi^2}{\frac{2f_c'}{E_c} \left(\frac{KL}{r_c} \right)^2} \end{aligned} \tag{2.66}$$

The ultimate buckling load of the hollow steel tube, P_{su}, was taken from steel design specifications in effect at the time (AISC 1963). When $kL/r_s > \sqrt{2\pi^2 E_s / f_y}$:

$$P_{su} = \frac{A_s \pi^2 E_s}{\left(\frac{kL}{r_s} \right)^2} \tag{2.67}$$

where E_s is determined from steel coupon tests. For $kL/r_s < \sqrt{2\pi^2 E_s / f_y}$, a parabolic approximation to the AISC equation was proposed for P_{su}:

$$P_{su} = f_y A_s \left[1 - \frac{f_y \left(\frac{kL}{r_s} \right)^2}{4\pi^2 E_s} \right] \tag{2.68}$$

Knowles and Park's equation to calculate the strength of an axially loaded concrete-filled steel column is simply the sum of, P_{cu}, given by Equation 2.66, and P_{su} from Equations 2.67 or 2.68, depending on the slenderness ratio of the steel tube columns.

2.4.2.5 Design Equations by Ruoquan (1987)

Ruoquan (1987) developed a design equation for axial load behaviour for long concrete-filled steel columns. The following assumptions were used:

- The column is assumed to be ideally straight, hinged at both ends; load acts on the ends in an axial direction; under critical state, the deflection curve of the column is sinusoidal.
- The load capacity of a short column, N_u, includes the effect of a confining force.
- The stress-strain relationship for steel is found by experimental data.
- The ratio of proportional limit to yield point is taken as 0.8.
- Creep and shrinkage effects are neglected.

Ruoquan uses the following equilibrium differential equation for the column at the critical state, N_{cr}:

$$N_{cr} = \frac{\pi^2}{L^2}(E_{st} I_s + E_{ct} I_c) \tag{2.69}$$

The equation can be rewritten by using $\alpha = A_s/A_c$ and slenderness ratio $\lambda = 2L/r$ where r is the inside radius of the steel shell:

$$N_{cr}=\frac{\pi^2 A_c}{\lambda^2}(E_{ct}+2\alpha E_{st}+1.5\alpha^2 E_{st}) \tag{2.70}$$

To characterize the modulus of the composite column, Φ is used:

$$\Phi=E_{ct}+2\alpha E_{st}+1.5\alpha^2 E_{st} \tag{2.71}$$

The modulus of elasticity for steel, E_{st} was taken from Bleich (1952),

$$\begin{aligned} E_{st} &= E_s && \text{when } f_s \le f_p \\ E_{st} &= E_s\frac{(f_s' - f_s)f_s}{(f_s' - f_p)f_p} && \text{when } f_p < f_s \le f_s' \end{aligned} \tag{2.72}$$

where f_s' is the specified yield strength of steel and f_p is the proportional limit of steel obtained from tensile tests (taken as $0.8f_s'$). The solution of this differential equation yields:

$$f_s = \frac{f_s'}{1+0.25\exp\left[5\left(1-\frac{E_s\epsilon_s}{0.8f_s}\right)\right]} \tag{2.73}$$

In short columns where a confining force from the steel on the concrete may be likely, the longitudinal yield stress, f_s' will drop to f_s'' and according to Mises's yield condition, it can be determined as

$$f_s''=\frac{1}{\alpha}\sqrt{\alpha f_s^2-3f_1^2}-f_1 \tag{2.74}$$

$$\epsilon_s = \frac{0.8f_s'}{E_s}\left(1-0.2\ln\left[5\left(\frac{f_s}{f_s'}-1\right)\right]\right) \tag{2.75}$$

where f_l is the confining force for a short concrete-filled steel column at ultimate state obtained from analysis or tests. When the column loses stability at the elasto-plastic stage, Ruoquan recommends using f_s'' instead of f_s' in Equation 2.73.

The uniaxial stress-strain curve for concrete was proposed by Hognestad (1951) with ϵ_c' equivalent to ϵ_o.

$$f_c = f_c'\left[2\frac{\epsilon_c}{\epsilon_c'} - \left(\frac{\epsilon_c}{\epsilon_c'}\right)^2\right] \tag{2.76}$$

The equation for the tangent modulus of concrete, E_{ct}, can be determined by differentiating Equation 2.76 with respect to strain.

$$E_{ct} = f_c'\left(\frac{2}{\epsilon_c'} - \frac{2\epsilon}{(\epsilon_c')^2}\right) \tag{2.77}$$

Since the equation proposed by Hognestad (1951) is for a uniaxial relationship and a confining force is present in some concrete-filled steel columns, a tri-axial stress-strain relationship of core concrete and a corresponding tangent modulus was developed by Ruoquan (1981) as outlined in the following equations:

$$f_c = f_o'\left(1.62\frac{\epsilon_c}{\epsilon_c'} - 0.62\left(\frac{\epsilon_c}{\epsilon_c'}\right)^2\right) \tag{2.78}$$

$$E_{tc} = f_o'\left[\frac{1.62}{\epsilon_c'} - \frac{1.24\epsilon}{(\epsilon_c')^2}\right] \tag{2.79}$$

in which the strength of the concrete core under a compressive load, f_o', and the corresponding strain, ϵ_c', are defined by:

$$f_o' = f_c'\left(1 + 5.487\left(\frac{f_1}{f_c'}\right)^{0.907}\right) \tag{2.80a}$$

$$\epsilon_c' = \left(2000 + 500\frac{\alpha f_s'}{f_c'}\right)\cdot 10^{-6} \tag{2.80b}$$

The stability coefficient, ν, for concrete-filled steel tubular columns under axial compressive loading is defined as,

$$\nu = \frac{N_{cr}}{N_u} \tag{2.81}$$

Ruoquan developed two methods to determine the column slenderness value that would define the behaviour of a composite column under axial load. The first method equates the load capacity of a short column, N_u, to the critical load of the column, the Euler Buckling load. The boundary slenderness ratio, λ_o along with the tangent modulus for concrete are given in the following equations:

$$N_{cr} = \frac{\pi^2 A_c E_{ct}}{\lambda_o^2} = N_u$$

$$E_{ct} = 0.38\frac{f_c'}{\epsilon_c'} \tag{2.82}$$

$$\lambda_o = \pi\sqrt{\frac{A_c E_{ct}}{N_u}}$$

The second method assumes that when the confining force is very small it may be neglected when the stress of the steel tube is lower than the proportional limit, f_p. Therefore, the strength of the column becomes the strength of the individual materials. Equating this load with the critical load of the column in Equation 2.70, the following slenderness ratio is produced:

$$N_{cr} = \frac{\pi^2 A_c}{\lambda_p^2}\Phi = (\alpha f_p + f_c)A_c$$

$$\lambda_p = \pi\sqrt{\frac{\Phi}{\alpha f_p + f_c}} \tag{2.83}$$

From the above analysis, there are three cases that may apply. When $\lambda < \lambda_o$, N_{cr} is equal to N_u and the stability of the column is not in question. When $\lambda_o < \lambda \leq \lambda_p$, N_{cr} must be calculated with consideration of the influence of the confining force. When $\lambda > \lambda_p$, the column can be designated a long column and the confining force will not be used in calculations of the critical load.

2.4.2.6 Design Equations by Kato (1996)

Kato (1996) developed a design equation for axially loaded concrete filled steel tubes from ISO (1994). As defined in this standard, the buckling strength of the column, N_c is defined by the general form:

$$N_c = gN_y \tag{2.84}$$

where N_y is the maximum compressive strength and g is the reduction coefficient given in terms of the relative slenderness $\bar{\lambda}$ which is defined as :

$$\bar{\lambda} = \sqrt{\frac{N_y}{N_{cr}}} \tag{2.85}$$

where N_{cr} is the Euler elastic buckling strength. Kato (1996) adopted this concept and changed the equation for N_y as well as $\bar{\lambda}$, using instead:

$$\begin{aligned} N_y &= A_s\sigma_y + A_c f_c \\ \bar{\lambda} &= \frac{kL}{\pi}\sqrt{\frac{A_s\sigma_y + A_c f_c}{E_s I_s + E_c I_c}} \end{aligned} \tag{2.86}$$

and:

$$\begin{aligned} g &= B(1-\sqrt{1-C}) \\ B &= \frac{1+\alpha(\bar{\lambda}-\bar{\lambda}_o)+\bar{\lambda}^2}{2\bar{\lambda}^2} \\ \bar{\lambda}_o &= 0.2 \\ C &= (B\bar{\lambda})^{-2} \end{aligned} \tag{2.87}$$

in which α varies depending on the degree of imperfections.

Table 2.1 is a summary of results from a number of different sources compared with Kato's equations. The value of α used in the calculations in Table 2.1 is 0.34, and an additional strength factor of 1.1 was used to multiply the concrete strength to take into the effects of confinement. The value of E_c, in MPa is

$$E_c = 2.0548*10^4 \text{ x } \sqrt{\frac{f_c}{19.6}} \quad (2.88)$$

and the value for E_s was taken as 200000 MPa.

2.4.2.7 Layer Models

Layer models have been used by researchers to calculate the moment capacity of a concrete-filled steel tube. The analysis is achieved by dividing the steel shell and the concrete core into individual sections. A curvature analysis is performed by assuming a strain diagram at the critical section. Full bond is assumed, therefore, the curvature is identical for both materials. By equating the sum of forces on all of the sections due to the applied loads, a static equilibrium state is satisfied. A number of different stress-strain relationships for concrete, steel, and confinement effect have been considered by different researchers.

2.4.2.7.1 Design Analysis by Prion and Boehme (1994)

Prion and Boehme (1994) developed a design method utilizing strain compatibility to predict the strength of concrete-filled steel columns. A variable stress block according to the concrete stress-strain relationship given by Hognestad (1951) and a full plastic moment carried by the steel shell was implemented in a computer program which numerically integrates the stresses to obtain the moment resistance for a given axial load. Increases in concrete strength resulting from confinement by the steel tube were neglected. Two different moment resistance values were calculated, one taking into account axial load, and another assuming no axial load. Prion and Boehme compared the theoretical calculations to their test data of columns with a D/t ratio of 92, and found the ultimate strength to be predicted well using this model with the exception of high axially loaded beam columns, shown in Figure 2.8. However, they recommend using a model that assumes no strain compatibility with the steel and concrete acting as independent materials, such as the model used by the Japanese code (Section 2.3.7), for post-ultimate strength analysis.

2.4.2.7.2 Design Analysis by Itani (1996)

Itani (1996) developed a design equation for concrete-filled steel columns assuming that full bond will develop between the steel shell and the concrete core (even though he recommends the use of shear studs throughout the length of the column because of the separation of the two materials in the elastic range due to the differences in Poisson's ratio). The stress-strain relationship of steel is represented by three stages; an elastic region, the yield plateau, and a strain hardening region and it is assumed that the steel will behave in the same manner in both tension and compression. The concrete model is based on the confined concrete model by Mander (1988). Since confinement of the concrete is taken into account, the steel shell is subjected to a biaxial state of stress. Longitudinal stress, f_s, develops due to the axial load and bending moment, whereas a circumferential stress, f_l', develops due to concrete confinement. Therefore,

$$f_s^2 + f_l'^2 + f_l' f_s = F_y^2 \tag{2.89}$$

2.4.2.7.3 Design Analysis by Hajjar and Gourley (1996)

Hajjar and Gourley (1996) developed an empirical polynominal equation to describe the interation diagram of beam-columns under bi-axial bending, calibrating their results on predictions obtained using a layer model that considered concrete confinement (increased strength and ductility in circular tubes, only increased ductility in rectangular tubes) and a bilinear stress-strain model with a yield strength of f_y. It was assumed that neglecting strain-hardening from the steel model indirectly made-up for the effect of lower yield strength under bi-axial bending. Accuracy of the resulting equations when compared with available experimental results is good, but its complexity makes it more suitable for implementation in computer programs than for a hand calculation method.

2.4.2.7.4 Design Analysis by Schneider (1998)

Schneider (1988) used a 3-dimensional non-linear finite-element analysis to study axially loaded concrete-filled tubes. The concrete core was modeled with 20-node elements having three translational degrees of freedom. The steel tube was modeled using 8-node elements having five

degrees of freedom at each node. Inelastic properties and nonlinear behaviour were used for this element but strain hardening was not considered. An additional element was used to represent the interface between the concrete core and the steel tube. Frictional forces developed on this element if the concrete and steel were in contact. In absence of contact between the two materials, no frictional forces were considered.

A wide array of D/t ratios and diameters were used in this study. The smaller diameters were matched to the experimental specimens tested in Sections 2.5.2.1.9 and 2.5.2.2.6 for comparison. The local buckling of the steel tube in this analysis was similar to the occurrence in the experimental specimens. The analytical study showed that for small diameter concrete-filled tubes, both the concrete core and the steel tube reached their specified nominal yield strength as the specimen reached the composite yield strength. However, in large diameter concrete-filled tubes, only the concrete core reached its compressive strength when the column reached its maximum strength due to the effect of biaxial stresses in the steel tube caused by the confining pressures on the concrete core.

2.5 Survey of past experimental studies

This section reviews the results of past experimental research on cyclic loading of concrete-filled steel tubes. Some relevant test results performed on non-cyclic hollow and filled columns, as well as cyclic hollow tubes are also presented. Many additional Japanese results exist but they are unavailable in the English literature. A comparative synthesis of this information follows in Section 2.7.

2.5.1 Non-cyclic tests of hollow steel sections

Non-cyclic tests on hollow steel sections, both circular and rectangular, have been reported by many researchers. It is generally agreed that a hollow circular steel column is the structural member with the most efficient cross-section to resist concentrically applied compressive loads if a significant distance exists between lateral supports.

Local buckling or overall buckling failure, either elastic or inelastic, are the most common failure modes of such columns. Column buckling is governed by the length-to-radius (L/r) ratio, where as the diameter-to-shell thickness (D/t) ratio governs shell local buckling. Additional information on the behaviour of monotonically loaded hollow tubes can be found in Galambos (1988). Some noteworthy results on hollow columns by Ghosh (1977) and Bridge and Webb (1992) who have investigated both hollow and filled columns are described in Section 2.5.2 for comparative purposes.

2.5.2 Non-cyclic tests of concrete-filled steel tubes

Most of the past experimental research on the behaviour of concrete-filled steel tubes subjected to monotonic loading has focused on the maximum strength attained and whether or not bond between the steel and concrete is maintained, without testing the column to complete column failure. The tests reviewed here investigated more fully the failure modes of these columns. Gardner and Jacobson (1967), Furlong (1967, 1968), Neogi et al. (1969), Knowles and Park (1969, 1970), Orito et al. (1987), Bridge and Webb (1992), Prion and Boehme (1994) and Schneider (1998) have all tested circular columns. Furlong (1967), Knowles and Park (1969, 1970), Shakir-Khalil and Zeghiche (1989, 1990), and Schneider (1998) performed tests on rectangular columns.

2.5.2.1 Circular columns

2.5.2.1.1 Gardner and Jacobson (1967)

Gardner and Jacobson (1967) tested ten long and eighteen stub concrete-filled steel tubes in axial compression. The diameter and thickness of the steel tubes ranged from 75 mm to 150 mm and 1.7 mm to 3.1 mm, respectively. This resulted in D/t ratios between 29.5 and 48. The steel strength varied from 363 MPa to 633 MPa and the concrete compressive strength from 21 MPa to 42 MPa. The properties for all columns tested are listed in Table 2.2. The columns were loaded through spherical ball seats that permitted movement in any direction. All specimens were capped on both ends by cement sulfur which extended over the steel tube and concrete core to effectively load both the steel tube and concrete core simultaneously.

No local buckling was observed in the long columns, only overall column buckling. Both the long columns and the stub columns yielded in the longitudinal direction first. Six of the stub columns were loaded using three different methods; steel only, concrete core only, and both steel and concrete, to investigate the effects of end conditions on the capacity of concrete-filled steel tubes. The three types of specimens are shown in Figure 2.9 after testing. Loading both the steel and the concrete produced a "barrel shape" failure in which 100% of the load was carried. Loading only the concrete core produced the same failure as loading both materials and the full load was also resisted. Local buckling occurred when only the steel tube was loaded and the specimen only resisted 40.2% of the total load carried when both materials were loaded together.

2.5.2.1.2 Test results from Furlong (1967,1968)

Furlong (1967) tested thirty two circular concrete-filled steel tubes. All specimens were 914 mm long, with outside dimensions ranging from 114 mm to 152 mm and steel thicknesses ranging from 1.55 mm to 3.18 mm. This produced a D/t ratio of 36 to 98. The steel shells ranged in yield strength from 290 to 414 MPa and the concrete cylinder strength ranged from 21 to 35 MPa. Nine specimens were tested with a concentric axial load, while the remaining twenty-two specimens were subjected to an axial load and a bending moment. In the bending moment tests, the axial force was held constant while moments were increased until failure occurred. Figure 2.10 shows the test set-up of the specimens. It can be seen that the ends of the column frame rigidly into the moment applicator beam, but the whole assembly rotates to model pin-pin boundary conditions. Test results for the axially loaded columns are presented in Table 2.3 and the results from the axial and bending tests are presented in Table 2.4. Parameters in this table are defined in Section 2.4.2.1.

Furlong (1967) observed the steel and concrete interaction by means of strain gauges. He assumed that if the ratio between the longitudinal strain and transverse strain were to sharply increase, the steel shell would be confining the concrete. The ratio was found not to increase significantly, and he concluded that the steel and concrete carried their loads independently. The steel walls were observed to resist increasing load without occurrence of local buckling until the

nominal yield strains were observed. It was concluded that the concrete was stabilizing the steel at this time.

Tests by Furlong (1967) on plain steel tubing revealed that the residual stresses in the cold-rolled and welded steel tubing used in these tests were such that proportional limits were typically lower than 50% of the nominal yield strength. That finding, along with the observation that the measured stiffness of concrete-filled steel tubes was less than the stiffness computed on the basis of transformed areas of component materials, lead Furlong (1968) to investigate more thoroughly the effectiveness of the bond between the steel and concrete.

Two different sets of specimens were considered. In the first series of "bonded" specimens, no special measures were taken to assure bond, but axle grease was applied to the inside of the steel shell in the second series of "unbonded" specimens in an attempt to prohibit bond. No significant difference was observed in the behaviour of the two different types of specimens, regardless of shape, concrete strength, or steel wall thickness, and it was concluded that no effective bond existed for any specimens. Furlong (1968) further concluded that any bond that may have originally existed must have broken due to the separation between the steel wall and the concrete core at relatively low axial loads. After tests were complete, sections of the shell were cut with an acetylene torch and removed cleanly without any evidence of concrete adhering to the steel. This occurred whether or not the insides of tubes had been greased before the concrete was cast.

2.5.2.1.3 Test results from Neogi et al. (1969)

The axially loaded circular members in tests performed by Neogi et al. (1969) consisted of mild steel tubes having nominal outside diameters of 140 mm or 168 mm, a thickness between 5 mm and 9.75 mm, and a length of 3327 mm (labeled series 'M' tests by Neogi et al.). By contrast, labeled series 'C' tests consisted of mild steel tubes having a nominal diameter of 127 mm, a steel thickness between 1.63 mm and 3.25 mm and lengths varying from 1410 mm to 2032 mm. This resulted in D/t ratios between 14 and 78. The steel yield strength ranged from

193 to 312 MPa, and the concrete cube strength ranged from 27 to 83 MPa. All specimens in these tests were loaded through hardened steel knife edges ensuring that practically pin-ended conditions were produced in the plane of bending. All specimens were capped such that the steel and concrete were loaded together at the ends. The length of the column, L, is the column length plus fittings, δ_i is the initial deflection at the midheight of the column, and e is the end eccentricity of the load. The test set up is illustrated in Figure 2.11. Results from the tests are presented in Table 2.5. Parameters in this table are defined in Section 2.4.2.2. For comparison, results from two other tests were reported by Neogi et al., namely those from Janss, and from Kato and Kanatani (1966) and are included in Table 2.5. All of Kato and Kanatani specimens were 2794 mm to 5970 mm long and had a diameter of 318 mm. Janss results are only reported in terms of normalized ratio.

All columns were observed to behave in a ductile manner. The final deflected shape of the columns was symmetrical and there was no local buckling of the tube. Neogi et al. observed that the behaviour of eccentrically-loaded circular columns having an L/D ratio greater than 15 showed no increase in concrete strength but they found an increase in the maximum load due to the tri-axial effect in the shorter columns. However, this tri-axial effect diminished as the eccentricity increased. After Neogi et al. finished testing, the steel shell was removed and the concrete was found to have retained its cohesion.

The experimental maximum loads, P_T are compared with the maximum load obtained with the deflected shape calculated by the finite difference method, P_{exact}, the cosine shape approximation, P_{cos}, and the maximum load carried by the hollow steel shell alone, P_{empty}, as defined in Section 2.4.2.2. Neogi et al. (1969) found that using a cosine deflected shape of the form expressed in Equation 2.57 in Section 2.4.2.2, the calculated maximum load differed by only 5% from the value produced by the finite difference method. They found that for L/D ratios greater than 15, triaxial effects were small.

2.5.2.1.4 Test results from Knowles and Park (1969)

Knowles and Park (1969) tested thirteen axially loaded hollow steel tubes and twelve axially loaded concrete-filled steel tubes. They also tested six hollow steel tubes and six concrete-filled steel tubes subjected to eccentric axial loads. The steel yield strength was 400 MPa for the steel shells of 89 mm diameter and 5.8 mm thick, and 482 MPa for the steel shells of 83 mm in diameter and 1.4 mm thick. The concrete tests showed a cylinder strength of 40 MPa. Eccentrically loaded columns were tested at both 7.6 mm and 25.4 mm initial eccentricities. The tubes were constructed of mild steel and lengths ranged from 305 mm to 1524 mm. All tests were performed using knife-edge hinges at each end to simulate pin joints as seen in Figure 2.12. To apply a eccentric load, the column was moved off-center on the recessed plate to achieve the initial eccentricity. The dimensions of the specimens were chosen to preclude failure by local buckling prior to attainment of the maximum axial capacity.

All the columns tested in axial compression failed by plastic column buckling. Some of the short thin-walled hollow tubes developed local buckling failure after the maximum load had been reached, but no local buckling occurred in the concrete-filled steel columns even beyond the point of failure after the maximum load was reached. After failure, all columns assumed a similar buckled shape, with a noticeable region of plasticity at mid-height. Some of the short columns did show an increase in strength, evident when the individual strengths of both materials are summed. The experimental loads of the axially loaded members are presented in Table 2.6. Parameters in this table are defined in Section 2.4.2.3.

The experimental loads of the axial and bending moment columns are presented in Table 2.7. Parameters in this table are defined in Section 2.4.2.3. When an eccentric load was applied, the hollow steel tubes showed no signs of local buckling failure prior to attainment of the ultimate load. The failure region of all columns was at mid-height corresponding to the location of maximum bending moment. The only columns which exhibited an increase in strength were the 813 mm tubes of 89 mm and 83 mm outside diameter tested with 7.6 mm initial eccentricity.

2.5.2.1.5 Test results from Knowles and Park (1970)

Knowles and Park (1970) collected data on concrete-filled steel columns from six researchers, for a total of ninety-eight specimens. The yield strength of the steel shells ranged from 269 to 605 MPa, and the cylinder strength of the concrete ranged from 20 to 66 MPa. The circular steel shells ranged from an outside diameter of 25.4 mm and thickness of 0.889 mm, to an outside diameter of 355.6 mm and a shell thickness of 4.7 mm. The characteristics and ultimate strengths of these axially loaded concrete-filled steel columns are presented in Table 2.8. Parameters in this table are defined in Section 2.4.2.3 and 2.4.2.4.

2.5.2.1.6 Test results from Orito et al. (1987)

Orito et al. (1987) tested three concrete-filled circular steel columns, Type S, A and B, all having the same dimensions and material properties. The diameter was 114.3 mm, length was 600.0 mm, and the shell thickness was 5.2 mm. The compressive strength of the concrete cylinder was 52 MPa, and the yield stress of the steel tube was 377 MPa. Type-S is a specimen simulating the unbonded concrete-filled steel column (UTC) with an antifriction asphalt material applied to the interface between the steel and concrete to reduce the transfer of axial load between the two materials. The load is applied directly to the core concrete. Type-A is a specimen simulating the bonded concrete-filled steel column (BTC) with the load applied to both the steel tube and concrete core. Type-B is a UTC specimen with no antifriction material between the steel and concrete, and the load is applied directly to the core concrete. The essential difference between each column is the response of the steel tube to the axial load. In the BTC specimen, the steel tube directly shares the axial load with the core concrete, whereas in the UTC specimens, the steel tube is used only to confine the core concrete.

Figure 2.13 shows the axial load and strain relationship for all specimens. The stiffness of the UTC (Type S) specimen was almost equal to the stiffness of the concrete core and lower than the BTC specimen. However, the UTC (Type S) specimen was able to withstand a larger axial load than the BTC specimen before the steel tube yielded under the confining pressures. The antifriction material proved effective by allowing the steel tube to function only as a

circumferential confining pressure. When no antifriction asphalt material was used, as in the UTC (Type B) specimen, the maximum axial load was not as high as the Type A specimen. A force transfer from the loaded concrete core to the steel tube occurred, thereby lowering the effective circumferential yield strength of the steel tube. As seen in Figure 2.13, the axial load - axial strain relationship for UTC (Type B) lies between those of UTC (Type S) and BTC (Type A).

2.5.2.1.7 Test results from Bridge and Webb (1992)

Bridge and Webb (1992) tested two circular composite columns and two circular bare steel tubes in axial compression. All columns were 750 mm long with an outside diameter of 250 mm and a steel shell thickness of 2.012 mm. The steel slenderness ratio of these columns, kL/r_s, was 8.6, and their kL/r_c value was 12. The columns were constructed with high strength concrete with a concrete strength of 59.5 MPa and mild steel having a yield strength of 260 MPa and ultimate strength of 344.3 MPa.

Although the magnitude of the buckling deformations was small, local buckling of the hollow steel tubes was observed by Bridge and Webb (1987) to form near mid-height prior to attainment of the maximum load. With further deformations into the post-ultimate region, the magnitude of the local buckles increased. For both hollow steel tubes, the buckling was not a single continuous outwards buckling around the tube but rather two distinct outwards buckles. Each buckled section was half the diameter and separated by about 50 to 70 mm; the half wavelength of the buckle measured 75 mm. Both concrete-filled tubes displayed a single continuous buckle around the tube near mid-height. However, the magnitude of the buckle was not constant around the tube. The half wavelength of the buckle measured 80 mm.

Bridge and Webb (1987) expressed concern that the concrete might shrink away from the tube, even though the likelihood is small in a sealed environment. Observations during the removal of the steel tube from a prototype column indicated that substantial bond stress does exist. However, the consequences of debonding are serious and they considered it careless to rely on bond alone to transfer the load. Bridge and Webb also noted that Shakir-Khalil (1991, 1992)

showed that the addition of a few shear connectors can increase the bond resistance of the steel-concrete interface. The use of nails was found to increase the bond strength more than the simple summation of the strength of the nail and concrete bond strength.

2.5.2.1.8 Test results from Prion and Boehme (1994)

Prion and Boehme (1994) tested 19 concrete-filled circular steel columns to investigate the effect of axial loads, axial and bending loads, and eccentric loads. All specimens had the same cross-sectional properties. The steel shell had an outside diameter of 152 mm and a wall thickness of 1.65 mm with a yield strength from 250 to 330 MPa steel with electric resistance welded longitudinal seams. Only high strength concrete was used, with a cylinder strength ranging from 73 MPa to 92 MPa. No mechanical shear connection was provided between the concrete and the steel and it was discovered that the concrete shrinkage resulted in a loss of bond in some specimens before they were tested. The experimental results are presented in Table 2.9. Parameters in this table are defined in Section 2.4.2.7.1.

Ten specimens with lengths from 500 to 900 mm were tested under concentric axial load. To test the existence and strength of the bond between the steel and concrete, some specimens were tested by applying the load on the steel and the concrete simultaneously (Type A-1), while others had loading plates that fit within the concrete's diameter to ensure that only the concrete was loaded (Type A-2). If no bond existed, the steel in Type A-2 specimens should be stressed in the circumferential direction only. However, no appreciable difference between the two types of specimens were noticed and all failed due to shear. Initially, a relatively abrupt decline in load-carrying capacity occurred, and then as the concrete wedges slid past each other, the steel shell acted in tension circumferentially, resulting in a ductile secondary failure mode. As can be seen in Table 2.9, their L/D ratio is very low, ie. between 3.3 and 5.9.

Various combinations of axial load and bending moment were applied to six specimens of 2120 mm effective length. While the axial load was maintained, two equal lateral forces were applied which resulted in a constant first-order moment in the test region. The monotonically

loaded columns are labeled C1. All columns failed in the centre by rupture of the steel tube in the tension zone after substantial cracking of the concrete and buckling of the steel in the compression zone. These specimens had a *L/D* ratio of 14, ie. much larger than for the Type A columns. The second-order moments resulting from the axial load acting about the displaced section centroid constituted about 20% of the total moment at ultimate.

Three concrete-filled steel columns were tested under eccentric loading (Type D). The effective length between inflection points was 1071 mm and the initial eccentricity varied from 11 to 15 mm. For the purpose of calculating moments, the lateral position of the specimen as well as strain readings on the tube surface was used. These columns did not exhibit the ductile behaviour observed in the beam-column specimens, but failed rather abruptly when lateral buckling occurred. Prion and Boehme suggested the brittle nature of the high strength concrete and the lack of proper confinement contributed to the premature and non-ductile failure.

It was concluded by Prion and Boehme that for short columns and beam-column specimens with high axial load-to-moment ratios, a sudden decline in load-carrying capacity beyond ultimate will develop. This is not good for earthquake design where ultimate design strength must be sustained into large plastic deformations. It was also shown that the failure mechanism of the short axially loaded columns was by shear failure and not by the lateral expansion of the concrete core on the steel. Therefore the design of short columns must take into account shear failure as well as compression failure.

2.5.2.1.9 Test results from Schneider (1998)

Schneider subjected three circular concrete-filled tubes to concentric axial compression. The diameter of all columns was 140 mm, and the thickness was 3 mm, 6.5 mm, and 6.68 mm for C1, C2 and C3, respectively. The *D/t* ratio ranged from 21 to 47 and the overall length of the columns was 635 mm. The specified yield strength of the steel was 317 MPa and the concrete compressive strength ranged from 23.8 MPa to 28.2 MPa. The properties of the columns are listed in Table 2.10. A stiffened end cap was attached at both ends of the steel tube to ensure the

concrete core and the steel tube would be loaded simultaneously. The axial load was applied at a slow rate to allow observation of the development of local buckling in the tubes. Axial deformations were measured at the mid-height of each column.

The test data for Specimen C3 was not recorded beyond a load of 1850 kN, corresponding to 92% yield, therefore, no comparison can be made with the ductility, however the yield strength to ultimate strength ratio was measured to be 35%. Specimens C1 and C2 exhibited significant strain hardening with a yield strength to ultimate strength ratio of 25% and 41%, respectively. Local buckling occurred late in the loading cycle for these columns, with an axial deformation ratio of 18 and 9 for columns C1 and C2, respectively. After examination of the columns, it was stated that local buckling of the column was due to a radial expansion of the steel tube. Figure 2.14 demonstrates the excellent ductility and strength attained during these tests in terms of axial compression versus deformation. The onset of local buckling is indicated on the respective graph. The load carried by the steel tube alone was calculated using the results from the longitudinal strain gages at mid-height of the columns. It was discovered that as the load increased toward the yield strength, the steel tube carried an increasingly larger percentage of the total load. After the yield strength had been reached, the steel began to resist less of the actual load. For Specimens C1 and C2, respectively, the steel tube carried 0.2 and 0.5 of the total load at the start of the test, 0.5 and 0.7 of the total load when the column reached its yield strength, and 0.42 and 0.55 of the total load at 125% of the yield strength. There was a decrease in the steel tube's share of load resistance for Specimen C2 at 20% of the yield strength but it began to increase again after this point.

2.5.2.2 Rectangular Columns

2.5.2.2.1 Test results from Furlong (1967)

Furlong (1967) tested twenty-two square columns, in addition to 32 circular columns. The testing procedure was similar to that described in Section 2.5.2.1.2 for the circular columns. The columns were 914 mm long, side widths of 101.6 mm and 127 mm, and steel thicknesses between 2.1 mm and 4.8 mm. This results in a D/t ratio ranging from 26 to 48. The steel yield strength

ranged from 331 MPa to 484 MPa, and the cylinder strength of concrete ranged from 23 to 45 MPa. Five columns were tested with a concentric axial load applied while seventeen specimens were subjected to an eccentrically applied axial load. Table 2.11 lists the axial load data for these columns, and Table 2.12 lists the data for bending and axial load. The parameters in these tables were defined in Section 2.4.2.1. There was no indication of an increase in concrete strength due to confinement in the axially loaded square specimens.

2.5.2.2.2 Test results from Knowles and Park (1969)

Knowles and Park (1969) also tested hollow and concrete-filled square columns. Their testing procedure was similar to that described earlier for their circular columns tests in Section 2.5.2.1.4. All hollow square columns had side lengths of 76 mm, thickness of 3.3 mm, and lengths varying between 305 mm and 1524 mm. The tubes had a yield strength of 323 MPa, and a cylinder strength of concrete of 41 MPa. The eccentrically loaded columns were tested with either 7.6 mm or 25.4 mm initial eccentricities.

The square concrete-filled columns behaved much like the circular concrete-filled columns, except for some weld splitting on the shortest of the 76.2 mm square tubes. However, no increase in strength due to confinement was noticed for the square columns under either axial or eccentric loading as per the reasoning of Knowles and Park (1969) for circular columns. The experimental results for the axially loaded members and eccentrically loaded members are presented in Tables 2.13 and 2.14 respectively. The parameters in these tables were previously defined in Section 2.4.2.3.

2.5.2.2.3 Test results from Knowles and Park (1970)

The square concrete-filled steel columns tested by Knowles and Park (1970) ranged from a side width of 76.2 mm and thickness of 3.3 mm, to a side width of 114.9 mm and thickness of 4.4 mm. The yield strength of the steel tubes ranged from 253 to 484 MPa, and the concrete cylinder strength ranged from 23 to 45 MPa. Knowles and Park (1970) also reviewed test data from Chapman and Neogi (1966) which is presented in Table 2.15.

When strains were measured on the axially loaded columns tested by Knowles and Park (1969) to investigate the likelihood of confinement, no evidence to indicate that any strength enhancement in the square column due to confinement was observed. However, Knowles and Park (1970) noted that specimen DF3, tested by Chapman and Neogi exhibited an experimental load much greater than predicted using the tangent modulus theory, and attributed this to an increase in the concrete strength due to some confinement as a result of the low kL/r_c value of 15 for this specimen and large thickness of the steel tube, 9.63 mm, for a tube width of 115 mm.

2.5.2.2.4 Test results from Shakir-Khalil and Zeghiche (1989)

Shakir-Khalil and Zeghiche (1989) investigated the behaviour of seven concrete-filled rectangular structural steel sections of 120 x 80 x 5 cross-section and 2760 mm long subjected to eccentric loading. The design strength of the steel shells ranged from 343 to 387 MPa, and the concrete design strength ranged from 40 to 45 MPa. All tests were performed by subjecting the columns to compressive forces applied at equal end eccentricities. The specimens were fixed at both ends to 75 mm thick loading plates which in turn were connected as pins to the loading apparatus. The test set-up is similar to that illustrated in Figure 2.11 in Neogi et al. (1967). The obtained carrying capacities, deflections, and failure loads for the tested columns are presented in Table 2.16. The design strength of structural steel is referred to as f_{sd}, and the characteristic 28-day cube strength of concrete is f_{cu}. P_u is the ultimate squash load, and M_{ux} and M_{uy} are the ultimate moments of resistance of the composite section.

A concentrically applied load was also applied to stub columns with a length of 200 mm and cross sectional properties the same as each of the seven specimens. The results of these tests are also presented in Table 2.16. The failure mode of the specimens was crushing failure and the steel wall was pushed out by the core concrete. When the steel shell of one specimen was removed, it was observed that the concrete had taken the deformed shape of the steel shell.

The effective buckling length, L_{ex} and L_{ey}, in the major and minor direction of the column are 3210 mm and 2940 mm, respectively. The mid-length lateral displacements at failure

perpendicular to the major and minor axes are δ_x and δ_y respectively, and the initial eccentricity about major and minor axes caused by the applied load is e_x and e_y respectively As is evident from Table 2.16, the δ_x/e_x and δ_y/e_y ratios are relatively large for columns subjected to small eccentricities. The moments at failure at the mid-height of the beam, $M_{\delta x}$ and $M_{\delta y}$, are calculated as the experimental failure load, P_{exp} multiplied by the total eccentricity about the major and minor axes, for example, $M_{\delta x} = P_{exp}(e_x + \delta_x)$. Failure for all of the specimens was by column buckling, with no sign of local buckling in the steel shells. Shakir-Khalil and Zeghiche (1989) concluded that in columns subjected to small eccentricities, secondary moments (P-Δ effects) play a large role and may even exceed the primary moment caused by the end eccentricities of the applied compressive load.

Tests were also performed by Shakir-Khalil and Zeghiche (1989) to investigate the bond between the steel shell and the concrete core. Specimens were 550 mm in length and filled with concrete until 50 mm from the top. An axial compressive load was applied to the concrete alone. The bond resistance was measured as the load required for the concrete core to move vertically relative to the steel section and thus, break the steel-concrete bond. These results are presented in Table 2.17.

2.5.2.2.5 Test results from Shakir-Khalil and Zeghiche (1990)

Shakir-Khalil and Zeghiche (1990) performed nine tests on two sizes of rectangular steel sections subjected to eccentric loading, with cross-sections of 120 x 80 x 5 and 150 x 100 x 5. The steel yield strength ranged from 340 to 362.5 MPa, and the concrete cylinder strength from 41 to 47 MPa. All columns tested were 3.0 m long and used the same set-up as Shakir-Khalil and Zeghiche (1989). The properties of the tested columns are listed in Table 2.18. All columns failed by overall buckling with no sign of local instability of the steel shell. When a section of steel was removed from one of the columns at mid-height at the corner of maximum tension, tension cracks were observed to have developed in the concrete at a right-angle to the longitudinal axis of the column. The concrete core was found to have remained intact even though the column had been loaded to failure. Whitewash was used on the steel to observe cracking in the outer shell. The

lowest ratio of applied load to failure load at which the whitewash was observed to flake off was 90%, whereas the highest ratio was 96%.

2.5.2.2.6 Test results from Schneider (1998)

Schneider tested five square and six rectangular shaped concrete-filled tubes under concentric axial compression. He also tested three circular columns described in Section 2.5.2.1.9. The square columns had an outside dimension of 127 mm while the rectangular columns had outside dimensions of 152 x 102 and 152 x 76. The thickness of the steel wall varied from 3 mm to 7.47 mm, the *w/t* ratio ranged from 17.0 to 50.8 and the overall length of all columns was 635 mm. The specified steel yield strength was 317 MPa and the concrete compressive strength ranged from 23.8 MPa to 30.5 MPa. The properties of these columns are listed in Table 2.10. The column load was applied at a slow rate to allow for observation of the development of local buckling in the tubes. Axial deformations were measured at the mid-height of each column.

Local buckling of the steel tube did not occur in any of the specimens before yield of the concrete-filled tube. Schneider found a correlation between the post yield behaviour of the columns and the respective *w/t* ratios. A graph of axial compression versus deformation is shown in Figure 2.15, local buckling is indicated on the respective graph. Specimen S5, having a *w/t* ratio of 17, exhibited strain hardening with an ultimate strength of 25% greater than its yield strength. Specimen R6, with a *w/t* ratio of 20.8, showed a small amount of strain hardening after the yield strength was reached. Local buckling occurred in these specimens between an axial deformation ratio of 7 and 8. The post yield behaviour of all other columns was described as strain softening and local buckling for these columns occurred between an axial deformation ratio of 2 and 6. The square columns exhibited local buckling on all faces equally while the local buckling was more pronounced on the broad face, rather than the narrow face of the rectangular columns. The columns with larger *w/t* ratios showed more local buckling with higher distortions than the columns with smaller *w/t* ratios. For each shape, the thicker the steel tube, the higher the axial deformations reached.

After testing, Specimen S3 was cut open near the local buckle to examine the concrete core. Diagonal cracks were visible in the concrete core, but very little space could be seen between the concrete and steel tube near the vicinity of the local buckle. It was determined that the concrete flowed plastically into the local buckle of the steel tube while still remaining cohesive.

2.5.3 Cyclic bending tests on hollow steel sections.

For illustration purposes, some cyclic test results on hollow steel sections are presented to provide perspective on the benefits of filling the sections with concrete. Of particular interest is the behaviour of the outer steel shell under cyclic loads. Tests by Usami et al. (1992) and Kitada et al. (1995) on hollow steel tubes and columns partially filled with concrete, and by Kawaguchi et al. (1987, 1992) and Ge and Usami (1994) on hollow steel tubes and fully filled steel tubes are reported later in Section 2.5.4 and Section 2.5.5, respectively. A few additional results of cyclic tested hollow sections are reported below.

2.5.3.1 Circular steel sections

Iura et al. (1997) tested six circular hollow steel columns subjected to cyclic loads. All columns have a diameter of 500 mm and a height of 1500 mm. The thickness of the steel shell varies from 3.07 mm to 5.60 mm, and the steel yield strength varies between 27 MPa to 31 MPa. The column is bolted to the rigid frame at the bottom and the axial and lateral load are applied at the top. The test set-up and test specimen are shown in Figure 2.16 and Figure 2.17, respectively.

The failure of all six columns was an "elephant foot mode", a failure in which local buckling occurs and the shell is pushed outwards all around the column. Iura et al. also studied the failure modes of hollow steel circular bridge piers after the Hanshin-Awaji earthquake in 1995. They found that the elephant foot failure mode was the most common. However, the diamond mode had been observed in a few piers. This mode occurs in the elastic range of thin circular columns, and has both inward and outward buckling of the steel shell.

2.5.3.2 Rectangular steel sections

Fukumoto and Kusama (1985) tested ten square box beams to obtain their load-deflection and M-ϕ relationship under cyclic bending. Six were built with plates of mild steel with a yield stress of 240 MPa, the others with high strength plates with a yield stress of 700 MPa. The square sections ranged in cross-section from 250 x 250 to 500 x 500 mm, all having a nominal plate thickness of 6 mm. The dimensions of the test specimens are presented in Table 2.19. The terminology used in the table is identical to the one defined in the illustration of the test set-up for Usami et al. (1992) in Figure 2.21. A loading beam was used to subject the test specimen to two point loads an equal distance from both ends, and cyclic bending was applied at an almost constant curvature ductility of 2.0. The resulting hysteretic loops form a symmetric spindle shape, but the peak load and beam stiffness in each cycle reduced as the number of cycles increased, as shown in Figure 2.18. The gap of peak loads between the first and second cycles is significant for the specimen with large b/t ratio. This phenomenal is most likely caused by the early occurrence of local instability of flange elements.

Watanabe et al. (1988) studied rectangular beam-columns simultaneously subjected to a constant axial force and a cyclic but slowly varying bending moment. The test consisted of three test specimens. Specimen A was unstiffened, Specimen B had a stiffened flange with $\gamma/\gamma^* = 1$, and Specimen C had a stiffened flange with $\gamma/\gamma^* = 3$ (where γ/γ^* is a stiffener flexural rigidity parameter whose complex meaning is described in Bruneau et al. 1995). Specimens were compared to an axial load bending moment interaction curve. The maximum bending moment of Specimen A occurred while the specimen remained fully elastic, the peak bending moment for Specimen B was in the elastic plastic range, while the peak bending moment for Specimen C exceeded the fully plastic curve. The axial load reduced the maximum strength by 18%, 10%, and 2% corresponding to Specimen A, B, and C, respectively. Elastic buckling occurred in the compression flange in Specimen A, then out-of plane deflections grew in the flange and web. In Specimen B and C, the flanges buckled just before the squash load was reached, plastification occurred in these flanges and the out-of-plane deformations increased. The buckling of the flanges occurred in both out-of-plane directions.

2.5.4 Cyclic partially filled

Japanese engineers frequently use rectangular hollow steel tubes for the bridge piers of elevated expressways. These columns are filled with concrete for a metre or two above the ground to improve the impact resistance from a vehicle. Usami et al. (1992), Ge and Usami (1994), Kitada et al. (1995), Goto et al. (1997), Itoh et al. (1997), and Otsuka et al. (1997) have tested the cyclic behaviour of such columns to investigate if the partial concrete fill improved ultimate strength and ductility.

Numerous other tests were conducted on rectangular and circular tubes partially filled with concrete for a few meters only, as done for the piers of many elevated expressways throughout Japan. Most of those results have not been published in English at this time. However, based on the limited information available (Toru Terayama, Senior Research Engineer, Earthquake Engineering Division, Public Works Research Institute, personnel communication), the tested composite circular columns appear to have been considerably ductile. The hysteretic curve for a 14 mm thick tube of 800 mm diameter, filled with concrete over its lower 2 meters, produced very stable hysteretic curves, as seen in Figure 2.19.

2.5.4.1 Test Results from Itoh et al. (1997)

Itoh et al. (1997) investigated the failure of two circular hollow steel piers partially filled with concrete after the Hanshin-Awaji earthquake in 1995. The piers in question were 16.5 meters in height and 2200 mm in diameter. Steel yield stress was 314 MPa for the first 4 metres from the base and 235 MPa for the rest of the column height. Concrete was filled up to the first 3.4 metres of the column. Diaphragms were located throughout the columns. In Pier P-584N, the thickness of the steel shell for the first 8 meters was 25 mm, and for the rest of the column was 19 mm. For Pier P-584S, the thickness of the steel for the first 8 meters was 28 mm, for the next 4 meters it was 21 mm, and for the rest of the column it was 19 mm.

Both of the columns failed at 8 meters above the foundation (far above the concrete-fill). This location coincided with the first change in thickness of the steel shell. The local buckle that

occurred at this location buckled outwards all around the tube. Failure shape of the two columns along with the original dimensions are shown in Figure 2.20.

2.5.4.2 Test results from Usami et al. (1992)

Usami et al. (1992) tested nine stiffened box columns with a D/b ratio equal to 2/3, and a nominal yield stress, σ_y, of 235 MPa. All columns were 1854 mm long except Specimen S2 which was 1354 mm in length. Two of these columns were partially filled with concrete: Specimen SS8 was 30% filled, while Specimen SS9 was 50% filled. At both ends of the test specimen, thick end plates were welded to secure the specimen to the loading plate. As can be seen in Figure 2.21, all columns were extremely stiffened at their base. Each specimen was subjected to a prescribed top horizontal displacement under a constant axial load of $0.2\ P/P_y$ as illustrated in Figure 2.22. Table 2.20 describes the geometry of the specimens, and Table 2.21 lists the ductility and energy-absorption obtained for the specimens during these tests. Definitions for the parameters used in this table can be found in Bruneau et al. (1995) and are briefly described here. The distance between interior horizontal diaphragms is l_d, the height over which longitudinal stiffeners have a greater stiffness is l_s, the concrete-fill length is l_c, and the height from the top of the bottom external stiffeners to the top of the column is h. The width and thickness of the stiffeners are designated b_s and t_s. R_f and R_w are calculated as the R_p value defined in Bruneau et al. (1995), using the flange and web dimensions respectively.

Longitudinal stiffeners of variable width were used in specimens SS3 and SS4, with a higher rigidity stiffener $(\gamma/\gamma^*=5)$ over the lower portion of the columns for a height of l_s above the lowest diaphragm, and a lower stiffener rigidity $(\gamma/\gamma^*=1)$ over the remaining column height. Specimen SS6 is a hybrid stiffened column, with 50% stronger steel (nominal yield strength of 353 MPa) used for the stiffeners only. Specimens SS1 - SS7 experienced local buckling in the flange plates at the base of the column during the cycles after the peak horizontal load was reached. Buckling deformations grew upon further cyclic loading because the plates could not fully straighten out under load reversal. Usami et al. (1992) found that these specimens lost their lateral resistance after cracking at the flange-web junction or when fracture in the flange material

became considerable. Specimens SS1-SS5 and SS7 all developed roughly the same ductility, however the hybrid specimen, SS6, exhibited approximately 1.5 times the ductility and 3 times the of energy absorption capacity compared to Specimen SS5 with the same dimensions but a uniform steel strength. The hysteresis curves for Specimens SS1 to SS9 are shown in Figure 2.23.

Specimens SS8 and SS9, with partial concrete-fill, exhibited good behaviour under the same applied cyclic load regions as for Specimens SS1 - SS7. Only slight local buckling occurred at the base of Specimen SS9. Specimen SS8 suffered moderate strength degradation with local buckling deformations developing in the steel panels just above the concrete-fill termination location. Testing for Specimen SS9 ended before the last three cycles were applied because of limitation in the stroke of the actuator. The maximum drift reached for both Specimen SS8 and SS9 was 3.3%. The decrease in the lateral stiffness was relatively gradual compared with equivalent hollow steel tubes. Specimen SS8 displayed twice the ductility and five times the energy absorption as compared to Specimen SS5 with the same dimensions but no concrete. The increased ductility, energy-absorption, and reduction of strength deterioration due to the concrete fill is quite noticeable in Figure 2.23 for Specimens SS8 and SS9. Because inward buckling of the steel plates is prevented by the concrete-fill, buckling was delayed and buckling deformations were of smaller magnitude.

After removing a portion of the flange plate by gas-cutting, Usami et al. (1992) observed that the concrete behind the severely buckled flange plates was crushed whereas concrete was undamaged elsewhere in the specimen. This lead Usami et al. to conclude that local plate buckling developed after the contained concrete had crushed under cyclic loading.

2.5.4.3 Test results from Ge and Usami (1994)

Ge and Usami (1994) performed cyclic tests on three hollow unstiffened steel box columns and twelve unstiffened steel box columns partially filled with concrete. All columns were constructed of steel having a nominal yield value of 235 MPa. The specimens were subjected to a prescribed repeated horizontal displacement and a constant axial load of $P/P_y = 0.2$. Table 2.22

lists the dimensions of the specimens and Figure 2.21 from Usami et al. (1992) shows a similar test set-up and the terminology used in Table 2.22. Specimens having names starting with UU in Table 2.22 are unstiffened steel box columns that were the first specimens tested with a steel slenderness ratio, $\bar{\lambda} > 0.4$, where $\bar{\lambda}$ is the slenderness parameter of the steel section. A later study into columns with a steel slenderness ratio, $\bar{\lambda} = 0.25$, was performed to investigate the behaviour of cyclic loading on shorter columns. These specimens have names starting with UC and are also unstiffened steel box columns with concrete-fill, the number in brackets after the specimen name represent the number of cycles at each load level. Concrete was poured from the bottom up to the desired height, and then a solid diaphragm was welded at that height, to ensure fully confined concrete. Specimens UC70-25-3[3]D and UC70-25-5[3]D did not have a diaphragm at the top of the concrete-fill. The ductility and energy absorption of the specimens are presented in Table 2.23 and the terminology has been defined in Section 2.5.4.2.

Figure 2.24 shows the hysteretic curves of some of the specimens tested. Local buckling first occurred in the flange plates at the column base for all specimens. In the hollow steel sections, buckling progressed into the webs. In the columns filled with concrete up to 30% of the height, local buckling developed above the diaphragm where there was no concrete-fill and most of the buckling deformations occurred there. When the columns were filled with concrete up to 50% of the height of the column, local buckling developed at the base and deformation characteristics in the inelastic range were good. For the two columns without the horizontal diaphragms acting to confine the concrete, local buckling occurred only at the base, regardless of the height of concrete-fill, and the ultimate load resistance was less than for the specimens having such a diaphragm. Columns filled with concrete up to 50% of the height always performed better than the columns with only 30% of the height filled with concrete. Some other noteworthy findings from Ge and Usami (1994) include:

- After testing, steel plates were cut and removed, and examination of the column revealed that the concrete was seriously crushed behind where the steel plates had buckled.
- It was concluded that longer columns (eg. UU5 compared to UU4) had smaller ductility capacity. As well, ductility appeared to reduce as the width-to-thickness ratio increased.

- The observed increase in strength and ductility was attributed to partially filling the hollow steel box with concrete.

2.5.4.4 Test results from Kitada et al. (1995)

Kitada et al. (1995) studied three rectangular stiffened steel specimens modeled at 1/3 scale from an actual bridge pier. One column, labeled H1, was tested in monotonic loading. Another column, labeled H2, was tested under cyclic loading, and the last column, labeled H3, had concrete-fill to 1100 mm (17% of height) and was also subjected to cyclic loading. The columns were 800 mm x 816 mm in cross-section and steel plates were 8 mm thick. All columns had sixteen 6 mm x 64 mm steel plate stiffeners per cross-section. The columns were 6400 mm long. Design parameters are presented in Table 2.24.

Specimen H2 subjected to cyclic horizontal loading failed by local buckling of the stiffened plate at the base of the column, whereas Specimen H3, tested in a similar manner failed by local buckling above the concrete fill. Results indicated that Specimen H3 developed a larger load resistance than Specimen H2, as shown in Figure 2.25. In addition, the slope of the curve in the post ultimate range was more gentle for Specimen H3 than for H2. The concrete was found effective in increasing both the strength and ductility. After the tests, Kitada (1992) concluded that larger ductility can be expected in concrete-filled columns if their failure mode is by plastic deformation of the concrete and steel, rather than local buckling of the steel cross-section.

2.5.4.5 Test results from Goto et al. (1997)

Goto et al. (1997) investigated two piers that were used for an elevated highway in the Hanshin Expressway Kobe line and were damaged in the Kobe earthquake. These piers consisted of a rectangular hollow section of dimension 2000 mm x 1500 with concrete-fill up to 2985 mm height as seen in Figure 2.26. Pier P-352 had a length of 8800 mm and web and flange thickness of 40 mm and 50 mm, respectively, and was of an unsymmetric T-shape. Pier P-353 had a length of 8600 mm and web and flange thickness of 35 mm and 33 mm, respectively and was of a symmetric T-shaped box pier.

Pier P-352 failed by plastic elongation of the anchor bolt on both the north and south side. Significantly large strains were recorded in the column footings, and in particular the anchor bolts. The location of the anchor bolt can be seen in Figure 2.26. The elongation of the anchor bolt appeared to have dissipated the energy caused by the seismic action and although the column leaned toward the south direction, there was no damage to the column itself. A large gravity moment was induced in Pier P-352 due to the unsymmetric configuration as seen in Figure 2.26, and this resulted in greater strain demands on the anchor bolts, leading to their failure. In comparison, no damage occurred in the anchor bolts of Pier P-353. Local buckling occurred in the south web panel above the concrete-fill in Pier P-352 and severe plastification occurred in the steel tube at this height. The thickness of the webs and flanges of Pier P-353 were smaller than P-352, and this may explain why web buckling occurred in Pier P-353.

A dynamic response analysis was performed to investigate if the failure modes could be reproduced analytically. In the analysis, it was determined that the steel in Pier P-353 had yielded above the concrete-fill, and more plastification had occurred as compared to Pier P-352. The analysis also produced strains on the anchor bolts that were approximately eight times greater in Pier P-352 than in Pier P-353. Therefore, this analysis confirmed the actual failure mode of both piers.

Goto et al. (1997) also analyzed two other columns, Pier A and Pier B. Pier A had a single anchor–beam type anchor bolts and a slenderness ratio of 19.1, while Pier B had a double anchor-beam type anchor bolts and a slenderness ratio of 6.2. They observed that by decreasing the column base restraint, the column experienced less damage while increasing the damage to the anchor bolts. Pier B sustained more damage due to the small slenderness ratio. They also found that there is a magnitude of base restraint that minimizes the sway displacement at the top of the column. It was concluded that, by choosing a reduced base restraint, the column and anchor bolts will experience less damage than when full base restraint is used.

2.5.4.6 Design results from Otsuka et al. (1997)

Otsuka et al. (1997) studied two large scale hollow rectangular steel piers, one with concrete-fill, type-ACON, and the other specimen with no concrete, type-A. The height of the concrete-fill was 1700 mm, and the total height of the column was 6000 mm. The width of the box was 800 mm and Figure 2.27 shows the column dimensions. The yield stress of the steel was 353 MPa, and the measured strength of the concrete was 14.7 MPa. A constant axial load was applied to the column, and the horizontal load was cycled three times at each specified displacement.

In the ACON specimen, fatique cracks were first observed in the toe of the base weld at the end of the first cycle of 2.8 δ_y, and local buckling occurred at the end of the 2nd cycle of 4.3 δ_y. There was no noticeable decline in strength until the first cycle of 5.3 δ_y, at which point, cracks increased in size and strength dropped. After analysis, it was discovered that the strength dropped due to low-cycle fatique and not by local buckling. In comparison with the hollow column, the ACON specimen experienced no local buckling in the stiffened plate and both the strength and the ductility was improved.

2.5.5 Cyclic tests of concrete-filled steel columns

Tests of concrete-filled steel columns under cyclic loading are the most relevant to the present study. Currently, there has been only a few tests performed to investigate the cyclic behaviour of concrete-filled steel tubes. Ghosh (1977), Prion and Boehme (1994), Boyd et al. (1995), and Alfawakiri (1997) studied the effect of cyclic loading on circular columns. Kitada (1992) has compared selected findings of Japanese researchers studying rectangular and circular cross-sections for a variety of different loading cases. Kawaguchi et al. (1987, 1992) and Ge and Usami (1994) have both studied the effects of cyclic loading on rectangular steel columns filled with concrete.

2.5.5.1 Circular columns

2.5.5.1.1 Test results from Ghosh (1977)

Ghosh (1977) tested two circular hollow steel tubes with one of the columns filled with concrete. The columns were 14.5 m in length, 320 mm in outside diameter, and 6 mm in steel wall thickness. The steel slenderness ratio of these columns was 129, and the kL/r_c value was 188. Each steel column was constructed from two pieces of pipe welded together with the joint 2.6 m from the top. The column was filled from the bottom by pumping the concrete through a porthole and valve assembly. Four 13 mm diameter holes were drilled through the steel cap in the top of the column in order to allow air to escape during pumping. The concrete cylinder compressive strength was 34 MPa at the time of testing and the steel shell had a yield strength of 365 MPa. The load was applied to the top and bottom end using bearing plates and the compression seats reacted against the beam at the top and the hydraulic jack on the bottom as shown in Figure 2.28.

When the axial load reached 267 kN, a moment of 90 kN·m was applied by pulling the columns at mid height. The vertical load on the column remained constant while the horizontal load on the concrete-filled column was released and reapplied several times in order to investigate repeated loading but without load reversal. The columns were finally axially loaded to 445 kN and 226 kNm in flexure. The columns were not tested to failure because of a limitation in the testing frame. It was observed that the deflections for the hollow column were approximately twice the deflections for the concrete-filled column at the same horizontal load. The steel shell was removed and the concrete was found to have remained intact. Tension cracks that occurred at the mid-height of the column closed completely on unloading and Ghosh (1977) reported that no cracks were easily observed on the concrete surface. Ghosh (1977) concluded that, for a column with a slenderness ratio of 129, filling with concrete is a viable way to increase the load and moment carrying capacity of a column without increasing its size, and a thinner-walled steel columns filled with concrete could be used at a considerable cost saving to provide a given desired strength.

2.5.5.1.2 Test results from Prion and Boehme (1994)

Prion and Boehme (1994) subjected three concrete-filled steel columns to cyclic loads. They also tested nineteen columns under monotonic loading as described in Section 2.5.2.1.8. The columns were both 2120 mm long, with an outside diameter of 152 mm, a steel shell 1.65 mm thick ($D/t = 92$) with a yield stress of 328 MPa, and a concrete cylinder strength of 92 MPa. One column, Specimen B2, was tested in the beam-column test set-up with no axial load. Two other columns, Specimens C2, were tested with axial loads applied. The specimens were cycled at a specified level of the yield deformation until failure, which occurred in all columns in four and half cycles. The properties of the three columns can be found in Table 2.9.

These cyclic tests demonstrated good ductility of the members. The resulting hysteretic curve for one of the C2 columns is shown in Figure 2.29. Prion and Boehme (1994) attributed the slight pinching observed in this hysteretic curve to the opening and closing of concrete cracks while the steel tube was yielding and buckling. It was concluded that the observed moment capacity deterioration after the first cycle could be attributed to the loss of concrete confinement. Fracture of the steel tube occurred on the tension side at a strain of approximately three times the yield strain when the specimens were loaded to failure after 4.5 cycles. Specimen B2 showed a slight decrease in strength after every cycle but the specimen exhibited good energy dissipation.

2.5.5.1.3 Test results from Kitada (1992)

Kitada (1992) summarized some of the Japanese research performed on short columns and beams subjected to axial force, flexure, combined compression and flexure, combined compression and shear, and torsion. Table 2.25 lists the dimensions and results of the tests reviewed by Kitada, and shows that the circular cross-section is better suited than the rectangular cross-section to sustain, in a ductile manner, numerous cycles of bending, or shear under constant compression. Prior to yielding of the steel shell, it was observed that the torsional rigidity of the circular composite column is similar to that of the steel column because the steel tube and concrete-fill behave as isolated components. This action is unlike the rectangular composite cross-section whose materials act together and therefore, the torsional rigidity is greater than the

hollow steel column. However, a considerable increase in ultimate torsional strength and ductility was observed in both circular and rectangular composite specimens, compared to steel specimens.

2.5.5.1.4 Test results from Boyd et al. (1995)

Tests by Boyd et al. (1995) were conducted on five circular composite column specimens subjected to cyclic inelastic lateral displacements under a constant axial load of 178 kN. All columns had a diameter of 203.2 mm and the steel shell thickness was either 1.91 or 2.77 mm. The steel shells were constructed of steel with a mean yield strength of either 283 MPa or 345 MPa, and filled with concrete of strength 31.7 MPa or 48.3 MPa. The footing of the column was attached to the laboratory strong floor with bolts in order to provide full fixity at the base as shown in Figure 2.30. The axial loads were maintained at a constant level and a lateral load was applied near the top of the column. The loading pattern for the flexure specimens consisted of two cycles at displacement ductility levels, μ, of ±1, ±2, ±4, ±6, and ±8. Table 2.26 summarizes the details of the columns and the test results.

Columns 1 and 2 were identical. Shear studs were welded to the interior surface of Column 3; these were 24 mm long sections of No. 3 Grade 60 reinforcing steel, and were placed on 100 mm centres. The steel shell was cut along its longitudinal axis, and studs were welded to the shell by a fillet weld around their circumference as shown in Figure 2.31. Boyd et al. found tensile coupons extracted from these specimens to be less ductile when they were tested with the studs attached. Columns 4 and 5 had larger D/t ratios and Column 5 had a higher strength concrete.

All columns exhibited stable behaviour and maintained, or exceeded, the ACI 318-89 predicted load capacity at a minimum displacement ductility of $\mu=6$. Although local buckling occurred in all of the shells, all test columns remained satisfactorily ductile and exceeded the ACI predicted flexural strengths, M_{ACI}, as described in Section 2.3.3, even though the thickness of the steel shells violated the thickness requirements of ACI 318-89 and AISC-LRFD 1986 codes. The comparison between M_{test} and M_{ACI} is presented in Table 2.26.

Figure 2.32 shows the hysteresis curves for all specimens tested by Boyd et al. Columns 1 and 2 buckled at $\mu=\pm 4$ and fractured at further cyclic loading. Column 3 displayed fractures at the top and bottom locations where buckles previously formed on each side. Because fracture did not occur in Column 4 or Column 5, Boyd et al. (1995) attributed this behaviour to their observations of the thin shell being more ductile than the thick shell. Prior to the fracture of the steel shell, the load carrying capacity of Columns 1 and 2 was higher than that of Column 4. Column 4 exhibited a greater displacement ductility while still maintaining its load-carrying capabilities and achieved this more effectively than Columns 1 and 2. Column 3 possessed a greater lateral load capacity than Columns 1 and 2 prior to steel shell fracture. Steel shell fracture occurred earlier in Column 3 than in Columns 1 and 2, which was attributed to the decreased material ductility.

Strain gauges were used to determine if bond existed at the interface between the steel shell and concrete core. Boyd et al. reported no significant increase in bond between the concrete core and the steel shell at low values of lateral displacement. As the lateral displacement increased, the shear studs appear to be productive as the ultimate strength of Column 3 only degraded by 4% while the strength of Columns 1 and 2 degraded by 12% and 7% respectively. Boyd et al. attributed the lesser strength degradation to a decrease in slip between the concrete core and the steel shell. Another advantage arising from the shear studs was that the energy dissipation for Column 3 was greater than that of Column 2.

2.5.5.1.5 Test results from Alfawakiri (1997)

Alfawakiri (1997) tested four concrete-filled steel tubes; one short column, 380 mm long, and three long beam-columns, 1655 mm long. All columns were constructed from a hot-formed seamless steel tube of diameter and thickness of 152 and 3 mm, respectively, with a tested yield strength of 330 MPa. The columns were filled with high strength concrete with a compressive strength between 72 and 90 MPa. The short column was tested in concentric axial loading, while the three long beam-columns were tested under cyclic loading. The beam columns were each welded to a thick steel base plate strengthed and made more rigid by adding two stiffeners to

achieve a fixed base connection. The assembly was then rigidly connected to a reinforced concrete base, itself attached to the strong floor of the laboratory. Displacement measurements taken on the steel base plate confirmed that the connection was rigid. Figure 2.33 shows the test set-up.

The concentrically loaded column resisted a load of 2157 kN. This compressive load was 1.17 times larger than the sum of the individual resistance of each of its components. Shear failure of the concrete core caused a brittle failure. Strain gauges attached in both the longitudinal and transverse direction indicated that the transverse strains were twice as great as longitudinal strains at $0.75P_{failure}$. Upon applying greater loads, a sharp increase in the tensile transverse strains occurred indicating effective lateral confinement of the concrete core.

A constant axial load was applied to the beam columns as the horizontal load was cycled. Each specimen was loaded with a different axial load ratio. Specimen FA1 was loaded with an axial load of $0.2P_o$, and the specimen reached its maximum moment resistance in both directions at a drift level of 4%. The test was stopped at a drift of 8%, at which time the lateral strength had reduced to 80% of the maximum reached. Because the stiffened base plate also stiffened the lower part of the column, the local buckle occurred 60 mm above the base plate. Yielding of the steel tube occurred at a drift level of 3%. The majority of the rotation in the column occurred at least 60 mm above the base plate.

Specimen FA2 was loaded with an axial load ratio of $0.5\ P_o$. The maximum moment resistance was reached at a drift of 3%, when the out-of-plane deflections become excessive and the test had to be stopped. Testing resumed at 3% drift but with a smaller axial load of $0.05P_o$. Local buckling on the positive and negative side of the column occurred at 5% and 6% drift, respectively. Testing ended at a drift of 10% when the steel tube fractured at the location of the buckles. The buckle occurred 90 mm and 100 mm above the base plate on the positive and negative side, respectively. Compression yielding of the steel tube in the hinging area occurred during cycling at 2% drift.

Specimen FA3 was loaded with an axial load ratio of $0.35\ P_o$ and the specimen reached its positive and negative maximum resistance at a drift level of 4% and 3%, respectively. The test was completed at a drift of 7% when the load resistance in the negative direction had reduced down to a minimal value. A local buckle was observed to occur 100 mm above the base plate during cycling at 5% drift. A buckle on the opposite side of the column, 410 mm above the base plate, was observed to occur during cycling at 6% drift. Compressive yield of the steel tube occurred during cycling at 2% drift and the sides of the column experienced compressive yield at 3% drift.

2.5.5.2 Rectangular columns

2.5.5.2.1 Test results from Kawaguchi et al. (1987, 1992)

Kawaguchi et al. (1987) tested 26 beam-column specimens (Table 2.27). Five different steels and three specimen sizes were used: 100 x 100 x 4.5 (width-to-thickness ratio of 22.2), 100 x 100 x 3.2 (width-to-thickness ratio of 31.3) and 100 x 100 x 2.3 (width-to-thickness ratio of 43.5). All specimens were 1048 mm long. The specimens labeled 'S' were hollow steel sections while the specimens labeled 'C' were concrete-filled steel tubes with a concrete compressive strength of approximately 22 MPa. The steel tubes were welded to a thick steel base plate. The specimens were tested under a constant axial load, and repeated horizontal load at a constant displacement amplitude. Different axial loads, P, as a fraction of the squash load of the composite column, P_y, were applied. The displacement amplitude ratio, α, was calculated as the ratio of the maximum displacement to the displacement at the occurrence of local buckling. The properties of all the specimens as well as the strain and displacement at the onset of local buckling are presented in Table 2.28; a 'C' is shown in the column titled "Corner Crack" if a weld crack appeared during testing.

The hysteretic curves for the horizontal load-displacement relationships for the hollow steel tubes and the concrete-filled steel columns are shown in Figure 2.34. Kawaguchi et al. (1992) have some noteworthy conclusions from these results and they include:

- The two faces perpendicular to the direction of horizontal load swelled out and the opposite two faces buckled inward for the hollow steel tubes, whereas in the concrete-filled steel tubes, all faces of the steel sections buckled outward. All local buckling occurred at the base of the tube.
- The displacement at first occurrence of local buckling, Δ_{cr}, was not influenced by the axial load ratio, and was greater in the concrete-filled steel columns than in the hollow steel tubes. The Δ_{cr} values for the C-series specimens with a D/t ratio of 22.2, 31.3, and 43.5 were approximately 1.25 to 1.4, 1.9, and 1.33-1.5 times greater than for the hollow steel tubes having the same width-to-thickness ratio and axial load ratio, respectively.
- The strength deterioration was less severe in the C-series specimens because concrete helped delay local buckling.
- The energy dissipation capacity for the C-series specimens was greater than for the S-series, for the same reasoning.

2.5.5.2.2 Test results from Ge and Usami (1994)

Ge and Usami (1994) subjected six concrete-filled square box stub columns with and without longitudinal stiffeners to a cyclic compressive load. For comparison, four hollow steel square box stub columns were also loaded to failure. Cross-section of the specimens varied from 213 to 345 mm and all steel boxes were constructed by welding 4.5 mm steel plates together. Columns without stiffeners ranged in height from 592 mm to 922 mm, and the height of the columns with stiffeners was 1316 mm. Specimen U12-HC was constructed from a high-performance concrete with a superflowing property, for which a high-early-strength low-heat cement was used. The measured dimensions of test specimens without stiffeners and with stiffeners are presented in Table 2.29 and Table 2.30, respectively. Parameters used in these tables were defined in 2.5.4.2.

Local buckling of the hollow columns occurred in their steel plates at the mid-section before their maximum load was reached and they buckled both inward and outward. In the concrete-filled columns, local buckling of the plates occurred just prior to attaining maximum

load, and then progressively grew. All plates buckled outward but the location varied. Cracks developed in some of the welds when the axial strains in the specimen became relatively large. Figure 2.35 shows specimens U12-S and U12-C after testing to failure. Local buckling can be easily seen in this figure. After testing, the webs plates were removed and the concrete behind the portion of plates which buckled was found to be seriously crushed, but concrete was undamaged elsewhere. Ge and Usami (1994) concluded that plate buckling probably developed after concrete was damaged.

Figure 2.36 shows the load versus axial strain for some of the columns tested in this study. Some hysteresis is visible in the unloading/reloading segments of these curves; this hysteresis was more evident in the later cycles. Ge and Usami interpreted this as a sign that the concrete-fill was damaged prior to attainment of the peak load resistance. The stiffened steel box columns had a higher compression capacity than the unstiffened steel box columns. The specimen with the higher strength concrete, U12-HC reached a higher strength but did not maintain this value over large deformations, as seen in Figure 2.36d. The ultimate strength of the two stiffened concrete-filled columns was considerably more than that of the unstiffened concrete-filled columns.

2.6 Comparison of analytical equations

The many different analytical expressions found in the literature suggest a lack of concensus on the best way to quantify the cyclic behaviour and ultimate strength of concrete-filled steel tube beam-columns. However, the equations reviewed in the previous sections share many similar attributes.

First, it is commonly reported that the ultimate axial strength of a concrete-filled steel column, or its squash load, can be calculated by adding the strengths of the two materials. Whether or not concrete confinement is considered in the calculation of the squash load produces slightly different results. Researchers who calculated the squash load with additional strength attributed to concrete confinement include Furlong (1967,1968), Ruoquan (1987), Kato (1996),

Itani (1996), and Hajjar and Gourley (1996). Knowles and Park (1969) have demonstrated that the concrete slenderness ratio must be less than 34.8 to achieve this additional strength.

The AISC LRFD (1984), ACI 318 (1995), and the CAN3-A23.3-M94 (1984) state that the steel strength shall be taken as the yield stress of the steel tube. However, Ruoquan (1987) and Itani (1996) have developed design equations that reduce the longitudinal steel stress and increase the attainable strength of the confined concrete. The stress-strain model used by these two researchers is a tri-linear model which takes into account the effect of strain hardening in steel. The CAN/CSA-S16.1-M94 is the only current design code that accommodates both an increase in concrete strength and a decrease in the longitudinal stress of steel.

Second, the most common method of calculating the buckling load of a concrete-filled steel column is by the tangent modulus load method and the Euler buckling load. Researchers who used this method include Furlong (1967, 1968), Knowles and Park (1969) and Ruoquan (1987). Among the other approaches used, Cai (1992) and Kato (1996) reduced the squash load by various ratios to achieve the strength of a long concrete-filled steel column. Neogi et al. (1967) analyzed the effect of eccentric loading on long concrete-filled steel column and found that equating the internal and external energy and using a deflection curve in the shape of a cosine wave, the strength of the column could be calculated.

There is no consensus on what constitutes the best method to analyze axial load and bending moment interaction. The thrust-moment interaction equation presented in Equation 2.46 was stated to be unconservative for slender columns but comparison with experimental results proved its adequacy (Knowles and Park (1970)). Much work remains to be done on this topic.

2.7 General observations on behaviour

This section synthesizes the research results presented in Section 2.5 on the behaviour of concrete-filled steel tubes subjected to both monotonic and cyclic loading. Characteristics of the general behaviour recognized by consensus are first described. The limits of the past studies are

then identified, followed by a summary of remaining contentious issues which have arisen out of the research.

2.7.1 Global observations

The additional ductility and energy absorption that concrete-filled columns possess is the predominant observation of all researchers studying these columns. For the most part, it is agreed that the strength of the composite column is at least equal to the sum of the strength of the steel shell and concrete core taken individually. The use of concrete-filled tubes enables a smaller hollow steel section to be used, because of the additional strength provided by the concrete core, as compared to a hollow steel column which is intended to resist all loads. Steel tubes filled with concrete also exhibit better energy absorption when subjected to cyclic loading. The additional ductility, energy absorption, and strength are significant benefits, and the concrete-filled steel tube appears to be a viable option for use as a bridge pier in high seismic regions.

2.7.1.1 Behaviour of concrete-filled steel columns subjected to non-cyclic loading

Concrete-filled steel columns have been observed to fail dominantly due to either global buckling or local buckling. In the columns which fail by local buckling, there is a distinct difference in behaviour between the hollow steel sections and the concrete-filled steel columns. Contrary to what is observed in hollow steel columns, no part of a concrete-filled steel column buckles inwards because the concrete core prevents movement of the shell in that direction. This delays buckling of concrete-filled steel columns compared to identical hollow steel columns.

Gardner and Jacobson (1967), Neogi et al. (1969), Knowles and Park (1969), and Shakir-Khalil and Zeghiche (1989, 1990) tested concrete-filled steel columns that failed due to global column buckling, and local buckling did not occur in any of these non-cyclic tests. However, Furlong (1967, 1968) and Schneider (1998) observed that local buckling occurred after the yield strain had been reached while Bridge (1987) observed that both the hollow steel sections and the concrete filled columns failed by local buckling before the maximum load was reached.

The D/t ratio for the columns that experienced local buckling were greater than 124. In comparison, the largest D/t ratio of the columns tested in which global column buckling failure occurred was 98. Therefore, the larger the D/t ratio, the greater the risk of local buckling becomes, similar to a hollow steel tube. Columns tested in axial and eccentric compression exhibit the greatest moment and curvature at the centre, with plasticity always found at the column's mid-height.

2.7.1.2 Behaviour of concrete-filled steel columns subjected to cyclic loading

Research has shown that hollow steel sections form symmetric pinched hysteretic energy dissipation diagrams when subjected to cyclic loads. The ability of a column to dissipate energy is equivalent to the area under its hysteretic curve. Partially filling a steel tube with concrete and subjecting it to cyclic loads produces a fuller hysteretic curve than a hollow steel section and also improves the ductility and strength deterioration of the hollow column. Completely filling the same steel tube with concrete and subjecting it to cyclic loads produces an even fuller hysteretic curve, more ductility, reduced strength deterioration and an increase in strength resistance over both the hollow column and the partially filled column.

Usami et al. (1992), Ge and Usami (1994), Kitada et al. (1995), and Otsuka et al. (1997) all concluded that partially filling a hollow steel section with concrete significantly increases the ductility and energy-absorption, and reduces the strength deterioration in the column. Findings from Usami et al. (1992), Ge and Usami (1994) and Goto et al. (1997) showed that filling the steel tube with concrete up to 30% of the height produced local buckling above the concrete-fill, however, 50% of the column height filled with concrete produced local buckling at the base. Failure to the column, in the form of local buckling, will occur when the moment resistance is less than the applied moment. The moment resistance of the column is smaller above the concrete-fill termination point, and if the ratio of applied moment to moment resistance is greater than one at this position before the base location, local buckling occurs above the concrete core.

Other failures were observed in partially filled steel tubes. Failure by local buckling was also seen by Itoh et al. (1997), however, location of the buckles coincided with a decrease in steel wall thickness, far above the concrete-fill. This local buckling failure was a result of the dimensions of the steel tube alone and the addition of concrete did not effect the overall failure. The second column investigated by Goto et al. (1997) failed by the plastic elongation of one of the anchor bolts due to unsymmetric loading conditions and Otsuka et al. (1997) found failure to his columns were caused by low-cycle fatigue. Kitada et al. (1995) suggested that larger ductility should be expected in concrete-filled steel columns if the failure mode is caused by plastic deformation of concrete-filled section instead of by local buckling of steel cross-section.

An extension to filling a hollow steel tube with concrete halfway up its height, is to completely fill the steel tube with concrete. Local buckling is delayed in concrete-filled columns because the steel tube is forced to buckle only outwards. Therefore, concrete-filled columns exhibit greater energy dissipation capacity and less strength deterioration than hollow steel columns because the occurrence of local buckling is delayed in the former. A concrete-filled column is able to sustain axial load after local buckling due to the contained concrete, thereby reducing the strength deterioration that occurs in hollow steel sections. It has been documented by researchers that the critical drift of the concrete-filled specimens is smaller than that for a steel section having the same width-thickness ratio and axial load ratio. In a review of experiments, Kitada (1992) found that circular cross-sections preform in a ductile manner when subjected to large cycles of bending or shear under constant compressive load.

Failure of concrete-filled steel columns subjected to cyclic loads is by severe local buckling or fractures near the buckles that cause a significant decrease in the resistance of the column. It was deduced by Boyd (1992) that a thinner walled tube possess more ductility than a thicker wall tube. In his experiments, the thinner wall tubes did not fracture, even at a ductility ratio of ± 8. It was also discovered by Boyd (1992) that shear studs reduce the ductility in the steel tube, and therefore, cause wall fractures sooner than in the columns without shear studs. Kawaguchi et al. (1987, 1997) tested rectangular concrete-filled steel columns and found that the first occurrence

of local buckling was not influenced by the axial load ratio applied to the column. One of the columns tested by Alfawakiri (1997) was subjected to a drift of 10% before final failure, while the other two failed at 8%, and 7%. Local buckling occurred approximately 100 mm above the base for all three columns due to the stiffened steel tube at the base. Three columns tested by Boyd (1992) failed during cycling at 6% drift and the two columns with larger D/t ratios failed during cycling at 8% drift. The columns subjected to cyclic tests by Prion and Boehme (1994) were cycled at 3% drift before failure. All of these columns have demonstrated good ductility.

2.7.2 Limits of past research

The research concerning concrete-filled steel tubes has by no means been exhausted. There are many areas that need to be aggressively researched in order to enhance the knowledge available about the seismic behaviour of these columns. Some of these are explored below.

2.7.2.1 Cyclic

The addition of concrete to hollow steel sections is a design concept that has recently gained popularity in high rise building construction. However, most of these structures are not in seismic active zones and therefore, many researchers have limited the scope of their study to determination of only the ultimate strength under monotonic loading. More testing must be performed on concrete-filled steel columns subjected to cyclic loading so that the behaviour of these columns can be better understood, and the implementation of this type of construction in high seismic regions can begin.

2.7.2.2 Size Limitations

The observations reported in this literature review is limited by the sizes of concrete-filled columns tested by previous researchers. The largest concrete-filled steel column subjected to monotonic loading was a circular column tested by Knowles and Park (1970) with a diameter of 355.6 mm and a steel thickness of 4.7 mm. The largest circular concrete-filled column subjected to cyclic loading has been tested by Ghosh (1977), with a diameter of 320 mm and a steel

thickness of 6 mm. A 345 x 345 x 4.5 mm square specimen tested by Ge and Usami (1994) is the largest rectangular column test under cyclic loading reported here. While the analytical solutions presented earlier imply that they are not limited by column sizes, this has not been experimentally verified. Hence, there is a need for cyclic tests on circular concrete-filled columns having moderate D/t ratios and large diameter steel tubes to determine the effect of concrete confinement on large steel tubes and the resistance of these columns to local buckling.

2.7.2.3 End Conditions

Testing in the laboratory must duplicate the conditions found in full scale implementation. Thus, composite columns need foundations capable to develop their full composite strength and have details that are likely to be implemented in practice.

The tests of concrete-filled columns under monotonic loads consisted of either axially loaded or eccentrically loaded specimens. Gardner and Jacobson (1967), Neogi et al. (1969), Ghosh (1977), Knowles and Park (1969, 1970), Shakir-Khalil and Zeghiche (1989, 1990), Orito et al. (1987), Prion and Boehme (1994) used knife edge connections to simulate pin-ended structures, Furlong (1967) used heavy end-fittings on the ends of the columns, and Schneider (1998) used a stiffened end cap at the base of the column. Plastic hinging occurred at mid-length of these columns, thus circumventing foundation-related issues.

When testing cyclic behaviour, various techniques were used to connect the base of the column to a rigid base. For partially concrete-filled tubes under cyclic bending moments, Ge and Usami (1994) braced the bottom of the column with triangular stiffeners to achieve a fixed end. Kawaguchi (1987), Ge and Usami (1994) and Alfawakiri (1997) welded the column to end plates. Ge and Usami (1994) also welded the column to end plates when subjecting their columns to cyclic axial loads. Boyd et al. (1995) cast the column into a thick concrete base anchored to the laboratory strong floor with bolts. Except for Boyd et al. (1995), the above configurations do not realistically represent the fixed end restraint details likely to be used for a pier foundation. Thus,

research is required to determine how the full composite strength of a concrete-filled circular steel tube can be transferred from the column to its foundation.

2.7.3 Contentious Issues

Adequacy of bond between the concrete and the steel, and of concrete tri-axially confined by the steel shell, are two factors that can have an impact on the cyclic loading of concrete-filled steel tubes, and for which researchers do not appear to agree. Although a resolution of these contention issues is beyond the scope of this study, it is important to be aware of the current debate and arguments.

2.7.3.1 Bond

An important issue in the design of composite columns is whether bond exists between the steel tube and concrete core. Some researchers claim that the adhesive bond between the concrete and the steel is sufficient to ensure full composite action of the two materials. Others argue that because of the differences in Poisson's ratio of steel and concrete, the two materials will separate upon loading and no transfer of load can exist.

Neogi et al. (1969), Ghosh (1977), Bridge and Webb (1992), and Shakir-Khalil and Zeghiche (1990) all observed that bond was retained between the steel and concrete after testing because they observed adhesion of the concrete to the steel when cutting and removing the steel shell after testing. Non-cyclic flexural tests by Lu and Kennedy (1994) on rectangular HSS under four-point bending also revealed that slippage between the steel and concrete was insignificant. No mechanical anchorage was used between the two materials, and full composite strength was reached.

Conversely, in tests designed to investigate bond strength, Furlong (1968), Knowles and Park (1970), Prion and Boehme (1994), and Boyd et al. (1995) found that the natural bond between the concrete core and the steel shell was not retained. Furlong (1968) tested columns with and without axle grease on the interface between the steel and concrete. Results from his

tests showed no difference in the behaviour of these columns. Knowles and Park (1970) loaded stub columns through the concrete only and found that there was little bond between the concrete and steel. Prion and Boehme (1994) discovered that the concrete had shrunk away from the steel shell prior to testing indicating that no bond existed for the entire test. Boyd et al. (1995) tested a column with shear studs and found they were effective at high lateral displacement values at producing greater energy dissipation and less strength degradation compared to columns without studs in which the natural bond was not retained.

2.7.3.2 Concrete Confinement

To order to derive the full benefits of a circular concrete-filled column, the concrete should be confined by the steel so that it is able to achieve a higher ultimate strength than unconfined concrete. It has been shown by Knowles and Park (1970) that for kL/r_c values less than 34.8, tri-axial confinement was likely. Neogi et al. (1969) noted higher than expected strength for eccentrically-loaded circular columns having an L/d ratio less than 15 and attributed this to tri-axial effects. However they also noted that the effectiveness of tri-axial concrete confinement diminished as the axial load eccentricity increased. Gardner and Jacobson (1967), Alfawakiri (1997) and Schneider (1998) also showed an increase in strength over the simple summation of independent strengths for circular concrete-filled steel tubes. A moment capacity deterioration after the 1st cycle in tests by Prion and Boehme (1994) was attributed to the loss of concrete confinement. Concrete confinement did not occur in any of the rectangular concrete-filled steel tubes owing to ineffectiveness of the steel tube to confine the concrete.

It is difficult to accurately determine at what stage the steel is offering no confinement to the concrete. This is partly a result of the unique properties of the two materials. Hence, it is difficult to judge experimentally when concrete confinement has taken place. Many national design codes do not allow an increase in the concrete strength regardless of the slenderness of the column, and those design codes that do allow a concrete strength increase use various equations to indicate when it is effective. Uncertainty remains as to when confined concrete can be relied upon to produce an increase in strength in concrete-filled steel tubes.

3.0.0 EXPERIMENTAL APPROACH

3.1 Selection of Specimen Sizes

The purpose of the experimental portion of this study is to design concrete-filled steel highway bridge piers capable of resisting moderate to severe earthquakes. Therefore, the test specimens must be indicative of full-scale bridge piers in North America. The test pier foundation must also incorporate an actual foundation design that can be implemented in practice.

3.1.1 Full-Scale Bridges Characteristics and Analysis

To ensure that the tested specimens had characteristics and dimensions representative of real prototypes, full-scale bridges and subsequent bridge piers were designed according to the Ontario Highway Bridge Design Code (MTO 1991) and the Canadian Highway Bridge Design Code (CSA 1999). In total, 1296 bridges were designed using a suite of different configurations, geometries, and parameters likely to be encountered in highway bridges situated in North America.

The bridges were designed as overpasses, capable of holding bi-directional traffic, to run perpendicular over a divided highway. The superstructure of all bridges was designed as a two span slab-on-girder bridge. The slab consisted of a 50 mm wearing surface and a 250 mm reinforced concrete deck slab. Concrete traffic barriers and sidewalk allowances were designed for both sides of the bridge. The girders were steel I-sections readily available through Canadian mills and placed at a center-to-center spacing of approximately 2 metres.

The following parameters were used in this parametric study:

- Bridges were simply supported or continuous over pier bent,
- Bridges consisted of 2, 4, or 6 traffic lanes,
- Individual spans had to accommodate an underpass highway of 1, 2, or 3 traffic lanes,
- Pier heights were 5, 6, or 8 meters,
- Pier bents had 1, 3, or 5 piers,

- Soil was Profile I ($S = 1.0$) or Profile IV ($S = 2.0$),
- Zonal acceleration ratio, A, was 0.15 (Shawinigan, Que.), 0.2 (Ottawa, Ont.), 0.3 (Vancouver, B.C.), 0.4 (Victoria, B.C.).

Eighteen different superstructures were designed using the first three parameters in the above list. The number of steel girders used in the superstructure was dependent on the number of design lanes on the bridge along with sidewalk and barrier clearances. The underlying highway, pier diameter (taken as 2 metres), and sloped abutments were all taken into consideration when determining the length of each bridge. Table 3.1 describes the eighteen different superstructures.

Using the bridge superstructures designed above, and the remaining four parameters in the list, 1296 bridges were designed. The pier height was taken as no less than five metres for minimum height clearance for the divided highway running under the bridge. A site coefficient, S, was used to consider variable soil condition around the substructure of the bridge. This coefficient is defined in Section 4.4.6.1 of the CSA 1999. Two soil conditions were used in this study: Profile I, defined as "rock of any characteristic, or stiff soil conditions were the soil depth is less than 60 m," and Profile IV, defined as "soft clays or silts greater than 12 m. in depth." Different zonal acceleration ratios, A, were also used to differentiate the seismic regions by using four different Canadian cities.

Loading cases considered, as defined in Section 2-5.1 of the "Ontario Highway Bridge Design Code" (MTO 1991), include fatigue limit states, serviceability limit states, and ultimate limit states. A number of ultimate limit states combinations were analysed including: live load alone; live load acting together with wind on the bridge and on the live load; and earthquake loads. Live loads were calculated as specified in Section 2-4.3 of MTO 1991 as either the OHBDC idealized five axle truck positioned on any design lane, or 70% of each axle of the OHBDC truck and a superimposed uniformly distributed load of 10 kN/m located within the 3.0 metre lane width. The loading case that produced the maximum loading effect was used for

design. A modification factor for the number of lanes loaded was also used. Dead load was obviously considered in all the above load cases and was calculated as the total weight of the superstructure in addition to one third of the weight of the pier bent.

Once the bridge superstructures were designed, all information necessary for the design of the bridge piers was available. The resulting lateral and axial loads produced different reactions on the pier depending on pier bent geometry and whether the bridge was simply supported or continuous over the pier bent. Clause 18.2 from the CAN/CSA-S16.1-M94 design specification (clause on the design of concrete-filled circular hollow structural sections) was used for the design of the concrete-filled steel pier.

Figure 3.1 shows how the axial and horizontal load were assumed to be resisted in a single pier bent. The horizontal load produces single curvature bending in the pier with zero moment at the top of the column. The corresponding moment at the base of the column was taken as equal to the height of the column multiplied by the horizontal force and divided by the response modification factor (R). The response modification factor is defined in Section 4.4.8.1 of CSA 1999 and given a value of 3.0 for single columns constructed of ductile reinforced concrete or ductile steel. The same R-factor was used here even though the type of construction considered here is not addressed by the CSA 1999. For seismic design, the single pier in this bent was designed to resist a shear force equal to the total horizontal load applied and an axial load equal to the reaction at the pier location caused by the dead load of the bridge. This approach was the same for both the simply supported bridges and the continuous bridges.

Figures 3.2 and 3.3 illustrates the design assumptions for pier bents having three and five piers, respectively. For both of these cases, the horizontal load put the piers into double curvature. First, the horizontal load acting on the bridge deck multiplied by the distance from the deck to the bottom of the girders, e, produces a resulting moment applied at the top of the pier cap. This moment resolves into a compression or tension force acting on the outside piers. Furthermore, each pier is subjected to an equal but opposite moment on either end of the column

equal to the horizontal load multiplied by half of the pier height divided by the number of piers and the response modification factor (R). This factor is defined in Section 4.4.8.1 of CSA 1999 and given a value of 5.0 for steel or composite steel and concrete pile bents having more than one column. P-Δ effects were also taken into account, therefore the effective length factor, k, was taken equal to 1. In addition, each pier was designed to resist a shear force equal to the total horizontal load divided by the number of piers and an axial load equal to the reaction at the pier from the dead load divided by the number of piers. A slight difference in calculations occurred between the simply supported and continuous bridges due to the different distances of the road surface to the pier bent, (on Figures 3.2 and 3.3 as "e") 1003 mm and 1053 mm, and calculation of the reaction at the pier due to the dead load. The center-to-center spacing of the piers in the three and five pier bent was taken as 4 and 2 metres, respectively.

Table 3.2 illustrates a design example for Bridge 2 (from Table 3.1) having 2 traffic lanes built over a divided highway having itself a total of 4 traffic lanes, with a single 5 metre pier built in Ottawa considering Profile I soil conditions. The resulting pier diameters and thicknesses are of interest.

3.1.2 Selection of Test Columns

Figure 3.4 a,b,c summarizes all the full-scale piers that were designed considering one pier, three piers, and five piers per bent, respectively, and Figure 3.4d combines all of the full-scale piers into one graph. It is hence observed that many pier sizes could be used for more than one design. Nonetheless, a more stringent criteria than bridge applicability alone was needed to select the four test piers that would be constructed for this project.

First, since the D/t ratio is an important parameter that relates to the local buckling resistance of hollow circular flexural members, it was retained as a parameter of significance. According to Section 11.1.1 of CAN/CSA.S16,1-M94, a circular hollow section of yield strength 350 MPa with a D/t ratio less than 37 is classified as a Class 1 section, a D/t ratio less than 51 is classified as a Class 2 and a D/t ratio less than 67 is classified as a Class 3 section.

Second, it has been noted by Knowles and Park (1969) that the kL/r_c value of a concrete-filled steel tube is an indicator of whether the concrete-fill is confined by the steel tube. Since Knowles and Park (1969) showed that a slenderness ratio, kL/r_c less than 35 is required to ensure concrete confinement, all tested columns were chosen among those from the above designs which would have such a value lower than 35.

Based on the parametric study results shown in Figure 3.4, and the observations on D/t and kL/r_c ratios, the following test specimen characteristics were selected:

1. $D/t = 35$ and $kL/r_c = 30$ (one pier), or 60 (multiple piers)
2. $D/t = 51$ and $kL/r_c = 30$ (one pier), or 60 (multiple piers)
3. $D/t = 51$ and $kL/r_c = 22$ (one pier), or 44 (multiple piers)
4. $D/t = 64$ and $kL/r_c = 22$ (one pier), or 44 (multiple piers)

These four columns are identified in Figure 3.5 a,b,c with the results from the parametric study for one, three and five piers per bent. Figure 3.5d illustrates the four columns along with columns previously tested by other researchers for comparison.

All specimens in the present study were tested as cantilevers. A full-scale pier in a single pier bent is also acting as a cantilever, and therefore, the test specimen shares the characteristics of the full-scale prototypes. However, a full-scale pier in a multiple pier bent is in double curvature. Therefore, if cantilever specimens are tested, they are representative of columns in the prototype from their base to the inflexion point at mid-height. This means that the kL/r_c value of the specimens must be doubled to permit comparison with the full-scale prototypes. Figure 3.6 shows this relationship between full-scale piers and tested specimens

Even with the criteria of realistic bridge applicability, and pre-selected D/t and kL/r_c values, there were still a number of full-scale piers that could meet the stated requirements for each of the four test columns. This allowed for a number of different scenarios, and permitted a

number of possible choices for each test column. Therefore, important parameters for the specimens and prototypes were matched as well as possible. The first two parameters to match were obviously the D/t and kL/r_c ratios. Test columns were selected from the catalogue of steel tubes produced by Ipsco, a major North American steel producer. Furthermore, to ensure proper consideration of the relative magnitude of axial forces present in the prototype composite piers during earthquakes, the ratios C_f/C_r, M_f/M_r, C_f/C_{rc} and C_r/C_{rc} were compared for the various possible prototypes to see which specimens could be tested to accommodate similar ratios. C_f and M_f are the axial load and moment applied to the column, respectively, and C_r, C_{rc}, and M_r are the axial resistance of the steel tube and composite cross-section, and the bending resistance of the composite cross section, respectively, as defined in CAN/CSA S16.1-M94 and in Section 2.3.4.

Restrictions with the test set-up (existing reaction frame components had to be used due to budget constraints) also impacted selection of the test specimens. The maximum axial and horizontal loads that could be applied were 2000 kN and 1000 kN, respectively, and the maximum height of the column was restricted to 2200 mm. Finally, the column with the larger diameter and for which all other selection conditions were met, was always chosen to permit study of larger diameter columns than had been previously tested.

With this criteria, the four test columns were chosen and labeled CFST ## where CFST refers to Concrete-Filled Steel Tube and the number refers to the D/t ratio of the steel tube. Therefore,

- CFST 51 has a 323.9 mm diameter and a 6.35 mm thickness
- CFST 34 has a 323.9 mm diameter and a 9.53 mm thickness
- CFST 64 has a 406.4 mm diameter and a 6.35 mm thickness
- CFST 42 has a 406.4 mm diameter and a 9.53 mm thickness

Note that it was originally intended to have two columns with the same D/t ratio of 51. Indeed, the fourth column was to have a D/t ratio of 51, a kL/r_c value of 30, and a 406.4 mm diameter

steel tube with a steel thickness of 7.53 mm was chosen. However, this size of steel tube could not be obtained in North America by the fabricators responsible for this study. Therefore, the same diameter tube was chosen but with a larger steel thickness, namely 9.53 mm thick. The new column has a D/t ratio of 42 and a kL/r_c value of 22.7. This column was identified as CFST 42. CFST 51, CFST 35, CFST 64 and CFST 42 were subjected to axial loads of 1600 kN, 2000 kN, 1000 kN, and 2000 kN respectively. The four column specimens and their comparable full-scale prototypes are identified in Table 3.3.

3.2 Design of Test Foundation

The objective in designing the foundation was to develop a design concept that provided full fixity and adequate strength to allow development of the column's composite strength. The proposed design idea consists of a foundation in which the concrete-filled steel tube is encased in concrete and the full composite moment strength of the column is resisted by steel components welded to the steel tube inside the concrete foundation.

A number of design ideas were considered, however; restrictions on size due to the test frame and cost of the total test columns narrowed the choices to one foundation design. The composite flexural strength was determined for all columns considered in this test program using a program written by the author to calculate the moment-curvature relationship of concrete-filled steel tubes. More information on this program can be found in Appendix A. Specimen CFST 42 was found to have the largest flexural strength, and all foundations were designed to be able to provide this resistance. Designing only one foundation simplified fabrication.

The proposed foundation design is shown in Figure 3.7. This system is described per its construction sequence. The bottom of the steel tube was welded to a 30 mm thick bottom plate. Two C channels with their flanges pointing away from the tube were placed alongside the steel tube on either side and welded longitudinally to the bottom plate. A 10 mm thick top plate with a hole cut out for the steel tube was then slipped over the column. The two longitudinal ends of the plate were welded to the top flange of the channels, in addition, the transverse ends of the plate

that were in contact with the flanges of the channels were also welded. The inside of the cut hole was welded to the column.

The channels and the top plate were used to transfer the entire composite moment from the column. The bottom plate was used to resist the tension and compression that was left in the tube when the load reached the bottom of the column. The load should significantly decrease at this location due to the load being transferred into the top plate or channels. No reinforcing bars were needed in the concrete foundation as the structural steel members were designed to transfer all forces. Four foundation bolts, two at each longitudinal end, were used to transfer the uplifting shear force and horizontal forces in the channel into the strong floor. The moment in the channels at the location of the bolts was zero. These bolts were longitudinally located 914 mm from the centerline of the column, and 914 mm from each other in the transverse direction. The concrete foundation and location of bolts is shown in Figure 3.8.

Due to size restrictions, the vertical load actuators sat on top of the foundation during testing. Four plastic tubes were set in the concrete on both the north and south sides of the columns for the bolts that attached the vertical actuators to the foundation. These bolt positions can be seen in Figure 3.8. The bolts run through the bottom portion of the actuator and the entire depth of the foundation. Therefore, when the vertical load was applied by the actuator to axially compress the specimens, the concrete foundation was subjected to the resulting high tension forces from the actuators. Because the steel tube ran the entire depth of the foundation creating an obstacle to what would have been the simplest path of reinforcement, a reinforcing cage was built around the column and through the channels to resist the forces caused by the actuators' upward pull. Figure 3.9 a,b,c show the front, side and top views of the reinforcing bar cage, respectively.

The foundation steel shapes and reinforcement were then positioned inside a prepared plywood formwork so that the underside of the bottom steel plate was 38 mm above the bottom

of the formwork. Concrete was then poured into the formwork, encasing the steel foundation to 260 mm above the top plate in concrete.

Note that this foundation design was also verified using SAP 90 to validate the hand calculations. Details on this analysis can be found in Appendix C.

3.3 Materials

3.3.1 Concrete

The concrete used in this study was ordered from a ready-mix plant in Ottawa, Ontario. Note that using the proposed foundation design, both the steel tube and the foundation for each specimen could be poured on the same day. The concrete remained in the steel tube and did not flow into the foundation because the column was welded all around the bottom plate. The concrete for Specimens CFST 64 and CFST 35 was poured from a first ready-mix truck, and Specimens CFST 51 and CFST 42 from a second on a different day. A square piece of plywood was laid on top of each column after it had been filled with concrete. This plywood held connection bolts that were embedded halfway into the concrete core during curing and that were to be used to attach a top loading beam to the specimens. After pouring was completed, the top of the foundation was covered with a layer of plastic to ensure proper curing. The plastic as well as all plywood forms were removed after two days.

Concrete taken from each ready-mix batch received was poured into a total of eighteen plastic cylinders having diameter and height of 150 mm and 300 mm, respectively. These concrete cylinders were also covered in plastic for two days but were kept in their plastic forms until they were tested. This attempted to duplicate the environment that the concrete experienced inside the steel tube.

The concrete cylinders were tested inside a compression test machine with a loading rate varying between 1500 N/sec and 3000 N/sec. From the first mix, three cylinders were tested at each of seven day, fourteen day, and twenty-eight day. In addition, three cylinders were tested

the day that CFST 35 was tested; CFST 64 was tested on the twenty-eighth day so no additional cylinders were tested. From the second mix, three cylinders were tested each at twenty-eight day, CFST 42 test day, and CFST 51 test day. The three compressive concrete cylinder strengths were averaged to arrive at a concrete strength on day of testing of 37, 40, 35, and 35 MPa for CFST 64, CFST 35, CFST 41, and CFST 52, respectively. Table 3.4 lists the concrete compressive strength on the various other days tested.

3.3.2 Steel

The specimen was constructed by a reputable steel fabricator in Toronto, Ontario. Along with the specimens, 500 mm long sections of the same four circular tubes used for the specimens were also shipped to the University of Ottawa. Steel coupons were machined out of these sections. Four coupons were machined from each tube. The seam weld ran longitudinally in the centre of one coupon for each specimen. This allowed investigation into whether the strength and ductility at the welded section was different than for the rest of the tube. The steel for the column was specified Grade C A500 (F_y = 350 MPa), while the plates and channels were specified to be 300W steel. Figures 3.10, 3.11, 3.12, and 3.13 show the force versus strain diagrams for Specimens CFST 64, CFST 34, CFST 42, and CFST 51, respectively.

The measured yield strength of the steel tubes was 449, 415, 505, 405 MPa for CFST 64, CFST 35, CFST 42, and CFST 51, respectively. Note that the yield strength of Grade C A500 steel is specified as 350 MPa. The mill certificates that accompanied the steel stated the yield strength to be between 350 MPa and 366 MPa. The tested yield strength of the steel ranged from 1.16 to 1.44 times stronger than ordered. The designer of hollow circular sections must be aware of this overstrength to effectively design structures that utilize the ductility of these sections. The measured yield strength, maximum strength, and fracture strength are listed in Table 3.5 along with their respective corresponding strain reading.

It is suggested by the Canadian Institute of Steel Construction that ASTM A500 steel not be substituted for the Grade 350W steel that is supplied by Canadian mills when ordering hollow

steel sections. This recommendation is made because the requirements on the steel thickness of the steel in the ASTM A500 are less stringent than the requirements on the Grade 350W steel. It was found that the steel tube thickness could be as much as 10% smaller than the specifications imply. The diameters of the four steel tubes that were used in this study were the exact size ordered. However, the steel tube thicknesses were indeed smaller than expected. The measured steel thickness for the test tubes was 5.5 mm, 7.5 mm, 9.5 mm, and 5.5 mm for CFST 64, CFST 34, CFST 42, and CFST 51. These actual steel thicknesses were in the order of 15%, 27%, 0%, and 15% smaller than the specified values of the steel tubes for CFST 64, CFST 34, CFST 42, and CFST 51.

The dimensions of the steel coupon are shown in Figure 3.14. The steel tube and the additional 508 mm tube section visually appeared to be longitudinally straight. However, when the steel coupons were machined from the steel tube section, an out-of-plane curvature was seen in the steel coupons. For the coupon with the weld down the length and a coupon without the weld, the arc length was 508 mm for each and the height at the mid-point of the coupon was 9.5 mm and 7 mm, respectively. This curvature is a result of coil memory. The hollow steel section is made out of the coiled sheet but rolled with a 90° direction change. Therefore, when the steel sheet is released, as in the case for cutting the coupons, the steel is free to revert back to its original rolled steel sheet shape.

3.4 Test Set-up

Tests were performed at the University of Ottawa Structures Laboratory. The laboratory floor is a 914 mm (3 ft) deep reinforced concrete slab. Holes of 75 mm (3 in) diameter run the entire depth of the floor and are spaced at 914 mm (3 ft) in both directions. Three independent hydraulic MTS actuators were used for loading each specimen, two for the vertical load and one for the horizontal load. The actuators were equipped with a swivel head on either end. The foundation was attached to the laboratory strong floor using four high strength bolts with diameter and length of 64 and 1800 mm, respectively. Figure 3.15 illustrates the front view from

the east side of the test assembly showing the vertical actuators, loading beam, spacers and the specimen and Figure 3.16 is a picture of the stet-up with the same view.

To permit testing of a column having a height of 2200 mm, the vertical load actuators were placed on top of the foundation. Four bolts running through the swivel head on the bottom of each actuator and through the entire foundation were needed to attach the vertical actuators to the foundation. To tighten the bolts under the foundation and to allow the foundation to sit flat on the floor, a recessed groove with a height and width of 38.1 mm and 850 mm, respectively, was formed out of the foundation running perpendicular to the channels and in the middle of the foundation. Once the bolts were tightened under the foundation, the vertical actuators were placed vertically over the bolts and the nuts tightened on the bottom swivel heads of the actuators.

A horizontal loading beam was used to transfer the vertical axial load from the actuators to the column. The loading beam was a square HSS section made by welding four plates together. Four holes at each end of the square beam were used to attach the loading beam to the vertical actuators. Eight additional holes were made in the middle of the beam to connect the loading beam to the column specimens. The loading beam is orientated north to south.

Two existing spacers were used to connect the loading beam to the column as shown in Figure 3.15. The first spacer was needed to allow the vertical actuators to fit between the loading beam assembly and the foundation. This spacer consisted of a 450 mm reinforced concrete cube. Eight plastic tubes were cast vertically inside to allow eight bolts to be slipped through the concrete spacer and tightened inside the loading beam and at the other end, the second spacer. This second spacer is an I-section with a height of 610 mm with is situated between the first spacer and the column. The web is oriented in the north and south direction. The top flange has eight holes that are spaced similarly to the holes in the first spacer. This allowed eight bolts to be run through the first spacer and tighten to, on one end, the loading beam, and on the other end, the I-section spacer. Two vertical plates were welded on each of the north and south sides of the

web to prevent buckling of the I-section. An additional vertical plate was welded in the middle of the two plates on the east for additional stiffness. The bottom flange also has eight bolt holes to attach the I-section to the column.

Eight bolts with a diameter and length of 19 and 305 mm respectively, were embedded halfway into the concrete-fill at the top of the column, with the threads visible. The loading beam and spacers were placed on top of these bolts and tightened into place. The vertical actuators were extended until they were in contact with the loading beam and attached to the ends of the loading beam by four bolts. The swivel head of the horizontal actuator was then bolted to the web on the west side of the I-section spacer. The other end of the actuator was attached to a reaction frame that consisted of a I-section column braced by rectangular HSS. This reaction frame was designed to resist the entire 1000 kN compression and tension capacity of the horizontal actuator. Figure 3.17 illustrates the side view of the reaction frame with the actuators and column.

For safety reasons and ease of assembly, three additional steel frames were used in the set-up. The first frame is located between the reaction frame and the specimen and shown in Figure 3.18. The 2950 mm high frame was attached to the strong floor with two bolts. It was mainly intended to provide an emergency support to protect the horizontal actuator if it accidentally fell due to collapse of the specimen. This emergency support also proved useful during the erection and dismantling of the test set-up necessary to test each specimen by making it possible to rest the horizontal actuator on a 4 x 4 piece of wood placed on top of that frame. The other two frames were situated on the north and south sides of the specimen and were bolted to the strong floor with two bolts, as shown in Figure 3.19. The specimens fit snugly between these two frames and the vertical actuators were tied to the frames during set-up and dismantling. During testing, the frames served as a protection against out-of-plane failure of the column. If this failure occurred, the actuators would be prevented from falling in the out-of-plane direction and the test could be safely stopped.

3.5 Instrumentation

3.5.1 Location of strain gauges

Thirty-six strain gauges were installed on all specimens. There were two different brands of strain gauges used in this study; EP-08-250BG-120 from Micro-Measurements Division and FAE-25-12-S6L from BLH Electronics, Inc. The locations of the thirty-six strain gauges are presented in Figure 3.20 and in Table 3.6 and 3.7. Here, the notation SG # is used, where SG means Strain Gauge and # is the corresponding number that can be found in the figure or tables previously defined.

The strain gauges on the channels were used to calculate the flexural moment in the channels. The results can then be compared to the values expected based on the assumptions used for the design of the foundation to determine if the forces and moments behaved as predicted. SG 1,2 and SG 7,8 should have results of similar magnitude as they are located at the same position but on the east and west sides respectively. SG 3,4 and SG 5,6 were positioned at the outside border of the panel zone in an attempt to measure the maximum moment resisted by the channels.

Strain gauges SG 9 and SG 12 were positioned on the bottom plate at the location of the largest predicted moment where the steel tube is in tension and is pulling the bottom plate upwards. The strain gauges on the top and bottom of the top plate, SG 11,15 and SG 14,16 were positioned to capture the shear force and moment transferred from the steel tube to the top plate at this location.

Strain gauges on the steel tube were positioned at various locations to investigate its behaviour. SG 10 and SG 13 were positioned at the bottom of the tube to record the amount of strain left in the steel tube after transfer had occurred through the concrete, the top plate, and the channels. SG 21-23 and SG 24-26 were attached to the steel tube inside the concrete foundation. These strain gauges were to determine whether the top of the concrete foundation acts as a fixed base or whether the maximum moment occurs somewhere else along the steel tube in the

foundation. The strain gauges were equally spaced between the top of the concrete foundation and the top steel plate. The strain gauges that were located above the concrete on the steel tube, SG 31-33 and SG 34-36, were positioned to determine the strain diagram for the lower portion of the column above the concrete foundation.

In addition to the longitudinal strain gauges on the steel tube, the steel tube was instrumented with eight transverse strain gauges. Four strain gauges, SG 17-20 were positioned on each of the four sides of the column immediately above the top plate. These strain gauges would indicate if the tube shrunk or expanded transversely inside the concrete foundation. The last four strain gauges, SG 27-29 were positioned immediately above the concrete foundation and were positioned to capture transverse expansion or contraction of the steel tube at the base.

3.5.2 Location of LVDTs

Four Low Voltage Displacement Transducers (LVDT) were used for all tests. Figure 3.21 shows the location of the four LVDT in relation to a test specimen. LVDT 1 measured the horizontal displacement at the base of the reaction frame. LVDT 2 measured the displacement of the foundation in the east-west direction (direction of horizontal loading). LVDT 3 measured the displacement of the concrete-filled steel tube immediately above the concrete foundation surface. It was discovered after the 1st test on CFST 64, that the middle of the local buckle occurred approximately 25 mm above this foundation surface. Therefore, to capture the magnitude of local buckling this LVDT was moved up to that position for all subsequent tests. LVDT 4 measured the column displacement at mid-height.

3.5.3 Location of Temposonic LVDTs

Figure 3.22 shows the location of the three temposonics Linear Variable Differential Transformer (LVDT) used for the tests. Temposonic LVDT 1 measured the column displacement at the horizontal actuator, 2200 mm above the concrete foundation. This temposonic LVDT was also used as the basis for reporting column displacements during the test. Temposonic LVDTs 2 and 3 measured the tip of the column displacement, approximately

1895 mm above the concrete foundation, on the north and south side of the column, respectively. This arrangement also made it possible to check that the column was not subjected to torsion during testing.

4.0.0 EXPERIMENTAL OBSERVATIONS

This chapter describes the four experiments performed in this study in the order they were tested. During each test, the behaviour of the specimen was recorded. Observations made during each test are discussed and force versus deflection diagrams are presented.

Here, a positive force or displacement corresponds to an extension of the horizontal actuator and the specimen is pushed towards the east. A negative force or displacement corresponds to retraction of the horizontal actuator and the specimens is pulled in the westward direction. During testing, two computer screens were available for monitoring the data. On the first screen, the horizontal actuator force was plotted against displacement at top of the column, as measured by Temposonic LVDT 1. The second screen numerically displayed the instantaneous strain gauge readings. Note that a grid was painted on each column for reference during the test to visually facilitate observation of local buckling. Each square in the grid for columns having diameter of 406 mm and 323.9 mm had a height and width of 50 mm and 45 mm, respectively.

4.1 Loading

In all tests, the axial load was first applied to the column. It was applied slowly and then held constant for the remaining duration of the test for each of the experiments. The vertical loads applied by each actuator was 960 kN for tests CFST 34 and CFST 42, and 800 kN for CFST 51. As for CFST 64, the south actuator was loaded with 487 kN and the north actuator was loaded with 513 kN. This is because during pouring of the concrete inside the steel tube, the temporary plywood spacer designed to keep the anchor bolts in proper position at the top of the pier was accidently bumped and displaced 4.7 mm towards the West and 15.3 mm towards the South. As a result, these connection bolts were no longer centered in the middle of the column. Analysis of the consequences of this small construction error, considering the unintended added torsion and flexure showed that adjusting the vertical axial applied forces with different load levels to counteract the effect of the misaligned bolts would provide an adequate solution to correct this problem.

After application of the axial load on each specimen, the procedure of the Applied Technology Council on "Guidelines for Cyclic Seismic Testing of Components of Steel Structures-ATC-24" (ATC 1992) was followed for all tests. In this procedure, the horizontal load is increased until a prescribed displacement at the height of the horizontal actuator is reached, then the load is reversed until the prescribed negative displacement is reached. This displacement is a function of the yield point, δ_y, of the column. The ATC 24 prescribed displacement history for the test is as follows:

1. 3 Cycles of loading at $0.25\ \delta_y \le \delta \le 0.5\ \delta_y$
2. 3 Cycles of loading at $0.6\ \delta_y \le \delta \le 0.8\ \delta_y$
3. 3 Cycles of loading at $\delta = \delta_y$
4. 3 Cycles of loading at $\delta = 2\delta_y$
5. 3 Cycles of loading at $\delta = 3\delta_y$
6. 3 Cycles of loading at $\delta = 4\delta_y$
7. 2 Cycles of loading at $\delta = 5\delta_y$
8. Testing shall be continued with 2 cycles of loading at δ equal to each of $5\delta_y$, $6\delta_y$, $7\delta_y$, etc.

Figure 4.1 illustrates the corresponding loading sequence followed here for each test.

The difficulty in this procedure lies in defining the yield strength of the composite column before testing has begun. A force-deflection diagram was calculated before each test using the program outlined in Appendix A to theoretically determine the yield deflection. However, during testing it became clear that the program overestimated the stiffness of the specimen, producing too small of a calculated yield displacement. Hence, another method had to be chosen to determine the yield displacement as testing proceeded. This was done with guidance by the ATC-24 document, which defines the yield force as the point when significant yielding has occurred. Therefore, an effective yield displacement was found by observing the force-displacement curve as the test was progressing, and determining when significant departure from elastic response started to occur. A visual estimate of the point at which a bilinear force displacement relationship would provide hysteretic energy equivalent to the extrapolated experimental one (based on

smooth projection of acquired results) was deemed adequate to define this point as the yield displacment. However, because the first method used underestimated the yield displacement, the specimen was cycled at three amplitudes of deformation before reaching the yield displacement instead of the ATC-24 recommended two. Since the specimen was still in the elastic range during the extra first three cycles, the additional cyclic loading was not deemed to be detrimental to the specimen.

For all tests, significant departure from the elastic curve occurred at approximately 1% drift. Therefore, the yield deformation was taken as 1% drift and the tests were continued using drift as the prescribed deformation instead of yield displacement. The length of the piston in the horizontal actuator restricted the tests to a maximum of 8% drift. Therefore, with one exception, whenever a specimen had not failed after two cycles at 7% drift, cycling was continued at 7% drift until failure occurred. The test was completed when fracture of the steel tube occurred.

4.2 CFST 64

Specimen CFST 64 has a diameter of 406.4 mm, a measured steel thickness of 5.5 mm, and a nominal steel thickness of 6.35 mm. The compressive concrete strength on the day of the test was 37 MPa and the steel strength of the hollow steel tube was 459 MPa. Figure 4.2 shows the experimental base moment versus drift graph.

During testing, no evidence of yielding or damage could be seen until the third positive cycle at $0.75\delta_y$ when slight cracking due to separation on the tension side at the interface of the steel tube and concrete foundation could be observed (Figure 4.3). During this cycle, the strain gauges on the steel tube had not reached yield, and the force-deflection plot still appeared to be a straight line. Deformation was increased to 22 mm, corresponding to 1% drift, for the next three cycles. Many of the strain gauges on the steel tube, both in and above the foundation, had reached yield in both tension and compression. The force-deflection curve had begun to deviate from the straight elastic line, and supported by information from the strain gauges, it was determined that the yield point had been reached.

Slight buckling on the east side of the column was observed during the second cycle at 2% drift. On the reverse, slight buckling was also seen on the west side but it was not as significant as the east side buckle. During the 1st cycles at 3% drift, it can be seen in Figures 4.4a and 4.4b that the buckle on the east side is more pronounced than on the west side. A maximum applied horizontal force of 164 kN was reached during the cycle at 3% drift. The buckle grew on the east side and did not completely straighten out during the negative cycle at 3% drift. Pinching in the hysteretic curve was visible starting at the second cycle of 3% drift. From then onward, the buckles on both sides of the column continued to grow with the steel remaining ductile in all subsequent cycles (Figures 4.5a, 4.5b, 4.6a, 4.6b, 4.7a, 4.7b, 4.8a, 4.8b) until the first cycle at 7% drift when a large gap opened between the column and the foundation at the west side. During the negative cycle, necking started to develop through the thickness of the steel shell and cracking was observed on the east side. The crack appeared to have penetrated through the tube. A drop in strength was visible in the force-deflection curve during the second positive cycle at 7% drift. Pulverized concrete spilled out through the crack in the buckle as it opened wider. After testing stopped, the crack on the upper portion of the buckle on the west side was measured to have a length of 47 mm and a width of 3 mm while the crack on the lower portion of the buckle had a length of 195 mm and a width of 22 mm. A side view of the failure surface for the east and west sides are shown in Figures 4.9a and 4.9b, respectively and the front view of the failure surface for the east and west sides are shown in Figures 4.10a and 4.10b. A global view of 7% drift is shown in Figure 4.11.

4.3 CFST 34

The CFST 34 specimen has a steel tube diameter of 323.9 mm, a measured thickness of 7.5 mm and a nominal thickness of 9.53 mm. The concrete strength the day of the test was 40 MPa, and the strength of the steel tube was 415 MPa. The experimental base moment versus drift graph obtained during testing is shown in Figure 4.12.

Behaviour remained essentially elastic until the third prescribed set of three loading cycles ($0.75\ \delta_y$), when some strain gauges indicated strains just below the yield strain. Deviation of the

force-displacement relationship from the elastic line also began to be noticeable. At a displacement of 22 mm, strain gauges started to indicate values greater than the yield strain, and there was deviation of the force-displacement curve from the elastic line. Using the criterion described in Section 4.1, it was decided to define the effective δ_y at 1% drift. Small longitudinal cracks in the paint were visible on the south east side from the base of the concrete foundation to the middle of the second grid line during the 2nd positive cycle at 1.0% drift. A very small buckle became visible on the west and east side of the column during the 2nd cycle at 3% drift for positive and negative forces, respectively (Figures 4.13a and 4.13b). A maximum load of 190 kN was reached at a deflection of 3% drift and the specimen continued to resist this load until the first cycle at 7% drift. Both buckles continued to grow during 4% drift as seen in Figure 4.14a and 4.14b for the east and west side, respectively. During the 1st negative cycle at 4% drift, the east buckle did not straighten out completely and the west buckle did not straighten out completely during the 2nd positive cycle at 4% drift.

During cycling at 5% and 6% drift, the buckles continued to grow. At 7% drift, the buckle around the column had become quite significant (Figure 4.15). After the second cycle had been completed at 7% drift and no cracking was observed, it was decided to attempt cycles at 8% drift. Unfortunately, readings from Temposonic LVDT 1 were lost while loading to negative 8% drift (the point of maximum retraction of the horizontal actuator). During loading at 6% and 7% drift, a deficiency in the experimental set-up prevented the smooth movement of the Temposonic LVDT 1 guide bar through its circular magnet. This added friction resulted in jaggedness in the shape of the force-deflection diagram of those drifts (Figure 4.12), and contributed to the loss of reliable readings from the temposonic LVDT. Upon discovery of this problem, the test was stopped, the horizontal actuator was returned to its zero starting position and the vertical actuators were unloaded. The strain gauges on the east and west side just above the foundation were removed to ascertain damage to the column. Longitudinal cracks on both the east and the west side were found approximately 2 mm up the column from the top of the concrete foundation and were estimated to be approximately 1 mm deep.

The test was restarted by loading each of the vertical actuators with 960 kN of force. Cyclic horizontal displacements were applied anew at 7% drift. During the 2nd positive cycle, miniature transverse cracks were visible on the east side. At the 2nd negative cycle, buckling had increased on both the east and west side. The transverse cracks on the east side joined together and the buckle on the west side pointed down instead of perpendicular to the column. Failure on the west side occurred when a large crack developed in the buckle and penetrated the steel during the 3rd positive cycle. The 25 mm crack opened up on the top of the first grid line, to a crack width of 3 mm (Figure 4.16b). Failure on the east side occurred during the 3rd negative cycle when a transverse crack on the bottom of the buckle penetrated the steel tube (Figure 4.16a). The 140 mm long crack had a height of 9 mm. The horizontal and vertical actuators were brought back to their respective starting positions and the vertical actuators were unloaded. Upon final inspection, a smaller crack was observed above the buckle on the east side after unloading. A global view of 7% drift is shown in Figure 4.17.

4.4 CFST 42

The CFST 42 specimen has a steel diameter of 406.4 mm, a measured steel thickness of 9.5 mm and a nominal steel thickness of 9.53 mm. The concrete strength on the day of testing was 35 MPa, and the steel coupon strength was 505 MPa. The experimentally obtained base moment versus drift diagram is shown in Figure 4.18. The Temposonic LVDT measuring the tip displacement did not record the positive drift greater than 3% correctly, due to unexpected friction. Results from other Temposonic LVDTs and the negative displacements were used to interpolate the positive drift values on Figure 4.18. This column had the largest predicted moment resistance.

As for the previous tests, significant yielding had not occurred when first departure from the elastic line of the force-displacement curve was observed at 15 mm (0.75 δ_y). Yielding in some strain gauges on the steel tube and departure from the elastic line occurred at 22 mm drifts, and, at this displacement, the deflection was deemed to be equal to δ_y, which also coincided with 1% drift. During the third negative cycle at 1% drift, a small opening on the foundation against

the east side of the column was found (Figure 4.19). A very slight buckle was seen on the east side between the first and second grid line during the 1st positive cycle at 2% drift (Figure 4.20). During the 2nd negative cycle at 2% drift, a slight decrease in strength was noticed in the force versus deflection diagram. However, no buckling could be seen. During the 3rd cycle at 2% drift, the gap between the column and the concrete foundation widened.

A maximum horizontal force of 400 kN was reached while cycling at 3% drift, and the specimen was able to resist this load until the end of cycling at 5% drift. The buckle on the east side had become more pronounced at 3% drift; it started at the third grid line and ended at the top of the concrete foundation (Figure 4.21a). It appeared to be at a maximum where the LVDT was situated. During the 3rd negative cycle at 3% drift, the buckle was visible on the west side (Figure 4.21b). The gap between the column and the foundation was measured to be 2 mm wide and grew during cycling at 4% drift. The buckles on both sides of the column continued to grow during 4% drift (Figures 4.22a and 4.22b). The west side buckle did not straighten out during the 1st cycle at 5% drift. At the end of cycling at 5% drift, no visible cracks were visible near either buckle. The column, however, appeared to be leaning slightly to the north, but there was no evidence of twisting. The buckle had grown to encompass the entire diameter of the column but appeared to be more pronounced on the north than on the south side (Figure 4.23).

During cycling at 6% drift, no cracks could be seen but the buckles on both sides had grown (Figure 4.24a and 4.24b). During the 2nd cycle at 7% drift, small hairline cracks on the west and east side could be seen. Cracking developed around the buckle and necking of the steel shell was observed during the 4th negative cycle on the west side. On the reverse cycle, the cracks began to join and necking occurred in the middle of the east side buckle (Figures 4.25a and 4.25b for east and west side, respectively). A bang was heard as the crack in the middle of the west buckle suddenly propagated to a length of 260 mm and fractured the steel shell. The load dropped to 60 kN at the 6th positive cycle. At the 6th negative cycle, another bang occurred and the crack in the middle of the east side buckle similarly propagated to a length of 233 mm and fractured the steel. The horizontal actuator was returned to its zero position and the vertical

actuators were unloaded. Cracks on the bottom of the buckle on both the west and east side had not penetrated the steel (Figure 4.26a and 4.26b). A global view of 7% drift is shown in Figure 4.27.

4.5 CFST 51

The CFST 51 specimen has a steel diameter of 323.9 mm, a measured thickness of 5.5 mm and a nominal thickness of 6.35 mm. The concrete strength on the day of testing was 35 MPa, and the steel coupon strength was 405 MPa. The experimentally obtained base moment versus drift diagram is shown in Figure 4.28.

Contrary to the previous tests, after the 3rd negative cycle at 0.75% drift, a very slight buckle was seen on the west side of the column. However, there was still no deviation of the force-displacement curve from the elastic straight line at this time, and no strain gauges on the steel tube indicated yielding. Therefore, the specimen was deemed to still be below the effective yield displacement. Similar to the previously tested specimens, observed data supported the effective yield displacement at 22 mm, corresponding to 1% drift. A small opening was visible on both the east and west side of the column between the steel tube and the concrete foundation during the 3rd cycle at 1% drift. A slight buckle began to develop on the east side during the 1st cycle to 2% drift (Figure 4.29). Pinching of the force-displacement curve during the 2nd negative cycle at 2% drift suggested that buckling was occurring somewhere in the steel tube. Upon closer examination the buckle on the west side was visible. Further cycling at 2% drift produced a larger gap at the steel tube and concrete foundation interface.

A maximum applied horizontal force of 155 kN was reached during cycling at 3% drift. The east side buckle became more significant by the 1st cycle to 3% drift (Figure 4.30a) and continued to grow during cycling at 3% drift, however, the buckle on the west side was smaller in comparison to the buckle on the east side (Figure 4.30b). The buckle on the east side completely straightened out upon load reversal until the 2nd negative cycle at 4% drift while the buckle on the west side fully straightened out upon such reversal until the 1st positive cycle to 5% drift. During

cycling at 4% and 5% drift, the buckles on both sides grew (Figures 4.31a, 4.31b, 4.32a, and 4.32b) and the buckle became visible around the entire circumference. However, no cracks were seen. The column leaned to the south slightly, and the buckle on the south side was typically larger than on the north side.

Vertical cracks became visible on top of the buckle on the west side during the 1st negative cycle at 6% drift (Figure 4.33a). After reversing the load, vertical cracks were seen on the north east side of the buckle and the vertical cracks on the west side had completely closed up. The buckle on the south west side began to droop and point down (Figure 4.33b). During the 1st cycle at 7% drift, the buckle on the east side also began to droop and point down instead of developing perpendicular to the column. The negative cycle produced horizontal cracks on the bottom and top of the buckle on the east side. During the next cycle, the horizontal and vertical cracks began to penetrate the thickness of the steel shell. The vertical cracks had completely opened up on the east side during the 4th positive cycle. Also on the east side, a transverse crack was noticed in the middle of the buckle, while necking had started on the buckle on the west side. After the next load reversal, the 4th negative cycle of 7% drift, a bang was heard and a through thickness fracture occurred in the middle of the buckle on the east side (Figure 4.34a). The length of the crack was 220 mm and its width was 20 mm. The vertical cracks had penetrated through the thickness of the steel and necking became severe on the west side (Figure 4.34b). Another loud bang was heard during the 5th positive cycle at 7% drift when fracture occurred along the center of the buckle on the west side. The crack length was 160 mm and the width was 13 mm. On the east side, two vertical cracks had completely penetrated the steel (Figure 4.35). The test was stopped at this point. A global view of 7% drift is shown in Figure 4.36.

4.6 Bond

Bond was also examined as part of the experimental study. As stated in Section 2.7.3.1, the existence of bond between the concrete core and the steel tube is under discussion by researchers. Although not a primary objective in this study, observations were made on the remaining bond of a concrete-filled column after failure.

To dispose of the specimens, one cut was made below the buckle on the steel tube. The column was then lifted off of the foundation. The concrete at this location was very weak and offered no resistance when the column was removed. Upon closer examination of the foundation, the concrete remaining in the steel tube was pulverized at the interface but quite cohesive and intact just below the foundation. This suggests that only the concrete behind the buckle experienced crushing while the remaining concrete core, above and below the buckle did not crush or fail.

An investigation into the bond remaining in the specimens was conducted on Specimen 51 before it was disposed. A circumferential cut was made, approximately 560 mm above the foundation. The bottom cut was made above the buckle, approximately 90 mm above the foundation. A vertical cut was made between these two horizontal lines. The column was then lifted off of the foundation. While still being supported, the column stood vertically on the ground. The column was tapped twice and the cut section fall off of the concrete core. The steel tube section is shown in Figure 4.37, and the remaining column is shown in Figure 4.38. The origin of the crack in the concrete core is not known, however, it is suspected that it was caused by the removal of the steel tube section. There were no signs of concrete cohesion on the steel tube. No concrete residue was left on the steel tube and the concrete core looks smooth. However, there was some white dust on the inside of the steel tube verifying that no significant concrete shrinkage occurred. The full bond strength was not retained at the end of testing for this column. This investigation was very limited and only looked at the bond after complete failure of both the steel and concrete.

5.0.0 ANALYSIS OF TESTED SPECIMENS BEHAVIOURS

In this section, the results obtained from the four tested specimens are evaluated. The behaviour of a concrete-filled steel tube is analyzed using two different sets of data recorded during the test: first, the displacement readings, and second, the strain gauge readings.

5.1 Shape of the Deflection of the Specimens

The deflections recorded during the test are examined below to determine if the column deflection was in the characteristic shape of a cantilevered column with a length corresponding to the effective height of the column.

The column deflections were measured at four different locations during the test. Figures 3.21 and 3.22 show the placement of the LVDTs and the temposonic LVDTs. LVDT's measured displacements between the column and the concrete foundation interface and at the mid-height of the column. At the top of the steel tube, results from the two temposonic LVDTs located on either side (Temposonic LVDT 2 and 3 on Figure 3.22) were averaged to give the column displacement at 1865 mm above the concrete foundation. The fourth column deflection point came from Temposonic LVDT 4, situated at the applied horizontal force height, corresponding to the total effective height of the column, 2200 mm above the concrete foundation.

The columns remained elastic until 1% drift during testing. Therefore, four column displacements for each specimen were plotted at each of 0.28% drift, 0.45% drift, 0.68% drift and 1% drift. The deflection of a cantilevered column caused by flexure is given in Equation 5.1,

$$\Delta_x = \frac{P}{6EI}(2L^3 - 3L^2x + x^3) \tag{5.1}$$

where Δ_x is the displacement at any distance x from the free end of the column, P is the horizontally applied load, L is the total length of the column, and EI is the stiffness of the column. The effective stiffness modulus, EI, for the composite column was calculated as the sum of the

individual stiffness from the steel tube and the concrete core. Since the deflection due to shear distortion amounts to less than 0.5% of the tip deflection due to flexure, this contribution is neglected in the deflection calculations. The experimentally obtained force at each drift level was used in Equation 5.1 to calculate the theoretical deflection. A line was drawn for each of the four drift levels as seen in Figures 5.1 to 5.4. This line significantly underestimates the actual deflection of the specimen for all but the deflection at 0.28% drift.

The difference between the experimental and analytical results indicates that Equation 5.1 does not fully predict the behaviour of the tested columns. A number of different approaches were used to duplicate the experimental results. The two solutions that produced the closest match of theoretical results to experimental data are discussed here. The first solution was to change the stiffness of the column to match the experimental tip deflection for each drift level. This curve matched the tested deflection points better than the original equation results but still did not produce an acceptable correlation.

The second approach was to replace the length, L, effective length, by $L+h$ were h is an additional length of column. The deflection curves corresponding to this approach are shown in Figures 5.5 to 5.8. In practical terms, this is equivalent to having a fixity point located in the concrete foundation and not at the top of the foundation. For Specimens CFST 64, CFST 34, and CFST 42, this approach provides a very good match to the data. The deflection of Specimen CFST 51 is matched particularly well except for the LVDT located at the column mid-height. The height of that LVDT was accurately measured prior to the test but, there is always a possibility that its location was incorrectly recorded. Figure 5.8 shows that if the location of that instrument was only 50 mm higher than measured, the match would be very good. It is noteworthy that as more horizontal load was applied, the fixity point moved further into the concrete foundation. To match the top displacement point, at 1% drift, the fixity point was calculated to be located in the foundation at a depth of 530 mm, 350 mm, 450 mm, and 310 mm for Specimens CFST 64, CFST 34, CFST 42, and CFST 51, respectively. The distance from the surface of the concrete foundation to the top of the top plate on the channels was only 300 mm.

This implies that, for all specimens at 1% drift, the steel foundation may have rotated as it reacted to the moments imposed.

Because Equation 5.1 is a purely linear elastic deflection equation, only the elastic portions of the test (0.28% to 1.0% drift) were analyzed. However, there may be partial plastification at 0.68% and 1.0% drift which could account for some of the discrepancies noted at these drifts. However, it remains true that results show there is not full fixity at $h = 0$.

5.2 Behaviour Recorded by Strain Gauges

The steel tubes and steel members in the foundation were instrumented with strain gauges for all four tests. Information on strain gauge locations can be found in Figure 3.20, in Tables 3.6 and 3.7, and Section 3.5.1. In the following paragraphs the measured strains are used to describe the specimen behaviour. In all cases, a positive strain corresponds to a tensile strain and a positive force corresponds to a push in the east direction as shown on the strain gauge positioning figures. Note that some of the strain gauges in the concrete foundation failed relatively early and collected rather limited data.

The figures in this section illustrate the strain envelope for the strain gauges, not the actual path. This means that only the largest strains reached at each yield cycle is plotted. When two or more cycles were applied at the same load level, the values at the end of each cycle was plotted, which explains why the curves on the following figures are jagged.

5.2.1 Behaviour of Channels

As shown on the sketch in Figure 5.9, the strain gauges on the channels were located taking into account symmetry and redundancy. Redundancy was obtained through the strain gauges in the middle of the channels, on the north channel (SG 3 and SG 4) and at the same location on the south channel (SG 5 and SG 6). Further using symmetry, the strain gauges on the west end of the north channel (SG 1 and SG 2) can be compared to the strain gauges on the east end of the north channel (SG 7 and SG 8) upon reversed loading of equal magnitude.

The moment at the base of the columns is transferred through the channels and resisted by the supports on both ends of the foundation. In the channels, these forces produce a constant shear force over the entire member and a maximum moment in the middle that decreases to zero at the ends.

Following this load path, the strains from gauges SG 1, SG 2, SG 7, and SG 8, located at the ends of the channels, were expected to be small because they were placed near the reaction points where the moment was expected to be close to zero. The strain gauges in the middle of the channels, SG 3 to SG 6, were located to permit calculation of the moment in the channels. To ensure that the strain gauges were not reading strains influenced by the panel zone, these gauges were placed at a distance of one radius of the steel tube away from the center line of the column.

The results from the strain gauges produced different results than were initially anticipated. The resistance moments in the channels were far smaller than anticipated. The strain gauges in the center of the channels did experience more strain than the gauges at the ends of the channels but the difference was small. The resistance moment in the channels never exceeded 17 kN-m (ie. 6% of the channels' plastic moment). In general, the strain gauges recorded strains of the same sign irrespectively of the direction of applied lateral load on the specimen. The small amount of strains in the concrete foundation suggests that the concrete in the foundation dissipated the stresses without a need for the channels. The information from the strain gauges are summarized in more detail in the following paragraphs. In all cases, reading accuracy is coarse due to the small strain magnitude compared to the resolution of the gauge readings of $\pm 20*10^{-6}$.

Figure 5.10 shows the strain gauges on CFST 64 in the middle of the channels. SG 3 and SG 5 record the same pattern except the north channel (SG 3) experiences larger strains, ($125*10^{-6}$ as compared to $90*10^{-6}$). The strain at both of these locations is in tension for both negative and positive force while zero force produces zero strain. The strains on the bottom of the north channel (SG 4), produce a cyclic pattern with a positive force producing a tensile strain. The

largest strains at this location are ±25 $*10^{-6}$. Figure 5.11 shows the strain gauges that recorded strains at the ends of the north channel. It appears that the strain gauge on the bottom of the north channel (SG 8) did not record strains during the test, while the strain gauge on the top of the north channel (SG 7) recorded positive strains for both a positive and negative force with a maximum strain of $300*10^{-6}$. For this specimen, the strain gauge on the east end of the north channel recorded larger strains than in the middle of the channel.

Figure 5.12 illustrates the strain gauge readings for the middle of the channels on CFST 34. Strain gauges SG 4 and 6 recorded the same behaviour, positive strain for positive force, except that the north channel (SG 4), experiences larger strain values, ranging from $70*10^{-6}$ to $-15*10^{-6}$ while the south channel (SG 6) recorded values from $45*10^{-6}$ to $0*10^{-6}$. The strains on the top of the south channel (SG 5) also follow the same pattern but the strains reach larger negative values than recorded at the bottom of the channels with maximum values of $20*10^{-6}$ and $-40*10^{-6}$. The strain gauges recording the strains on the ends of the channel are shown in Figure 5.13. The strains on the bottom of the north channel follow an opposite pattern for the west end (SG 2) and the east end (SG 8). A positive force produces a compressive strain on the east end and a tensile strain on the west end. Values range from $15*10^{-6}$ to $-25*10^{-6}$ for both locations. Strains on the top of the east end (SG 7) are in tension for both a positive and negative force with a maximum value of $40*10^{-6}$.

Figure 5.14 illustrates the strain readings for the middle of the channels on CFST 42. The strains on the top of the north channel (SG 3) are in tension for both positive and negative force with a maximum strain of $150*10^{-6}$. The corresponding strains on the bottom of the north channel (SG 4) are in compression for positive force and in tension for negative force. A second acquisition system was used for the ends of the north channels on CFST 42 and for the middle of the south channel. The bottom of the south channel (SG 6) recorded compressive strains for both positive and negative forces. The top of the south channel (SG 5) does not appear to have recorded conclusive data due to the degree of accuracy in the secondary data acquistion system. Figure 5.15 shows the strain gauge readings for the ends of the north channel of CFST 42. The

strain gauge on the top of the west end of the north channel (SG1) recorded tensile strains for both positive and negative forces with a maximum strain of $110*10^{-6}$. The strain gauges on the bottom of the west end (SG 2) and the top of the east end (SG7) of the north channel recorded very small values and as with SG5, may not have recorded values above the gauge resolution.

Figure 5.16 shows the strain readings in the middle of the channels on CFST 51. The strains on the top (SG 3) and bottom (SG 4) of the north channel followed the same pattern as in CFST 42. The strain readings are smaller on this specimen in comparison with CFST 42, with maximum values of $70*10^{-6}$ and $20*10^{-6}$ to $-30*10^{-6}$ for SG 3 and 4, respectively. Figure 5.17 shows the strain readings for the west end of the north channel. The top (SG 1) and bottom (SG 2) of the north channel on the west end recorded negative strains for positive force and positive strains for negative force. The range of strain values are $-20*10^{-6}$ to $100*10^{-6}$ and $-200*10^{-6}$ to $800*10^{-6}$, respectively.

5.2.2 Behaviour of Top and Bottom Plates

A diagram of the strain gauge location and numbering for the plates and bottom of the steel tube is shown in Figure 5.18. Recall that when a positive force was applied to the specimen, the column was subjected to tension on the west side and compression on the east side. Consequently, the west side of the column pulls up on the bottom plate at the same time as the east side of the column pushes it. Elsewhere, as the tube elongates under tensile strains, the west side of the top plate lifts, resulting in flexural compression and tension on that plates's top and bottom respectively. Reversed flexural strains are expected on the east side of the top plate. This is concurrent with expected compressive strains on the west side and tensile strains on the east side due to possible lateral displacement of the tube.

The strain gauges on the bottom plates only worked for CFST 64 and CFST 34, Figures 5.19 and 5.20, respectively. Regardless of the horizontal force direction, the plate was always in compression. However, with a positive force, the strains were small on the east side and in maximum compression on the west side of the bottom plate.

The analysis of the top plates in the foundation suggested that if the fixity point was above the top plates then the only stresses in the column would be tension and compression. With a positive force, the east side of the column would be in compression, therefore squeezing downwards, and the west side of the column would be stretching upwards. As the column moved this way, the top plates would follow. Therefore, on the west plate, the top would be in compression and the bottom in tension with the east plate experiencing the opposite. All foundations reacted this way during the tests. There was no yielding in the plates during any of the tests and the maximum strain reached was 800$\mu\epsilon$. Figures 5.21, 5.22, 5.23, and 5.24 show the strains experienced on the top plate by CFST 64, CFST 34, CFST 42, and CFST 51, respectively.

5.2.3 Behaviour of Column Encased in Concrete Foundation

The foundation design assumed that full fixity was achieved near the top of the concrete foundation. If this was the case, the strains in the column within the concrete foundation would either: a) remain constant from the top of the concrete to the top plate and channels and decrease thereafter, or b) decrease as the distance within the concrete foundation increased.
Eight strain gauges were located on each column within the foundation; four on the east and four on the west side of the column. Three of the gauges on each side were spaced at 100 mm starting 50 mm from the top plate and up and the last gauge on either side was placed 40 mm above the bottom plate. The strain gauge numbering can be seen in Figure 5.18 and Figure 5.25.

Figure 5.26 shows the occurrence of tension yielding on the steel tubes for all specimens (gauges just above the bottom plate are not shown in Figure 5.26 as they all remained elastic and reached no more than $900*10^{-6}$ mm/mm). Tension yielding occurred in the strain gauges between 1% and 2% drift except for SG 26 on CFST 64 which yielded at approximately 0.45% drift but failed at 0.68% drift. No yielding due to compression was recorded, however strains reached values as high as 80% of yield strain in compression. Some of the gauges failed at approximately 2% drift, disallowing a more through analysis of the occurrence of yield in the steel tube in the

concrete foundation. Figures 5.27a, 5.28a, 5.29a, and 5.30a illustrate the strain along the steel tube on the east side, both within the concrete foundation and above, for columns CFST 64, CFST 34, CFST 42, and CFST 51, respectively. The west side is shown in Figures 5.27b, 5.28b, 5.29b, and 5.30b for columns CFST 64, CFST 34, CFST 42, CFST 51, respectively. The results from the strain gauges indicate that the strains decreases as the distance below the concrete surface increases for all four tests in both tension and compression. A more through examination of each specimen with respect to the longitudinal strain gauges encased in concrete follows.

On the east side of Specimen CFST 64, none of the strain gauges yielded (or survived until sufficiently large drifts to record yield). Figure 5.27a illustrates the decreasing strains as the distance from the top of the concrete foundation increased for both positive and negative force. On the west side of Specimen CFST 64, the strain gauge just below the concrete foundation (SG 26) recorded yielding during the 0.45% drift, however, this strain gauge failed during cycling at 0.68% drift. However, it can be seen in Figure 5.27b that this strain gauge recorded the largest strain values on the west side. The two strain gauges just above the top plate (SG 24 and SG 21) recorded the least amount of strain for both sides of the columns.

On the east side of Specimen CFST 34, the strain gauges recorded yielding just above the top plate (SG 21) at approximately 1% drift, in the middle of the foundation (SG 22) at approximately 2% drift, and no yielding was noted just below the top of the concrete foundation (SG 23). On the west side of Specimen CFST 34, the strain gauge in the middle of the foundation (SG 25) and just below the top of the concrete foundation (SG 26) recorded yield at approximately 2% drift. However, the strains are larger just below the top of the concrete foundation as seen in Figure 5.28b.

On the east side of the specimen, strain gauges recorded yield in the middle of the foundation (SG 22) at approximately 1% drift, and above the top plate (SG 21) at approximately 2% drift. The strain gauge recording data below the top of the concrete foundation (SG 23) failed during cycling at 1% drift. As the distance within the concrete foundation increases, the

strain readings decrease, as shown in Figure 5.29a. The strain gauge located just below the top of the concrete foundation (SG 26) was the only gauge to record information on the west side of Specimen CFST 42. This gauge failed during cycling at 1% drift and did not record yield before failure.

The only gauge to record yield on the east side of Specimen CFST 51 was located just below the top of the concrete foundation (SG 23) and yielding occurred at approximately 2%. On the west side, no yield was recorded in any gauge but the two gauges closest to the top of the concrete foundation failed during cycling at 1% drift. Figures 5.30a and 5.30b show the strains decreasing as the distance from the top of the concrete foundation increased for the east and west side, respectively.

It was originally considered that the strain gauges located at the bottom of the columns would record both tension and compression. However, all working strain gauges only recorded tension forces that increased as the test progressed and the gauges never yielded, all strains were less than $900*10^{-6}$ (45% of yield strain). At this position in the foundation, the concrete may be resisting all of the compression strains while the steel is resisting only the tensile strains.

The strain gauge readings on the east side can be seen in Figures 5.27a and 5.30a for columns CFST 64, and CFST 51, respectively and on the west side of the column, Figures 5.29b, and 5.30b for columns CFST 42, and CFST 51, respectively. None of the other strain gauges were working. It can be seen that the strain remaining in the column at the bottom is significantly lower than the strains recorded elsewhere in the column. The strain gauges on the west side experienced larger tensile strains for a positive horizontal force than for a negative force, while

the opposite was true for the east side. The larger tensile strain corresponds to the side of the column that is experiencing the tensile forces.

5.2.4 Behaviour of Column Transversely Encased in Concrete Foundation

It has been stated and experimentally proven that a concrete-filled steel tube will not buckle inward because the concrete core pushes the steel to buckle outward. However, inside the concrete foundation, there is concrete on both sides of the steel tube. Four strain gauges measured the transverse strains on the steel tube in the foundation. They were placed around the tube 23 mm above the top plate on the north, south, east, and west directions. Figure 5.31 illustrates the locations of the strain gages. No transverse yielding was recorded in any of the steel tubes, furthermore, strains did not exceed 40% of the yield strain.

The strains for Specimen CFST 64 are shown in Figure 5.32. The strains on the north (SG 18) and on the south (SG 20) sides are approximately equal but of opposite signs, always in tension and compression, respectively. In comparison, the strains on the east (SG 17) and the west (SG 19) sides follow a cyclic pattern with a positive force producing compressive strain and tensile strain, respectively. On both the east and west sides, as the number and magnitude of cycles increase, and after longitudinal yielding of the steel tube, the compressive strains progressively reduce, and eventually even become tensile strains.

The strains for Specimen CFST 34 can be seen in Figure 5.33. Both the north (SG 18) and the south (SG 20) sides produce strains that are in tension for both positive and negative forces with a maximum tensile strain of $200*10^{-6}$ and $230*10^{-6}$ for the north and south, respectively. The strains on the west side (SG 19) produce a cyclic pattern and are in compression under a positive force. This strain gauge recorded compressive strains as large as $300*10^{-6}$, and recorded tensile forces of $25*10^{-6}$. The strain gauge on the east side was not working during this test.

The strains for Specimen CFST 42 are shown in Figure 5.34. The strains on the east side (SG 17) are always in tension while the strains on the opposite side, the west side (SG 19) are always in compression. The strains on the north side (SG 18) are also always in tension but the

values are much smaller compared to the strains on the east side. The strains on the south side (SG 20) start in compression but by 1% drift have shifted to tension.

The strains for Specimen CFST 51 are shown in Figure 5.35. The strains on the west side (SG 19) are in tension for both positive and negative forces and reach a maximum strain of $450*10^{-6}$. The strains on the south side (SG 20) are cyclic and a positive force produces tensile strains. These strains are in the order of 8 times smaller than the strains on the west side. The strain gauges on the east and north sides were not working during this test.

5.2.5 Behaviour of Longitudinal Column above the Concrete Foundation

The portion of the steel tube above the foundation was instrumented with three strain gauges on both the east and west side. The gauges were placed 200 mm apart starting from 35 mm above the concrete foundation. Strain gauge locations are shown in Figure 5.25. As with any cantilever column, the moment (and the strain) should be greatest at the foundation and decrease linearly toward zero at the tip of the column. Gauges located at the concrete foundation (SG 31 and SG 34) should experience the largest strain values as this location corresponds to the plastic rotation point. Yielding of the steel tube occurred in both compression and tension between 1% and 2% drift. Figure 5.36 outlines the drift level that corresponded to the yield of each of the strain gauges.

On the east side of Specimen CFST 64, the strain gauges located at the foundation (SG 31) yielded at approximately 1% in compression and the two strain gauges located higher on the steel tube (SG 32 and SG 33) yielded at approximately 2% in compression. The strains at 200 mm and 400 mm above the foundation were of comparable values. In tension, the strains were greatest at 200 mm above the foundation (SG 32) and the steel yielded at approximately 1% drift. At 400 mm above the foundation (SG 33) and at the base of the foundation (SG 31), the strain gauges gave results of comparable magnitude until they yielded at approximately 2% drift. The strain readings can be seen in Figure 5.27a. On the west side, the strain gauges located on top of the foundation (SG 34) and at 200 mm above the foundation (SG 35) yielded at

approximately 1% drift in both tension and compression while the strain gauge located at 400 mm above the foundation yielded at approximately 2% in both tension and compression. Figure 5.27b shows the strain on the steel tube decreasing as the distance from the foundation increases.

For the remaining three specimens, all yielding occurred in compression at approximately 1% drift and in tension at approximately 2% drift. On the east and west sides of Specimen CFST 34, the compressive strains decreased as the height increased from the top of the concrete foundation. However, in tension, the gauge on top of the foundation on the west side (SG 34) did not yield in compression and the other gauges recorded values that were similar in magnitude for all other locations. The strain gauge readings can be seen in Figure 5.28a and 5.28b. The strain readings on Specimens CFST 42 and CFST 51 behaved more as expected, with decreasing strain as a function of height from the top of the foundation, these can be seen in Figures 5.29a, 5.29b, 5.30a, and 5.30b, respectively.

5.2.6 Behaviour of Column Transversely above the Concrete Foundation

As mentioned previously, a steel tube filled with concrete does not have the ability to buckle inwards because of the concrete-fill. Therefore, the failure mechanism of the steel tube is to buckle outwards. Strain gauges SG 27, SG 28, SG 29, and SG 30 are located on the east, north, west, and south faces of the columns, respectively, as seen in Figure 5.37. All four specimens developed a continuous buckle 50 mm above the concrete foundation. The strain gauges were located just below that buckle at 20 mm above the concrete foundation. Figures 5.38 to 5.41 represent the transverse strains recorded on Specimens CFST 64, CFST 34, CFST 42, and CFST 51, respectively. A more indepth look at each of the specimen follows.

In Specimen CFST 64, a positive force produces a tensile strain on the east side (SG 27), and a compressive strain on both the west and south sides (SG 29 and SG 30). The strain gauge on the north side was not working during this test. The strain on the east side (SG 27) exhibited a cyclic pattern under elastic loading, however, once the longitudinal strains reached yield, the

transverse strains on the east side remained in tension for both positive and negative forces. The strain on the west side (SG 29) was also cyclic but the strains remained in compression for all positive forces. The strain on the south side (SG 30) was in compression for both positive and negative force. Tensile yielding occurred on the west side (SG 29) at 2% and on the south side (SG 30) at 5% while no yielding occurred on the east side.

In Specimen CFST 34, positive and negative forces produced a tensile strain in all strain gauges. Tensile yielding occurred on the west side (SG 29) at 2%, the east side (SG 27) at 4%, and the north (SG 28) and south (SG 30) sides at 4% and 3%, respectively.

Specimen CFST 42 behaved similarly to Specimen CFST 34, with all strain gauges recording tensile forces. Tensile yielding occurred on the west side (SG 29) at 2%, the east side (SG 27) at 3%, and the north (SG 28) and south (SG 30) sides at 5% and 6%, respectively.

In Specimen CFST 51, a positive force produced tensile strains on the east side (SG 27), and compressive strains on the west (SG 28) and the north (SG 29) sides. The strain gauge on the south side was not working during this test. All three strain gauges exhibit a cyclic pattern with both tensile and compressive strains. The strain gauge on the west side (SG 29) failed during cycling at 1% without showing existence of yielding. Tensile yielding occurred on the east side (SG 27) at 2%, and the north side (SG 28) at 2% drift. The east side (SG 27) is the only gauge in all four specimens to yield in compression, occurring at 1% drift.

All gauges, except the gauge on the east side (SG 27) on CFST 51, yielded in tension between drifts of 2% and 6%. SG 27 yielded in compression during cycling of 1% drift. In most cases yielding occurred first on the east and west sides of the column. These are the directions of loading and therefore experienced more significant stresses and local buckling. It is interesting to note that compressive strains developed in the steel tube in two instances even though they were filled with concrete. This remains unexplained. However, at failure of all specimens, strain gauges were all recording tensile strain.

5.2.7 Summary of Strain Gauge Results

The foundation design worked well by transferring the moment from the steel tube before it reached the bottom plate. This was verified by the significant decrease in strain on the steel tube from the top plate to the bottom of the steel tube. However, the decrease in strain on the steel tube from the top of the concrete foundation to the top plate shows that some of the moment was taken by the concrete in the foundation before the forces reached the top plate, therefore, the steel sections used in the foundation detail were in excess of the sections needed. This is partially because the original design analysis assumed that the unreinforced concrete foundation would act only to confine the steel sections, and this was not completely true.

5.3 Analysis of Second Order Effects

The applied moment on a column can be greater than the applied horizontal force multiplied by the length of the column if there is also an axial load applied. This effect is termed P-Δ, or second order effects. The first order moment is given by the applied horizontal force multiplied by the length of the column. The applied horizontal force is equal to the horizontal actuator force and the horizontal component of the axial load actuator, P_H.

The second order effects occur when the tip deflection increases due to the horizontal force applied to the cantilevered column. As a result, the axial force is now eccentric with respect to the base and an additional moment comprised of the axial force multiplied by the tip deflection must be considered. Therefore, the total base moment is the summation of the first and second order moments. A diagram illustrating the first and second order moments for the tests performed here is shown in Figure 5.42. The second order moment is the vertical component, P_v, of the axial load multiplied by the deflection.

All columns tested in this experiment were subjected to axial loads. All analyses, until now reported the base moment which was calculated encompassing second order effects. Due to the testing set-up used in this study, the horizontal actuator remains horizontal with respect to the specimen during the entire test duration. On the other hand, the vertical actuators rotate to follow

the column since the top swivel head is attached to the top of the specimen and the bottom swivel head is attached to the top of the concrete foundation. This set-up should ensure that the axial force runs directly to the base of the column. However, the line of the vertical actuator meets the column center-line at a distance of 240 mm from the top of the concrete foundation because the bottom swivel head of the actuators rotates about this position. Since the line of force of the vertical actuator runs almost to the base of the column, the moment caused by this actuator is very small. Therefore, the total base moment including second order effects is equivalent to horizontal actuator multiplied by the column height.

Figures 5.43a, 5.44a, 5.45a, and 5.46a illustrates the difference between the total horizontal force and the horizontal actuator on Specimens CFST 64, CFST 34, CFST 42, and CFST 51, respectively. Due to the test set-up, there is a significant difference in the applied horizontal force and the actual horizontal force that was resisted by the specimens. At 2% drift, the horizontal component of the vertical actuator decreased the horizontal force to 91%, 77%, 89%, and 76% of the horizontal actuator force for Specimens CFST 64, CFST 34, CFST 42, and CFST 51, respectively. During the first cycle at 7% drift, the horizontal component of the vertical actuator decreased the horizontal force to 66%, 23%, 57% and 18% of the horizontal actuator force. The two columns with the smaller diameter steel tube, CFST 34 and CFST 51 show the greatest decrease in actual horizontal force applied. Both of these columns resisted smaller applied horizontal force but the axial load was high in both of these columns, namely, 1820 kN and 1600 kN, respectively. The effects of the horizontal component of the vertical actuator were the smallest for Specimen CFST 64, which had the smallest applied axial load of 1000 kN.

Figures 5.43b, 5.44b, 5.45b, and 5.46b illustrate the difference between the first order moments and the first order and second order moments for CFST 64, CFST 34, CFST 42, and CFST 51, respectively. In all four cases, the first order moment is significantly smaller than the total moment. At 7% drift, the second order moment is 37%, 57%, 38%, and 85% of the total moment for CFST 64, CFST 34, CFST 42, and CFST 51, respectively. The vertical component of the axial load is 1000 kN, 1920 kN, 1920 kN, and 1600 kN for CFST 64, CFST 34, CFST 42,

and CFST 51, respectively. CFST 34 and CFST 51 have the greatest second order moments in relation to the total moments due to the large axial force which is the cause of second order effects and the small horizontal force.

6.0.0 DESIGN EQUATIONS FOR FLEXURAL CAPACITY

The expected moment capacity of the specimens was estimated in a number of ways during the early stages of this project, particularly to effectively design the foundation and test set-up. However, following the testing program, a through examination of the predicted maximum moments is warranted. In the following sections, such analyses are carried out and compared to the test results. Improved design equations are then proposed for inclusion in the Canadian design standard for steel structures (CAN/CSA-S16.1).

6.1 Code Comparisons

There are a number of national codes and standards that provide equations for the design of concrete-filled steel tubes (Section 2.3). However, there does not appear to be one unique method to calculate compressive or moment resistance. In this section, the adequacy of selected codes is investigated by comparing their predicted column strength with experimental data. The codes and standards considered here are the CAN/CSA-S16.1-M94, AISC LRFD 1994, and the Eurocode 4 1994. Although proper terminology for the CAN/CSA-S16.1-M94 is a "Standard", and for the AISC LRFD 1994 is "Specifications", all documents will be called "codes" here, inferring that these documents are referenced by other enforceable codes, but also to keep the following text unburdened by such subtle differences.

6.1.1 Code Comparisons of Axial Resistance with Previous Research

Table 6.1 lists available experimental data on axially loaded columns, P_f, along with the corresponding calculated axial resistance for each respective code equation, P_r, and the ratio of the experimental to theoretical axial resistance, P_f/P_r. However, for the comparison here, no safety factors were considered in any of the code equations. The CAN/CSA-S16.1-M94 equation for axial compression is found in Section 2.3.4.1 and Equation 2.14. The corresponding AISC LRFD 1994 equation has been presented in Section 2.3.2.1 and Equation 2.3, and the Eurocode 4 1994 equation is found in Section 2.3.8.1 and Equation 2.28.

It is shown in Table 6.1 that the CAN/CSA-S16.1-M94 and the Eurocode 4 1994 equations produce close but different results, the Canadian code giving up to 18% greater and 16% lower values for different combinations of characterizing parameters. However, the average ratio of experimental to theoretical axial load capacity for the entire data set considered, are nearly the same and relatively close to unity for the two codes, being 1.14 and 1.13 for the Canadian and European codes, respectively, with corresponding standard deviations of 0.24 and 0.22. Both of these codes consider the effect of concrete confinement in circular tubes but do it in significantly different ways, which partly accounts for the differences observed for individual results. The experimental to theoretical axial resistance ratio calculated by the AISC LRFD 1994 was, on average, 1.26. This ratio is larger than obtained using the other two codes. This code does not allow for a significant increase in strength due to concrete confinement as compared with the previous two codes. Detailed calculations for each of the 3 codes are presented in Appendix D.

6.1.2 Code Comparison of Beam-Columns Capacities

No safety factors were used in the following calculations. The equation for calculating beam-columns capacities per CAN/CSA-S16.1-M94 is found in Section 2.3.4.2. Equation 2.16 is used with C_f equal to the applied axial load and solving for M_f. The value of $\left(\frac{\omega_1}{1 - \frac{(C_f - \tau' C_r')}{C_e}} \right)$ is taken as equal to 1.0 for all calculations.

The Eurocode 4 1994 procedure and equations are found in Section 2.3.8.2. An axial force strength diagram is constructed using Equations 2.36 and 2.37. To account for slenderness and imperfections, a reduction coefficient is calculated using Equation 2.33. Graphically, the concept can be illustrated by constructing a non-dimensional axial force diagram, with a shaded triangular region on the left of the diagram and sized as a function of the slenderness factor. For a given axial load applied, the length from the right side of that triangle to the right edge of the interaction diagram gives the usable moment resistance, as calculated by Equation 2.39. Although the Eurocode procedure specifies that the value of this length can not be greater than 1.0, this restriction has been lifted for all calculations here as it appears to be only a constraint introduced

to ensure conservative design. The final member resistance is calculated from Equation 2.40, neglecting the 0.9 factor as it appears to be another safety factor.

The calculation of the moment resistance from the AISC LRFD 1994 comes from Section 2.3.2.2 and Equation 2.7. The applied axial load is used for the value of P_u and the equation is solved for M_u.

6.1.2.1 Comparison with Results for Specimens

Interaction curves were developed using the code procedures outlined above for the four specimens tested in this project. Figures 6.1 to 6.4 show these curves and Table 6.2 summarizes the theoretical and tested moment resistance for the four columns studied. These graphs and table effectively show the benefits and disadvantages of the three codes. The interaction curves labeled CAN/CSA-S16.1-M99 (Proposal A) and CAN/CSA-S16.1-M99 (Proposal B) will be described in detail in Section 6.3. Note that the Eurocode 4 moment resistance at a given axial force level is the length of the horizontal line ranging from the strength interaction curve on the right and the diagonal line on the left side of the graph.

For all four of the specimens tested here, the best prediction of maximum moment is given by the Eurocode. That interaction curve is derived somewhat following the principles of an axial force-moment interaction diagram for reinforced concrete which explains its particular shape. The experimental to calculated moment resistance using Eurocode is 1.33, 1.10, 1.01, and 1.17 for CFST 64, CFST 34, CFST 42, and CFST 51, respectively. The AISC LRFD bilinear interaction curve predicts a smaller axial resistance load and a smaller resistant moment than the Eurocode. It underestimates the strength of the four specimens by 1.64, 1.90, 1.36, and 2.25 for CFST 64, CFST 34, CFST 42, and CFST 51, respectively. CAN/CSA-S16.1-M94 also predicted extremely conservative values of maximum moment resistance, namely 1.88, 1.74, 1.53, and 1.95 for CFST 64, CFST 34, CFST 42, and CFST 51, respectively. These low values from the Canadian code can be explained by the peculiar shape of the interaction curve shown on the figures. This results from the fact that, once the value of $C_f - \tau' C_r'$ in Equation 2.16 becomes

less than zero, the axial force - moment interaction curve is simply the moment resistance of the steel section acting alone (i.e. non-composite). Therefore, at the point that $C_f - \tau' C_r' \leq 0$ the moment resistance is constant for all values of C_f below this axial force. This truncates the interaction curve in the manner shown in the figures, such that for specimens with low applied axial forces, the moment capacity of the composite section is grossly underestimated, as seen for all tested specimens.

6.1.2.2 Comparison with Previous Research Data

Table 6.3 lists the circular concrete-filled steel tube columns that were subjected to both axial and bending loads from the previous research reviewed in Section 2.5.5, as well as from the current study, along with their moment capacity calculated using the three codes and procedures described above. This table allows for a more through study of the three codes than can be accomplished from the limited data produced by the four specimens tested in this study. Tables 6.4 to 6.6 present more detailed information for the same data, ASIC LRFD 1994, CAN/CSA-S16.1-M94, and Eurocode 4 1994, respectively.

The columns tested in the current study were chosen to investigate different steel tube classes with respect to concrete-filled steel tubes. However, as explained earlier, the steel tube thickness were smaller than the nominal sizes and the steel yield strengths for greater than the nominal strengths. When the class calculation was performed on the actual dimensions, the columns fall into different classes. All calculations on the four columns tested in this study have been using the actual dimensions. However, in Table 6.3, Marson (1999) nominal is the title for the nominal values for the columns tested in this study.

Table 6.4 shows that the average experimental to theoretical moment resistance calculated per the AISC LRFD is 3.90 with a standard deviation of 4.20. Table 6.5 shows the CAN/CSA-S16.1-M94, with an average experimental to theoretical moment resistance of 1.79 and a standard deviation of 0.64. Table 6.6 for the Eurocode 4 (1994) shows an average experimental to theoretical moment resistance of 1.10, with a standard deviation of 0.32.

Again, the AISC is the most conservative and has a large standard deviation. The CAN/CSA-S16.1-M94 produced better results than the AISC equations, but the ratio of 1.79 shows theoretical values almost twice as conservative as those obtained during experimental studies. The Eurocode 4 1994 best captured the behaviour.

In light of the significant deviation from the average values, especially using AISC LRFD and CAN/CSA-S16.1-M94, a closer examination of the data was performed, the results were segregated as a function of the different loading types and D/t ratios, to determine if the equations work better for certain parameters. The type of loading method is indicated in the first column of Table 6.3 using an arbitrary letter code. Four different methods have been used in the past to apply bending moments to concrete-filled steel tubes. In Type A, the bending moment is produced by applying an eccentric load to the column, producing a uniform moment along the entire length of the column. Note that Type A specimens cannot be subjected to a constant axial load for moments of varying magnitude. The bending moment in Type B columns is produced by applying two transverse loads close to the middle of the column to achieve a maximum moment in the center region. A horizontal load is applied to the tip of a cantilever for the Type C columns, producing a maximum moment at the base of the column. All columns tested using the Type C load application were subjected to cyclic bending moments. The bending moment for Type D columns was produced in the same manner as Type B columns but applied in a cyclic manner. The effect of loading set-up on the columns is considered in Figures 6.5 to 6.10 along with other parameters.

Table 6.7 is Table 6.3 sorted according to the steel tube classes using the actual values of the four columns tested in this study. Table 6.8 sorts the four tested columns in this study by their nominal steel tube classes. Figures 6.5, 6.6, and 6.7 are graphical representations of the $D/t*F_y$ ratio, the experimental to theoretical ratio, and the loading method for AISC LRFD (1994), CAN/CSA-S16.1-M94, and Eurocode 4 (1994), respectively. Vertical lines in these figures represent the limits for classes 1,2,3 defined by Clause 11.2 of CAN/CSA-S16.1-M94 and class 4 defined by Clause 18.2 of the same standard. Note that Clause 18.2 permits the use of class 4

sections for concrete-filled steel tubes provided $D/t \leq 28000\ F_y$, which is delimited by the fourth vertical line in Figures 6.5 to 6.7. Figures 6.8, 6.9, and 6.10 illustrate the effect of axial load ratio to the experimental to calculated moment resistance ratio for the same three codes. The axial load ratio is defined as the axial force applied to the beam-column divided by the compressive resistance of the column when no moment is applied. The notation of M_f and M_r in these graphs represent the experimental and theoretical moment resistances, respectively.

For the CAN/CSA-S16.1-M94 in Figure 6.6, better results are obtained for the Type A loading condition, with an experimental to theoretical ratio of 1.48. The code is most conservative when a column is axially loaded and a bending moment is induced in the middle by two point loads, as is the case for Type B and Type D loading, where ratios of 2.65 and 3.02 are respectively obtained. However, these columns all have a $D/t*F_y$ ratio of 30000, which is larger than the limit of 28000 permitted by the code for Class 4 concrete-filled structures. The columns that were loaded as Type C had an experimental to theoretical ratio of 1.87. Overall, the code equations are considerably conservative for all types of loading. Looking at the results as a function of their steel section classes is a better and more significant comparison. For specimens within the steel Classes 1, 2, 3, 4 (permitted by Clause 18.2 of CAN/CSA-S16.1-M94), and Class 4 (as defined by Clause 11.2 of CAN/CSA-S16.1-M94), the experimental to theoretical ratios are 1.02, 1.66, 1.53, 1.95 and 2.07, respectively. Hence, as the D/t ratio of the steel tube increases, the equations become more conservative.

The equations from the Eurocode produced the best results out of the three codes considered here. The ratios of experimental to theoretical moment resistance were 1.07, 1.15, 1.19 , and 1.24 for loading of Type A, B, C, and D, respectively. The ratios were 0.91, 1.20, 1.01, 1.18 and 1.04 for steel tube Classes 1, 2, 3, 4 (permitted by Clause 18.2 of CAN/CSA-S16.1-M94), and Class 4 (as defined by Clause 11.2 of CAN/CSA-S16.1-M94). The categories of D/t ratios here are still taken from the CAN/CSA-S16.1-M94; the Eurocode does not have such an explicit size restriction but rather states that local buckling should be taken into account

above a $D/t*F_y$ ratio of 21150. However, the effects of local buckling were not considered in the Eurocode strength calculations presented here.

The AISC LRFD 1994 did not produce as favourable results as either the CAN/CSA-S16.1-M94 or Eurocode 4. The ratios of M_f/M_r were 4.16, 4.43, 2.09, and 4.04, for Type A, B, C, and D, respectively and the ratios of M_f/M_r were 1.36, 3.32, 1.36, 2.25, 5.22 for Class 1, 2, 3, 4 (as defined by Clause 18.6 of CAN/CSA-S16.1-M94), and Class 4 (as defined by Clause 11.2 of CAN/CSA-S16.1-M94).

As seen in Figure 6.8, as the amount of axial load applied on the column increases, so does the ratio of experimental to calculated moment resistance for AISC LRFD (1994). Therefore, the AISC LRFD equation works well for small axial forces but becomes extremely conservative for larger compressive forces. This is a consequence of having a straight interaction curve in which the axial ratio plus the moment ratio must be equal to one, i.e. the available moment resistance rapidly diminishes when larger axial loads are imposed on the column. The scatter in Figures 6.9 and 6.10 shows no trend, signifying that the accuracy of the CAN/CSA-S16.1-M94 and Eurocode 4 (1994) equations does not depend on the axial load ratio.

It is noteworthy that all three codes produced conservative results or slightly unconservative results within the variability expected for this type of calculations. However, all codes produces grossly unconservative results for two of the four Class 1 columns Knowles and Park (1969) tested under Type A loading and an initial eccentric load of 7.62 mm and 25.4 mm with an average M/M_r ratio on the order of 0.5. Closer examination of Knowles and Park's data did not reveal any peculiar characteristic which would explain the unusually poor comparison between experimental results and theoretical computations for these 2 columns and the nature of this discrepancy remains unresolved.

6.2 Maximum Moment using the Moment-Curvature Program

A theoretical loading envelope was developed using the computer program described in Appendix A. The program calculates a moment versus drift curve from the structural characteristics of the concrete-filled steel tube. The method used is a classic moment- curvature procedure in which the steel tube and the concrete core are divided into layers. The program calculates each layer's individual area, center of gravity, and the stress, and force corresponding to a given curvature and neutral axis location. Forces from all layers are summed together and the neutral axis is iteratively moved until the sum becomes equal to the applied axial force. The corresponding moment at each curvature is then calculated. Finally, the force is taken as the moment divided by the height of the column and the deflection is calculated by integration of the curvature diagram.

For the initial determination of the moment versus drift diagram, the actual dimensions of the steel tube and the strengths found from testing the steel coupons and the concrete cylinders were used in the calculations. The concrete model used was a confined concrete model by Mander et al. (1998) and the steel model was a bilinear stress-strain relationship.

The stiffness and maximum force calculated by the program with the above assumptions are compared to the test data in Figures 6.11 to 6.14. Note that the program only calculates cross-sectional strength, and cannot model the local buckling of the steel tube that occurred during testing after the maximum moment was reached. When comparing the program results to the experimental data, the yield moment and the maximum moment were overestimated and the deflections were significantly underestimated for all specimens using the design information for the steel and concrete strengths. To investigate the differences between the calculated and experimental moments, deflections and stiffnesses, a closer examination into the deflection calculations and the material properties of the composite column is undertaken. A detailed analysis of the deflection calculation is performed first.

The deflection at the top of the column was calculated as the second moment of the curvature diagram. Example moment and curvature diagrams are shown for Specimen CFST 64 in Figure 6.15 at a curvature of 0.0006 and a moment of 601 kN·m. The deflection can be calculated from this graph as the area under the curvature curve multiplied by the distance from the tip of the column to the centroid of the area. Even though the curvatures due to yielding are very large at the base of the column, the plastic hinge length is relatively small and the calculated deflections remain smaller than the experimental deflections.

In Section 5.1 the theoretical equation for a cantilever column was also shown to underestimate the experimentally obtained tip deflection. It was found that increasing the total effective length of the column by h in Equation 5.1, provided a reasonable solution. For the studied elastic behaviour, this procedure worked well, and the location of the fixity point for all columns was found to be between the top of the concrete foundation and the bottom of the steel plate in the foundation, but its location varied as a function of the applied moment. However, implementing such a variable effective height concept in the program was not practical and there is not enough corroborating data to properly model it. Nonetheless, a simpler form of this concept was used to determine the corrected tip deflection. The two assumptions used in the calculation of the new deflections are :

- the maximum moment occurs at the concrete foundation,
- the column moment linearly decreases from the top of the concrete foundation to the top steel plate.

Figures 6.16 to 6.19 and 6.20 to 6.23 demonstrate the distribution of the strain along the column at various drift levels for positive force and negative force, respectively for each specimen. Each symbol represents one strain gauge reading on the steel tube. The assumption that the maximum moment occurs at the top of the concrete foundation is demonstrated in these figures. Despite the variance found from the strain gauge information, a linear decrease in strain from the top of the concrete foundation to the top plate seems a reasonable approximation of the strain distribution on all of the specimens tested.

The new tip deflection is calculated as in Figure 6.15 except the maximum moment was assumed to decrease to zero at the top plate in the foundation. The moment distribution on the column is illustrated in Figure 6.24. The new deflections calculated using this method produce results that match the actual test results better. Figures 6.25 to 6.28 show the envelope from the experimental data along with the original deflection curve and the improved deflection curves for Specimens CFST 64, CFST 34, CFST 42, and CFST 51, respectively.

The capacity predicted by the computer program for Specimen CFST 64 is only 1.03 times greater than the actual resistance of the column. The stiffness of the column is also better modeled as shown by the deflection values. Incidentally, this column was loaded with an axial load of 1000 kN, corresponding to 12% of its squash load, the smallest of all the axial loads. The computer program did not predict the flexural strength of the other three specimens as well. The results from the program for Specimens CFST 34, 42, and 51 were 1.15, 1.16, and 1.07 times greater than the actual resistance of the tested column. The axial loads on these three columns were 1820 kN, 1820 kN, and 1600 kN for CFST 34, 42, and 51, respectively, corresponding to 25%, 16%, and 28% of their squash load.

While elastic deflection is better modeled by this new approach, the flexural strength of the columns remains poorly estimated. This suggested the need to review the material models considered. Until now, all analyses used a confined concrete model by Mander et al. (1988). Such a model will overestimate the concrete strength if the entire concrete core is not confined by the steel tube. A number of different stress-strain relationships were investigated to define the behaviour of the test specimens. The following concrete axial compression stress-strain models were considered:

Model 1 - confined concrete model [Mander et al. (1988)] (described previously),

Model 2 - unconfined concrete model [Hognestad (1951)],

Model 3 - confined concrete model [Saatcioglu and Ravzi (1992)],

Model 4 - unconfined concrete model with high ductility,

Model 5 - unconfined concrete model with CISC provisions,

Model 6 - unconfined concrete model with high ductility and CISC provisions,

Model 7 - reduced confined concrete model [Mander et al. (1988)].

A description of each model and the rationale that led to their consideration follows. Figures 6.29 to 6.32 shows the resulting force-tip displacement curves for Specimens CFST 64, CFST 34, CFST 42, and CFST 51, respectively, for the six different models. Table 6.9 compares the numerical results for different curves and the test results.

To investigate if the strength of the composite material was the simple summation of the strength of the steel tube and the strength of the concrete core the unconfined concrete model proposed by Hognestad (1951) was used (Model 2 above). Figures 6.29 to 6.32 illustrate the results of this attempt for the four tested specimens. From these curves it is clear that the steel tube is an effective method of concrete confinement as the composite strength is 0.86, 0.81, 0.91, and 0.70 of the test results which confirms that the steel tube is providing some measure of concrete confinement.

In another attempt to quantify the effect of concrete confinement, the model proposed by Saatcioglu and Razvi (1992) was used (Model 3). Results from the analysis give curves that essentially followed the Mander confined concrete model curves and overestimated the strength by 1.03, 1.17, 1.19, and 1.09, as seen in Figures 6.29 to 6.32 for Specimens CFST 64, CFST 34, CFST 42, and CFST 51. From the results of both Mander et al. (1988) and Saatcioglu and Razvi (1992) and the absence of bond at the end of the tests, as discussed in Section 4.6, it was concluded that a fully confined concrete model overestimated the strength of a concrete-filled steel tube.

An alternative approach consisted of altering the stress-strain relationship of the concrete core previously examined. Model 4 assumed that the steel tube confined the concrete core in such a way that the ductility was significantly improved and the strength of the concrete was f_c', instead of the usual concrete column strength of 0.85 f_c'. The unconfined concrete model was used, but when the concrete strength reached f_c', the strength remained at this level without a

descending branch. This concrete model resembles the elastic-perfectly-plastic model of the steel tube. The plastic portion of the curve is assumed to result from the steel tube providing confinement to the concrete core. The curves resulting from these analyses can be seen in Figures 6.29 to 6.32. The strength attained by this curve is greater than the strength predicted using the simple unconfined concrete model, but still underestimates the resistance of the test specimens of 0.92, 0.92, 0.99, and 0.87 of the test results for Specimens CFST 64, CFST 34, CFST 42, and CFST 51, respectively.

Hognestad's unconfined concrete model was used again in model five. This time however, it was modified using the provisions of the CAN/CSA S16.1-M94. This code was described in Section 2.3.4, with τ and τ' defined as the steel and concrete modification factors, respectively, and described as:

$$\begin{aligned} \tau &= \frac{1}{\sqrt{1+\rho_s+\rho_s^2}} \\ \tau' &= 1+\left(\frac{25\rho_s^2\tau}{(D/t)}\right)\left(\frac{F_y}{0.85f_c'}\right) \\ \rho_s &= 0.02(25-L/D) \end{aligned} \tag{6.1}$$

The steel factor ($\tau \leq 1.0$) signifies that during confinement, the steel tube acts in a biaxial stress state and therefore, a loss in available longitudinal steel strength occurs. The concrete factor ($\tau' \geq 1.0$) takes into account the additional strength gained by the concrete core due to the confinement of the steel tube. The program therefore was altered to multiply the steel and concrete stress at each layer by τ and τ', respectively. The values of τ were 0.804, 0.817, 0.804, and 0.817 for Specimens CFST 64, CFST 34, CFST 42, and CFST 51, respectively. The values of τ' were 1.587, 1.756, 2.22, and 1.618 for Specimens CFST 64, CFST 34, CFST 42, and CFST 51, respectively. The results of this analysis, shown in Figures 6.29 to 6.32, demonstrate that this approach underestimates the strength of the columns, 0.81, 0.86, 0.92, and 0.81 of the test results. Calculated strengths are closer to the test specimen results for Specimens CFST 34,

CFST 42, and CFST 51 than when the unmodified unconfined concrete model is used (Model 2), but not Specimen CFST 64. The difference in results from the two approaches for these four specimens, however, is small.

Model 6 was developed along the same idea as Model 5, except that, instead of using the simple unconfined concrete model, the unconfined concrete model with high ductility of Model 4 was used. The CAN/CSA S16.1-M94 equations increase the concrete strength of a composite column. However, using the unconfined concrete model of Hognestad, the concrete core cannot maintain the yield strength and subsequently fails due to concrete crushing. Using this modified model, the increase in concrete strength proposed by the CAN/CSA S16.1-M94 should produce the effect intended by this code. Figures 6.29 to 6.32 show the results of this trial. This approach only slightly underestimates the strength of the specimens at 0.86, 0.94, 0.97, and 0.90 of the test results (i.e. a reasonable range in a design perspective). Interestingly, the additional concrete strength did not dominate the calculations. Instead, it was the decrease in steel strength that has the most noticeable impact in the calculations.

In a final attempt to identify the behaviour of the tested specimens, a confined concrete model was modified. The stress-strain relationship proposed by Mander et al. increases the maximum concrete strength to as much as $2.8*f_c'$. Since it has been shown that the confined concrete model overestimates the strength of these composite columns, a reduction in the maximum concrete strength reached in that model may approach the experimentally obtained composite column behaviour. A sensitivity analysis was performed to see the effect of reducing the maximum concrete strength in intervals of 10%. Figures 6.33, 6.34, 6.35, and 6.36 illustrate this analysis. Using this method, best matches are obtained for Specimens CFST 64, CFST 34, CFST 42, and CFST 51, respectively, when the maximum concrete compressive strength is reduced to 80%, 60%, 40%, and 70% of the maximum confined concrete strengths. However, these reductions in concrete compressive strength are arbitrary, not uniform, and are not based on any defensible physical model. Therefore, this method is not appropriate to be used as an analysis tool.

Based on the rational that a theoretical method should be conservative, the best model from the above detailed analyses carried out on a limited number of specimens seems to be the unconfined model with high ductility (Model 6). The ratio of experimental to calculated maximum horizontal force ranged from 0.87 to 0.99.

6.3 Proposed New Equations for CAN/CSA-S16.1.

As shown in Figures 6.1 to 6.4, the current CAN/CSA-S16.1-94 design equation for a concrete-filled steel tube severely underestimates the moment capacity of a beam-column when the applied axial force is less than the compressive resistance from the concrete core alone. CAN/CSA-S16.1-M94 has two methods for the design of composite columns. In the first method (Clause 18.6.1), the moment resistance of the composite section is considered in calculations. However, use of this method is only permitted for rectangular CFST sections. This method depends on the moment resistance of a composite section, M_{rc}, in Clause 18.5 of CAN/CSA-S16.1-M94. The value of M_{rc} in this clause is only given for rectangular sections because the research in support of these equations was performed for rectangular sections only. An example on how to calculate the moment resistance for rectangular CFST sections is documented in Picard and Beaulieu (1997). The second calculation method presented in CAN/CSA-S16.1-94 (Clause 18.6.2) assumes that bending is resisted by the steel section alone. It is applicable to any concrete-filled tube section, and is by default the only method permissible for circular concrete-filled steel tubes. The commentary for this clause states that "a lower bound solution is retained for the design of circular hollow structural sections filled with concrete, until expressions such as those for rectangular hollow structural sections are developed". This more conservative method is the one that has been used in Figures 6.1 to 6.4.

In this section, new equations are proposed to calculate the strength of circular concrete-filled steel tube beam-columns with better results than by the current Clause 18.6.2 of CAN/CSA-S16.1-M94. These equations are formulated in a format compatible with the Canadian code to facilitate their potential implementation in future editions of that standard.

6.3.1 Bending Resistance

The moment resistance of a circular section is recalculated using the approach outlined in Picard and Beaulieu (1997) to consider the effect of both the concrete core and the steel tube. Using the same terminology as in this paper, and the diagram in Figure 6.37, the following equations define the forces acting on the composite section.

$$T_r = A_{st} F_y \tag{6.2}$$

$$T_r = T_{\max} - C_r \tag{6.3}$$

$$T_r = C_r + C_r' \tag{6.4}$$

$$T_{\max} = A_s F_y \tag{6.5}$$

where T_r is the tensile force in the steel tube, A_{st} is the area of tensile steel, F_y is the yield strength of the steel tube, T_{max} is the total force if the entire steel tube is in tension, C_r is the axial compressive resistance of the steel tube, C'_r is the axial compressive resistance of the compressed concrete core and A_s is the total area of steel. To solve for the neutral axis location, h, in Figure 6.37, the above four equations are combined to produce one equation,

$$2A_{st}F_y = A_s F_y + C_r' \tag{6.6}$$

The terms in the above equation are defined below:

$$A_{st} = (2\pi R^* - L^*)t \tag{6.7}$$

$$L^* = \overline{A} R^*$$

$$A_s = 2\pi R^* t \tag{6.8}$$

$$C_r' = A_{conc} f_c' = \left(\frac{LR}{2} - \frac{c(R-a)}{2} \right) f_c' \tag{6.9}$$

$$L = \overline{A} R$$

$$a = \frac{c}{2} \tan \frac{\overline{A}}{4}$$

$$c = 2R \sin \frac{\overline{A}}{2}$$

where L^* is the arc length of the tube in compression measured at mid-thickness of the steel tube, $\overline{A}$ is the angle in radians from the centre of the tube and sustaining the arc L^*, R^* is the radius of the steel tube to the center-line of the steel tube, L is the arc length in compression measured on the inside face of the steel tube, and R is the outer steel tube radius, all variables are shown in Figure 6.37. Substituting these terms into Equation 6.6, simplifying by saying $R \cong R^*$ and $L \cong L^*$, and expressing in terms of $\overline{A}$, the equation becomes:

$$\frac{2\pi RtF_y + \left(R^2\sin\frac{\overline{A}}{2} - R^2\sin^2\frac{\overline{A}}{2}\tan\frac{\overline{A}}{4}\right)f_c'}{\frac{R^2f_c'}{2} + 2RtF_y} = \overline{A} \tag{6.10}$$

There is no closed form solution for the above equation so an iterative solution is required to obtain $\overline{A}$. Once the value for $\overline{A}$ is found, C_r, C'_r, and T_s can be calculated. Figure 6.37 illustrates how these three forces act on the composite section to produce the composite resistance moment, M_{rc}. The distances from the neutral axis for C_r, C'_r, and T_s, are y_{sc}, y_c, and y_{st}, respectively. These terms are outlined in the following equations.

$$y_{sc} = \frac{Rc}{L} \tag{6.11}$$

$$y_c = \frac{c^3}{6[RL - c(R-a)]} \tag{6.12}$$

$$y_{st} = \frac{Rc}{2\pi R - L} \tag{6.13}$$

From simple statics, M_{rc} is defined as:

$$M_{rc} = C_r e + C'_r e' \tag{6.14}$$

$$e = y_{st} + y_{sc}$$

$$e' = y_{st} + y_c$$

6.3.2 Interaction Curve for Axial Compression and Bending Resistance - Proposal A

Availability of the above equations for M_{rc} for circular concrete-filled steel tubes makes it possible for users of CAN/CSA-S16.1-M94 to use Clause 18.6.1 and consider the composite section to calculate the moment resistance of these composite columns. Clause 18.6.1 is similar to the axial compression and bending equations for steel members found in Clause 13.8 of CAN/CSA-S16.1-M94. The interaction equation for concrete-filled tubes subjected to both axial compression and bending moment is:

$$\frac{C_f}{C_{rc}} + \frac{B\,\omega_1 M_f}{M_{rc}\left(1 - \frac{C_f}{C_{ec}}\right)} = 1.0 \tag{6.15}$$

where C_f is the applied axial force on the column, and C_{rc} is the axial resistance of a concrete-filled steel column as defined in Equation 2.14 and rewritten here for convenience:

$$C_{rc} = \tau C_r + \tau' C_r' \tag{6.16a}$$

$$C_r' = 0.85\phi_c f_c' A_c \lambda_c^{-2}\left[\sqrt{1+0.25\lambda_c^{-4}} - 0.5\lambda_c^{-2}\right] \tag{6.16b}$$

$$\lambda_c = \frac{kL}{r_c}\sqrt{\frac{f_c'}{\pi^2 E_c}} \tag{6.16c}$$

$$C_r = \phi A_s F_y (1+\lambda_s^{2n})^{\left(-\frac{1}{n}\right)} \tag{6.16d}$$

$$\lambda_s = \frac{kL}{r_s}\sqrt{\frac{F_y}{\pi^2 E_s}} \tag{6.16e}$$

M_f is the applied moment on the column, C_{ec} is the Euler buckling strength of a concrete-filled steel tube and B is defined as:

$$B = \frac{C_{rco} - C_{rcm}}{C_{rco}} = 1 - \frac{C_{rcm}}{C_{rco}} \tag{6.17}$$

where C_{rco} is the compressive resistance as calculated by Equation 6.16a with $\lambda = 0$, and C_{rcm} is the compressive resistance of the concrete core alone with no slenderness effect taken into account. As seen in Figure 6.38, the moment capacity with no axial force applied and a neutral axis location of h above the center of gravity is the same moment capacity for an axial force equal to C_{rcm} and a neutral axis location of h below the center of gravity. As seen in the equations in Figure 6.38, M_{rc} is equal to M_{rcm}.

Figure 6.39 shows the effect of B for values of B equal to 1.0, 0.85, 0.75, and 0.5. CAN/CSA-S16.1 states that $B=1.0$ can conservatively be used, but, as shown on Figure 6.39, this can be grossly conservative. The factor B changes a straight line interaction curve into a bilinear interaction curve. As B decreases, a column can resist more axial force in addition to resisting its full plastic moment. For the actual column, in which $\lambda=0$, the interaction curve is automatically adjusted downward by the ratio C_f/C_{rc} with C_{rc} calculated by Equation 6.16. In that case, the greatest axial force that can be resisted in addition to the full moment is C_{rcm} reduced by the ratio C_{rc} / C_{rco}.

The interaction curve using Equation 6.15 for the four specimens tested in this study is shown in Figures 6.1 to 6.4 as CAN/CSA-S16.1-99 (Proposal A). As suspected, the moment resistance calculated relying on the composite section is in much better agreement with the experimental results than those values calculated earlier using the model where flexural resistance is provided by the steel tube alone, as done in CAN/CSA-S16.1-94. For this interaction curve, the experimental to calculated ratio are 1.20, 1.15, 1.02, and 1.28 for Specimens CFST 64, CFST 34, CFST 42, and CFST 51, respectively. These ratios are much smaller than the values of 1.88, 1.74, 1.53, and 1.94 for Specimens CFST 64, CFST 34, CFST 42, and CFST 51, respectively calculated using Clause 18.6.2 relying on the steel tube alone for moment capacity.

6.3.3 Interaction Curve for Axial Compression and Bending Resistance - Proposal B

It is well known that reinforced concrete columns can have a moment resistance at small axial forces greater than the maximum moment capacity of a section with no axial load applied, and this interaction diagram is usually represented by a polygon with three straight lines. This concept also works for concrete-filled steel sections and is incorporated into the Eurocode 4 1994. The interaction curve specified by the Eurocode produce slightly better results than Proposal A equations presented in the previous sections. (Recall that the experimental to calculated moment resistance for the Eurocode was 1.13, 1.10, 1.01, and 1.17 for Specimens CFST 64, CFST 34, CFST 42, and CFST 51, respectively.)

The second proposal for making the Canadian code equations more effective, Proposal B, utilizes this concept. To obtain a tri-linear interaction diagram, one more point is added to the interaction curve developed in Proposal A, namely the point (C_{rhc}, M_{rhc}). C_{rhc} is the axial force needed for the neutral axis to be at the same position as the center of gravity of the composite section, which also gives the maximum moment resistance, M_{rhc}. As shown in Figure 6.40, the axial force at C_{rhc} corresponds to half of the force at C_{rcm} or half of the concrete core strength, designated C_{rhc}. The moment, M_{rhc} and force C_{rhc} at this location can be calculated as:

$$\begin{aligned} C_{rhc} &= 0.5\pi R_c^2 f_c' \\ M_{rhc} &= \frac{2}{3} f_c' R_c^3 + 4 F_y R_c^2 t \end{aligned} \tag{6.18}$$

where R_c is the radius of the concrete core. Hence, the three line interaction diagram for the composite section shown in Figure 6.41, can be drawn using the following four points:

$$
\begin{aligned}
C_A &= C_{rco} = \tau A_s F_y + \tau' 0.85 f_c' A_c & M_A &= 0 \\
C_C &= C_{rcm} = A_c f_c' & M_C &= M_{rc} \\
C_D &= C_{rhc} = 0.5 A_c f_c' & M_D &= M_{rhc} = \frac{2}{3} f_c' R_c^3 + \frac{4}{3} F_y R_c^2 t \\
C_B &= C_0 = 0 & M_B &= M_{rc}
\end{aligned}
\tag{6.19}
$$

The interaction diagram shown in Figure 6.41 is a cross-sectional strength interaction curve. It does not consider slenderness or stability of the member. Slenderness and stability decrease the maximum axial load and moment that a column can resist. The Eurocode 4 1994 method to modify the strength interaction curve into a stability interaction curve is shown in non-dimensional form in Figure 6.42. All notation is described in Section 2.3.8.2. To simply describe Figure 6.42, a diagonal line is drawn from the strength interaction diagram at the value of maximum axial resistance of the column, χ, defined by the column buckling limit to the point χ_n. The bending moment that can coexist with the applied axial force, χ_d is taken from the graph as the distance, μ, from the strength interaction curve to the slenderness effects line. Unfortunately, this approach is of a format incompatible with CAN/CSA-S16.1. However, the concept of defining a tri-linear interaction diagram from the above four points, as done in Eurocode 4 1994, has been used to develop a stability curve for Proposal B.

The method proposed here requires that the strength interaction curve using Equation 6.19 be developed, and C_{rc} from Equation 6.16 also be calculated. For simplicity sake, the method proposed here assumes that, if the Eurocode approach was used, the diagonal line from the point on the interaction curve at C_{rc} is extended to the point of zero axial force and zero moment. This can be seen in Figure 6.43, where the left hand side of the diagonal line is equivalent to the moment capacity that is "lost", M_L due to slenderness. Because of the above simplification, this moment "lost" can be subtracted from the strength interaction curve in Figure 6.44 to produce a stability interaction curve of a format more compatible with North American practice. At C_{rc}, the entire moment resistance on the strength curve is "lost" due to

slenderness, and the moment resistance on the stability curve is zero. At zero axial force, there is no loss in moment capacity and the moment resistance of the strength curve is the same as the moment resistance of the stability curve. In between these two extreme axial loads, the moment resistance from the strength curve is linearly reduced as a function of the axial load to produce the stability interaction curve.

Following this approach, three different stability interaction curves can be drawn for a single strength interaction curve depending on the slenderness of the column. In the following, the same points defined by Equation 6.19 are used to draw the stability interaction curve, with the difference that some values of moments must be replaced by the values of M^* listed below.

1. In Figure 6.45, if $C_{rc} > C_{rcm}$, a three line stability interaction curve is developed with:

$$M_L = \frac{M_{rc}(C_{rc} - C_{rco})}{(C_{rcm} - C_{rco})}$$

$$\text{therefore} \quad M_{rc}^* = M_{rc} - \frac{M_L C_{rcm}}{C_{rc}} \tag{6.19}$$

$$\text{and} \quad M_{rhc}^* = M_{rhc} - \frac{M_L C_{rhc}}{C_{rc}}$$

To determine the moment resistance of the composite section, M_r, the value of C_f is plotted on the vertical axis and the value of M_r is read off of the stability interaction curve in Figure 6.45 or from the equations below:

$$\text{If } C_f \geq C_{rcm} \quad M_r = \frac{M_{rcm}^*(C_{rc} - C_f)}{(C_{rc} - C_{rcm})}$$

$$\text{If } C_f \geq C_{rhc} \quad M_r = M_{rhc}^* - \frac{(M_{rhc}^* - M_{rcm}^*)(C_{rhc} - C_f)}{(C_{rhc} - C_{rcm})} \tag{6.20}$$

$$\text{If } C_f \geq C_0 \quad M_r = M_{rhc}^* - \frac{(M_{rhc}^* - M_{rc})(C_f)}{C_{rhc}}$$

2. In Figure 6.46, if $C_{rc} > C_{rhc}$, a two line stability interaction curve is developed with:

$$M_L = M_{rhc} - \frac{(M_{rhc} - M_{rc})(C_{rhc} - C_{rc})}{(C_{rhc} - C_{rcm})}$$

$$\text{therefore} \quad M^*_{rhc} = M_{rhc} - \frac{M_L C_{rhc}}{C_{rc}} \tag{6.21}$$

To determine the moment resistance of the composite section, M_r, the value of C_f is plotted on the vertical axis and the value of M_r is read off of the stability interaction curve in Figure 6.46 or from the equations below:

$$\text{If } C_f \geq C_{rhc} \quad M_r = \frac{M^*_{rhc}(C_{rc} - C_f)}{(C_{rc} - C_{rhc})}$$

$$\text{If } C_f \geq C_0 \quad M_r = M_{rc} - \frac{(M_{rc} - M^*_{rhc}) C_f}{C_{rhc}} \tag{6.22}$$

3. In Figure 6.47, if $C_{rc} > C_0$, a one line stability interaction curve is developed with:

$$M_L = M_{rc} + \frac{(M_{rhc} - M_{rc}) C_{rc}}{C_{rhc}} \tag{6.23}$$

To determine the moment resistance of the composite section, M_r, the value of C_f is plotted on the vertical axis and the value of M_r is read off of the stability interaction curve in Figure 6.47 or from the equation below:

$$M_r = M_{rc} + \frac{C_f(M_{rhc} - M_{rc})}{C_{rhc}} - \frac{M_L C_f}{C_{rc}} \tag{6.24}$$

Figures 6.45, 6.46, and 6.47 show the three different stability interaction curves that may develop from the same strength interaction curve, depending on the slenderness of the beam-column.

Using CAN/CSA-S16.1-99 (Proposal B) with the four tested specimens produces the stability curves shown in Figures 6.1, 6.2, 6.3, and 6.4 as CAN/CSA-S16.1-99 (Proposal B) for Specimens CFST 64, CFST 34, CFST 42, and CFST 51, respectively. The ratio of experimental to calculated moment resistance for Proposal B is 1.14, 1.17, 1.04, and 1.25, for Specimens CFST 64, CFST 34, CFST 42, and CFST 51, respectively, which is in good agreement with the test data. All four of the specimens have a three line interaction curve with the four axial points visible, however, the moment, M^*_{rhc} is less than M_{rc} for Specimen CFST 42 and nearly equal to M_{rc} for Specimen CFST 34. This shows that, in spite of its greater complexity, Proposal B can sometimes be more conservative than Proposal A.

The advantage of Proposal B over Proposal A is the ability to predict greater moment capacity when a beam-column is subjected to low axial forces particularly for members of low slenderness. Both of the proposed interaction curves, (Proposals A and B), are identical from C_{rc}, compressive resistance of the column, to C_{rcm}, compressive resistance of the column that can coexist with M_{rc}. From this point on the graph, the second line of Proposal B starts and continues to C_{rhc}, the compressive resistance corresponding to the maximum moment resistance, with a greater slope than the first line. On the contrary, the first line of Proposal A continues past C_{rcm} until the moment reaches M_{rc}. This axial force will be less than C_{rcm}, thereby predicting a greater moment resistance than Proposal B for these axial forces. The axial load at which the moment resistance becomes equal to the maximum moment is dependent on the factor B in Equation 6.15, as seen in Figure 6.39.

6.3.4 Comparison of the New S16.1 Equations with Previous Research

The calculations required by Proposal B are more intensive than the calculations for Proposal A, and the advantages of Proposal B do not outweigh these additional calculations for the four specimens tested in this study. These specimens all had low slenderness ratios and low axial load ratio. Consideration of only these four specimens did not permit exploring the two new proposals to their full extent. However, the previous research that has been performed on

concrete-filled steel tubes as beam-columns can provide more evidence as to the effectiveness of the new equations.

Table 6.2 shows a comparison between the original CAN/S16.1-M94 and Proposal A and Proposal B for the four specimens tested here. The standard deviation for the experimental to calculated moment resistance is 0.16, 0.07, and 0.08, and the average is 1.78, 1.17 and 1.15 for CAN/S16.1-M94 Clause 18.6.2, Proposal A and Proposal B, respectively. Table 6.10 shows a comparison between these three equations for all of the previously tested beam columns outlined in Table 6.3. The standard deviation of the experimental to calculated moment resistance is 0.64, 0.37, and 0.34, and the average is 1.79, 1.03 and 1.20 for CAN/S16.1-M94 Clause 18.6.2, Proposal A and Proposal B, respectively. As was discussed in Section 6.1.2.2, investigating the effectiveness of the different equations as a function of their steel section classes is a better and more significant comparison. Table 6.11 compares the previously tested specimens, along with the four tested specimens here, with respect to their respective classes. The equations of CAN/CSA-S16.1 M94 produced specimens within steel Classes 1, 2, 3, 4 (permitted by Clause 18.2 of CAN/CSA-S16.1M94) and Class 4 (as defined by Clause 11.2 of CAN/CSA-S16.1-M94), with experimental to theoretical ratios of 1.02, 1.66, 1.53, 1.95, and 2.07, respectively. For Proposal A, the experimental to theoretical ratios are 1.12, 1.21, 1.26, 1.23, 0.79, and for Proposal B, the ratios are 0.82, 1.20, 1.04, 1.25, 1.27, respectively. The experimental to theoretical ratios of Class 1 are influenced by the extremely applied moment of the two columns by Knowles and Park as discussed in Section 6.1.2.2. Table 6.12 highlights the averages and standard deviation from the three national codes and the two new proposals.

However, it appears that the additional calculations required to construct a three line interaction curve is unnecessary and the bilinear axial compression and bending moment interaction curve approach, Proposal A, works reasonably well. However, both of the two new design equations, namely Proposal A and Proposal B have been submitted for consideration by the CAN/CSA S16.1 sub-committee on composite columns for the 1999 edition of the code.

7.0 SUMMARY AND CONCLUSION

7.1 Summary

A literature review was performed to collect data on the behaviour of concrete-filled steel tubes under axial load, combined axial and bending forces, and cyclic forces. Experimental data shows that a steel tube filled with unreinforced concrete generally has a ductile behaviour; the steel tube acts to confine and strengthen the concrete core which resists axial load and in turn, the concrete core prevents premature local buckling of the steel tube allowing it to resist more bending forces. This survey of past experimental studies also revealed that while a significant number of axial compression tests have been conducted, there has been far fewer flexural cyclic tests. From the results of seven researchers who have looked at forty-nine circular columns subjected to both axial and bending forces, only twelve columns have been subjected cyclic loading. Furthermore, in these studies, the largest circular concrete-filled column subjected to cyclic loading had a diameter of 320 mm and a steel shell thickness of 6 mm. Most researchers welded the base of the steel tube to a thick steel plate (sometimes with thick base stiffeners) rather than providing a base connection representative of what could be encountered or constructed in the field. It also appears that the adequacy of the bond between the two materials during cyclic testing, and whether the concrete core becomes tri-axially confined by the steel tube, remain contentious unresolved issues.

This study tested four concrete-filled steel tubes under cyclic loading, with two of the columns having greater diameters than had been previously tested. The steel tube of the test specimens had the following sizes: HSS 324 x 6.5, HSS 324 x 9.5, HSS 406 x 6.5, and HSS 406 x 9.5, and was filled with normal strength concrete. Analytical work was performed to ensure that the test columns chosen would be representative of full-scale bridge piers found in North America. A foundation detail was designed to ensure that the full moment capacity of the composite column could be developed at its base without failure of the foundation. To achieve this, the steel tube was welded longitudinally to the steel plate, and a smaller top plate with a hole in

the middle was slipped down and welded to the top flanges of the two channels. This assembly was designed to distribute the full plastic moment from the composite column to the ends of the channels, relying on the strength of the steel alone, and was then entirely encased in a concrete foundation.

The four specimens were tested under a constant axial load and subjected to an increasing cyclic horizontal force applied at the top of the column. The columns were subjected to two or three cycles at each specified drift levels ranging from 0.25% to 7% drift. All four columns sustained drifts of 7% before failure occurred. Local buckling began to develop near the base of the columns during the cycles at 2% - 3% drift levels. These buckles grew during the following cycles. During the cycles at 7%, large transverse cracks opened near the buckles and caused a significant drop in moment carrying capacity of the column; this was defined as failure. The foundation design was successful in allowing the composite column to reach its full moment carrying capacity during the tests.

Analysis of test results showed that, in all cases, the maximum moment location of the concrete-filled columns was below the top of the concrete foundation. Using information from the strain gauges positioned on the steel tube, the maximum moment appeared to occur at the most, 100 mm into the concrete foundation. The strain gauge results indicated that the steel sections used in the foundation were subjected to insignificant stresses, and that the concrete foundation likely provided most of the resistance. The P-Δ effects on the four tested specimens were significant, and show that these should be considered in analysis.

Subsequent analytical work lead to two new proposed design equations. These produce axial-flexure interaction equations in much better agreement with the existing data than the equations for circular concrete-filled steel tubes currently used by the Canadian CAN/CSA-S16.1-M94 standard, or American AISC LRFD 1994 Specifications. A computer program was also written to investigate the behaviour of the four tested specimens. Many models were considered but with poor correlation with the data. Using an unconfined concrete model with high ductilility

(caused by the confinement of the steel tube) and a bilinear stress-strain model for the steel tube, a good representation of the force-displacement envelope for the four specimens was obtained.

7.2 Recommendations for Future Research

The results from this study have been encouraging. However, these results also show that improvements can be made in the foundation design to make it both more effective and economical. More experimental study on concrete-filled steel tubes involving cyclic tests, with larger diameter specimens, and optimized foundation design, are recommended.

7.2.1 Foundation design

The foundation detail can be improved, particularly to reduce the size of the channels and transfer plates, if the design concept of the base assembly also relies on the concrete rather than on the steel alone. This can translate into smaller required base channels, itself an important improvement to the concept. Using the conservative design approach followed for these tests, the size of the channels that would be needed to accommodate large diameter concrete-filled steel columns could become excessive, beyond the largest available rolled section sizes. A "leaner" foundation detail may also permit a simpler test set-up, and eliminate the need for local reinforcing in the concrete foundation under the actuator's reaction points. This will further simplify the foundation construction, as it will only consist of steel components fabricated off-site and placed in rectangular shoring that is filled with unreinforced concrete. Likewise, the amount of concrete cover above the top plate of the foundation in this study was dictated by the reinforcement needed in the foundation for cross-width transfer of the actuator's reaction points. New research could also seek to determine the required thickness of the concrete cover needed above the top of the steel base assembly. Since this concrete braces the top plate against buckling when pushed on by the concrete-filled steel tube, its failure could jeopardize the seismic performance of that detail, and due attention must be paid to this point.

Future tests will also require that instrumentation be placed around the area of maximum moment in the tube to more accurately capture the moment gradient along the tube's base than what was done in this study.

7.2.2 Cyclic and full-scale testing

The two new proposed design axial-flexure interaction equations appear to predict reasonably well the behaviour of the tested columns. However, additional tests on concrete-filled steel columns under axial and bending moments, especially cyclic testing, will provide more data to validate these equations. In particular, there is a need to test large-scale columns. For concrete-filled steel tubes to become commonly used in bridge piers, there will be a necessity for full-scale tests of actual-size specimens. Size-effects could be significant with respect to concrete confinement in large-diameter columns, and local buckling of steel tubes having large D/t ratios.

7.2.3 Bond strength and concrete confinement

More tests are also needed to fully understand the issues of bond and tri-axial effects. Full composite action of the steel tube and concrete core requires the development of shear at the interface between the two materials, either through friction, bond strength, or by artificial means such as shear studs. The specimens tested in this study clearly developed composite action, because their moment resistance exceeded that of the steel tube alone. However, after the tests, when a part of the steel tube was cut from the column, there was no evidence of bond between the concrete core and the steel tube. These two contradictory observations along with the discrepancy between previous researchers on this same topic illustrate a need for further research.

In some cases, tri-axial effects are seen in the concrete core. With low D/t and L/D ratios, the steel tube effectively confines the concrete core, increasing the strength of the concrete beyond its unconfined compressive resistance. However, as the size of the column increases, it is unclear whether concrete confinement will still be as effective. This study has shown that slightly larger specimens can still maintain concrete confinement. However, larger specimens must be tested to fully investigate the issue of concrete confinement.

7.3 Conclusions

In this study, four concrete-filled steel tubes were subjected to both an axial load and a cyclic bending moment. The diameter of these columns were 324 mm and 406 mm, with a D/t ratio ranging from 34 to 64. Based on the work conducted, it is concluded that:

- The ductility of all tested columns was good, all columns being able to reach drifts of 7% before a significant loss in moment capacity occurred as a result of cracks opening on the local buckles.
- The maximum flexural strength of all columns was reached at approximately 4% drift and was larger than the moment resistance of the steel tube alone.
- Flexural strength deterioration after the maximum strength was reached was slow until fracture occurred during cycling at 7% drift.
- The favourable hysteretic curves produced from the tests showed good energy dissipation for all columns.
- The foundation detail worked well, ensuring that full moment resistance capacity of the concrete-filled steel column could be developed during testing.
- Data shows that the proposed foundation detail could be significantly optimized.
- No significant bond was seen between the steel tube and the concrete core after testing had been completed.
- New design equations have been developed for combined axial and bending moments, and correlate well with the results from this test and from tests by other researchers.
- The proposed new axial-flexure interaction equations for design should be considered for implementation in the next edition of the CAN/CSA-S16.1 standard.

Overall, this study demonstrates that concrete-filled steel tubes can be a viable alternative to bridge piers in North America, up to the column sizes tested in this study. However, more knowledge will permit significantly reduce the foundation sizes, better understand details of the behaviour, and investigate whether larger columns would exhibit the same good behaviour.

REFERENCES

Alfawakiri, F. "Behavior of High Strength Concrete Filled Circular Steel Tube Beam-Columns"Thesis in partial fulfillment of the requirements for the Master of Applied Science Degree at the University of Ottawa. 1997

American Association of State Highway and Transportation Officials. (AASHTO). "AASHTO's LRFD Bridge Design Specifications " 1994

American Concrete Institution, "Standard Building Code Requirements for Reinforced Concrete," ACI 318-63

American Concrete Institution, "Standard Building Code Requirements for Reinforced Concrete," ACI 318-89

American Institute of Steel Construction. (AISC) "Specification for the Design, Fabrication and Erection of Structural Steel for Buildings." New York, 1963

American Institute of Steel Construction. (AISC) "Commentary for the Design, Fabrication and Erection of Structural Steel for Buildings." New York, 1963

American Institute of Steel Construction. (AISC) "Manual of Steel Construction, Load and Resistance Factor Design,". New York, 1986

American Institute of Steel Construction. (AISC) "Manual of Steel Construction, Load and Resistance Factor Design,". New York, 1994

Applied Technology Council "Guidelines for Cyclic Seismic Testing of Components of Steel Structures-ATC-24." 1992

Australian Standard AS4100-1990. "Steel Structures." Standards Australia, Sydney. 1990

Basu, A. K. and Hill, W. F. "A More Exact Computation of the Failure Loads of Composite Columns," *Proceedings, Institution of Civil Engineers*, Vol.40, May 1968, pp 37-60

Bauer, C. J. "New Standards for Innovative Composite Construction," *The Construction Specifier*, April 1988, pp 84-89

Beedle, L.S. et al. (Editors) "Stability of Metal Structures. A World View" 2nd ed. Structural Stability Research Council Bethlehem.Pa. 1989

Bleich, L. "Buckling Strength of Metal Structures." Engineering Societies Nonographs, 1952

Boehme, J. "Behaviour of Circular Steel tubes Filled with High Strength Concrete Subjected to Bending" *B. Sc. Thesis. Department of Civil Engineering, University of Toronto*. Toronto, Ontario. 1988

Boehme, J. "Strength of Thin-Walled Circular Steel Tubes filled with High Strength Concrete." *M.A.Sc. Thesis. Department of Civil Engineering, University of Toronto*. Toronto, Ontario. 1989

Boyd, P., Cofer, W. F., and McLean, D. I. "Seismic Performance of Steel-Encased Concrete Columns under Flexural Loading" *ACI Structural Journal.* Vol. 92, No.3 pg 355 - 364 May-June 1995.

Bradford, M.A., and Gilbert, R.I. "Nonlinear Behaviour of Slender Concrete-Filled RHS Columns" Uniciv Report No. R-284. The University of New South Wales Kensington NSW Australia June 1991

Bradford, M. "Design Strength of Slender Concrete-Filled Rectangular Steel Tubes", ACI Structural Journal Vol. 93 No. 2 March-April 1996

Bridge, R., and Webb, J. 'Thin Walled Circular Concrete Filled Steel Tubular Columns' *Composite Construction in Steel and Concrete II*, ASCE, Potosi, Missouri June 14-19, 1992.

British Standards Institution, Steel Girder Bridges, Part 3B Stresses. Part 4 "Design and Construction." BS153: Parts 3B and 4; 1958

Bruneau, M., Wilson, J. C., and Tremblay, R. 'Performance of Steel Bridges during the 1995 Hyogo-ken Nanbu (Kobe Japan) Earthquake' *Canadian Journal of Civil Engineering*. Vol. 23, No. 3, 1996

CECS 28:90. "Specification for the Design and Construction of Concrete-Filled Steel Tubular Structures." 1991 (in Chinese)

Cai, S. 'Chinese Standard for concrete-filled Tube Columns'. *Composite Construction in Steel and Concrete II*, ASCE, Potosi, Missouri June 14-19, 1992.

Canadian Institute of Steel Construction (CSIC) "Handbook of Steel Construction" 6th edition. CAN/CSA-S16.1-94 1995

Canadian Standards Association (CSA) "Design of Concrete Structures for Buildings" CAN3-A23.3-M84, 1984

Canadian Standards Association (CSA) "CSA Standard for the Design of Highway Bridges CAN/CSA-S6-88. 1988

CECS 28:90. "Specification for the Design and Construction of Concrete-Filled Steel Tubular Structures." 1991 (in Chinese)

Chapman, J.C. and Neogi, P.K. "Research on Concrete Filled Tubular Columns," Progress to October 31, 1964, Jan. 31, 1964, Nov. 30, 1965 and April 30, 1966. Engineering Structures Laboratories, Civil Engineering Department, Imperial College, London.

Computers & Structures Inc. "SAP 90 - A series of Computer Programs for the Finite Element Analysis of Structures" California, 1992

Desayi, P, and Krishnan, S., "Equation for the Stress-Strain Curve of Concrete," *ACI Journal Proc.*, Vol. 61, No. 3, March 1964.

Eurocode No. 3 "Design of Steel Structures." Part 1, edited draft, Issue 5, November, Commission of the European Communities, Brussells. 1990

Eurocode No. 4 "Design of composite Steel and Concrete Structures." Part 1, Revised draft, Issue 1, October, Commission of the European Communities, Brussells. 1990

Fukumoto, Y., and Kusama, H. 'Cyclic Bending Tests of Thin-Walled Box Beam' *Proceedings of JSCE Structural Eng./Earthquake Eng.* Vol.2, No. 1, April 1985

Furlong, R. W. 'Strength of Steel -Encased Concrete Beam-Columns'. *Journal of the Structural Division, Proceedings of the American Society of Civil Engineering.* Vol. 93 October 1967. pp113-124.

Furlong, R. W. 'Design of Steel -Encased Concrete Beam-Columns'. *Journal of the Structural Division, Proceedings of the American Society of Civil Engineering.* Vol. 96 January 1968. pp267-281.

Furlong, R.W. "AISC Column Design Logic Makes Sense for Composite Columns, Too". *AISC Engineering Journal* Vol. 13 No.1 First Quarter, 1976. pp1-7.

Furlong, R.W.; "Steel-Concrete Composite Columns"; Chapter 6 of Handbook of Composite Construction Engineering by Sabnis,G.M. (Ed.); Litton Educational Publishing, 1979, pp. 211-229

Galambos T. V.(editor) "Guide to Stability Design Criteria for Metal Structures." 4th edition, John Wiley & Sons, New York. 1988.

Gardner, N.J. and Jacobson, E.R., "Structural Behaviour of Concrete Filled Steel Tubes," *Proceedings, American Concrete Institute*, vol. 64, No. 7, July, 1967. pp 404-413

Gardner, N.J. and Jacobson, E.R., "Structural Behaviour of Concrete Filled Steel Tubes," Discussion, *Proceedings, American Concrete Institute*, Vol. 65, No. 1, Jan., 1968, pp 66-69

GBJ 68-84. "Common Unified Design Standard For Building Structures." China National Standard. China Building Industry Press, Beijing. 1984 (in Chinese)

GBJ 17-88. "Code for Design of Steel Structures" China National Standard. China Building Industry Press, Beijing. 1989 (in Chinese)

GBJ 10-89. "Code for Design of Concrete Structures" China National Standard. China Building Industry Press, Beijing. 1989 (in Chinese)

Ge, H., and Usami, T. "Development of Earthquake-Resistant Ultimate Strength Design Method for Concrete-Filled Steel Structures." *NUCE Research Report, No. 9401.* Department of Civil Engineering, Nagoya University. March 1994.

Ghosh, R. 'Strengthening of Slender Hollow Steel Columns by Filling with Concrete'. *Canadian Journal of Civil Engineering.* Vol 4 No. 2 pp 127-133. June 1977.

Goto, Y., Miyashita, S., and Iwamoto, M. "Effect of Column Base Restraint on Seismic Behavior of Bridge Pier". *STESSA 1997*, pp. 51 - 58.

Hajjar, J., and Gourley, B. 'Representation of Concrete-Filled Steel Tube Cross-Section Strength.' *Journal of Structural Engineering*, Vol.122 No. 11, Nov 1996

Hajjar, J., and Gourley, B. "A Cyclic Nonlinear Model for Concrete-Filled Tubes. I: Formulation." ASCE, Journal of Structural Engineering. Vol 123 No. 6 June 1997. Pp 736-733

Hajjar, J., Gourley, B., and Olson, M. "A Cyclic Nonlinear Model for Concrete-Filled Tubes. II: Verification." ASCE, Journal of Structural Engineering. Vol 123 No. 6 June 1997. Pp 745-754.

Hajjar, J. and Schiller, P. "A distributed Plasticity Model for Cyclic Analysis of Concrete-Filled Steel Tube Beam-Columns and Composite Frames." *Engineering Structures*, Vol. 20, Nos. 4-6, pp. 398-412. 1998

Hognestad, E. (1951) "A study of Combined Bending and Axial Load in Reinforced Concrete Members," Bulletin Series No. 399, Univ, Illinois Engineering. Experimental Station, Urban, Ill

ISO/DIS 10721, Steel Structures - materials and design (this draft was approved on 2 December 1994 as an international standard)

Itani, A. M. "Future Use of Composite Steel-concrete Columns in Highway Bridges". *ASCE, Third Quarter*, 1996

Iura, M., Kumagai, Y., and Komaki, O. "Tests on Stiffened Cylindrical Columns Subjected to Cyclic Lateral Loads", *Stability and Ductility of Steel Structures*, Nagoya, Japan, Vol. 1, pp. 245-250. July 29-31, 1997.

Iyengar, H.S.; "Recent Developments in Mixed Steel-Concrete Systems"; *ASCE*, Composite and Mixed Construction, Edited by C.W.Roeder, December 1984, pp. 173-184

Janss, J. "Composite Steel -Concrete Construction. Part 3. Tests on Concrete Filled Tubular Columns" Report published by the Centre of Scientific Research and Industrial Techniques of Metal Fabrication (CRIF), Brussels.

Japan Road Association, (JRA) "Japanese Specifications for Highway Bridges, Part V: seismic design" Tokyo, Japan 1990

Kato,B. and Kanatani, H. "Experimental Studies on Concrete Filled Steel Tubular Columns", Steel Structures Laboratory Report, Department of Architecture, Faculty of Engineering, Tokio University. October 1966

Kato, B. "Column Curves of Steel-Concrete Composite Members" *Journal of Constructional Steel Research* Vol. 39, No. 2 pp 121- 135. September 1996

Kawaguchi, J., Morino, S., Atsumi, H, and Yamamoto, S. 'Strength Deterioration Behaviour of Concrete-Filled Steel Tubular Beam-Columns'. *Composite Construction in Steel and Concrete II*, ASCE, Potosi, Missouri June 14-19, 1992.

Kawaguchi, J., Morino, S. and Machida, T. "Energy Dissipation Capacity of CFT Beam Columns Failing in Local Buckling", STESSA 1997.

Kerensky, O. and Dallard, N. "The Four-Level Interchange between M4 and M5 Motorways at Almodsbury",*Proceedings, The Institution of Civil Engineers*, Vol. 40 July, 1968. Pp295-322

Kishada, H., Akahori, K., and Ishimoto, K. "Flexural Behaviour of Concrete Filled Steel Pipe Piles with Special Reference to Concrete Strength" *Japanese Society of Steel Construction*, Vol. 18, No. 197, pp 31-42, December 1992 (in Japanese)

Kitada, T., Yoshida, Y., and Nakai, H. " Fundamental Study on Elastoplastic Behaviour of Concrete Filled Steel Short Tubular Columns." Memoirs of Faculty of Engineering, Osaka City University, Vol. 28, pp 237-253, 1987

Kitada, T., Nakai, H., Yoshikawa, M. and Higashida, T. "Experimental Study on Ultimate Strength of Concrete Filled Circular Members Subjected to Bending and Torsion" *Proceedings of Annual Conference*, Kansai Branch of JSCE. PpI-46-1-2. June 1991 (in Japanese)

Kitada, T. and Nakai, H. "Experimental Study on Ultimate Strength of Concrete Filled Square Steel Short Members Subjected to Compression or Torsion." *Proceedings of Third International conference on Steel-Concrete Composite Structures*, Fukuoka, Japan, September 1991 (to be published)

Kitada, T., Nakai, H., Saimura, Y, and Kanzaki, A. "Experimental Study on Ultimate Strength of Concrete Filled Box Members Subjected to Torsion." Proceedings of JSCE (in Japanese) (to be published as of 1992.)

Kitada, T. "Ductility and Ultimate Strength of Concrete-Filled Steel Members", Stability and Ductility of Steel Structures Under Cyclic Loading, ed. Fukumoto, U., Lee, G. CRC Press 1992. pp 139-148

Kitada, T., Nanjo, A., and Okashiro, S. "Limits States and Design Methods Considering Ductility of Steel Piers for Bridges under Seismic Load", *EASEC-5 Building for the 21st Century. The Fifth East Asia-Pacific Conference on Structural Engineering and Construction Gold Coast*, Queensland, Australia, 25-27 July 1995

Kitada, T. "Ultimate Strength and Ductility of State-of-the-Art Concrete-Filled Steel Bridge Piers in Japan". *Engineering Structures*, Vol. 20, Nos. 4-6, pp 347-354. 1998.

Kloppel, V.K. and Goder, W. "Traglastversuche mit ausbetonierten Stahlrohen and Aufstellumn einer Bemessungsformel," Der Sthahlbau, Berlin, Vol. 26, No.1, Jan 1957

Knowles , R.B. "Steel Tube Columns Infilled with Concrete," Thesis presented to the University of Canterbury, at Christchurch, New Zealand, in 1967, in partial fulfillment of the requirements for the degree of Master of Engineering

Knowles, R. B., and Park, R. 'Strength of Concrete Filled Steel Tubular Columns'. *Journal of Structural Division, Proceedings of the American Society of Civil Engineering.* Vol. No ST12 December, 1969. pp 2565 - 2586.

Knowles, R. B., and Park, R. "Axial Load Design For Concrete Filled Steel Tubes". *Journal of the Structural Division. Proceedings of the American Society of Civil Engineers.* Vol. 96 ST10. October 1970. pp 2125 - 2152

Kumar, S., and Usami, T. "A Note on the Evaluation of Damage in Steel Structures under Cyclic Loading"

Lu, Q. and Kennedy, L. "The flexural Behaviour of Concrete-Filled Hollow Structural Sections" *Canadian Journal of Civil Engineering* Vol. 21, No. 1 February 1994.

Mander,J., Priestley, M., and Park, R. "Observed Stress-Strain Behavior of Confined Concrete." *Journal of Structural Engineering*. ASCE, Vol. 114, No. 8. 1988

Ministry of Transportation of Ontario (MTO). "Ontario Highway Bridge Design Code" 1991

Morino, S., Kawaguchi, J., Yasuzaki, C., and Kanazawa, S. "Behaviour of Concrete-Filled Steel Tubular Three-Dimensional Subassemblages". *Composite Construction in Steel and Concrete II*, ASCE, Potosi, Missouri June 14-19, 1992.

Neogi, P. K., Sen, H. K., and Chapman, J. C. "Concrete-Filled Tubular Steel Columns under Eccentric Loading" *The Structural Engineer*. Vol 47, No. 5, May 1969.

Ohno, T. and Nishioka, T. "An Experimental Study on Energy Absorption Capacity of Columns in Reinforced Concrete Structures", *Proceedings of JSCE, Structural Eng./Earthquake Eng.* Vol. 1, No. 2, October 1984. Pp 23-33.

Orito, Y., Sato, T. Tanaka, N., and Watanabe, Y. "Study on the Unbonded Steel Tube Concrete Structure." *Composite Construction in Steel and Concrete*. ASCE, Henniker, New Hampshire. June 7-12, 1987

Otsuka, H., Egawa, S., Tajima, H., and Takena, K., "Failure Mechanism of Steel Rectangular Piers Under Cyclic Loading" *Stability and Ductility of Steel Structures*, Nagoya, Japan, Vol. 1, pp. 213-220. July 29-31, 1997.

Park, R. J. T., Priestly, M. J. N., and Walpole, W. R. 'Reinforced Concrete Bridge Piles." *Bulletin of the New Zealand National Society for Earthquake Engineering*, V. 16, No, 2. June 1983

Picard, A. and Beaulieu, D. "Resistance of Concrete-Filled Hollow Structural Sections" *Canadian Journal of Civil Engineering*, V. 24, pp 785-789. 1997

Popovics, S. "A Numerical Approach to the Complete Stress-Strain curve of Concrete" *Cement and Concrete Research*, Vol. 3, No. 5, pp 583-589. 1973

Preiswerk, M. "Application of New Methods of Construction on the High Mountain Transmission Line which crosses the Col du Nufenen" *The International Conference on Large Electric Systems*, 12th session, Vol.2 No. 220. 1948

Prion, H. and Boehme, J. "Beam-Column Behaviour of Steel Tubes Filled with High Strength Concrete" *Canadian Journal of Civil Engineering*, Vol. 21, No. 2, April 1994

Richart, F.E., Brandtzaeg, A., and Brown, R.L. "A Study of the Failure of Concrete Under Combined Compressive Stresses." University of Illinois Engineering Experiment Station Bulletin 185, Nov. 1929.

Roik, K.; Bergmann, R.; "Composite Columns - Design and examples for Construction"; Composite and Mixed Construction, by Roeder, C.W. (Ed.); Proceedings of US/Japan Joint Seminar, Seattle, July 1984, ASCE, 1985, pp. 267-278

Ruoquan, H. "Behaviour and Stress Strain Relation of Concrete Core", *Journal of Architectural and Civil Engineering Institute*, No. 1, 1981.

Ruoquan, H. "Behaviour of Long Concrete Filled Steel Columns". *Composite Construction in Steel and Concrete*. ASCE, Henniker, New Hampshire. June 7-12, 1987

Saatcioglu, M. Razvi, S.R. "Strength and ductility of confined concrete." *Journal of Structural Engineering-ASCE*. Vol 118, No. 6, Jun 1992. p 1590-1607

Sakino, K., and Ishibashi, H., "Experimental Studies on concrete Filled Square Steel Tubular Short Columns Subjected to Cyclic Shearing Force and Axial Force." *Transactions of the Architectural Institute of Japan* (Tokyo), No. 353, July 1985, pp 81-89.

Sakino, K., and Tomii, M. "Hysteretic Behaviour of Concrete Filled Square Shell Tubular Beam-Columns Failed in Flexure." *Transactions of the Japan Concrete Institute* (Tokyo), V.3, 1981, pp. 439-446.

Sakurai, T., Kato, K., Uno, Y, Chu, K., and Kusama, H. "Experimental Study on Strength of Concrete Filled Steel Square Beams under Alternating Bending." *Journal of Structural Engineering*, (Japan Society of civil engineers), Vol. 34A, pp 265-274, March 1988 (in Japanese)

Salani, H.J. and Sims, J.R. "Behaviour of Mortar Filled Steel Tubes in Compression." *Proceedings, American Concrete Institute*, Vol. 61, No. 10, Oct. 1964, pp 1271-1283

Schneider, S. P. "Axially Loaded Concrete-Filled Steel Tubes" *Journal of Structural Engineering*, October 1998, pp 1125-1138.

Sen, H.K. "Triaxial Effects in Concrete-Filled Tubular Steel Columns." PhD thesis, University of London, July 1969.

Shakir-Khalil, H., and Zeghiche, J. "Experimental Behaviour of Concrete-Filled Rolled Rectangular Hollow-Section Columns" *The Structural Engineer*. Vol. 67 No. 19, 3 October 1989.

Shakir-Khalil, H. "Bond Strength in Hollow Concrete-Filled Steel Hollow Sections." Proceddings, International Conference on Steel and Aluminum Structures, Composite Steel Structures, Singapore, pp 157-168. 1991

Shakir-Khalil, H. "Push-out Tests on Concrete-Filled Steel Hollow Sections." Tubular Structures, 4th International Symposium, Delft, pp 402-411 1992.

Shakir-Khalil, H., and Zeghiche, J. "Further Tests on Concrete-Filled Rectangular Hollow-Section Columns" *The Structural Engineer*. Vol. 67 No. 19, 3 October 1990.

Shams, M. and Saadeghvaziri, M. "State of the Art of Concrete-Filled Steel Tubular Columns", ACI Structural Journal. Vol. 94, No. 5 September – October 1997.

Standards Association of Australia. (SAA) "Rules for the Use of Normal Reinforced Concrete Buildings." CA2-1963

Tarics, A. G. "Concrete-Filled Steel Columns for Multistory Construction," *Modern Steel Construction*. Vol. 12, AISC 1972, pp 12-15

Tomii, M. and Sakino, K. "A State of Art Report on concrete Filled Steel Tube Structures -- Part 1. Elasto-Plastic Behaviour of Members --, Concrete Journal , Vol.13, No. 2, pp 26-40, February 1974 (in Japanese)

Usami, T., Mizutani, S., Aoki, T., and Yoshito, I. "Steel and Concrete-Filled Steel Compression Members under Cyclic Loading" Stability and Ductility of Steel Structures Under Cyclic Loading. ed. Fukumoto, Y., and Lee, G. CRC Press, Inc. 1992. pg 123-138

Viest, I. M., Colaco, J. P., Furlong, R. W., Griffis, L. G., Leon, R. T., and Wyllie, L. A. Jr. "Composite Construction Design for Buildings" Co-published by the American Society of Civil Engineers and McGraw-Hill. New York. 1997

Vogeli, R. "Steel Tube Pylons Filled with Concrete", *The International Conference on Large Electric Systems*, 12th session, Vol.2 No. 221. 1948

Vogeli, R. "New Transmission Lines with Concrete Filled Steel Tube Towers", *The International Conference on Large Electric Systems*, Vol.2 No. 223. June-July 1950

Wang, Y. and Moore, D. "A Design Method for Concrete-Filled, Hollow Section, Composite Columns" *The Structural Engineer*, Vol. 75 No. 21 November 1997.

Watanabe, E., Usami, T., and Haseqagwa, A. "Strength and Design of Steel Stiffened Plates - A Literature Review of Japanese Contributions" In Inelastic Instability of Steel Structures and Structural Elements. Edited by Y. Fujita and T.V. Galamabos. U.S. - Japan Seminar, Tokyo, Japan. pp 225-236. 1981

Watanabe, E., Emi, S., Isami, H., and Yamanouchi, T. "An Experimental Study on Strength of Thin-Walled Steel Box Beam-Columns Under Repetitive Bending", *Japan Society of Civil Engineers (Proc. Of JSCE No.392/I-9), Structural eng. /Earthquake Eng.* Vol.5 No.1, 21s-29s, April 1988.

Watanabe, E., Sugiura, K., Maekawa, Y., Tomita, M. and Nishibayashi, M. "Pseudo-Dynamic Test on Steel Bridge Piers and Seismic Damage Assessment", *EASEC-5 Building for the 21st Century. The Fifth East Asia-Pacific Conference on Structural Engineering and Construction Gold Coast*, Queensland, Australia, 25-27 July 1995

Webb, J. and Peyton J. "Composite Concrete Filled Steel Tube Columns" *Proceedings, 2nd National Structures Conference*, The Institution of Engineers, Austrailia, Adelaide, pp. 181-185. 1990

Zhong, S. and Zhang, S. 'A New Method From China to Determine Load-Carrying Capacity for CFST Members' *Composite Construction in Steel and Concrete II*, ASCE, Potosi, Missouri June 14-19, 1992.

TABLES

Table 2.1: Concrete-filled circular columns as compared to Kato (1996)

No.	Diameter (mm)	t (mm)	kL (cm)	σ_y (MPa)	f_c (MPa)	$\bar{\lambda}$	N_{cal} (kN)	N_{test} (kN)	$\frac{N_{test}}{N_{cal}}$
CFT Working Group (1993)									
1	165.2	4.1	66.1	353	40.9	0.178	1599	1562	0.976861
2	165.2	4.1	132.2	353	40.9	0.357	1516	1412	0.931398
3	165.2	4.1	198.2	353	40.9	0.535	1397	1372	0.982105
4	165.2	4.1	297.4	353	40.9	0.802	1171	1147	0.979505
5	165.2	4.1	396.5	353	40.9	1.069	902	1019	1.129712
6	165.2	4.1	495.6	353	40.9	1.337	675	782	1.158519
Masuo, K. et al. (1991)									
7	190.7	5.5	115.0	505	48.3	0.3	2821	3148	1.115916
8	190.7	5.5	345.0	505	48.3	0.901	2101	2133	1.015231
9	267.4	6.4	160.0	461	48.3	0.292	4966	5188	1.044704
10	267.4	6.4	480.0	461	48.3	0.876	3568	3903	1.09389
11	190.7	5.5	115.0	505	55.9	0.307	2987	3063	1.025444
12	190.7	5.5	230.0	505	55.9	0.613	2532	2612	1.031596
13	190.7	5.5	345.0	505	55.9	0.92	1889	2059	1.089995
14	267.4	6.4	160.0	461	55.9	0.299	5280	5181	0.98125
15	267.4	6.4	320.0	461	55.9	0.598	4451	4534	1.018647
16	267.4	6.4	480.0	461	53.5	0.89	3323	3626	1.091183
Sasaki, R (1984)									
17	114.3	3.1	67.0	348	53.5	0.272	896	898	1.002232
18	114.3	3.1	67.0	348	53.5	0.272	896	904	1.008929
19	114.3	3.1	67.0	348	53.5	0.272	896	910	1.015625
20	114.3	3.1	102.0	348	53.4	0.414	842	888	1.054632
21	114.3	3.1	102.0	348	53.4	0.414	842	849	1.008314
22	114.3	3.1	102.0	348	53.4	0.414	842	845	1.003563
23	114.3	3.1	133.5	348	56.0	0.547	809	784	0.969098
24	114.3	3.1	133.5	348	56.0	0.547	809	773	0.955501
25	114.3	3.1	133.5	348	56.0	0.547	809	794	0.981459
26	114.3	3.1	204.0	348	57.5	0.841	643	617	0.959565
27	114.3	3.1	204.0	348	57.5	0.841	643	649	1.009331
28	114.3	3.1	204.0	348	57.5	0.841	643	688	1.069984
29	114.3	3.1	270.0	340	57.5	1.107	471	516	1.095541
30	114.3	3.1	270.0	340	57.5	1.107	471	537	1.140127
31	114.3	3.1	270.0	340	57.5	1.107	471	536	1.138004
32	114.3	3.1	337.0	340	63.1	1.409	345	401	1.162319
33	114.3	3.1	337.0	340	63.1	1.409	345	362	1.049275
34	114.3	3.1	337.0	340	63.1	1.409	345	379	1.098551
35	114.3	3.1	372.0	340	55.1	1.513	286	320	1.118881
36	114.3	3.1	372.0	340	55.1	1.513	286	293	1.024476
37	114.3	3.1	372.0	340	55.1	1.513	286	305	1.066434

Table 2.2: Axial load data for circular columns [Gardner and Jacobson (1967)]

Specimen #	Diameter (mm)	Thickness (mm)	Length (mm)	f_y (MPa)	f_c (MPa)	D/t	Yield Strength (MPa)	Ultimate Strength (MPa)
Stub columns								
3	100.90	3.05	202	605	13	33	1054	1112
4	100.90	3.05	202	605	31	33	1068	1068
8	119.88	4.03	239	452	34	30	1201	1201
9	119.85	4.06	239	452	30	30	1157	1201
10	119.88	4.06	239	452	26	30	1097	1112
13	151.43	3.15	302	415	21	48	1065	1201
14	151.40	3.12	302	415	23	48	1144	1201
15	151.38	4.89	302	633	42	31	—	2909
16	151.35	4.86	302	633	43	31	—	2914
19	75.83	1.69	151	363	25	45	343	356
22	75.85	1.66	151	363	41	46	—	435
23	75.83	1.69	151	363	26	45	—	372
Long columns								
1	100.88	3.05	1512	605	34		none	818
2	100.93	3.07	1512	605	31		none	801
5	119.7	4.06	1042	452	34		1060	1157
6	119.88	4.06	1042	452	30		981	1093
7	119.88	4.06	1042	452	26		926	950
11	151.40	3.12	1663	415	21		916	839
12	151.50	3.12	1663	415	23		879	881
18	75.88	1.69	1512	363	25		none	245
21	75.83	1.71	605	363	41		—	411
22	75.88	1.71	605	363	26		—	330

Table 2.3: Axial load data for circular columns [Furlong (1967)]

Diameter inches	t inches	F_y kips/in^2	A_s in^2	f_c' kips/in^2	A_c in^2	P_o kips	P_u kips	$\frac{P_u}{P_o}$
4.5	0.125	60.0	1.73	4.20	14.17	163.4	160	0.979
4.5	0.125	60.0	1.73	4.20	14.17	163.4	170	1.040
6.0	0.061	48.0	1.18	3.05	27.10	134.9	153.4	1.137
6.0	0.061	48.0	1.18	3.75	27.10	152.8	162.2	1.062
6.0	0.061	48.0	1.18	3.75	27.10	152.8	164.8	1.079
5.0	0.095	42.0	1.40	5.10	17.91	142.1	141	0.992
5.0	0.095	42.0	1.40	5.10	17.91	142.1	140	0.985
5.0	0.095	42.0	1.40	5.10	17.91	142.1	148	1.042

Table 2.4: Bending plus axial load data for circular columns [Furlong (1967)]

Diameter inches	t inches	F_y kips/in^2	A_s in^2	f_c' kips/in^2	A_c in^2	P_o kips	M_o kips-in	P_u kips	M_u kips-in	$\frac{P_u}{P_o}$	$\frac{M_u}{M_o}$
4.50	0.125	60.0	1.73	4.20	14.17	163.4	143	100	100	0.612	0.699
4.50	0.125	60.0	1.73	4.20	14.17	163.4	143	90	106	0.551	0.741
4.50	0.125	60.0	1.73	4.20	14.17	163.4	143	75	131	0.459	0.916
4.50	0.125	60.0	1.73	4.20	14.17	163.4	143	50	141	0.306	0.986
4.50	0.125	60.0	1.73	4.20	14.17	163.4	143	25	144	0.153	1.007
6.00	0.061	48.0	1.18	3.75	27.10	152.8	100.8	127.6	88	0.835	0.873
6.00	0.061	48.0	1.18	3.75	27.10	152.8	100.8	94.8	157.6	0.620	1.563
6.00	0.061	48.0	1.18	3.75	27.10	152.8	100.8	64.3	152.7	0.421	1.515
6.00	0.061	48.0	1.18	3.05	27.10	134.9	100.8	30.6	143.4	0.227	1.423
6.00	0.061	48.0	1.18	3.05	27.10	134.9	100.8	30.4	133.1	0.225	1.320
5.00	0.095	42.0	1.40	5.10	17.90	142.1	96.6	127.8	78.0	0.899	0.807
5.00	0.095	42.0	1.40	5.10	17.90	142.1	96.6	120.0	112.0	0.844	1.159
5.00	0.095	42.0	1.40	5.10	17.90	142.1	96.6	90.0	141.0	0.633	1.460
5.00	0.095	42.0	1.40	5.10	17.90	142.1	96.6	19.0	140.0	0.134	1.449
5.00	0.095	42.0	1.40	5.10	17.90	142.1	96.6	18.5	126.4	0.130	1.308
5.00	0.095	42.0	1.40	5.10	17.90	142.1	96.6	77.6	140.5	0.546	1.454
5.00	0.095	42.0	1.40	5.10	17.90	142.1	96.6	68.8	150.5	0.484	1.558
5.00	0.095	42.0	1.40	5.10	17.90	142.1	96.6	60.0	156.0	0.422	1.615
5.00	0.095	42.0	1.40	5.10	17.90	142.1	96.6	58.6	155.5	0.412	1.610
5.00	0.095	42.0	1.40	5.10	17.90	142.1	96.6	39.3	145.6	0.277	1.507
5.00	0.095	42.0	1.40	5.10	17.90	142.1	96.6	20.0	140.8	0.141	1.458
5.00	0.095	42.0	1.40	5.10	17.90	142.1	96.6	9.8	130.0	0.069	1.346

Table 2.5: Experimental maximum loads of various specimens [Neogi et al. (1969)]

Specimen	L in.	D in.	t in.	e in.	δ_i in.	σ_1 tonf/in^2	f_{cu} lbf/in$_2$	$\frac{L}{D}$	$\frac{D}{t}$	$\frac{e}{D}$	P_T (tons)	$\frac{P_T}{P_{exact}}$	$\frac{P_{cos}}{P_{exact}}$	$\frac{P_{cos}}{P_{empiv}}$
M1	131	6.67	0.201	1.875	—	20.0	8060	19.64	33.18	0.281	62.4	1.027	0.973	1.659
M2	131	6.66	0.207	1.500	—	20.0	7840	19.67	32.17	0.225	70.4	1.033	0.973	1.636
M3	131	6.65	0.223	1.875	—	19.1	6160	19.67	29.82	0.282	60.2	1.030	0.974	1.501
M4	131	6.63	0.258	1.875	—	19.3	5510	19.76	25.70	0.283	62.74	1.015	0.974	1.384
M5	131	6.66	0.283	1.875	—	20.2	4640	19.67	23.53	0.282	65.5	1.000	0.977	1.293
M6	131	6.66	0.287	1.500	—	20.2	4810	19.67	23.21	0.225	74.1	1.010	0.977	1.301
M7	130	6.65	0.347	1.875	—	20.9	4790	19.54	19.16	0.282	75.0	0.984	0.975	1.230
M8	131	5.52	0.378	1.250	0.224	17.7	6030	23.73	14.60	0.226	55.0	0.993	0.957	1.207
M9	131	5.52	0.384	1.250	0.147	17.7	3920	23.73	14.38	0.226	55.0	1.014	0.963	1.147
M10	131	5.55	0.197	1.250	0.040	19.0	6180	23.60	28.17	0.225	41.8	1.021	0.966	1.431
C5	55.5	5.01	0.072	0.250	0.019	12.5	12100	11.08	69.58	0.05	96.8	1.230	0.987	3.885
C6	55.5	5.00	0.112	0.250	0.015	17.5	12100	11.10	44.64	0.05	104.9	1.160	0.960	2.487
C7	67.5	5.00	0.068	0.250	0.022	12.5	10890	13.50	73.53	0.05	85.4	1.300	0.986	3.566
C8	67.5	5.00	0.119	0.250	0.022	17.5	10890	13.50	42.02	0.05	80.7	0.989	0.973	2.233
C9	80.0	5.01	0.070	0.625	—	12.5	7280	15.97	71.57	0.125	35.5	0.923	0.977	2.112
C10	80.0	5.00	0.128	0.625	—	17.5	7280	16.00	39.06	0.125	52.8	1.015	0.979	1.725
C11	80.0	5.00	0.064	0.875	—	12.5	7730	16.00	78.13	0.175	34.5	1.051	0.966	2.142
C12	80.0	5.00	0.128	0.875	—	17.5	7730	16.00	39.06	0.175	50.5	1.068	0.977	1.711
Kato and Kanatani (1966)														
AC7	216.60	12.52	0.276	2.754				17.3	45.42	0.220	231	0.932	0.957	2.047
AC10	216.60	12.52	0.276	3.931				17.3	45.42	0.314	191	0.926	0.959	1.968
AC20	216.60	12.52	0.276	7.863				17.3	45.42	0.628	120	0.983	0.953	1.672
AB20	235.38	12.52	0.276	7.863				18.8	45.42	0.628	120	1.024	0.951	1.651
BC7	111.43	12.52	0.276	2.754				8.9	45.42	0.220	313	0.983	0.980	2.308
BC10	110.18	12.52	0.276	3.931				8.8	45.42	0.314	254	0.963	0.974	2.194
BC20	110.18	12.52	0.276	7.863				8.8	45.42	0.628	149	1.000	0.973	1.788
BB20	130.21	12.52	0.276	7.863				10.4	45.42	0.628	153	1.061	0.966	1.766
Janss														
1								20.4	36.4	0.0250	193			1.023
2								15.5	36.4	0.0144	232			1.001
3								10.4	36.4	0.0065	271			1.140
4								4.4	36.4	0.0011	310			1.221
5								4.4	36.4	0.0011	319			1.265
6								4.4	36.4	0.0011	23			1.273
8/1								45.5	25.3	0.0105	17			1.355
8/2								45.5	25.3	0.0105	16			1.046
8/3								45.5	25.3	0.0105	26			0.953
9/1								30.2	25.3	0.0105	31			0.902
9/2								30.2	25.3	0.0105	32			0.920
9/3								30.2	25.3	0.0105	32			0.925
10/1								20.4	25.3	0.0105	41			0.894
10/2								20.4	25.3	0.0105	46			0.994
10/3								20.4	25.3	0.0105	46			0.998
11/1								15.4	25.3	0.0105	50			0.996
11/2								15.4	25.3	0.0105	50			1.000
11/3								15.4	25.3	0.0105	56			1.132
12/1								10.4	25.3	0.0105	59			1.136

M2	131	6.66	0.207	1.500	—	20.0	7840	19.67	32.17	0.225	70.4	1.033	0.973	1.636
12/2								10.4	25.3	0.0105	57			1.126
12/3								10.4	25.3	0.0105	60			1.165
13/1								5.3	25.3	0.0015	72			1.230
13/2								5.3	25.3	0.0015	71			1.270
13/3								5.3	25.3	0.0015	75			1.344

Table 2.6: Failure load of axially loaded circular specimens [Knowles and Park (1969)]

Tube Size	kL inches	Steel tube		Concrete Core		Theoretical	Experimental	Experimental / Theoretical
		Slenderness ratio	f_{su} lb/in^2	Slenderness ratio	f_{cu} lb/in^2	$f_{su}+f_{cu}$ lb/in^2	Max. Stress lb/in^2	
Experimental failure loads of axially loaded concrete-filled steel tubes								
3.50 in OD	68	58.6	111000	89.5	23900	134900	138200	1.022
t = 0.23 in	56	48.3	116000	73.7	30800	146800	160000	1.096
	44	37.9	123900	57.9	36100	160000	160800	1.004
	32	27.6	128500	42.2	41300	169800	206500	1.217
	20	17.25	134300	26.35	42400	176700	223000	1.263
	20	17.25	134300	26.35	42400	176700	200000	1.132
3.25 in OD	68	60.2	27700	86.6	28200	55900	50500	0.902
t = 0.055 in	56	49.6	30350	71.4	33800	64150	66200	1.031
	44	38.9	33100	56.1	39400	72500	80000	1.103
	32	28.3	35800	40.7	44300	80100	90000	1.123
	20	17.7	38650	25.45	45700	84050	110000	1.292
	10	8.85	41700	12.73	45700	87400	119200	1.363
Experimental failure loads of axially loaded hollow steel tubes								
3.50 in OD	68	58.6	47000	——	——	——	46200	0.983
t = 0.23 in	56	48.3	49500	——	——	——	51000	1.030
	44	37.9	52500	——	——	——	51600	0.983
	32	27.6	54500	——	——	——	63400	1.163
	20	17.25	57000	——	——	——	69900	1.226
	9	7.76	77000	——	——	——	81300	1.053
3.25 in OD	68	60.2	50200	——	——	——	53100	1.058
t = 0.055 in	56	49.6	55000	——	——	——	53800	0.978
	44	38.9	60000	——	——	——	61100	1.019
	32	28.3	649000	——	——	——	65000	1.002
	20	17.7	70000	——	——	——	71200	1.017
	9	7.96	75800	——	——	——	77400	1.021
	9	7.96	75800	——	——	——	76800	1.013

Table 2.7: Failure load of eccentrically loaded specimens [Knowles and Park (1969)]

Tube	L inches	P_u pounds	P_o pounds	$\frac{P_u}{P_o}$	e_i inches	e inches	$M_u = P_u e$, pounds·inch	M_o pounds·inch	$\frac{M_u}{M_o}$	$\frac{P_u}{P_o} + \frac{M_u}{M_o}$
Experimental failure loads of eccentrically loaded concrete-filled steel tubes										
3.50 in. OD t = 0.23 in	32	124600	206500	0.604	0.30	0.76	94700	144300	0.656	1.260
	56	105450	160000	0.660	0.30	0.66	69600	144300	0.482	1.142
	32	43800	206500	0.212	1.00	1.30	57000	144300	0.395	0.607
	44	43000	160800	0.268	1.00	1.20	51600	144300	0.357	0.625
3.25 in. OD	32	37750	90000	0.753	0.30	0.77	52200	55000	0.950	1.703
t = 0.055 in.	32	20000	90000	0.222	1.00	1.15	23000	55000	0.418	0.640
Experimental failure loads of eccentrically loaded hollow steel tubes										
3.50 in. OD t = 0.23 in.	32	90900	149250	0.609	0.30	0.75	68200	143000	0.477	0.086
	56	80100	120300	0.666	0.30	0.62	49700	143000	0.348	1.014
	32	39500	149250	0.265	1.00	1.45	57300	143000	0.401	0.666
	44	39325	121800	0.323	1.00	1.25	49200	143000	0.344	0.667
3.25 in. OD t = 0.055 in	32	28300	35800	0.790	0.30	0.50	14150	39350	0.390	1.180
	32	15000	35800	0.419	1.00	1.38	20700	39350	0.527	0.946

Table 2.8: Axially loaded concrete-filled steel tube specimens [Knowles and Park (1970)]

Test Number	D inches	t inches	kL inches	f_c' lb/in^2	$E_s \times 10^6$ lb/in^2	f_y lb/in^2	$\frac{kL}{r_c}$	P_{uc} kips	P_{cu} kips	P_u kips	P_{test}, kips	$\frac{P_{test}}{P_u}$
Kloppel and Goder (1957)												
7	3.740	0.492	55.91	2940	29.87	39830	81.14	184.3	13.39	197.7	212.9	1.077
8	3.740	0.502	55.91	2940	29.87	39540	81.73	186.2	13.13	199.3	210.8	1.058
9	3.740	0.488	55.91	2940	29.87	39540	89.91	181.9	13.50	195.4	203.9	1.044
10	3.740	0.496	33.86	2940	29.87	39830	49.28	195.6	16.55	212.2	228.8	1.078
11	3.740	0.500	33.86	2940	29.87	39540	49.43	195.5	16.45	212	226.6	1.069
12	3.740	0.500	33.86	2940	29.87	39540	49.43	195.5	16.45	212	232.4	1.096
13	3.740	0.504	77.95	2940	29.87	40390	114.4	174.8	9.30	184.1	199.3	1.083
14	3.740	0.492	77.95	2940	29.87	39970	113.1	170.1	9.57	179.7	203.9	1.135
15	3.740	0.496	77.95	2940	29.87	40540	113.5	173.1	9.58	182.7	206.1	1.128
41	3.740	0.144	33.86	3620	29.87	47360	39.22	74.71	33.01	107.7	147.5	1.369
42	3.740	0.145	33.86	3620	29.87	56040	39.25	88.62	32.96	121.6	154.3	1.269
43	3.740	0.134	33.86	3620	29.87	48640	39.01	71.83	33.39	105.2	147.5	1.402
44	3.740	0.152	55.91	3620	29.87	47360	65.06	74.64	28.59	103.2	127.4	1.234
45	3.740	0.154	55.91	3620	29.87	56040	65.14	88.01	28.50	116.5	136.2	1.169
46	3.740	0.141	55.91	3620	29.87	48640	64.68	71.55	29.02	100.6	129.4	1.287
47	3.740	0.148	77.95	3620	29.87	47360	90.53	67.17	22.34	89.51	120.6	1.347
48	3.740	0.149	77.95	3620	29.87	46040	90.60	77.46	22.29	99.75	127.2	1.275
49	3.740	0.138	77.95	3620	29.87	48640	90.00	64.15	22.74	86.89	109.6	1.261
63	8.504	0.160	87.40	3320	29.87	41250	42.72	167.5	169.1	336.6	230.0	0.683
64	8.504	0.162	87.40	3320	29.87	43380	42.74	178.0	168.9	346.9	412.4	1.189
65	8.504	0.159	87.40	4320	29.87	41820	42.71	168.9	218.1	387	514.6	1.33
66	8.504	0.162	87.40	4320	29.87	41530	42.74	170.7	217.7	388.4	503.3	1.296
69	8.504	0.238	87.40	3320	29.87	56470	43.55	334.3	162.3	496.6	553.4	1.114
70	8.504	0.235	87.40	3320	29.87	48040	43.52	333.7	162.5	496.2	544.3	1.097
71	8.504	0.256	87.40	4320	29.87	42810	43.74	274.6	207.0	481.6	630.6	1.309
72	8.504	0.248	87.40	4320	29.87	48740	43.66	361.0	207.9	568.9	659.2	1.159
73	3.740	0.152	77.95	3490	29.87	48210	90.72	69.70	21.63	91.33	112.0	1.226
74	3.740	0.134	77.95	3490	29.87	48930	89.80	62.71	22.30	85.01	106.3	1.25
75	3.740	0.141	77.95	3490	29.87	51490	90.18	68.81	20.25	89.06	106.3	1.194
76	3.740	0.147	77.95	3490	29.87	47360	90.49	66.83	20.05	86.88	92.81	1.068
83	4.764	0.144	41.34	3060	29.87	42810	36.94	87.22	47.33	134.6	156.3	1.162
84	4.764	0.147	41.34	3060	29.87	47510	36.99	98.58	47.15	145.7	167.8	1.151
85	4.764	0.148	41.34	3510	29.87	44660	37.00	93.30	53.95	147.3	188.1	1.277
86	4.764	0.157	41.34	3510	29.87	47360	37.17	105.1	53.46	158.6	194.9	1.229
89	4.764	0.221	41.34	3060	29.87	49920	38.26	153.0	44.01	197	224.4	1.139
90	4.764	0.213	41.34	3060	29.87	49780	38.13	147.6	44.33	191.9	228.8	1.192
91	4.764	0.215	41.34	3510	29.87	47930	38.16	143.5	50.60	194.1	247.1	1.273
92	4.764	0.219	41.34	3510	29.87	46650	38.23	142.2	50.41	192.6	242.5	1.259
95	4.764	0.146	90.95	3060	29.87	42810	81.35	80.51	36.40	116.9	144.0	1.232
96	4.764	0.148	90.95	3060	29.87	47510	81.42	89.23	36.31	125.5	141.5	1.127
97	4.764	0.146	90.95	3510	29.87	44660	81.35	83.52	40.60	124.1	156.3	1.259
98	4.764	0.152	90.95	3510	29.87	47360	81.58	91.49	40.28	131.8	169.8	1.289
101	4.764	0.224	90.95	3060	29.87	49920	84.28	137.6	32.96	170.6	176.8	1.037
102	4.764	0.216	90.95	3060	29.87	49780	93.98	133.0	33.29	166.3	183.4	1.103
103	4.764	0.222	90.95	3510	29.87	47930	64.20	131.9	36.80	168.7	196.4	1.164
104	4.764	0.214	90.95	3510	29.87	46650	83.91	124.8	37.17	162	194.5	1.201
Salani and Sims (1964)												
30F	2.00	0.065	42	4040	29.5	76000	89.84	22.65	7.205	29.86	27.10	0.908
42F	3.00	0.065	42	3950	29.5	76000	58.54	40.68	22.62	63.3	72.00	1.137

9	3.740	0.488	55.91	2940	29.87	39540	89.91	181.9	13.50	195.4	203.9	1.044
49F	1.00	0.035	42	4035	29.5	76000	180.65	2.05	0.650	2.7	3.54	1.311
50F	1.00	0.035	42	4035	29.5	76000	180.65	2.05	0.650	2.7	3.49	1.293
51F	1.50	0.109	42	4035	29.5	76000	131.05	19.08	2.082	21.16	25.40	1.2
52F	1.50	0.109	42	4035	29.5	76000	131.05	19.08	2.082	21.16	24.00	1.134
71F	2.75	0.049	42	4040	29.5	76000	63.35	27.61	18.99	46.6	51.90	1.114
Gardner & Jacobson (1967)												
1	4.003	0.121	30.00	4950	30.03	87760	63.81	111.2	45.31	156.5	184.0	1.176
2	4.005	0.122	60.00	4520	30.03	87760	63.81	112.2	41.93	154.1	180.0	1.168
5	4.750	0.161	41.34	4990	217.78	65500	37.34	146.1	74.62	220.7	260.0	1.178
6	4.757	0.161	41.34	4290	27.78	65500	37.29	146.4	64.62	211	245.6	1.164
7	4.757	0.161	41.34	3760	27.78	65500	37.29	146.4	56.81	203.2	213.5	1.051
11	6.008	0.124	66.00	3030	29.50	60210	45.83	130.8	75.87	206.7	211.0	1.021
12	6.012	0.124	66.00	3030	29.50	60210	45.80	130.9	83.68	214.6	198.0	0.923
18	3.011	0.067	60.00	3620	28.68	52690	83.42	27.60	16.85	44.45	55.00	1.237
20	3.009	0.068	24.00	5930	28.68	52690	33.41	32.29	37.59	69.88	92.50	1.324
21	3.011	0.068	23.99	3760	28.68	52690	33.39	32.31	24.06	56.37	74.25	1.317
Chapman and Neogi (1966)												
A1	14.00	0.440	74.0	5520	29.0	51500	21.95	955.5	743.3	1699	2576.0	1.516
A4	14.00	0.440	74.0	4760	29.0	51500	21.95	955.5	639.9	1595	2408.0	1.509
A5	14.00	0.186	74.0	3040	29.0	40100	21.13	321.2	442.6	763.8	790.7	1.035
A6	14.00	0.314	82.0	3400	29.0	51500	21.54	688.4	476.4	1165	1671.0	1.435
B1	5.011	0.064	28.0	9600	29.0	53750	19.66	52.99	179.0	232	289.0	1.246
B1X	5.011	0.064	28.0	9600	29.0	47700	19.66	47.0	179.0	226	289.0	1.279
B2	5.002	0.116	28.0	9600	29.0	53750	20.05	95.20	172.0	267.2	293.5	1.098
B2X	5.002	0.116	28.0	9600	29.0	47700	20.05	84.57	172.0	256.6	293.5	1.144
DF1	5.514	0.381	16.0	4660	29.0	38500	13.47	235.9	82.57	318.5	663.0	2.082
DF1X	5.514	0.381	16.0	4660	29.0	39000	13.47	238.9	82.57	321.5	663.0	2.062
DF2	5.527	0.194	16.0	4740	29.0	41900	12.45	135.8	98.25	234.1	410.0	1.752
DF2X	5.527	0.194	16.0	4740	29.0	43200	12.45	140.0	98.25	238.3	410.0	1.721
SC1	6.621	0.178	32.0	4560	29.0	43200	20.43	154.5	140.2	294.7	451.0	1.53
SC2	6.628	0.178	32.0	6200	29.0	43200	20.41	154.7	192.7	347.4	502.0	1.445
SC3	6.621	0.178	32.0	6260	29.0	43200	20.43	154.5	192.3	346.8	475.0	1.37
SC4	6.625	0.176	32.0	3340	29.0	43200	20.40	152.9	103.0	255.9	392.0	1.532

Table 2.9: Experimental results for circular columns [Prion and Boehme (1994)]

Specimen #	Type	length (mm)	L/D (D=152 mm)	F_y (MPa)	f_c' (MPa)	Axial Load P (kN)		Moment (kNm)			P_{exp} / P_u	M_{exp} / M_u	M_{exp} / M_{uo}
						Predicted P_u	Experimental P_{exp}	Predicted		Experimental			
								M_{uo}	M_u				
B1	A1	900	5.92	270	73	1483	1550	—	—	—	1.045	—	—
B3	A1	900	5.92	270	73	1483	1458	—	—	—	0.983	—	—
B5	A1	500	3.29	270	73	1483	1548	—	—	—	1.044	—	—
B7	A1	500	3.29	270	73	1483	1448	—	—	—	0.977	—	—
BP9	A1	660	4.34	328	85	1737	1863	—	—	—	1.072	—	—
BP10	A1	660	4.34	328	85	1737	1895	—	—	—	1.091	—	—
B2	A2	900	5.92	270	75	1517	1458	—	—	—	0.961	—	—
B4	A2	900	5.92	270	75	1517	1548	—	—	—	1.02	—	—
B6	A2	500	3.29	270	75	1517	1548	—	—	—	1.02	—	—
B8	A2	500	3.29	270	75	1517	1587	—	—	—	1.046	—	—
BP16	B2	2120	13.95	328	92	1867	—	16.5		21.0			1.270
B11	C1	2120	13.95	328	92	1859	470	16.5	30.3	29.7	0.253	0.98	1.8
B12	C1	2120	13.95	328	92	1859	570	16.5	30.9	32.1	0.307	1.039	1.9455
B13	C1	2120	13.95	328	92	1859	670	16.5	30.9	28.5	0.36	0.922	1.7273
B14	C1	2120	13.95	328	92	1859	820	16.5	30.1	29.2	0.441	0.97	1.7697
B15	C1	2120	13.95	328	92	1859	970	16.5	27.7	30.5	0.522	1.101	1.8485
B17	C1	2120	13.95	328	92	1859	270	16.5	26.7	30.1	0.145	1.127	1.8242
BP18	C2	2120	13.95	328	92	1859	270	16.5	26.7	30.8	0.145	1.154	1.8667
BP19	C2	2120	13.95	328	92	1859	670	16.5	30.9	34.8	0.36	1.126	2.1091
BP20	D	1071	7.05	328	92	1859	1273	16.5	20.1	21.4	0.685	1.065	1.297
BP21	D	1071	7.05	328	92	1859	1451	16.5	14.7	13.8	0.781	0.939	0.8364
BP22	D	1071	7.05	328	92	1859	1309	16.5	19.1	15.9	0.704	0.83	0.9636

Table 2.10: Properties of tested specimens [Schneider (1998)]

Shape	Outer nominal diameter (mm)	Actual dimensions (mm)	Actual wall thickness (mm)	D/t ratio	L/D ratio	Steel Properties			Concrete Properties		
						A_s (mm²)	F_y (MPa)	E_s (MPa)	A_c (mm²)	F_y (MPa)	E_c (MPa)
C1	140	140.8	3.00	47.0	4.3	1297	285	189475	14258	28.2	25599
C2	140	141.4	6.50	21.7	4.3	2755	313	206011	12968	23.8	23528
C3	140	140.0	6.68	21.0	4.4	2794	537	205322	12581	28.2	25599
S1	127 x 127	127.3 x 127.3	3.15	40.4	4.8	1535	356	180518	14645	30.5	26611
S2	127 x 127	126.9 x 126.9	4.34	29.2	4.8	2077	357	190164	13935	26.0	24609
S3	127 x 127	126.9 x 127.0	4.55	27.9	4.8	2174	322	205322	13871	23.8	23528
S4	127 x 127	125.3 x 126.5	5.67	22.3	4.8	2684	312	203944	13097	23.8	23528
S5	127 x 127	126.8 x 127.2	7.47	17.0	4.8	3426	347	204633	12516	23.8	23528
R1	76 x 152	76.6 x 152.3	3.00	50.8	4.0	1316	430	190164	10323	30.5	26611
R2	76 x 152	76.5 x 152.8	4.47	34.2	4.0	1923	383	213590	9677	26.0	24609
R3	102 x 152	101.8 x 152.4	4.32	35.3	4.0	2077	413	214968	13355	26.0	24609
R4	102 x 152	102.8 x 152.7	4.57	33.4	4.0	2200	365	206044	13419	23.8	23528
R5	102 x 152	101.3 x 151.4	5.72	26.5	4.0	2671	324	204633	12581	23.8	23528
R6	102 x 152	102.1 x 152.4	7.34	20.8	4.0	3381	358	205322	12000	23.8	23528

Table 2.11: Axial load data for square columns [Furlong (1967)]

Side Length inches	t inches	F_y kips/in²	A_s in²	f'_c kips/in²	A_c in²	P_o kips	P_u kips	$\frac{P_u}{P_o}$
5.00	0.189	70.3	3.64	6.50	21.36	393.8	360.0	0.914
4.00	0.084	48.0	1.33	3.40	14.67	110.8	117.8	1.063
4.00	0.084	48.0	1.33	3.40	14.67	110.8	109.8	0.991
4.00	0.125	48.0	1.95	4.18	14.05	149.1	150.0	1.006
4.00	0.125	48.0	1.95	4.18	14.05	149.1	152.0	1.019

Table 2.12: Bending plus axial load data for square columns [Furlong (1967)]

Side length inches	t inches	F_y kips/in^2	A_s in^2	f_c' kips/in^2	A_c in^2	P_o kips	M_o kips·in	P_u kips	M_u kips·in	$\frac{P_u}{P_o}$	$\frac{M_u}{M_o}$
5.00	0.189	70.3	3.64	6.50	21.36	393.8	461	250	310	0.635	0.672
5.00	0.189	70.3	3.64	6.50	21.36	393.8	461	150	365	0.381	0.792
5.00	0.189	70.3	3.64	6.50	21.36	393.8	461	150	430	0.381	0.933
5.00	0.189	70.3	3.64	6.50	21.36	393.8	461	100	450	0.254	0.976
4.00	0.084	48.0	1.33	3.40	14.67	110.8	93.2	84	44.3	0.758	0.475
4.00	0.084	48.0	1.33	3.40	14.67	110.8	93.2	74	44.6	0.668	0.479
4.00	0.084	48.0	1.33	3.40	14.67	110.8	93.2	54.4	91.7	0.491	0.984
4.00	0.084	48.0	1.33	3.40	14.67	110.8	93.2	20.2	104.9	0.182	1.126
4.00	0.084	48.0	1.33	3.40	14.67	110.8	93.2	20.1	114.1	0.181	1.224
4.00	0.125	48.0	1.95	4.18	14.05	149.0	137.0	98.4	119	0.660	0.869
4.00	0.125	48.0	1.95	4.18	14.05	149.0	137.0	68.8	162	0.462	1.182
4.00	0.125	48.0	1.95	4.18	14.05	149.0	137.0	67.7	162	0.454	1.182
4.00	0.125	48.0	1.95	4.18	14.05	149.0	137.0	58.6	190	0.393	1.387
4.00	0.125	48.0	1.95	4.18	14.05	149.0	137.0	29.0	209	0.195	1.526
4.00	0.125	48.0	1.95	4.18	14.05	149.0	137.0	28.8	193	0.193	1.409
4.00	0.125	48.0	1.95	4.18	14.05	149.0	137.0	9.0	165	0.060	1.204
4.00	0.125	48.0	1.95	4.18	14.05	149.0	137.0	0.0	204	0.000	1.489

Table 2.13: Failure load of axially loaded square specimens [Knowles and Park (1969)]

Tube	kL inches	Steel tube		Concrete Core		Theoretical	Experimental	Experimental / Theoretical
		Slenderness ratio	f_{su} pounds/in^2	Slenderness ratio	f_{cu} pounds/in^2	$f_{su}+f_{cu}$ lb/in^2	Max. Stress lb/in^2	
Experimental failure loads of axially loaded concrete-filled steel tubes								
3.00 in square t = 0.131 in	68	58.6	57500	89.7	37200	84700	80000	0.945
	56	48.3	59000	70.0	32900	91900	86600	0.942
	44	37.9	59800	55.7	38200	98000	95000	0.969
	32	27.6	63500	40.5	42800	106300	104000	0.977
	20	17.25	68100	25.35	43800	111900	113700	1.016
	10	8.63	76900	12.68	44200	121100	115000	0.950
Experimental failure loads of axially loaded hollow steel tubes								
3.00 in square t = 0.131 in	68	58.6	38900	——	——	——	39600	1.018
	56	48.3	39900	——	——	——	40000	1.002
	44	37.9	41000	——	——	——	41400	1.010
	32	27.6	42900	——	——	——	42600	0.993
	20	17.25	46100	——	——	——	45800	0.994
	9	7.76	52500	——	——	——	54500	1.038
	9	7.76	52500	——	——	——	54500	1.038

Table 2.14: Failure load of eccentrically loaded square specimens [Knowles and Park (1969)]

Tube	L inches	P_u pounds	P_o pounds	$\frac{P_u}{P_o}$	e_i inches	e inches	$M_u = P_u e$, pounds-inch	M_o pounds-inch	$\frac{M_u}{M_o}$	$\frac{P_u}{P_o} + \frac{M_u}{M_o}$
Experimental failure loads of eccentrically loaded concrete-filled steel tubes										
3.00 in. square t =0.131 in	32	77750	104000	0.747	0.30	0.485	37700	98800	0.382	1.129
	56	63200	86600	0.730	0.30	0.71	44900	98800	0.455	1.185
	32	48650	104000	0.468	1.00	1.32	64200	98800	0.650	1.118
	56	35150	86600	0.406	1.00	1.45	51000	98800	0.516	0.922
Experimental failure loads of eccentrically loaded hollow steel tubes										
3.00 in. square t =0.131 in.	32	52250	63000	0.814	0.30	0.50	25625	95000	0.270	1.084
	56	44800	59100	0.759	0.30	0.56	23750	95000	0.250	1.009
	32	35000	63000	0.556	1.00	1.212	42500	95000	0.449	1.005
	56	32800	59100	0.555	1.00	1.37	44900	95000	0.474	1.029

Table 2.15: Axially loaded square concrete-filled steel tube specimens [Knowles and Park (1970)]

Test Number	D inches	t inches	kL inches	f'_c lb/in²	$E_s \times 10^6$ lb/in²	f_y lb/in²	$\frac{KL}{r_c}$	P_{eu} kips	P_{cu} kips	P_u kips	P_{test}, kips	$\frac{P_{test}}{P_u}$
Chapman and Neogi (1966)												
DF3	4.500	0.379	16.0	4660	29.0	36850	14.81	229.6	65.20	294.8	549.0	1.863
DF4	4.522	0.173	16.0	4660	29.0	36850	13.27	110.6	81.17	191.8	201.6	1.051

Table 2.16: Carrying capacity, deflections and failure loads of tested rectangular columns. [Shakir-Khalil and Zeghiche (1989)]

Column #	A_s mm²	f_{sd} MPa	f_{cu} MPa	e_x mm	e_y mm	Stub Column Tests			δ_x mm	δ_y mm	P_{exp} kN	M_{2x} kN·m	M_{2y} kN·m
						P_o kN	M_{ox} kN·m	M_{oy} kN·m					
1	1883	386.3	44	0	0	950	31.6	23.3	2.0	6.0	600	1.2	3.6
2	1883	386.6	40	24	0	950	31.5	23.3	21.8	0.12	393	18.0	—
3	1869	384.7	40	60	0	900	31.3	23.1	33.0	1.62	232	21.6	0.4
4	1869	384.7	44	0	16	910	31.45	23.2	0.93	26.0	260	0.2	10.9
5	1870	343.3	43	0	40	900	28.2	20.8	0.35	38.0	210	0.1	16.4
6	1870	343.3	45	24	16	900	28.3	20.8	12.0	26.0	268	9.6	11.3
7	1855	357.5	44	60	40	920	29.3	21.6	21.0	36.0	160	13.0	12.2

Table 2.17: Results of tests on bond on rectangular columns [Shakir-Khalil and Zeghiche (1989)]

Column #	f_{sd} MPa	f_{cu} MPa	Failure Load kN	Area of interface $mm^2 \cdot 10^3$	Bond Strength MPa
1	386.3	44	80.0	216	0.37
2	386.6	40	57.0	219	0.26
3	384.7	40	67.5	218	0.31
4	384.7	44	64.0	221	0.29
5	343.3	43	60.0	214	0.28
6	343.3	45	67.5	218	0.31
7	357.5	44	70.0	219	0.32

Table 2.18: Properties of tested rectangular columns [Shakir-Khalil and Zeghiche (1990)]

Column #	A_s mm^2	f_{sd} MPa	f_{cu} MPa	e_x mm	e_y mm	Stub Column Tests			δ_x mm	δ_y mm	P_{exp} kN	$M_{\delta x}$ kN·m	$M_{\delta y}$ kN·m	$M_{\delta x}$ kN·m	$M_{\delta y}$ kN·m
						P_u kN	M_{ux} kN·m	M_{uy} kN·m							
1	1855	7260	357.5	41.6	0	8	200	850	29.2	21.5	1.0	19.3	407.2	0.4	11.1
2	1827	7280	341.0	42.6	12	8	200	900	28.0	20.6	12.0	18.4	348.0	8.3	9.2
3	1827	7280	341.0	46.2	42	28	200	920	28.1	20.6	20.8	26.4	198.5	12.5	10.8
4	1866	7240	362.5	42.4	24	40	200	950	29.6	21.9	10.1	36.9	206.8	7.0	15.9
5	1866	7340	362.5	40.8	60	16	200	955	29.6	21.8	20.2	25.1	209.8	16.8	8.6
6	2239	12140	346.7	46.0	0	0	100 200	1370 1210	45.6	33.3	2.8	4.2	1003.0	2.8	4.6
7	2239	12000	346.7	46.2	15	10	100 200	1340 1200	45.5	33.3	8.0	9.8	596.2	13.7	11.8
8	2260	12060	340.0	46.6	45	30	100 200	1300 1190	44.8	32.7	18.9	27.5	329.2	21.1	18.9
9	2260	12010	340.0	47.2	75	50	100 200	1320 1200	44.8	32.7	22.6	31.4	254.6	24.8	20.7

Table 2.19: Dimensions of Test Specimens [Fukumoto and Kusama (1985)]

Specimen	B (mm)	D (mm)	t (mm)	A (mm^2)	b/t	M_u (kNm)
B-40-1	263.3	234.7	5.54	5515	43.6	144
B-40-2	263.0	235.0	5.60	5569	43.1	153
B-60-1	383.3	354.7	5.68	8375	63.7	258
B-60-2	382.9	354.6	5.72	8427	63.1	265
B-80-1	503.1	474.4	5.62	10974	85.7	389
B-80-2	503.1	474.6	5.62	10971	85.7	402
BH-40-1	262.2	234.8	6.00	5958	40.0	311
BH-40-2	262.2	234.8	5.99	5949	40.1	311
BH-60-1	381.9	354.2	5.98	8805	60.2	493
BH-60-2	382.6	354.2	5.96	8780	60.5	529

Table 2.20: Measured Dimensions of Test Specimens [Usami et al. (1992)]

Specimen	L (mm)	h (mm)	l_d (mm)	B (mm)	D (mm)	t (mm)	b_s (mm)	t_s (mm)	γ/γ_{req}	l_s (mm)	l_c (mm)	$\bar{\lambda}$	R_f	R_w
SS1	1854	1671	296	312	202	4.51	44.0	4.36	3.23	1854	—	0.490	0.430	0.427
SS2	1854	1216	296	309	201	4.51	44.0	4.36	3.23	1854	—	0.356	0.426	0.425
SS3	1854	1671	296	311	202	4.51	50.0	4.31	5.03	556	—	0.495	0.429	0.426
SS4	1854	1671	296	311	202	4.51	50.0	4.31	5.03	927	—	0.495	0.429	0.426
SS5	1854	1671	196	311	202	4.51	50.0	4.31	5.03	1854	—	0.495	0.429	0.427
SS6	1854	1671	296	312	202	4.51	50.0	6.25	5.39	1854	—	0.521	0.446	0.427
SS7	1854	1671	148	310	202	4.51	50.0	4.31	13.6	1854	—	0.495	0.428	0.427
SS8	1854	1671	296	311	201	4.51	44.0	4.36	1.13	1854	556	0.49	0.429	0.424
SS9	1854	1671	296	311	201	4.51	38.0	4.39	0.98	1854	927	0.487	0.430	0.424

Table 2.21: Ductility and energy-absorption capacity [Usami et al. (1992)]

Test Specimen	H_{yo} (kN)	δ_{yo} (mm)	$\frac{H_{max}}{H_{yo}}$	$\frac{\delta_m}{\delta_{yo}}$	$\frac{H_y}{H_{yo}}$	$\frac{\delta'}{\delta_{yo}}$	μ_m	μ	$\frac{\sum E_i}{E_e}$	Remarks
SS1	60.0	12.7	1.14	2.36	0.80	3.92	2.95	3.66	122	——
SS2	82.4	6.73	1.22	3.09	0.80	5.59	3.86	5.01	182	$\lambda = 0.4$
SS3	60.7	12.74	1.12	2.30	0.80	4.42	2.88	4.24	103	ls = 0.3h
SS4	60.7	12.74	1.17	2.36	0.80	4.45	2.95	5.03	109	ls = 0.3h
SS5	60.7	12.71	1.12	2.38	0.80	4.30	2.98	4.47	94	——
SS6	69.7	13.63	1.14	3.33	0.78	7.09	4.27	6.99	308	Hybrid
SS7	60.7	12.74	1.16	2.35	0.80	4.13	2.94	4.31	90	ld = 0.5b
SS8	60.0	12.70	1.53	4.92	0.80	7.73	6.45	11.70	5.06	lc = 0.3h
SS9	60.0	12.80	1.53	5.05	0.80	9.72*	6.31	14.92*	1040	lc = 0.5h

* = Extrapolated data.

Table 2.22: Dimensions of Specimens [Ge and Usami (1994)]

Specimen	B (mm)	D (mm)	L (mm)	h (mm)	l_d (mm)	h_{rib}	l_c (mm)	$\bar{\lambda}$	R_f	R_w	H_{max}	δ_m
UU0	170	110	854	762	306	228	—	0.362	0.664	0.430	42.1	11.1
UU1	169	111	854	762	306	228	—	0.362	0.664	0.430	41.8	11.6
UU2	170	111	854	762	229	228	229	0.362	0.664	0.430	55.0	20.0
UU3	170	111	854	762	381	228	381	0.362	0.664	0.430	53.6	23.3
UU4	170	111	854	762	381	228	381	0.362	0.664	0.430	55.3	24.4
UU5	170	110	1354	1216	365	365	365	0.577	0.664	0.430	31.9	30.8
UU6	214	145	1154	1035	394	311	—	0.381	0.854	0.575	43.2	11.25
UU7	214	145	1154	1035	311	311	311	0.381	0.854	0.575	60.2	15.3
UC70-40-3[0]	235	156	1354	1216		122	365	0.429	0.750		94.9	39.7
UC70-25-3[0]	235	157	953	788		150	236	0.276	0.750		154.6	16.58
UC70-25-3[3]	235	157	952	788		150	125	0.276	0.750		157.7	14.0
UC70-25-5[3]	235	157	954	788		150	394	0.276	0.750		160.8	20.26
UC70-25-3[3]D	235	156	952	788	—	150	236	0.278	0.750		130	14.8
UC70-25-5[3]D	235	157	952	788	—	150	394	0.277	0.750		132.1	15.3
UC90-40-5[3]	296	202	1753	1578		160	789	0.434	0.961		115.8	24.6

Table 2.23: Ductility and Energy-Absorption Capacity [Ge and Usami (1994)]

Test Specimen	H_{yo} (kN)	δ_{yo} (mm)	$\frac{H_{max}}{H_{yo}}$	$\frac{\delta_m}{\delta_{yo}}$	$\frac{H_y}{H_{yo}}$	$\frac{\delta'}{\delta_{yo}}$	μ_m	μ	$\hat{E}$
UU0	35.7	4.33	1.18	2.56	1.0	5.23	2.58	3.68	111
UU1	35.7	4.33	1.17	2.69	0.8	3.78	3.36	3.68	77
UU2	35.7	4.33	1.54	4.62	0.8	8.37	5.78	9.54	536
UU3	35.7	4.33	1.50	5.39	0.8	12.02	6.74	12.50	1088
UU4	35.7	4.33	1.55	5.63	0.8	11.54	8.29	12.90	1237
UU5	22.3	11.08	1.43	2.78	0.8	10.50	3.48	8.10	505
UU6	46.6	6.25	0.99	1.80	0.64	3.19	1.80	3.35	72
UU7	46.6	6.25	1.38	2.45	0.64	5.60	2.45	7.05	225
UC70-40-3[0]	65.9	8.57	1.44	4.40	0.76		4.14		13
UC70-25-3[0]	102.4	3.58	1.51	4.63	0.76		4.41		14
UC70-25-3[3]	102.4	3.58	1.54	3.92	0.76		3.68		20
UC70-25-5[3]	102.4	3.58	1.57	5.66	0.76		5.62		99
UC70-25-3[3]D	101.6	3.60	1.28	4.11	0.76		3.72		23
UC70-25-5[3]D	102.4	3.58	1.29	4.26	0.76		3.84		30
UC90-40-5[3]	83.3	11.33	1.39	2.17	0.55		3.92		30

Table 2.24: Design parameters [Kitada et al. (1995)]

Column	R_p	R_h	$\frac{\gamma}{\gamma_*}$	$\frac{\sigma_c}{\sigma_y}$	$\frac{H_u}{H_y}$	$\frac{\delta_u}{\delta_y}$	Particulars
H1	0.35	0.71	0.58	0.104	1.14	2.46	Monotonic loading
H2	0.35	0.71	0.58	0.104	1.20	2.02	Cyclic loading
H3	0.35	0.71	0.58	0.104	1.32	2.52	Partially filled with concrete

Table 2.25: Dimensions and summarization of tests [Kitada (1992)]

Shape	Diameter (mm)	Width (mm)	Thickness (mm)	Test	Remarks	Ref
Circular	114.3	——	5	Compressive load and axial displacement under 3 types of load conditions.(load the steel, load the concrete, and load the composite)	The composite structure carried more load than either the steel or the concrete.	Kitada et al. (1987)
Square	——	320	4.5	Compressive load and axial strain for the steel shell, concrete core and composite section.	The composite column had a higher ultimate strength and a substantial increase in ductility over the steel or concrete. Composite effect js not as great as for the circular columns.	Kitada and Nakai (1991)
Circular	300	—	3.2	P - δ of composite beam	With slip restricted, the composite pipe retains its strength well into the ultimate range, whereas with slip not restricted, there is a large drop in the load carrying capacity after the ultimate load has been reached.	Kishida et al. (1982)
Square	—	200	4.5	P - δ of composite beam with cyclic loading	P/P_y = 1.0, δ/δ_y = 1.6 The decrease of load-carrying capacity of a steel section under cyclic loading is reduced when the section is filled with concrete.	Sakurai et al. (1988)
Circular	168	—	5.2	Composite beam with P/P_y = 0.57 and bending moment applied	Converging at 625 tf*cm, and curvature of 0.05 and failure has not occurred. A good ductile design.	Sen (1969)
Square	——	100	2.3	Composite beam with P/P_y = 0.52 and bending moment applied	The moment versus curvature diagram was linear until ultimate of 120 tf*cm at a curvature of 0.08 and the moment decreased after this point with additional curvature. Not as ductile as the circular section.	Tomii and Sakino (1974)
Circular	139.8	—	4.5	Torsional moment and rate of twisting angle	The steel alone reached T/T_{pc} = 0.6 at Θ / Θ_y = 2.25, while the composite beam reached 1.0 at Θ / Θ_y = 4.75.	Kitada et al. (1991)
Rectangular	—	154 x 114		Torsional moment and rate of twisting angle	The steel alone reached T/T_{pc} = 0.8 while the composite beam reached 1.0	Kitada et al. (to be published)

Table 2.26: Summary of column details and testing [Boyd et al. (1995)]

Column #	D mm	t mm	$\frac{D}{t}$	Shear studs	f_c' MPa	f_y MPa	Shell buckles @	Fracture @	M_{test} kN·m	M_{ACI} kN·m	$\frac{M_{test}}{M_{ACI}}$
1	203.2	2.77	73	No	31.7	345	1st cycle: $\mu=\pm4$	2nd cycle: $\mu=\pm6$	67.8	51.5	1.12
2	203.2	2.77	73	No	31.7	345	1st cycle: $\mu=\pm4$	2nd cycle: $\mu=\pm8$	67.4	51.5	1.11
3	203.2	2.77	73	Yes	31.7	345	1st cycle: $\mu=\pm2$	1st cycle: $\mu=\pm6$	76.6	51.5	1.26
4	203.2	1.91	107	No	31.7	283	1st cycle: $\mu=\pm4$	no fracture	49.2	35.9	1.16
5	203.2	1.91	107	No	48.3	283	2nd cycle: $\mu=\pm2$	no fracture	52.1	38.1	1.16

Table 2.27: Material Properties [Kawaguchi et al. (1992)]

Material	Steel Properties					Concrete Properties
	Yield Stress MPa	Tensile Strength MPa	Compressive Strength in Stub Column Test MPa	$E_s \cdot 10^3$ MPa	Elongation of steel by tensile test %	f_c' MPa
A	332	403	402	190	29.9	23.6
B	443	487	500 (22S.... = 472)	206	12.8	21.7
C	384	459	—	194	26.7	24.8
D	399	433	386	201	25.9	—
E	324	414	414 (31S2010 = 334)	171	23.5	22.6

Table 2.28: Details and strain and displacement at local buckling of rectangular columns [Kawaguchi et al. (1992)]

Specimen	Material	t (mm)	D (mm)	l (mm)	D/t	P (kN)	P/P_y (%)	Δ_{cr} (mm)	Δ_{max} (mm)	Δ_{max}/Δ_{cr}	ϵ_{cr} (%)	Corner Crack
22S0510	A	4.31	100.10	1048	23.2	27.4	5.0	83	83	1.00	1.20	C
22Si010	A	4.31	100.09	1049	23.2	54.9	10.0	57	57	1.00	1.36	
22S1510	A	4.21	100.14	1048	23.8	80.5	15.0	52	52	1.00	1.25	
22S2010	A	4.21	100.13	1048	23.8	107.3	20.0	50	50	1.00	1.13	
22C1510	A	4.31	100.16	1048	23.2	117.6	15.8	72	72	1.00	1.75	
22C2010	A	4.31	100.04	1048	23.2	156.8	21.0	70	70	1.00	1.50	
22C2510	A	4.21	100.19	1048	23.8	196.0	26.7	65	65	1.00	1.67	
22C3010	A	4.21	100.13	1048	23.8	235.2	32.0	60	60	1.00	1.30	
22S0513	A	4.31	100.16	1049	23.2	27.4	5.0	54	70.2	1.30	1.10	C
22S1013	A	4.31	100.13	1049	23.2	54.9	10.1	59	76.7	1.30	1.06	C
22S1513	B	4.34	99.66	1043	23.0	110.0	15.0	54	70.2	1.30	1.00	
22S2013	B	4.34	99.79	1049	23.0	146.8	20.0	57	74.1	1.30	1.21	
22C1512	B	4.34	99.75	1047	23.0	152.9	16.7	72	84.0	1.17	1.98	C
22C2012	B	4.34	99.76	1048	23.0	215.6	23.6	71	85.3	1.20	2.04	C
22C2512	B	4.34	99.74	1048	23.0	249.9	27.4	72	87.4	1.21	2.01	
22C3012	B	4.34	99.73	1049	23.0	303.8	33.3	73	87.4	1.20	2.22	
22C2508	C	4.31	100.04	1047	23.2	210.1	25.0	46	55	0.8	1.60	
22C2506	C	4.31	100.03	1047	23.2	210.1	25.0	33	41	0.6	0.93	
31S0510	D	2.95	99.80	1049	33.8	22.8	5.0	39	39	1.00	2.29	C
31S1010	D	2.95	99.81	1049	33.8	45.6	10.0	36	36	1.00	1.39	
31S1510	D	2.95	99.90	1049	33.9	68.4	15.0	33	33	1.00	1.68	
31S2010	E	2.99	99.55	1048	33.3	74.9	20.0	32	32	1.00	0.74	
31C1510	E	2.99	99.55	1049	33.3	85.9	15.0	62	62	1.00	1.08	
31C2010	E	2.99	99.69	1048	33.3	114.9	20.0	62	62	1.00	1.48	
31C2510	E	2.99	99.49	1048	33.3	143.1	25.0	59	59	1.00	1.21	
31C3010	E	2.99	99.63	1048	33.3	172.1	30.0	55	55	1.00	1.16	
43S0510					43.0	15.8	5	30	30	1.00	0.49	
43S1010					43.0	31.7	10	24	24	1.00	0.46	
43S1510					43.0	47.1	15	21	21	1.00	0.52	
43S2010					43.0	63.2	20	21	21	1.00	0.40	
43C1510					43.0	89.2	15.9	32	32	1.00	0.54	
43C2010					43.0	114.6	21.2	28	28	1.00	0.17	
43C2510					43.0	150.9	27	28	28	1.00	0.17	
43C3010					43.0	196.3	34.4	19	19	1.00	0.18	
43C1512					43.0	71.1	15	24	29.04	1.21	0.23	
43C2012					43.0	97.4	20	22	25.96	1.18	0.18	
43C2512					43.0	122.3	25	20	25	1.25	0.22	
43C3012					43.0	127.4	26.1	17	20.06	1.18	0.19	
43C2506					43.0	118.6	25.0	12	7.2	0.60	0.17	
43C2508					43.0	98.0	20.1	-11	-8.8	0.80	0.03	

Table 2.29: Measured Dimensions of Rectangular Specimens without stiffeners [Ge and Usami (1994)]

Specimen	b (mm)	B (mm)	A_s (mm^2)	A_c (mm^2)	L (mm)	r (mm)	b/t	R_p with k=4.0	P_u (kN)
U9-S	197	213	3654	—	592	81.0	43.7	0.844	821
U9-C	196	213	3654	37100	592	29.5	43.7	0.839	1845
U12-S	263	279	4842	—	789	108.0	58.3	1.126	803
U12-C	263	279	4842	66800	790	36.2	58.3	1.126	3070
U12-HC	263	279	4842	66800	789	36.2	58.3	1.126	3999
U15-S	329	345	6030	—	988	118.0	73.0	1.409	805
U15-C	329	345	6030	105300	988	39.8	73.0	1.409	3275

Table 2.30: Measured Dimensions of Rectangular Specimens with Stiffeners [Ge and Usami (1994)]

Specimen	b (mm)	B (mm)	b_s (mm)	t_s (mm)	A_s (mm^2)	A_c (mm^2)	r (mm)	$\frac{\gamma_1}{\gamma_1^*}$	R_p with k = 16	P_u (kN)
S75-S(1)	328	344	38.1	4.36	6714	—	132.0	1.11	0.702	1598
S75-C(1)	328	345	38.0	4.36	6714	104616	43.3	1.11	0.702	5030
S75-C(0.35)	329	344	25.1	4.34	6480	104850	43.1	0.35	0.705	5158

Table 3.1: Bridge superstructures

Bridge	Length (m)	Width (m)	# of girders	Simply-Supported(SS) or Continuous (Cont.)	Dead Load (kN/m)
1	12.3	92	5	S.S.	119
2	19.8	92	8	S.S.	195
3	27.3	92	11	S.S.	266
4	12.3	84.5	5	S.S.	119
5	19.8	84.5	8	S.S.	193
6	27.3	84.5	11	S.S.	266
7	12.3	99.5	5	S.S.	120
8	19.8	99.5	8	S.S.	197
9	27.3	99.5	11	S.S.	267
10	12.3	92	5	Cont..	118
11	19.8	92	8	Cont.	192
12	27.3	92	11	Cont.	263
13	12.3	84.5	5	Cont.	117
14	19.8	84.5	8	Cont.	191
15	27.3	84.5	11	Cont.	263
16	12.3	99.5	5	Cont.	119
17	19.8	99.5	8	Cont.	195
18	27.3	99.5	11	Cont.	266

Table 3.2: An example of applicable full-scale piers for a particular bridge.

T	V	H	D	t	ρ	C_{fcr}	M_{fmr}	Δ
1.12	8964	1606	600	81.18	0.468	0	1	388
1.06	8964	1667	650	59.19	0.331	0	1	347
1.01	8964	1728	700	45.81	0.245	0	1	312
0.96	8964	1788	750	36.51	0.185	0	1	282
0.9	8964	1857	800	30.14	0.145	0	1	252
0.86	8964	1927	850	25.13	0.115	0	1	225
0.81	8964	2003	900	21.27	0.09	0	1	201
0.76	8964	2088	950	18.48	0.08	0	0.98	177
0.68	8964	2236	1000	19.45	0.08	0	0.8	144
0.64	8964	2341	1050	17.89	0.07	0	1	125
0.6	8964	2438	1100	15.97	0.06	0	1	112

where T = period of the pier.
V = the axial load applied to the pier
H = the horizontal load applied to the pier
D = Diameter of the steel tube
t = Thickness of the steel tube
ρ = the amount of the steel per cross sectional area
C_{fcr} = The ratio of the applied axial force to the axial resistance as per Section 18 of CAN/CSA-S16.1-M94
M_{fmr} = The ratio of the applied moment to the moment resistance of the column
Δ = Deflection expected at tip of pier due to horizontal force

Table 3.3: Full-scale columns with matching test column.

Specimen #	**Axial load kN**	**Height mm**	**D mm**	**t mm**	$\frac{D}{t}$	$\frac{kL}{r_c}$	$\frac{C_f}{C_{rc}}$	$\frac{C_r}{C_{rc}}$
Full Scale	8056	6000	1150	17.74	64.83	21.53	0.20	0.48
CFST 64	1000	154	406.4	6.35	64.00	21.34	0.20	0.49
Full-Scale	12114	6000	900	25.52	25.4	28.26	0.34	0.61
CFST 34	1600	2200	323.9	9.53	34.35	28.21	0.34	0.62
Full-Scale	13234	6000	1100	24.9	44.18	22.85	0.28	0.56
CFST 42	1850	2200	406.4	9.53	42.64	22.72	0.28	0.56
Full-Scale	5426	6000	900	18	50	27.78	0.19	0.55
CFST 51	700	2200	323.9	6.35	51.01	27.63	0.19	0.54

Table 3.4: Concrete cylinder strength

Mix #	Day	Concrete Strength (MPa)			Average Strength (MPa)
		#1	#2	#3	
1	7	31.67	33.39	35.34	33.47
	14	34.56	36.98	34.75	35.43
	28	38.39	35.45	36.92	36.92
	CFST 64	38.39	35.45	36.92	**36.92**
	CFST 35	38.69	41.53	41.31	**40.51**
2	35	31.02	30.76	31.23	31.00
	CFST 42	36.14	34.43	34.78	**35.12**
	CFST 51	34.47	35.55	35.16	**35.06**

Table 3.5: Steel coupon strength

Test #	Yield		Maximum		Yield (weld)		Maximum (weld)	
	σ_y	ϵ_y	σ_y	ϵ_y	σ_y	ϵ_y	σ_y	ϵ_y
CFST 64	442	0.003	562	0.35	565	0.006	698	NR
CFST 34	415	0.0024	515	0.40	565	0.0046	638	0.18
CFST 41	505	0.0043	595	0.30	666	0.0052	766	NR
CFST 51	400	0.0034	543	0.35	545	0.0047	633	0.17

where NR = not recorded

Table 3.6: Strain gauges for CFST 64 and CFST 42

Strain Gauge #	Strain Gauge Name	Strain Gauge Location
		Strain Gages on Channels are located 40 mm from the tip of the channel
1	Top North West Channel	225 mm from the west end of the channel
2	Bottom North West Channel	225 mm from the west end of the channel
3	Top North Channel	834 mm from west end of channel
4	Bottom North Channel	834 mm from west end of channel
5	Top South Channel	834 mm from west end of channel
6	Bottom South Channel	834 mm from west end of channel
7	Top North East Channel	225 mm from the east end of the channel
8	Bottom North East Channel	225 mm from the east end of the channel
9	East Bottom Plate	203 mm from channel and 245 mm from end of plate
10	East Longitudinal Column at Bottom Plate	203 mm from channel and 30 mm from bottom plate
11	Bottom East Top Plate	203 mm from channel and 245 mm from end of plate
12	West Bottom Plate	203 mm from channel and 245 mm from end of plate
13	West Longitudinal Column at Bottom Plate	203 mm from channel and 30 mm from bottom plate
14	Bottom West Top Plate	203 mm from channel and 245 mm from end of plate
15	Top East Top Plate	277 mm from channel and 245 mm from end of plate
16	Top West Top Plate	277 mm from channel and 245 mm from end of plate
17	East Transverse Column above Top Plate	on east line and 15 mm above top plate
18	North Transverse Column above Top Plate	on north line and 15 mm above top plate

19	West Transverse Column above Top Plate	on west line and 15 mm above top plate
20	South Transverse Column above Top Plate	on south line and 15 mm above top plate
21	East Longitudinal Column	on east line and 35 mm above the top plate
22	East Longitudinal Column	on east line and 135 mm above the top plate
23	East Longitudinal Column	on east line and 235 mm above the top plate
24	West Longitudinal Column	on west line and 35 mm above the top plate
25	West Longitudinal Column	on west line and 135 mm above the top plate
26	West Longitudinal Column	on west line and 235 mm above the top plate
27	East Transverse Column above Concrete Foundation	on east line and 15 mm above concrete foundation
28	North Transverse Column above Concrete Foundation	on north line and 15 mm above concrete foundation
29	West Transverse Column above Concrete Foundation	on west line and 15 mm above concrete foundation
30	South Transverse Column above Concrete Foundation	on south line and 15 mm above concrete foundation
31	East Longitudinal Column	on east line and 35 mm above concrete foundation
32	East Longitudinal Column	on east line and 135 mm above concrete foundation
33	East Longitudinal Column	on east line and 235 mm above concrete foundation
34	West Longitudinal Column	on west line and 35 mm above concrete foundation
35	West Longitudinal Column	on west line and 135 mm above concrete foundation
36	West Longitudinal Column	on west line and 235 mm above concrete foundation

Table 3.7: Strain gauges for CFST 34 and CFST 51

Strain Gauge #	Strain Gauge Name	Strain Gauge Location
		Strain Gages on Channels are located 40 mm from the tip of the channel
1	Top North West Channel	225 mm from the west end of the channel
2	Bottom North West Channel	225 mm from the west end of the channel
3	Top North Channel	875 mm from west end of channel
4	Bottom North Channel	875 mm from west end of channel
5	Top South Channel	875 mm from west end of channel
6	Bottom South Channel	875 mm from west end of channel
7	Top North East Channel	225 mm from the east end of the channel
8	Bottom North East Channel	225 mm from the east end of the channel
9	East Bottom Plate	162 mm from channel and 286 mm from end of plate
10	East Longitudinal Column at Bottom Plate	162 mm from channel and 30 mm from bottom plate
11	Bottom East Top Plate	162 mm from channel and 286 mm from end of plate
12	West Bottom Plate	162 mm from channel and 286 mm from end of plate
13	West Longitudinal Column at Bottom Plate	162 mm from channel and 30 mm from bottom plate
14	Bottom West Top Plate	162 mm from channel and 286 mm from end of plate
15	Top East Top Plate	236 mm from channel and 286 mm from end of plate
16	Top West Top Plate	236 mm from channel and 286 mm from end of plate
17	East Transverse Column above Top Plate	on east line and 15 mm above top plate
18	North Transverse Column above Top Plate	on north line and 15 mm above top plate

19	West Transverse Column above Top Plate	on west line and 15 mm above top plate
20	South Transverse Column above Top Plate	on south line and 15 mm above top plate
21	East Longitudinal Column	on east line and 35 mm above the top plate
22	East Longitudinal Column	on east line and 135 mm above the top plate
23	East Longitudinal Column	on east line and 235 mm above the top plate
24	West Longitudinal Column	on west line and 35 mm above the top plate
25	West Longitudinal Column	on west line and 135 mm above the top plate
26	West Longitudinal Column	on west line and 235 mm above the top plate
27	East Transverse Column above Concrete Foundation	on east line and 15 mm above concrete foundation
28	North Transverse Column above Concrete Foundation	on north line and 15 mm above concrete foundation
29	West Transverse Column above Concrete Foundation	on west line and 15 mm above concrete foundation
30	South Transverse Column above Concrete Foundation	on south line and 15 mm above concrete foundation
31	East Longitudinal Column	on east line and 35 mm above concrete foundation
32	East Longitudinal Column	on east line and 135 mm above concrete foundation
33	East Longitudinal Column	on east line and 235 mm above concrete foundation
34	West Longitudinal Column	on west line and 35 mm above concrete foundation
35	West Longitudinal Column	on west line and 135 mm above concrete foundation
36	West Longitudinal Column	on west line and 235 mm above concrete foundation

Table 6.1: Axially loaded columns with code compressive resistances (k=1.0 in all cases).

Name	Length (mm)	D (mm)	t (mm)	kL/r_s	Fy (MPa)	fc' (MPa)	Pf (kN)	CAN/CSA-S16.1 Pr (kN)	CAN/CSA-S16.1 Pf/Pr	AISC LFRD Pr (kN)	AISC LFRD Pf/Pr	Eurocode 4 Pr (kN)	Eurocode 4 Pf/Pr
Kato (1996)													
CFT Working Group (1993)													
1	661	165.2	4.1	11.6	353	40.9	1562	1840.1	0.85	1388.7	1.12	1779	0.88
2	1322	165.2	4.1	23.2	353	40.9	1412	1645.0	0.86	1339.3	1.05	1506	0.94
3	1982	165.2	4.1	34.8	353	40.9	1372	1419.4	0.97	1261.1	1.09	1400	0.98
4	2974	165.2	4.1	52.2	353	40.9	1147	1071.6	1.07	1101.1	1.04	1231	0.93
5	3965	165.2	4.1	69.6	353	40.9	1019	815.4	1.25	910.8	1.12	973	1.05
6	4956	165.2	4.1	87.0	353	40.9	782	626.0	1.25	761.2	1.03	718	1.09
Masuo, K. et al (1991)													
7	1150	190.7	5.5	17.6	505	48.3	3148	3378.2	0.93	2566.2	1.23	2950	1.07
8	3450	190.7	5.5	52.7	505	48.3	2133	1862.6	1.15	1941.8	1.10	2110	1.01
9	1600	267.4	6.4	17.3	461	48.3	5188	5624.4	0.92	4364.9	1.19	5075	1.02
10	4800	267.4	6.4	52.0	461	48.3	3903	3253.4	1.20	3364.1	1.16	3700	1.05
11	1150	190.7	5.5	17.6	505	55.9	3063	3537.8	0.87	2721.3	1.13	3114	0.98
12	2300	190.7	5.5	35.1	505	55.9	2612	2745.4	0.95	2442.5	1.07	2691	0.97
13	3450	190.7	5.5	52.7	505	48.3	2059	1862.6	1.11	1941.8	1.06	2110	0.98
14	1600	267.4	6.4	17.3	461	48.3	5181	5624.4	0.92	4364.9	1.19	5075	1.02
15	3200	267.4	6.4	34.7	461	48.3	4534	4472.2	1.01	3958.8	1.15	4387	1.03
16	4800	267.4	6.4	52.0	461	48.3	3626	3253.4	1.11	3364.1	1.08	3700	0.98
Sasaki, R (1984)													
17	670	114.3	3.1	17.0	348	53.5	898	969.0	0.93	772.5	1.16	911	0.99
18	670	114.3	3.1	17.0	348	53.5	904	969.0	0.93	772.5	1.17	911	0.99
19	670	114.3	3.1	17.0	348	53.5	910	969.0	0.94	772.5	1.18	911	1.00
20	1020	114.3	3.1	25.9	348	53.4	888	882.2	1.01	744.1	1.19	823	1.08
21	1020	114.3	3.1	25.9	348	53.4	849	882.2	0.96	744.1	1.14	823	1.03
22	1020	114.3	3.1	25.9	348	53.4	845	882.2	0.96	744.1	1.14	823	1.03
23	1335	114.3	3.1	33.9	348	56	784	807.6	0.97	727.6	1.08	812	0.97
24	1335	114.3	3.1	33.9	348	56	773	807.6	0.96	727.6	1.06	812	0.95
25	1335	114.3	3.1	33.9	348	56	794	807.6	0.98	727.6	1.09	812	0.98
26	2040	114.3	3.1	51.9	348	57.5	617	601.2	1.03	634.2	0.97	702	0.88
27	2040	114.3	3.1	51.9	348	57.5	649	601.2	1.08	634.2	1.02	702	0.92
28	2040	114.3	3.1	51.9	348	57.5	688	601.2	1.14	634.2	1.08	702	0.98
29	2700	114.3	3.1	68.6	340	57.5	516	451.5	1.14	517.3	1.00	536	0.96
30	2700	114.3	3.1	68.6	340	57.5	537	451.5	1.19	517.3	1.04	536	1.00
31	2700	114.3	3.1	68.6	340	57.5	536	451.5	1.19	517.3	1.04	536	1.00
32	3370	114.3	3.1	85.7	340	63.1	401	354.7	1.13	429.2	0.93	392	1.02
33	3370	114.3	3.1	85.7	340	63.1	362	354.7	1.02	429.2	0.84	392	0.92
34	3370	114.3	3.1	85.7	340	63.1	379	354.7	1.07	429.2	0.88	392	0.97
35	3720	114.3	3.1	94.6	340	55.1	320	298.1	1.07	342.9	0.93	328	0.97
36	3720	114.3	3.1	94.6	340	55.1	293	298.1	0.98	342.9	0.85	328	0.89
37	3720	114.3	3.1	94.6	340	55.1	305	298.1	1.02	342.9	0.89	328	0.93
Furlong (1967)													
1	914	114.3	3.2	23.3	413.7	29	711.68	840.1	0.85	654.7	1.09	725	0.98
2	914	114.3	3.2	23.3	413.7	29	756.16	840.1	0.90	654.7	1.15	725	1.04

Name	Length (mm)	D (mm)	t (mm)	kL/r_s	Fy (MPa)	fc' (MPa)	Pf (kN)	CAN/CSA-S16.1		AISC LFRD		Eurocode 4	
								Pr (kN)	Pf/Pr	Pr (kN)	Pf/Pr	Pr (kN)	Pf/Pr
Furlong (1967)													
3	914	152.4	1.5	17.1	330.9	21	682.32	666.5	1.02	536.1	1.27	657	1.04
4	914	152.4	1.5	17.1	330.9	25.9	721.47	738.9	0.98	606.5	1.19	735	0.98
5	914	152.4	1.5	17.1	330.9	25.9	733.03	738.9	0.99	606.5	1.21	735	1.00
6	914	127	2.4	20.7	289.6	35.2	627.17	731.5	0.86	601.8	1.04	702	0.89
7	914	127	2.4	20.7	289.6	35.2	622.72	731.5	0.85	601.8	1.03	702	0.89
8	914	127	2.4	20.7	289.6	35.2	658.3	731.5	0.90	601.8	1.09	702	0.94
Knowles and Park (1969)													
1	1727	88.9	5.8	58.6	400	40	614.74	518.5	1.19	562.7	1.09	603	1.02
2	1422	89	5.8	48.2	400	39.6	711.72	620.8	1.15	621.3	1.15	669	1.06
3	1118	89	5.8	37.9	400	39	715.27	743.4	0.96	670.7	1.07	716	1.00
4	813	89	5.8	27.6	400	41.8	918.56	886.1	1.04	722.4	1.27	759	1.21
5	508	89	5.8	17.2	400	40.9	991.95	1009.1	0.98	749.7	1.32	874	1.14
6	508	89	5.8	17.2	400	40.9	889.64	1009.1	0.88	749.7	1.19	874	1.02
7	1727	82.55	1.4	60.2	483	41.3	224.64	218.2	1.03	235.0	0.96	255	0.88
8	1422	82.6	1.4	49.5	483	37	294.47	255.5	1.15	254.8	1.16	285	1.03
9	1118	82.6	1.4	38.9	483	40.9	355.86	321.3	1.11	294.1	1.21	330	1.08
10	813	82.6	1.4	28.3	483	40.9	400.34	377.6	1.06	317.7	1.26	350	1.14
11	508	82.6	1.4	17.7	483	40.9	489.3	426.6	1.15	334.9	1.46	391	1.25
12	254	82.6	1.4	8.8	483	40.9	530.23	462.4	1.15	343.5	1.54	452	1.17
Gardner & Jacobson (1967)													
1	762	101.7	3.1	21.8	605.1	34.1	818.43	987.0	0.83	744.4	1.10	803	1.02
2	1524	101.7	3.1	43.7	605.1	31.2	800.64	649.6	1.23	613.4	1.31	668	1.20
5	1050	120.7	4.1	25.5	451.6	34.4	1156.5	1148.9	1.01	909.1	1.27	976	1.18
6	1050	120.8	4.1	25.4	451.6	29.6	1092.4	1112.9	0.98	873.4	1.25	937	1.17
7	1050	120.8	4.1	25.4	451.6	25.9	949.65	1083.8	0.88	844.8	1.12	907	1.05
11	1676.4	152.6	3.2	31.7	415.1	20.9	938.53	1015.1	0.92	845.4	1.11	905	1.04
12	1676.4	152.7	3.2	31.7	415.1	20.9	880.7	1016.3	0.87	846.3	1.04	906	0.97
18	1524	76.5	1.7	57.6	363.3	25	244.64	172.3	1.42	178.9	1.37	200	1.23
20	609.6	76.4	1.7	23.1	363.3	40.9	411.44	338.4	1.22	276.6	1.49	311	1.32
21	609.3	76.5	1.7	23.0	363.3	25.9	330.26	288.1	1.15	227.4	1.45	258	1.28
Knowles and Park (1970)													
Kloppel and Goder (1957)													
7	1420.1	95	12.5	48.1	274.6	20.3	946.98	838.8	1.13	833.2	1.14	874	1.08
8	1420.1	95	12.8	48.3	272.6	20.3	937.64	845.9	1.11	842.3	1.11	883	1.06
9	1420.1	95	12.4	48.1	272.6	20.3	906.95	829.9	1.09	823.6	1.10	864	1.05
10	860	95	12.6	29.2	274.6	20.3	1017.7	1067.9	0.95	914.3	1.11	1410	0.72
11	860	95	12.7	29.2	272.6	20.3	1007.9	1065.7	0.95	913.6	1.10	948	1.06
12	860	95	12.7	29.2	272.6	20.3	1033.7	1065.7	0.97	913.6	1.13	948	1.09
13	1979.9	95	12.8	67.3	278.5	20.3	886.49	685.6	1.29	750.8	1.18	796	1.11
14	1979.9	95	12.5	67.1	275.6	20.3	906.95	671.0	1.35	733.6	1.24	779	1.16
15	1979.9	95	12.6	67.2	279.5	20.3	916.73	680.3	1.35	744.6	1.23	790	1.16
41	860	95	3.7	26.6	326.5	25	656.08	563.8	1.16	450.4	1.46	492	1.33
42	860	95	3.7	26.6	386.4	25	686.33	641.0	1.07	507.2	1.35	545	1.26
43	860	95	3.4	26.5	335.4	25	656.08	543.8	1.21	434.3	1.51	475	1.38
44	1420.1	95	3.9	44.1	326.5	25	566.68	454.4	1.25	426.1	1.33	461	1.23

Name	Length (mm)	D (mm)	t (mm)	kL/r_e	Fy (MPa)	fc' (MPa)	Pf (kN)	CAN/CSA-S16.1 Pr (kN)	CAN/CSA-S16.1 Pf/Pr	AISC LFRD Pr (kN)	AISC LFRD Pf/Pr	Eurocode 4 Pr (kN)	Eurocode 4 Pf/Pr
Kloppel and Goder (1957)													
45	1420.1	95	3.9	44.1	386.4	25	605.82	506.8	1.20	474.7	1.28	513	1.18
46	1420.1	95	3.6	43.9	335.4	25	575.57	439.3	1.31	411.2	1.40	446	1.29
47	1979.9	95	3.8	61.4	326.5	25	536.43	343.4	1.56	366.2	1.47	400	1.34
48	1979.9	95	3.8	61.4	317.4	25	565.79	338.6	1.67	360.7	1.57	394	1.43
49	1979.9	95	3.5	61.2	335.4	25	487.5	330.6	1.47	352.1	1.38	385	1.26
63	2220	216	4.1	29.6	284.4	22.9	1023.0	1599.6	0.64	1351.1	0.76	1499	0.68
64	2220	216	4.1	29.6	299.1	22.9	1834.4	1647.1	1.11	1386.5	1.32	1533	1.20
65	2220	216	4	29.6	288.3	29.8	2288.9	1774.4	1.29	1523.6	1.50	1692	1.35
66	2220	216	4.1	29.6	286.3	29.8	2238.7	1788.9	1.25	1535.1	1.46	1704	1.31
69	2220	216	6.1	29.9	389.4	22.9	2461.5	2498.5	0.99	2043.2	1.20	2179	1.13
70	2220	216	6	29.9	331.2	22.9	2421.1	2207.4	1.10	1821.8	1.33	1968	1.23
71	2220	216	6.5	30.0	295.2	29.8	2804.9	2317.7	1.21	1950.9	1.44	2123	1.32
72	2220	216	6.3	29.9	336.1	29.8	2932.1	2473.2	1.19	2066.2	1.42	2231	1.31
73	1979.9	95	3.9	61.4	332.4	24.1	498.18	349.9	1.42	373.1	1.34	406	1.23
74	1979.9	95	3.4	61.1	337.4	24.1	472.82	323.3	1.46	343.7	1.38	375	1.26
75	1979.9	95	3.6	61.2	355	24.1	472.82	343.5	1.38	366.5	1.29	399	1.19
76	1979.9	95	3.7	61.3	326.5	24.1	412.82	335.4	1.23	356.9	1.16	389	1.06
83	1050	121	3.7	25.3	295.2	21.1	695.22	705.2	0.99	559.5	1.24	630	1.10
84	1050	121	3.7	25.3	327.6	21.1	746.37	761.3	0.98	599.9	1.24	669	1.12
85	1050	121	3.8	25.3	307.9	24.2	836.67	765.5	1.09	610.0	1.37	681	1.23
86	1050	121	4	25.4	326.5	24.2	866.92	825.8	1.05	654.5	1.32	725	1.20
89	1050	121	5.6	25.7	344.2	21.1	998.13	1057.3	0.94	826.9	1.21	901	1.11
90	1050	121	5.4	25.7	343.2	21.1	1017.7	1027.7	0.99	803.7	1.27	878	1.16
91	1050	121	5.5	25.7	330.5	24.2	1099.1	1033.3	1.06	814.6	1.35	891	1.23
92	1050	121	5.6	25.7	321.6	24.2	1078.6	1023.8	1.05	808.4	1.33	886	1.22
95	2310.1	121	3.7	55.7	295.2	21.1	640.51	465.0	1.38	473.9	1.35	523	1.22
96	2310.1	121	3.8	55.7	327.6	21.1	629.22	499.3	1.26	510.5	1.23	562	1.12
97	2310.1	121	3.7	55.7	307.9	24.2	695.22	491.3	1.42	503.7	1.38	556	1.25
98	2310.1	121	3.9	55.8	326.5	24.2	755.27	522.2	1.45	536.6	1.41	590	1.28
101	2310.1	121	5.7	56.6	344.2	21.1	786.41	669.1	1.18	693.0	1.13	751	1.05
102	2310.1	121	5.5	56.5	343.2	21.1	815.76	652.0	1.25	674.5	1.21	732	1.11
103	2310.1	121	5.6	56.6	330.5	24.2	873.39	659.6	1.32	684.6	1.28	743	1.18
104	2310.1	121	5.4	56.5	321.6	24.2	865.14	634.5	1.36	657.3	1.32	715	1.21
Salani and Sims (1964)													
30F	1066.8	50.8	1.7	61.4	524	27.9	120.54	109.6	1.10	119.9	1.01	128	0.95
42F	1066.8	76.2	1.7	40.5	524	27.2	320.26	282.7	1.13	256.7	1.25	282	1.14
49F	1066.8	25.4	0.9	123.1	524	27.8	15.75	10.7	1.48	10.6	1.49	11	1.40
50F	1066.8	25.4	0.9	123.1	524	27.8	15.52	10.7	1.45	10.6	1.47	11	1.38
51F	1066.8	38.1	2.8	85.2	524	27.8	112.98	73.3	1.54	84.6	1.34	81	1.39
52F	1066.8	38.1	2.8	85.2	524	27.8	106.75	73.3	1.46	84.6	1.26	81	1.31
71F	1066.8	69.9	1.2	43.9	524	27.9	230.85	191.7	1.20	180.5	1.28	201	1.15

Name	Length (mm)	D (mm)	t (mm)	kL/r_s	Fy (MPa)	fc' (MPa)	Pf (kN)	CAN/CSA-S16.1 Pr (kN)	CAN/CSA-S16.1 Pf/Pr	AISC LFRD Pr (kN)	AISC LFRD Pf/Pr	Eurocode 4 Pr (kN)	Eurocode 4 Pf/Pr
Furlong (1967)													
3	914	152.4	1.5	17.1	330.9	21	682.32	666.5	1.02	536.1	1.27	657	1.04
4	914	152.4	1.5	17.1	330.9	25.9	721.47	738.9	0.98	606.5	1.19	735	0.98
5	914	152.4	1.5	17.1	330.9	25.9	733.03	738.9	0.99	606.5	1.21	735	1.00
6	914	127	2.4	20.7	289.6	35.2	627.17	731.5	0.86	601.8	1.04	702	0.89
7	914	127	2.4	20.7	289.6	35.2	622.72	731.5	0.85	601.8	1.03	702	0.89
8	914	127	2.4	20.7	289.6	35.2	658.3	731.5	0.90	601.8	1.09	702	0.94
Knowles and Park (1969)													
1	1727	88.9	5.8	58.6	400	40	614.74	518.5	1.19	562.7	1.09	603	1.02
2	1422	89	5.8	48.2	400	39.6	711.72	620.8	1.15	621.3	1.15	669	1.06
3	1118	89	5.8	37.9	400	39	715.27	743.4	0.96	670.7	1.07	716	1.00
4	813	89	5.8	27.6	400	41.8	918.56	886.1	1.04	722.4	1.27	759	1.21
5	508	89	5.8	17.2	400	40.9	991.95	1009.1	0.98	749.7	1.32	874	1.14
6	508	89	5.8	17.2	400	40.9	889.64	1009.1	0.88	749.7	1.19	874	1.02
7	1727	82.55	1.4	60.2	483	41.3	224.64	218.2	1.03	235.0	0.96	255	0.88
8	1422	82.6	1.4	49.5	483	37	294.47	255.5	1.15	254.8	1.16	285	1.03
9	1118	82.6	1.4	38.9	483	40.9	355.86	321.3	1.11	294.1	1.21	330	1.08
10	813	82.6	1.4	28.3	483	40.9	400.34	377.6	1.06	317.7	1.26	350	1.14
11	508	82.6	1.4	17.7	483	40.9	489.3	426.6	1.15	334.9	1.46	391	1.25
12	254	82.6	1.4	8.8	483	40.9	530.23	462.4	1.15	343.5	1.54	452	1.17
Gardner & Jacobson (1967)													
1	762	101.7	3.1	21.8	605.1	34.1	818.43	987.0	0.83	744.4	1.10	803	1.02
2	1524	101.7	3.1	43.7	605.1	31.2	800.64	649.6	1.23	613.4	1.31	668	1.20
5	1050	120.7	4.1	25.5	451.6	34.4	1156.5	1148.9	1.01	909.1	1.27	976	1.18
6	1050	120.8	4.1	25.4	451.6	29.6	1092.4	1112.9	0.98	873.4	1.25	937	1.17
7	1050	120.8	4.1	25.4	451.6	25.9	949.65	1083.8	0.88	844.8	1.12	907	1.05
11	1676.4	152.6	3.2	31.7	415.1	20.9	938.53	1015.1	0.92	845.4	1.11	905	1.04
12	1676.4	152.7	3.2	31.7	415.1	20.9	880.7	1016.3	0.87	846.3	1.04	906	0.97
18	1524	76.5	1.7	57.6	363.3	25	244.64	172.3	1.42	178.9	1.37	200	1.23
20	609.6	76.4	1.7	23.1	363.3	40.9	411.44	338.4	1.22	276.6	1.49	311	1.32
21	609.3	76.5	1.7	23.0	363.3	25.9	330.26	288.1	1.15	227.4	1.45	258	1.28
Knowles and Park (1970)													
Kloppel and Goder (1957)													
7	1420.1	95	12.5	48.1	274.6	20.3	946.98	838.8	1.13	833.2	1.14	874	1.08
8	1420.1	95	12.8	48.3	272.6	20.3	937.64	845.9	1.11	842.3	1.11	883	1.06
9	1420.1	95	12.4	48.1	272.6	20.3	906.95	829.9	1.09	823.6	1.10	864	1.05
10	860	95	12.6	29.2	274.6	20.3	1017.7	1067.9	0.95	914.3	1.11	1410	0.72
11	860	95	12.7	29.2	272.6	20.3	1007.9	1065.7	0.95	913.6	1.10	948	1.06
12	860	95	12.7	29.2	272.6	20.3	1033.7	1065.7	0.97	913.6	1.13	948	1.09
13	1979.9	95	12.8	67.3	278.5	20.3	886.49	685.6	1.29	750.8	1.18	796	1.11
14	1979.9	95	12.5	67.1	275.6	20.3	906.95	671.0	1.35	733.6	1.24	779	1.16
15	1979.9	95	12.6	67.2	279.5	20.3	916.73	680.3	1.35	744.6	1.23	790	1.16
41	860	95	3.7	26.6	326.5	25	656.08	563.8	1.16	450.4	1.46	492	1.33
42	860	95	3.7	26.6	386.4	25	686.33	641.0	1.07	507.2	1.35	545	1.26
43	860	95	3.4	26.5	335.4	25	656.08	543.8	1.21	434.3	1.51	475	1.38
44	1420.1	95	3.9	44.1	326.5	25	566.68	454.4	1.25	426.1	1.33	461	1.23

Table 6.2: Experimental to calculated ratios for tested specimens using National codes

Code	CFST 64 P = 1000 kN		CFST 34 P = 1820 kN		CFST 42 P = 1820 kN		CFST 51 P = 1600 kN	
	Strength (kN m)	Calculated / Tested	Strength (kN m)	Calculated / Tested	Strength (kN m)	Calculated / Tested	Strength (kN m)	Calculated / Tested
Test Data	591		444		928		356	
AISC LRFD (1994)	362	1.64	234	1.90	681	1.36	158	2.25
CAN/S16.1-M94	314	1.88	255	1.74	608	1.53	182	1.95
Eurocode 4 (1994)	522	1.33	402	1.10	918	1.01	304	1.17
CAN/S16.1-M99 (Proposal A)	492	1.20	387	1.15	911	1.02	278	1.28
CAN/S16.1-M99 (Proposal B)	519	1.14	380	1.17	897	1.04	284	1.25

Table 6.3: Experimental axial and bending moments compared with code equations

	Name	Length (mm)	D (mm)	t (mm)	D/t*Fy	kL/r$_s$	Fy (MPa)	fc' (MPa)	Pf (kN)	Mf (kNm)	CAN/CSA-S16.1-M94		AISC LRFD 1994		Eurocode 4 1994	
											Mr (kNm)	Mf/Mr	Mr (kNm)	Mf/Mr	Mr	Mf/Mr
Prion and Boehme (1994)																
B	BP16	2120	152	1.65	30216	39.9	328	92	0	21	10.9	1.93	12.2	1.72	17.3	1.21
B	B11	2120	152	1.65	30216	39.9	328	92	470	29.7	10.9	2.74	8.8	3.39	27.4	1.08
B	B12	2120	152	1.65	30216	39.9	328	92	570	32.1	10.9	2.96	7.7	4.17	28.2	1.14
B	B13	2120	152	1.65	30216	39.9	328	92	670	28.5	10.9	2.63	6.6	4.29	28.9	0.99
B	B14	2120	152	1.65	30216	39.9	328	92	820	29.2	10.9	2.69	5.0	5.79	29.0	1.01
B	B15	2120	152	1.65	30216	39.9	328	92	970	30.5	10.9	2.81	3.4	8.85	22.5	1.35
B	B17	2120	152	1.65	30216	39.9	328	92	270	30.1	10.9	2.77	10.9	2.76	24.1	1.25
D	BP18	2120	152	1.65	30216	39.9	328	92	270	30.8	10.9	2.84	10.9	2.83	24.1	1.28
D	BP19	2120	152	1.65	30216	39.9	328	92	670	34.8	10.9	3.21	6.6	5.24	28.9	1.20
A	BP20	1071	152	1.65	30216	20.1	328	92	1273	21.4	10.0	2.13	2.3	9.4	21.9	0.98
A	BP21	1071	152	1.65	30216	20.1	328	92	1451	13.8	10.0	1.38	0.7	20.6	16.6	0.83
A	BP22	1071	152	1.65	30216	20.1	328	92	1309	15.9	10.0	1.59	2.0	8.15	20.8	0.76
Furlong (1967)																
A	9	914	113.4	3.15	14891	23.4	413.64	29.0	444.8	11.2	13.1	0.85	5.4	2.06	10.0	1.12
A	10	914	113.4	3.15	14891	23.4	413.64	29.0	400.3	11.9	13.1	0.90	6.7	1.78	11.9	1.00
A	11	914	113.4	3.15	14891	23.4	413.64	29.0	333.6	14.7	13.1	1.12	8.5	1.72	14.6	1.01
A	12	914	113.4	3.15	14891	23.4	413.64	29.0	222.4	15.8	13.1	1.20	11.6	1.36	18.0	0.88
A	13	914	113.4	3.15	14891	23.4	413.64	29.0	111.2	16.1	13.1	1.23	14.5	1.12	18.7	0.87
A	14	914	151.2	1.54	32549	17.3	330.91	25.9	567.6	9.9	8.1	1.21	0.8	13.09	6.6	1.50
A	15	914	151.2	1.54	32549	17.3	330.91	25.9	421.7	17.7	9.2	1.91	3.9	4.58	14.4	1.23
A	16	914	151.2	1.54	32549	17.3	330.91	25.9	286.0	17.1	9.2	1.85	6.7	2.54	17.1	1.00
A	17	914	151.2	1.54	32549	17.3	330.91	21.0	136.1	16.1	9.2	1.74	9.6	1.68	16.3	0.99
A	18	914	151.2	1.54	32549	17.3	330.91	21.0	135.2	14.9	9.2	1.62	9.6	1.56	16.3	0.92
A	19	914	126	2.39	15239	20.9	289.55	35.2	568.5	8.7	6.0	1.45	0.5	17.83	4.5	1.95
A	20	914	126	2.39	15239	20.9	289.55	35.2	533.8	12.6	7.5	1.69	1.2	10.57	6.2	2.03
A	21	914	126	2.39	15239	20.9	289.55	35.2	400.3	15.8	8.7	1.82	3.9	4.08	12.6	1.25
A	22	914	126	2.39	15239	20.9	289.55	35.2	84.5	15.7	8.7	1.80	9.8	1.6	14.1	1.11
A	23	914	126	2.39	15239	20.9	289.55	35.2	82.3	14.2	8.7	1.63	9.9	1.44	14.1	1.01
A	24	914	126	2.39	15239	20.9	289.55	35.2	345.2	15.7	8.7	1.81	5.0	3.16	13.5	1.17
A	25	914	126	2.39	15239	20.9	289.55	35.2	306.0	16.9	8.7	1.94	5.8	2.93	14.1	1.20

	Name	Length (mm)	D (mm)	t (mm)	D/t*Fy	kL/r_s	Fy (MPa)	fc' (MPa)	Pf (kN)	Mf (kNm)	CAN/CSA-S16.1-M94		AISC LRFD 1994		Eurocode 4 1994	
											Mr (kNm)	Mf/Mr	Mr (kNm)	Mf/Mr	Mr	Mf/Mr
Furlong (1967)																
A	26	914	126	2.39	15239	20.9	289.55	35.2	266.9	17.5	8.7	2.01	6.6	2.67	14.7	1.19
A	27	914	126	2.39	15239	20.9	289.55	35.2	260.7	17.4	8.7	2.00	6.7	2.61	14.8	1.18
A	28	914	126	2.39	15239	20.9	289.55	35.2	174.8	16.3	8.7	1.88	8.4	1.94	15.4	1.06
A	29	914	126	2.39	15239	20.9	289.55	35.2	89.0	15.8	8.7	1.81	9.8	1.61	14.2	1.11
A	30	914	126	2.39	15239	20.9	289.55	35.2	43.6	14.6	8.7	1.67	10.2	1.43	13.5	1.08
Knowles and Park (1969)																
A	13	806.4	88.2	5.84	6039	27.6	400	40.9	554.2	10.7	8.7	1.24	4.0	2.68	6.0	1.78
A	14	1411.2	88.2	5.84	6039	48.3	400	40.9	469.1	7.9	4.0	1.96	4.3	1.81	7.0	1.13
A	15	806.4	88.2	5.84	6039	27.6	400	40.9	194.8	6.4	13.3	0.48	13.0	0.50	16.8	0.38
A	16	1108.8	88.2	5.84	6039	38.0	400	40.9	191.3	5.8	13.9	0.42	12.8	0.46	16.9	0.34
A	17	806.4	82.55	1.40	28541	28.1	483	40.9	167.9	3.3	3.8	0.87	2.4	1.39	5.4	0.61
A	18	806.4	82.55	1.40	28541	28.1	483	40.9	89	2.6	3.8	0.69	3.6	0.72	6.1	0.43
Alfawakiri (1997)																
C	FA1	1605	152.4	3.40	14792	30.5	330	89.4	400	49.2	21.26	2.32	20.0	2.46	32.1	1.53
C	FA2	1605	152.4	3.40	14792	30.5	330	72	100	37.3	21.26	1.75	23.9	1.56	33.4	1.12
C	FA3	1605	152.4	3.40	14792	30.5	330	75.7	700	49.1	21.26	2.31	12.6	3.89	38.9	1.26
Marson(1999)																
C	CFST 64	2200	406.4	5.50	27635	15.5	442	37	1000	592	314.3	1.88	361.8	1.64	522.0	1.13
C	CFST 34	2200	323.9	7.50	17922	19.7	415	40.5	1820	444	254.7	1.74	233.8	1.90	400.6	1.11
C	CFST 42	2200	406.4	9.50	21603	15.7	505	35	1820	928	608.1	1.53	681.5	1.36	914.8	1.01
C	CFST 51	2200	323.9	5.50	23556	19.5	400	35	1600	356	182.3	1.95	158.2	2.25	302.2	1.18
									Average			**1.79**		**3.90**		**1.10**
									Standard Deviation			**0.64**		**4.20**		**0.32**
Marson(1999) nominal																
C	CFST 64	2200	406.4	6.53	21783	15.6	350	30	1000	592	294.0	2.01	334	1.77	481.8	1.23
C	CFST 34	2200	323.9	9.53	11896	19.8	350	30	1820	444	269.5	1.65	236	1.88	381.6	1.16
C	CFST 42	2200	406.4	9.53	14926	15.7	350	30	1820	928	422.7	2.20	438	2.12	668.9	1.39
C	CFST 51	2200	323.9	6.53	17853	19.6	350	30	1600	356	269.5	1.32	158	2.26	289.6	1.23

The letter in the first column is the type of bending moment loading condition

Table 6.4: AISC LRFD (1994) equations for experimental axial and bending moments

Name	Length mm	D mm	t mm	k	Fy MPa	fc' MPa	Pf kN	Mf kNm	Rm mm	Fmy MPa	Em MPa	λ	Mr kNm	Mf/Mr	Pf/Pn
Prion and Boehme (1994)															
BP16	2120	152	1.65	1.00	328	92	0	21	53.2	2070.5	632229	0.5	12.2	1.72	0.00
B11	2120	152	1.65	1.00	328	92	470	30	53.2	2070.5	632229	0.5	8.8	3.39	0.36
B12	2120	152	1.65	1.00	328	92	570	32	53.2	2070.5	632229	0.5	7.7	4.17	0.44
B13	2120	152	1.65	1.00	328	92	670	29	53.2	2070.5	632229	0.5	6.6	4.29	0.52
B14	2120	152	1.65	1.00	328	92	820	29	53.2	2070.5	632229	0.5	5.0	5.79	0.63
B15	2120	152	1.65	1.00	328	92	970	31	53.2	2070.5	632229	0.5	3.4	8.85	0.75
B17	2120	152	1.65	1.00	328	92	270	30	53.2	2070.5	632229	0.5	10.9	2.76	0.21
BP18	2120	152	1.65	1.00	328	92	270	31	53.2	2070.5	632229	0.5	10.9	2.83	0.21
BP19	2120	152	1.65	1.00	328	92	670	35	53.2	2070.5	632229	0.5	6.6	5.24	0.52
BP20	1071	152	1.65	1.00	328	92	1273	21	53.2	2070.5	632229	0.1	2.3	9.40	0.83
BP21	1071	152	1.65	1.00	328	92	1451	14	53.2	2070.5	632229	0.1	0.7	20.60	0.95
BP22	1071	152	1.65	1.00	328	92	1309	16	53.2	2070.5	632229	0.1	2.0	8.15	0.86
Furlong (1967)															
9	914	113	3.15	1.00	414	29	445	11	39.0	616.9	289854	0.1	5.4	2.06	0.69
10	914	113	3.15	1.00	414	29	400	12	39.0	616.9	289854	0.1	6.7	1.78	0.63
11	914	113	3.15	1.00	414	29	334	15	39.0	616.9	289854	0.1	8.5	1.72	0.52
12	914	113	3.15	1.00	414	29	222	16	39.0	616.9	289854	0.1	11.6	1.36	0.35
13	914	113	3.15	1.00	414	29	111	16	39.0	616.9	289854	0.1	14.5	1.12	0.17
14	914	151	1.54	1.00	331	26	568	10	52.9	854.8	445162	0.1	0.8	13.09	0.94
15	914	151	1.54	1.00	331	26	422	18	52.9	854.8	445162	0.1	3.9	4.58	0.70
16	914	151	1.54	1.00	331	26	286	17	52.9	854.8	445162	0.1	6.7	2.54	0.47
17	914	151	1.54	1.00	331	21	136	16	52.9	757.0	421099	0.1	9.6	1.68	0.25
18	914	151	1.54	1.00	331	21	135	15	52.9	757.0	421099	0.1	9.6	1.56	0.25
19	914	126	2.39	1.00	290	35	568	9	43.7	660.5	348845	0.1	0.5	17.83	0.96
20	914	126	2.39	1.00	290	35	534	13	43.7	660.5	348845	0.1	1.2	10.57	0.90
21	914	126	2.39	1.00	290	35	400	16	43.7	660.5	348845	0.1	3.9	4.08	0.68
22	914	126	2.39	1.00	290	35	85	16	43.7	660.5	348845	0.1	9.8	1.60	0.14
23	914	126	2.39	1.00	290	35	82	14	43.7	660.5	348845	0.1	9.9	1.44	0.14
24	914	126	2.39	1.00	290	35	345	16	43.7	660.5	348845	0.1	5.0	3.16	0.58
25	914	126	2.39	1.00	290	35	306	17	43.7	660.5	348845	0.1	5.8	2.93	0.52
26	914	126	2.39	1.00	290	35	267	17	43.7	660.5	348845	0.1	6.6	2.67	0.45
27	914	126	2.39	1.00	290	35	261	17	43.7	660.5	348845	0.1	6.7	2.61	0.44
28	914	126	2.39	1.00	290	35	175	16	43.7	660.5	348845	0.1	8.4	1.94	0.29
29	914	126	2.39	1.00	290	35	89	16	43.7	660.5	348845	0.1	9.8	1.61	0.15
30	914	126	2.39	1.00	290	35	44	15	43.7	660.5	348845	0.1	10.2	1.43	0.07
Knowles and Park (1969)															
13	806.4	88.2	5.84	1.00	400	41	554	11	29.2	505.8	239345	0.2	4.0	2.68	0.78
14	1411.2	88.2	5.84	1.00	400	41	469	8	29.2	505.8	239345	0.5	4.3	1.81	0.76
15	806.4	88.2	5.84	1.00	400	41	195	6	29.2	505.8	239345	0.2	13.0	0.50	0.27
16	1108.8	88.2	5.84	1.00	400	41	191	6	29.2	505.8	239345	0.3	12.8	0.46	0.28
17	806.4	82.6	1.4	1.00	483	41	168	3	28.7	970.6	381415	0.2	2.4	1.39	0.53
18	806.4	82.6	1.4	1.00	483	41	89	3	28.7	970.6	381415	0.2	3.6	0.72	0.28
Alfawakiri (1997)															
FA1	2050	152	3.4	1.00	330	89	400	49	52.7	1125.0	400038	0.4	20.0	2.46	0.29
FA2	2050	152	3.4	1.00	330	72	100	37	52.7	970.2	379518	0.4	23.9	1.56	0.08
FA3	2050	152	3.4	1.00	330	76	700	49	52.7	1003.2	384073	0.4	12.6	3.89	0.55
Marson(1999)															
CFST 64	2200	406	5.5	1.00	442	37	1000	592	141.8	999.5	418052	0.1	361.8	1.64	0.15
CFST 34	2200	324	7.5	1.00	415	41	1820	444	111.9	761.1	329375	0.1	233.8	1.90	0.33
CFST 42	2200	406	9.5	1.00	505	35	1820	928	140.4	801.0	319051	0.1	681.5	1.36	0.20
CFST 51	2200	324	5.5	1.00	400	35	1600	356	112.6	815.8	367223	0.1	158.2	2.25	0.37
													Average	**3.90**	
													Standard Deviation	**4.20**	

Table 6.5: CAN/CSA-S16.1-M94 equations for experimental axial and bending moments

Name	Length (mm)	D (mm)	t (mm)	D/t*fy	k	Fy (MPa)	fc' (MPa)	kL/ rs	kL/ rc	tau	tau'	w1	U1	Pf (kN)	Mf (kNm)	Mz	Mf/ Mr	Pf/ Pr
Prion and Boehme (1994)																		
BP16	2120	152	1.65	30216	1.00	328	92	40	56	0.89	1.05	1	1	0	21	11	1.93	0.00
B11	2120	152	1.65	30216	1.00	328	92	40	56	0.89	1.05	1	1	470	30	11	2.74	0.36
B12	2120	152	1.65	30216	1.00	328	92	40	56	0.89	1.05	1	1	570	32	11	2.96	0.44
B13	2120	152	1.65	30216	1.00	328	92	40	56	0.89	1.05	1	1	670	29	11	2.63	0.52
B14	2120	152	1.65	30216	1.00	328	92	40	56	0.89	1.05	1	1	820	29	11	2.69	0.63
B15	2120	152	1.65	30216	1.00	328	92	40	56	0.89	1.05	1	1	970	31	11	2.81	0.75
B17	2120	152	1.65	30216	1.00	328	92	40	56	0.89	1.05	1	1	270	30	11	2.77	0.21
BP18	2120	152	1.65	30216	1.00	328	92	40	56	0.89	1.05	1	1	270	31	11	2.84	0.21
BP19	2120	152	1.65	30216	1.00	328	92	40	56	0.89	1.05	1	1	670	35	11	3.21	0.52
BP20	1071	152	1.65	30216	1.00	328	92	20	28	0.82	1.12	1	1	1273	21	10	2.13	0.75
BP21	1071	152	1.65	30216	1.00	328	92	20	28	0.82	1.12	1	1	1451	14	10	1.38	0.86
BP22	1071	152	1.65	30216	1.00	328	92	20	28	0.82	1.12	1	1	1309	16	10	1.59	0.77
Furlong (1967)																		
9	914	113.4	3.15	14891	1.00	413.6	29.0	23	32	0.83	2.11	1	1	445	11	13	0.85	0.54
10	914	113.4	3.15	14891	1.00	413.6	29.0	23	32	0.83	2.11	1	1	400	12	13	0.90	0.49
11	914	113.4	3.15	14891	1.00	413.6	29.0	23	32	0.83	2.11	1	1	334	15	13	1.12	0.41
12	914	113.4	3.15	14891	1.00	413.6	29.0	23	32	0.83	2.11	1	1	222	16	13	1.20	0.27
13	914	113.4	3.15	14891	1.00	413.6	29.0	23	32	0.83	2.11	1	1	111	16	13	1.23	0.14
14	914	151.2	1.54	32549	1.00	330.9	25.9	17	24	0.81	1.45	1	1	568	10	8	1.21	0.77
15	914	151.2	1.54	32549	1.00	330.9	25.9	17	24	0.81	1.45	1	1	422	18	9	1.91	0.57
16	914	151.2	1.54	32549	1.00	330.9	25.9	17	24	0.81	1.45	1	1	286	17	9	1.85	0.39
17	914	151.2	1.54	32549	1.00	330.9	21.0	17	24	0.81	1.55	1	1	136	16	9	1.74	0.20
18	914	151.2	1.54	32549	1.00	330.9	21.0	17	24	0.81	1.55	1	1	135	15	9	1.62	0.20
19	914	126	2.39	15239	1.00	289.5	35.2	21	29	0.82	1.48	1	1	568	9	6	1.45	0.79
20	914	126	2.39	15239	1.00	289.5	35.2	21	29	0.82	1.48	1	1	534	13	7	1.69	0.74
21	914	126	2.39	15239	1.00	289.5	35.2	21	29	0.82	1.48	1	1	400	16	9	1.82	0.56
22	914	126	2.39	15239	1.00	289.5	35.2	21	29	0.82	1.48	1	1	85	16	9	1.80	0.12
23	914	126	2.39	15239	1.00	289.5	35.2	21	29	0.82	1.48	1	1	82	14	9	1.63	0.11
24	914	126	2.39	15239	1.00	289.5	35.2	21	29	0.82	1.48	1	1	345	16	9	1.81	0.48
25	914	126	2.39	15239	1.00	289.5	35.2	21	29	0.82	1.48	1	1	306	17	9	1.94	0.42
26	914	126	2.39	15239	1.00	289.5	35.2	21	29	0.82	1.48	1	1	267	17	9	2.01	0.37
27	914	126	2.39	15239	1.00	289.5	35.2	21	29	0.82	1.48	1	1	261	17	9	2.00	0.36
28	914	126	2.39	15239	1.00	289.5	35.2	21	29	0.82	1.48	1	1	175	16	9	1.88	0.24
29	914	126	2.39	15239	1.00	289.5	35.2	21	29	0.82	1.48	1	1	89	16	9	1.81	0.12
30	914	126	2.39	15239	1.00	289.5	35.2	21	29	0.82	1.48	1	1	44	15	9	1.67	0.06
Knowles and Park (1969)																		
13	806.4	88.2	5.84	6039	1.00	400	40.9	28	37	0.84	2.61	1	1	554	11	9	1.24	0.63
14	1411	88.2	5.84	6039	1.00	400	40.9	48	64	0.91	1.56	1	1	469	8	4	1.96	0.76
15	806.4	88.2	5.84	6039	1.00	400	40.9	28	37	0.84	2.61	1	1	195	6	13	0.48	0.22
16	1109	88.2	5.84	6039	1.00	400	40.9	38	50	0.87	2.03	1	1	191	6	14	0.42	0.26
17	806.4	82.55	1.4	28541	1.00	483	40.9	28	39	0.85	1.46	1	1	168	3	4	0.87	0.44
18	806.4	82.55	1.4	28541	1.00	483	40.9	28	39	0.85	1.46	1	1	89	3	4	0.69	0.24
Alfawakiri (1997)																		
FA1	1605	152.4	3.4	14792	1.00	330	89.4	30	42	0.85	1.17	0.6	1	400	49	21	2.32	0.23
FA2	1605	152.4	3.4	14792	1.00	330	72	30	42	0.85	1.21	0.6	1	100	37	21	1.75	0.06
FA3	1605	152.4	3.4	14792	1.00	330	75.7	30	42	0.85	1.20	0.6	1	700	49	21	2.31	0.44
Marson(1999)																		
CFST 64	2200	406.4	5.5	32660	1.00	442	37	16	22	0.80	1.59	0.6	1	1000	592	314	1.88	0.12
CFST 34	2200	323.9	7.5	17922	1.00	415	40.5	20	27	0.82	1.76	0.6	1	1820	444	255	1.74	0.26
CFST 42	2200	406.4	9.5	21603	1.00	505	35	16	22	0.80	2.22	0.6	1	1820	928	608	1.53	0.15
CFST 51	2200	323.9	5.5	23556	1.00	400	35	20	27	0.82	1.62	0.6	1	1600	356	182	1.95	0.29
																	Average	**1.79**
																	Standard Deviation	**0.64**

Table 6.6: Eurocode 4 (1994) equations for experimental axial and bending moments

Name	Length mm	D mm	t mm	e mm	ecc	Fy MPa	fc' MPa	Pf kN	Mf kNm	n2	n1	χ	Cai d	Cai n	Mr kNm	Mf/ Mr	Pf/Pr
Prion and Boehme (1994)																	
BP16	2120	152	1.65	0.00	0	328	92	0	21	1	0	0.81	0.00	0.00	17.3	1.21	0.00
B11	2120	152	1.65	63.19	0	328	92	470	30	1	0	0.81	0.25	0.20	27.4	1.08	0.25
B12	2120	152	1.65	56.32	0	328	92	570	32	1	0	0.81	0.31	0.20	28.2	1.14	0.31
B13	2120	152	1.65	42.54	0	328	92	670	29	1	0	0.81	0.36	0.20	28.9	0.99	0.36
B14	2120	152	1.65	35.61	0	328	92	820	29	1	0	0.81	0.44	0.20	29.0	1.01	0.44
B15	2120	152	1.65	31.44	0	328	92	970	31	1	0	0.81	0.52	0.20	22.5	1.35	0.52
B17	2120	152	1.65	111.48	0	328	92	270	30	1	0	0.81	0.15	0.15	24.1	1.25	0.15
BP18	2120	152	1.65	114.07	0	328	92	270	31	1	0	0.81	0.15	0.15	24.1	1.28	0.15
BP19	2120	152	1.65	51.94	0	328	92	670	35	1	0	0.81	0.36	0.20	28.9	1.20	0.36
BP20	1071	152	1.65	16.81	1	328	92	1273	21	1	0	0.95	0.69	0.24	21.9	0.98	0.69
BP21	1071	152	1.65	9.51	1	328	92	1451	14	0.98	0.09	0.95	0.78	0.24	16.6	0.83	0.78
BP22	1071	152	1.65	12.15	1	328	92	1309	16	0.99	0.05	0.95	0.71	0.24	20.8	0.76	0.71
Furlong (1967)																	
9	914	113	3.15	25.20	1	414	29	445	11	1	0	0.97	0.62	0.24	10.0	1.12	0.62
10	914	113	3.15	29.68	1	414	29	400	12	1	0	0.97	0.56	0.24	11.9	1.00	0.56
11	914	113	3.15	44.02	1	414	29	334	15	1	0	0.97	0.47	0.24	14.6	1.01	0.47
12	914	113	3.15	71.06	1	414	29	222	16	1	0	0.97	0.31	0.24	18.0	0.88	0.31
13	914	113	3.15	145.15	1	414	29	111	16	1	0	0.97	0.16	0.16	18.7	0.87	0.16
14	914	151	1.537	17.38	1	331	26	568	10	1	0	0.99	0.83	0.25	6.6	1.50	0.83
15	914	151	1.537	41.89	1	331	26	422	18	1	0	0.99	0.62	0.25	14.4	1.23	0.62
16	914	151	1.537	59.85	1	331	26	286	17	1	0	0.99	0.42	0.25	17.1	1.00	0.42
17	914	151	1.537	118.09	1	331	21	136	16	1	0	0.99	0.23	0.23	16.3	0.99	0.23
18	914	151	1.537	110.33	1	331	21	135	15	1	0	0.99	0.22	0.22	16.3	0.92	0.22
19	914	126	2.394	15.38	1	290	35	568	9	1	0	0.98	0.84	0.24	4.5	1.95	0.84
20	914	126	2.394	23.52	1	290	35	534	13	1	0	0.98	0.79	0.24	6.2	2.03	0.79
21	914	126	2.394	39.48	1	290	35	400	16	1	0	0.98	0.59	0.24	12.6	1.25	0.59
22	914	126	2.394	185.68	1	290	35	85	16	1	0	0.98	0.13	0.13	14.1	1.11	0.13
23	914	126	2.394	172.18	1	290	35	82	14	1	0	0.98	0.12	0.12	14.1	1.01	0.12
24	914	126	2.394	45.63	1	290	35	345	16	1	0	0.98	0.51	0.24	13.5	1.17	0.51
25	914	126	2.394	55.13	1	290	35	306	17	1	0	0.98	0.45	0.24	14.1	1.20	0.45
26	914	126	2.394	65.52	1	290	35	267	17	1	0	0.98	0.40	0.24	14.7	1.19	0.40
27	914	126	2.394	66.87	1	290	35	261	17	1	0	0.98	0.39	0.24	14.8	1.18	0.39
28	914	126	2.394	93.36	1	290	35	175	16	1	0	0.98	0.26	0.24	15.4	1.06	0.26
29	914	126	2.394	177.41	1	290	35	89	16	1	0	0.98	0.13	0.13	14.2	1.11	0.13
30	914	126	2.394	334.29	1	290	35	44	15	1	0	0.98	0.06	0.06	13.5	1.08	0.06
Knowles and Park (1969)																	
13	806.4	88.2	5.842	19.31	1	400	41	554	11	1	0	0.95	0.70	0.24	6.0	1.78	0.70
14	1411	88.2	5.842	16.76	1	400	41	469	8	1	0	0.84	0.59	0.21	7.0	1.13	0.59
15	806.4	88.2	5.842	33.01	1	400	41	195	6	1	0	0.95	0.25	0.24	16.8	0.38	0.25
16	1109	88.2	5.842	30.48	1	400	41	191	6	1	0	0.90	0.24	0.23	16.9	0.34	0.24
17	806.4	82.6	1.397	19.54	1	483	41	168	3	1	0	0.93	0.45	0.23	5.4	0.61	0.45
18	806.4	82.6	1.397	29.21	1	483	41	89	3	1	0	0.93	0.24	0.23	6.1	0.43	0.24
Alfawakiri (1997)																	
FA1	2050	152	3.4	123.12	0	330	89	400	49	1	0	0.85	0.20	0.20	32.1	1.53	0.20
FA2	2050	152	3.4	372.94	0	330	72	100	37	1	0	0.87	0.06	0.06	33.4	1.12	0.06
FA3	2050	152	3.4	70.12	0	330	76	700	49	1	0	0.86	0.39	0.22	38.9	1.26	0.39
Marson(1999)																	
FST 6	2200	406	5.5	591.80	0	442	37	1000	592	1	0	0.99	0.13	0.13	522.0	1.13	0.13
FST 3	2200	324	7.5	243.96	0	415	41	1820	444	1	0	0.97	0.30	0.24	400.6	1.11	0.30
FST 4	2200	406	9.5	509.89	0	505	35	1820	928	1	0	0.99	0.18	0.18	917.8	1.01	0.18
FST 5	2200	324	5.5	222.50	0	400	35	1600	356	1	0	0.98	0.33	0.24	302.2	1.18	0.33

ecc indicates if a column was subjected to an eccentric load (1)

Average 1.10

Standard Deviation 0.32

Table 6.7: Axial and bending moments compared by D/t values

									CAN/CSA S16.1-M94		AISC LRFD 1994		Eurocode 4 1994	
Name	Length mm	D mm	t mm	D/t*Fy	Fy MPa	fc' MPa	Pf (kN)	Mf (kNm)	Mr (kNm)	Mf/Mr	Mr (kNm)	Mf/Mr	Mr (kNm)	Mf/Mr
Class 1 sections														
Knowles and Park (1969)														
13	806.4	88.2	5.842	6039	400	41	554.2	10.7	8.7	1.24	4.0	2.68	6.0	1.78
14	1411.2	88.2	5.842	6039	400	41	469.1	7.9	4.0	1.96	4.3	1.81	7.0	1.13
15	806.4	88.2	5.842	6039	400	41	194.8	6.4	13.3	0.48	13.0	0.50	16.8	0.38
16	1108.8	88.2	5.842	6039	400	41	191.3	5.8	13.9	0.42	12.8	0.46	16.9	0.34
								AVERAGE		**1.02**		**1.36**		**0.91**
								STANDARD DEVIATION		**0.63**		**0.94**		**0.59**
Class 2 sections														
Marson(1999)														
CFST 34	2200	323.9	7.5	17922	415	41	1820	444.0	254.7	1.74	233.8	1.90	400.6	1.11
Alfawakiri (1997)														
FA1	1605	152.4	3.4	14792	330	89	400	49.2	21.3	2.32	20.0	2.46	32.1	1.43
FA2	1605	152.4	3.4	14792	330	72	100	37.3	21.3	1.75	23.9	1.56	33.4	1.12
FA3	1605	152.4	3.4	14792	330	76	700	49.1	21.3	2.31	12.6	3.89	38.9	1.26
Furlong (1967)														
9	914	113.4	3.15	14891	414	29	444.8	11.2	13.1	0.85	5.4	2.06	10.0	1.12
10	914	113.4	3.15	14891	414	29	400.3	11.9	13.1	0.90	6.7	1.78	11.9	1.00
11	914	113.4	3.15	14891	414	29	333.6	14.7	13.1	1.12	8.5	1.72	14.6	1.01
12	914	113.4	3.15	14891	414	29	222.4	15.8	13.1	1.20	11.6	1.36	18.0	0.88
13	914	113.4	3.15	14891	414	29	111.2	16.1	13.1	1.23	14.5	1.12	18.7	0.87
19	914	126	2.394	15239	290	35	568.5	8.7	6.0	1.45	0.5	17.83	4.5	1.95
20	914	126	2.394	15239	290	35	533.8	12.6	7.5	1.69	1.2	10.57	6.2	2.03
21	914	126	2.394	15239	290	35	400.3	15.8	8.7	1.82	3.9	4.08	12.6	1.25
22	914	126	2.394	15239	290	35	84.5	15.7	8.7	1.80	9.8	1.60	14.1	1.11
23	914	126	2.394	15239	290	35	82.3	14.2	8.7	1.63	9.9	1.44	14.1	1.01
24	914	126	2.394	15239	290	35	345.2	15.7	8.7	1.81	5.0	3.16	13.5	1.17
25	914	126	2.394	15239	290	35	306.0	16.9	8.7	1.94	5.8	2.93	14.1	1.20
26	914	126	2.394	15239	290	35	266.9	17.5	8.7	2.01	6.6	2.67	14.7	1.19
27	914	126	2.394	15239	290	35	260.7	17.4	8.7	2.00	6.7	2.61	14.8	1.18
28	914	126	2.394	15239	290	35	174.8	16.3	8.7	1.88	8.4	1.94	15.4	1.06
29	914	126	2.394	15239	290	35	89.0	15.8	8.7	1.81	9.8	1.61	14.2	1.11
30	914	126	2.394	15239	290	35	43.6	14.6	8.7	1.67	10.2	1.43	13.5	1.08
								AVERAGE		**1.66**		**3.32**		**1.20**
								STANDARD DEVIATION		**0.40**		**3.79**		**0.29**
Class 3 sections														
Marson(1999)														
CFST 51	2200	323.9	5.5	23563	400	35	1600	356.0	182.3	1.95	158.2	2.25	302.2	1.18
CFST 42	2200	406.4	7.5	27364	505	35	1820	928.0	608.1	1.53	681.5	1.36	914.8	1.01
								AVERAGE		**1.74**		**1.81**		**1.10**
								STANDARD DEVIATION		**0.21**		**0.44**		**0.08**
Class 4 sections Permitted by Clause 18.6														
Marson(1999)														
CFST 64	2200	406.4	6.5	27635	442	37	1000	591.0	314.3	1.88	361.8	1.64	522.0	1.13
								AVERAGE		**1.88**		**1.64**		**1.13**
								STANDARD DEVIATION		**0.00**		**0.00**		**0.00**

									CAN/CSA S16.1-M94		AISC LRFD 1994		Eurocode 4 1994	
Name	Length mm	D mm	t mm	D/t*Fy	Fy MPa	fc' MPa	Pf (kN)	Mf (kNm)	Mr (kNm)	Mf/Mr	Mr (kNm)	Mf/Mr	Mr (kNm)	Mf/Mr
Class 4														
Knowles and Park (1969)														
17	806.4	82.55	1.397	28541	483	41	167.9	3.3	3.8	0.87	2.4	1.39	5.4	0.61
18	806.4	82.55	1.397	28541	483	41	89	2.6	3.8	0.69	3.6	0.72	6.1	0.43
Prion and Boehme (1994)														
BP16	2120	152	1.65	30216	328	92	0	21.0	10.9	1.93	12.2	1.72	17.3	1.21
B11	2120	152	1.65	30216	328	92	470	29.7	10.9	2.74	8.8	3.39	27.4	1.08
B12	2120	152	1.65	30216	328	92	570	32.1	10.9	2.96	7.7	4.17	28.2	1.14
B13	2120	152	1.65	30216	328	92	670	28.5	10.9	2.63	6.6	4.29	28.9	0.99
B14	2120	152	1.65	30216	328	92	820	29.2	10.9	2.69	5.0	5.79	29.0	1.01
B15	2120	152	1.65	30216	328	92	970	30.5	10.9	2.81	3.4	8.85	22.5	1.35
B17	2120	152	1.65	30216	328	92	270	30.1	10.9	2.77	10.9	2.76	24.1	1.25
BP18	2120	152	1.65	30216	328	92	270	30.8	10.9	2.84	11.0	2.83	24.1	1.28
BP19	2120	152	1.65	30216	328	92	670	34.8	10.9	3.21	6.6	5.24	28.9	1.20
BP20	1071	152	1.65	30216	328	92	1273	21.4	10.0	2.13	2.3	9.40	21.9	0.98
BP21	1071	152	1.65	30216	328	92	1451	13.8	10.0	1.38	0.7	20.60	16.6	0.83
BP22	1071	152	1.65	30216	328	92	1309	15.9	10.0	1.59	2.0	8.15	20.8	0.76
Furlong (1967)														
14	914	151.2	1.537	32549	331	26	567.6	9.9	8.1	1.21	0.8	13.09	6.6	1.50
15	914	151.2	1.537	32549	331	26	421.7	17.7	9.2	1.91	3.9	4.58	14.4	1.23
16	914	151.2	1.537	32549	331	26	286.0	17.1	9.2	1.85	6.7	2.54	17.1	1.00
17	914	151.2	1.537	32549	331	21	136.1	16.1	9.2	1.74	9.6	1.68	16.3	0.99
18	914	151.2	1.537	32549	331	21	135.2	14.9	9.2	1.62	9.6	1.56	16.3	0.92
							AVERAGE			**2.08**		**5.41**		**1.04**
							STANDARD DEVIATION			**0.73**		**4.79**		**0.25**

Table 6.8: Nominal values for tested specimens compared by D/t values

									CAN/CSA S16.1-M94		AISC LRFD 1994		Eurocode 4 1994	
Name	Length mm	D mm	t mm	D/t*Fy	Fy MPa	fc' MPa	Pf (kN)	Mf (kNm)	Mr (kNm)	Mf/Mr	Mr (kNm)	Mf/Mr	Mr (kNm)	Mf/Mr
Class 1 sections														
Marson (1999) nominal														
CFST 34	2200	323.9	9.53	11896	350	30	1820	444.0	269.5	1.65	236.0	1.88	381.6	1.16
Class 2 sections														
Marson(1999) nominal														
CFST 42	2200	406.4	9.53	14926	350	30	1820	928.0	422.7	2.20	438.0	2.12	668.9	1.23
CFST 51	2200	323.9	6.5	17853	350	30	1600	356.0	269.5	1.32	159.0	2.26	289.6	1.23
Class 3 sections														
Marson(1999)														
CFST 64	2200	406.4	6.5	21783	350	30	1000	591.0	294.0	2.01	334.0	1.77	481.8	1.23

Table 6.9: Comparison of different material stress-strain relationships with test curve.

Step #	Researcher	Type of Concrete or Modification	CFST 64		CFST 34		CFST 42		CFST 51	
			Strength (kN)	Calculated / Tested	Strength (kN)	Calculated / Tested	Strength (kN)	Calculated / Tested	Strength (kN)	Calculated / Tested
Test Data			591	1.0	444	1.0	928	1.00	356	1.0
1	Mander et al. (1988)	Confined concrete	607	1.03	513	1.15	1074	1.16	383	1.07
2	Hognestad (1951)	Unconfined concrete	510	0.86	359	0.81	845	0.91	251	0.70
3	Saatcioglu and Razvi (1992)	Confined concrete	607	1.03	521	1.17	1109	1.19	387	1.09
4	Hognestad (1951)	high ductility	545	0.92	403	0.92	920	0.99	310	0.87
5	Hognestad (1951)	CISC provisions	480	0.81	383	0.86	851	0.92	288	0.81
6	Hognestad (1951)	high ductility and CISC provisions	506	0.86	418	0.94	900	0.97	321	0.90

Table 6.10: Comparison of new proposals for CAN/S16.1

												Original					Proposal A					Proposal B	
Name	Length mm	D mm	t mm	k	Fy MPa	fc' MPa	Pf kN	Mf kNm	tau	tau'	Mr kNm	Mf/Mr	Crco kN	Crcm	B	P/Pr	Mr kNm	Mf/Mr	Crhc kN	Mrc kNm	Mrhc kNm	Mr kNm	Mf/Mr
Prion and Boehme (1994)																							
BP16	2120	152	1.65	1.00	328	92	0	21.0	0.89	1.05	10.9	1.93	1843	1598	0.13	0.00	37.5	0.56	799	17.1	37.4	17.1	1.23
B11	2120	152	1.65	1.00	328	92	470	29.7	0.89	1.05	10.9	2.74	1843	1598	0.13	0.25	37.5	0.79	799	17.1	37.4	20.0	1.48
B12	2120	152	1.65	1.00	328	92	570	32.1	0.89	1.05	10.9	2.96	1843	1598	0.13	0.31	37.5	0.85	799	17.1	37.4	20.7	1.55
B13	2120	152	1.65	1.00	328	92	670	28.5	0.89	1.05	10.9	2.63	1843	1598	0.13	0.36	37.5	0.76	799	17.1	37.4	21.3	1.34
B14	2120	152	1.65	1.00	328	92	820	29.2	0.89	1.05	10.9	2.69	1843	1598	0.13	0.44	37.5	0.78	799	17.1	37.4	21.1	1.38
B15	2120	152	1.65	1.00	328	92	970	30.5	0.89	1.05	10.9	2.81	1843	1598	0.13	0.53	37.5	0.81	799	17.1	37.4	14.4	2.11
B17	2120	152	1.65	1.00	328	92	270	30.1	0.89	1.05	10.9	2.77	1843	1598	0.13	0.15	37.5	0.80	799	17.1	37.4	18.8	1.60
BP18	2120	152	1.65	1.00	328	92	270	30.8	0.89	1.05	10.9	2.84	1843	1598	0.13	0.15	37.5	0.82	799	17.1	37.4	18.8	1.64
BP19	2120	152	1.65	1.00	328	92	670	34.8	0.89	1.05	10.9	3.21	1843	1598	0.13	0.36	37.5	0.93	799	17.1	37.4	21.3	1.64
BP20	1071	152	1.65	1.00	328	92	1273	21.4	0.82	1.12	10.0	2.13	1843	1598	0.13	0.69	37.5	0.57	799	17.1	37.4	17.3	1.24
BP21	1071	152	1.65	1.00	328	92	1451	13.8	0.82	1.12	10.0	1.38	1843	1598	0.13	0.79	37.5	0.37	799	17.1	37.4	11.6	1.19
BP22	1071	152	1.65	1.00	328	92	1309	15.9	0.82	1.12	10.0	1.59	1843	1598	0.13	0.71	37.5	0.42	799	17.1	37.4	16.1	0.99
Furlong (1967)																							
9	914	113.4	3.15	1.00	414	29	444.8	11.2	0.83	2.11	13.1	0.85	1052	261	0.75	0.42	9.1	1.23	130	19.0	18.8	11.6	0.97
10	914	113.4	3.15	1.00	414	29	400.3	11.9	0.83	2.11	13.1	0.90	1052	261	0.75	0.38	10.2	1.17	130	19.0	18.8	12.9	0.92
11	914	113.4	3.15	1.00	414	29	333.6	14.7	0.83	2.11	13.1	1.12	1052	261	0.75	0.32	11.8	1.24	130	19.0	18.8	15.0	0.98
12	914	113.4	3.15	1.00	414	29	222.4	15.8	0.83	2.11	13.1	1.20	1052	261	0.75	0.21	14.5	1.09	130	19.0	18.8	17.4	0.91
13	914	113.4	3.15	1.00	414	29	111.2	16.1	0.83	2.11	13.1	1.23	1052	261	0.75	0.11	15.0	1.08	130	19.0	18.8	18.1	0.89
14	914	151.2	1.537	1.00	331	26	567.6	9.9	0.81	1.45	8.1	1.21	833	446	0.47	0.68	7.8	1.26	223	14.5	18.4	7.2	1.38
15	914	151.2	1.537	1.00	331	26	421.7	17.7	0.81	1.45	9.2	1.91	833	446	0.47	0.51	14.5	1.22	223	14.5	18.4	12.9	1.37
16	914	151.2	1.537	1.00	331	26	286.0	17.1	0.81	1.45	9.2	1.85	833	446	0.47	0.34	15.8	1.08	223	14.5	18.4	15.9	1.08
17	914	151.2	1.537	1.00	331	21	136.1	16.1	0.81	1.55	9.2	1.74	763	362	0.52	0.18	14.3	1.12	181	14.3	17.1	15.7	1.02
18	914	151.2	1.537	1.00	331	21	135.2	14.9	0.81	1.55	9.2	1.62	763	362	0.52	0.18	14.3	1.04	181	14.3	17.1	15.7	0.95
19	914	126	2.394	1.00	290	35	568.5	8.7	0.82	1.48	6.0	1.45	848	406	0.52	0.67	5.5	1.58	203	13.5	15.8	5.5	1.60
20	914	126	2.394	1.00	290	35	533.8	12.6	0.82	1.48	7.5	1.69	848	406	0.52	0.63	6.8	1.85	203	13.5	15.8	6.7	1.87
21	914	126	2.394	1.00	290	35	400.3	15.8	0.82	1.48	8.7	1.82	848	406	0.52	0.47	11.6	1.36	203	13.5	15.8	11.4	1.39
22	914	126	2.394	1.00	290	35	84.5	15.7	0.82	1.48	8.7	1.80	848	406	0.52	0.10	13.7	1.15	203	13.5	15.8	14.0	1.12
23	914	126	2.394	1.00	290	35	82.3	14.2	0.82	1.48	8.7	1.63	848	406	0.52	0.10	13.7	1.04	203	13.5	15.8	14.0	1.01
24	914	126	2.394	1.00	290	35	345.2	15.7	0.82	1.48	8.7	1.81	848	406	0.52	0.41	13.7	1.15	203	13.5	15.8	12.3	1.28
25	914	126	2.394	1.00	290	35	306.0	16.9	0.82	1.48	8.7	1.94	848	406	0.52	0.36	13.7	1.23	203	13.5	15.8	13.0	1.30
26	914	126	2.394	1.00	290	35	266.9	17.5	0.82	1.48	8.7	2.01	848	406	0.52	0.31	13.7	1.28	203	13.5	15.8	13.6	1.28
27	914	126	2.394	1.00	290	35	260.7	17.4	0.82	1.48	8.7	2.00	848	406	0.52	0.31	13.7	1.27	203	13.5	15.8	13.7	1.27
28	914	126	2.394	1.00	290	35	174.8	16.3	0.82	1.48	8.7	1.88	848	406	0.52	0.21	13.7	1.19	203	13.5	15.8	14.5	1.12
29	914	126	2.394	1.00	290	35	89.0	15.8	0.82	1.48	8.7	1.81	848	406	0.52	0.10	13.7	1.15	203	13.5	15.8	14.0	1.12
30	914	126	2.394	1.00	290	35	43.6	14.6	0.82	1.48	8.7	1.67	848	406	0.52	0.05	13.7	1.07	203	13.5	15.8	13.8	1.06

											Original						Proposal A				Proposal B	
Name	Length mm	D mm	t mm	k	Fy MPa	fc' MPa	Pf kN	Mf kNm	tau	tau'	Mr kNm	Mf/Mr	Crco kN	Crcm kN	B	P/Pr	Mr kNm	Mf/Mr	Crhc kN	Mrc kNm	Mrhc kNm	Mr kNm	Mf/Mr
Knowles and Park (1969)																							
13	806.4	88.2	5.842	1.00	400	41	554.2	10.7	0.84	2.61	8.7	1.24	1192	188	0.84	0.46	6.4	1.68	94	19.9	17.3	8.7	1.23
14	1411.2	88.2	5.842	1.00	400	41	469.1	7.9	0.91	1.56	4.0	1.96	1192	188	0.84	0.39	4.2	1.88	94	19.9	17.3	5.7	1.38
15	806.4	88.2	5.842	1.00	400	41	194.8	6.4	0.84	2.61	13.3	0.48	1192	188	0.84	0.16	13.5	0.48	94	19.9	17.3	18.4	0.35
16	1108.8	88.2	5.842	1.00	400	41	191.3	5.8	0.87	2.03	13.9	0.42	1192	188	0.84	0.16	12.9	0.45	94	19.9	17.3	17.5	0.33
17	806.4	82.55	1.397	1.00	483	41	167.9	3.3	0.85	1.46	3.8	0.87	497	204	0.59	0.34	4.9	0.68	102	5.5	6.2	4.8	0.69
18	806.4	82.55	1.397	1.00	483	41	89	2.6	0.85	1.46	3.8	0.69	497	204	0.59	0.18	5.1	0.51	102	5.5	6.2	5.6	0.47
Alfawakiri (1997)																							
FA1	1605	152.4	3.4	1.00	330	89	400	49.2	0.85	1.17	21.3	2.32	2241	1489	0.34	0.18	46.0	1.07	744	33.8	47.9	36.2	1.36
FA2	1605	152.4	3.4	1.00	330	72	100	37.3	0.85	1.21	21.3	1.75	1995	1199	0.40	0.05	40.4	0.92	599	33.2	43.4	33.7	1.11
FA3	1605	152.4	3.4	1.00	330	76	700	49.1	0.85	1.20	21.3	2.31	2047	1260	0.38	0.34	41.6	1.18	630	33.3	44.4	34.6	1.42
Marson(1999)																							
CFST 64	2200	406.4	5.5	1.00	442	37	1000	591.0	0.80	1.59	314.3	1.88	9646	4543	0.53	0.10	491.6	1.20	2272	492	581	518.5	1.14
CFST 34	2200	323.9	7.5	1.00	415	41	1820	444.0	0.82	1.76	254.7	1.74	8321	3035	0.64	0.22	341.6	1.30	1518	387	411	379.8	1.17
CFST 42	2200	406.4	9.5	1.00	505	35	1820	928.0	0.80	2.22	608.1	1.53	******	4126	0.72	0.12	739.3	1.26	2063	911	925	896.6	1.04
CFST 51	2200	323.9	5.5	1.00	400	35	1600	356.0	0.82	1.62	182.3	1.95	6419	2691	0.58	0.25	261.1	1.36	1346	278	312	284.0	1.25
											Average	**1.79**					**Average**	**1.049**			**Average**	**1.20**
											Standard Deviation	**0.64**					**Standard Deviation**	**0.346**			**Standard Deviation**	**0.34**
Marson(1999) nominal																							
CFST 64	2200	406.4	6.5	1.00	350	30	1000	591.0	0.80	1.68	286.2	2.07	8498	3645	0.57	0.12	433.2	1.36	1823	433	517	467.2	1.26
CFST 34	2200	323.9	9.5	1.00	350	30	1820	444.0	0.82	2.09	269.5	1.65	7902	2190	0.72	0.23	323.6	1.37	1095	365	400	351.7	1.26
CFST 42	2200	406.4	9.5	1.00	350	30	1820	928.0	0.80	1.99	422.7	2.20	******	3535	0.67	0.17	548.4	1.69	1768	682	670	643.9	1.44
CFST 51	2200	323.9	6.5	1.00	350	30	1600	356.0	0.82	1.75	183.2	1.94	6188	2277	0.63	0.26	251.6	1.41	1138	268	305	268.8	1.32

Table 6.11: Comparison of new proposals for CAN/S16.1 with respect to D/t ratios

Name	L	D	t	D/t*Fy	k	Fy	fc'	Pf	Mf	tau	tau'	Original Mr	Original Mf/Mr	Crco	Crcm	B	P/Pr	Proposal A Mr	Proposal A Mf/Mr	Crhc	Mrc	Mrhc	Proposal B Mr	Proposal B Mf/M
	mm	mm	mm			MPa	MPa	kN	kNm			kNm		kN	kN			kNm		kNm	kNm	kNm	kNm	
Class 1 sections																								
Knowles and Park (1969)																								
13	806.4	88.2	5.84	6039	1	400	41	554.2	10.7	0.84	2.61	8.7	1.24	1192	188	0.84	0.46	6.4	1.68	94	19.9	17.3	8.7	1.23
14	1411	88.2	5.84	6039	1	400	41	469.1	7.9	0.91	1.56	4.0	1.96	1192	188	0.84	0.39	4.2	1.88	94	19.9	17.3	5.7	1.38
15	806.4	88.2	5.84	6039	1	400	41	194.8	6.4	0.84	2.61	13.3	0.48	1192	188	0.84	0.16	13.5	0.48	94	19.9	17.3	18.4	0.35
16	1109	88.2	5.84	6039	1	400	41	191.3	5.8	0.87	2.03	13.9	0.42	1192	188	0.84	0.16	12.9	0.45	94	19.9	17.3	17.5	0.33
												Average	**1.02**					**Average**	**1.12**				**Average**	**0.82**
												Standard Deviation	**0.63**					**Standard Deviation**	**0.66**				**Standard Deviation**	**0.49**
Class 2 sections																								
Marson(1999)																								
CFST 34	2200	324	7.5	17922	1	415	41	1820	444.0	0.82	1.76	254.7	1.74	8321	3035	0.64	0.22	342	1.30	1518	387	411	379.8	1.17
Alfawakiri (1997)																								
FA1	1605	152	3.4	14792	1	330	89	400	49.2	0.85	1.17	21.3	2.32	2241	1489	0.34	0.18	46.0	1.07	744	33.8	47.9	36.2	1.36
FA2	1605	152	3.4	14792	1	330	72	100	37.3	0.85	1.21	21.3	1.75	1995	1199	0.40	0.05	40.4	0.92	599	33.2	43.4	33.7	1.11
FA3	1605	152	3.4	14792	1	330	76	700	49.1	0.85	1.20	21.3	2.31	2047	1260	0.38	0.34	41.6	1.18	630	33.3	44.4	34.6	1.42
Furlong (1967)																								
9	914	113	3.15	14891	1	414	29	444.8	11.2	0.83	2.11	13.1	0.85	1052	261	0.75	0.42	9.1	1.23	130	19.0	18.8	11.6	0.97
10	914	113	3.15	14891	1	414	29	400.3	11.9	0.83	2.11	13.1	0.90	1052	261	0.75	0.38	10.2	1.17	130	19.0	18.8	12.9	0.92
11	914	113	3.15	14891	1	414	29	333.6	14.7	0.83	2.11	13.1	1.12	1052	261	0.75	0.32	11.8	1.24	130	19.0	18.8	15.0	0.98
12	914	113	3.15	14891	1	414	29	222.4	15.8	0.83	2.11	13.1	1.20	1052	261	0.75	0.21	14.5	1.09	130	19.0	18.8	17.4	0.91
13	914	113	3.15	14891	1	414	29	111.2	16.1	0.83	2.11	13.1	1.23	1052	261	0.75	0.11	15.0	1.08	130	19.0	18.8	18.1	0.89
19	914	126	2.39	15239	1	290	35	568.5	8.7	0.82	1.48	6.0	1.45	848	406	0.52	0.67	5.5	1.58	203	13.5	15.8	5.5	1.60
20	914	126	2.39	15239	1	290	35	533.8	12.6	0.82	1.48	7.5	1.69	848	406	0.52	0.63	6.8	1.85	203	13.5	15.8	6.7	1.87
21	914	126	2.39	15239	1	290	35	400.3	15.8	0.82	1.48	8.7	1.82	848	406	0.52	0.47	11.6	1.36	203	13.5	15.8	11.4	1.39
22	914	126	2.39	15239	1	290	35	84.5	15.7	0.82	1.48	8.7	1.80	848	406	0.52	0.10	13.7	1.15	203	13.5	15.8	14.0	1.12
23	914	126	2.39	15239	1	290	35	82.3	14.2	0.82	1.48	8.7	1.63	848	406	0.52	0.10	13.7	1.04	203	13.5	15.8	14.0	1.01
24	914	126	2.39	15239	1	290	35	345.2	15.7	0.82	1.48	8.7	1.81	848	406	0.52	0.41	13.7	1.15	203	13.5	15.8	12.3	1.28
25	914	126	2.39	15239	1	290	35	306.0	16.9	0.82	1.48	8.7	1.94	848	406	0.52	0.36	13.7	1.23	203	13.5	15.8	13.0	1.30
26	914	126	2.39	15239	1	290	35	266.9	17.5	0.82	1.48	8.7	2.01	848	406	0.52	0.31	13.7	1.28	203	13.5	15.8	13.6	1.28
27	914	126	2.39	15239	1	290	35	260.7	17.4	0.82	1.48	8.7	2.00	848	406	0.52	0.31	13.7	1.27	203	13.5	15.8	13.7	1.27
28	914	126	2.39	15239	1	290	35	174.8	16.3	0.82	1.48	8.7	1.88	848	406	0.52	0.21	13.7	1.19	203	13.5	15.8	14.5	1.12
29	914	126	2.39	15239	1	290	35	89.0	15.8	0.82	1.48	8.7	1.81	848	406	0.52	0.10	13.7	1.15	203	13.5	15.8	14.0	1.12
30	914	126	2.39	15239	1	290	35	43.6	14.6	0.82	1.48	8.7	1.67	848	406	0.52	0.05	13.7	1.07	203	13.5	15.8	13.8	1.06
												Average	**1.66**					**Average**	**1.22**				**Average**	**1.20**
												Standard Deviation	**0.40**					**Standard Deviation**	**0.19**				**Standard Deviation**	**0.24**

												Original						Proposal A					Proposal B	
Name	L	D	t	D/t*Fy	k	Fy	fc'	Pf	Mf	tau	tau'	Mr	Mf/Mr	Crco	Crcm	B	P/Pr	Mr	Mf/Mr	Crhc	Mrc	Mrhc	Mr	Mf/Mr
	mm	mm	mm			MPa	MPa	kN	kNm			kNm		kN	kN			kNm		kNm	kNm	kNm	kNm	
Class 3 sections																								
Marson(1999)																								
CFST 51	2200	324	5.5	23556	1	400	35	1600	356.0	0.82	1.62	182.3	1.95	6419	2691	0.58	0.25	261	1.36	1346	278	312	284.0	1.25
CFST 42	2200	406	9.5	21603	1	505	35	1820	928.0	0.80	2.22	608.1	1.53	14603	4126	0.72	0.12	739	1.26	2063	911	925	896.6	1.04
												Average	**1.74**					**Average**	**1.31**				**Average**	**1.14**
												Standard Deviation	**0.21**					**Standard Deviation**	**0.05**				**Standard Deviation**	**0.11**
Class 4 sections Permitted by Clause 18.6																								
Marson(1999)																								
CFST 64	2200	406	5.5	32660	1	442	37	1000	591.0	0.80	1.59	314.3	1.88	9646	4543	0.53	0.10	492	1.20	2272	492	581	518.5	1.14
												Average	**1.88**					**Average**	**1.20**				**Average**	**1.14**
												Standard Deviation	**0.00**					**Standard Deviation**	**0.00**				**Standard Deviation**	**0.00**
Class 4																								
Knowles and Park (1969)																								
17	806.4	82.6	1.4	28541	1	483	41	167.9	3.3	0.85	1.46	3.8	0.87	497	204	0.59	0.34	4.9	0.68	102	5.5	6.2	4.8	0.69
18	806.4	82.6	1.4	28541	1	483	41	89	2.6	0.85	1.46	3.8	0.69	497	204	0.59	0.18	5.1	0.51	102	5.5	6.2	5.6	0.47
Prion and Boehme (1994)																								
BP16	2120	152	1.65	30216	1	328	92	0	21.0	0.89	1.05	10.9	1.93	1843	1598	0.13	0.00	37.5	0.56	799	17.1	37.4	17.1	1.23
B11	2120	152	1.65	30216	1	328	92	470	29.7	0.89	1.05	10.9	2.74	1843	1598	0.13	0.25	37.5	0.79	799	17.1	37.4	20.0	1.48
B12	2120	152	1.65	30216	1	328	92	570	32.1	0.89	1.05	10.9	2.96	1843	1598	0.13	0.31	37.5	0.85	799	17.1	37.4	20.7	1.55
B13	2120	152	1.65	30216	1	328	92	670	28.5	0.89	1.05	10.9	2.63	1843	1598	0.13	0.36	37.5	0.76	799	17.1	37.4	21.3	1.34
B14	2120	152	1.65	30216	1	328	92	820	29.2	0.89	1.05	10.9	2.69	1843	1598	0.13	0.44	37.5	0.78	799	17.1	37.4	21.1	1.38
B15	2120	152	1.65	30216	1	328	92	970	30.5	0.89	1.05	10.9	2.81	1843	1598	0.13	0.53	37.5	0.81	799	17.1	37.4	14.4	2.11
B17	2120	152	1.65	30216	1	328	92	270	30.1	0.89	1.05	10.9	2.77	1843	1598	0.13	0.15	37.5	0.80	799	17.1	37.4	18.8	1.60
BP18	2120	152	1.65	30216	1	328	92	270	30.8	0.89	1.05	10.9	2.84	1843	1598	0.13	0.15	37.5	0.82	799	17.1	37.4	18.8	1.64
BP19	2120	152	1.65	30216	1	328	92	670	34.8	0.89	1.05	10.9	3.21	1843	1598	0.13	0.36	37.5	0.93	799	17.1	37.4	21.3	1.64
BP20	1071	152	1.65	30216	1	328	92	1273	21.4	0.82	1.12	10.0	2.13	1843	1598	0.13	0.69	37.5	0.57	799	17.1	37.4	17.3	1.24
BP21	1071	152	1.65	30216	1	328	92	1451	13.8	0.82	1.12	10.0	1.38	1843	1598	0.13	0.79	37.5	0.37	799	17.1	37.4	11.6	1.19
BP22	1071	152	1.65	30216	1	328	92	1309	15.9	0.82	1.12	10.0	1.59	1843	1598	0.13	0.71	37.5	0.42	799	17.1	37.4	16.1	0.99
Furlong (1967)																								
14	914	151	1.54	32549	1	331	26	567.6	9.9	0.81	1.45	8.1	1.21	833	446	0.47	0.68	7.8	1.26	223	14.5	18.4	7.2	1.38
15	914	151	1.54	32549	1	331	26	421.7	17.7	0.81	1.45	9.2	1.91	833	446	0.47	0.51	14.5	1.22	223	14.5	18.4	12.9	1.37
16	914	151	1.54	32549	1	331	26	286.0	17.1	0.81	1.45	9.2	1.85	833	446	0.47	0.34	15.8	1.08	223	14.5	18.4	15.9	1.08
17	914	151	1.54	32549	1	331	21	136.1	16.1	0.81	1.55	9.2	1.74	763	362	0.52	0.18	14.3	1.12	181	14.3	17.1	15.7	1.02
18	914	151	1.54	32549	1	331	21	135.2	14.9	0.81	1.55	9.2	1.62	763	362	0.52	0.18	14.3	1.04	181	14.3	17.1	15.7	0.95
												Average	**2.08**					**Average**	**0.81**				**Average**	**1.28**
												Standard Deviation	**0.61**					**Standard Deviation**	**0.25**				**Standard Deviation**	**0.29**

												Original						Proposal A					Proposal B	
Name	L mm	D mm	t mm	D/t*Fy	k	Fy MPa	fc' MPa	Pf kN	Mf kNm	tau	tau'	Mr kNm	Mf/Mr	Crco kN	Crcm kN	B	P/Pr	Mr kNm	Mf/Mr	Crhc kNm	Mrc kNm	Mrhc kNm	Mr kNm	Mf/M
Class 1 sections																								
Marson (1999) nominal																								
CFST 34	2200	324	9.5	11896	1	350	30	1820	444.0	0.82	2.09	269.5	1.65	7902	2190	0.72	0.23	324	1.37	1095	365	400	351.7	1.26
Class 2 sections																								
Marson (1999) nominal																								
CFST 42	2200	406	9.5	14926	1	350	30	1820	928.0	0.80	1.99	422.7	2.20	10718	3535	0.67	0.17	548	1.69	1768	682	670	643.9	1.44
CFST 51	2200	324	6.5	17853	1	350	30	1600	356.0	0.82	1.75	183.2	1.94	6188	2277	0.63	0.26	252	1.41	1138	268	305	268.8	1.32
Class 3 sections																								
Marson (1999) nominal																								
CFST 64	2200	406	6.5	21783	1	350	30	1000	591.0	0.80	1.68	286.2	2.07	8498	3645	0.57	0.12	433	1.36	1823	433	517	467.2	1.26

Table 6.12: Comparison of all code equations with respect to D/t ratios

Class	AISC LFRD 1994		Eurocode 4 1994		CAN/CSA-S16.1 M94		Proposal A		Proposal B	
	ave.	σ	ave.	σ	ave.	σ	ave.	σ	ave.	σ
1	1.36	0.94	0.91	0.59	1.02	0.63	1.12	0.66	0.82	0.49
2	3.32	3.79	1.20	0.29	1.66	0.40	1.22	0.19	1.20	0.24
3	1.81	0.44	1.10	0.08	1.74	0.21	1.31	0.05	1.14	0.11
4 (permitted by Clause 18.6)	1.64	0.00	1.13	0.00	1.88	0.00	1.20	0.00	1.14	0.00
4	5.41	4.79	1.04	0.25	2.08	0.61	0.81	0.25	1.28	0.29

FIGURES

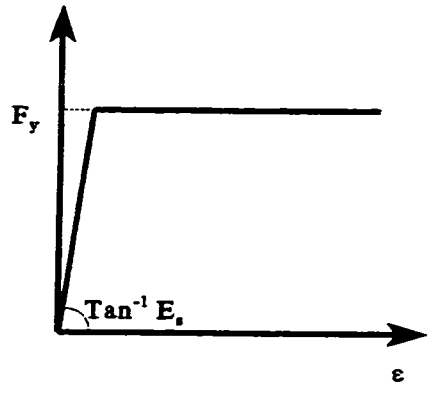

Figure 2.1a: The simplified stress-strain relationship of steel - bilinear stress strain curve

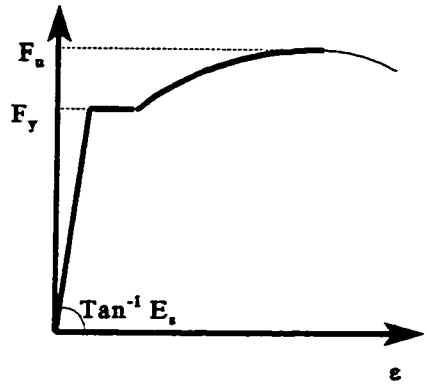

Figure 2.1b: The stress-strain relationship of steel.

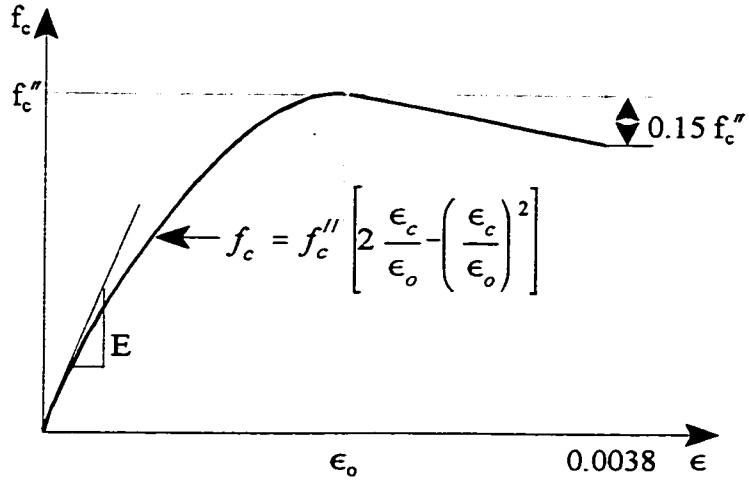

Figure 2.1c: The stress-strain relationship of unconfined concrete [modified Hognestad (1951)].

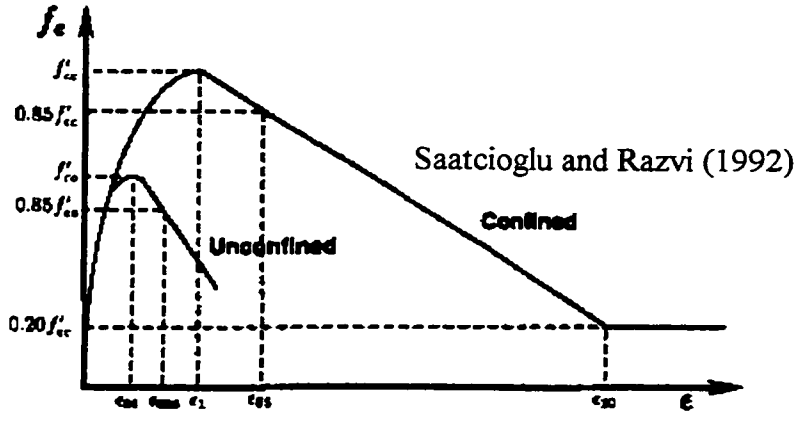

Figure 2.1d: Various stress-strain relationships for confined concrete.

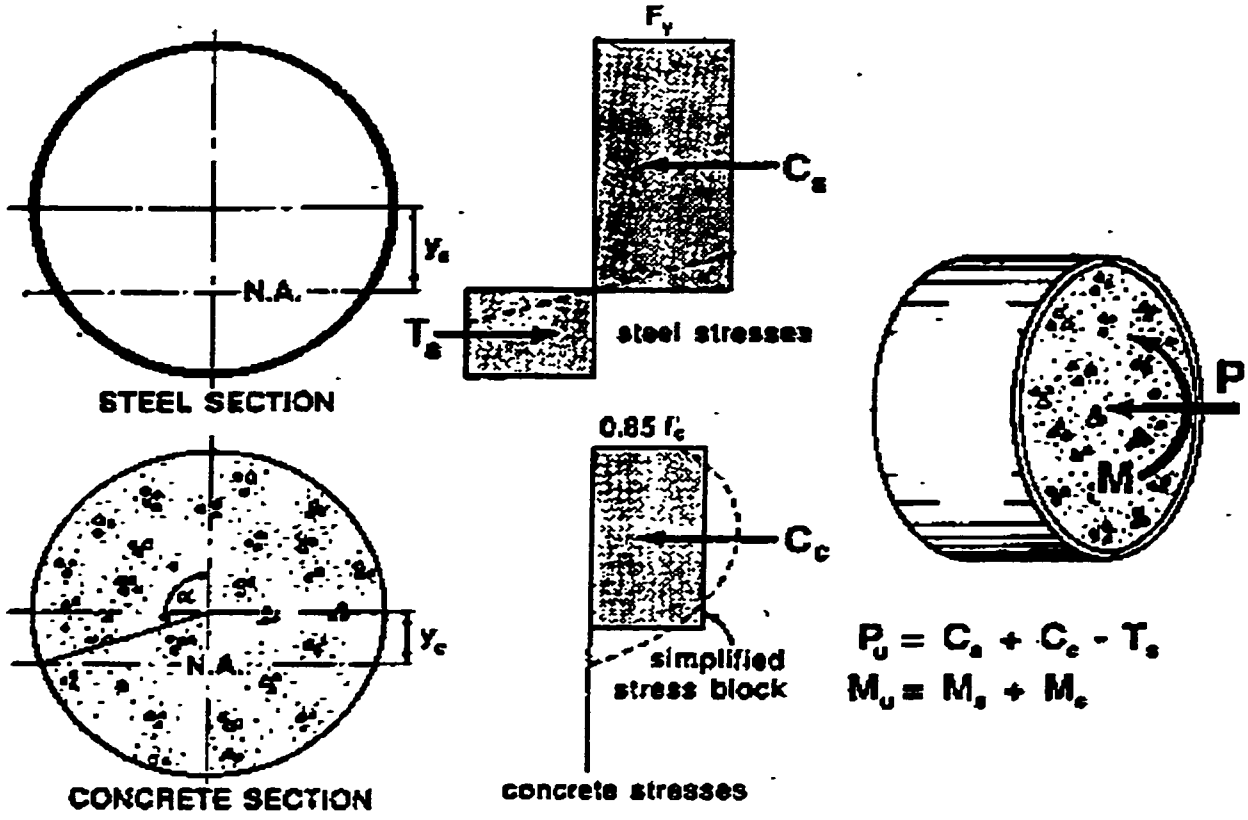

Figure 2.2: Superposition model [Prion and Boehme (1994)].

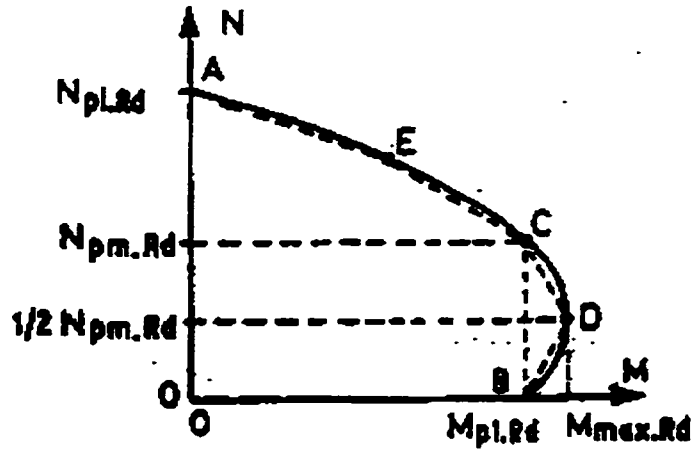

Figure 2.3: Interaction curve for compression and bending [Eurocode 4 (1994)]

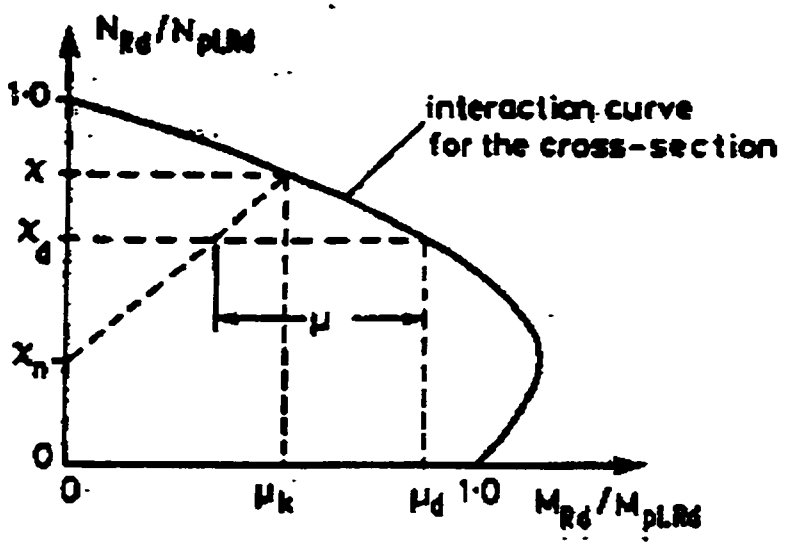

Figure 2.4: Design procedure for compression and bending [Eurocode 4 (1994)]

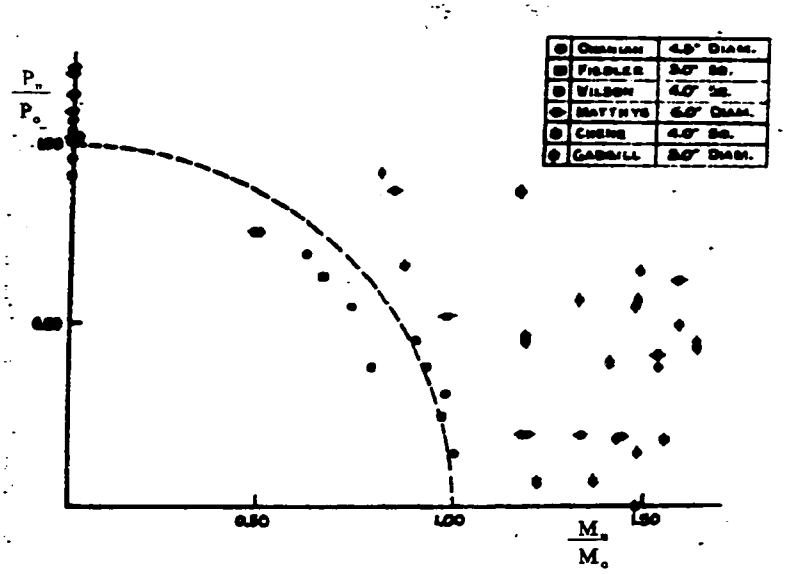

Figure 2.5: Interaction diagram for concrete-filled columns [Furlong (1967)]

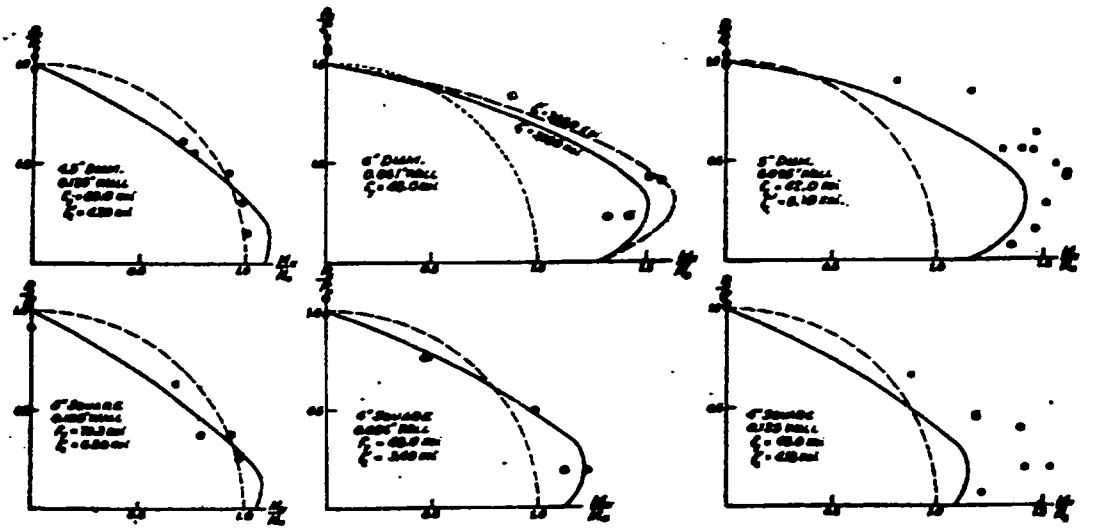

Figure 2.6: Composite column capacity using reinforced concrete design [Furlong (1967)].

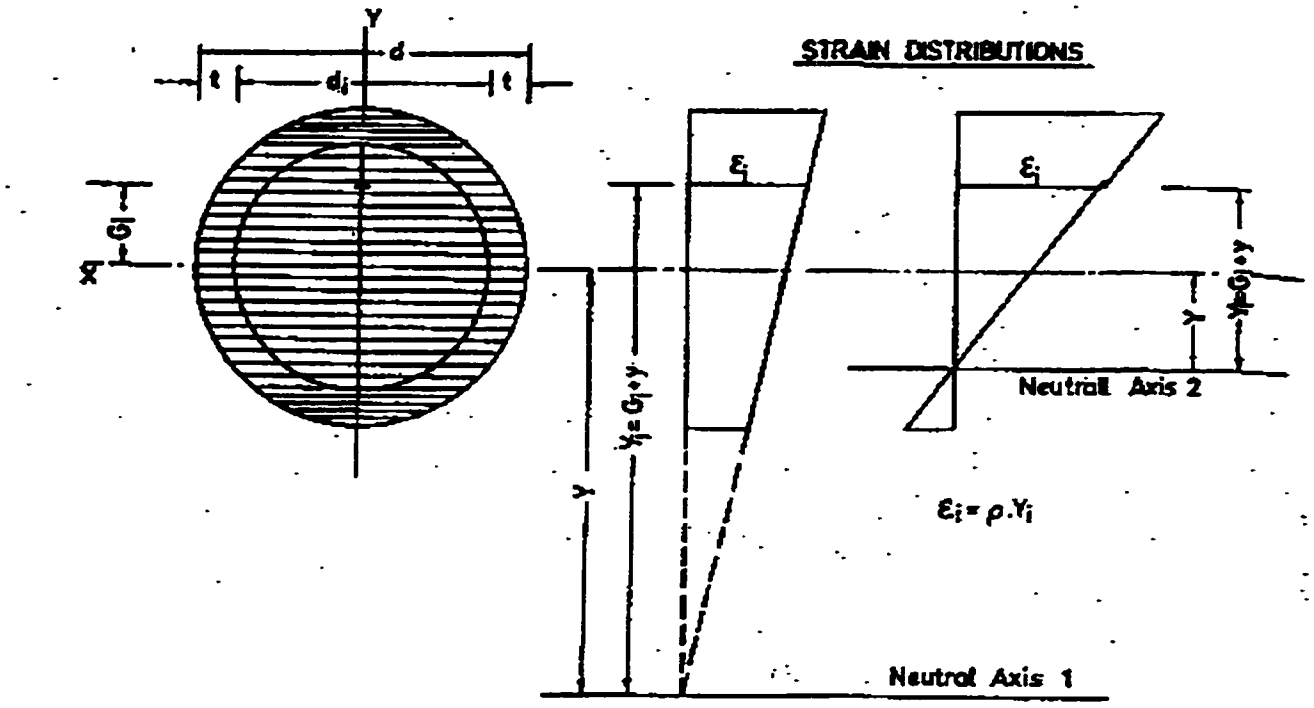

Figure 2.7: The analytical set-up of a concrete-filled steel column [Neogi et al. (1969)].

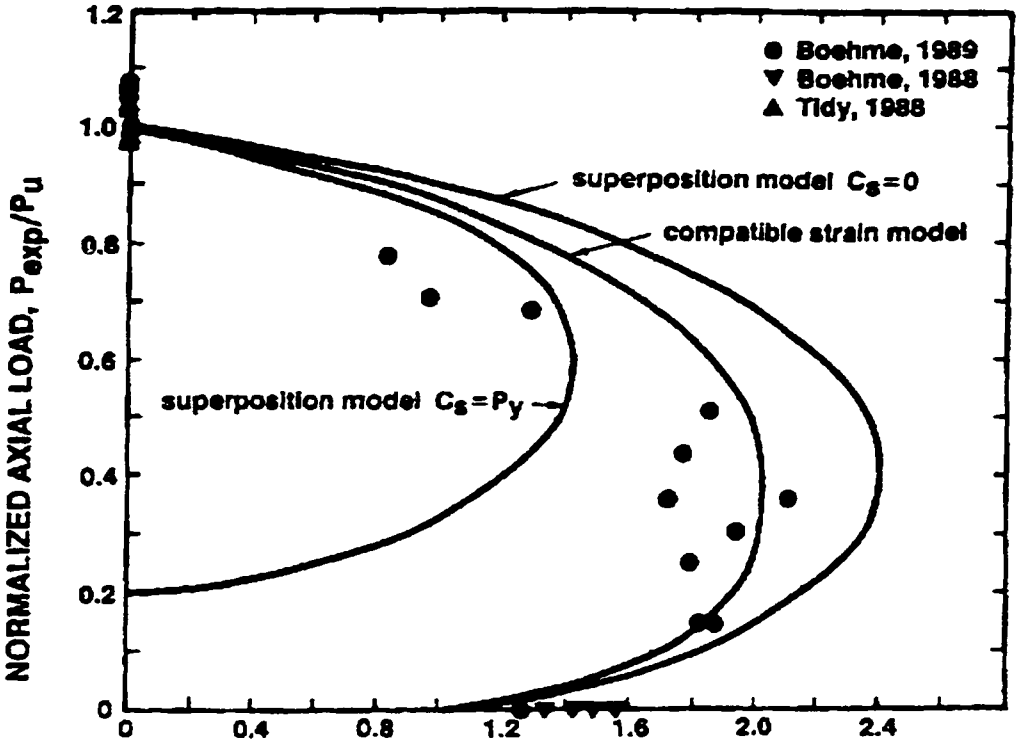

Figure 2.8: Axial load - bending moment interaction diagram [Prion and Boehme (1994)].

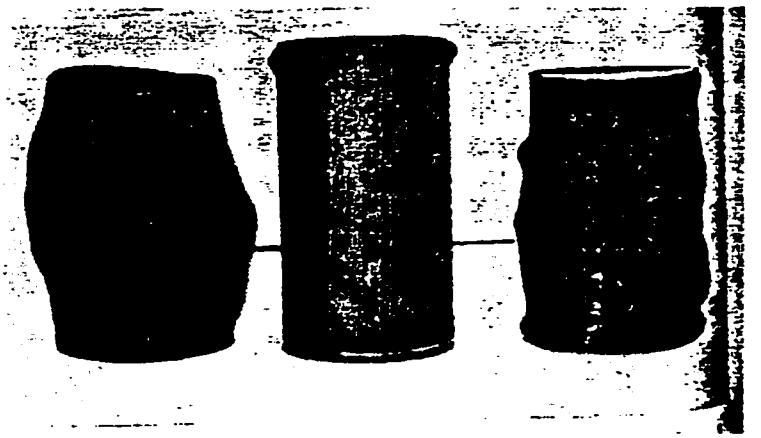

Figure 2.9: Variation of failures [Gardner and Jacobson (1967)].
Left - concrete only loaded
Centre - steel only loaded
Right - concrete and steel loaded

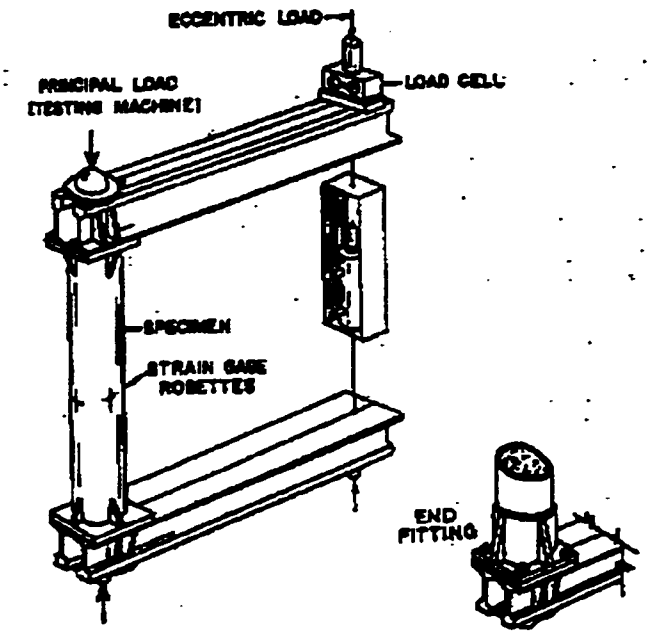

Figure 2.10: Arrangement of specimen and testing apparatus [Furlong (1967)].

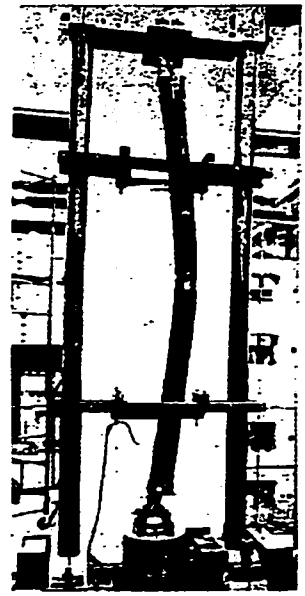

Figure 2.11: Test set-up [Neogi et al. (1969)].

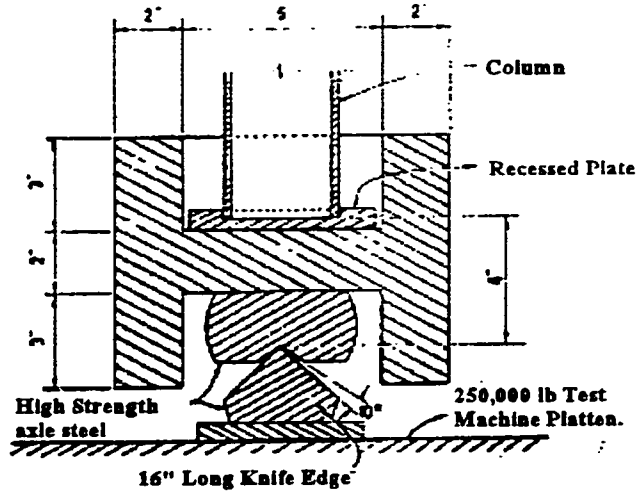

Figure 2.12: End loading device for columns [Knowles and Park (1969)].

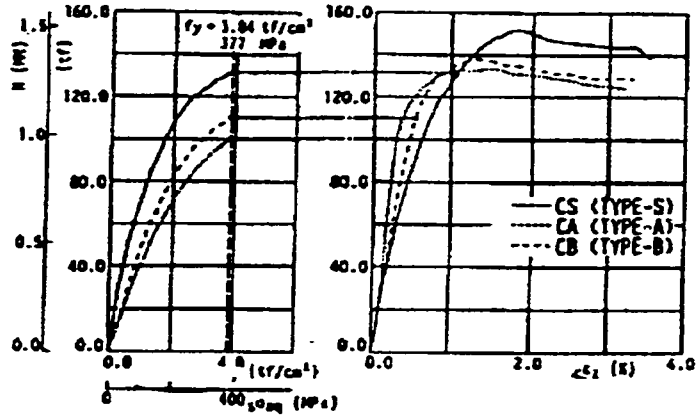

Figure 2.13: Axial load - strain relationship [Orito et al. (1987)].

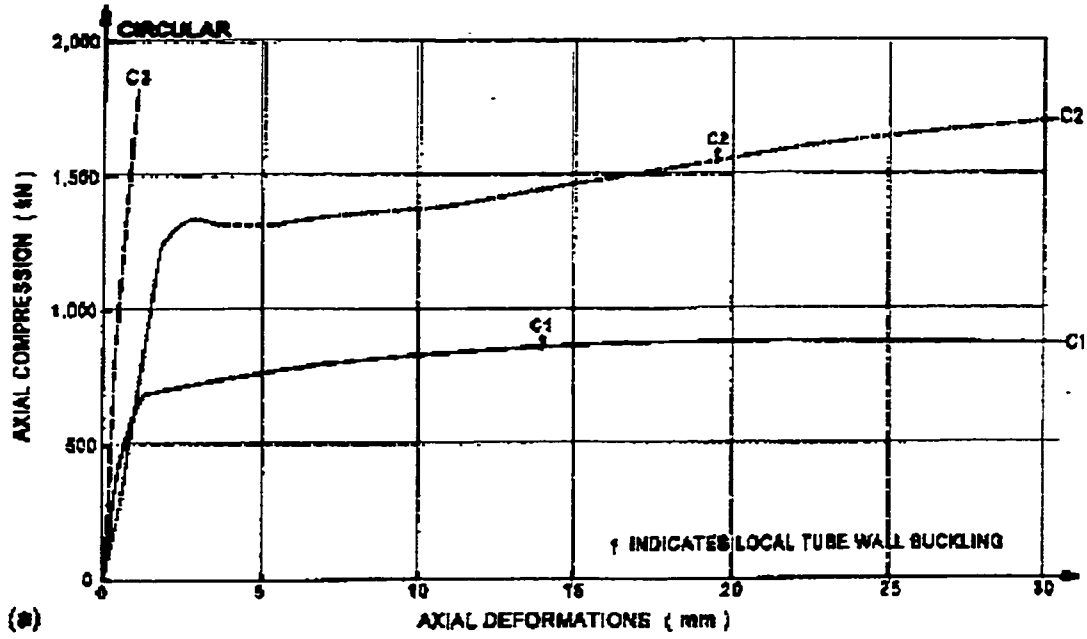

Figure 2.14: Force versus Displacement for Circular Columns [Schneider (1998)].

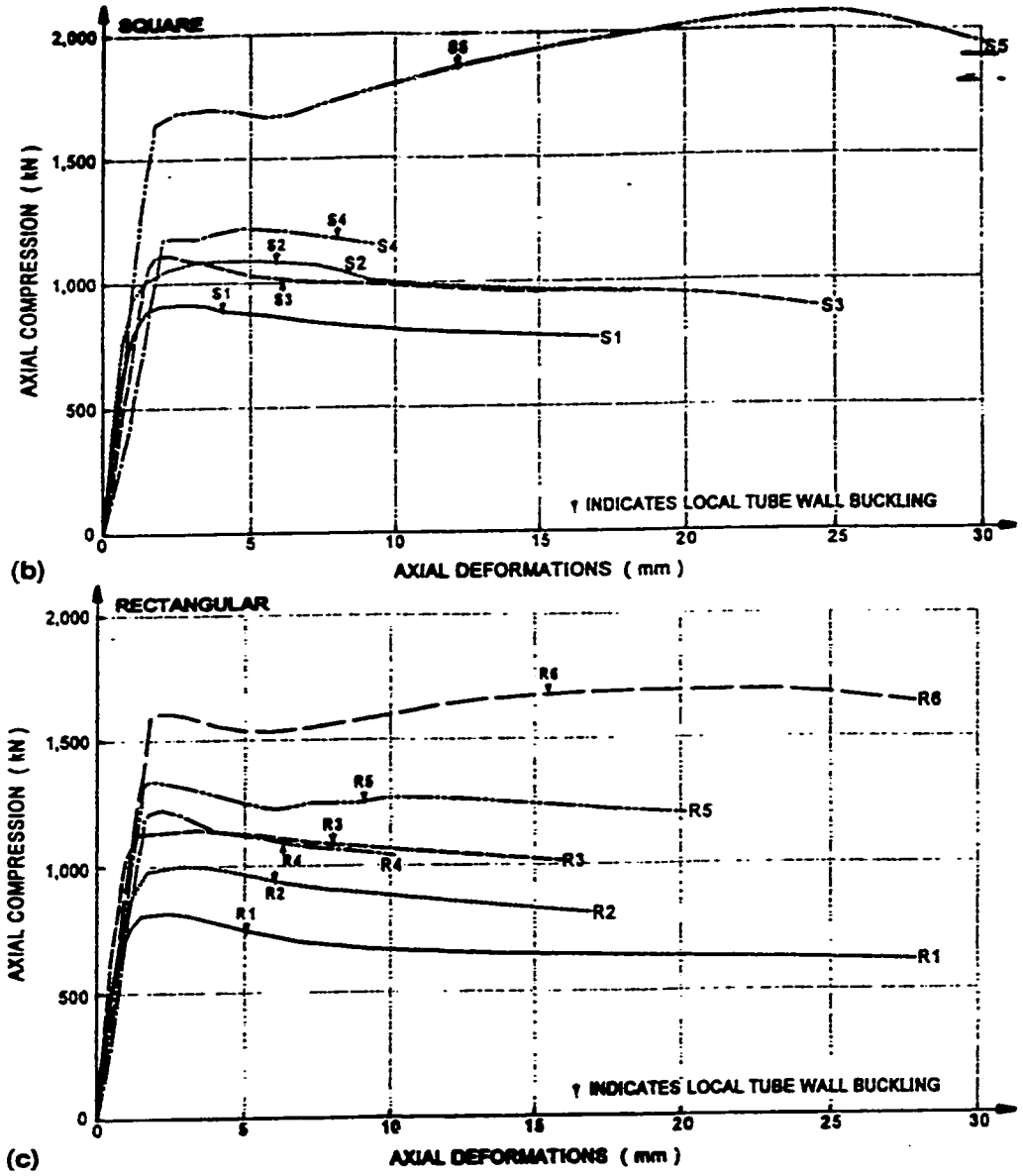

Figure 2.15: Force versus deflection a) square and b) rectangular columns [Schneider (1998)].

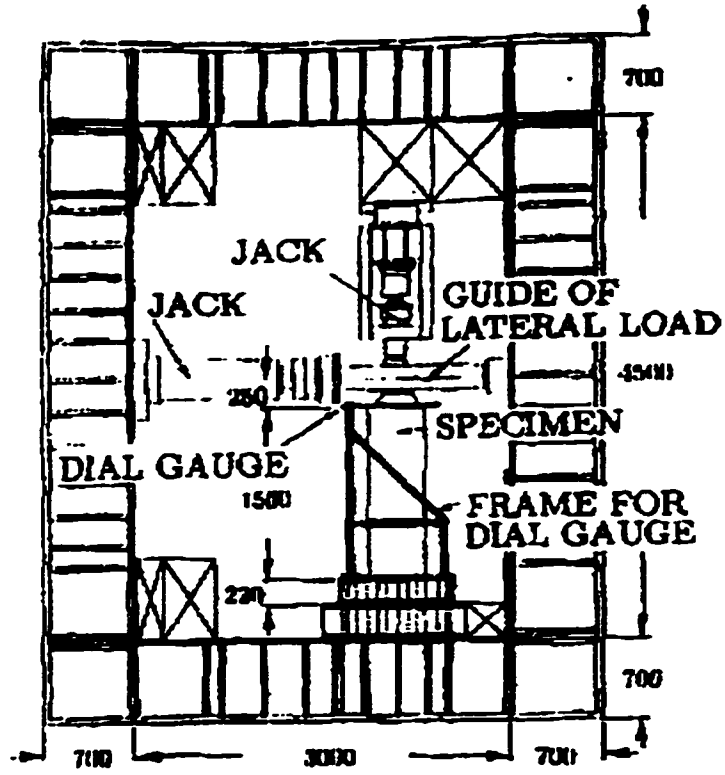

Figure 2.16: Test set-up [Iura et al. (1997)].

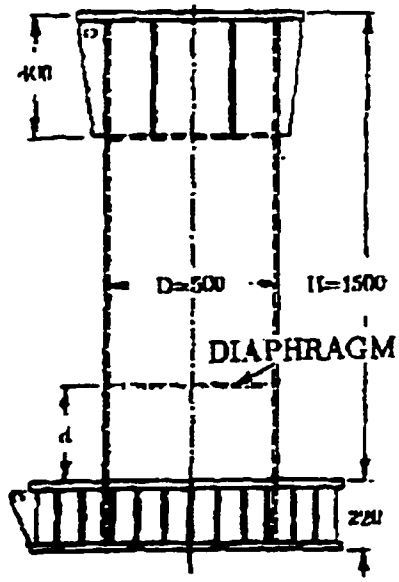

Figure 2.17: Test specimen [Iura et al. (1997)].

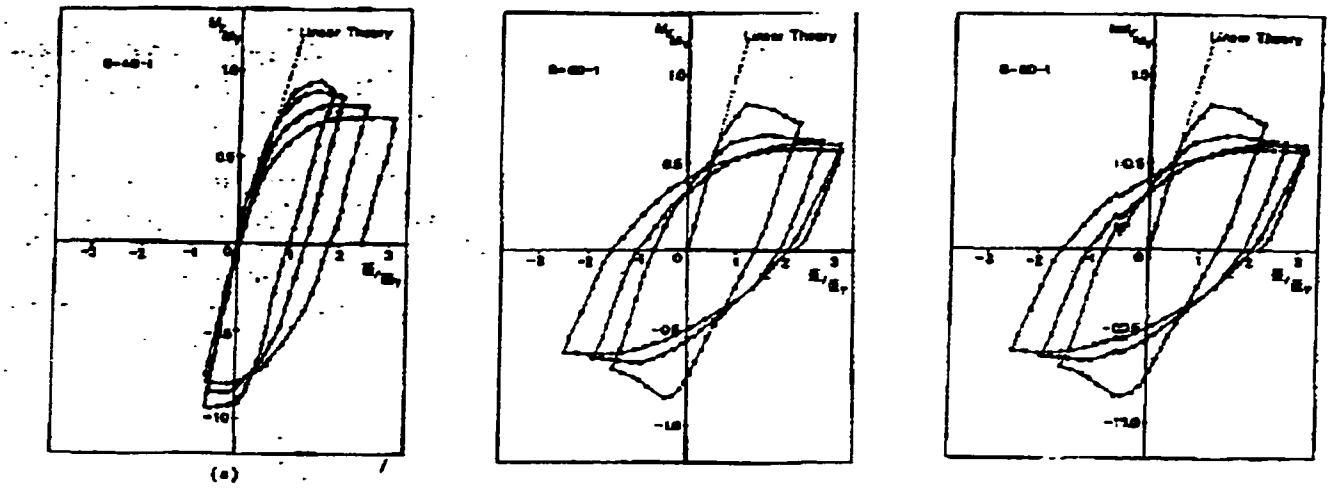

Figure 2.18: Cyclic moment-curvature hysteretic curves [Fukomoto and Kusama (1985)].

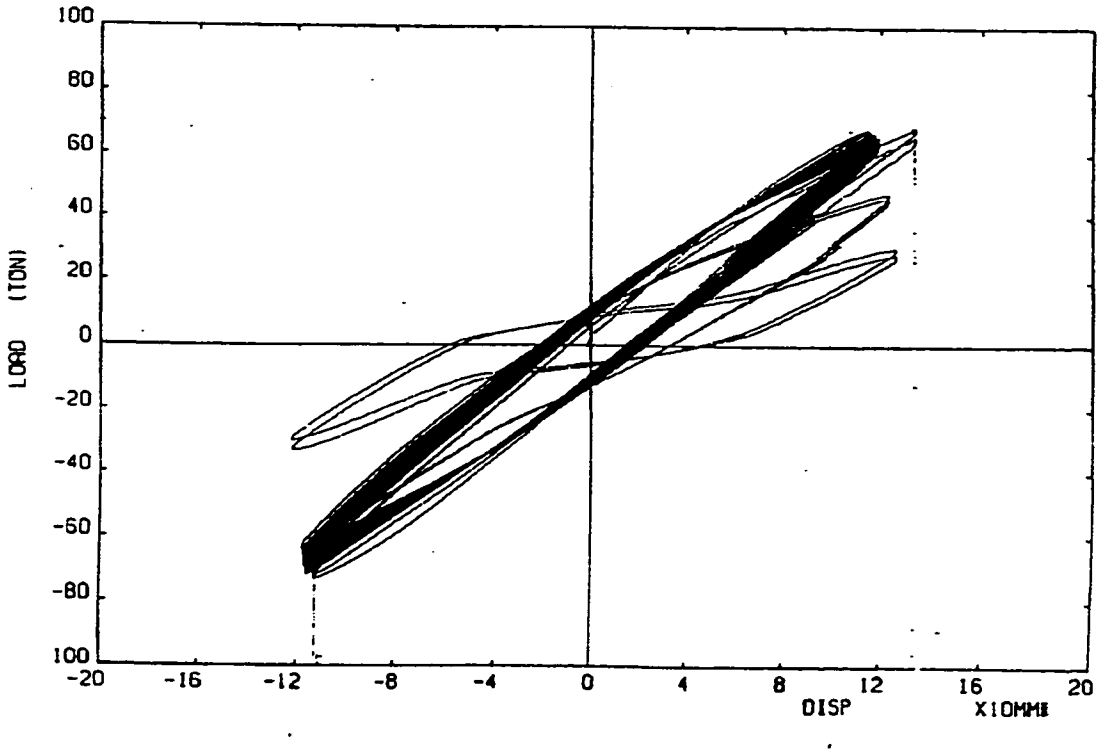

Figure 2.19: Hysteretic curve for specimen HL5 [Terayama (1997)].

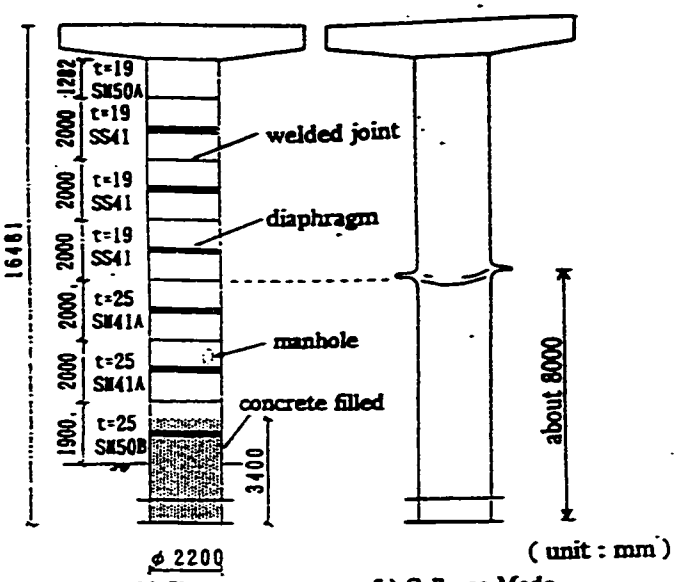

Fig. 1 Shape and Collapse Mode of Pier P−584N

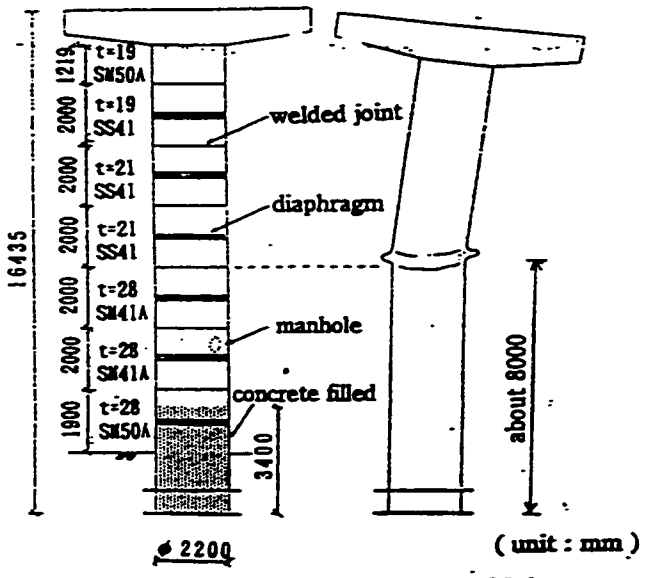

Fig. 2 Shape and Collapse Mode of Pier P−584S

Figure 2.20: Failure shape of columns [Itoh et al. (1997)].

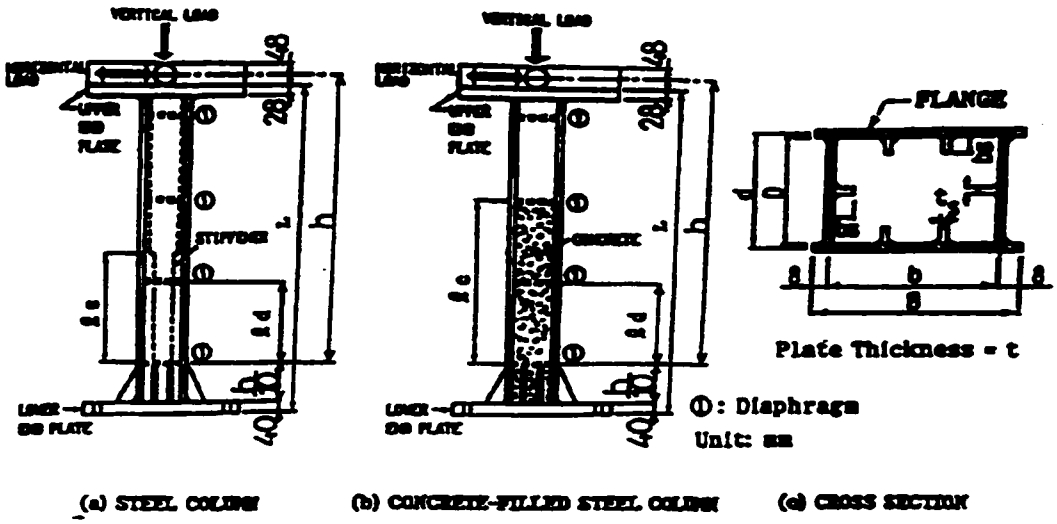

Figure 2.21: Test set-up [Usami et al. (1992)].

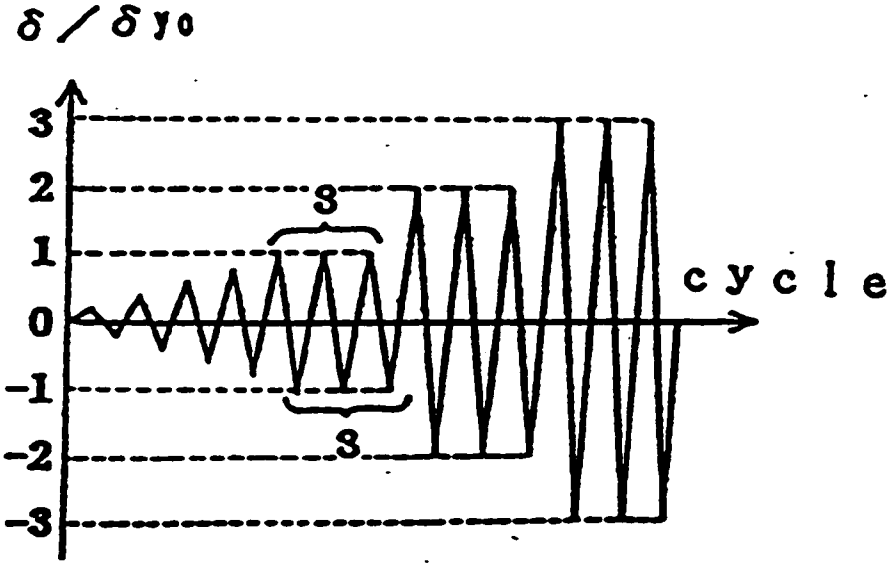

Figure 2.22: Displacement history of cyclic loading [Usami et al. (1992).

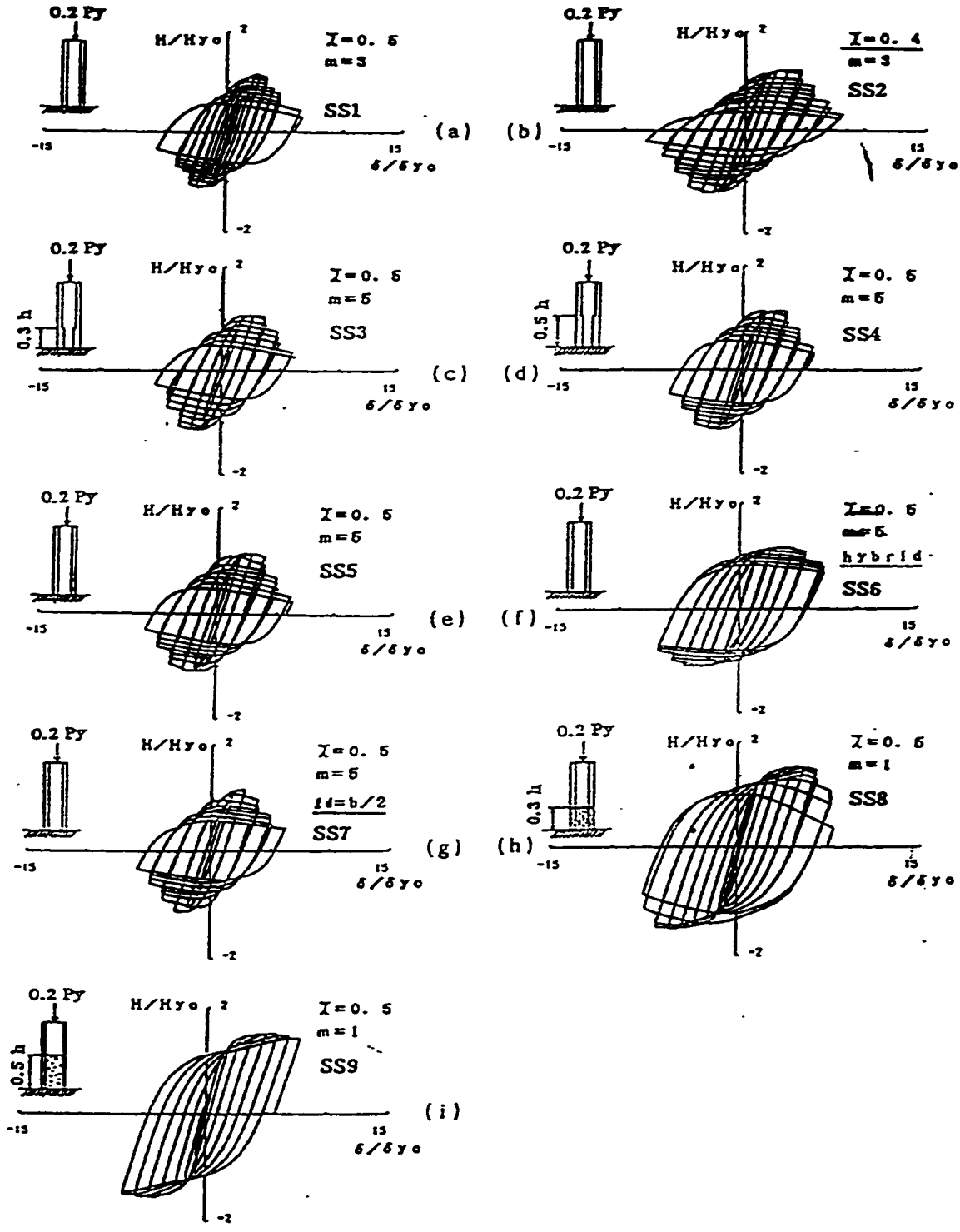

Figure 2.23: Horizontal load versus displacement hysteretic curves [Usami et al. (1992)]

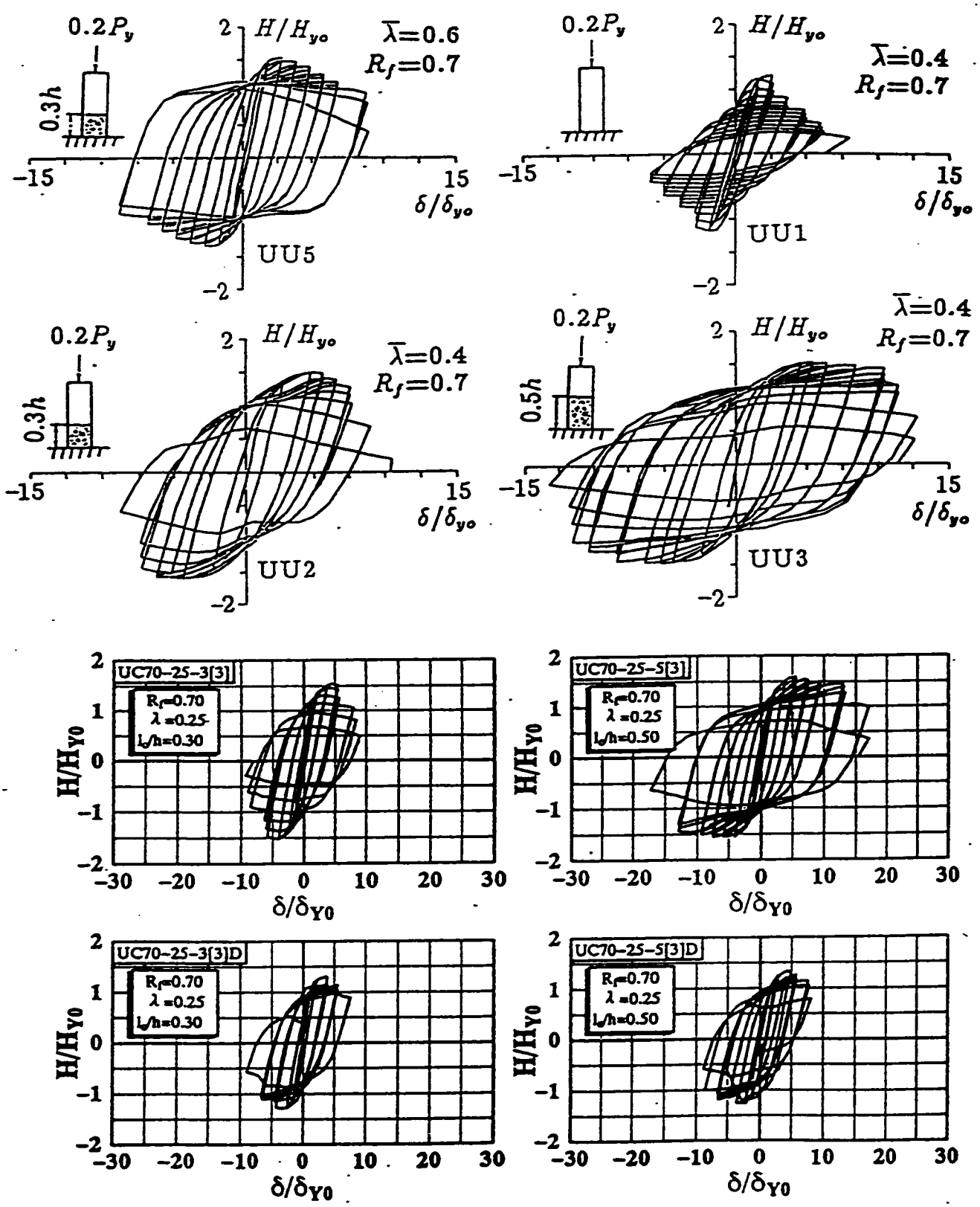

Figure 2.24: Horizontal load versus displacement hysteretic curves [Ge and Usami (1994)].

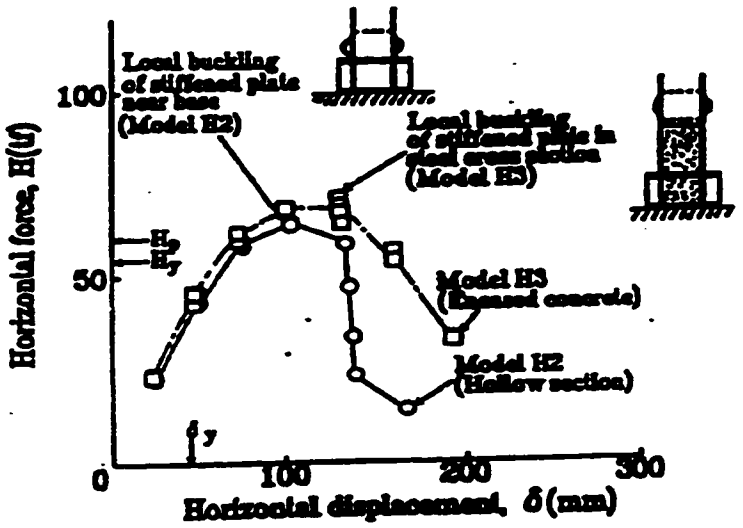

Figure 2.25: Horizontal force versus horizontal displacement curves [Kitada et al. (1995)].

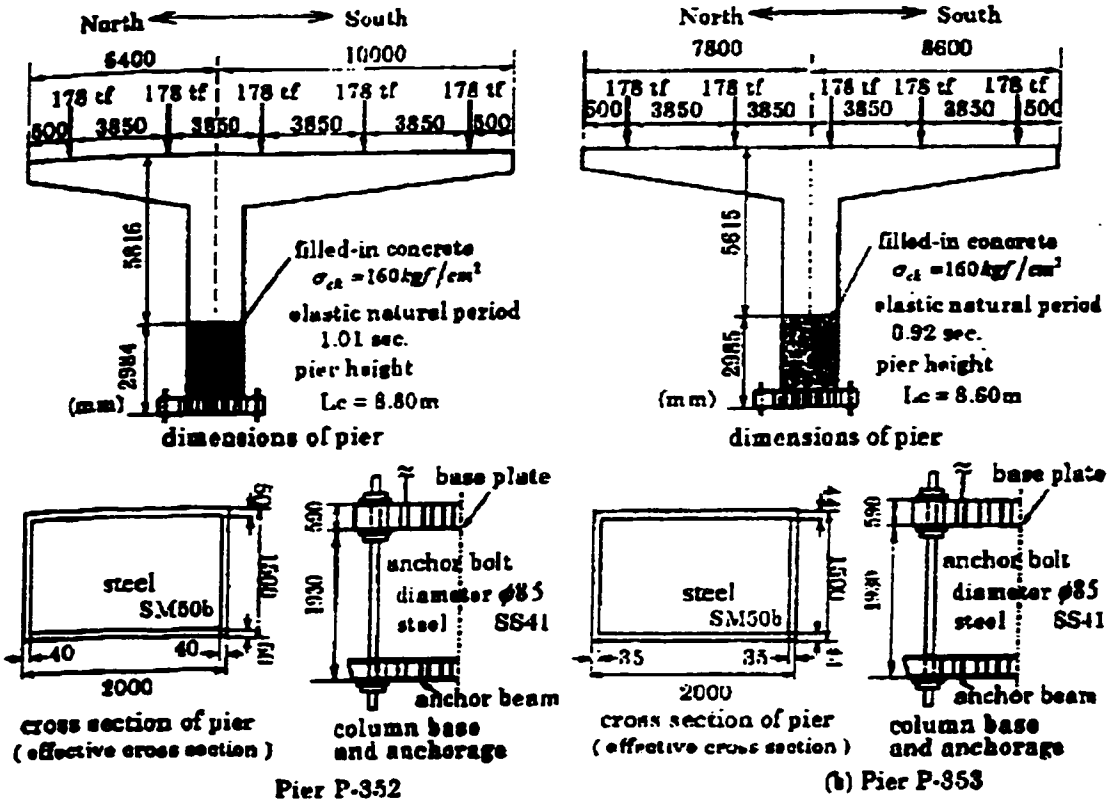

Figure 2.26: Structural dimensions of bridge piers [Goto et al. (1997)].

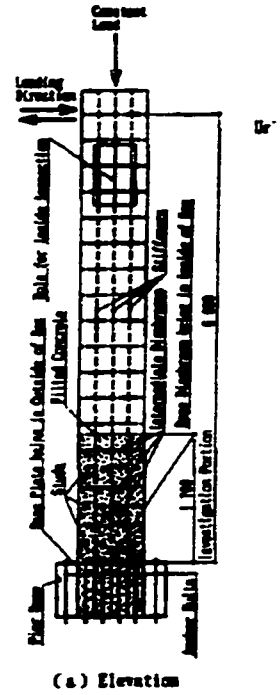

Figure 2.27: Column dimension [Otsuka et al. (1997)].

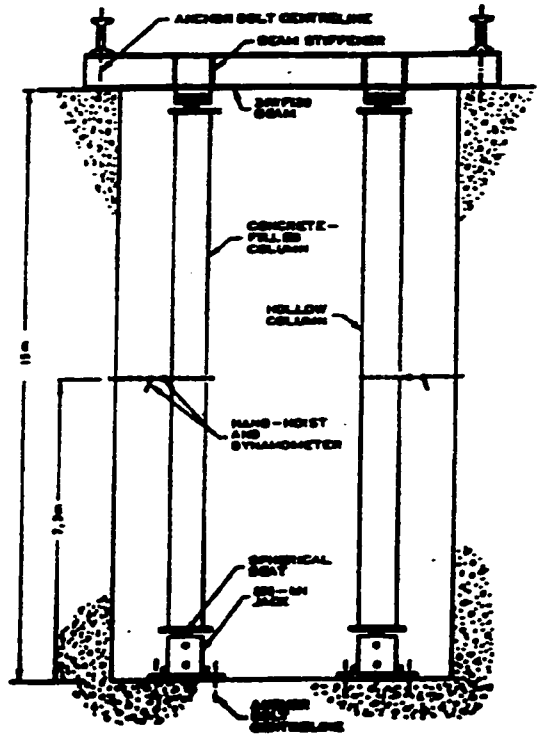

Figure 2.28: Test set-up [Ghosh et al. (1997)].

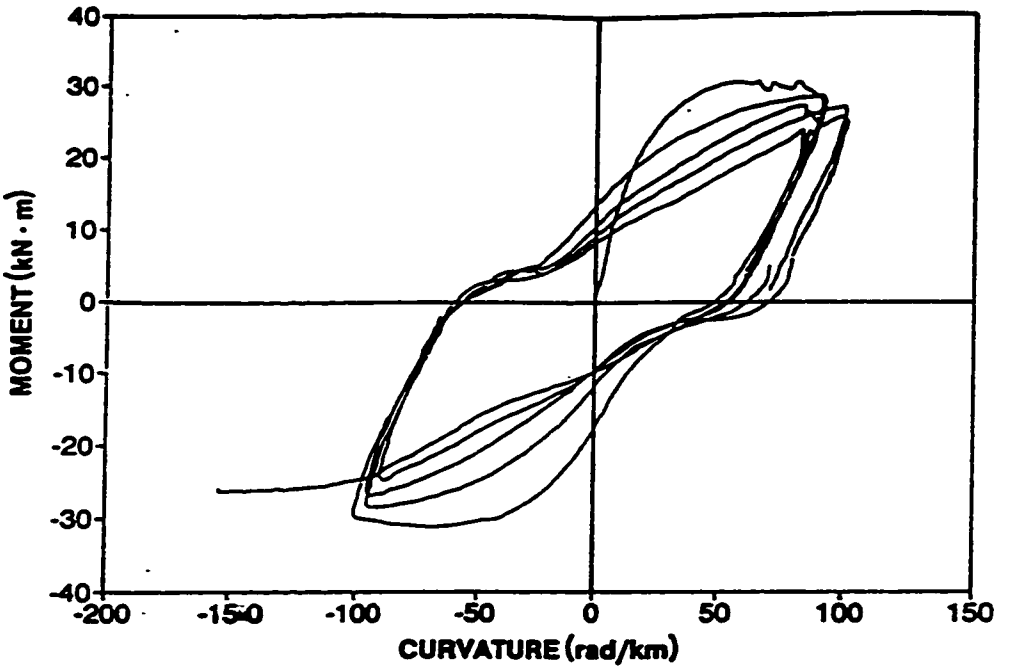

Figure 2.29: Hysteretic behaviour of beam-column specimen [Prion and Boehme (1994)].

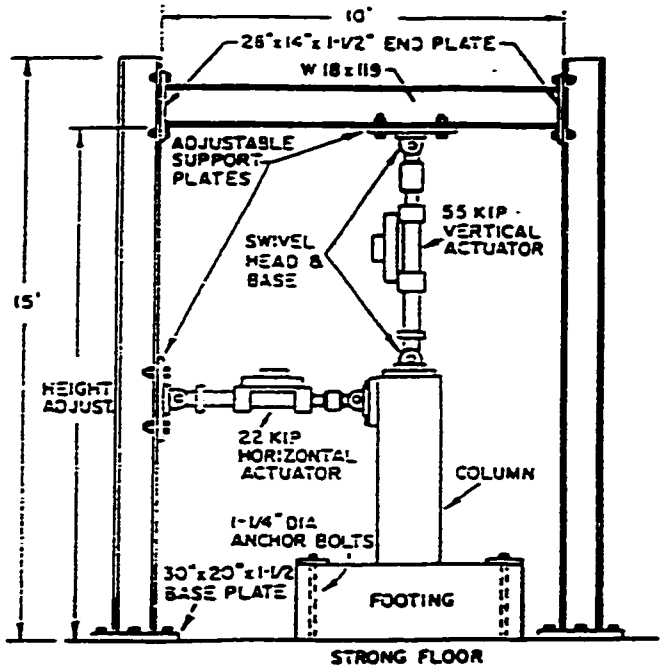

Figure 2.30: Test set-up [Boyd et al. (1995)].

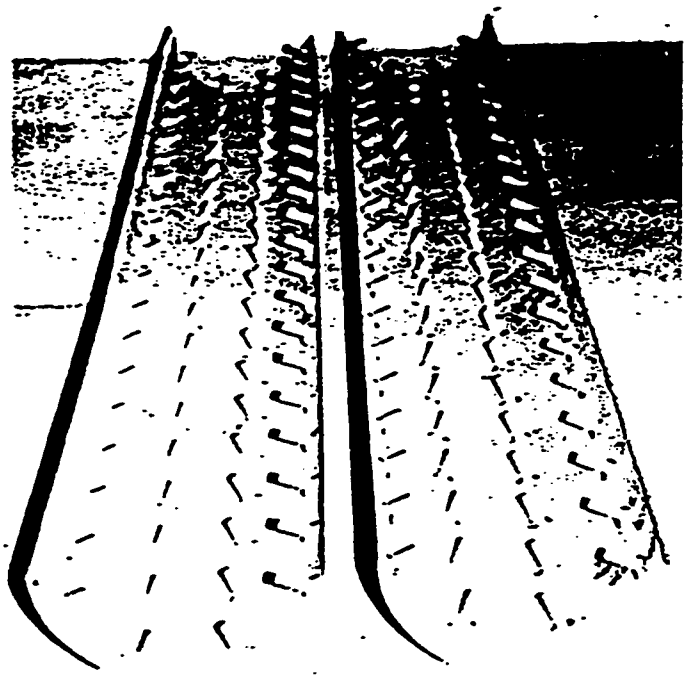

Figure 2.31: Studded shell halves of Specimen 3 prior to welding the shell back together [Boyd et al. (1992)].

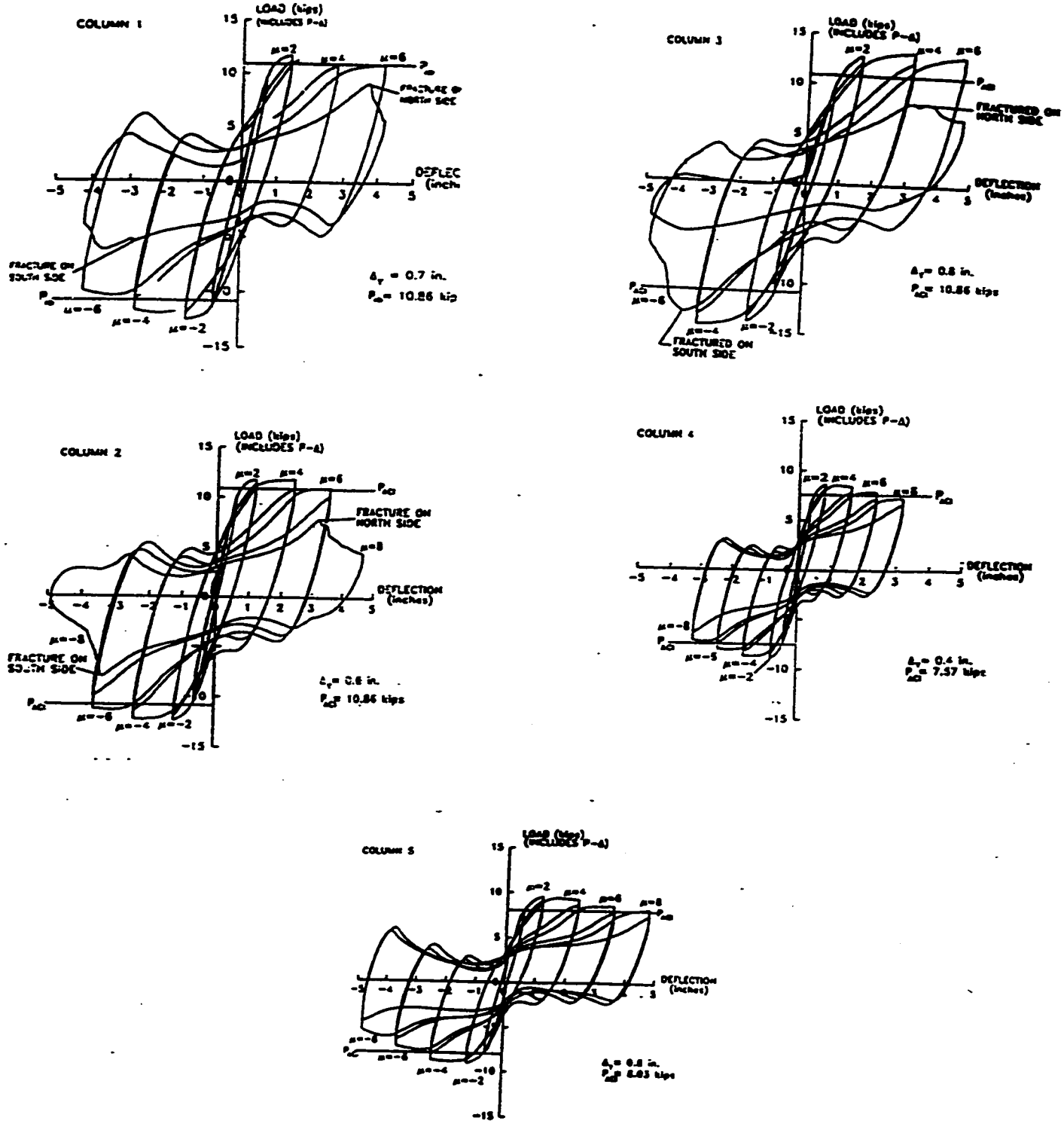

Figure 2.32: Lateral load-displacement hysteresis curves [Boyd et al. (1995)].

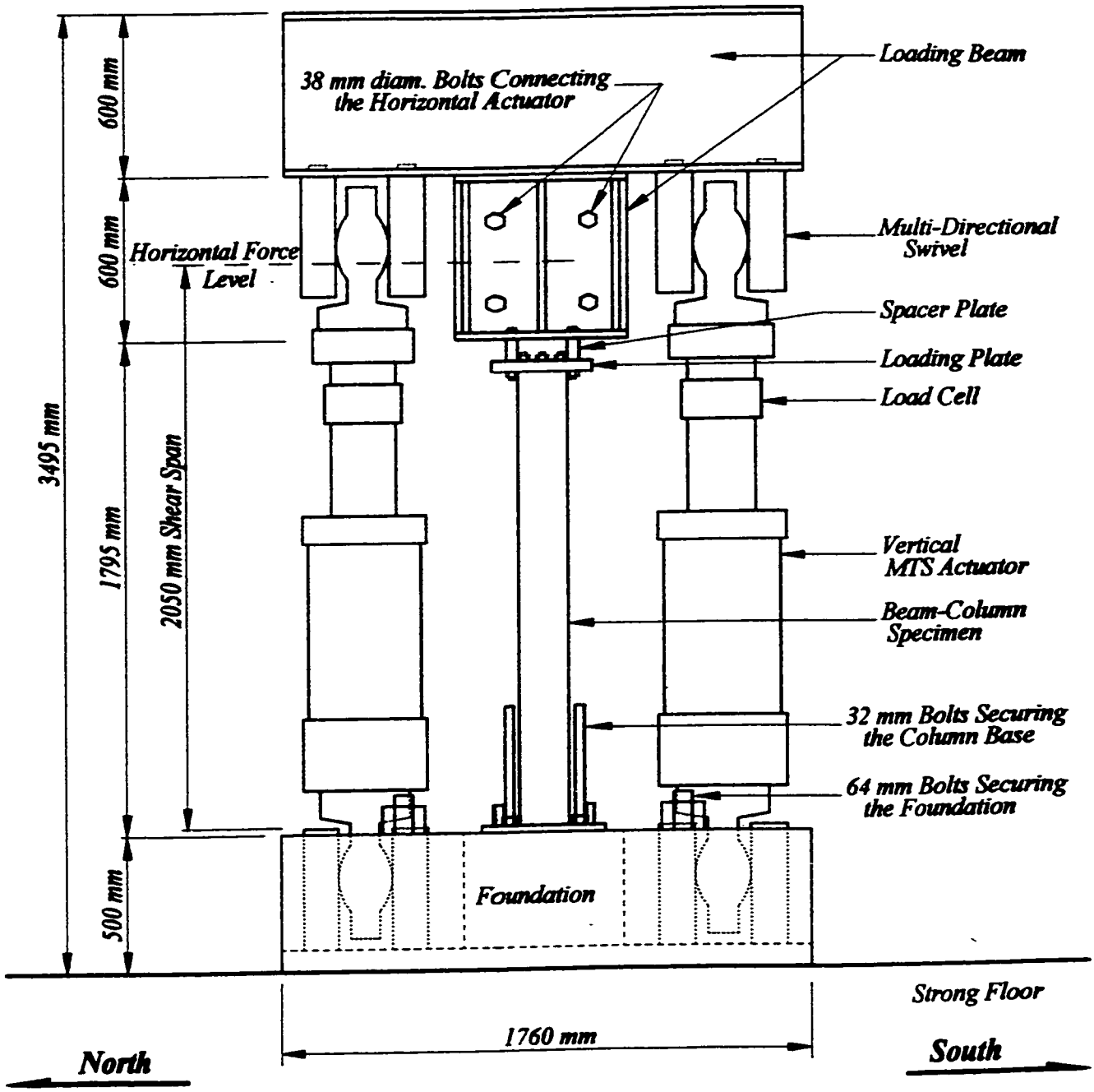

Figure 2.33: Test set-up [Alfawakìri (1997)]

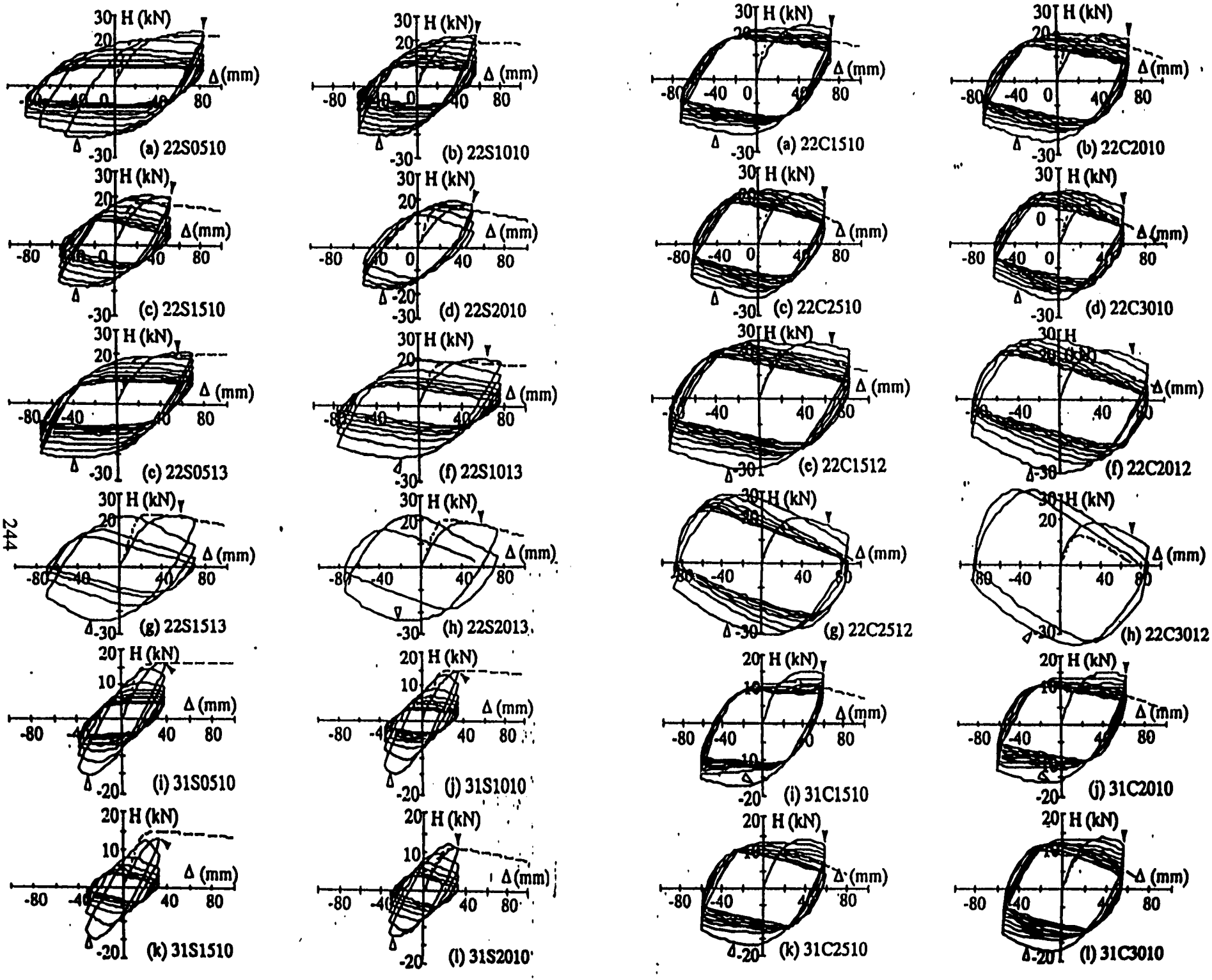

Figure 2.34: Horizontal load - displacement hysteretic curves [Kawaguchi et al. (1992)].

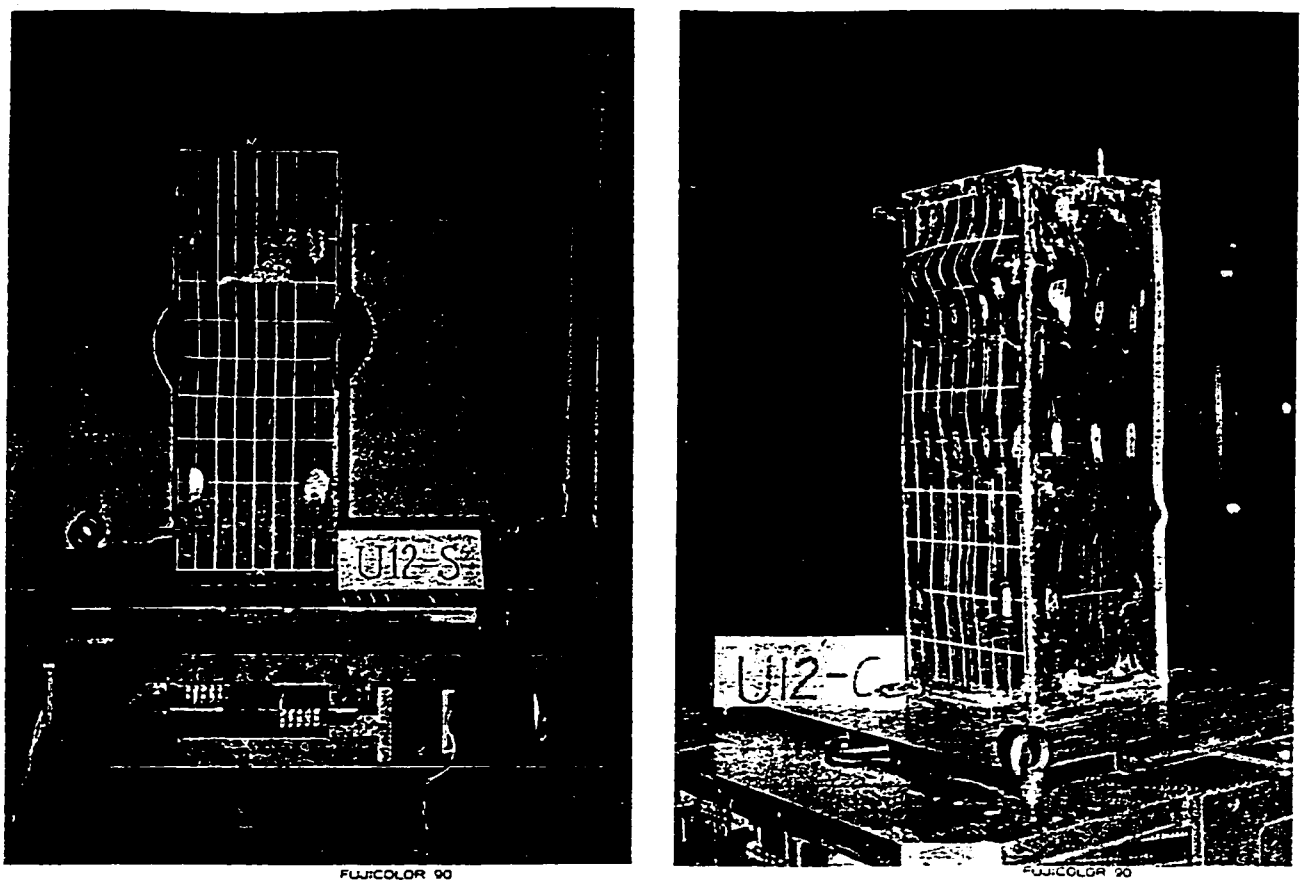

Figure 20: Typical failure experiences of test specimens [Ge and Usami (1994)]

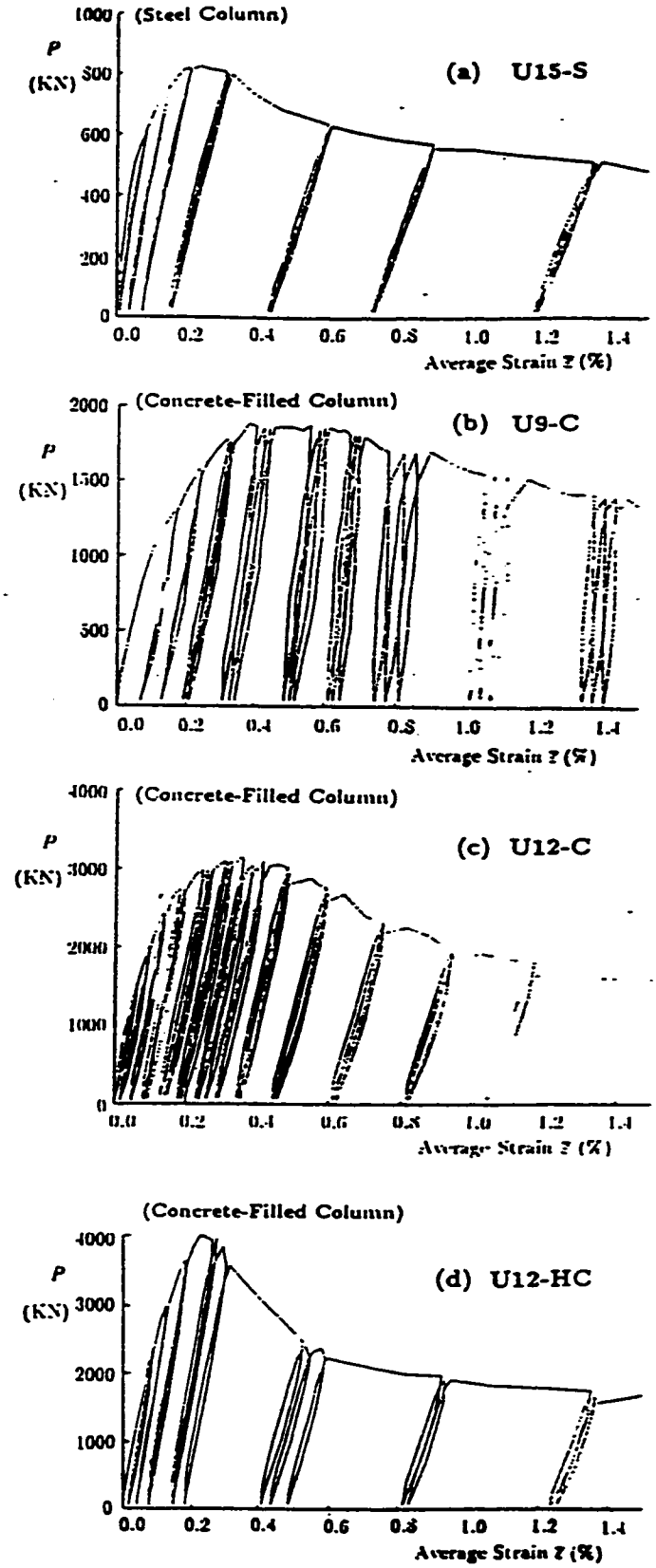

Figure 2.36: Load versus strain curves under cyclic compression loads [Ge and Usami (1994)].

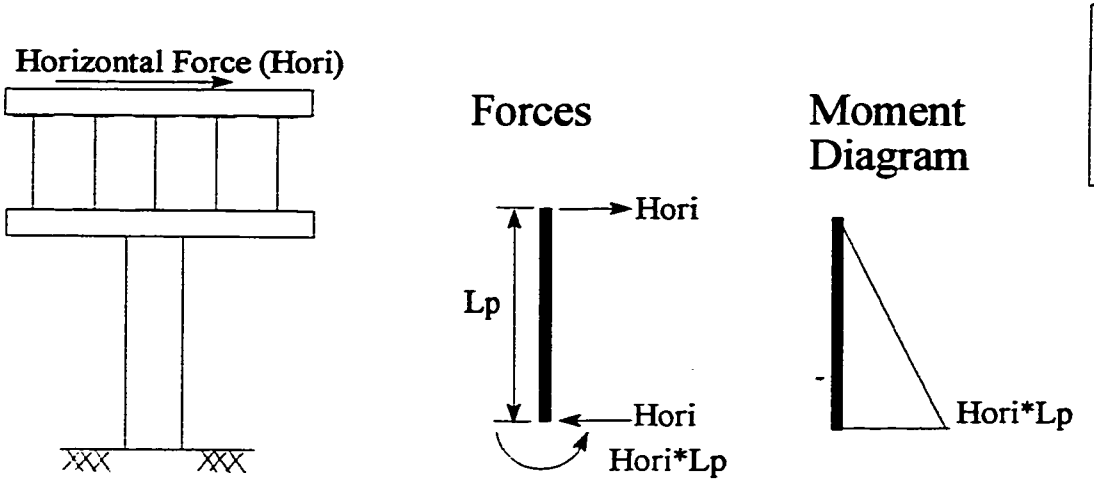

Figure 3.1: Axial and horizontal forces on one pier

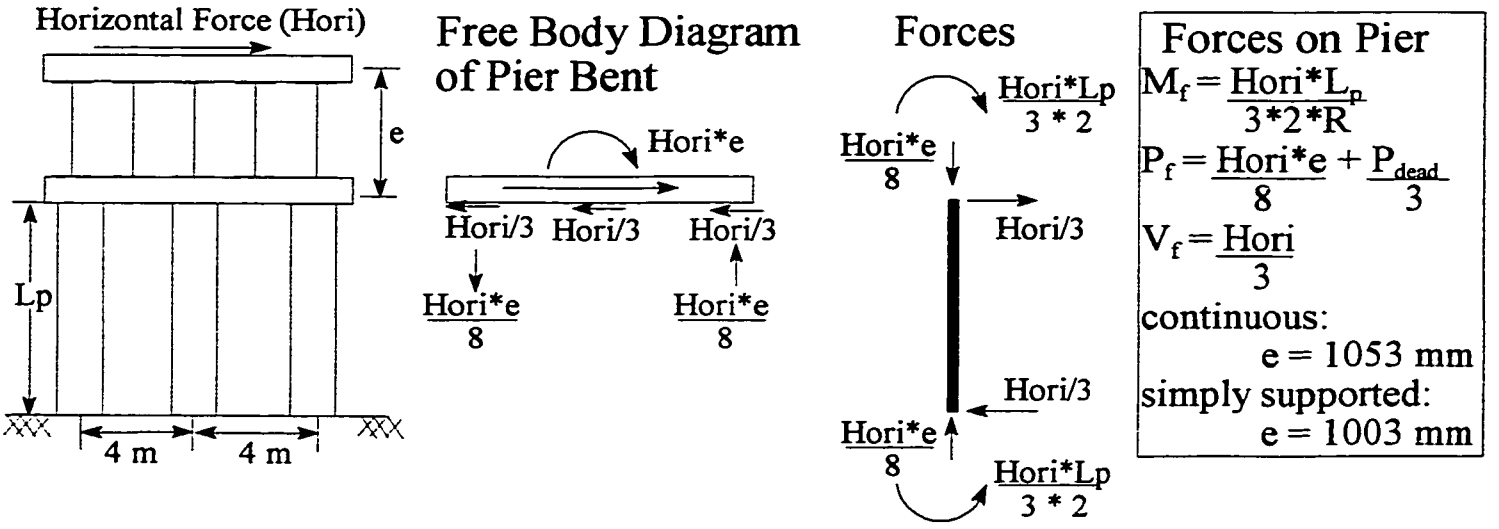

Figure 3.2: Axial and horizontal forces on three piers

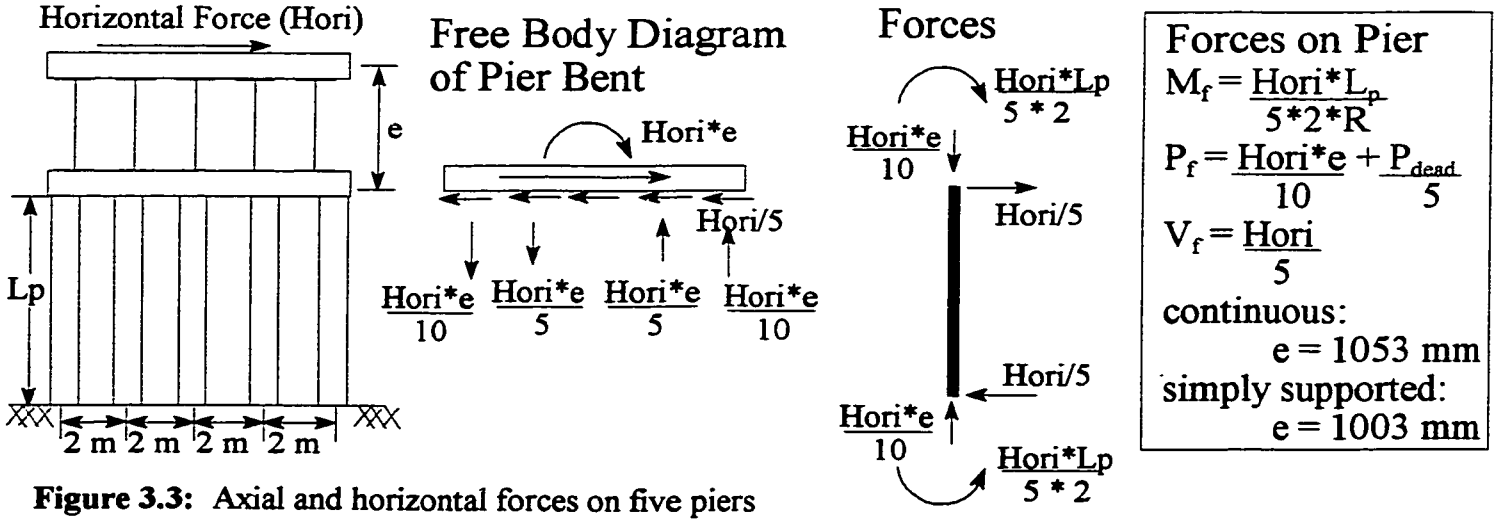

Figure 3.3: Axial and horizontal forces on five piers

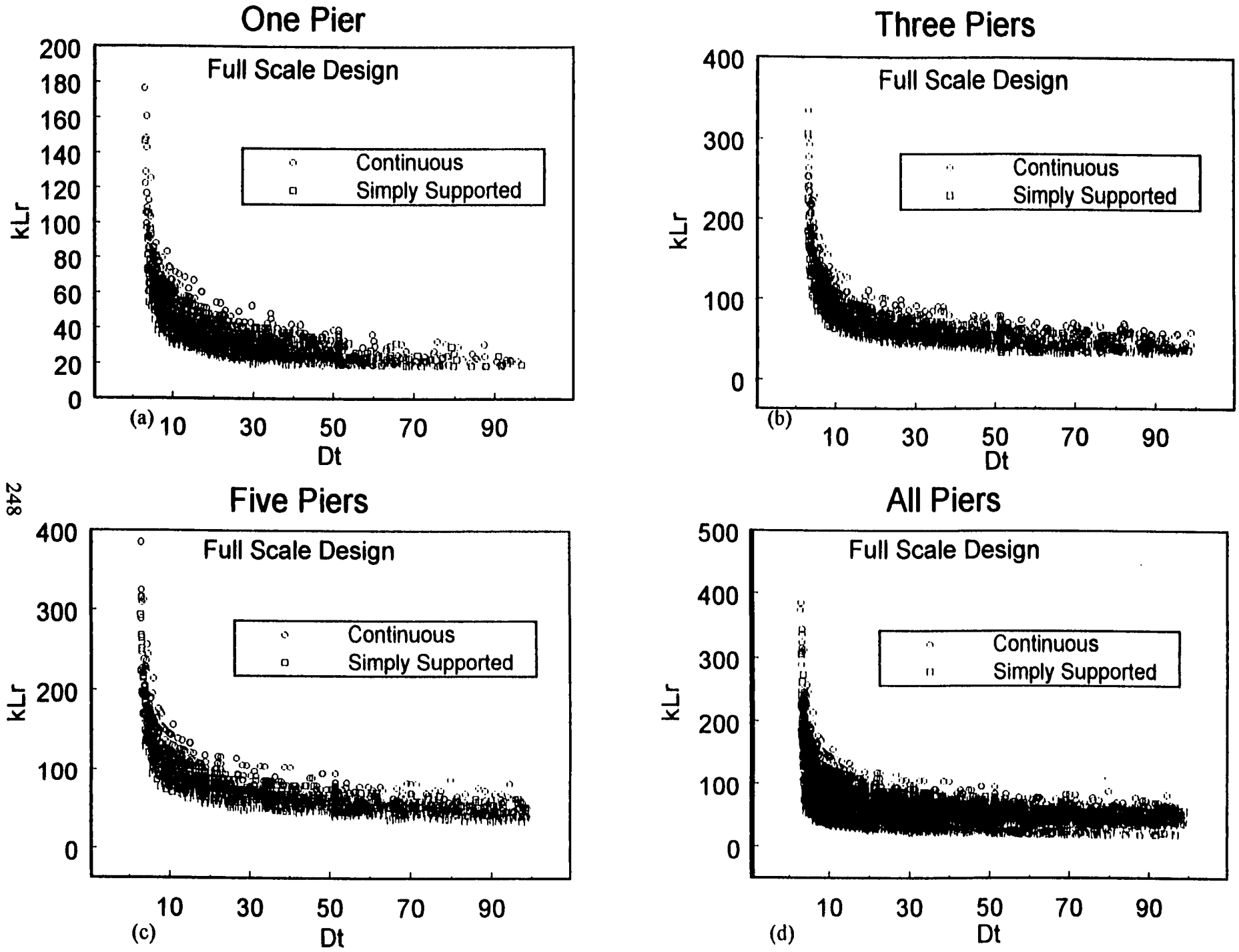

Figure 3.4: Full-scale bridge piers according to number of piers in bent

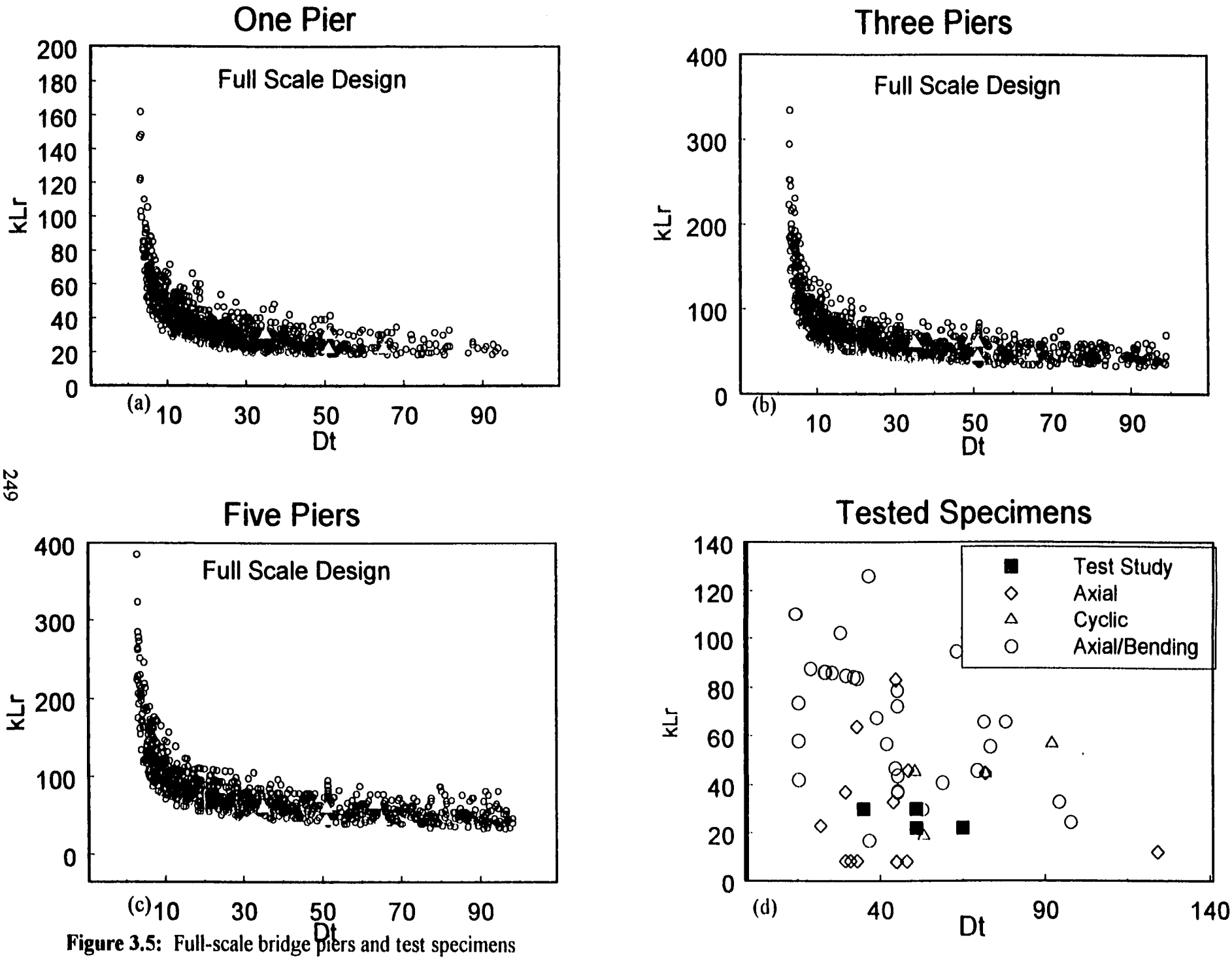

Figure 3.5: Full-scale bridge piers and test specimens

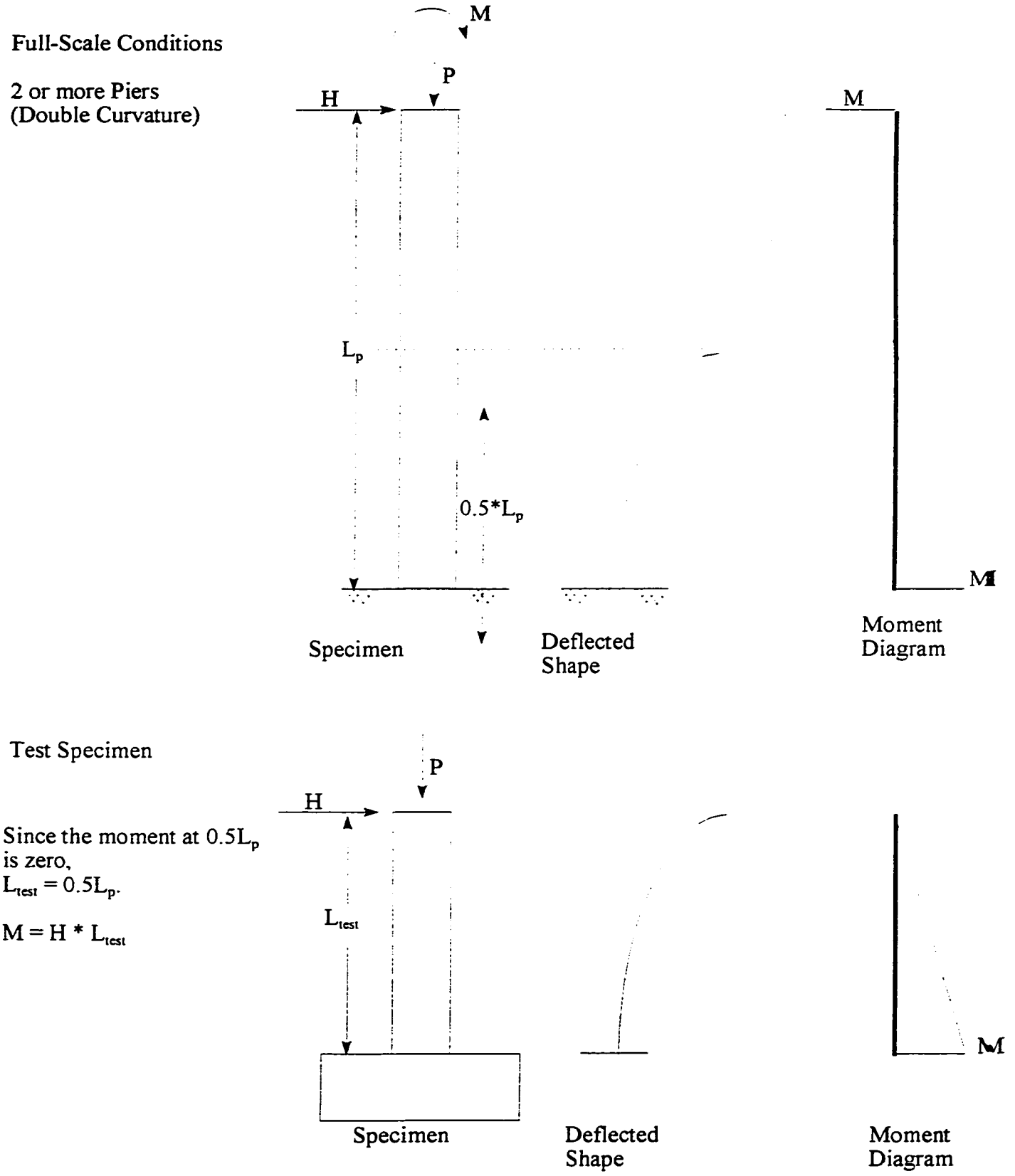

Figure 3.6: Full-scale pier compared to tested column

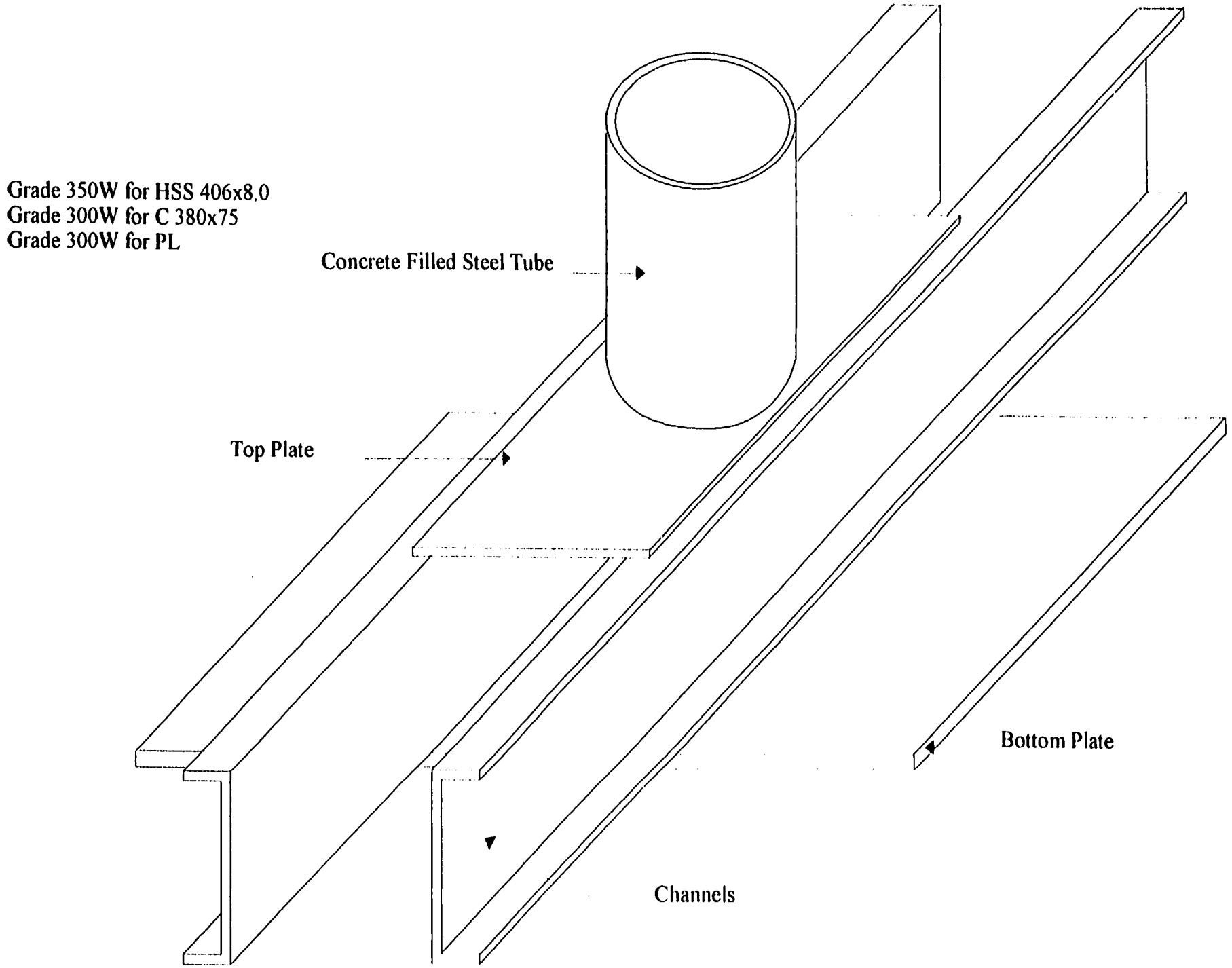

Figure 3.7: 3D view of steel tube and steel foundation

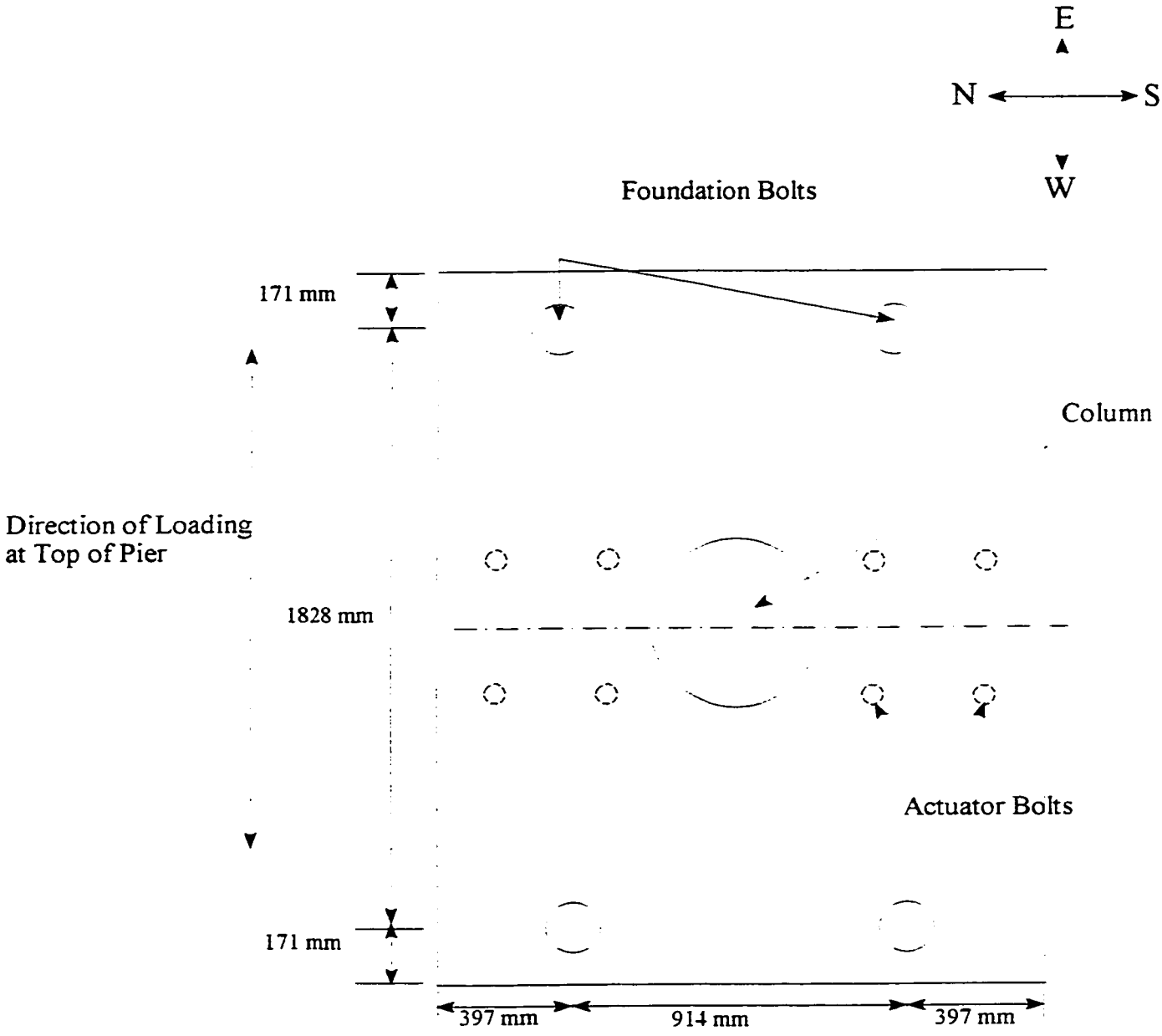

Figure 3.8: Top view of specimen with foundation and actuator bolts

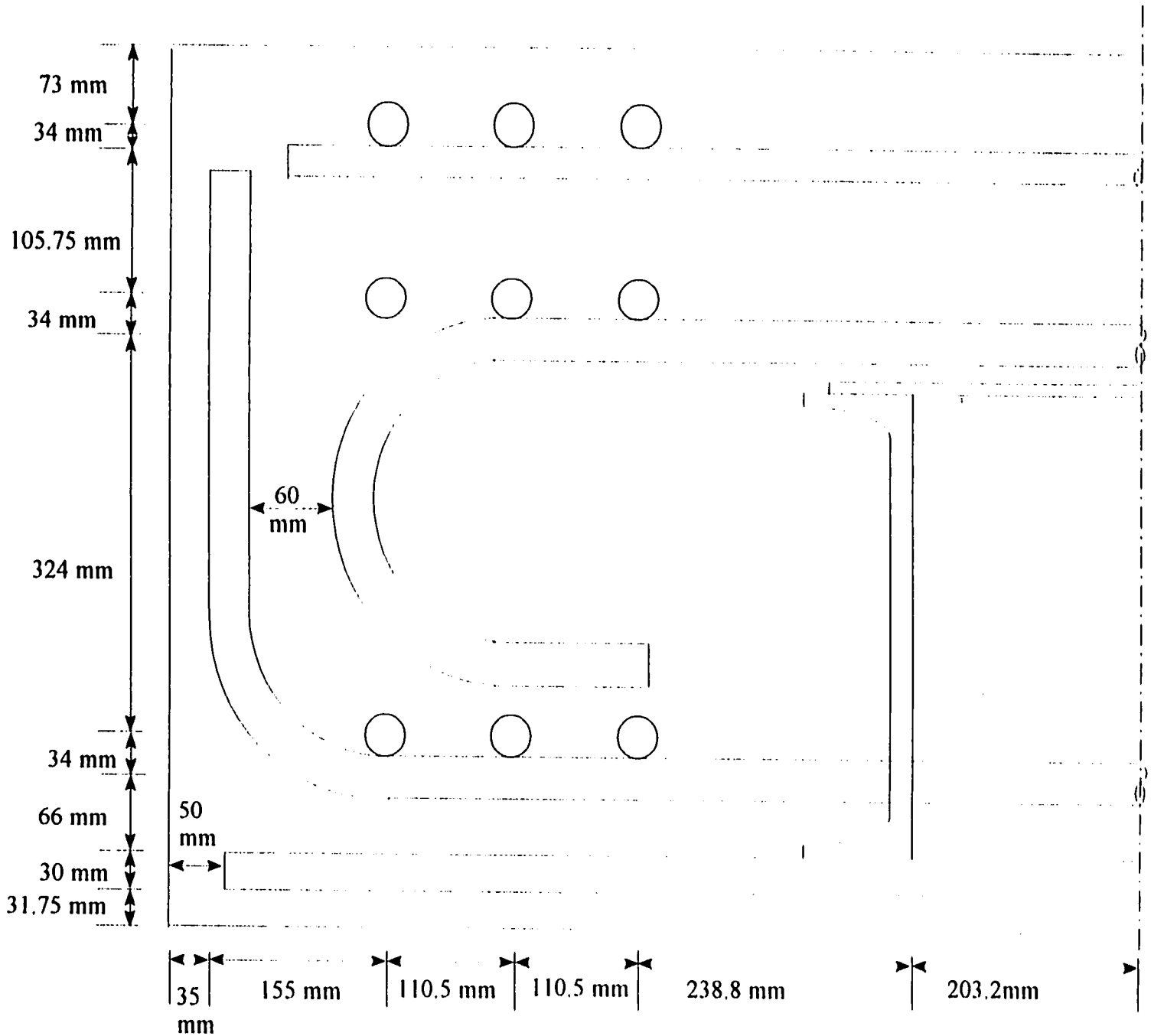

Figure 3.9a: Front view of reinforcement

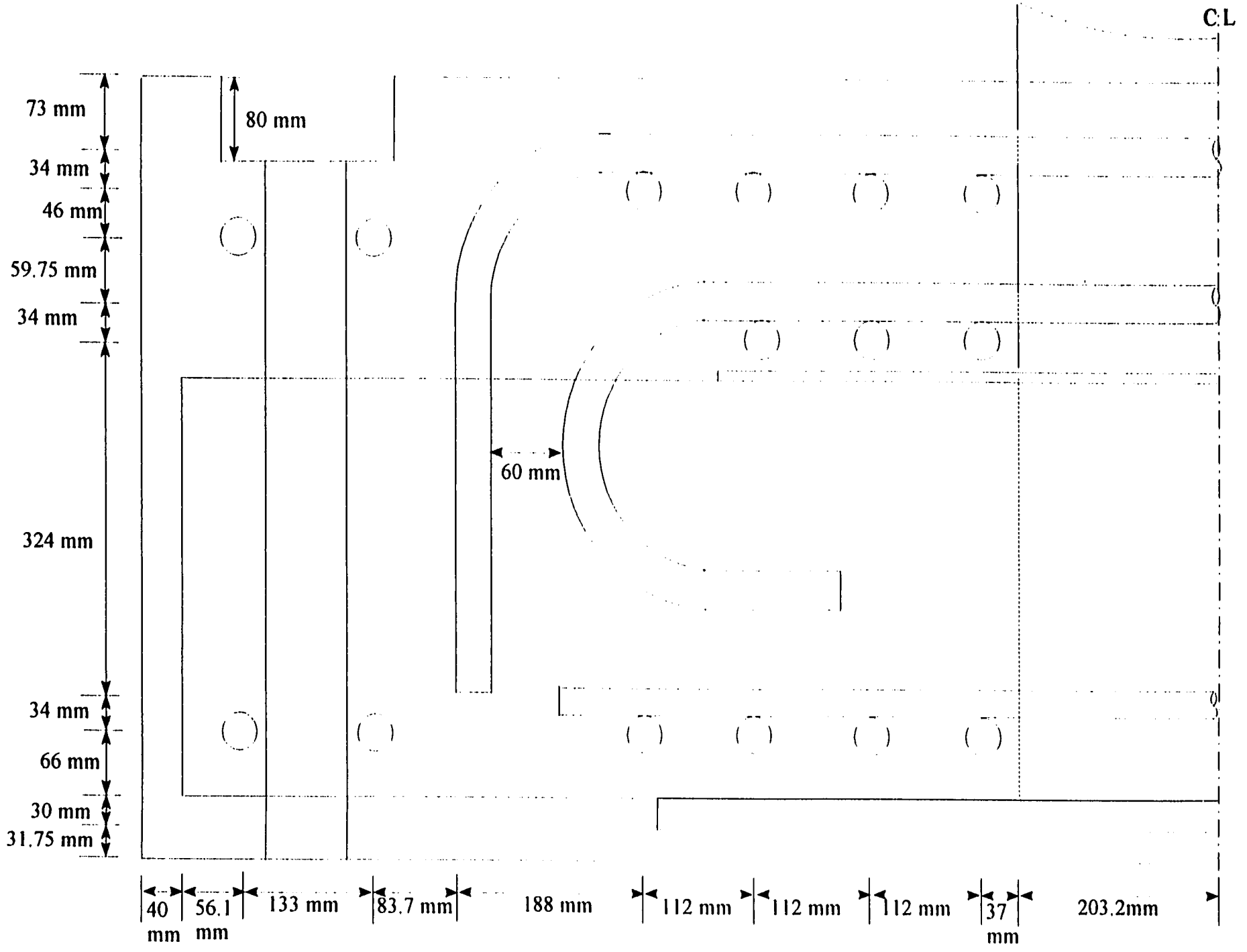

Figure 3.9b: Side view of reinforcement

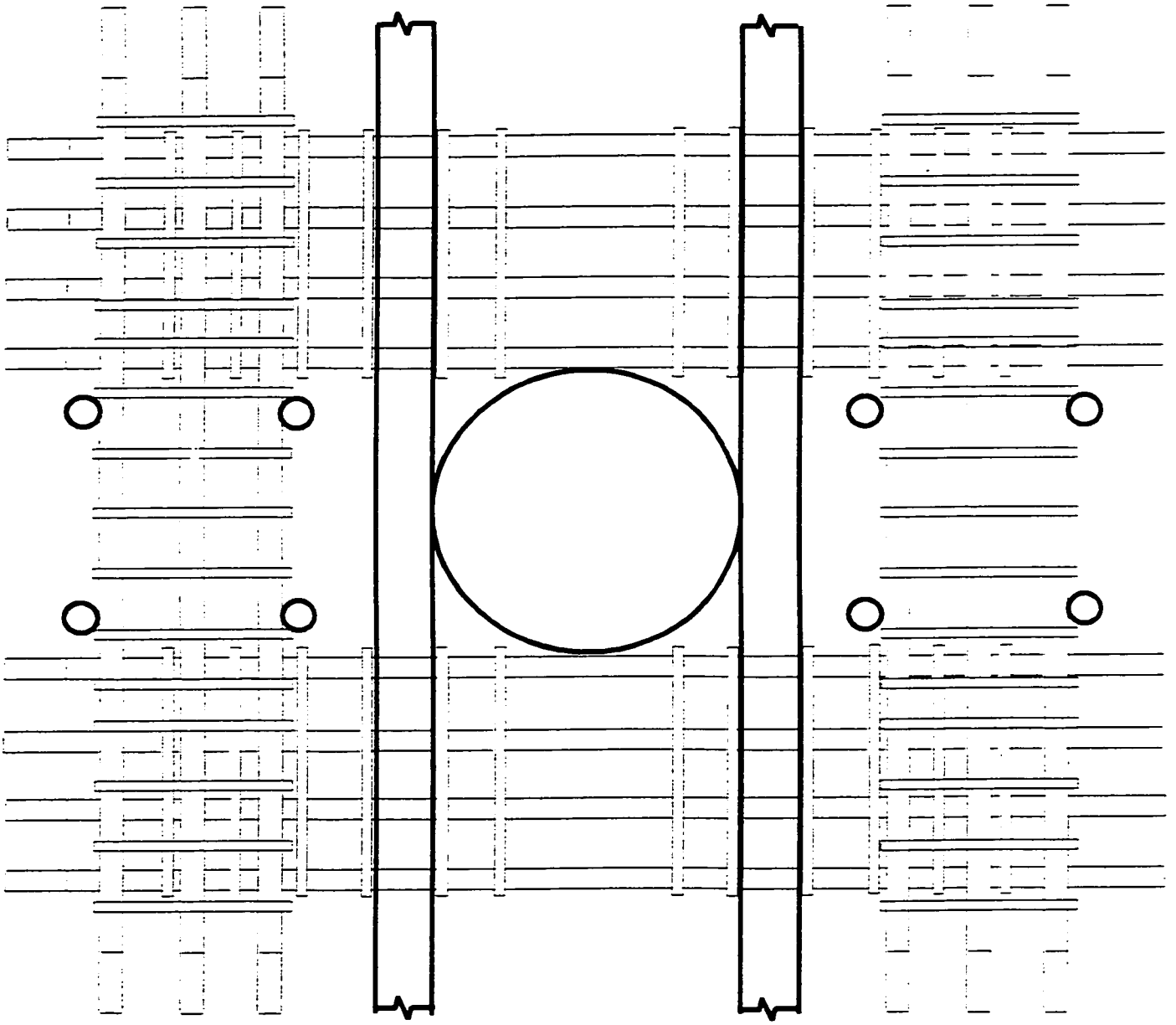

Figure 3.9c: Top view of reinforcement

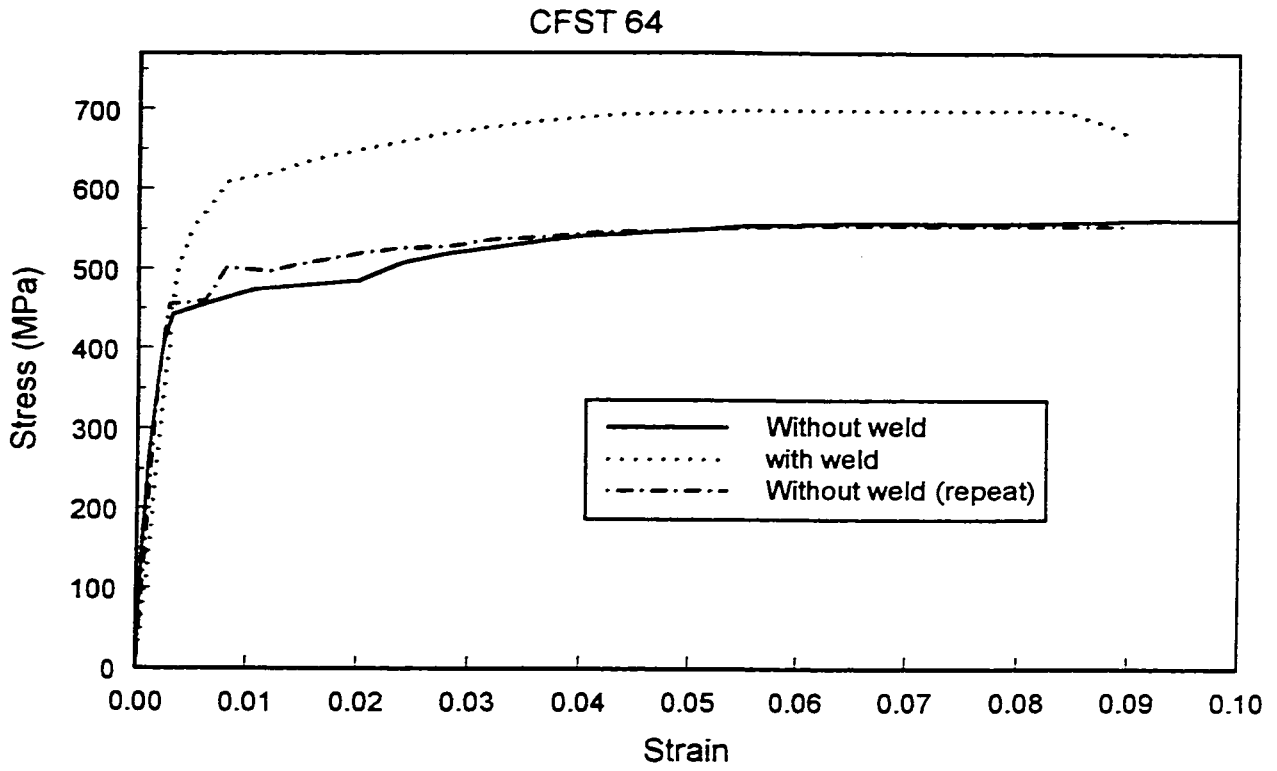

Figure 3.10: Steel coupon strengths for CFST 64

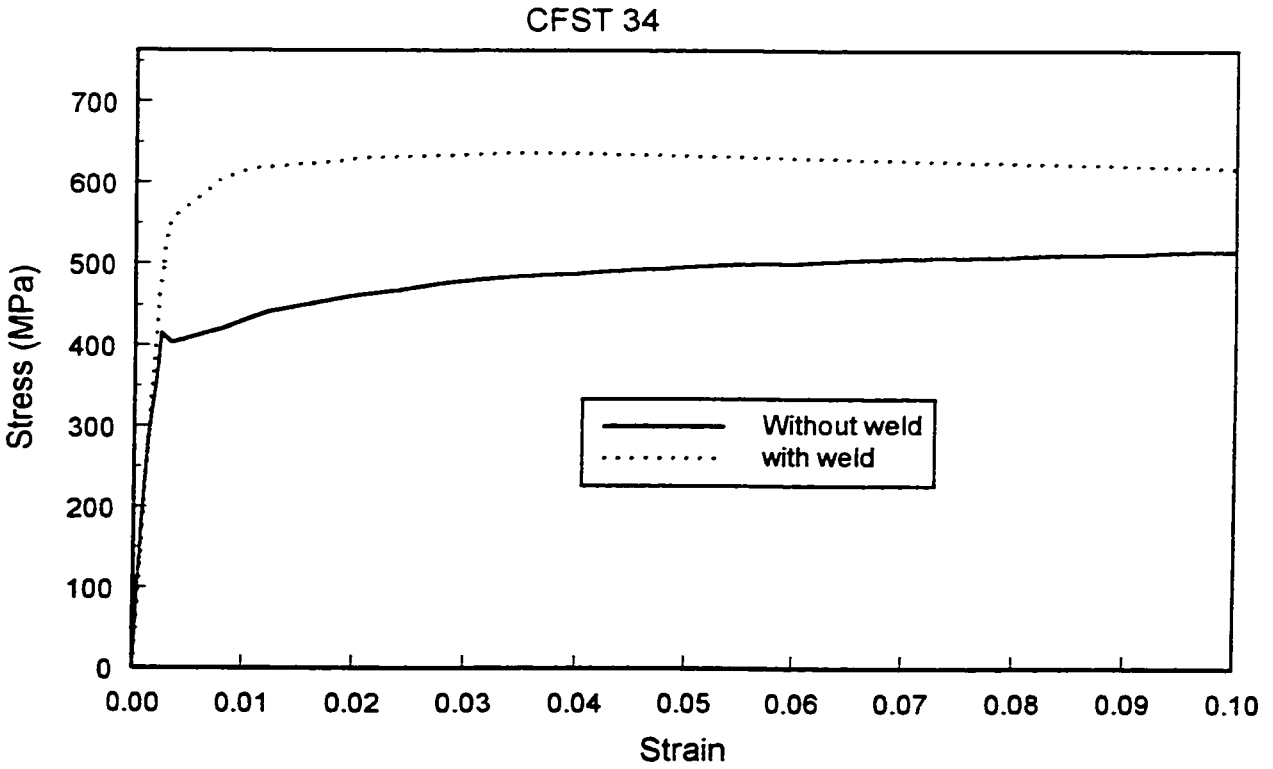

Figure 3.11: Steel coupon strengths for CFST 34

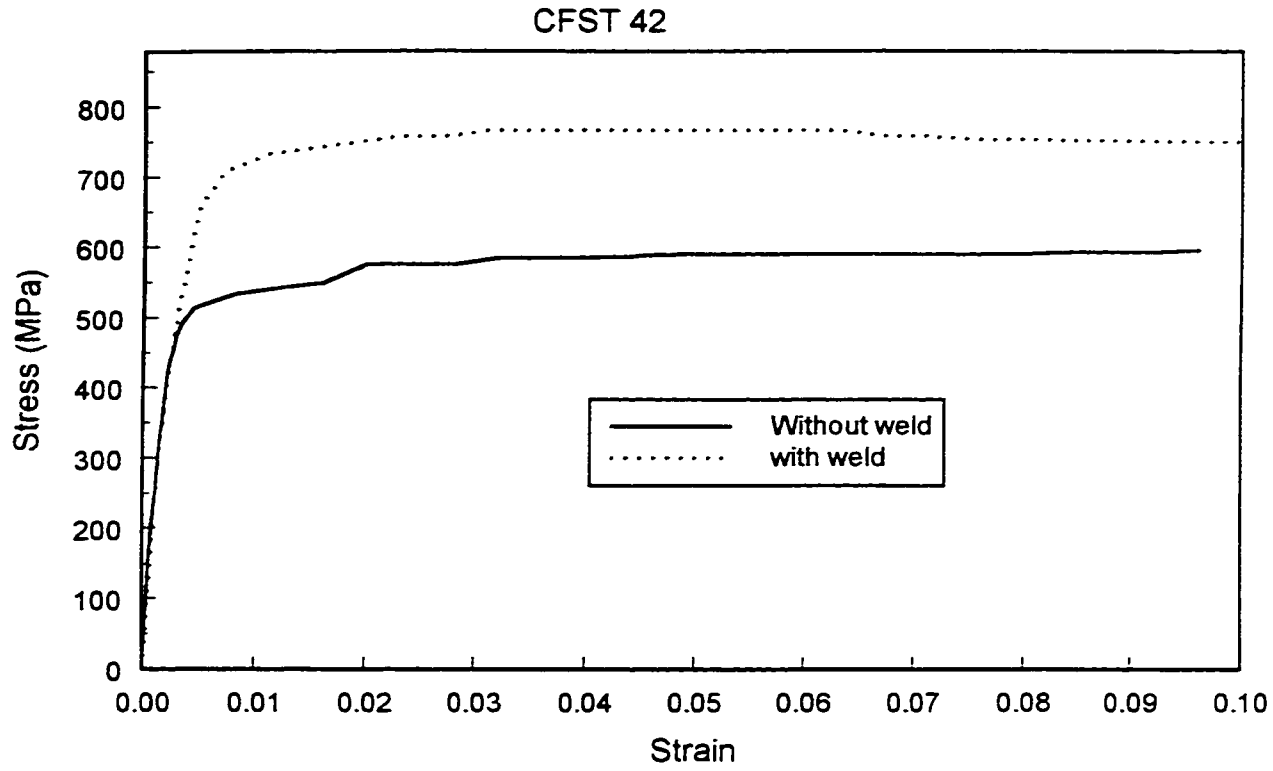

Figure 3.12: Steel coupon strengths for CFST 42

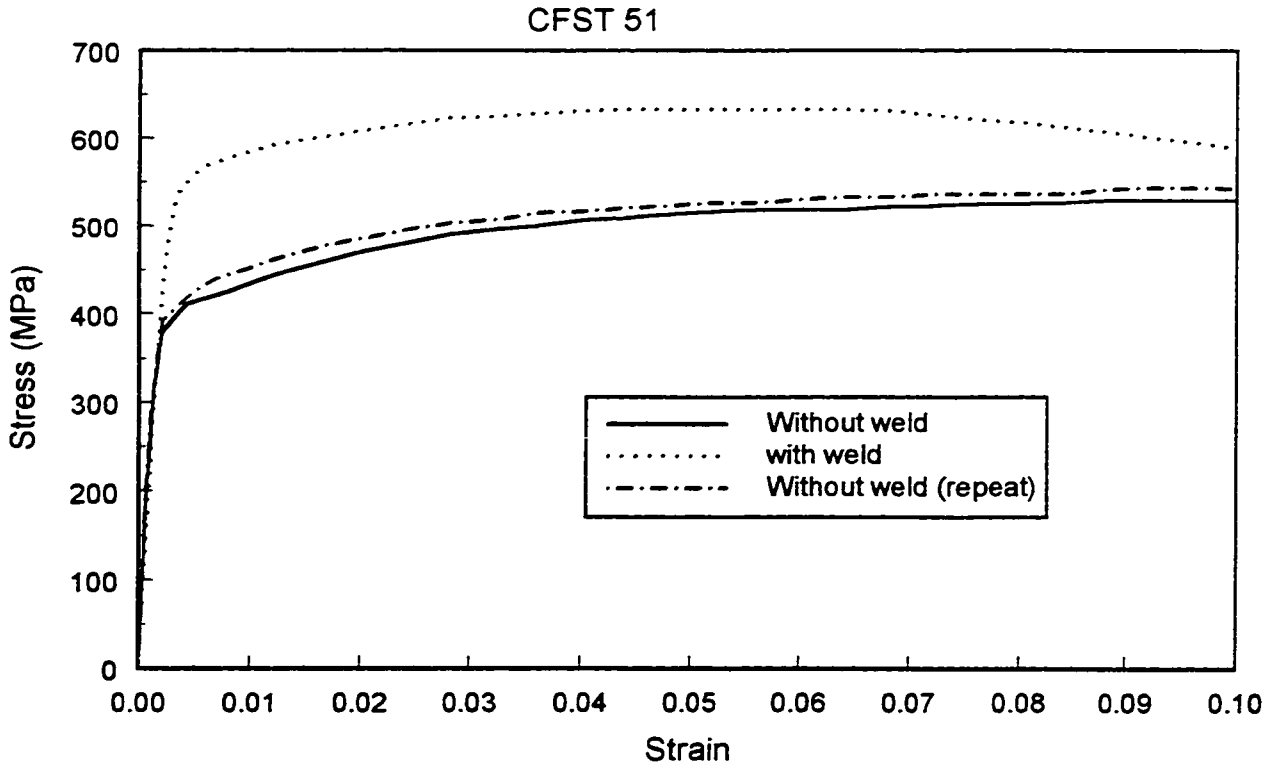

Figure 3.13: Steel coupon strengths for CFST 51

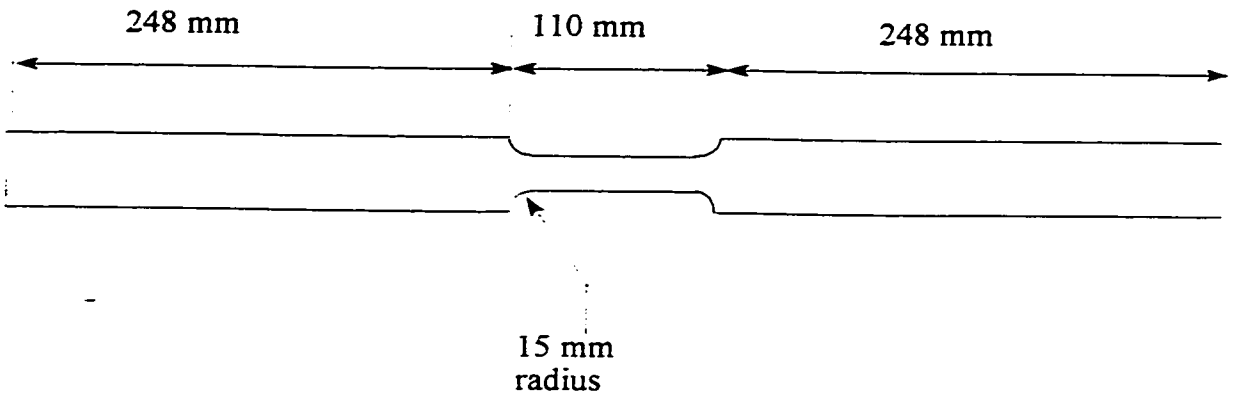

Figure 3.14: Steel coupon tension specimen

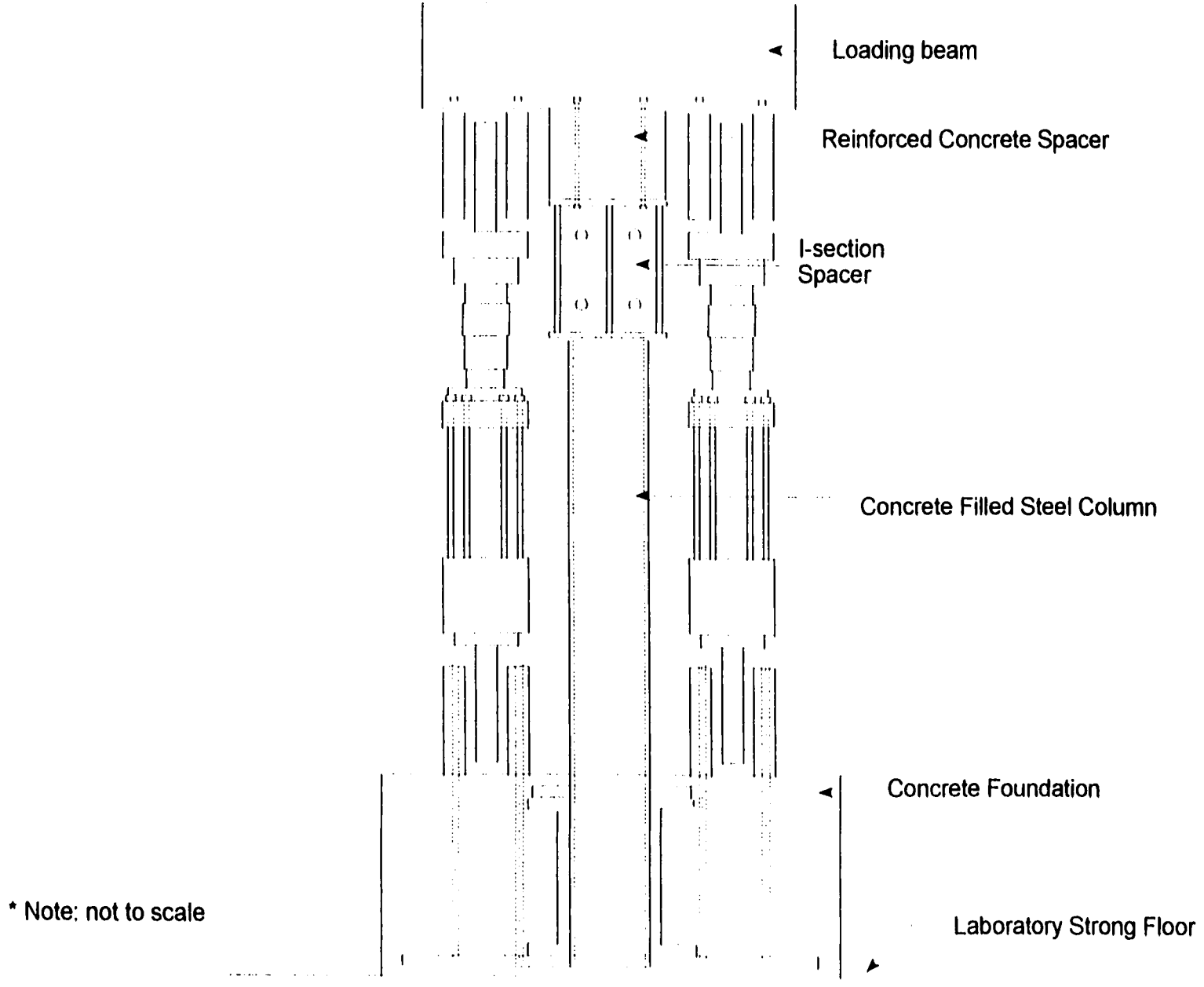

Figure 3.15: Test set-up for east view

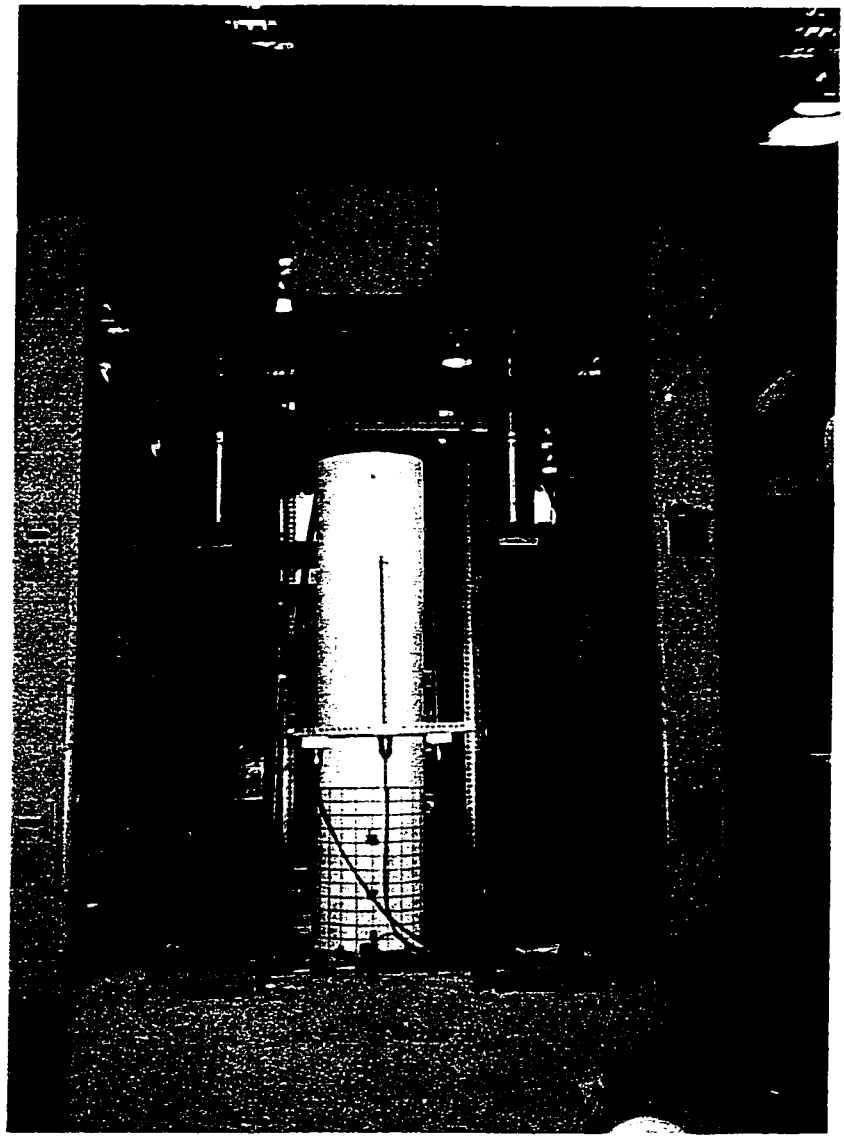

Figure 3.16: Picture of the front view of test set-up

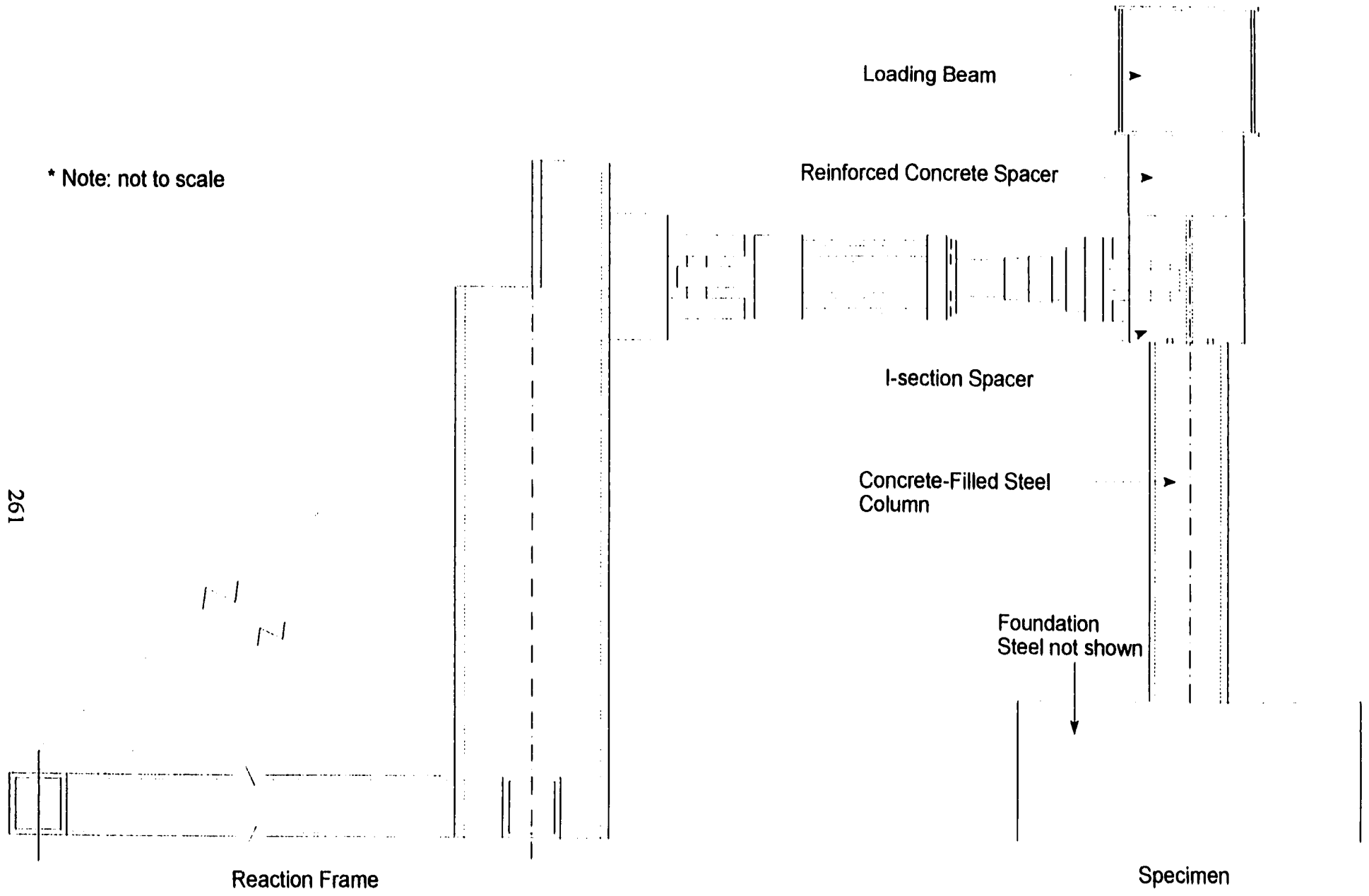

Figure 3.17: Side view of reaction frame with actuators and specimen

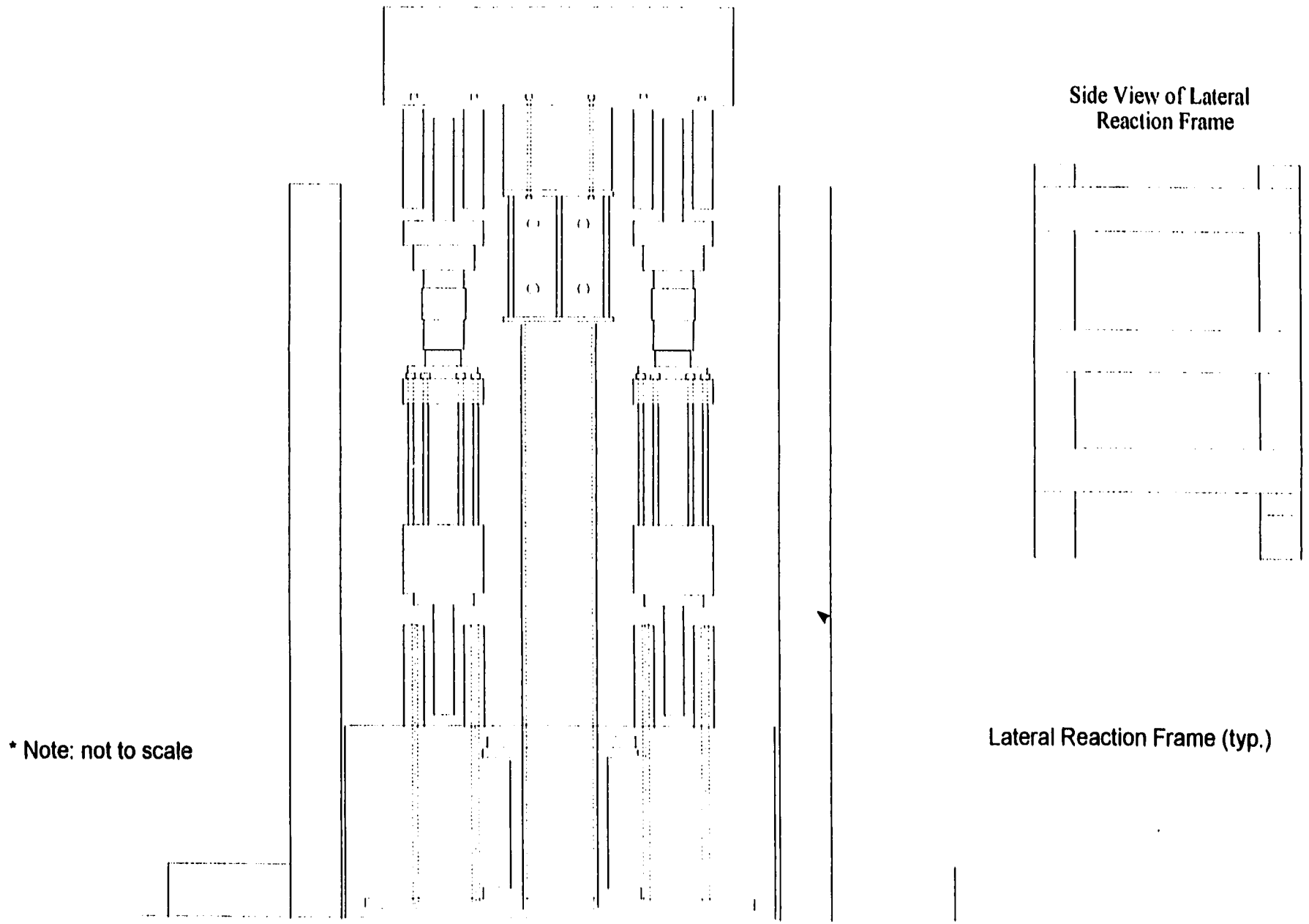

Figure 3.18: Test set-up with lateral reaction frames added for safety

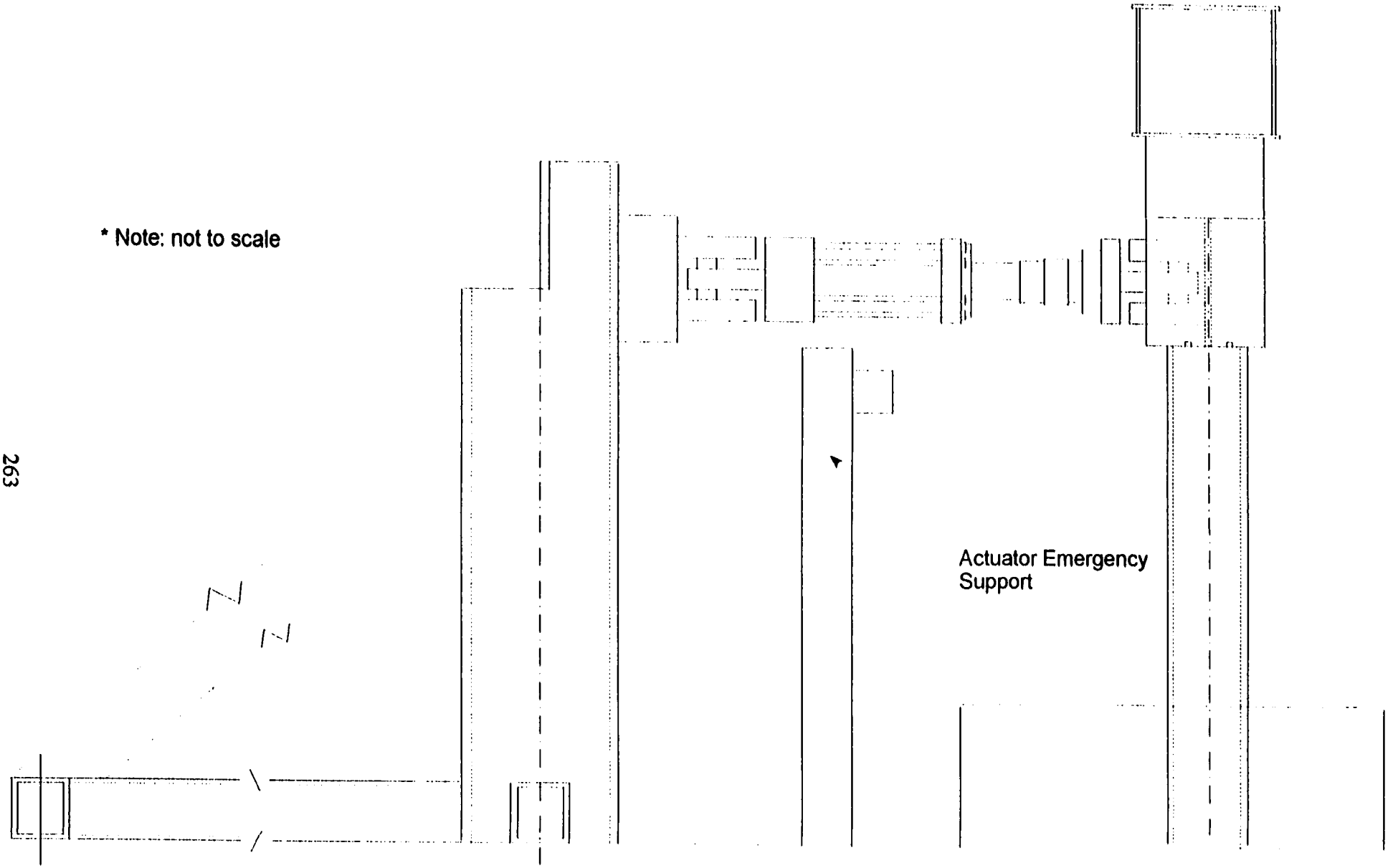

Figure 3.19: Horizontal actuator with safety frame

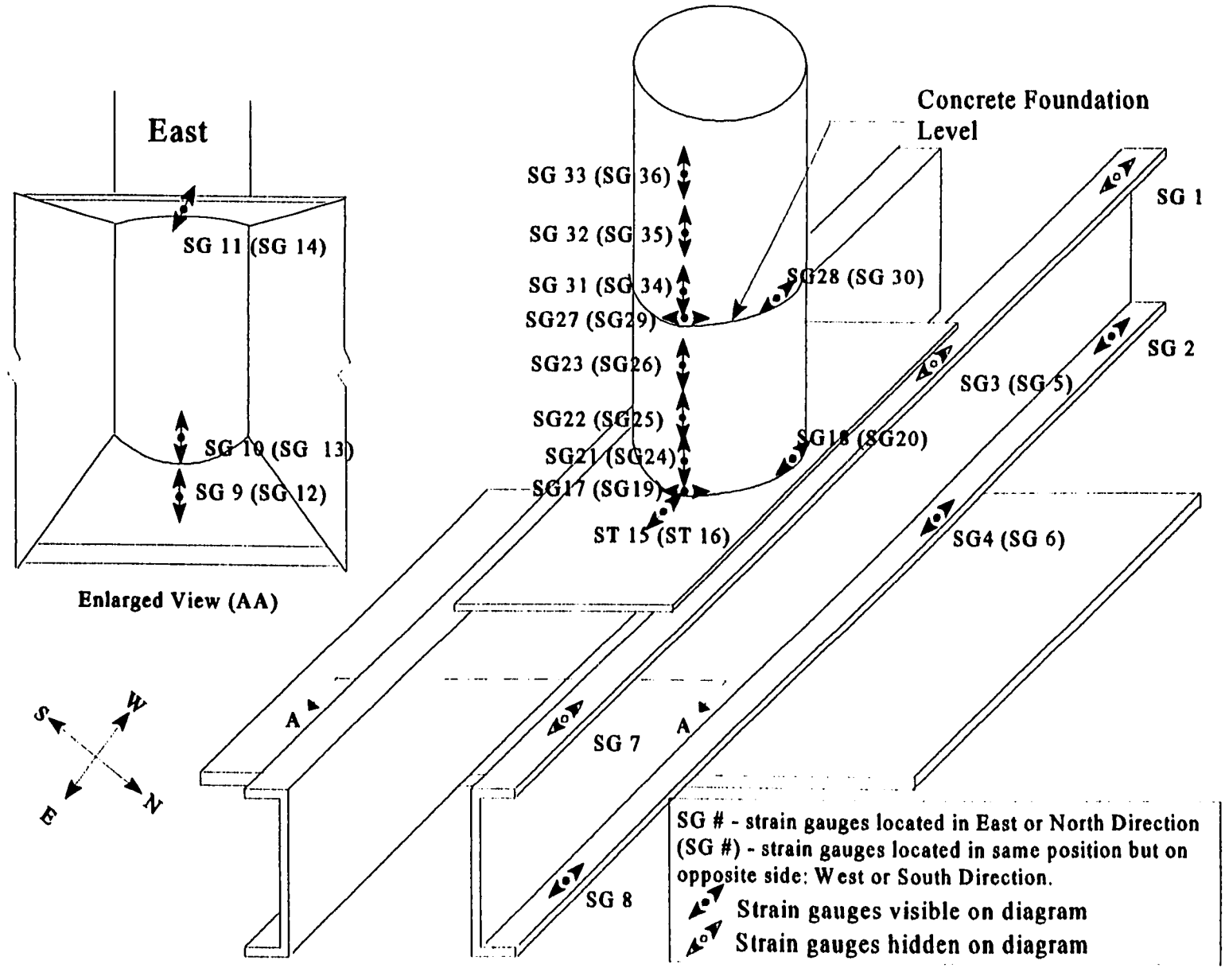

Figure 3.20: Location of strain gauges

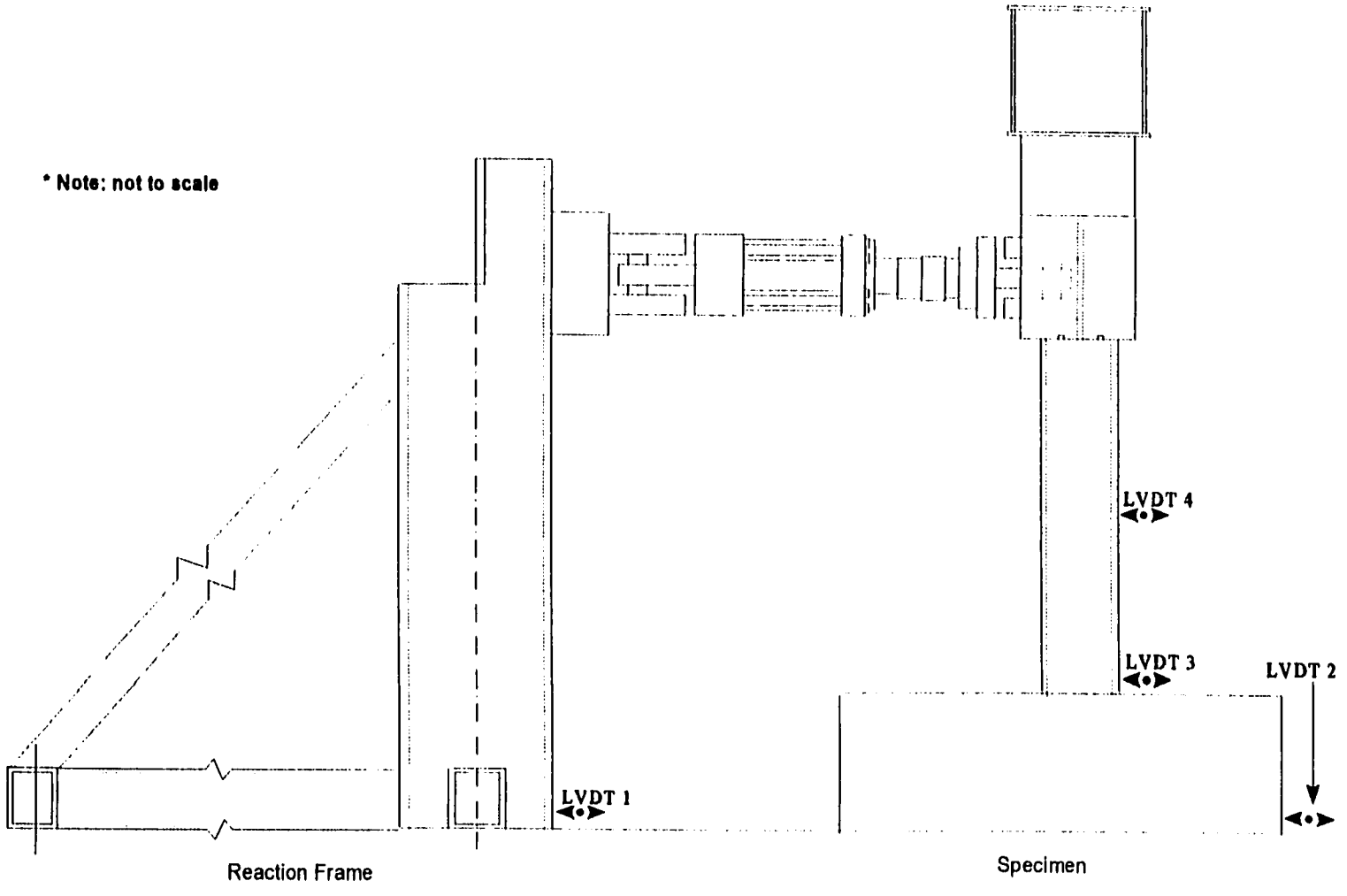

Figure 3.21: Positioning of LVDT's

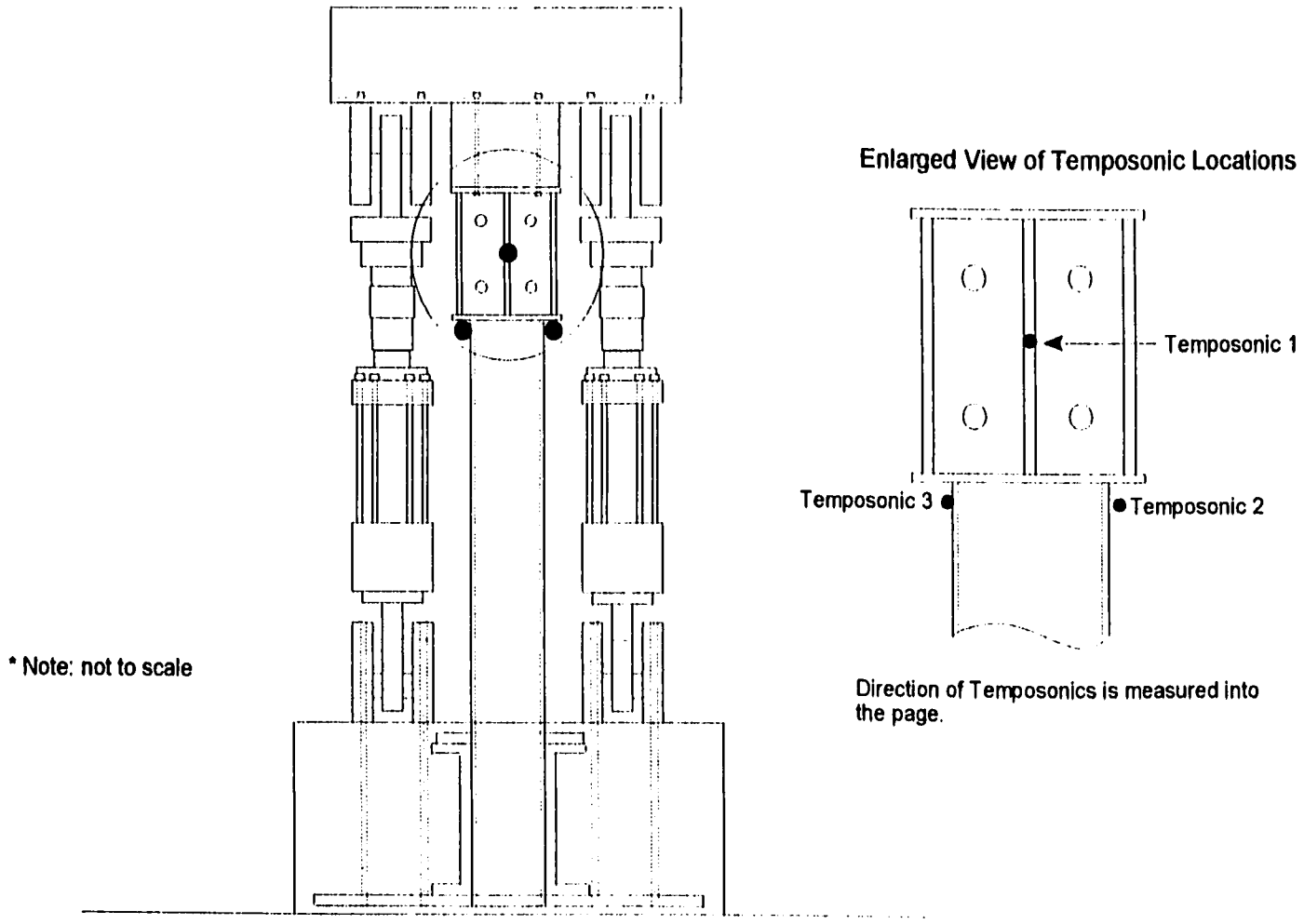

Figure 3.22: Positioning of temposonic LVDTs

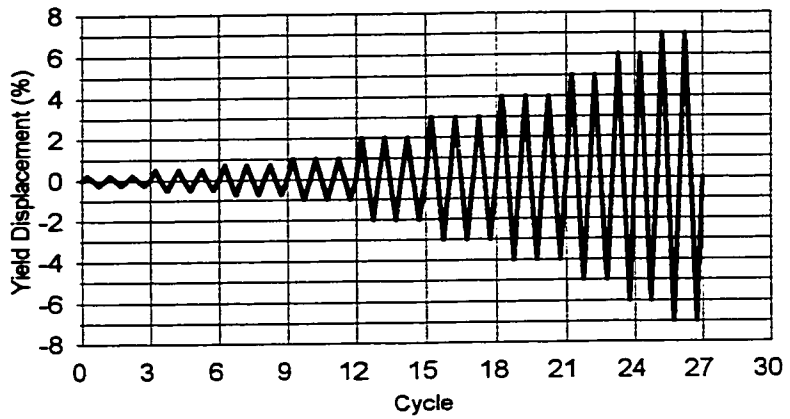

Figure 4.1: Loading sequence

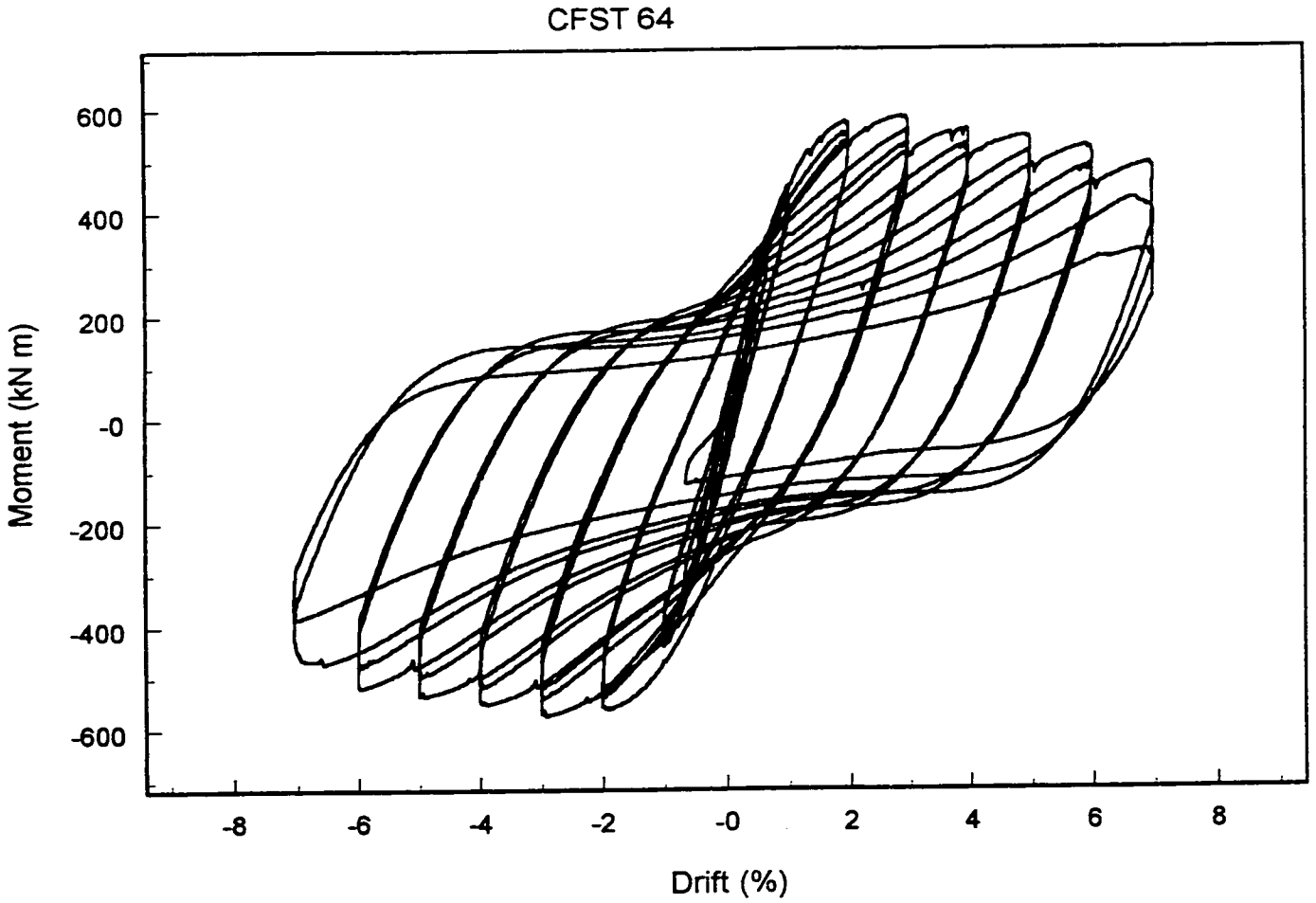

Figure 4.2: Base moment versus drift - CFST 64

Figure 4.3: Cracking at interface of steel tube and concrete foundation - CFST 64

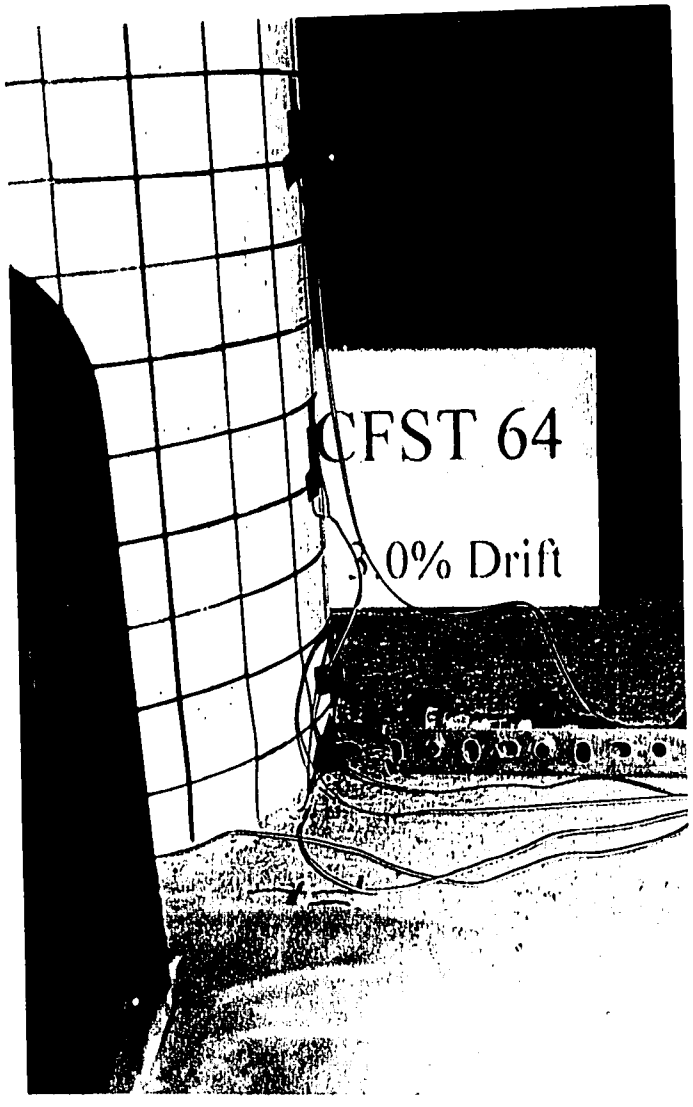

Figure 4.4a: 1st cycle at 3% drift in east direction - CFST 64

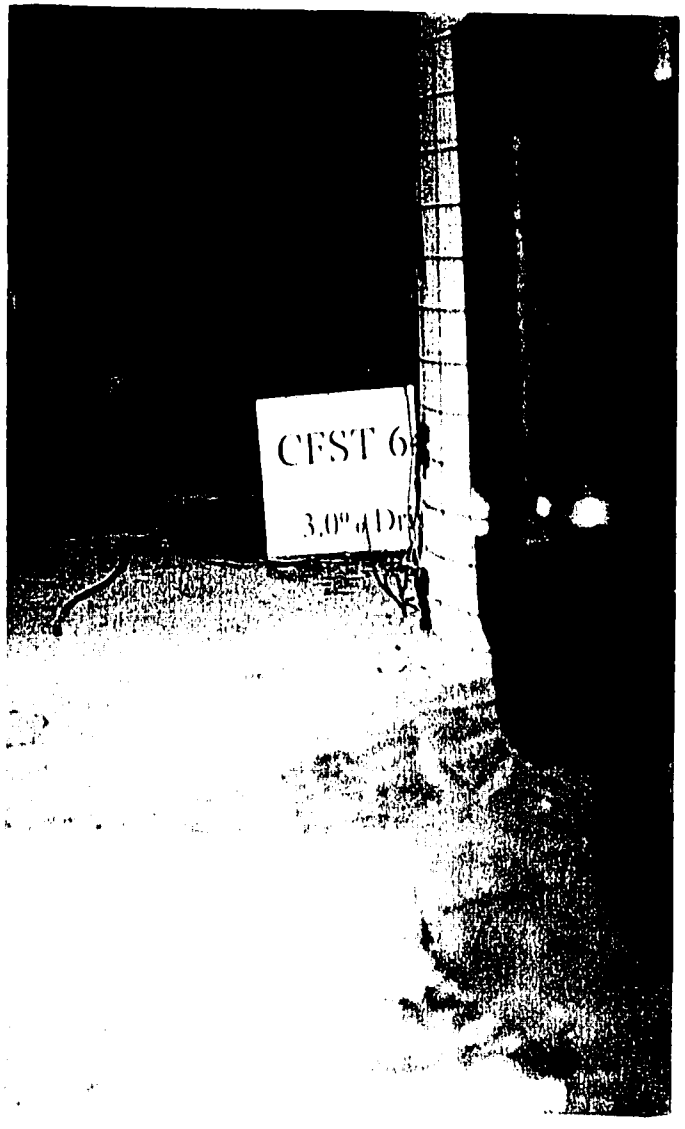

Figure 4.4b: 1st cycle at 3% drift in west direction - CFST 64

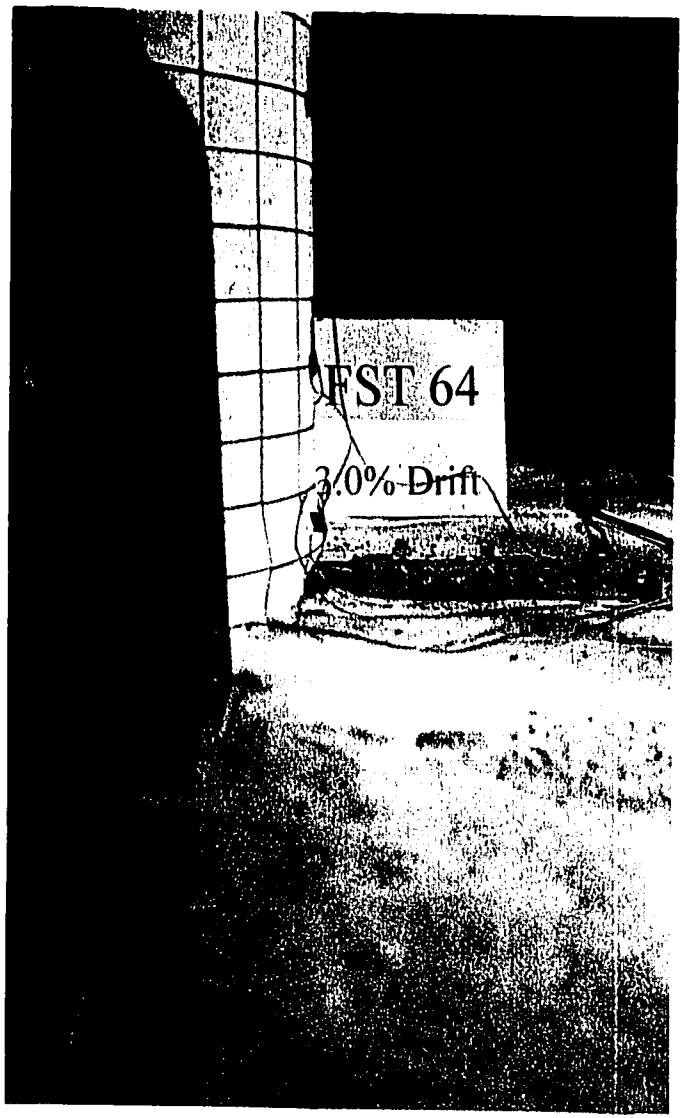

Figure 4.5a: 3rd cycle at 3% drift in east direction - CFST 64

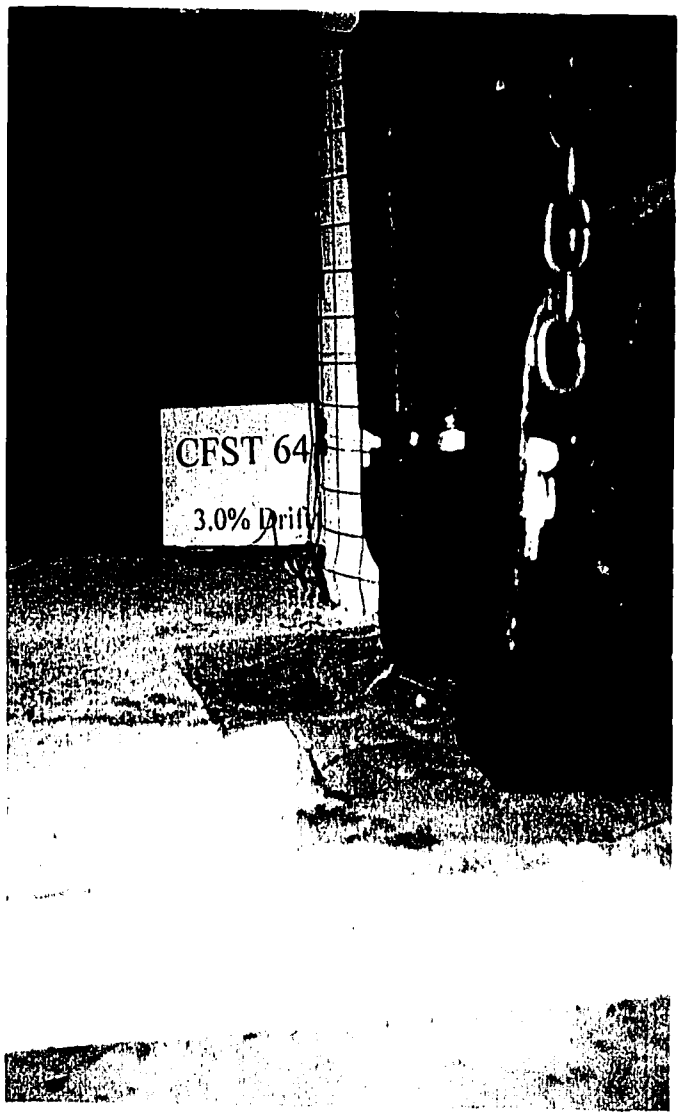

Figure 4.5b: 3rd cycle at 3% drift in west direction - CFST 64

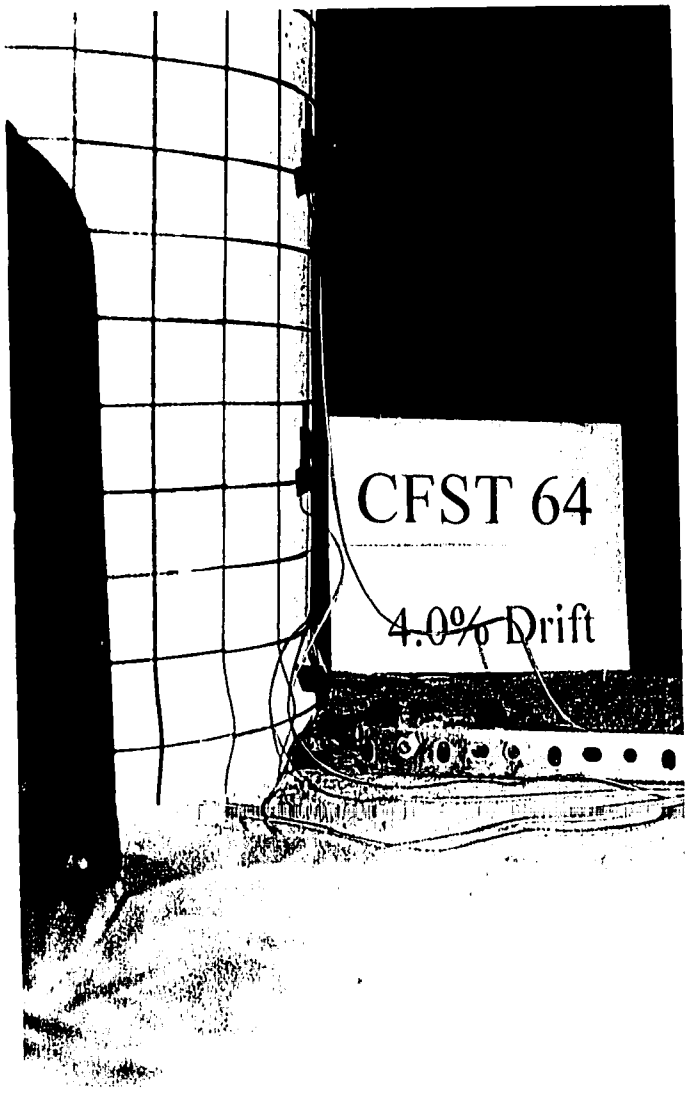

Figure 4.6a: 4% drift in east direction - CFST 64

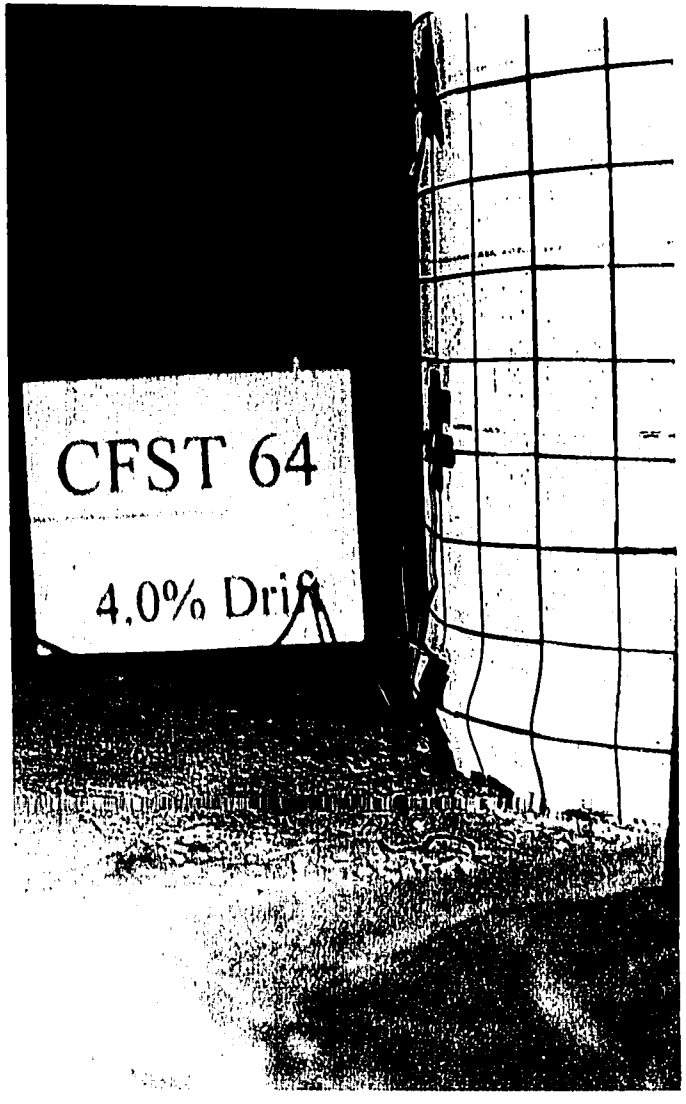

Figure 4.6b: 4% drift in west direction - CFST 64

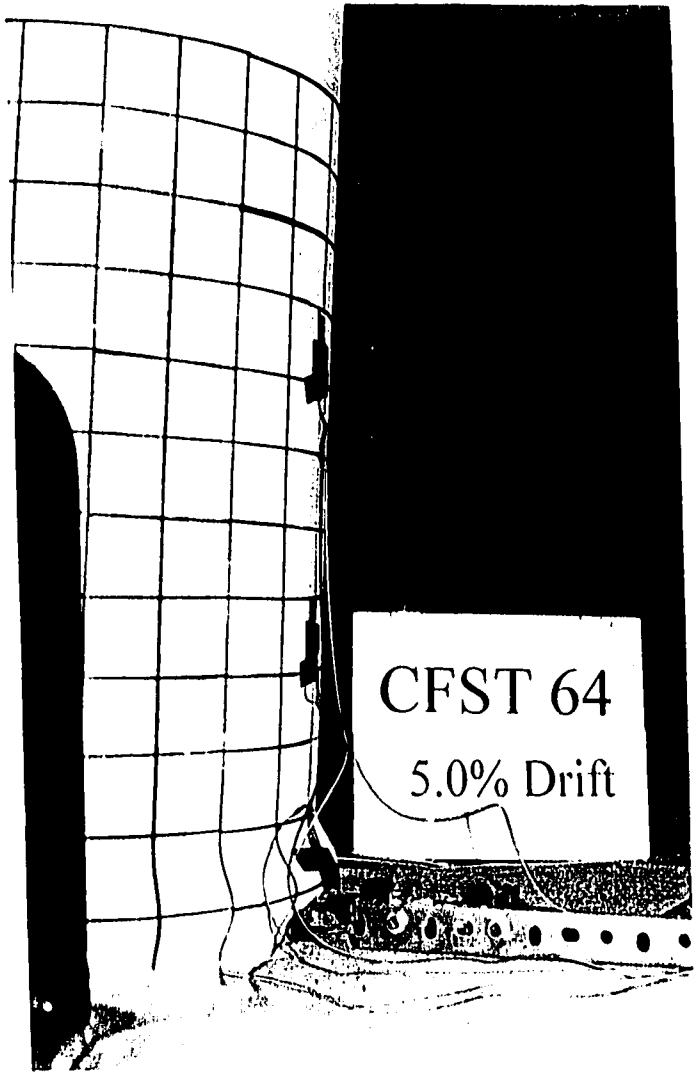

Figure 4.7a: 5% drift in east direction - CFST 64

Figure 4.7b: 5% drift west direction - CFST 64

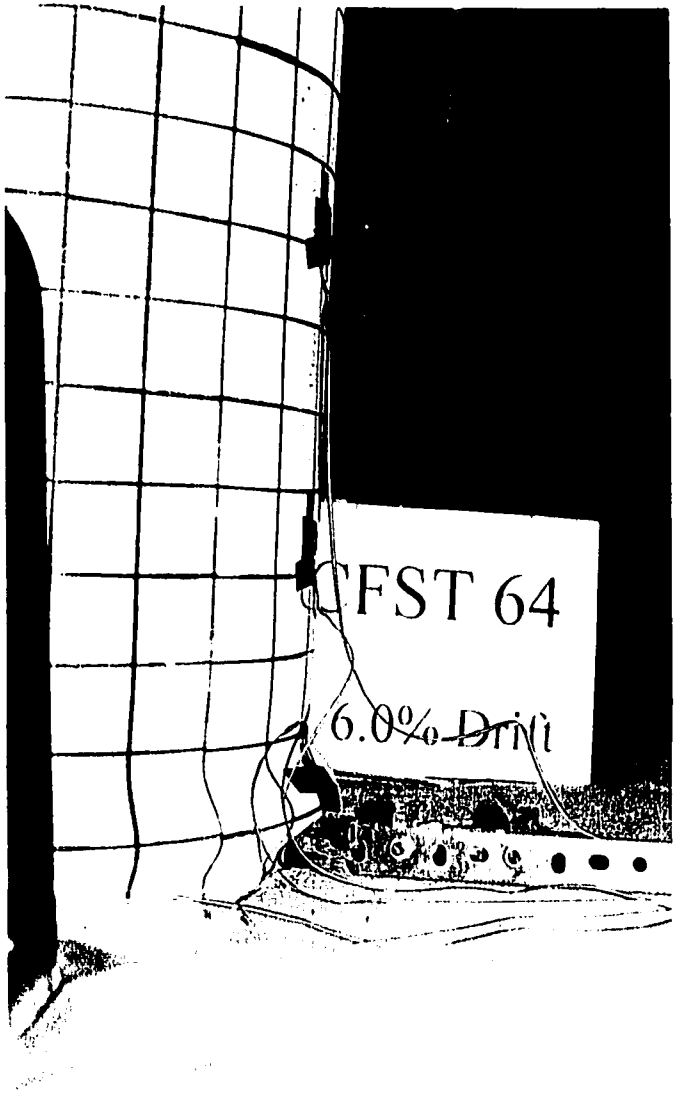

Figure 4.8a: 6% drift in east direction - CFST 64

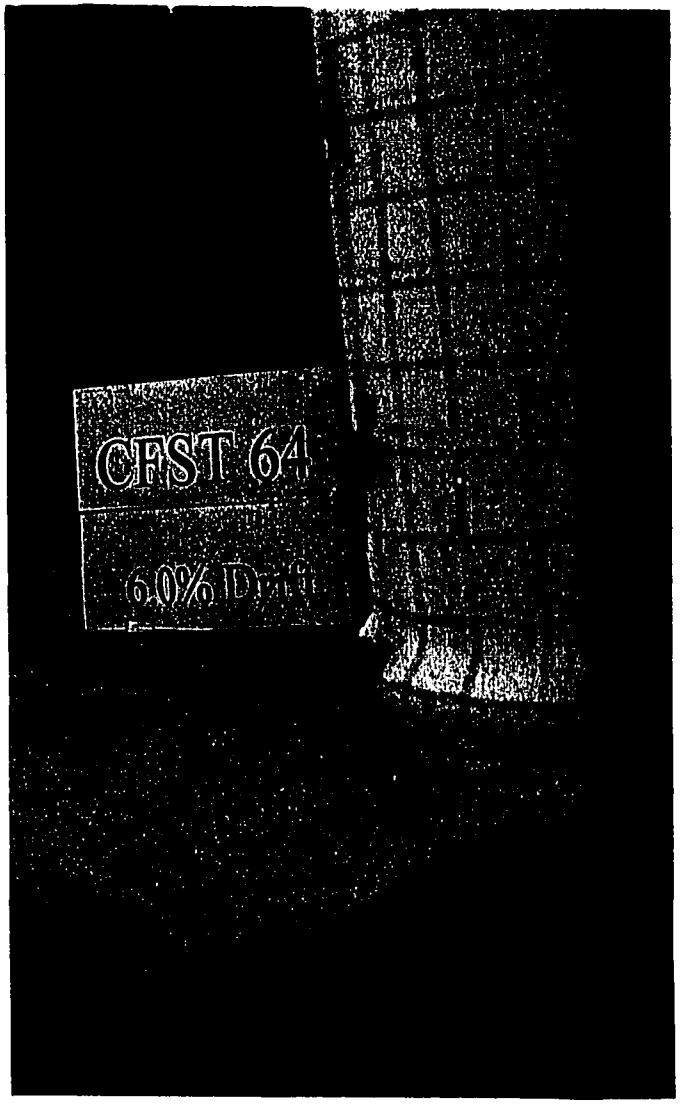

Figure 4.8b: 6% drift in west direction - CFST 64

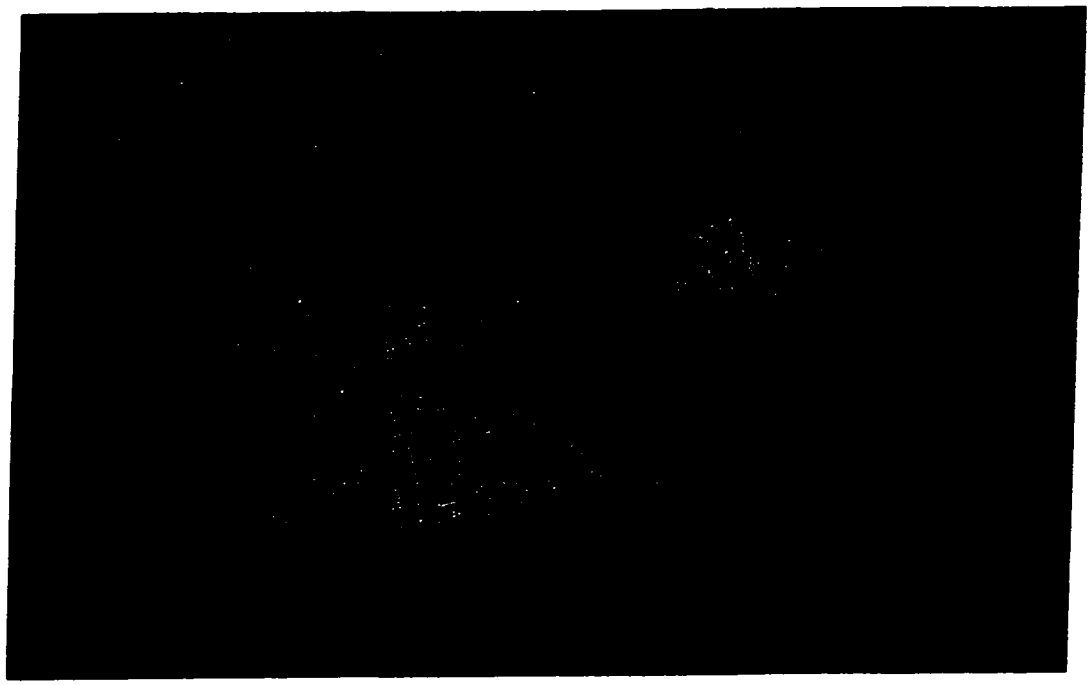

Figure 4.9a: Side view of failure surface in east direction - CFST 64

Figure 4.9b: Side view of failure surface in west direction - CFST 64

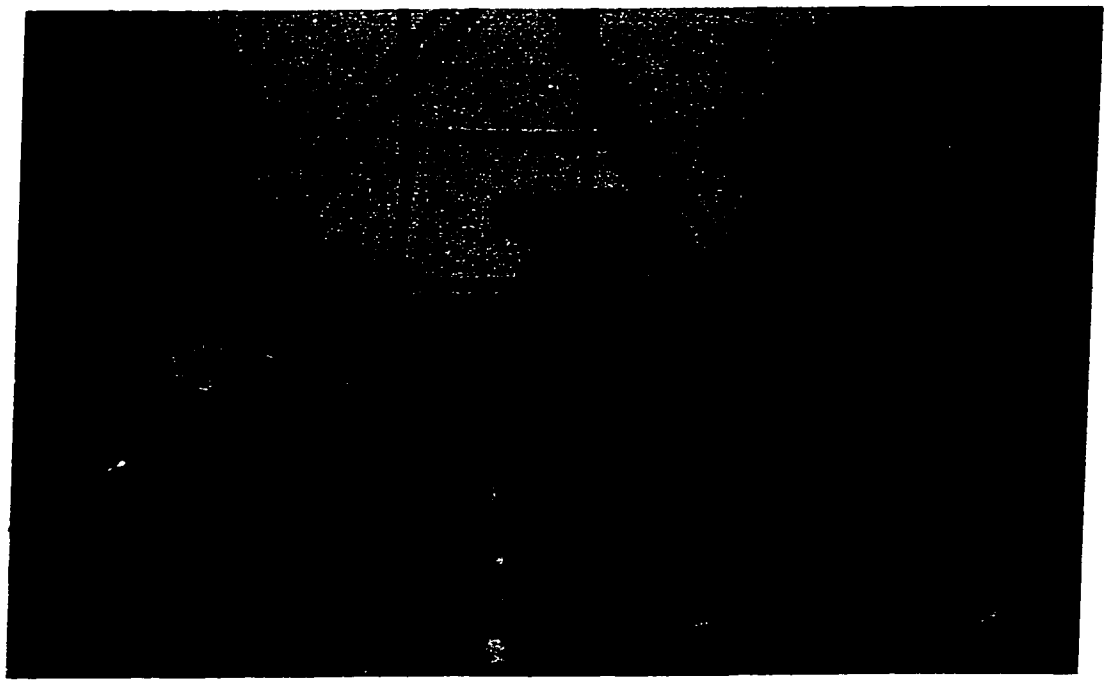

Figure 4.10a: Front view of failure surface in east direction - CFST 64

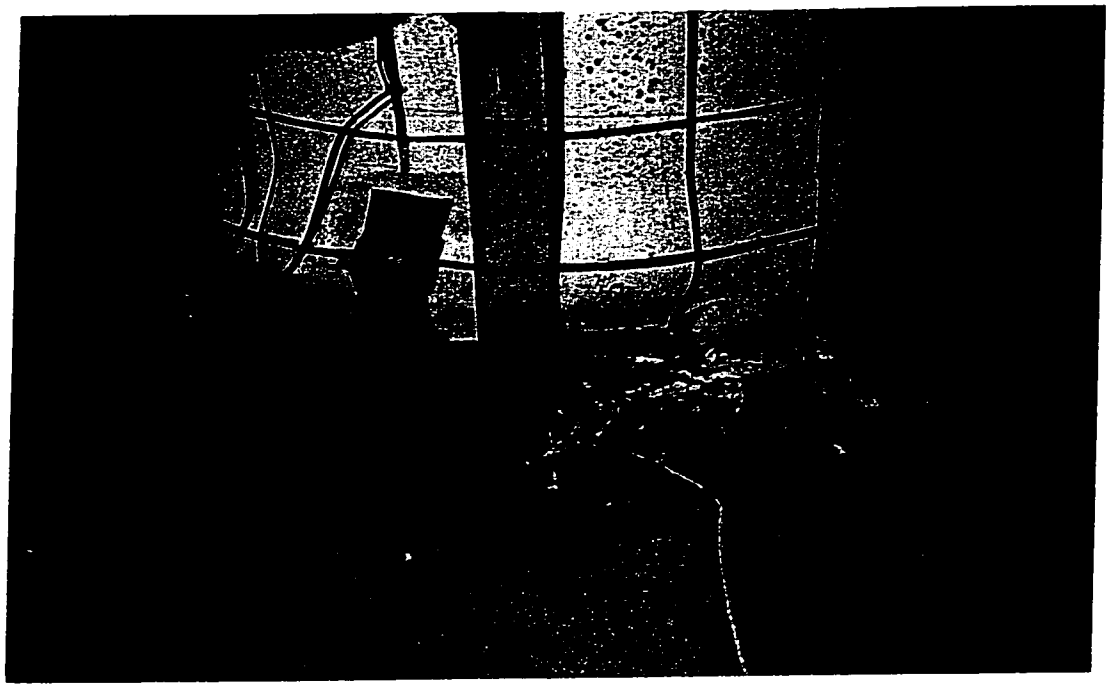

Figure 4.10b: Front view of failure surface in west direction - CFST 64

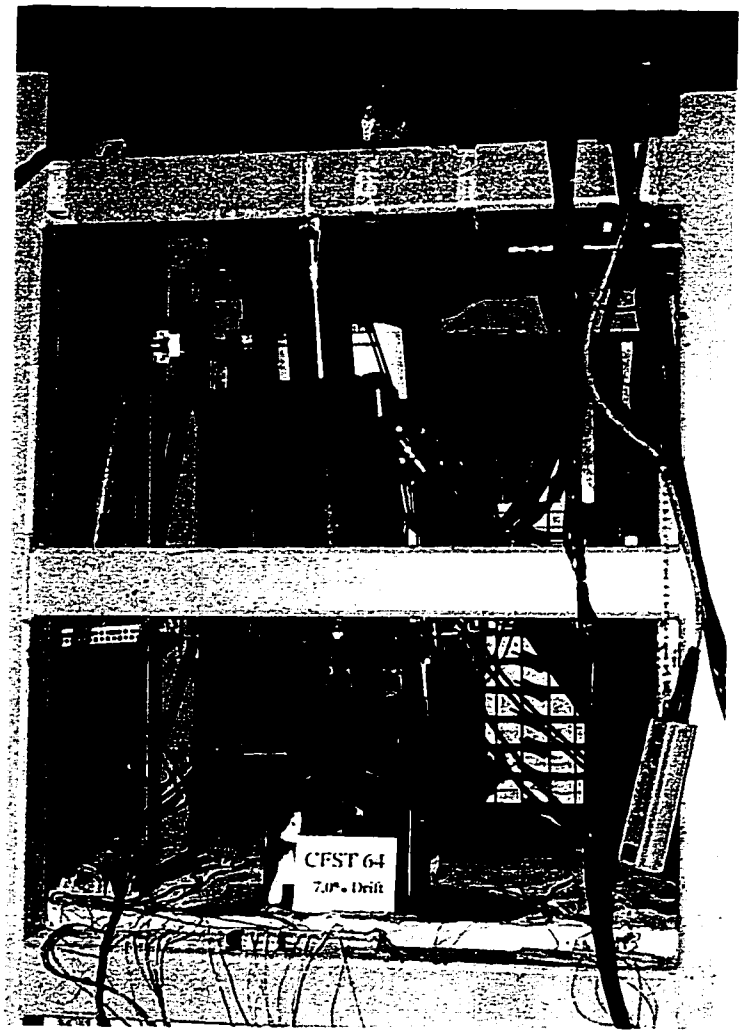

Figure 4.11: Global view of 7% drift - CFST 64

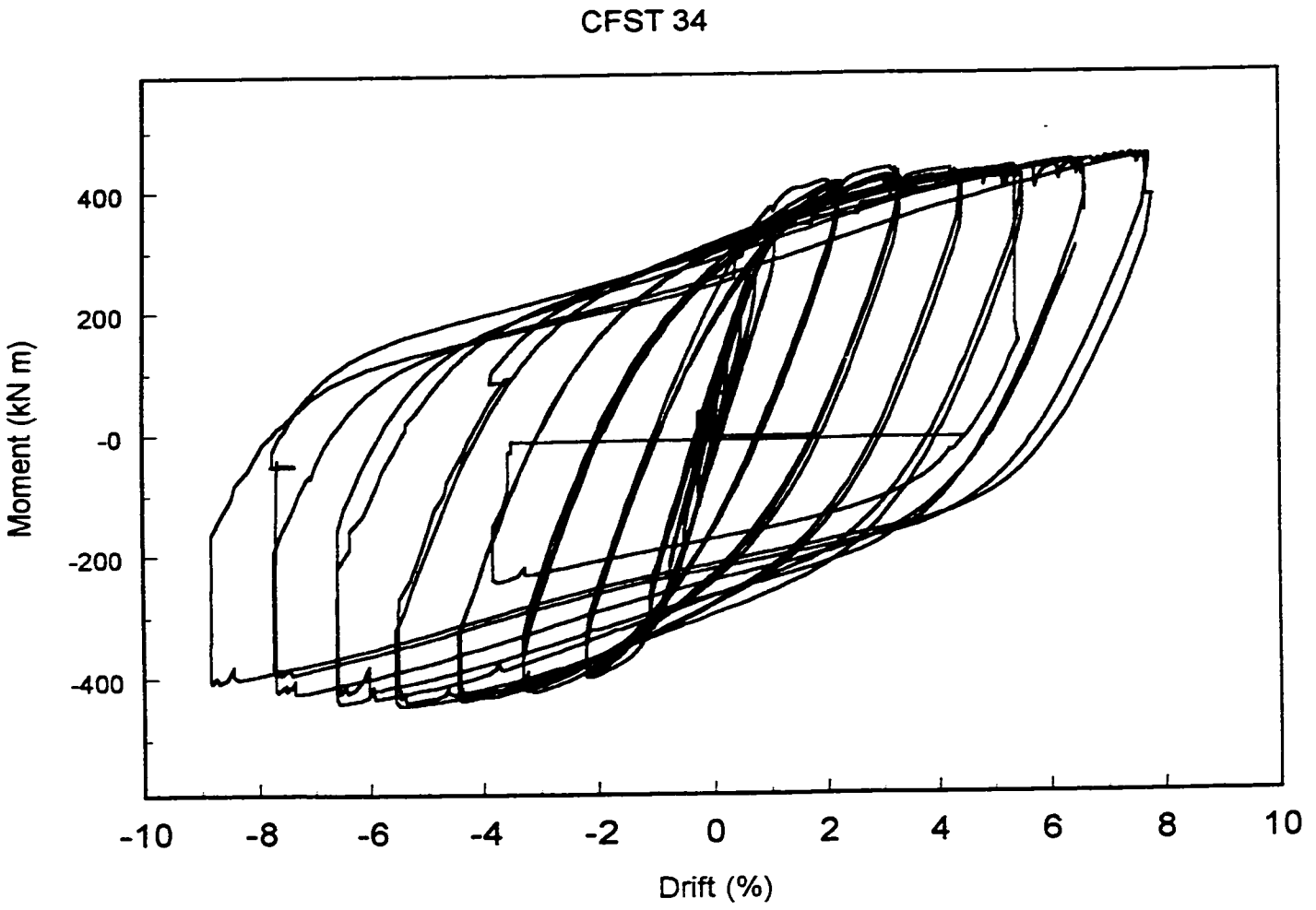

Figure 4.12: Base moment versus drift for CFST 34

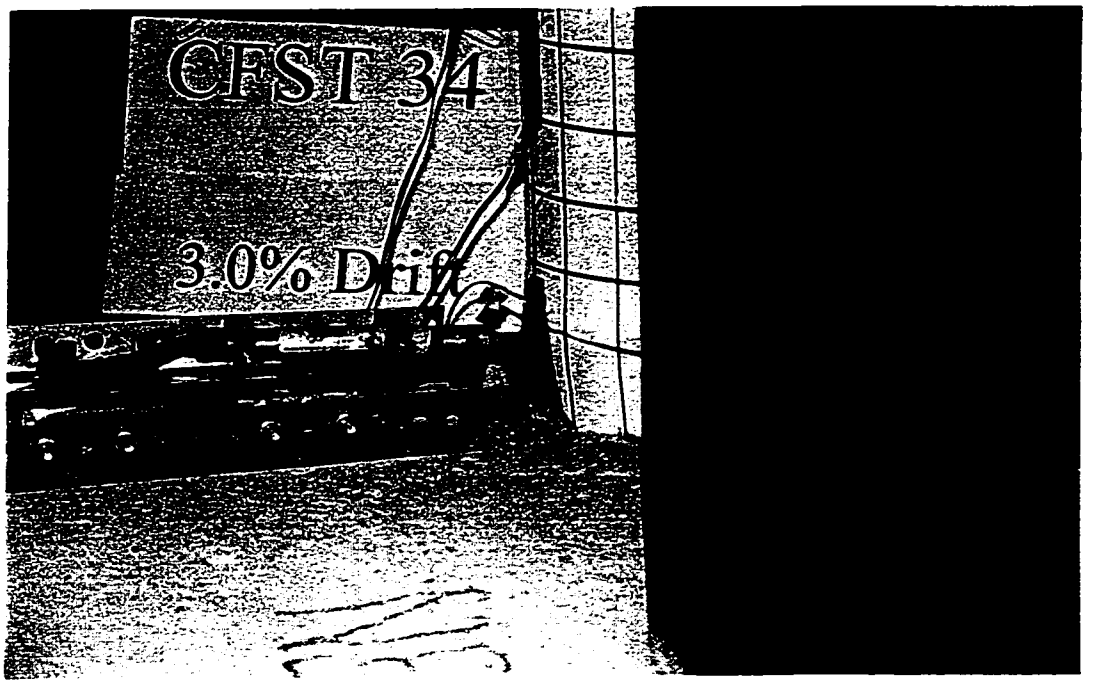

Figure 4.13a: 3% drift in east direction - CFST 34

Figure 4.13b: 3% drift on west side - CFST 34

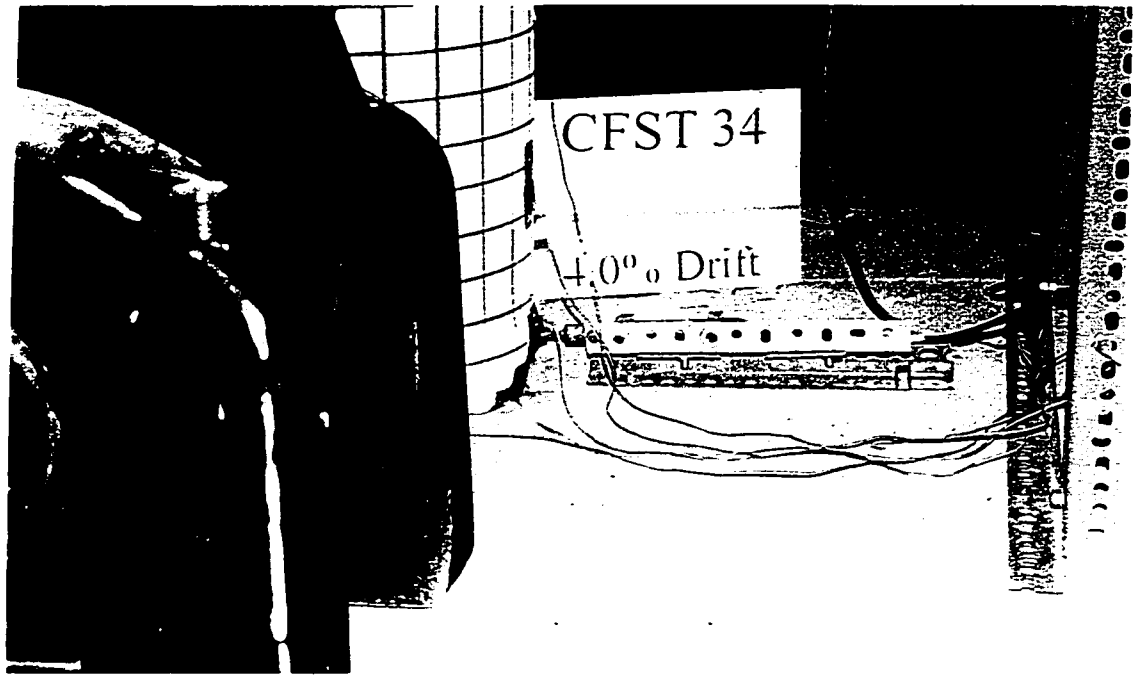

Figure 4.14a: 4% drift in east direction - CFST 34

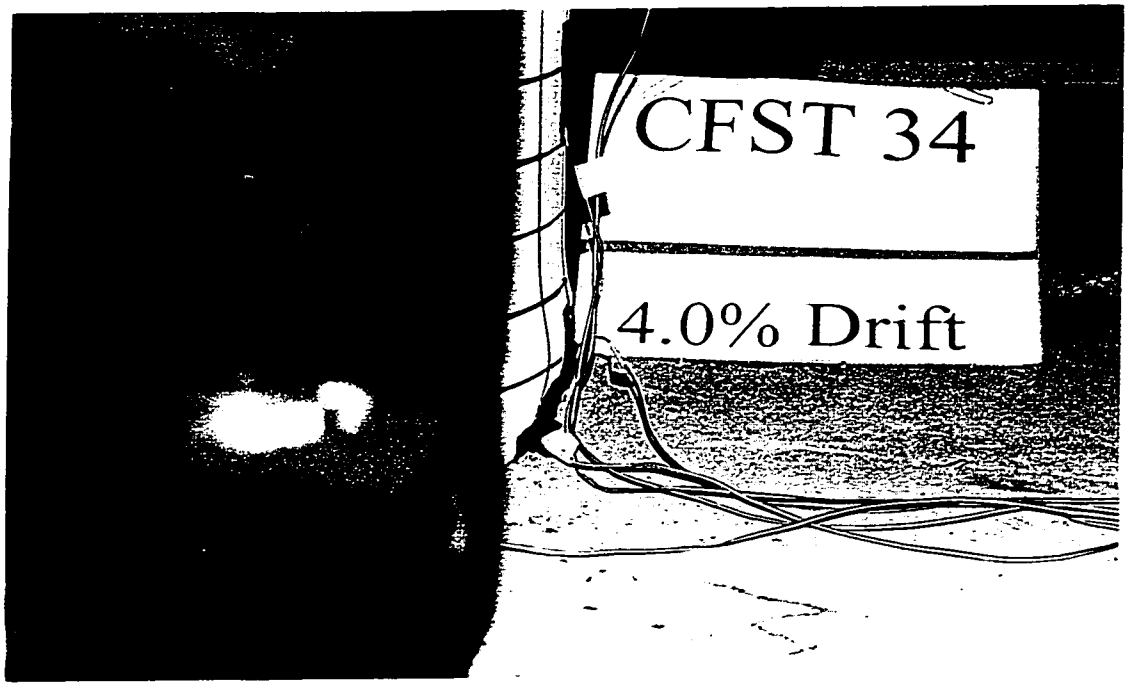

Figure 4.14b: 4% drift on west side - CFST 34

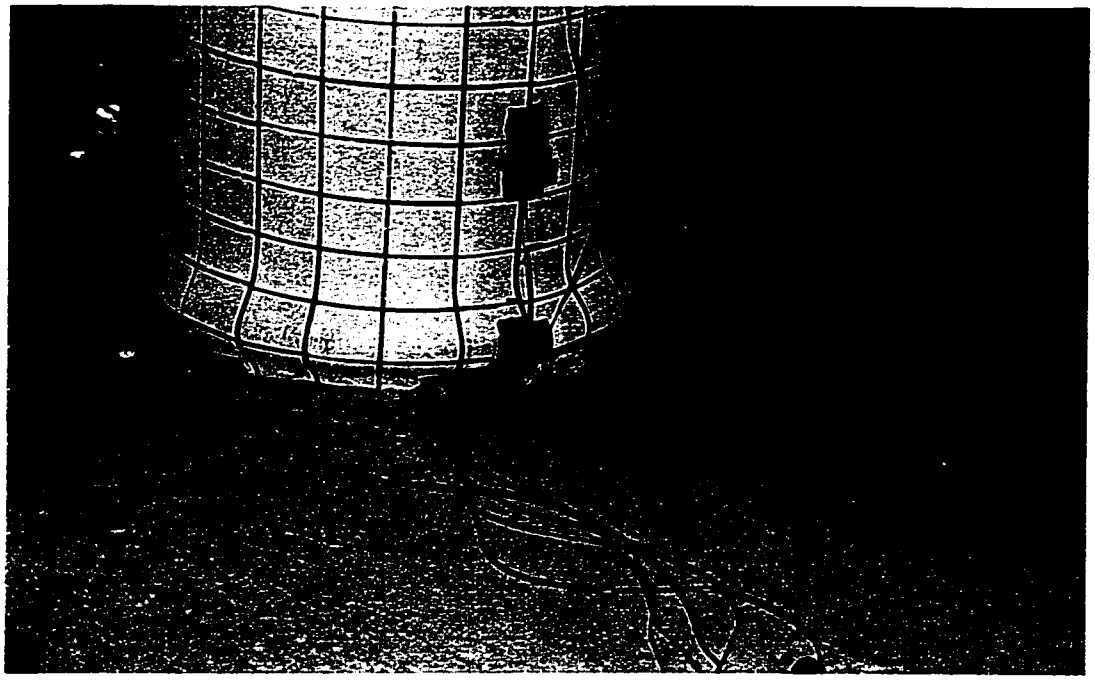

Figure 4.15: 7% drift, buckle encompassing entire column - CFST 34

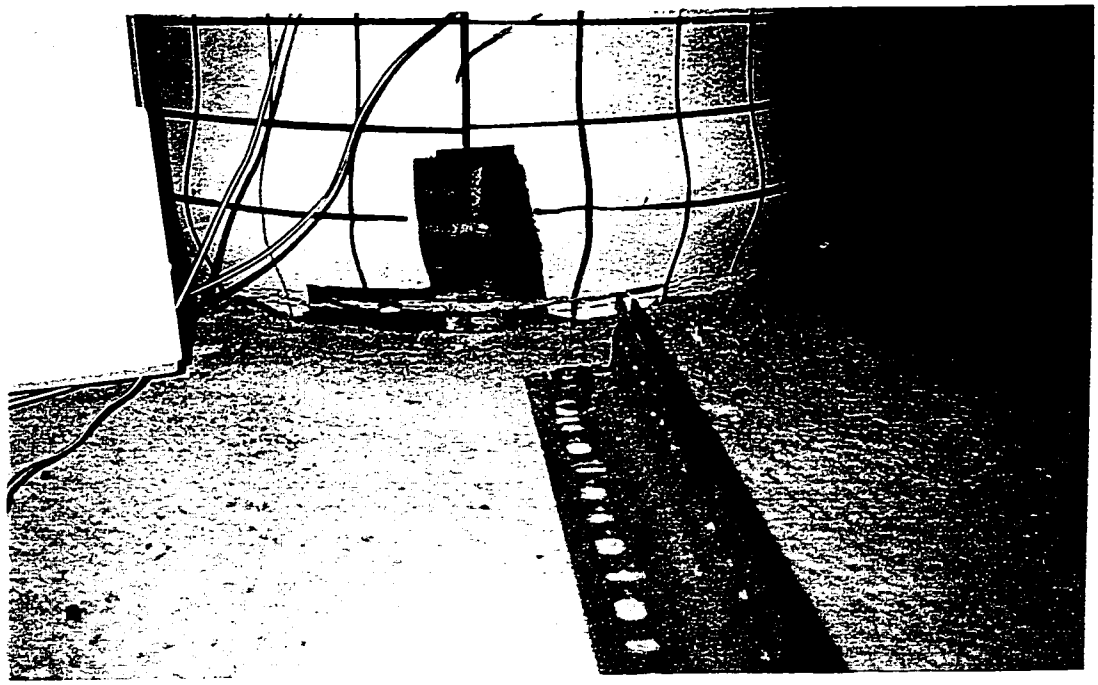

Figure 4.16a: Failure in east direction - CFST 34

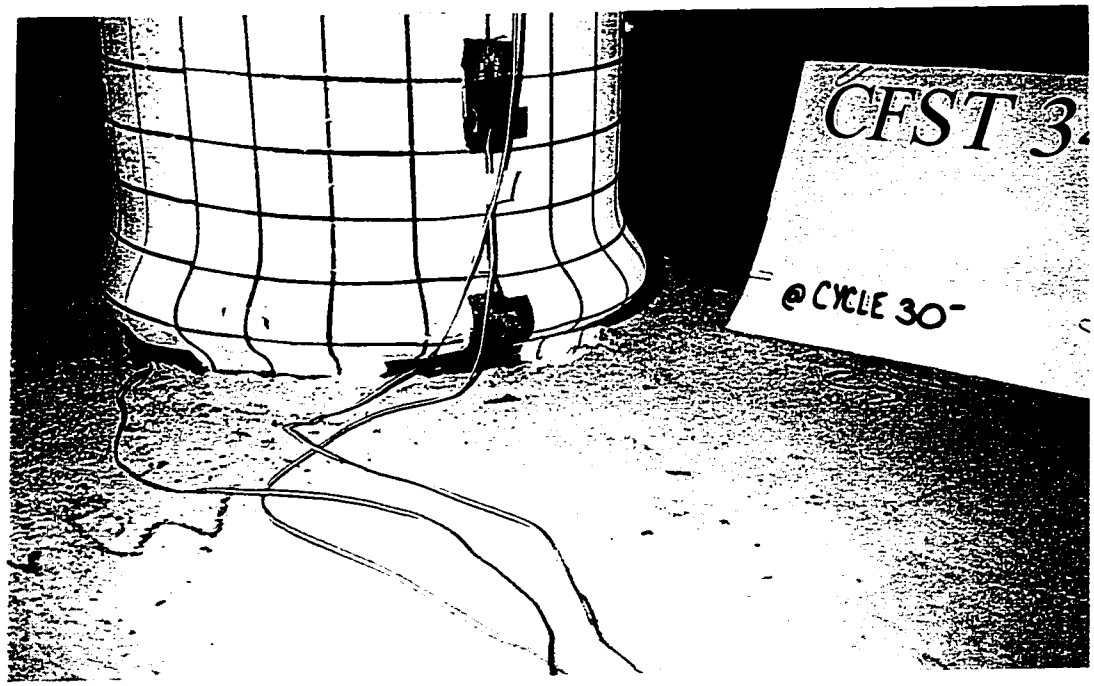

Figure 4.16b: Failure on west side - CFST 34

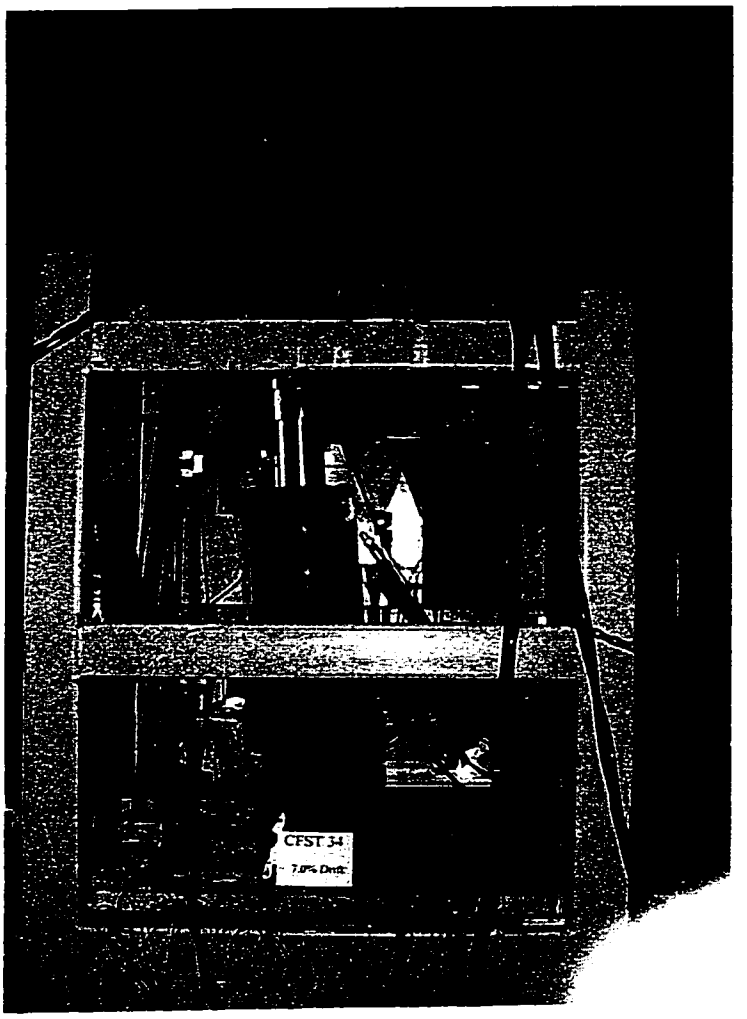

Figure 4.17: Global view of 7% drift - CFST 34

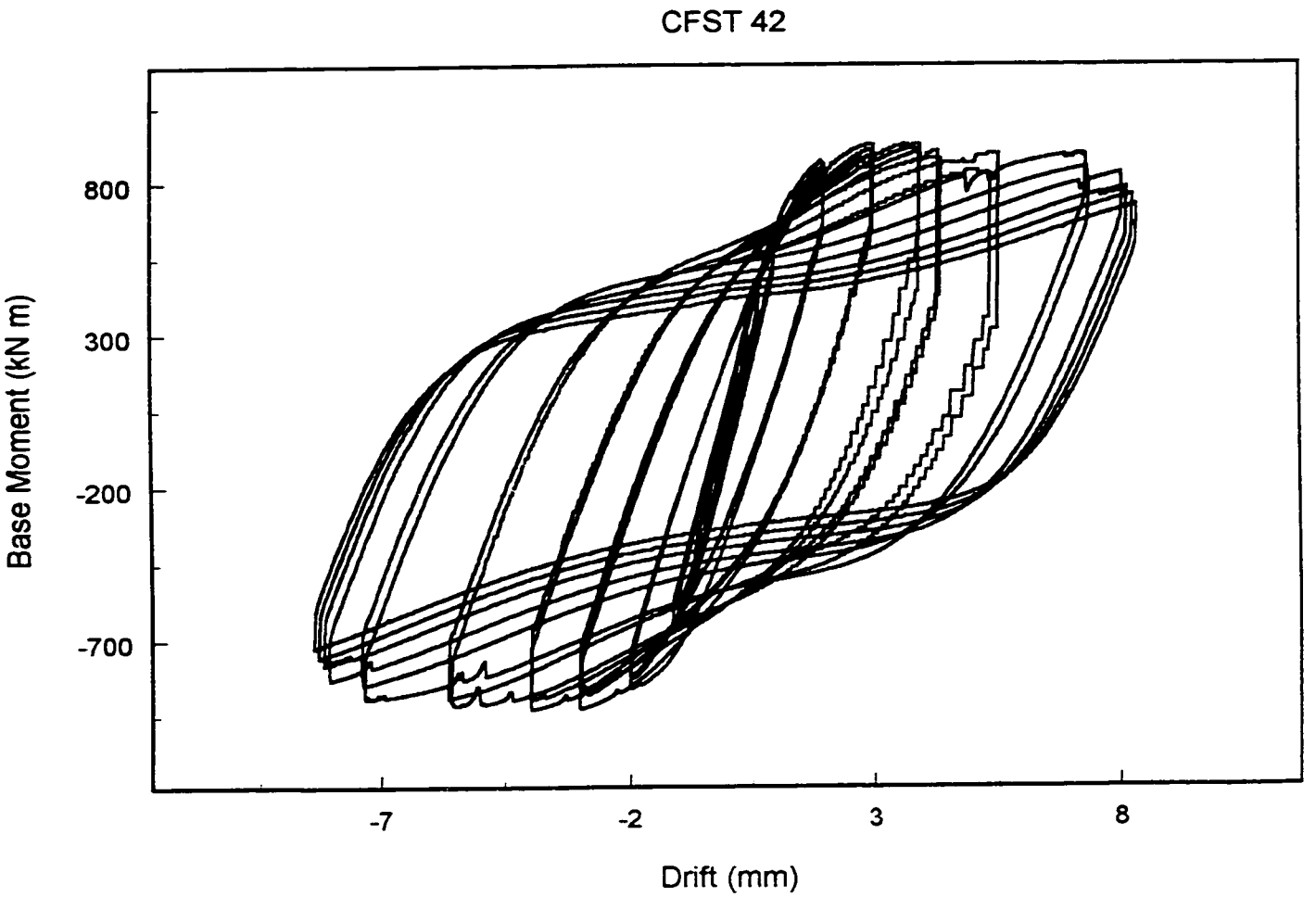

Figure 4.18: Base moment versus drift - CFST 42

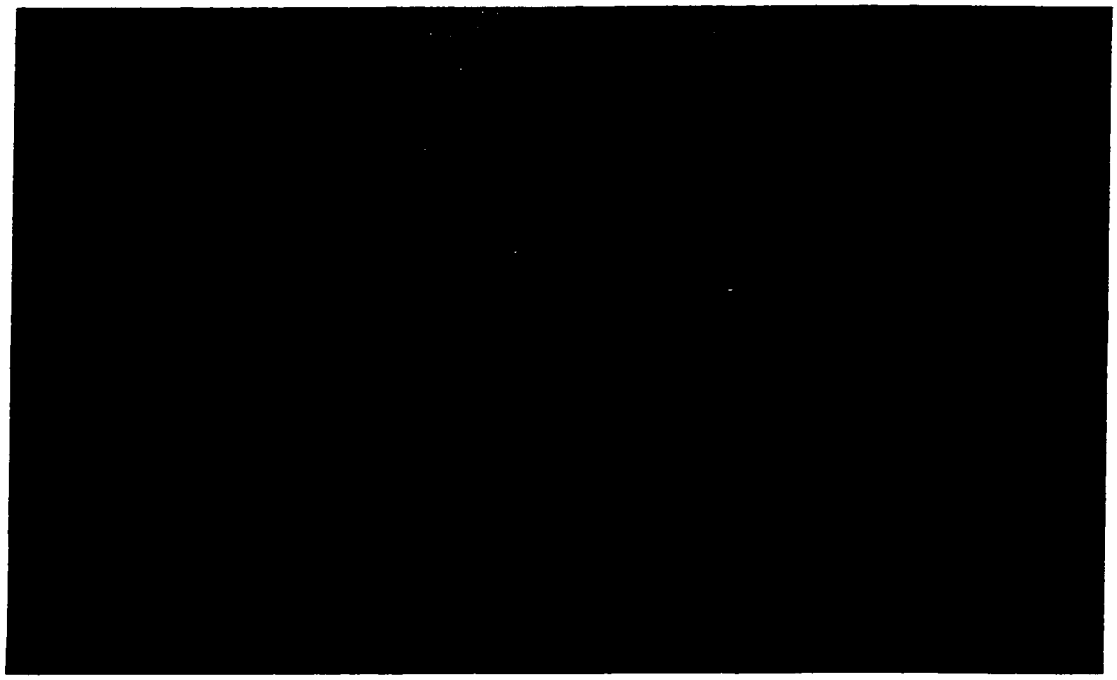

Figure 4.19: 1% drift in east direction - CFST 42

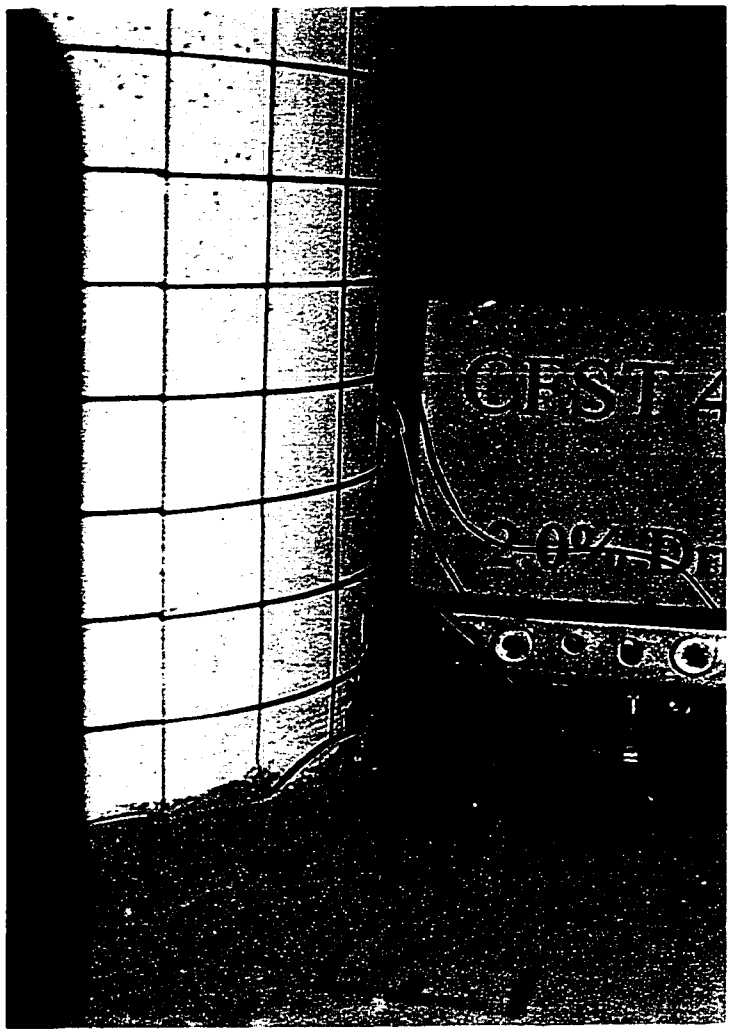

Figure 4.20: 2% drift on east side - CFST 42

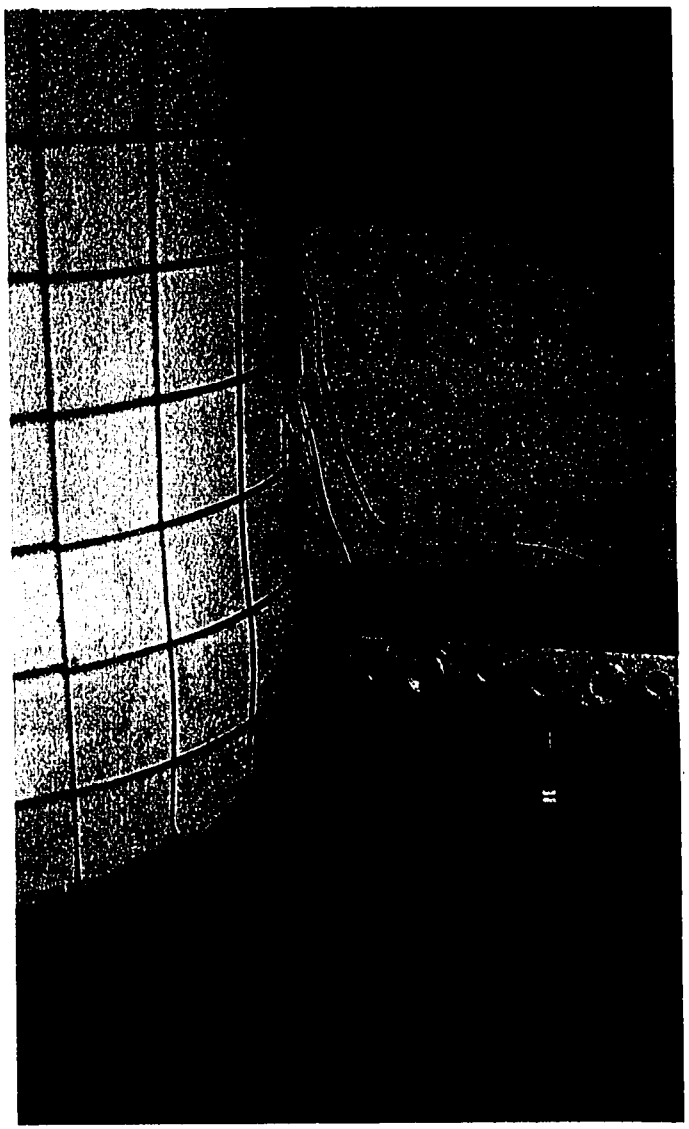

Figure 4.21a: 3% drift in east direction - CFST 42

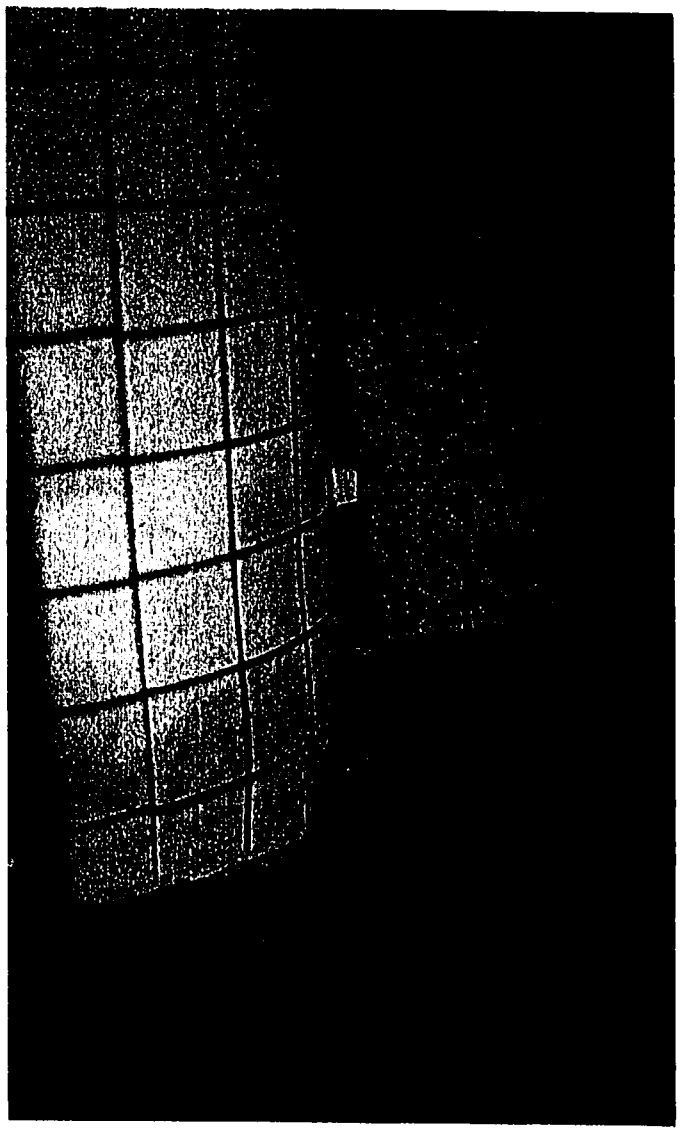

Figure 4.21b: 3% drift in west side - CFST 42

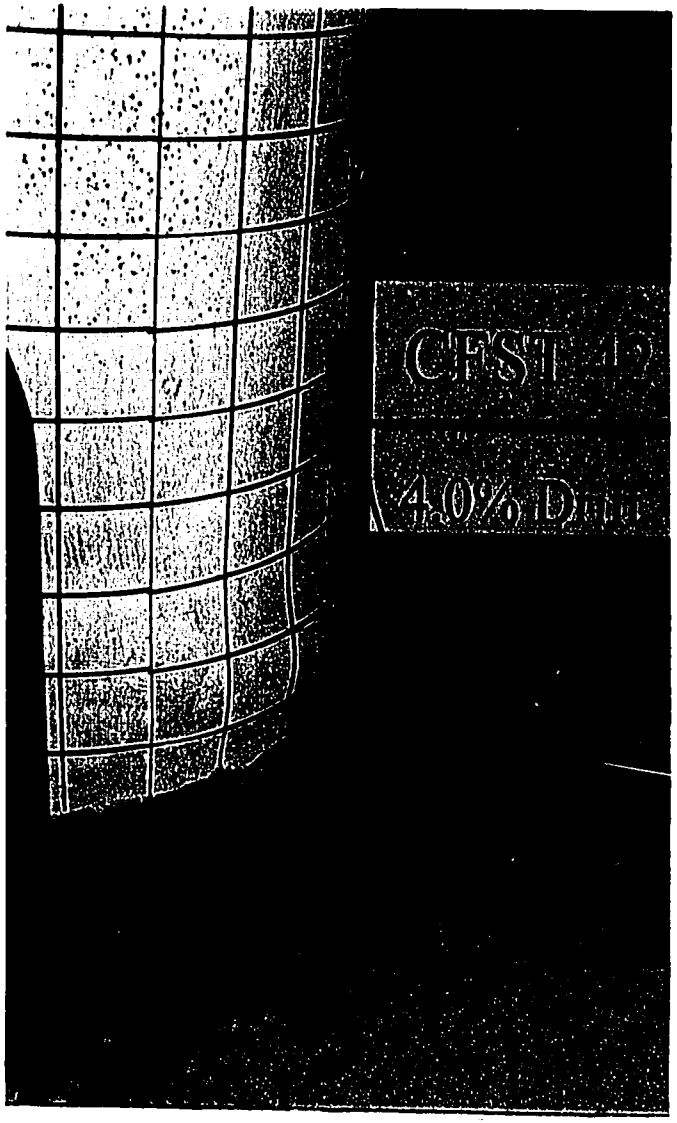

Figure 4.22a: 4% drift in east direction - CFST 42

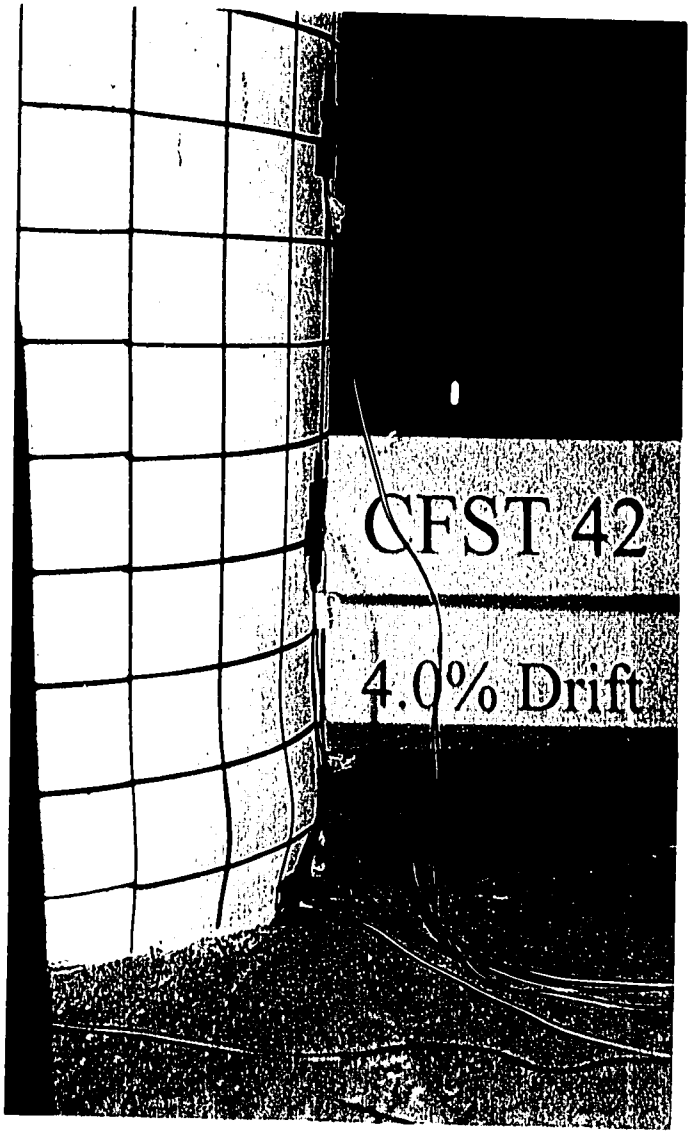

Figure 4.22b: 4% drift on west side - CFST 42

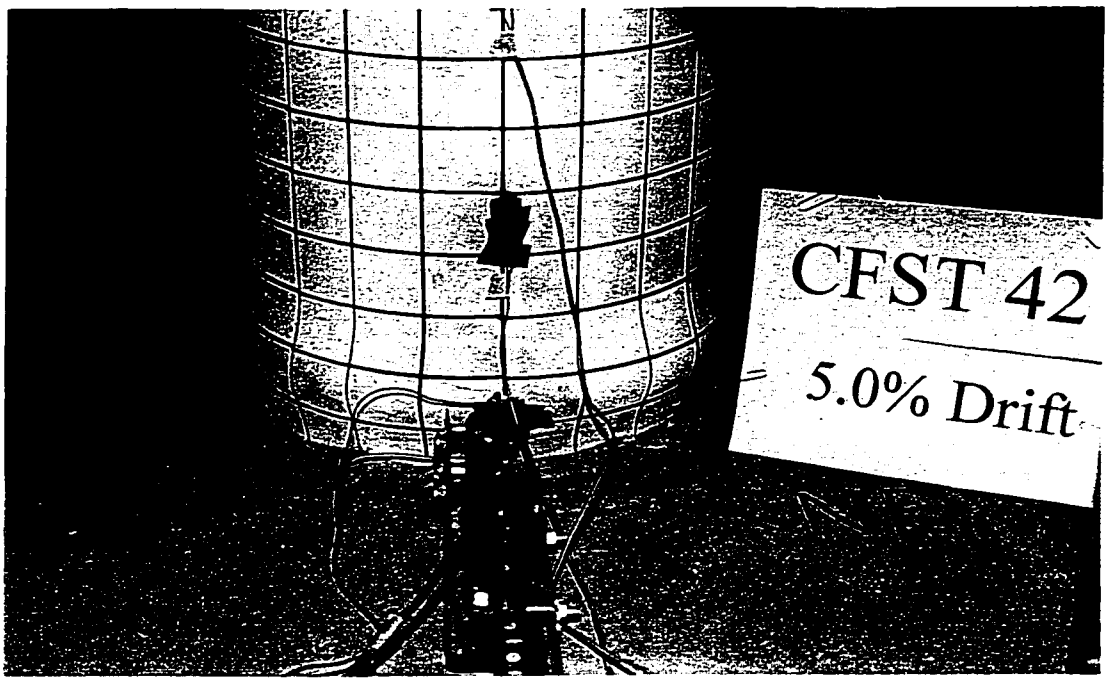

Figure 4.23: 5% drift buckle encompassing entire column - CFST 42

Figure 4.24a: 6% drift in east direction - CFST 42

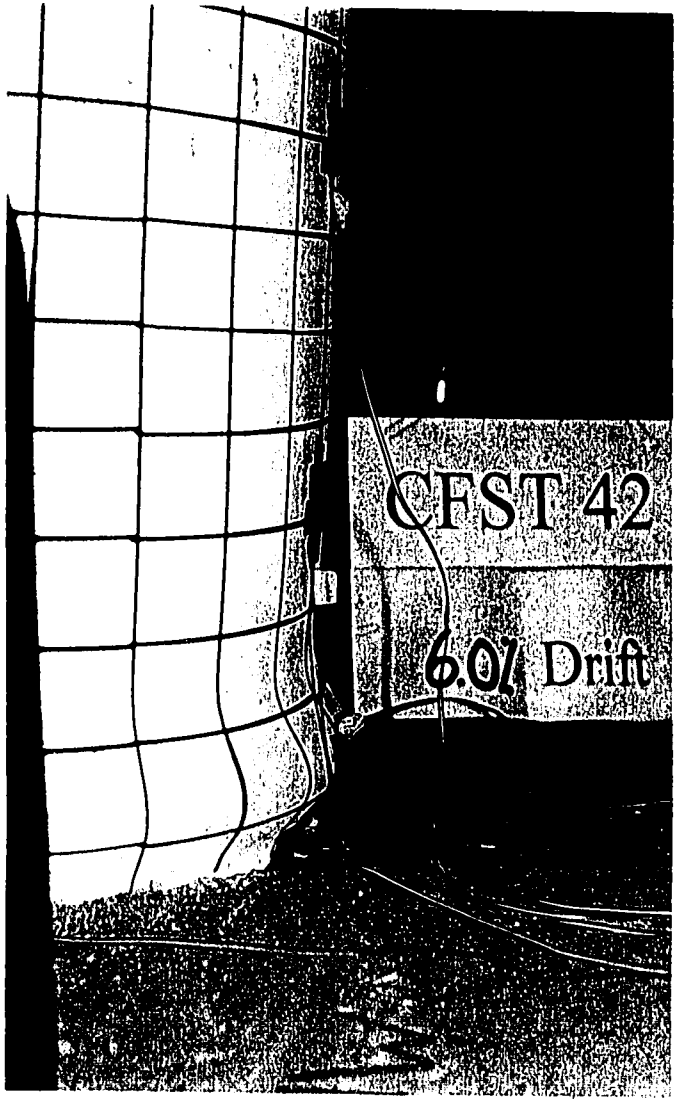

Figure 4.24b: 6% drift in west side - CFST 42

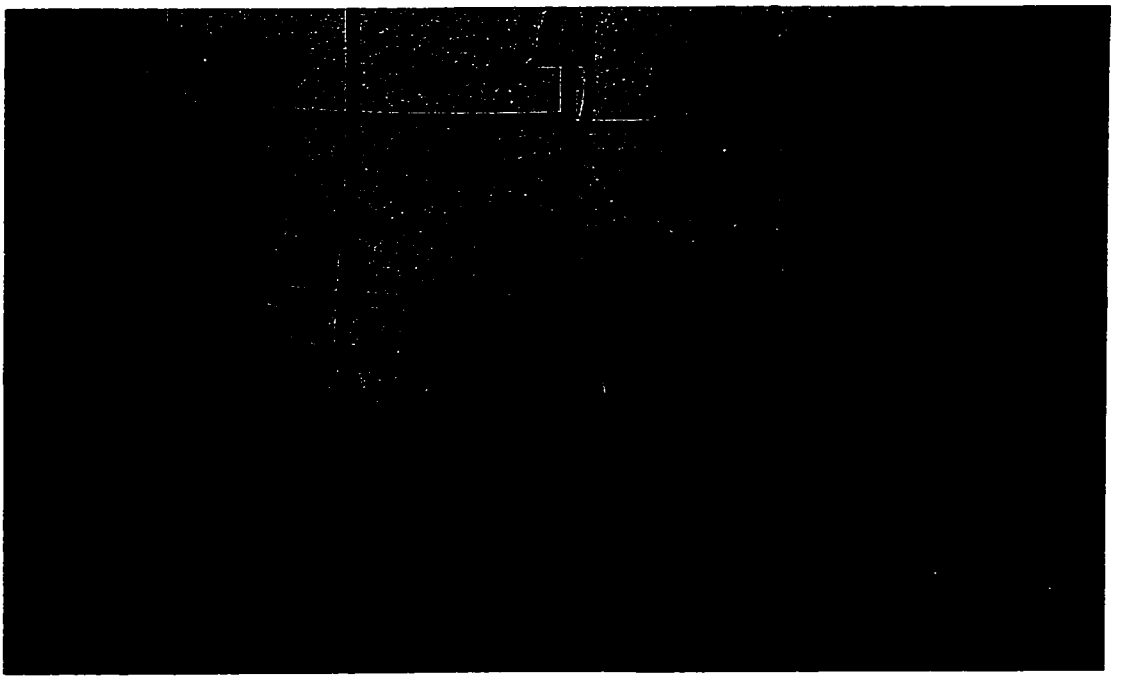

Figure 4.25a: 7% drift in east direction - CFST 42

Figure 4.25b: 7% drift on west side - CFST 42

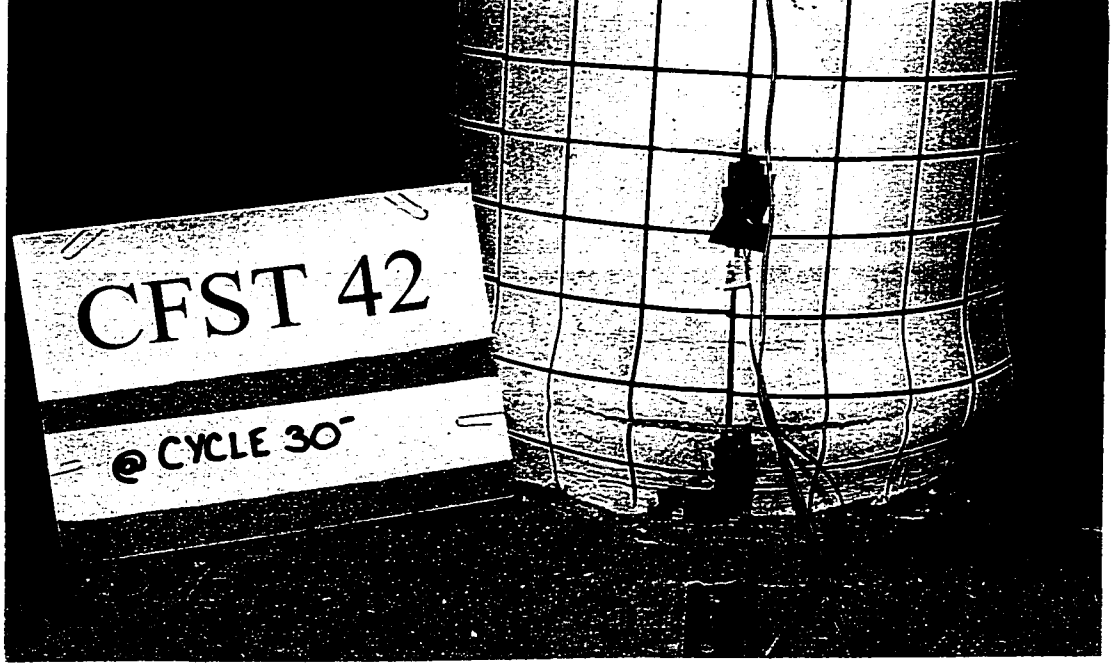

Figure 4.26a: Failure in east direction - CFST 42

Figure 4.26b: Failure on west side - CFST 42

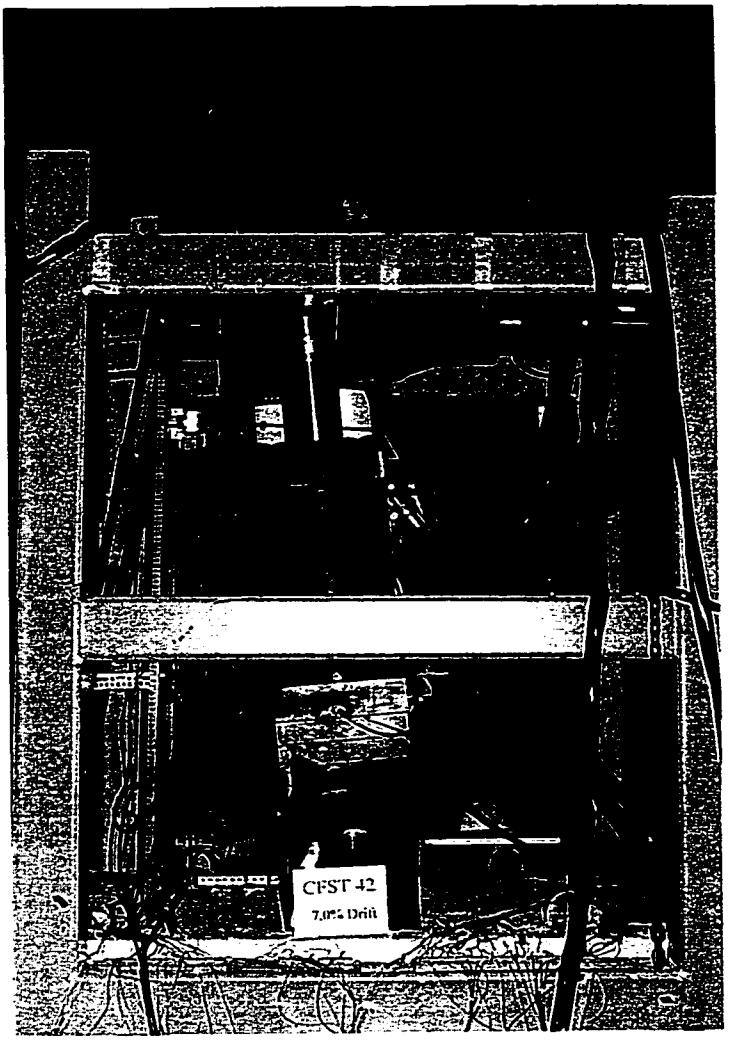

Figure 4.27: Global view of 7% drift - CFST 42

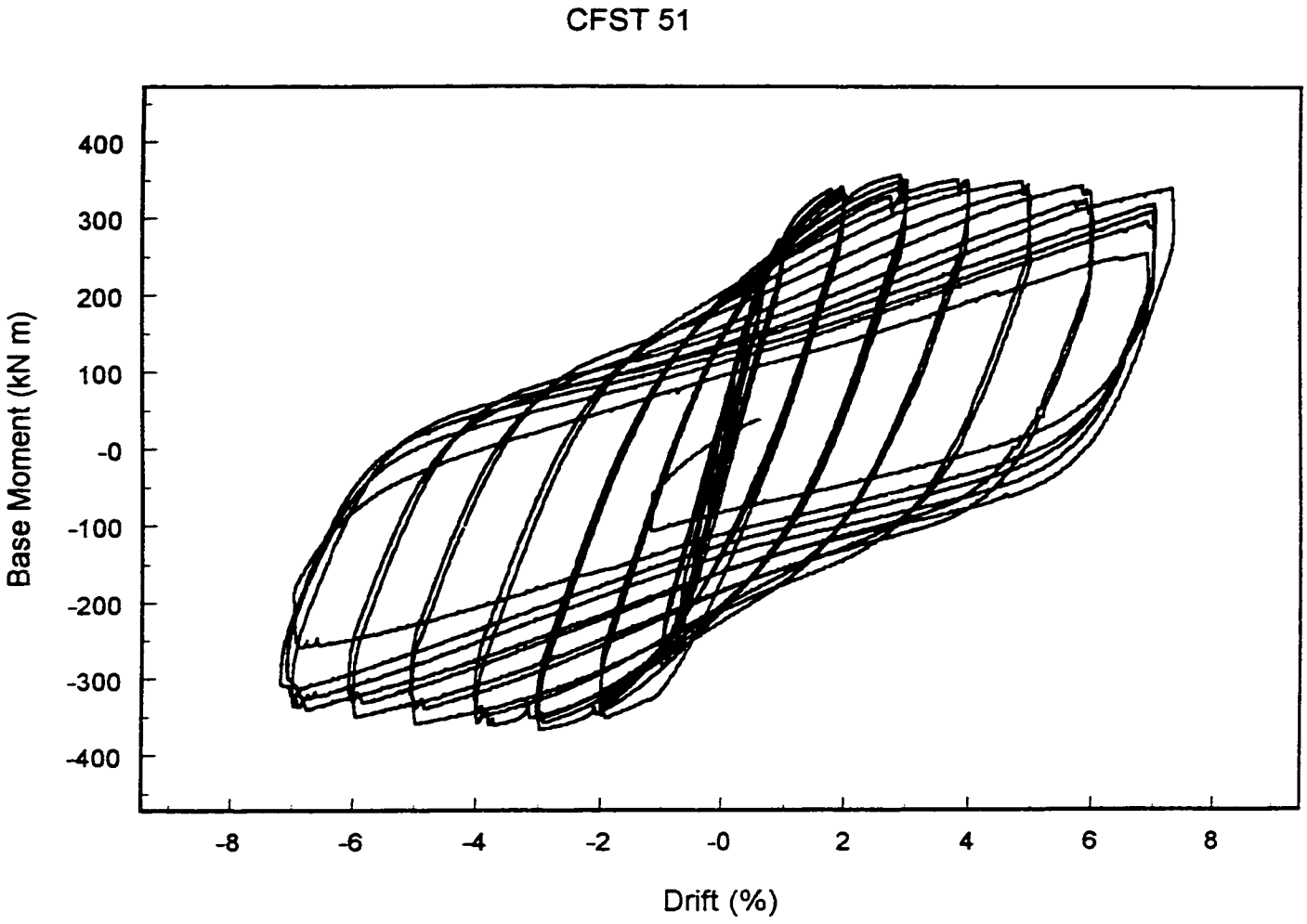

Figure 4.28: Base moment versus drift - CFST 51

Figure 4.29: 2% drift in east direction - CFST 51

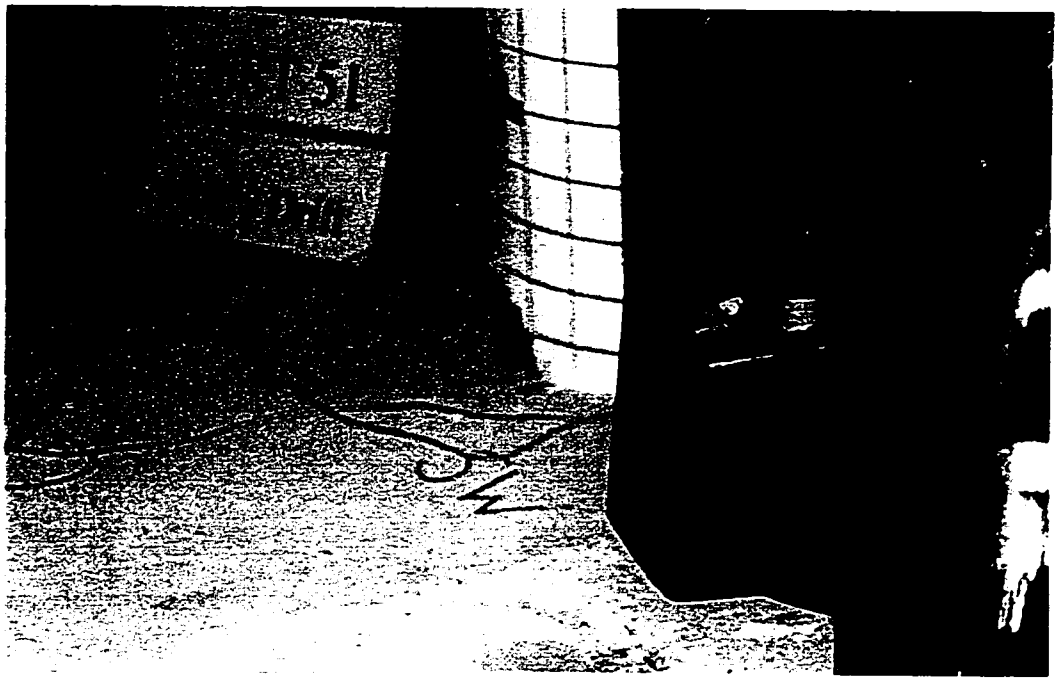

Figure 4.30a: 3% drift in east side - CFST 51

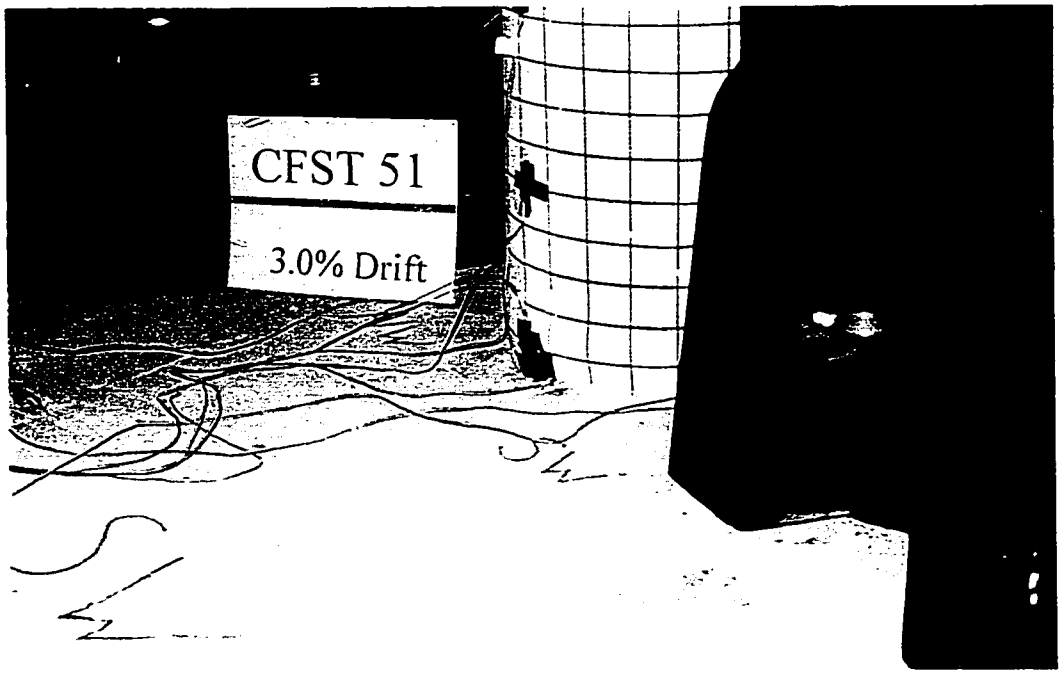

Figure 4.30b: 3% drift in west side - CFST 51

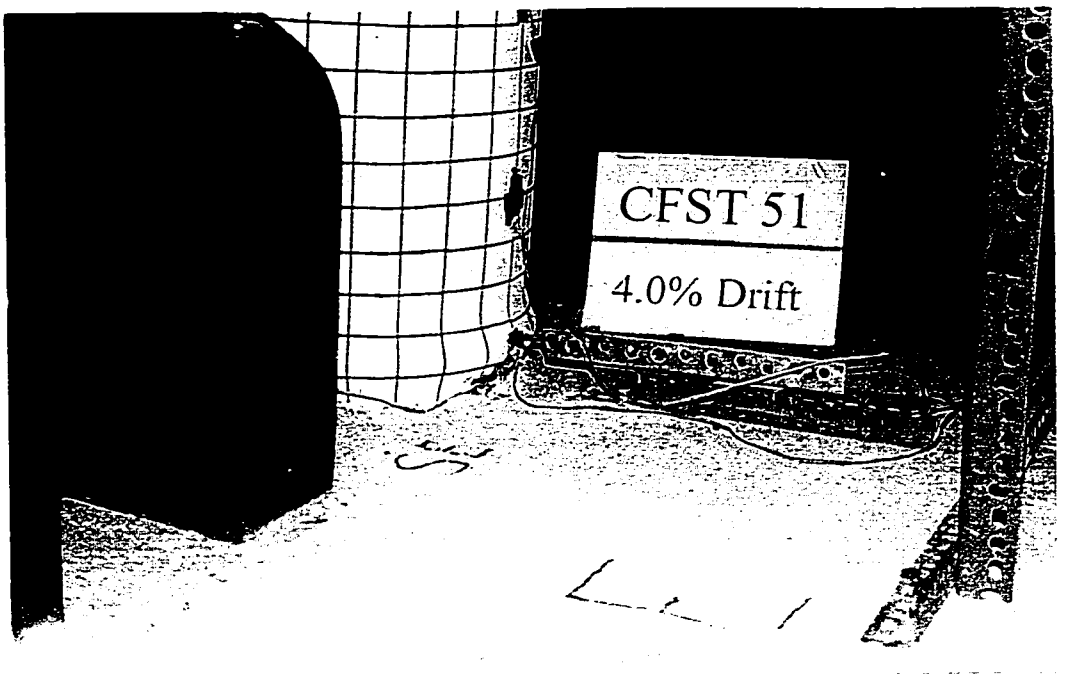

Figure 4.31a: 4% drift in east side - CFST 51

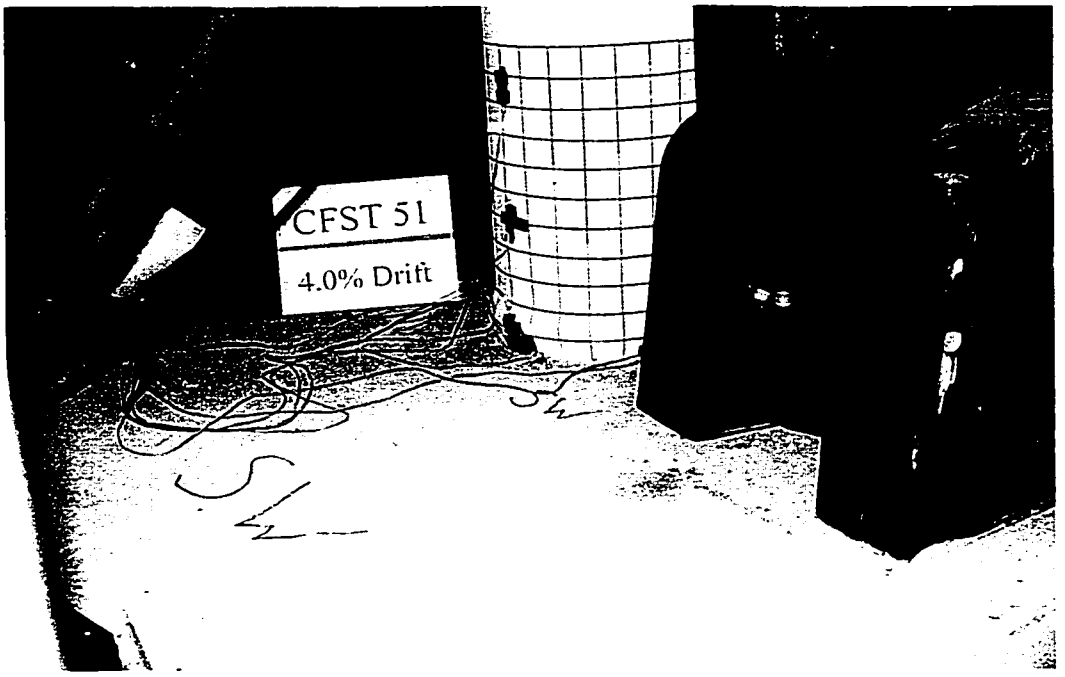

Figure 4.31b: 4% drift in west side - CFST 51

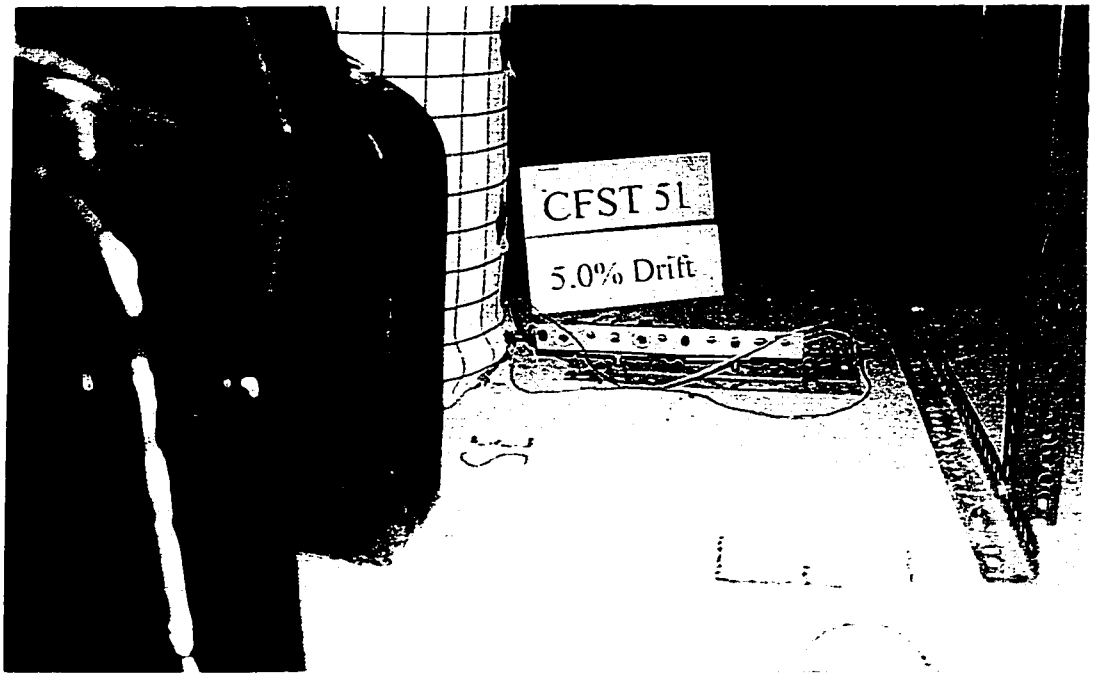

Figure 4.32a: 5% drift in east side - CFST 51

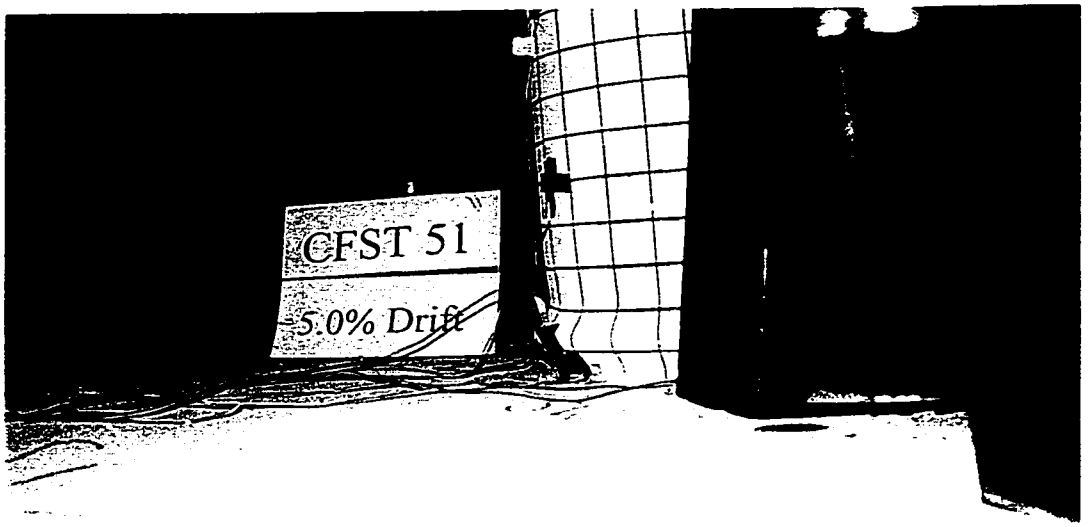

Figure 4.32b: 5% drift in west side - CFST 51

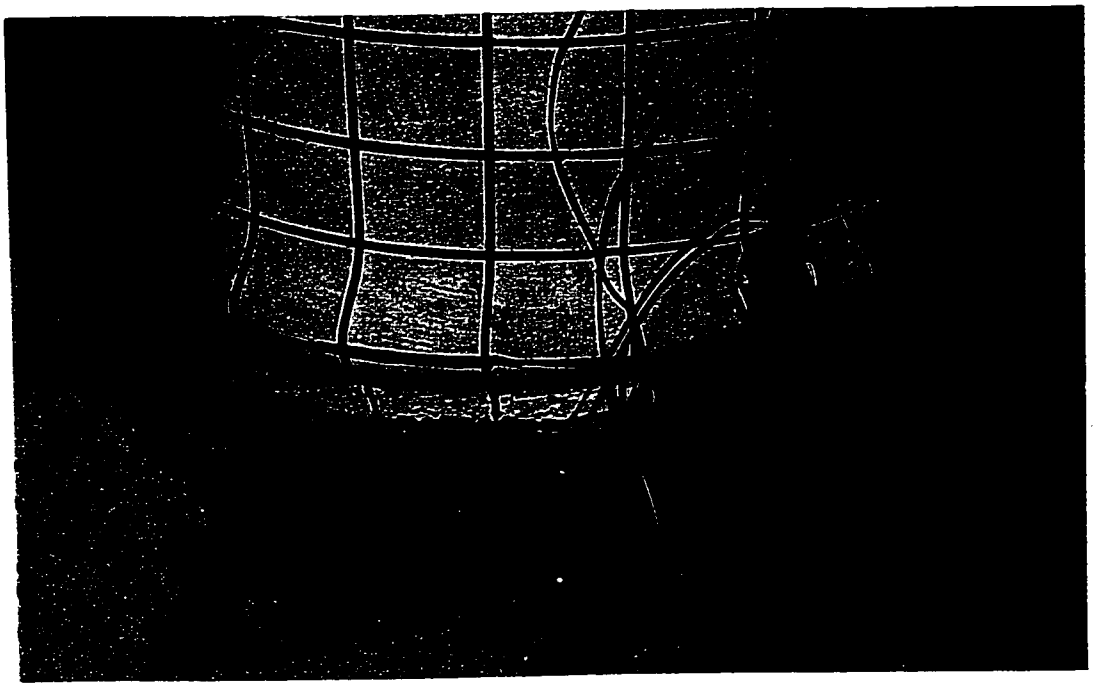

Figure 4.33a: Vertical cracks at 6% drift in west side - CFST 51

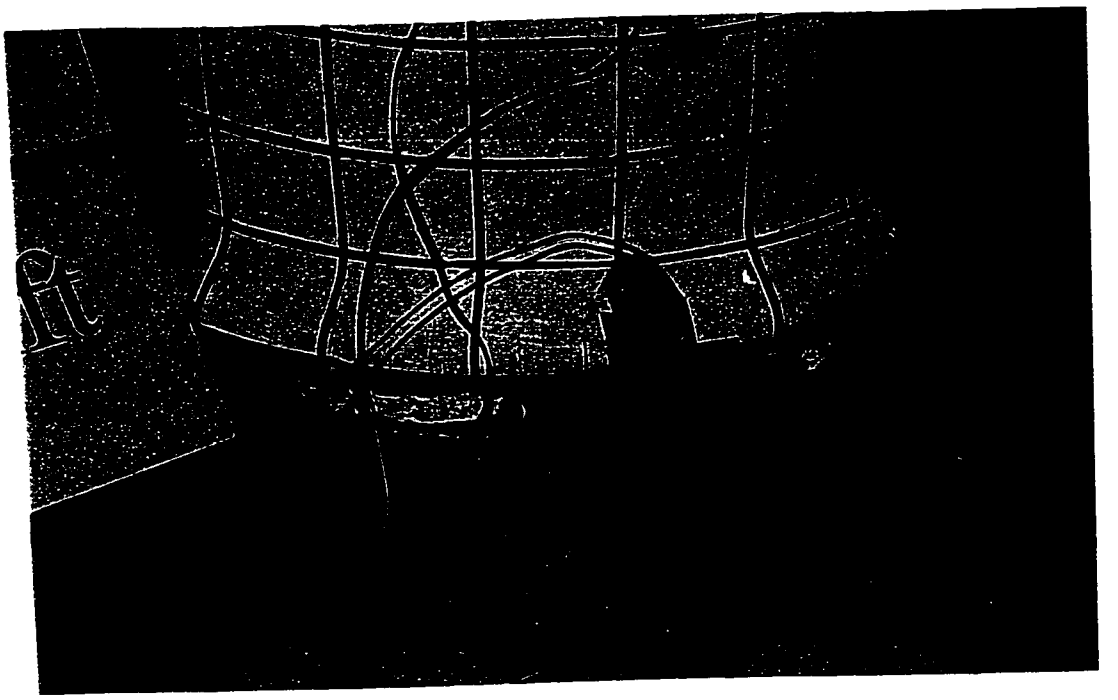

Figure 4.33b: 6% drift in west side - CFST 51

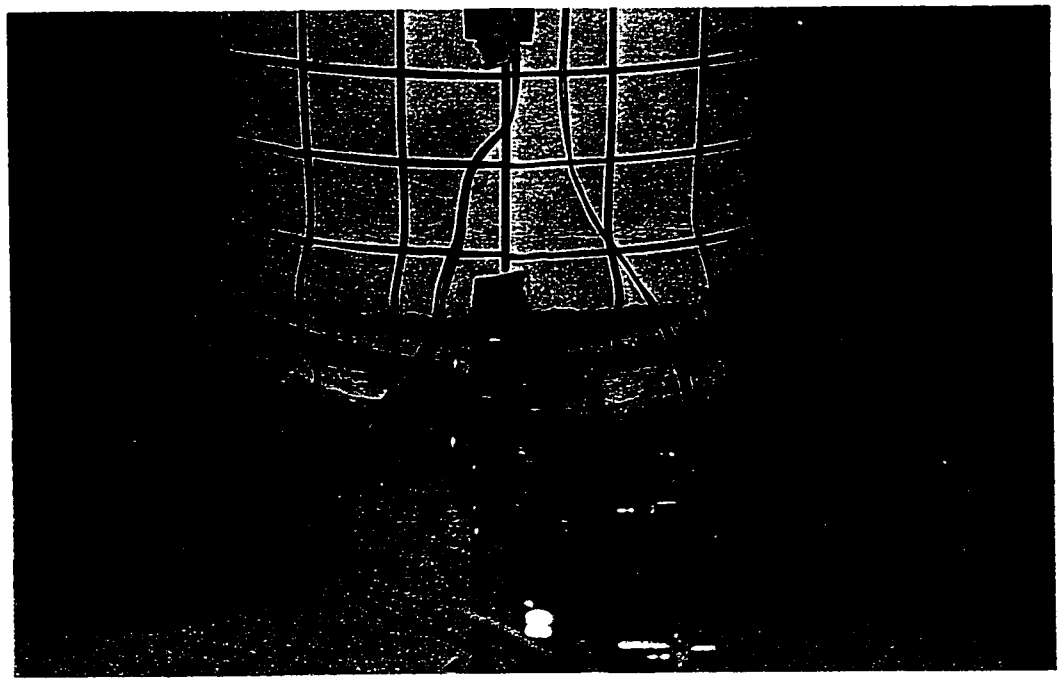

Figure 4.34a: Failure in east side - CFST 51

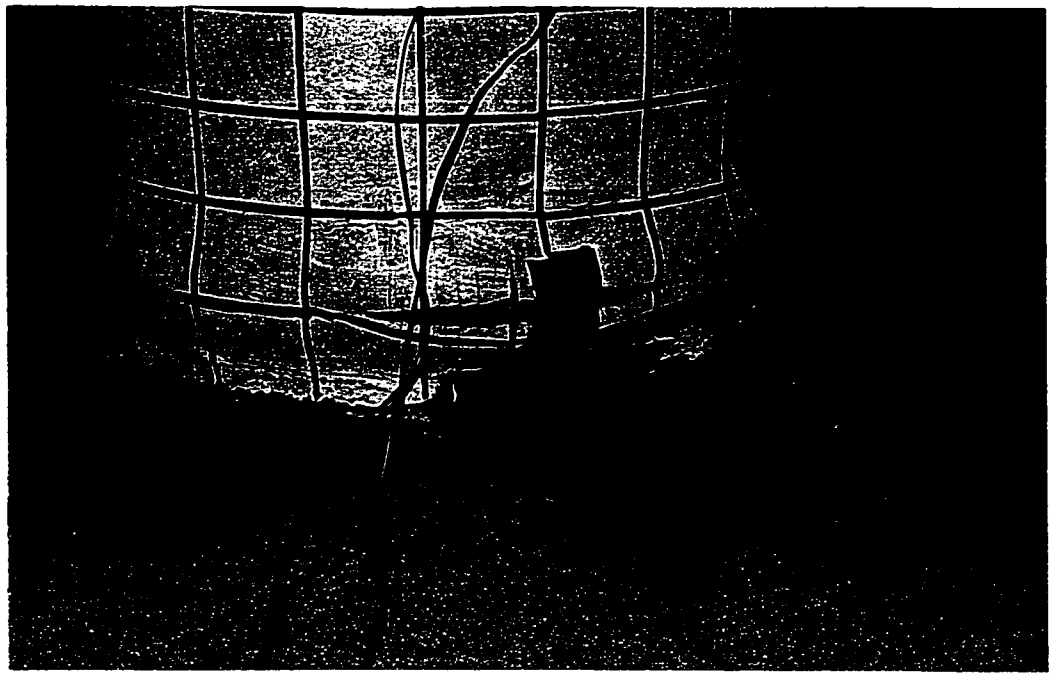

Figure 4.34b: Failure in west side - CFST 51

Figure 4.35: Penetrated vertical cracks in east side - CFST 51

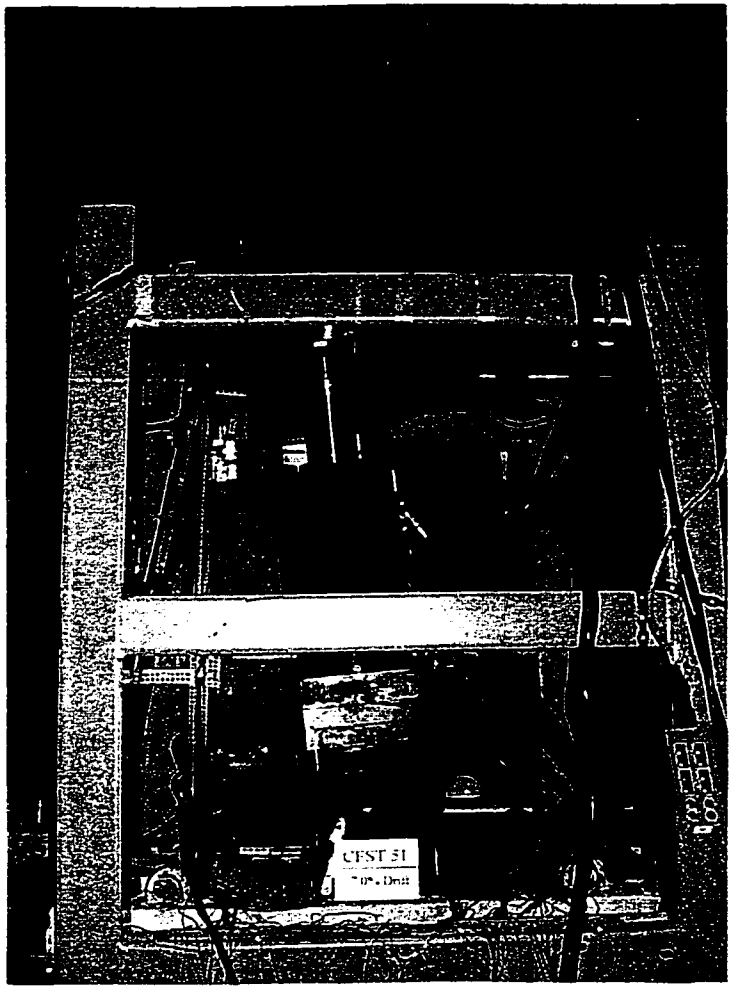

Figure 4.36: Global view of 7% drift - CFST 51

Figure 4.37: Steel section after removal from column

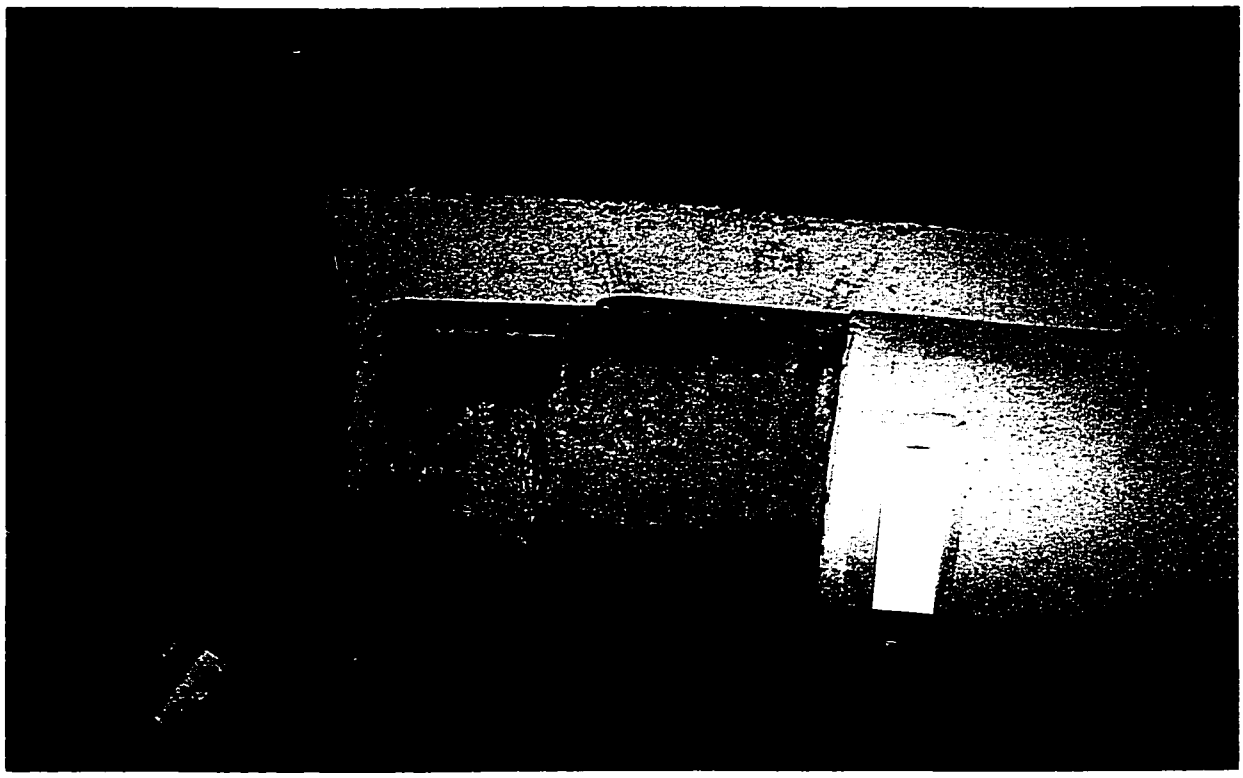

Figure 4.38: Column and concrete core after removal of steel section

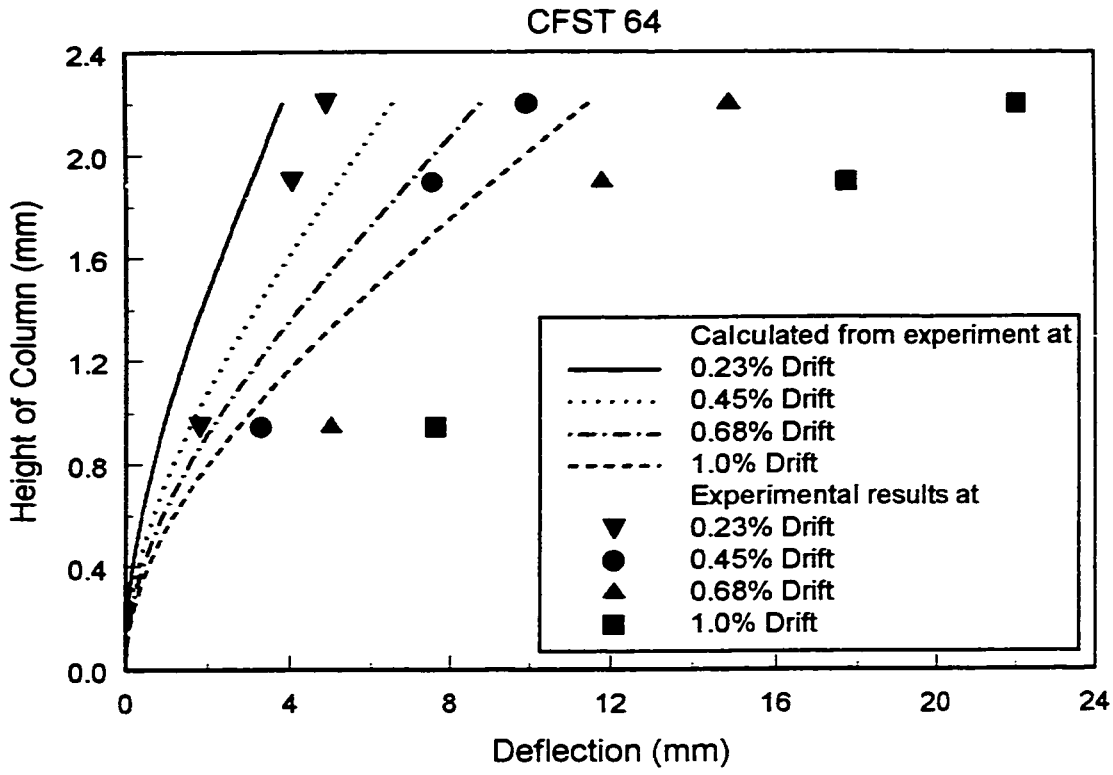

Figure 5.1: Theoretical deflected shape of CFST 64 with experimental deflections

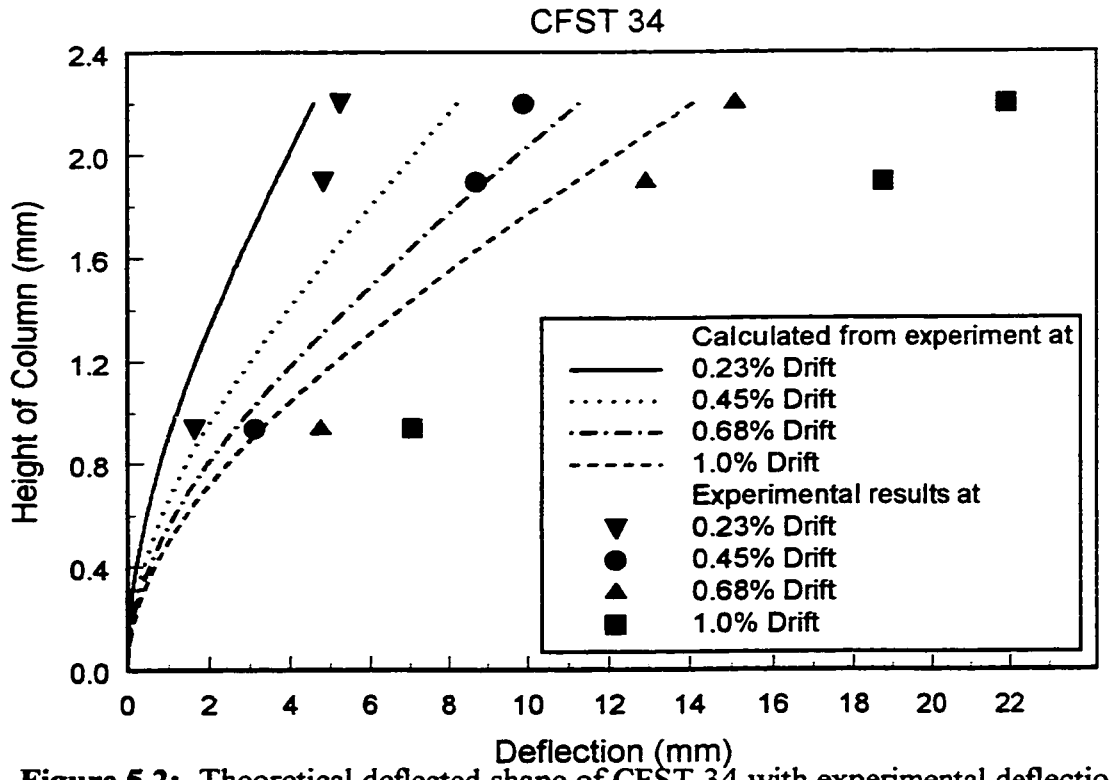

Figure 5.2: Theoretical deflected shape of CFST 34 with experimental deflections

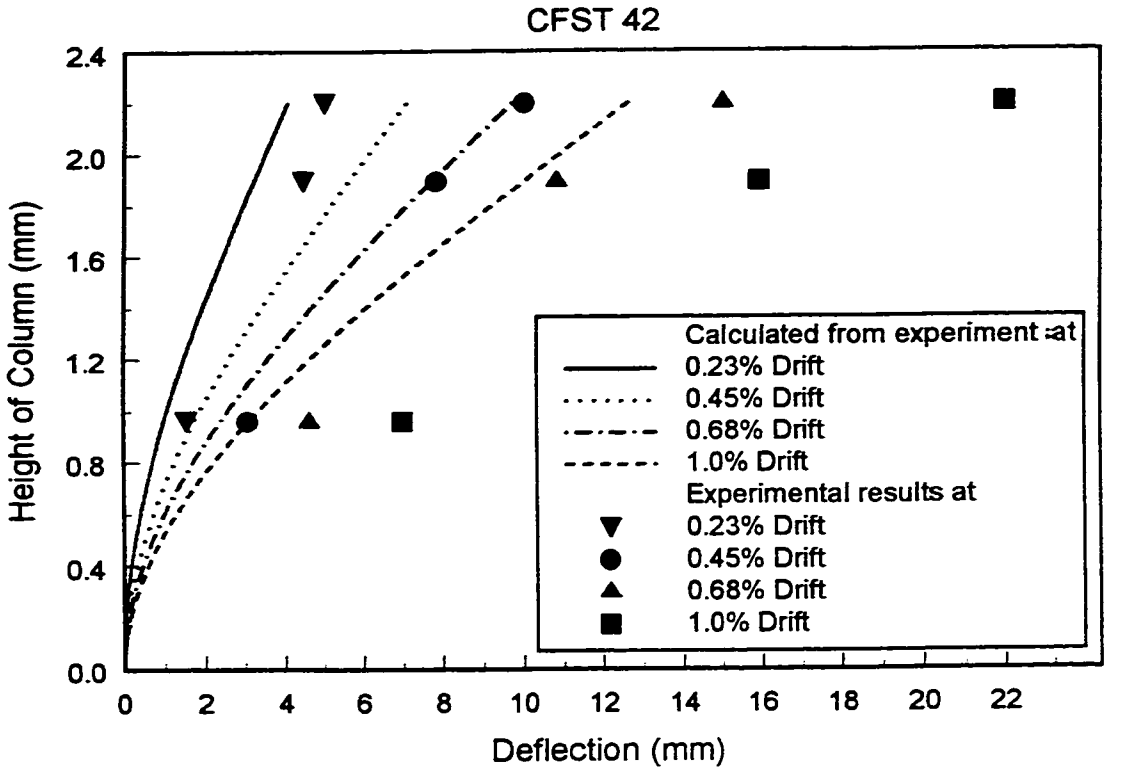

Figure 5.3: Theoretical deflected shape of CFST 42 with experimental deflections

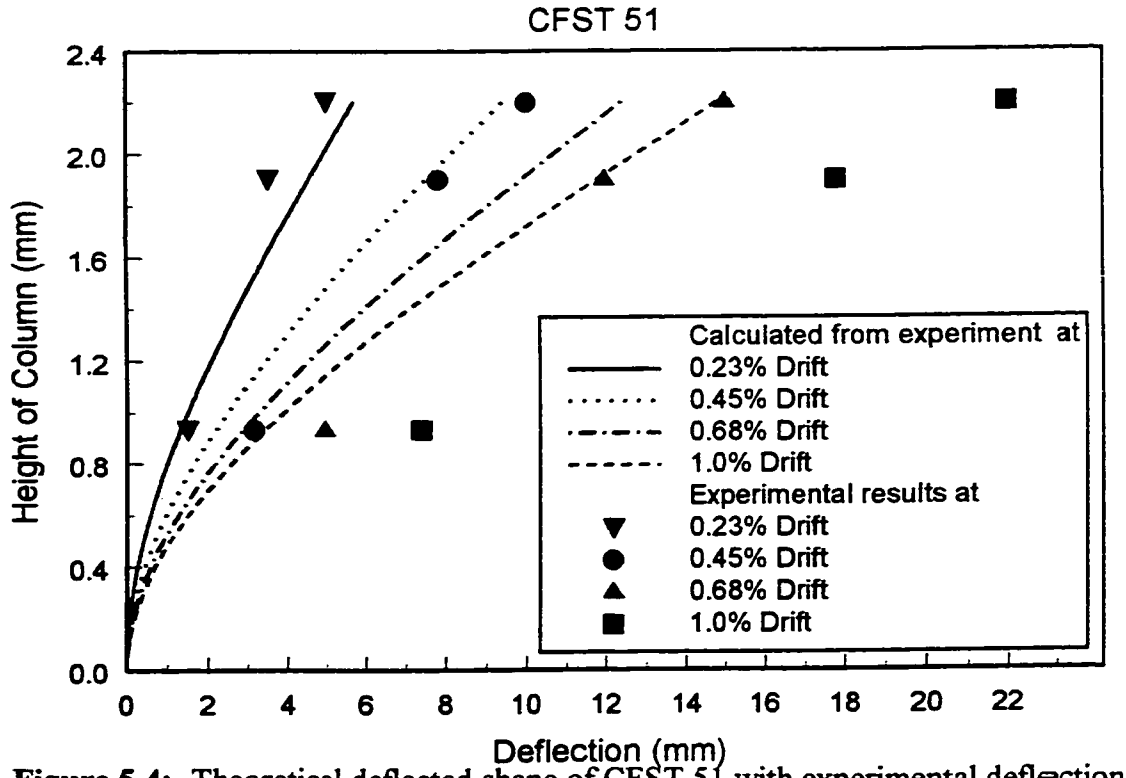

Figure 5.4: Theoretical deflected shape of CFST 51 with experimental deflections

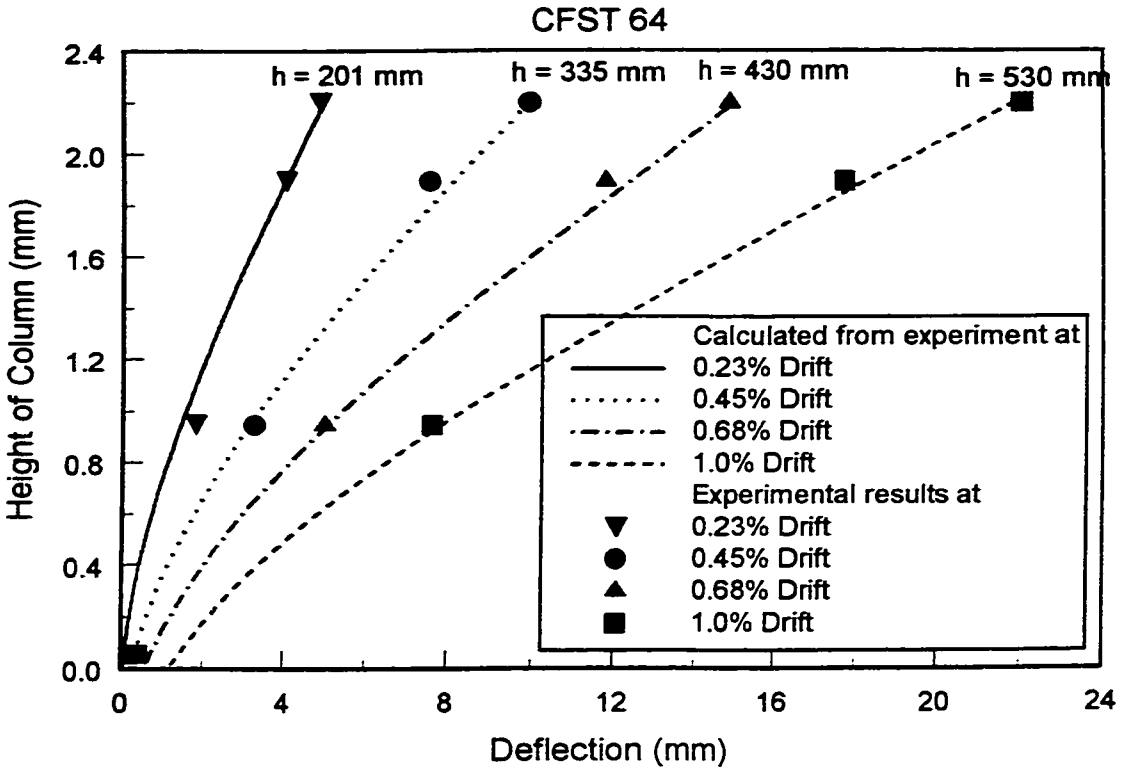

Figure 5.5: Theoretical deflected shape of CFST 64 with effective length increased

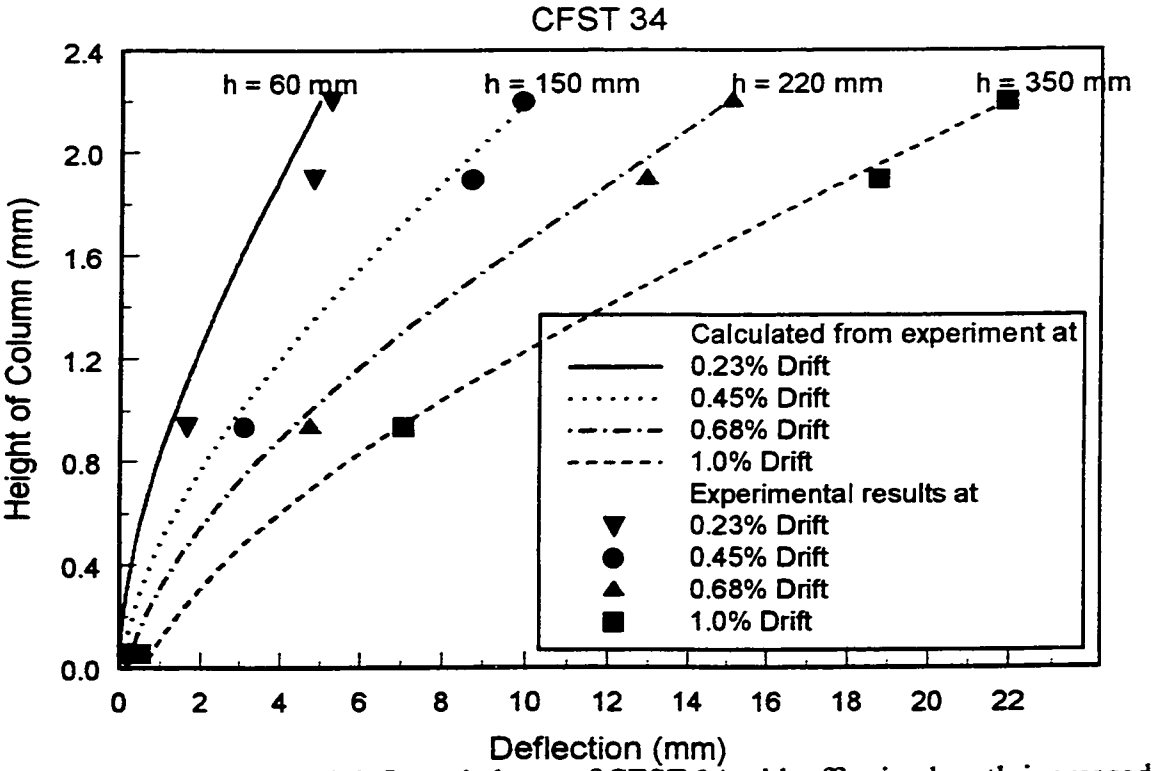

Figure 5.6: Theoretical deflected shape of CFST 34 with effective length increased

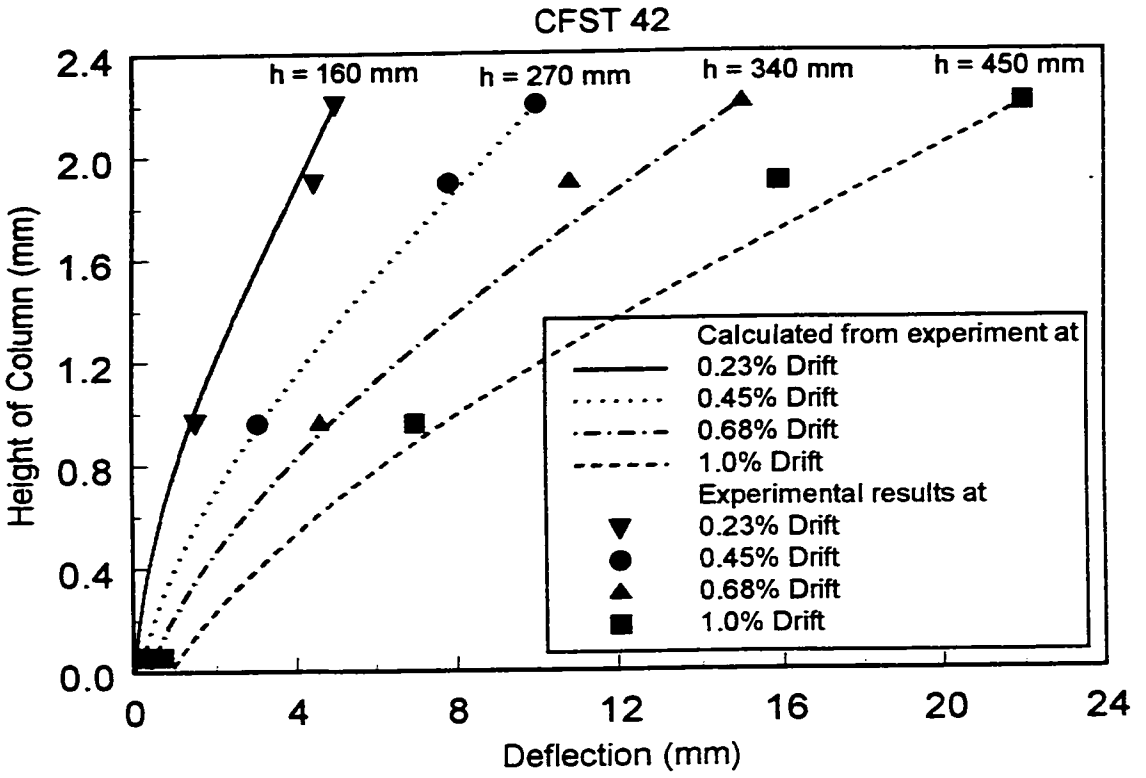

Figure 5.7: Theoretical deflected shape of CFST 42 with effective length increased

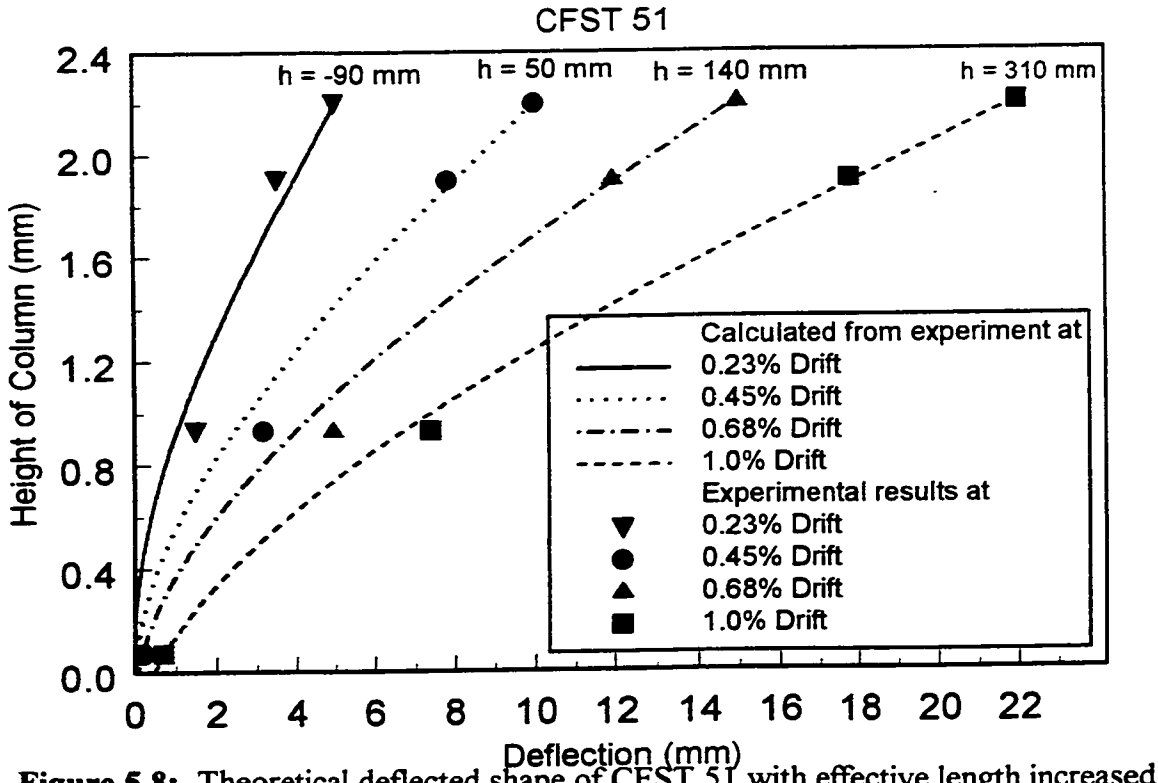

Figure 5.8: Theoretical deflected shape of CFST 51 with effective length increased

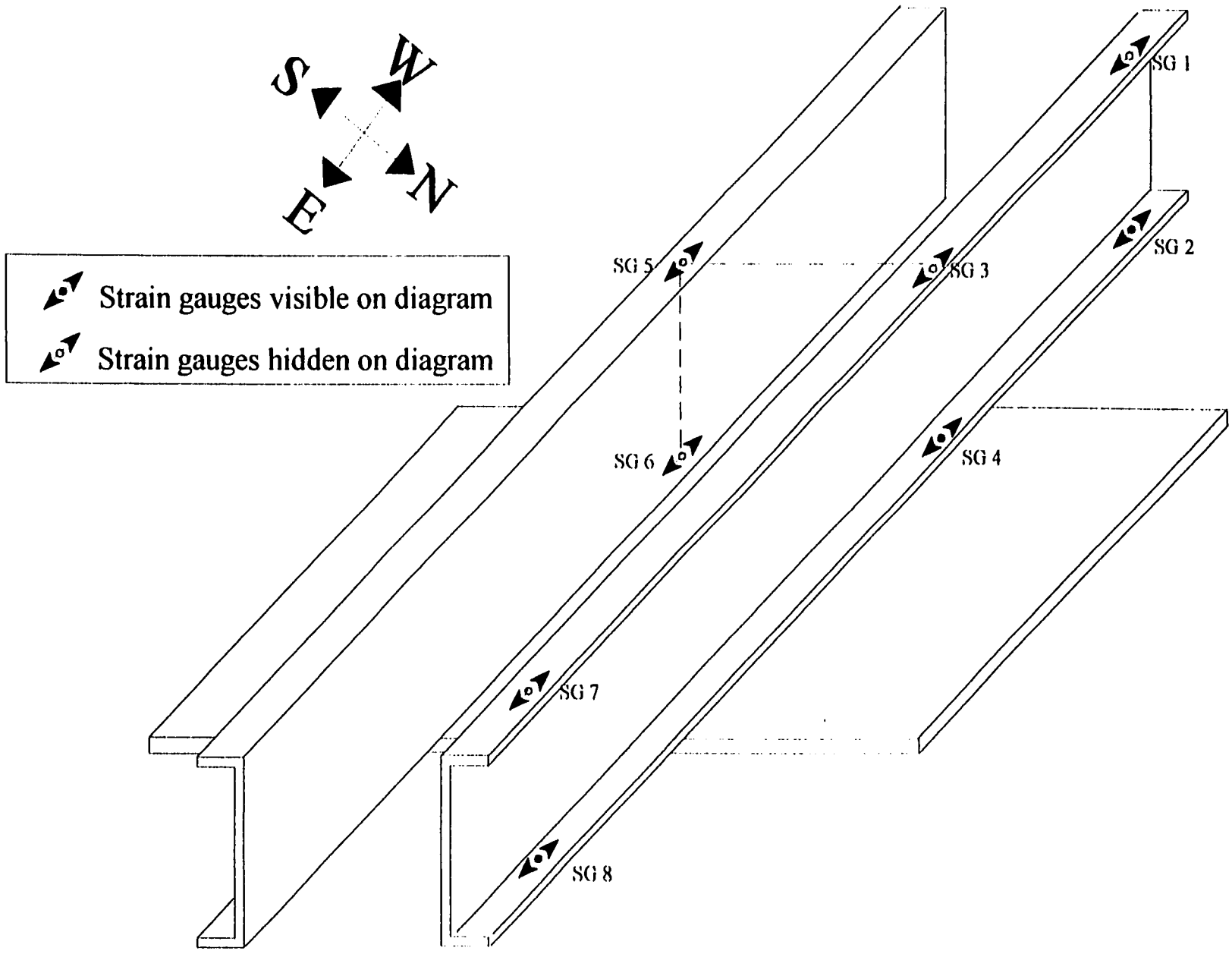

Figure 5.9: Location of strain gauges on the channels

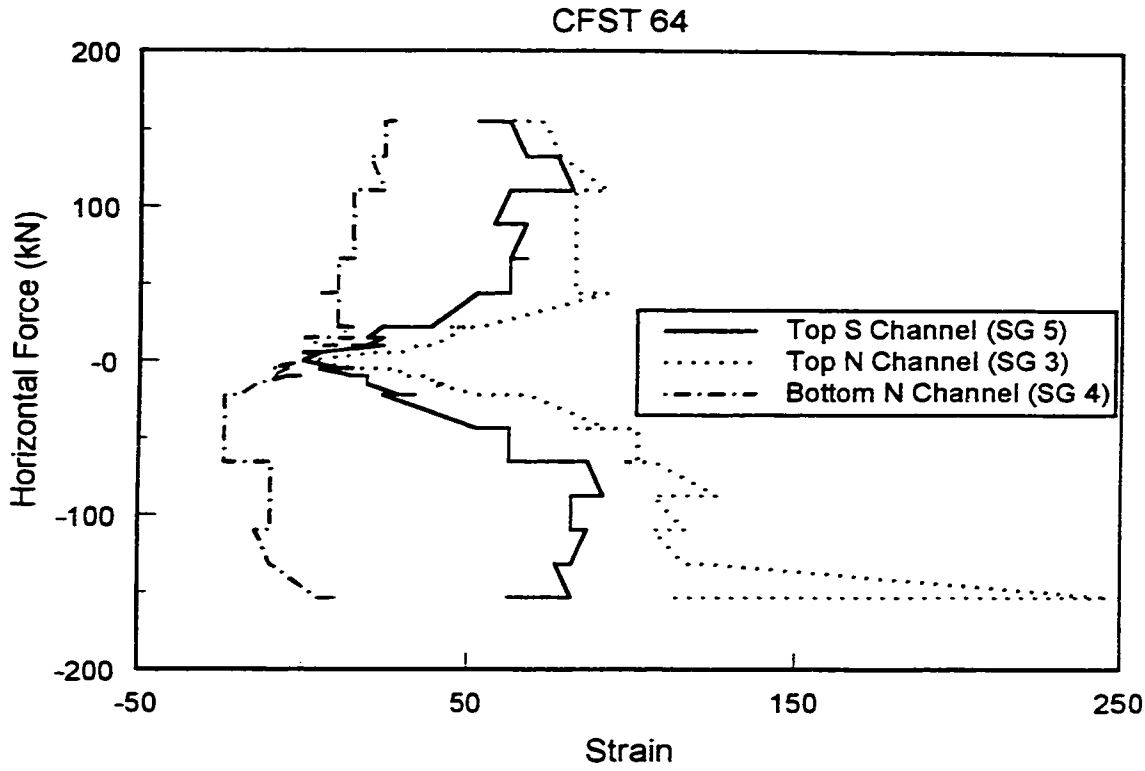

Figure 5.10: Strain gauge readings in middle of channels on CFST 64

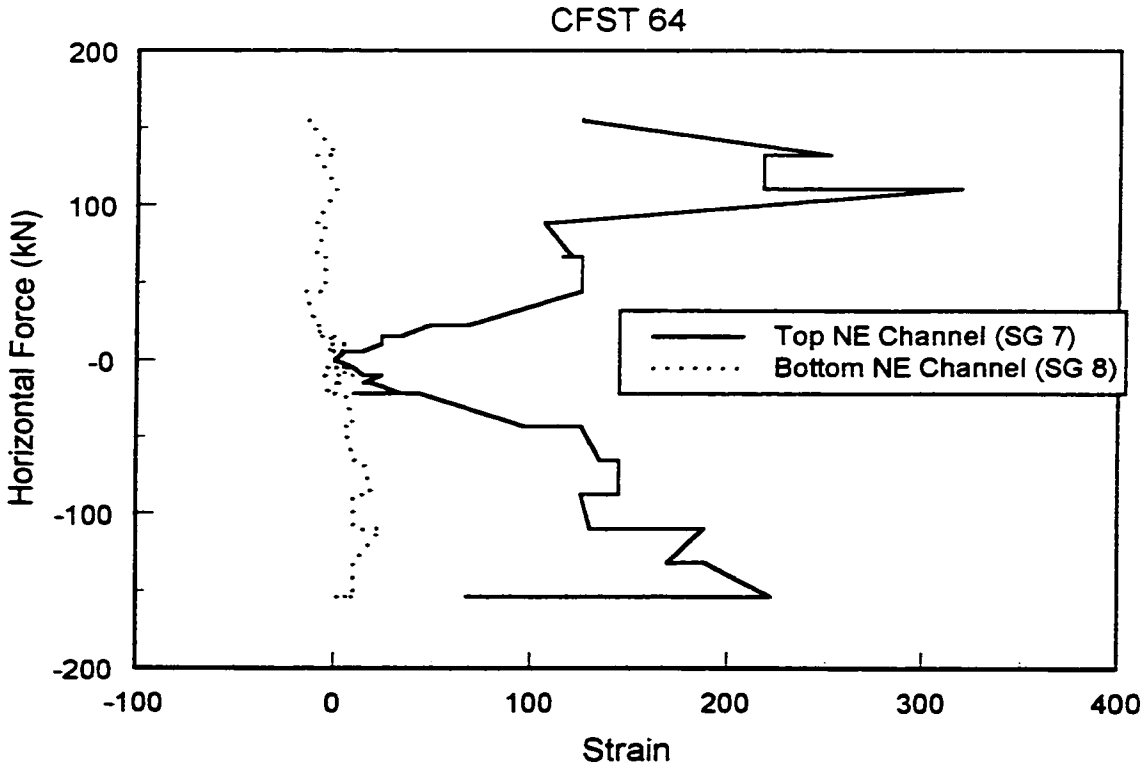

Figure 5.11: Strain gauge readings on ends of channels on CFST 64

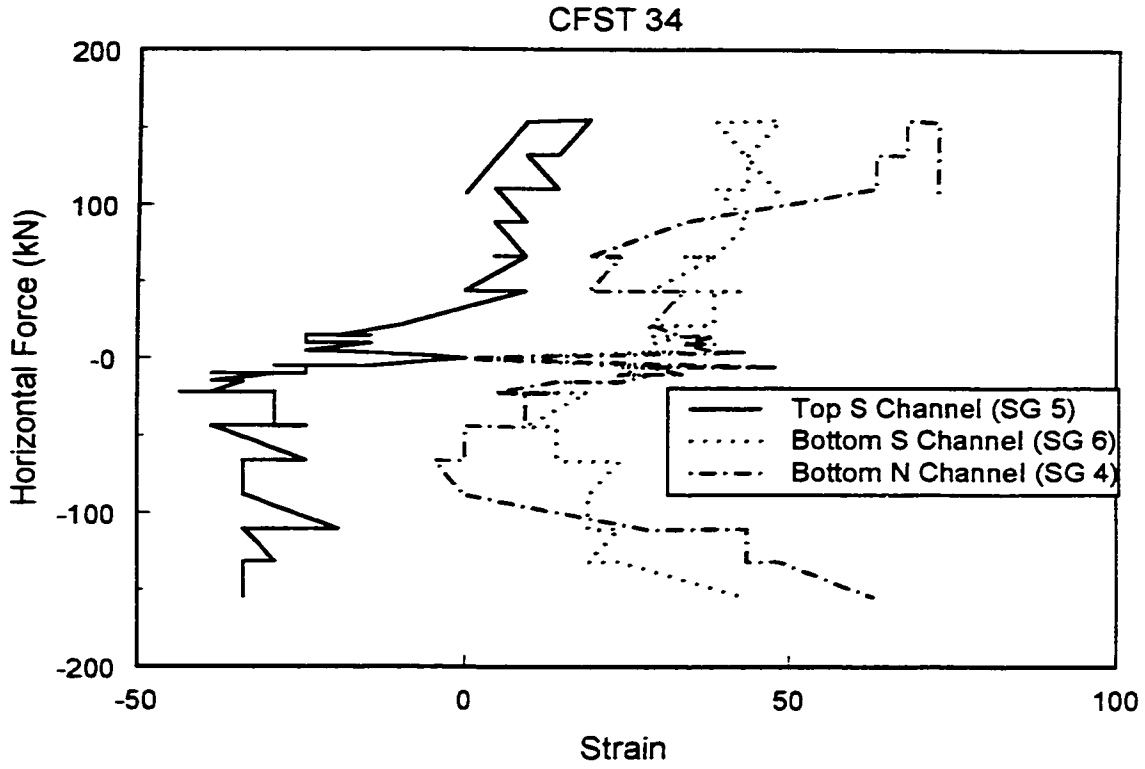

Figure 5.12: Strain gauge readings in middle of channels on CFST 34

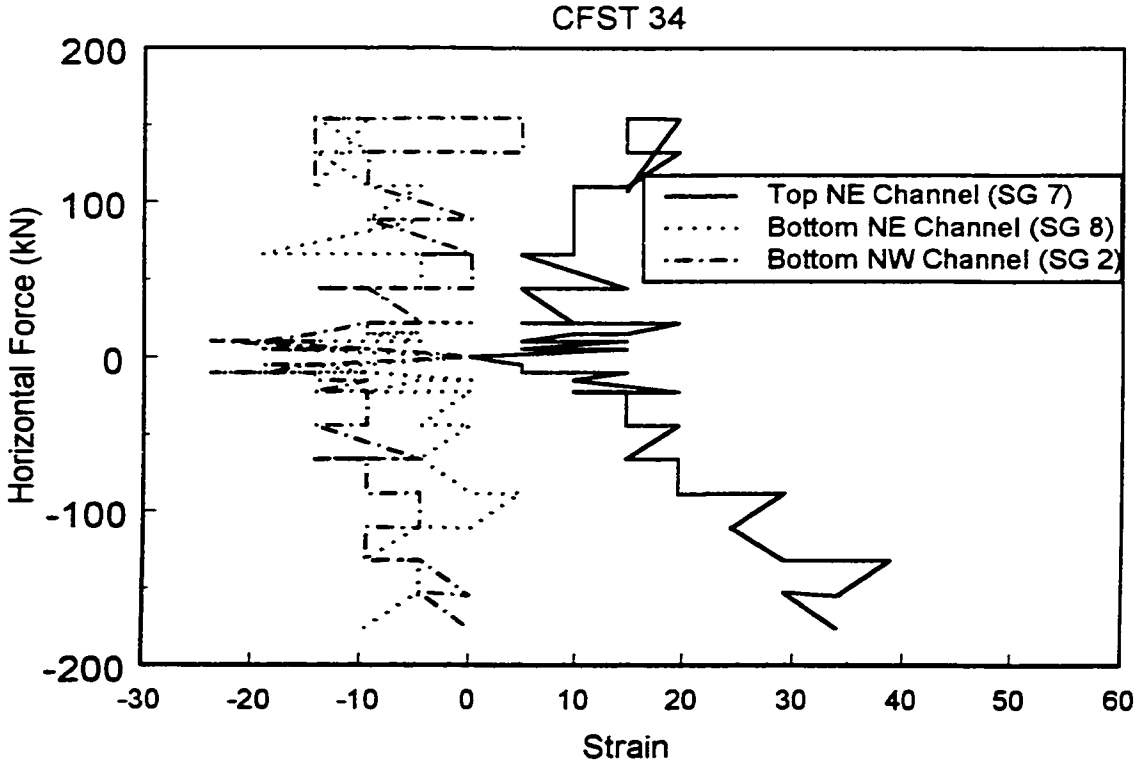

Figure 5.13: Strain gauge readings on ends of channels on CFST 34

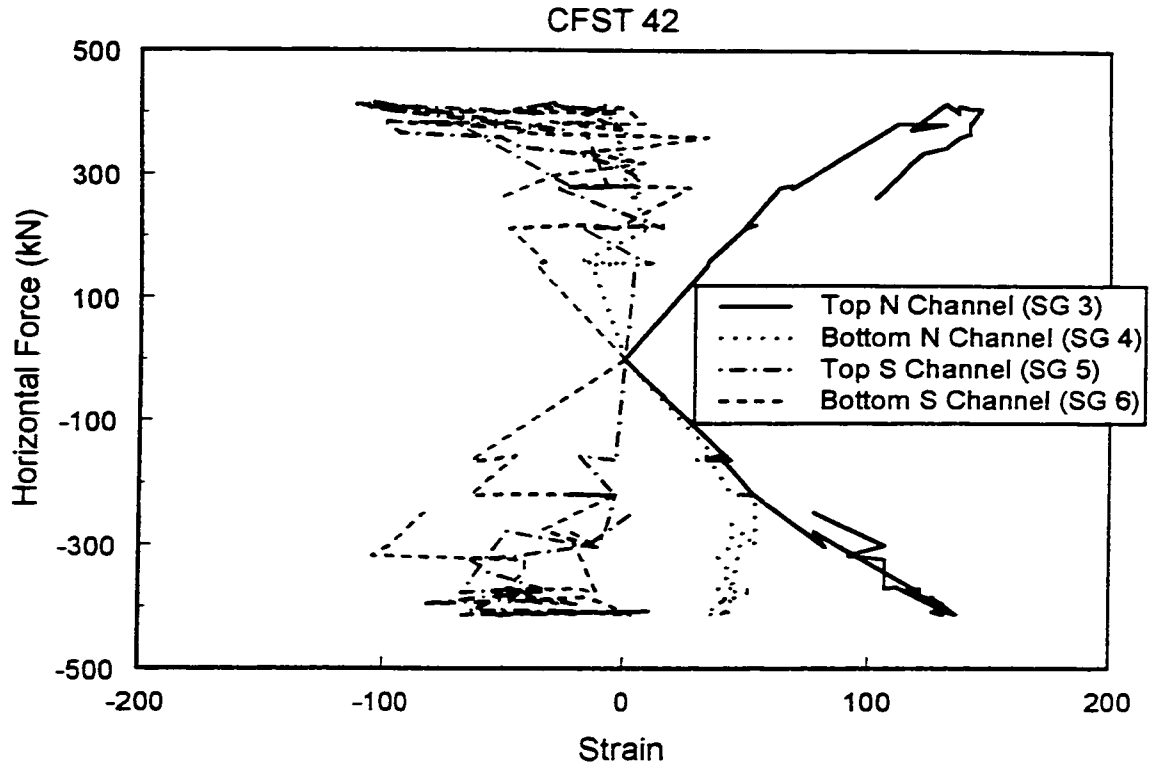

Figure 5.14: Strain gauge readings in middle of channels on CFST 42

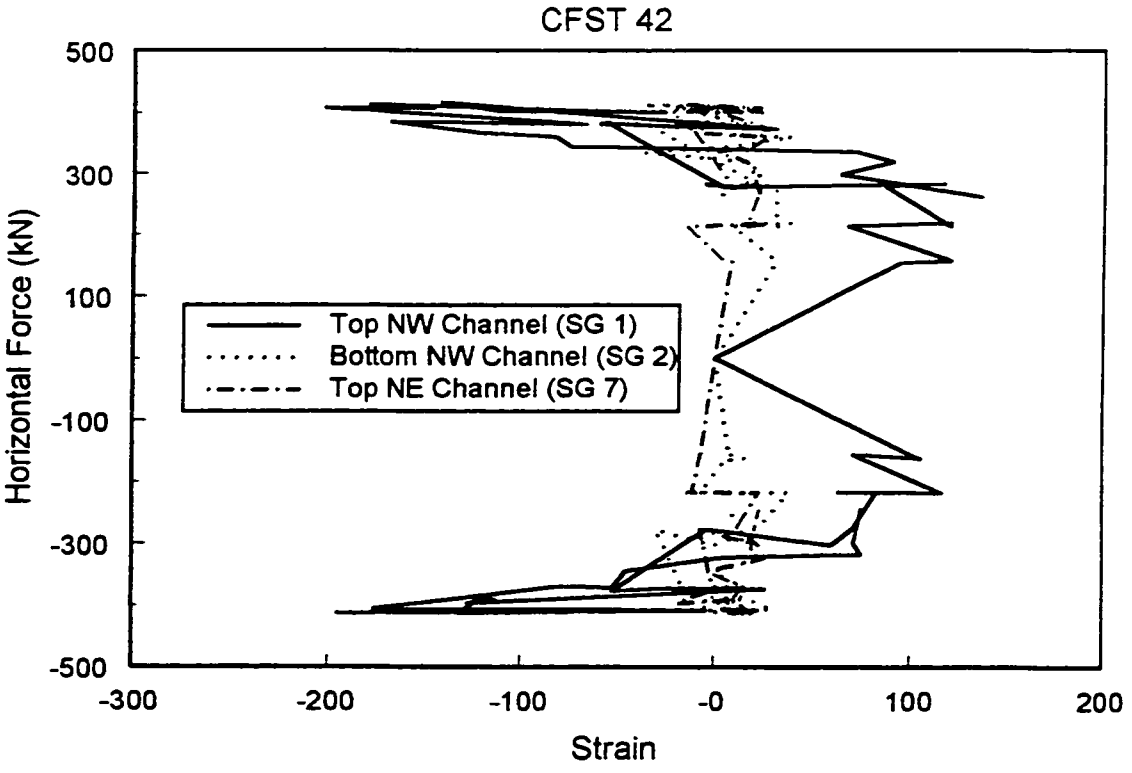

Figure 5.15: Strain gauge readings on ends of channels on CFST 42

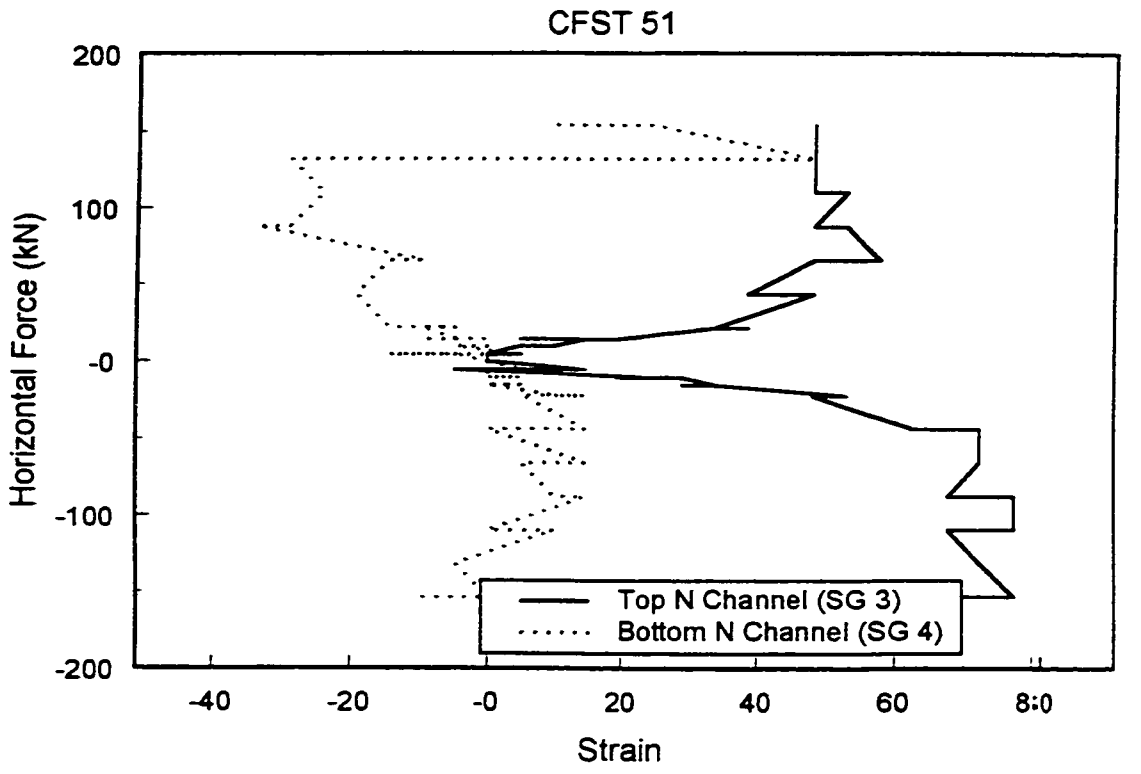

Figure 5.16: Strain gauge readings in middle of channels on CFST 51

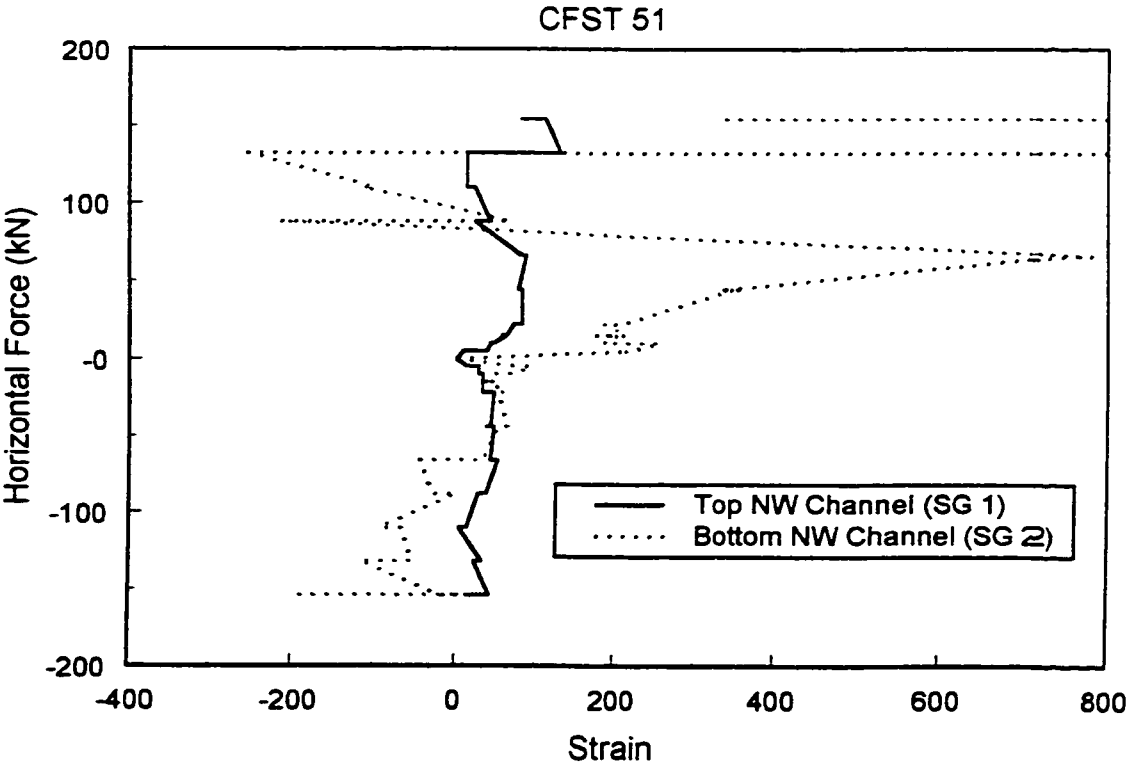

Figure 5.17: Strain gauge readings on ends of channels on CFST 51

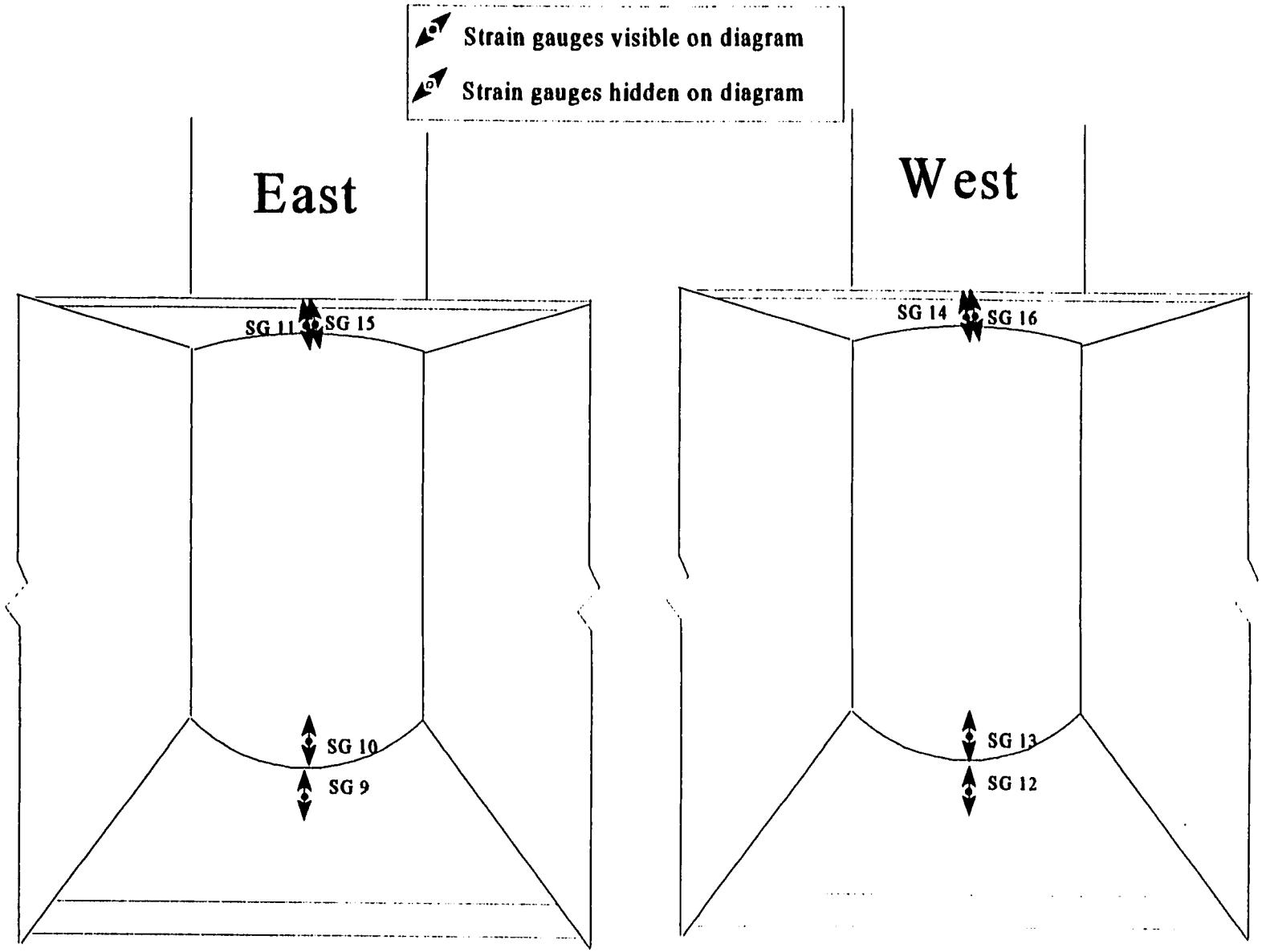

Figure 5.18: Location of strain gauges on the plates and bottom of the column

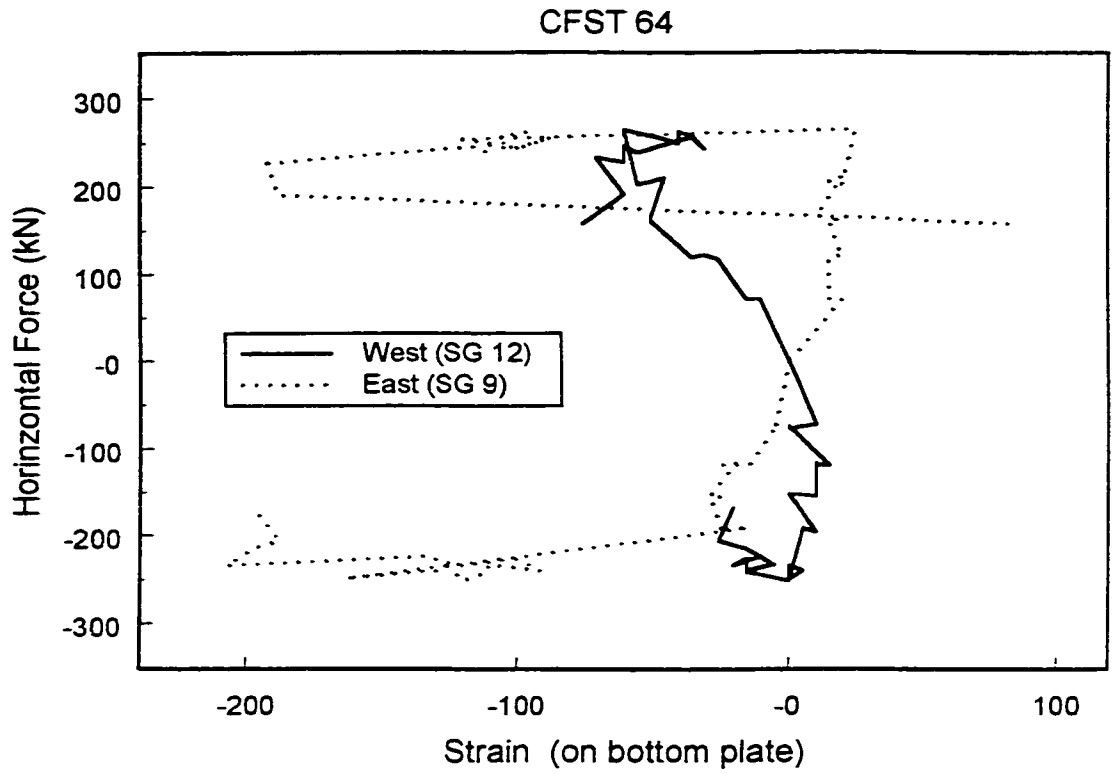

Figure 5.19: Strain gauge readings on the bottom plate on CFST 64

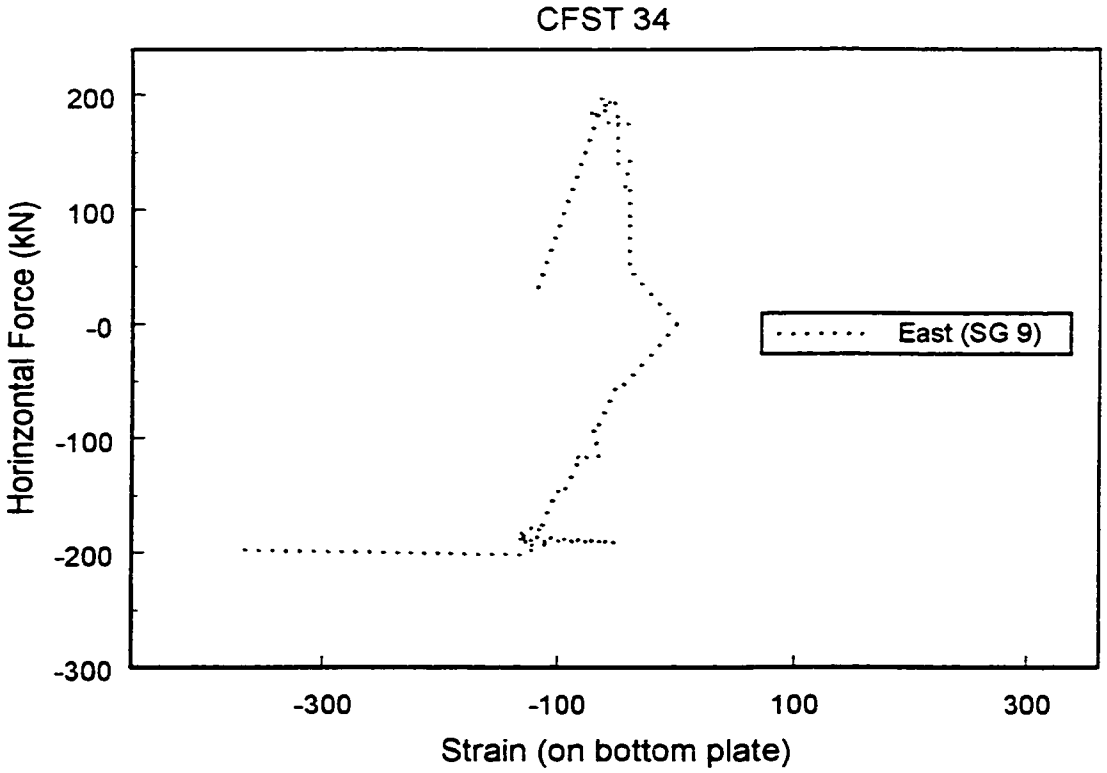

Figure 5.20: Strain gauge readings on the bottom plate on CFST 34

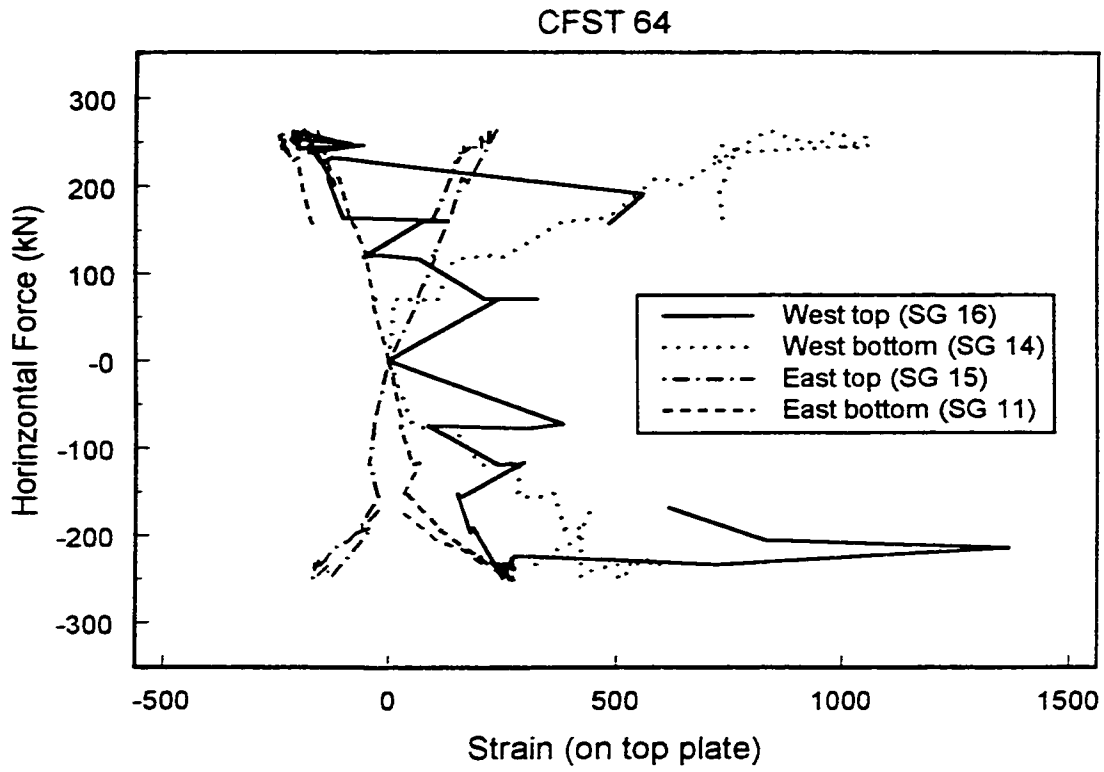

Figure 5.21: Strain gauge readings on the top plate on CFST 64

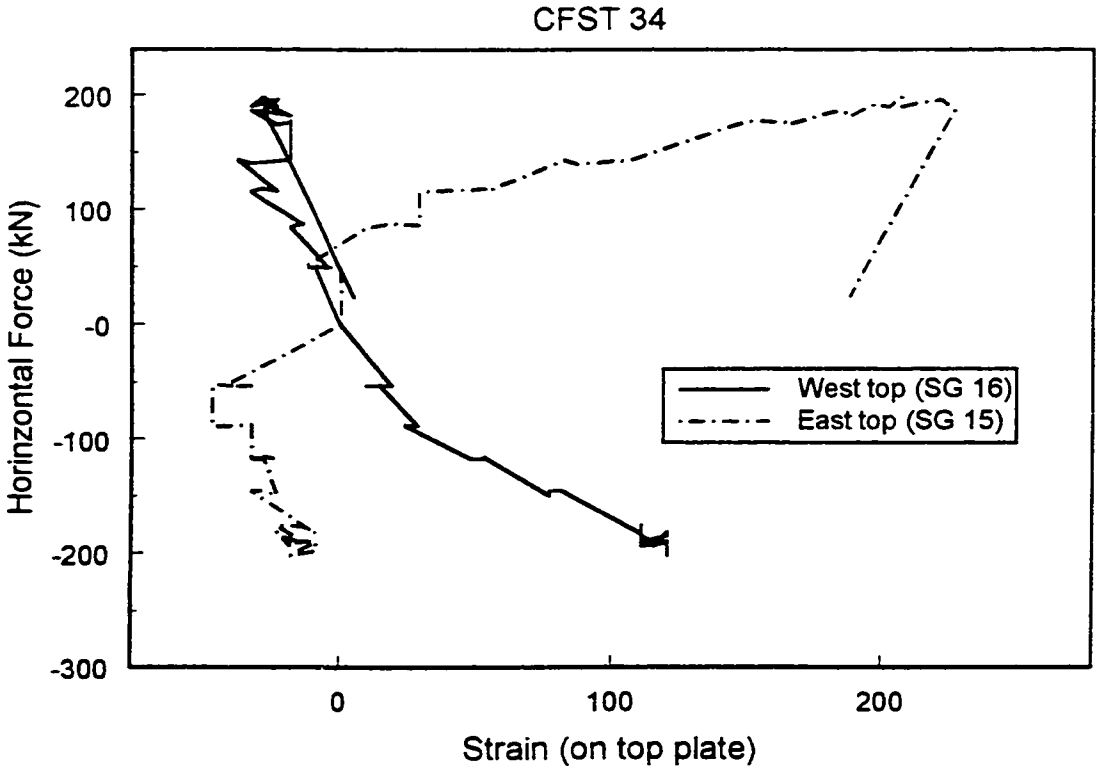

Figure 5.22: Strain gauge readings on the top plate on CFST 34

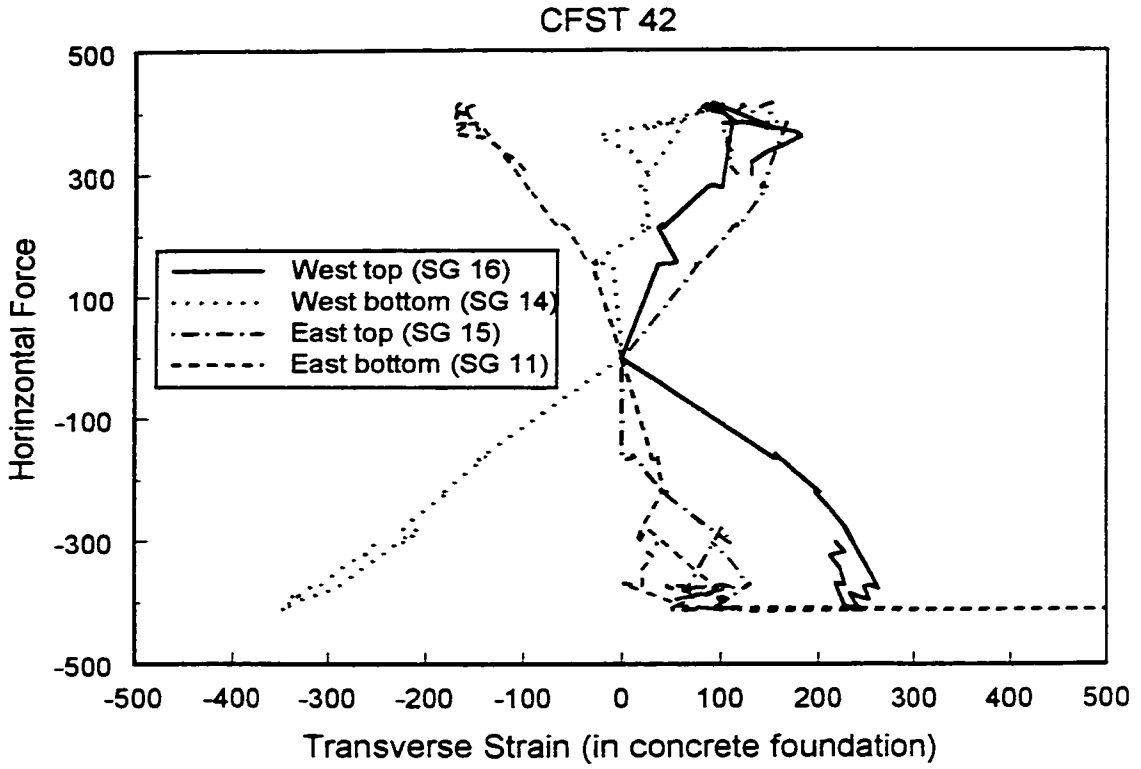

Figure 5.23: Strain gauge readings on the top plate on CFST 42

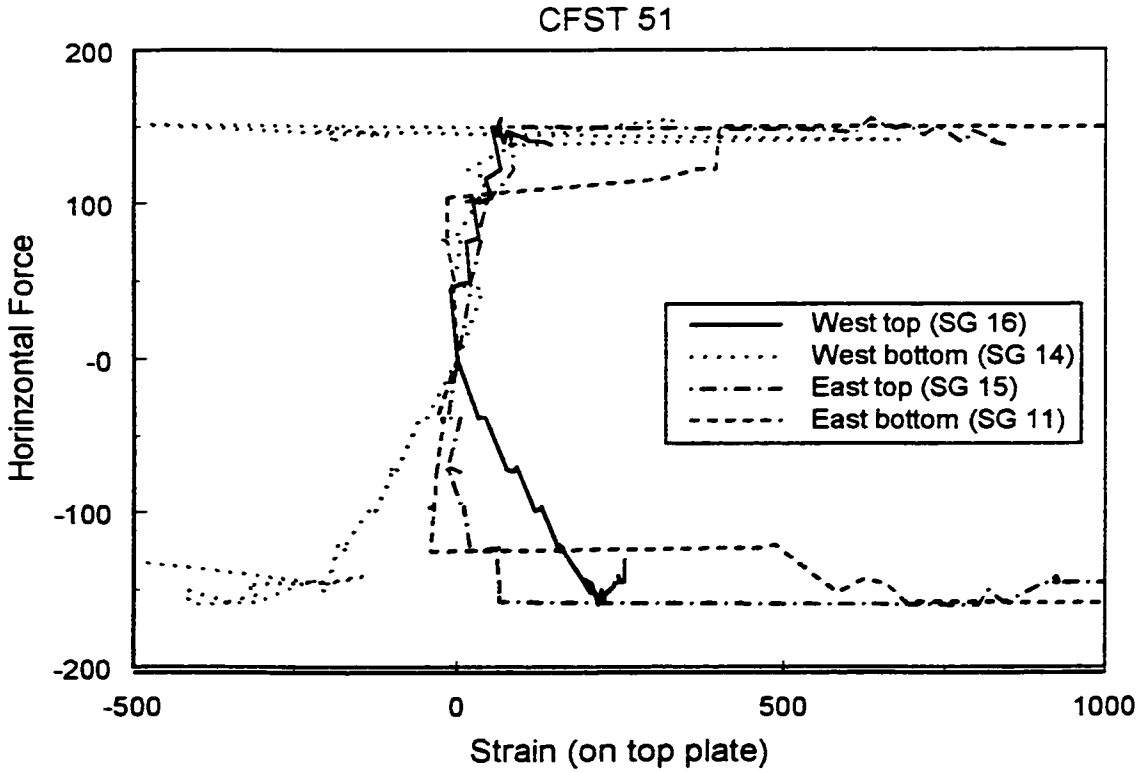

Figure 5.24: Strain gauge readings on the top plate on CFST 51

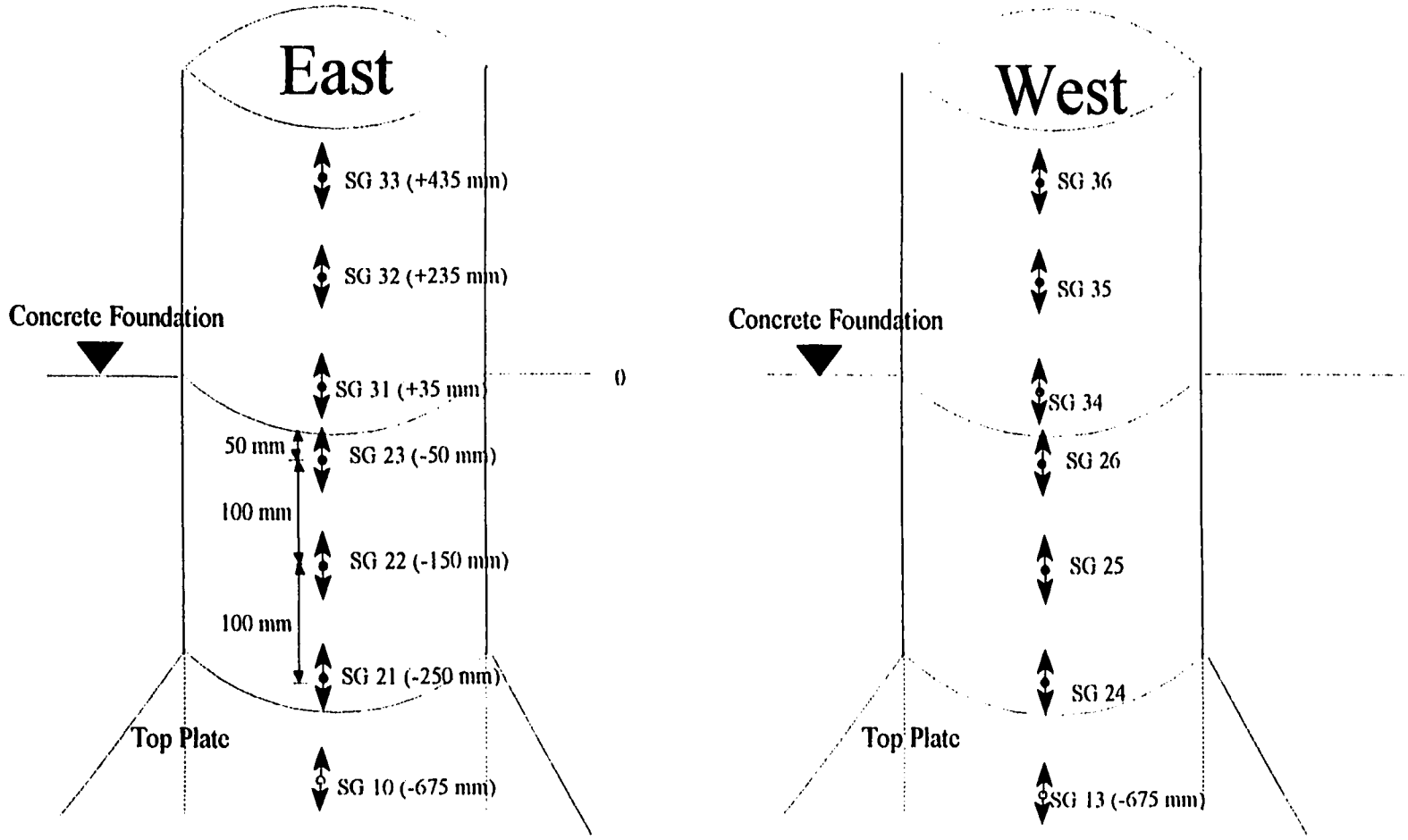

Figure 5.25: Location of longitudinal strain gauges on the steel tube

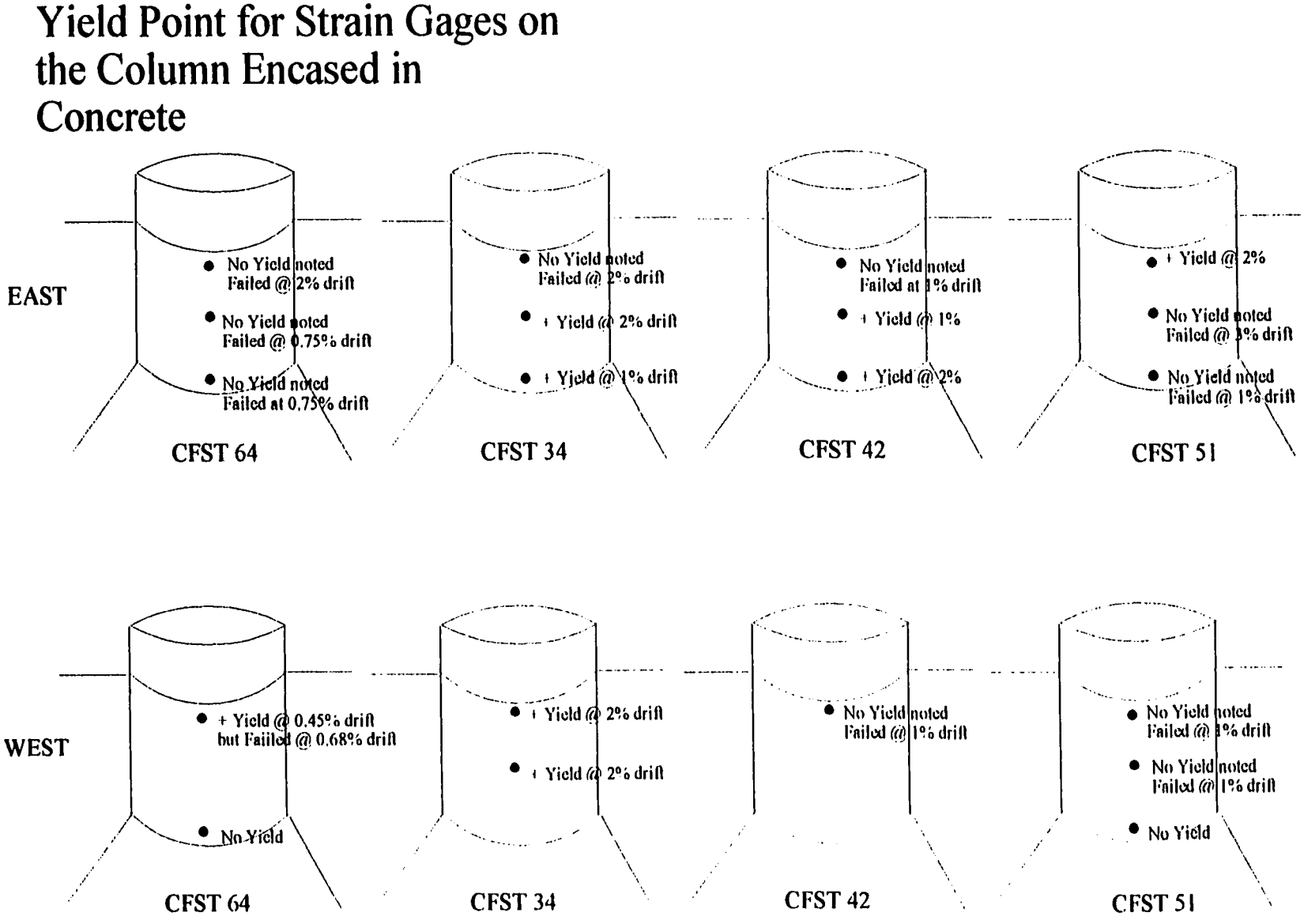

Figure 5.26: Yielding of longitudinal strain gauges on the steel tube encased in concrete

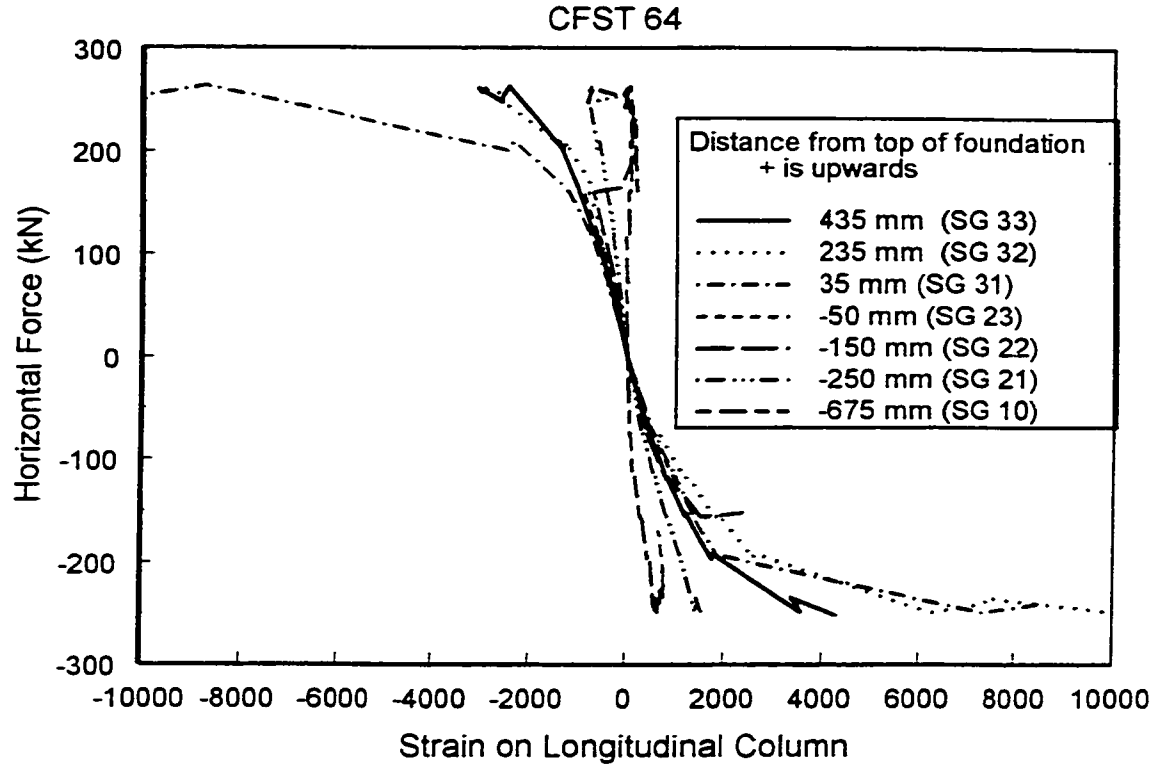

Figure 5.27a: Strain gauge reading of longitudinal strain on east side of CFST 64

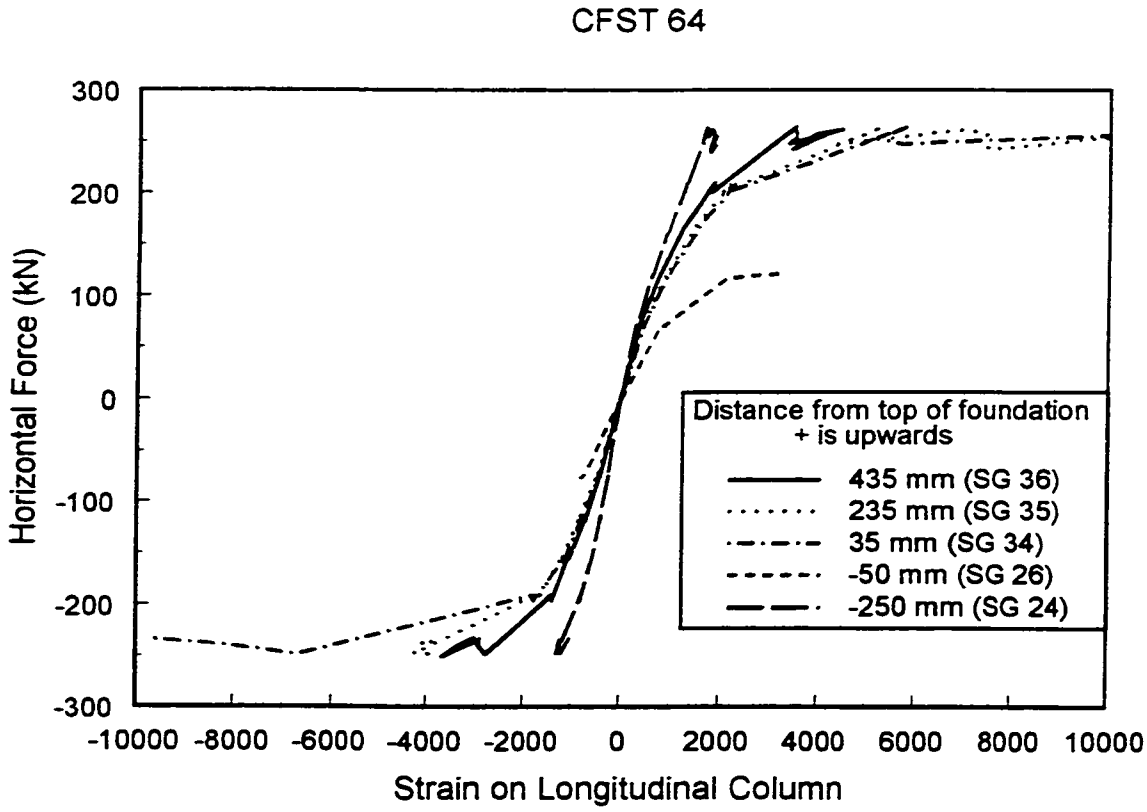

Figure 5.27b: Strain gauge reading of longitudinal strain on west side of CFST 64

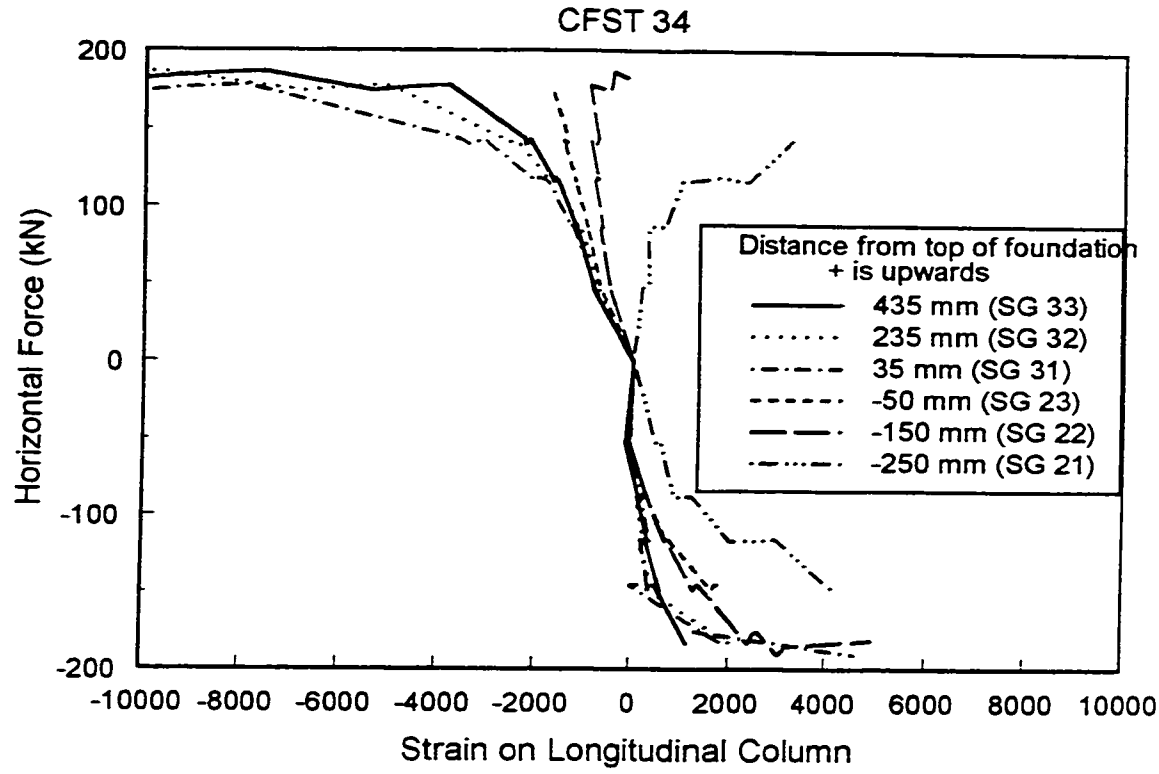

Figure 5.28a: Strain gauge reading of longitudinal strain on east side of CFST 34

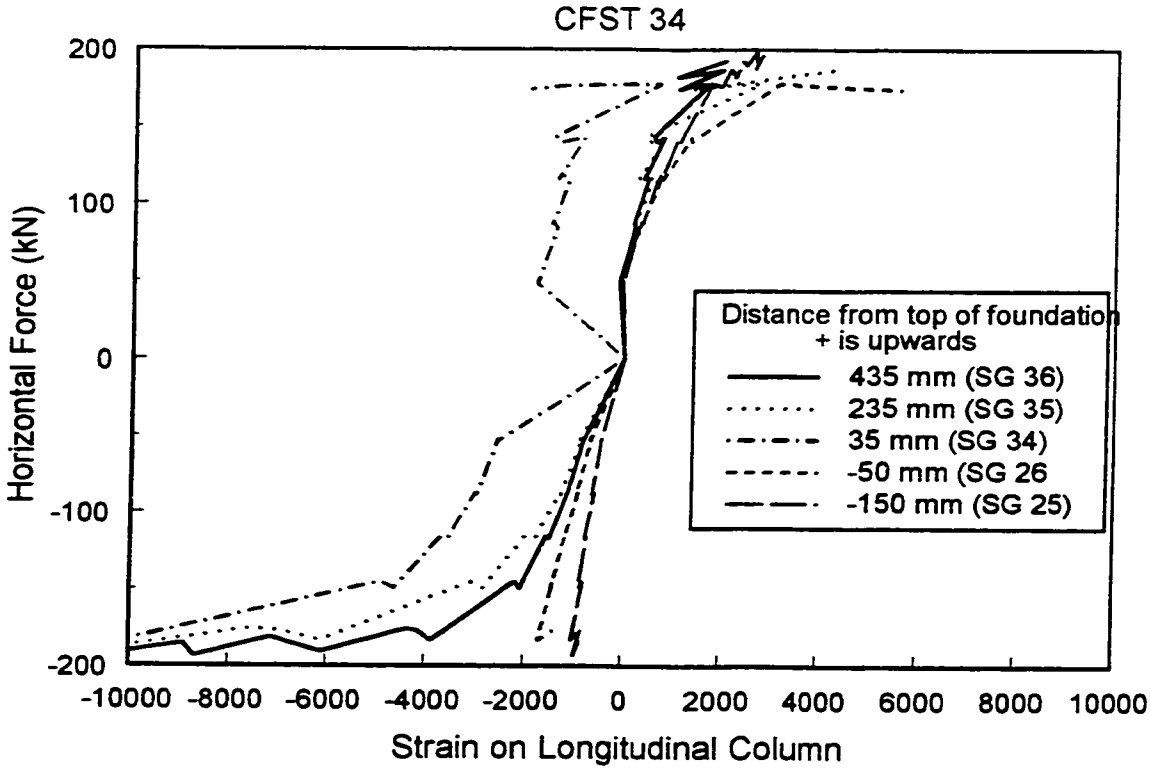

Figure 5.28b: Strain gauge reading of longitudinal strain on west side of CFST 34

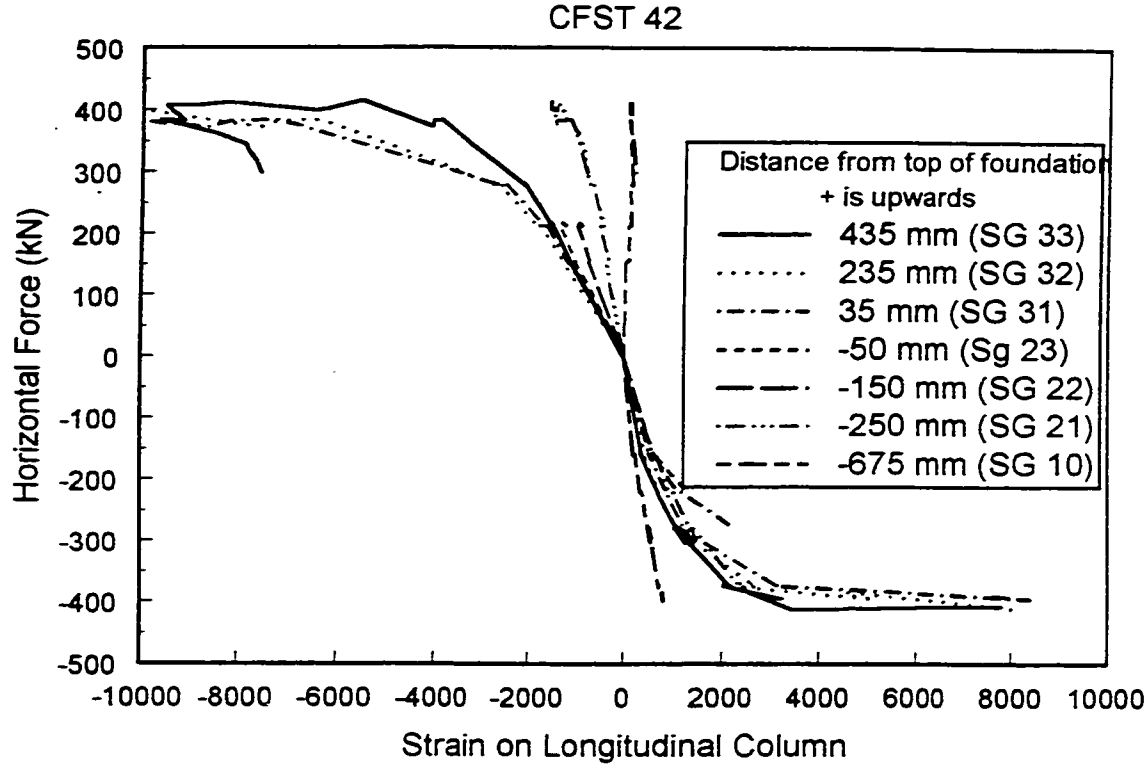

Figure 5.29a: Strain gauge reading of longitudinal strain on east side of CFST 42

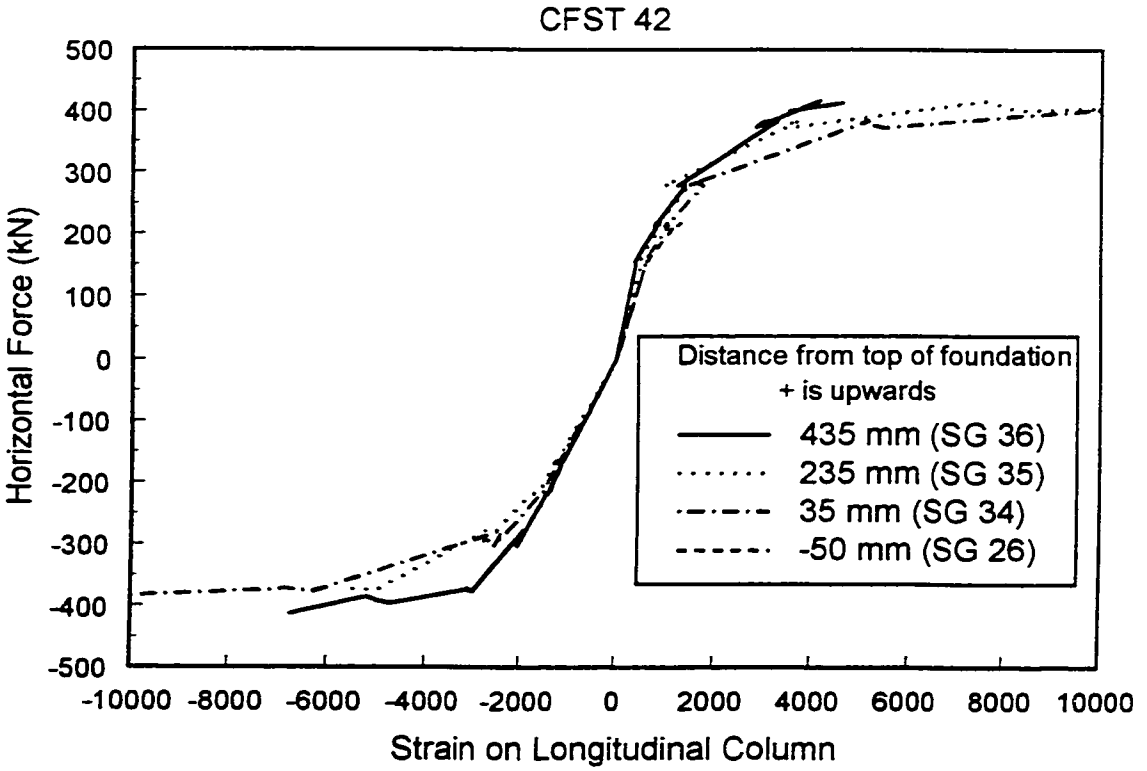

Figure 5.29b: Strain gauge reading of longitudinal strain on west side of CFST 42

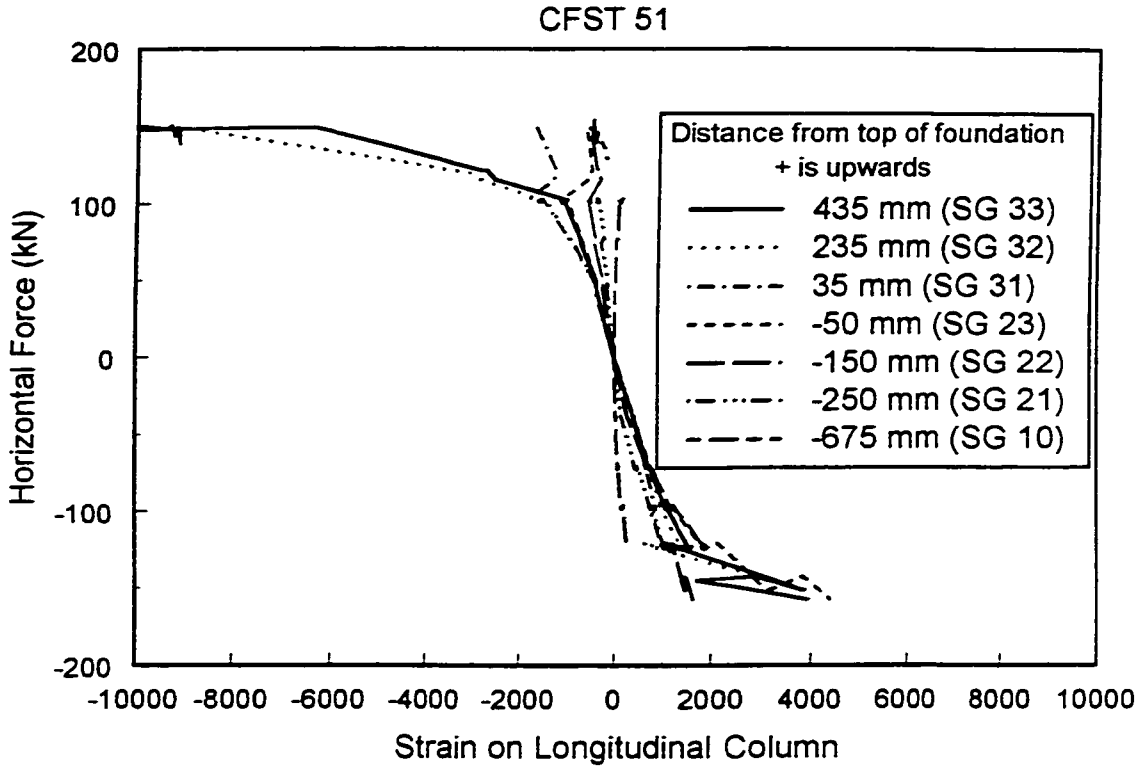

Figure 5.30a: Strain gauge reading of longitudinal strain on east side of CFST 51

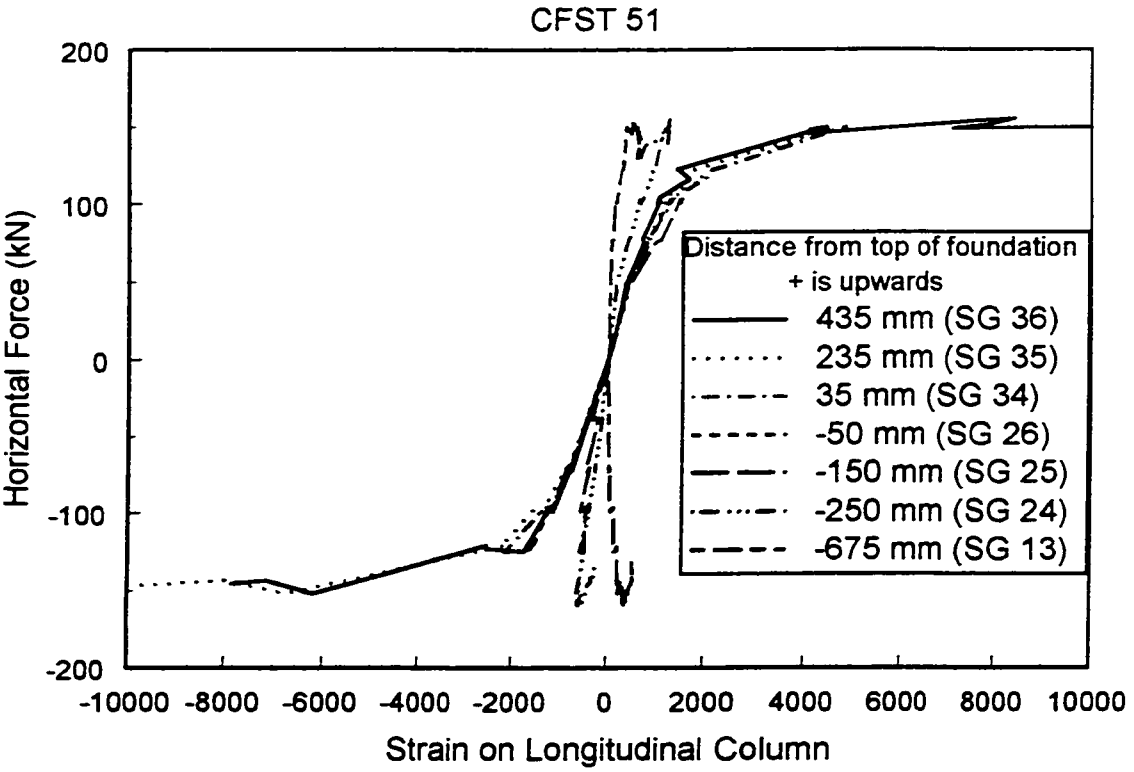

Figure 5.30b: Strain gauge reading of longitudinal strain on west side of CFST 51

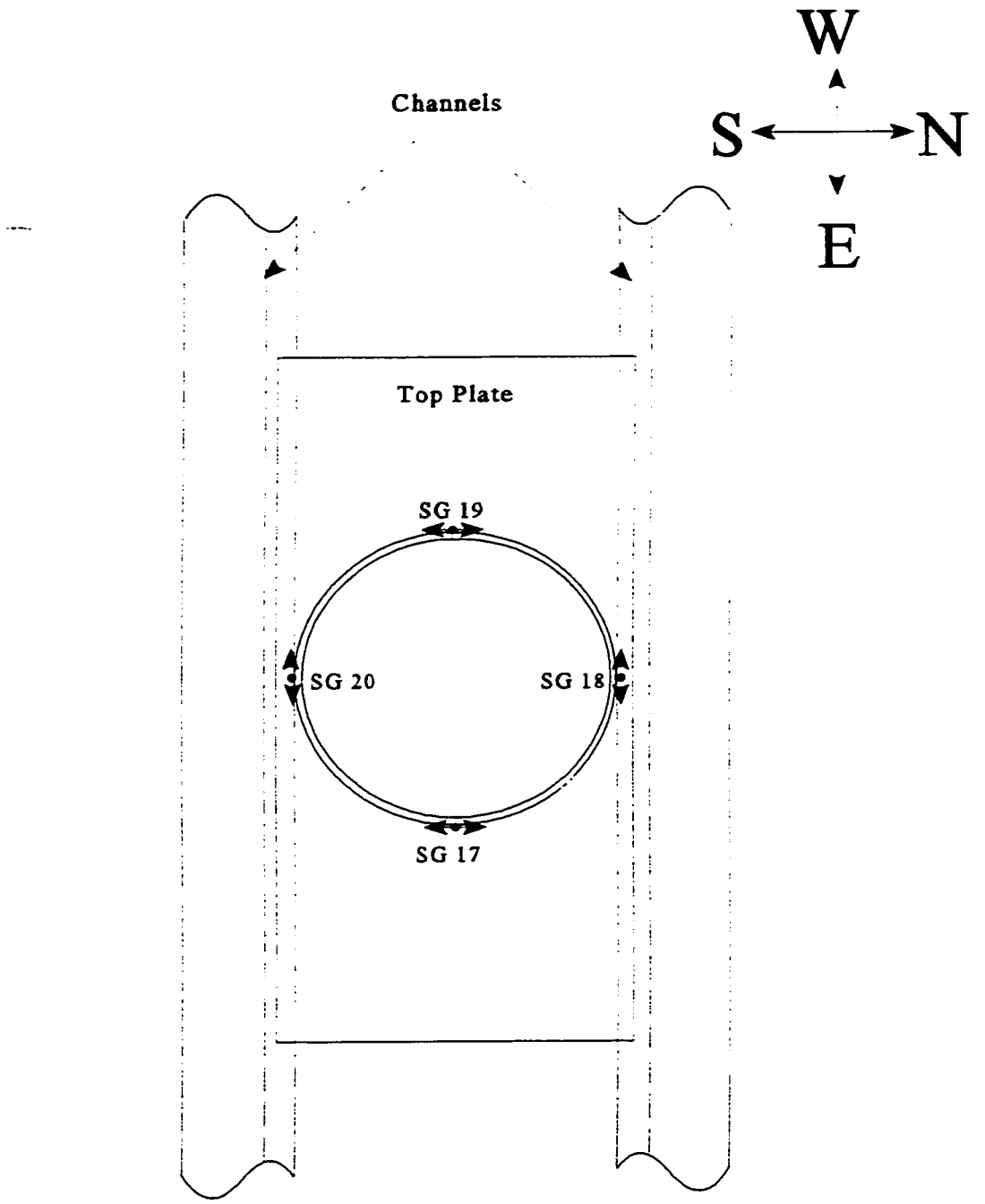

Figure 5.31: Location of transverse strain gauges on the steel tube encased in concrete

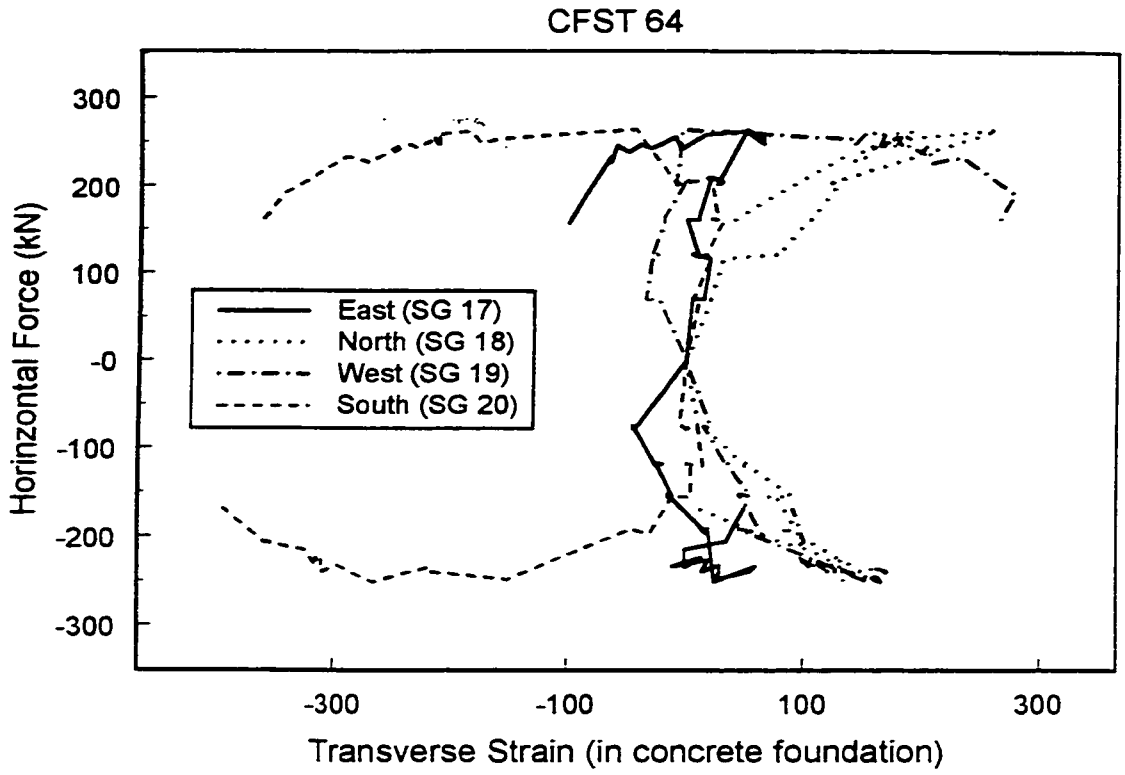

Figure 5.32: Transverse strain on the steel tube encased in concrete on CFST 64

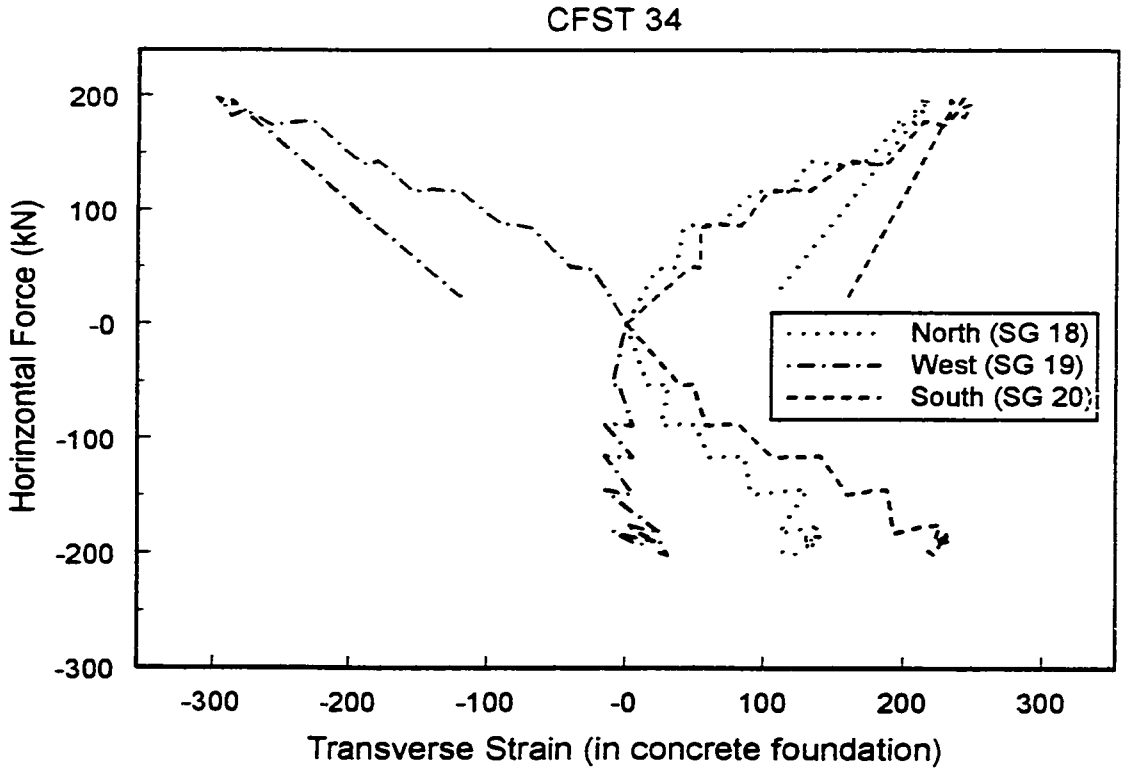

Figure 5.33: Transverse strain on the steel tube encased in concrete on CFST 34

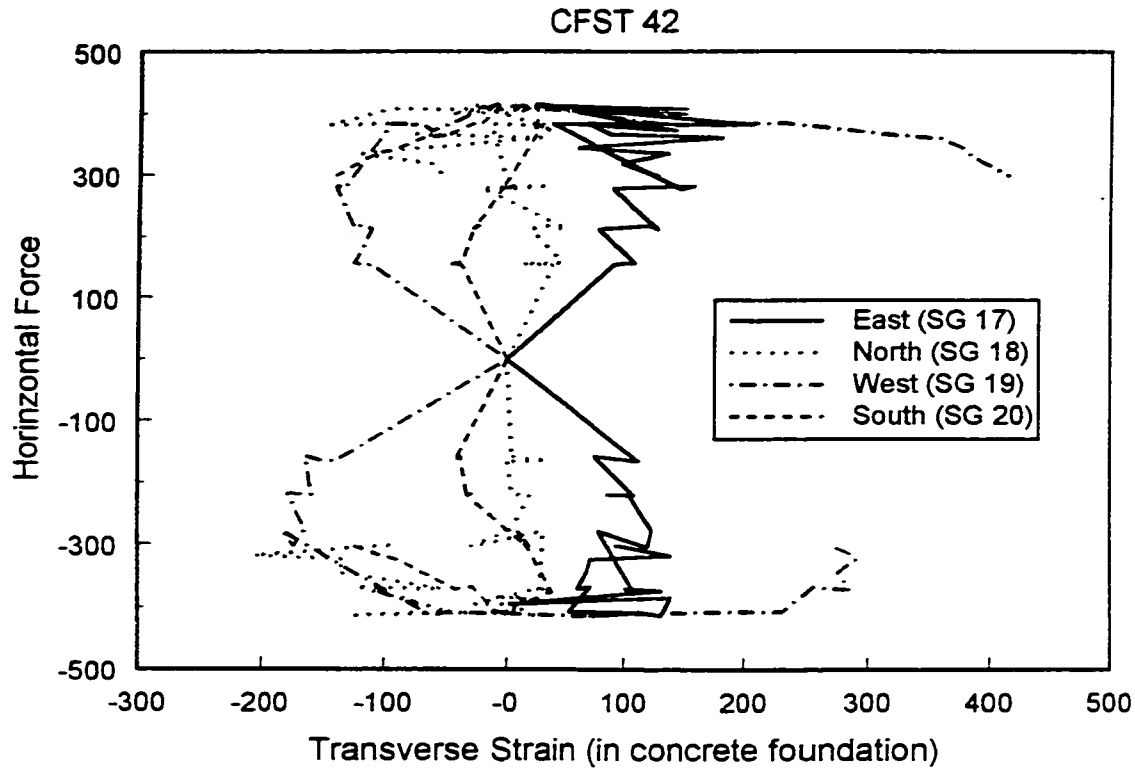

Figure 5.34: Transverse strain on the steel tube encased in concrete on CFST 42

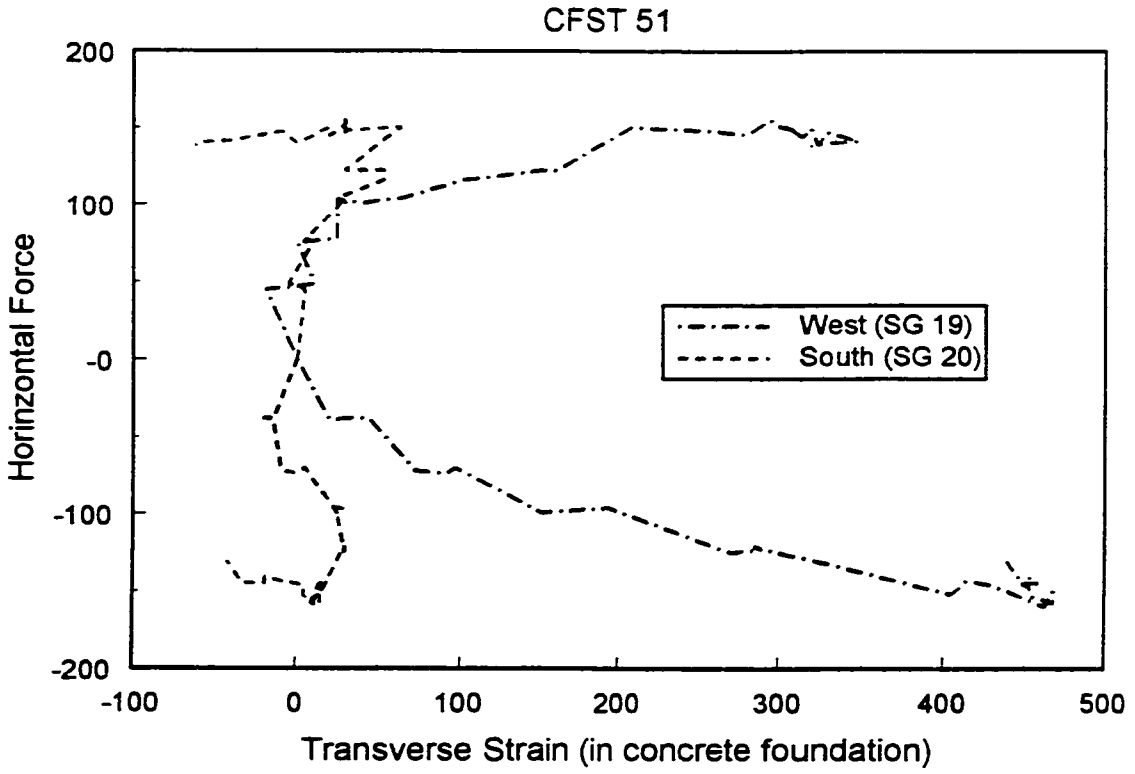

Figure 5.35: Transverse strain on the steel tube encased in concrete on CFST 51

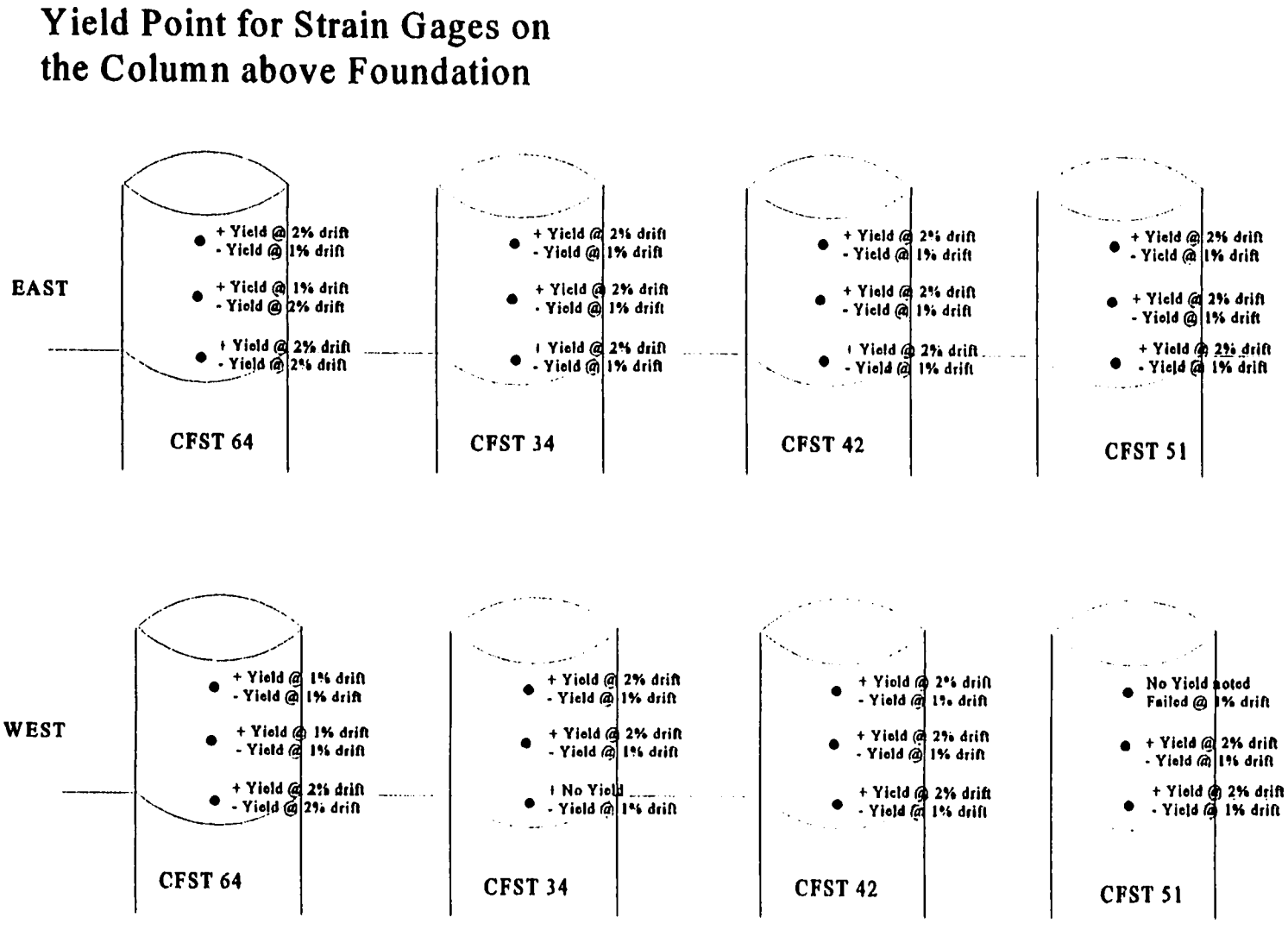

Figure 5.36: Yielding of longitudinal strain gages on the steel tube

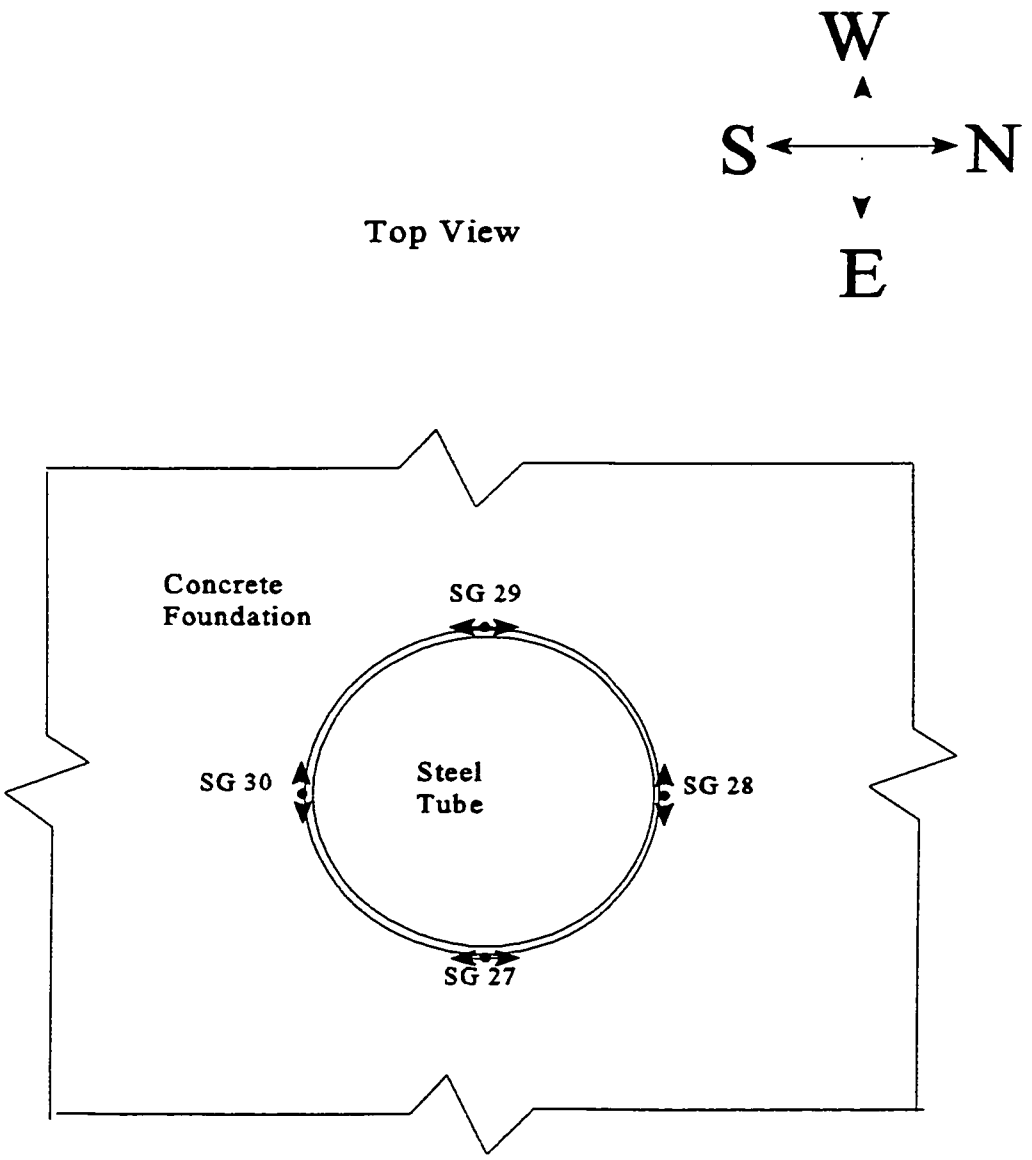

Figure 5.37: Location of transverse strain gages on the steel tube

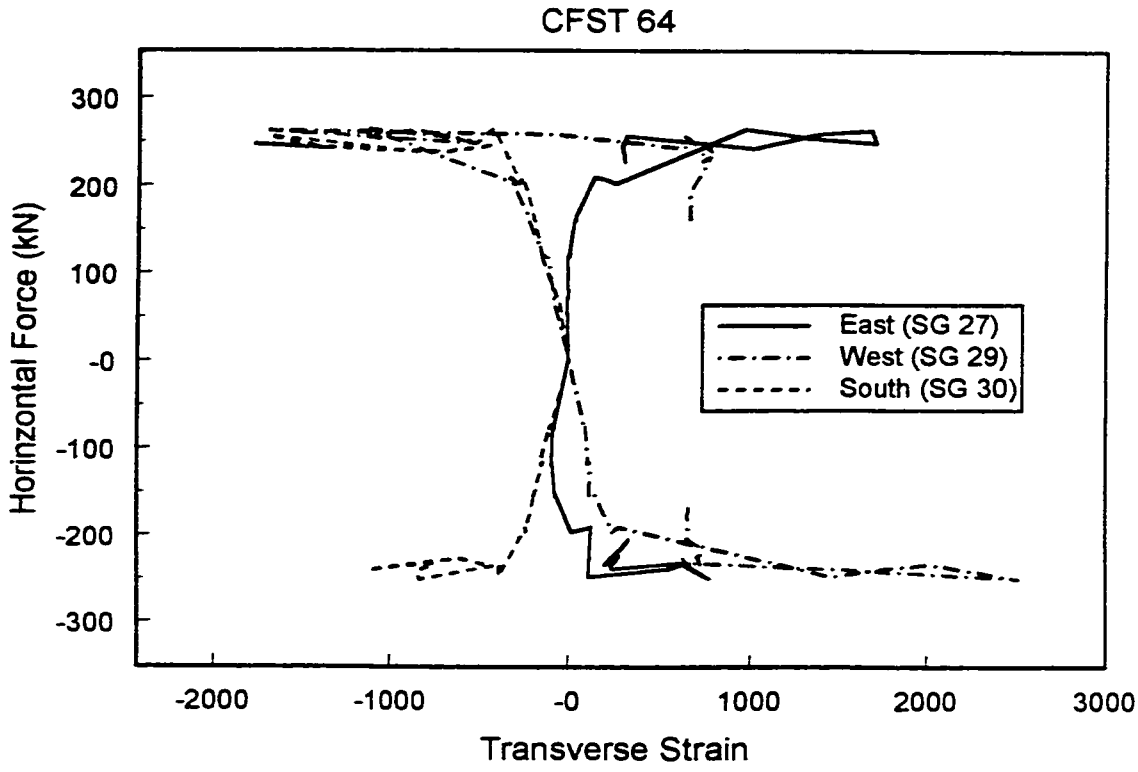

Figure 5.38: Transverse strain on the steel tube above foundation on CFST 64

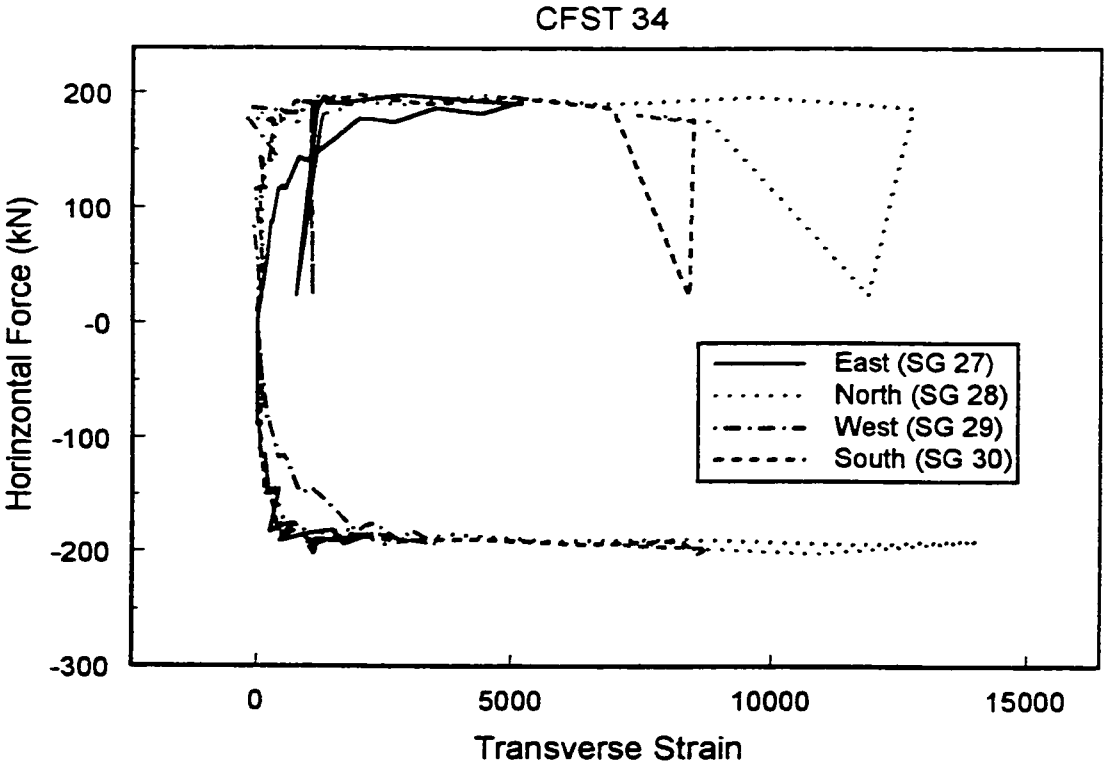

Figure 5.39: Transverse strain on the steel tube above foundation on CFST 34

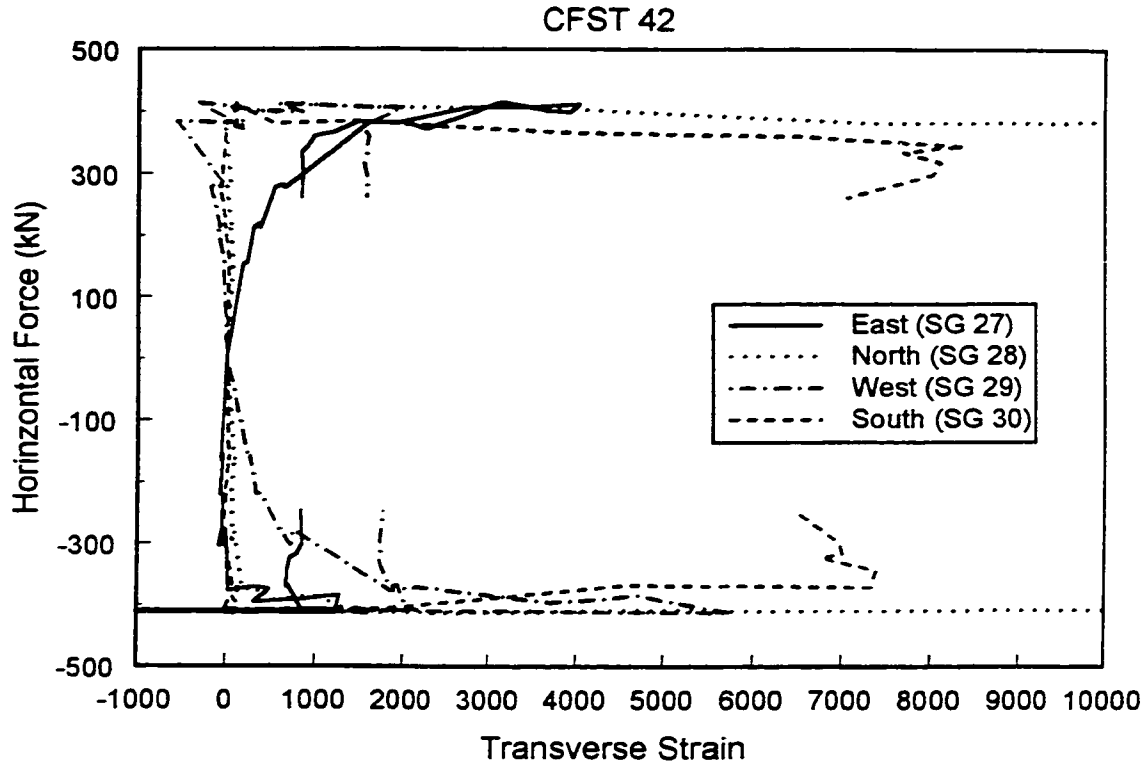

Figure 5.40: Transverse strain on the steel tube above foundation on CFST 42

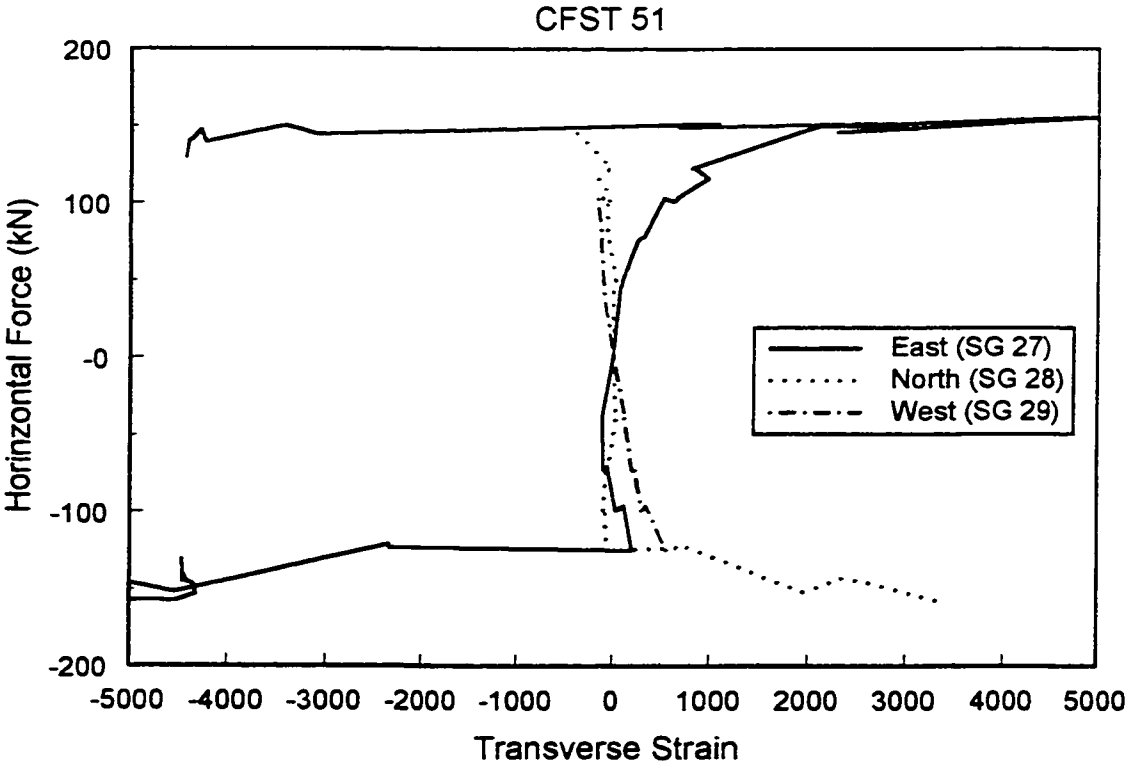

Figure 5.41: Transverse strain on the steel tube above foundation on CFST 51

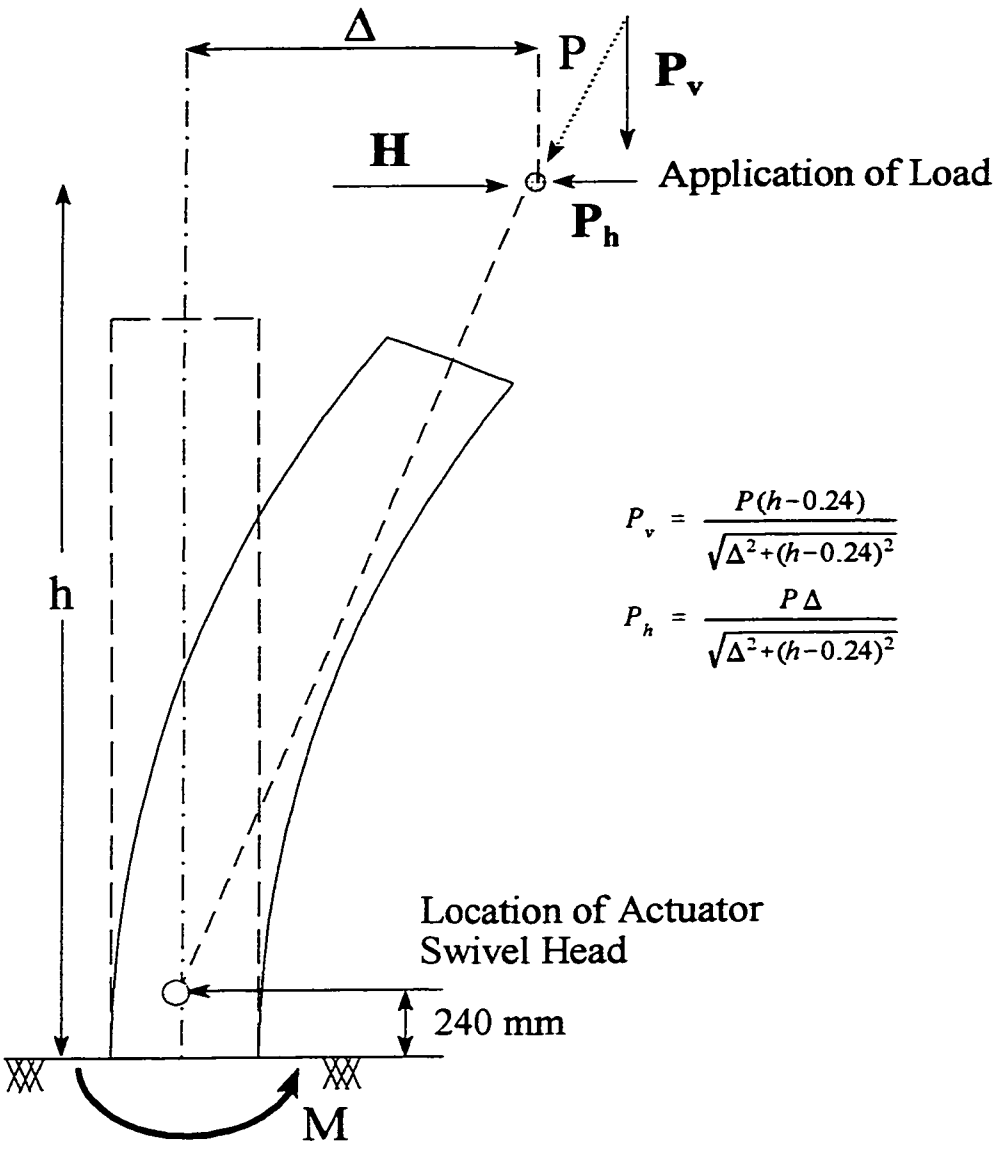

Horizontal Force (H_T) = H -P_h

First Order Moment

$M = H_T h$

First and Second Order Moments

$M = H_T h + P_v \Delta$

Figure 5.42: Illustration of P-Δ effects

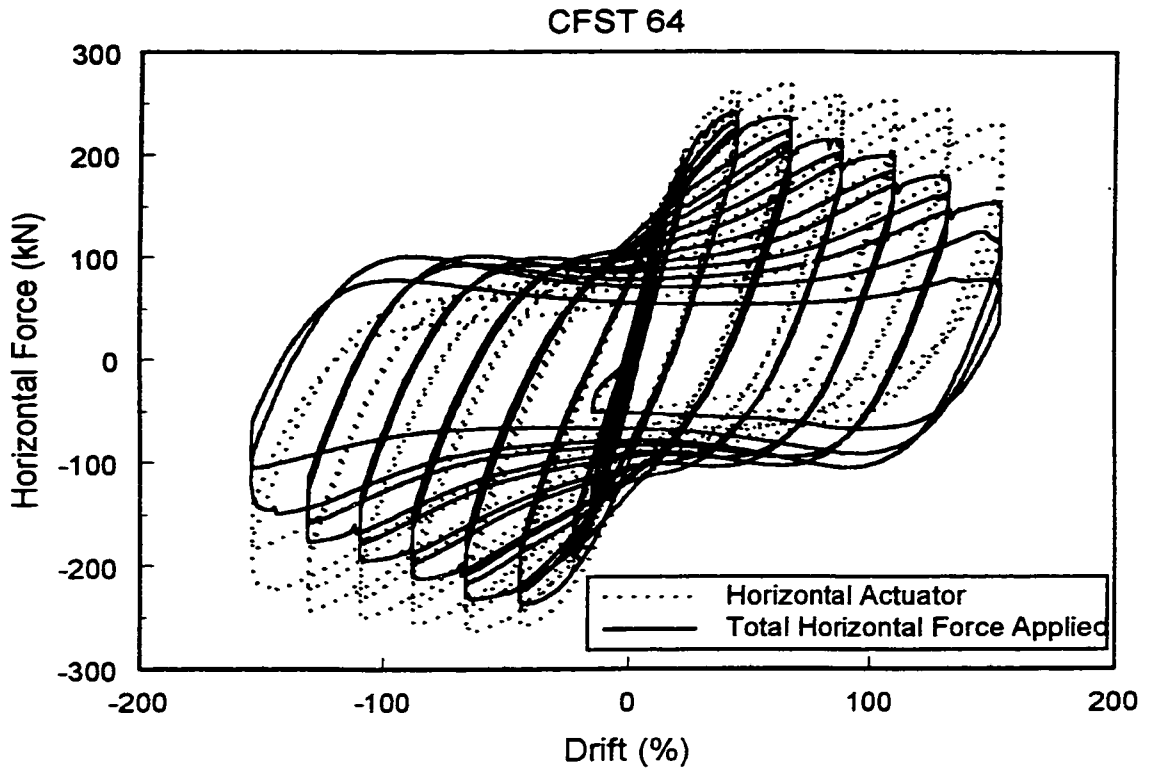

Figure 5.43a: Horizontal actuator and total horizontal force versus drift for CFST 64

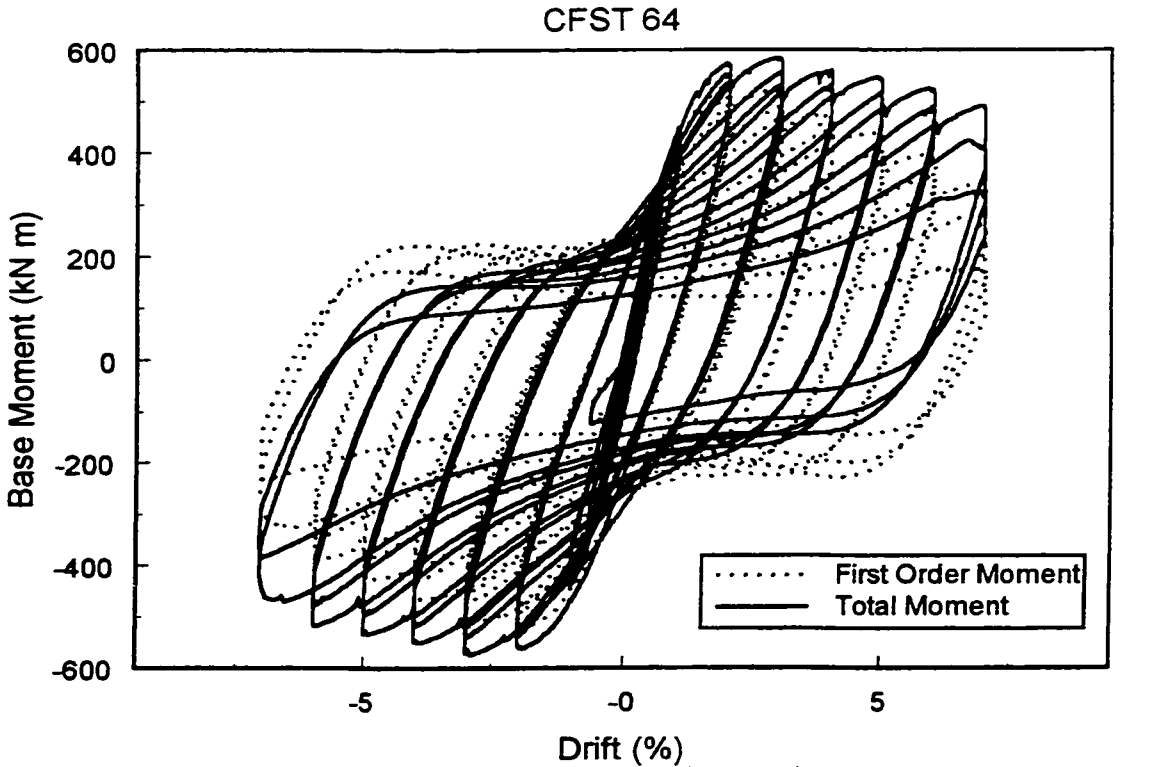

Figure 5.43b: Moment versus drift with and without P-Δ effects for CFST 64

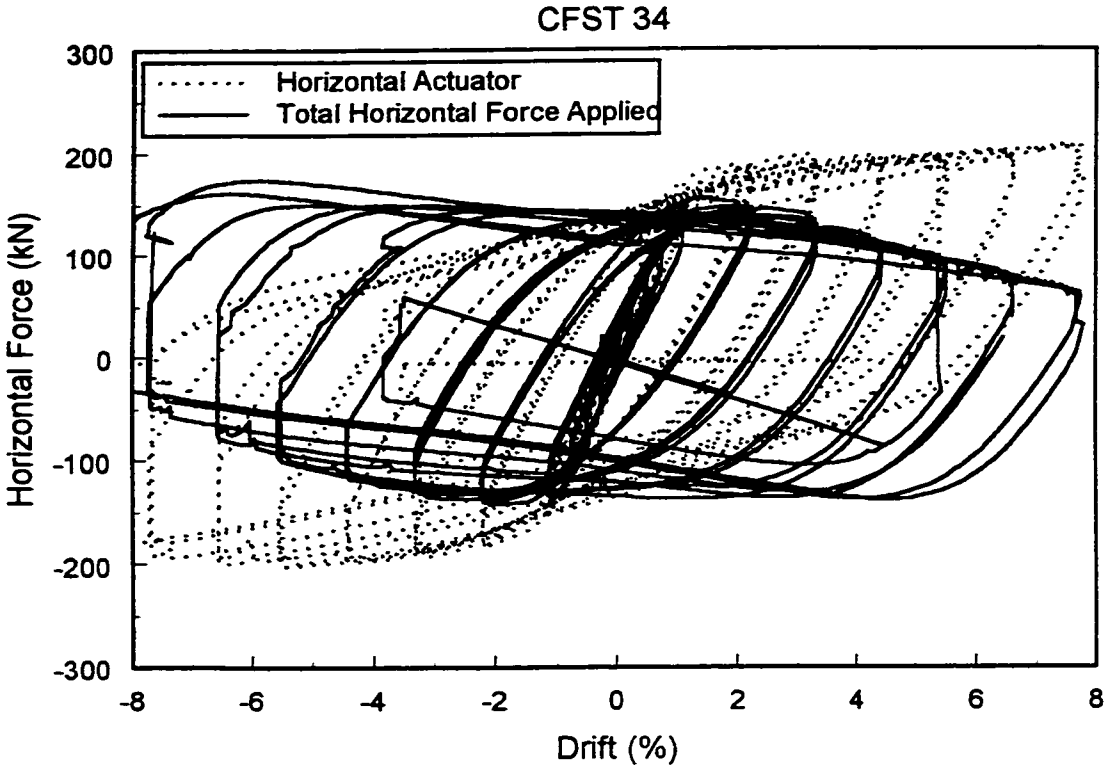

Figure 5.44a: Horizontal actuator and total horizontal force versus drift for CFST 34

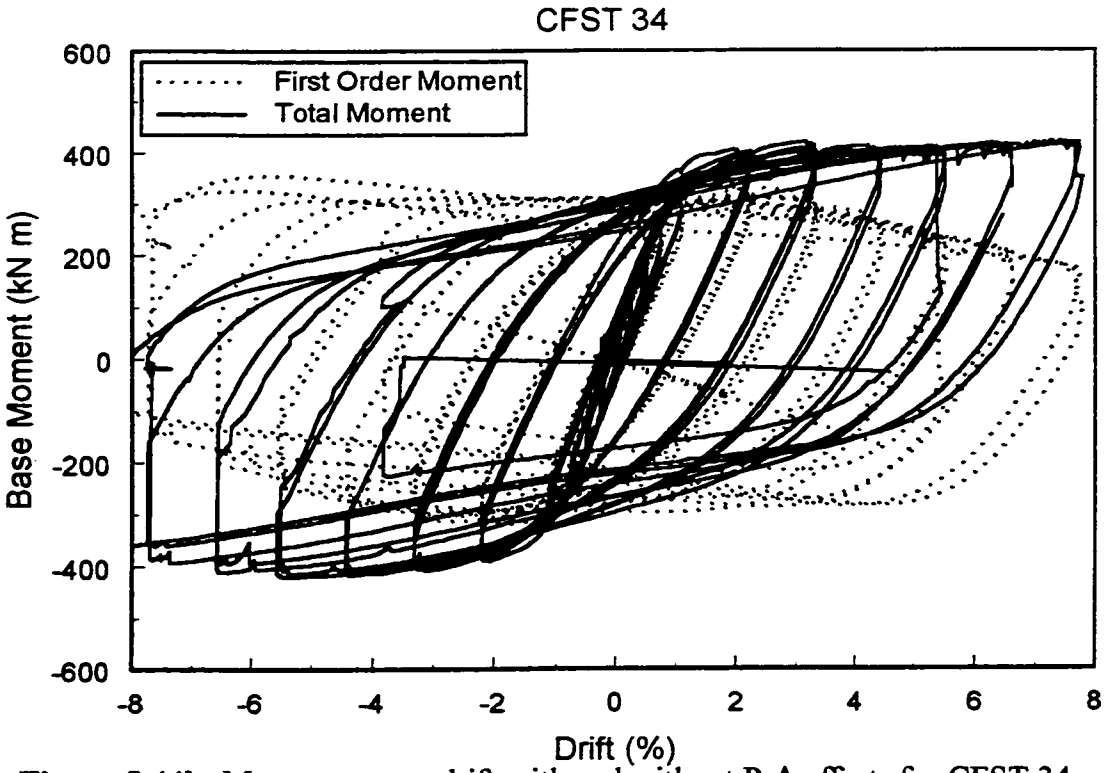

Figure 5.44b: Moment versus drift with and without P-Δ effects for CFST 34

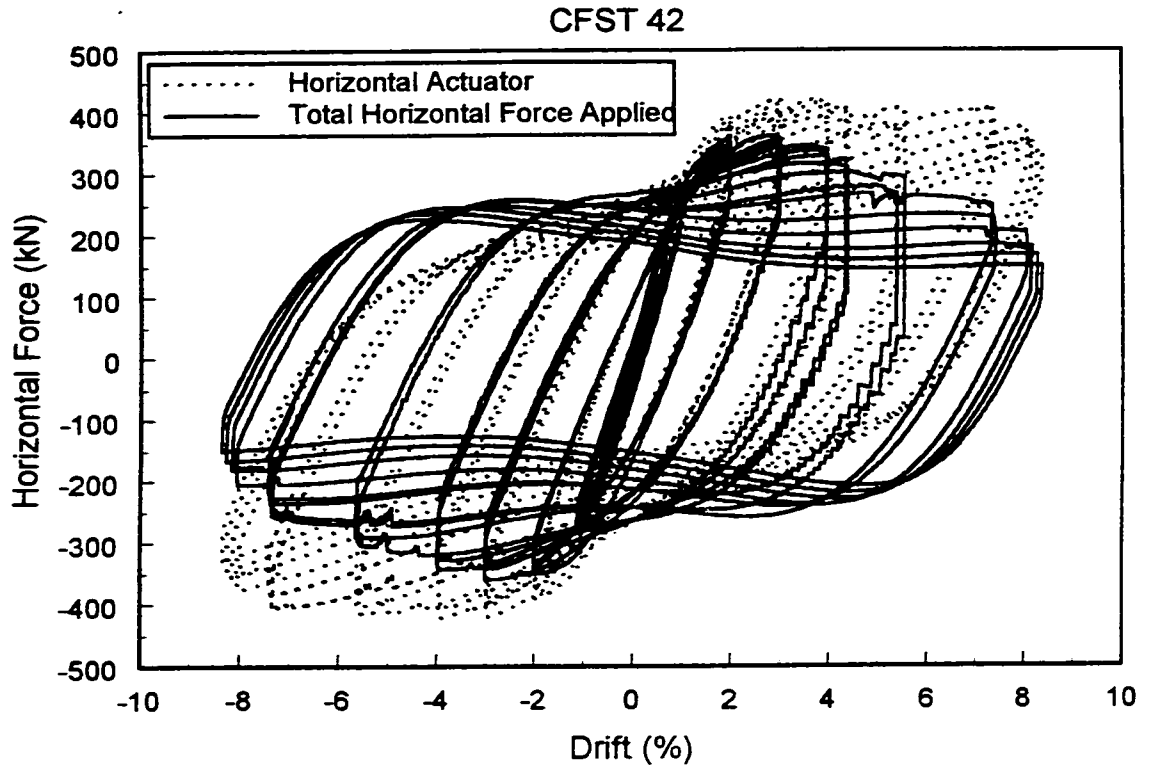

Figure 5.45a: Horizontal actuator and total horizontal force versus drift for CFST 42

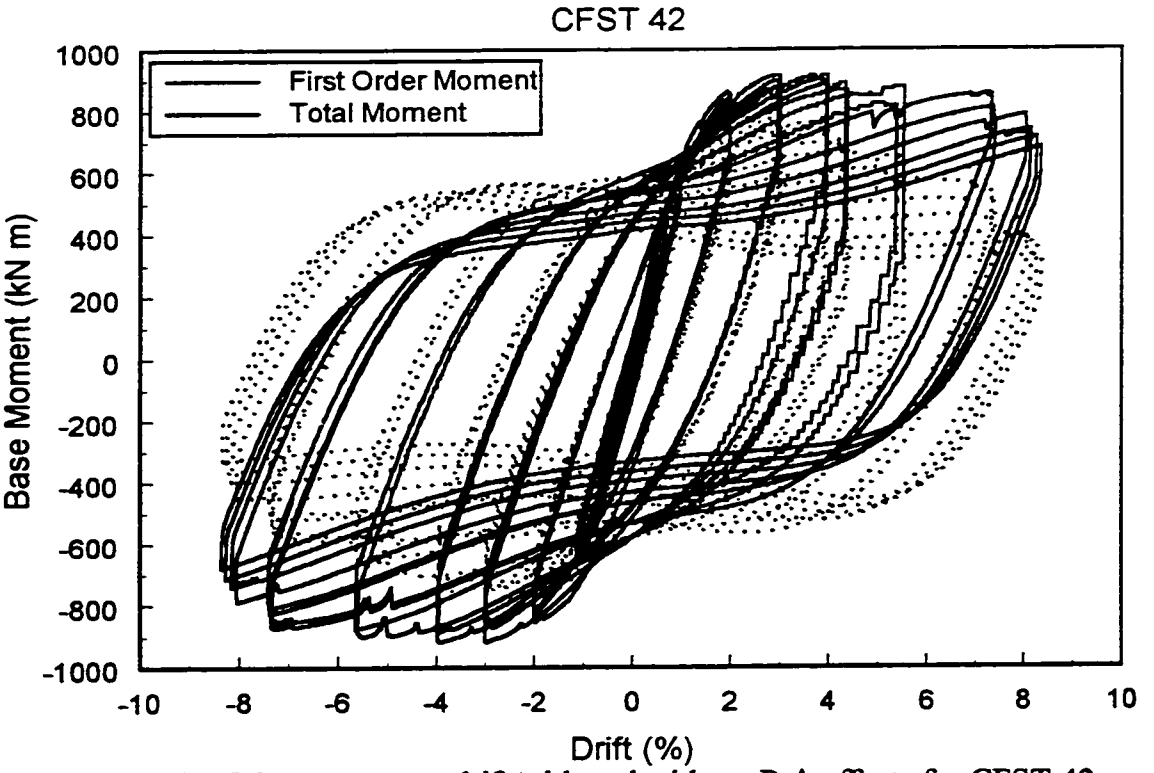

Figure 5.45b: Moment versus drift with and without P-Δ effects for CFST 42

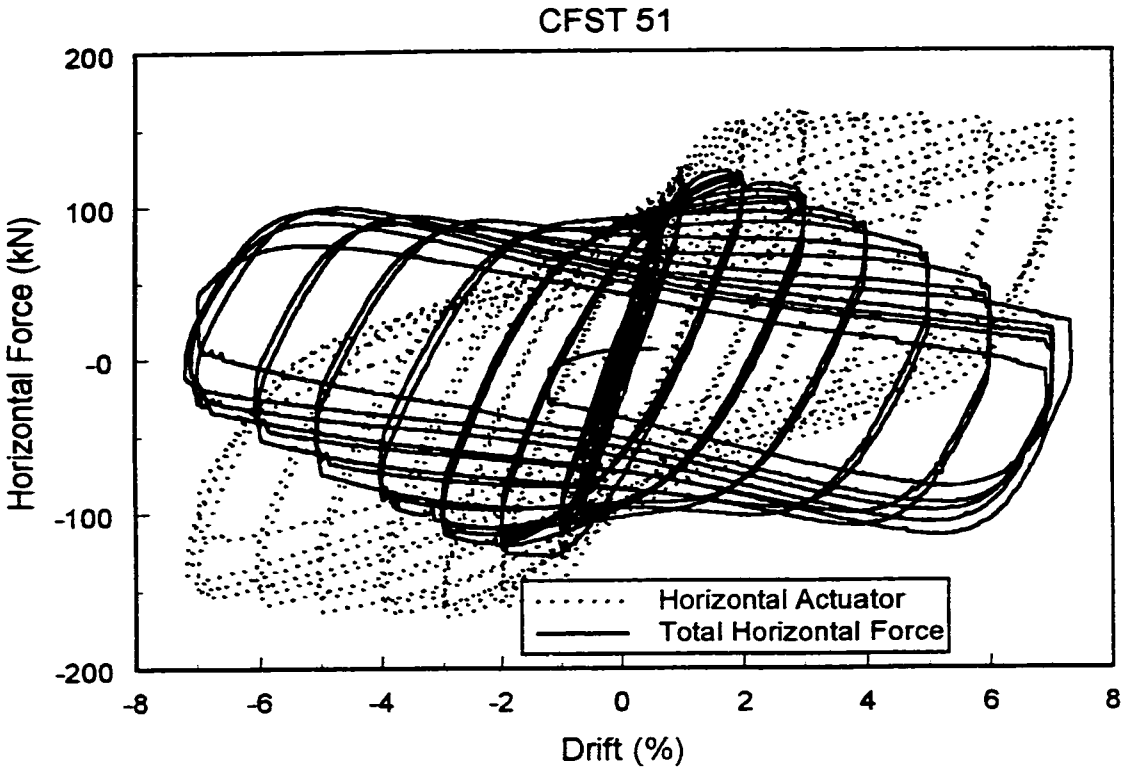

Figure 5.46a: Horizontal actuator and total horizontal force versus drift for CFST 51

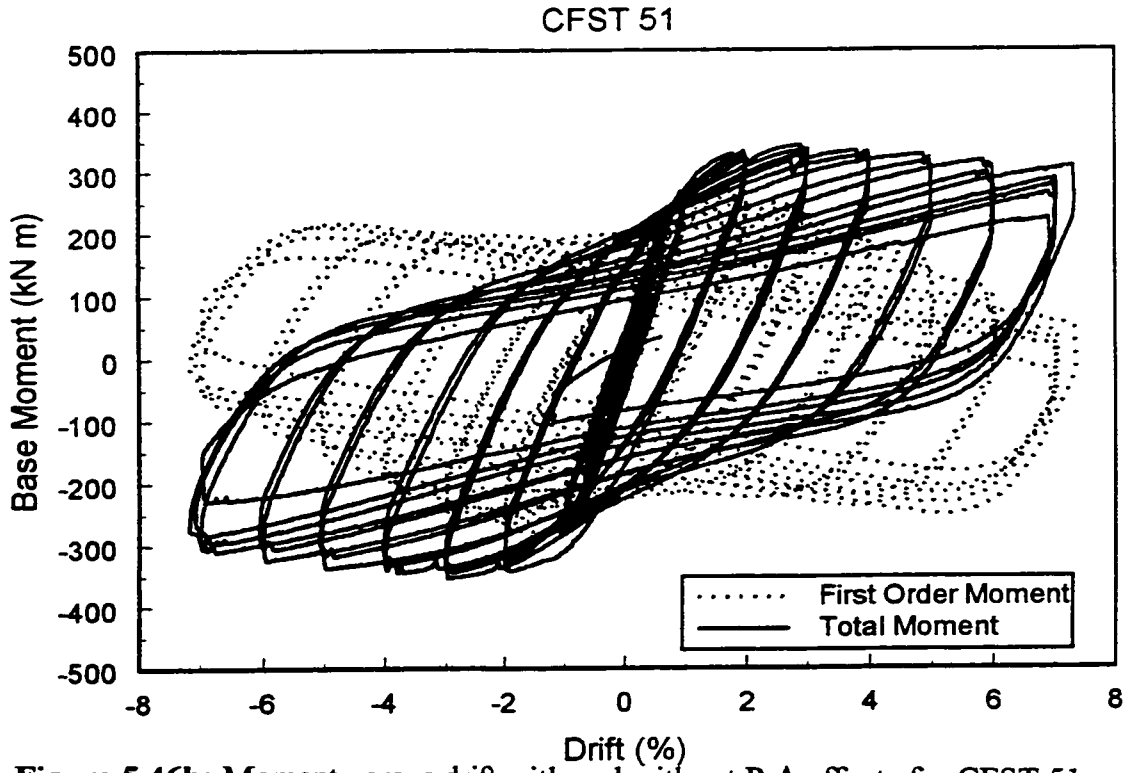

Figure 5.46b: Moment versus drift with and without P-Δ effects for CFST 51

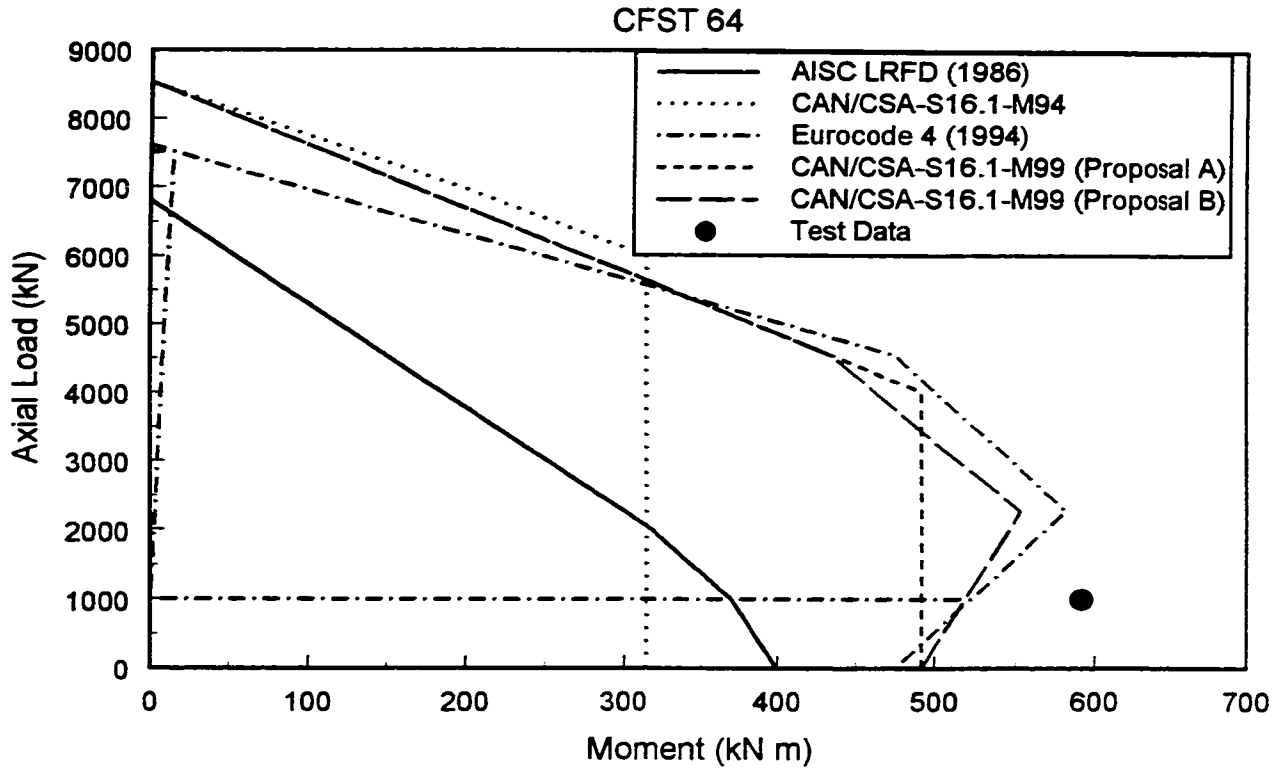

Figure 6.1: Compression and bending interaction curves based on national codes for CFST 64

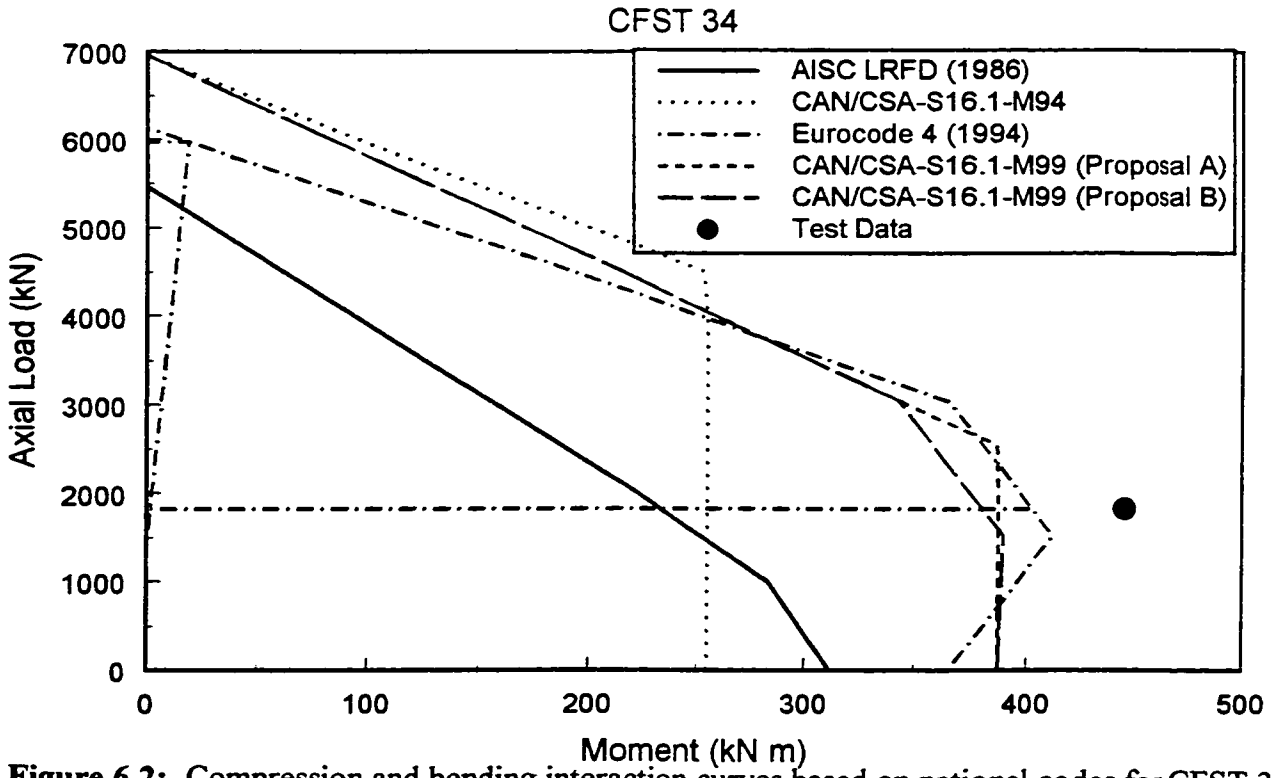

Figure 6.2: Compression and bending interaction curves based on national codes for CFST 34

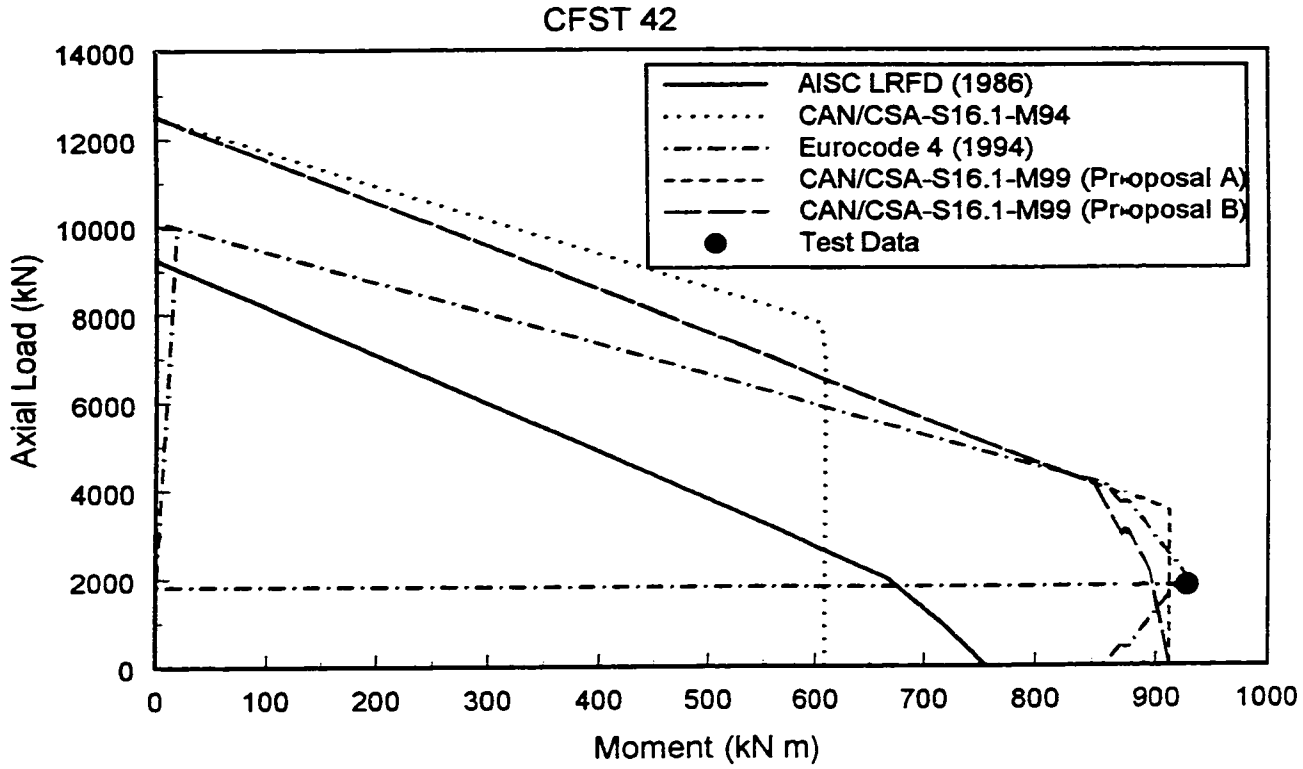

Figure 6.3: Compression and bending interaction curves based on national codes for CFST 42

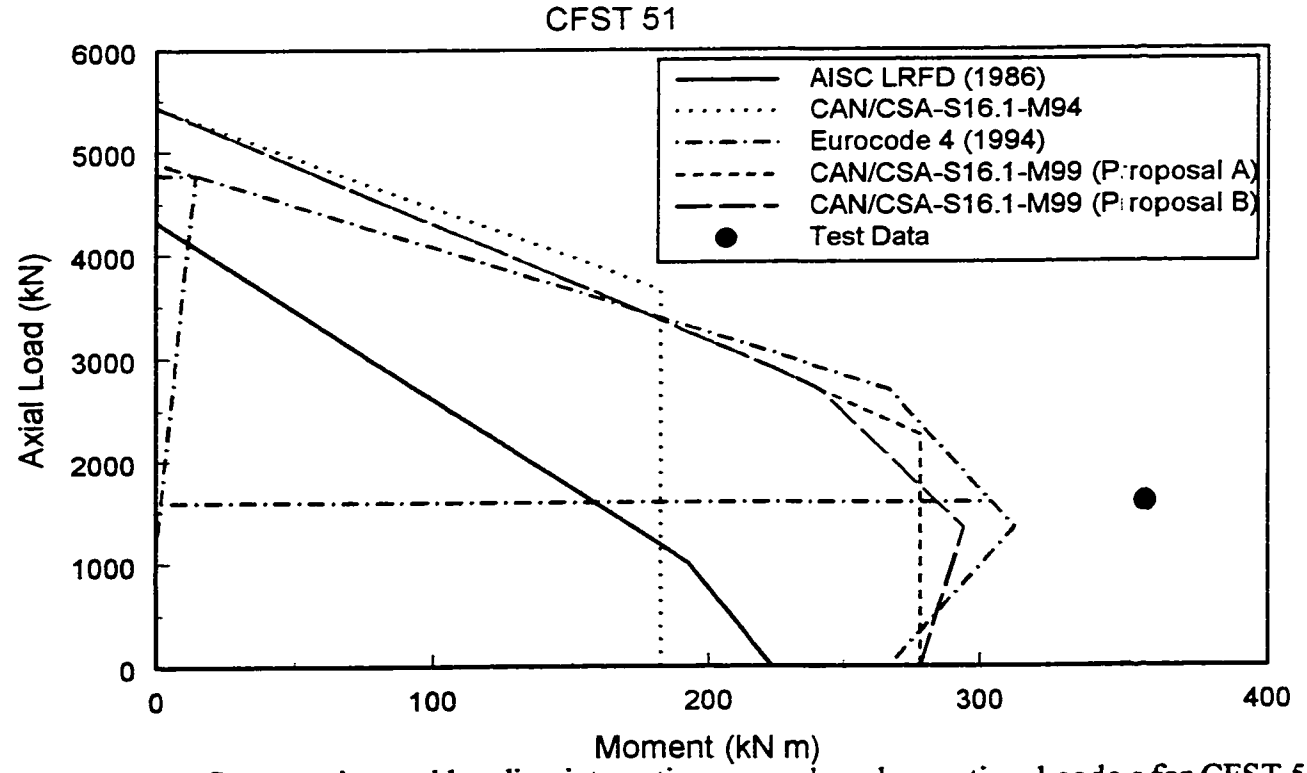

Figure 6.4: Compression and bending interaction curves based on national codes for CFST 51

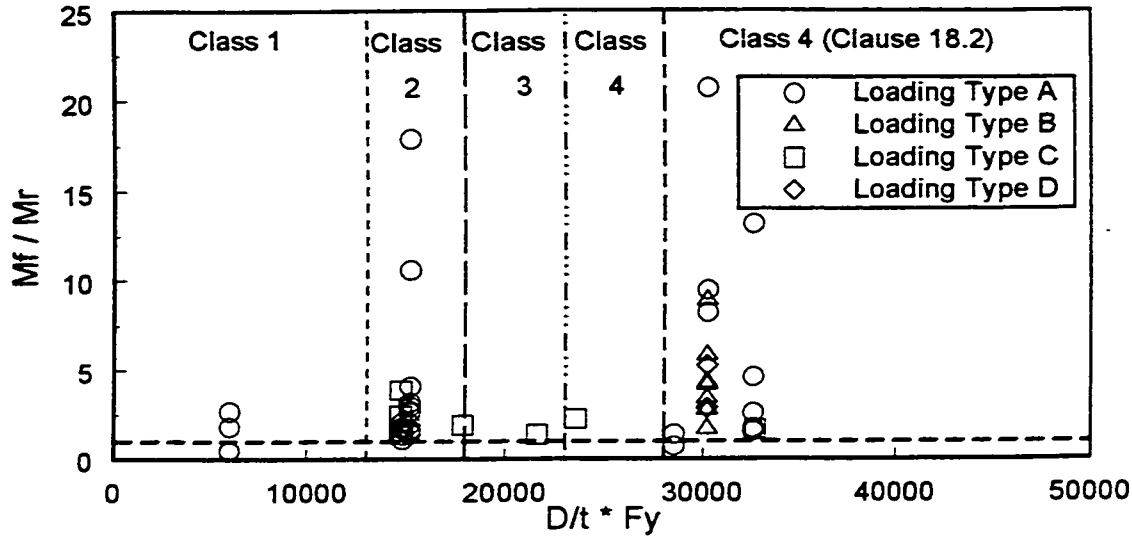

Figure 6.5: Comparison of moment resistance of experimental columns -AISC LRFD (1994)

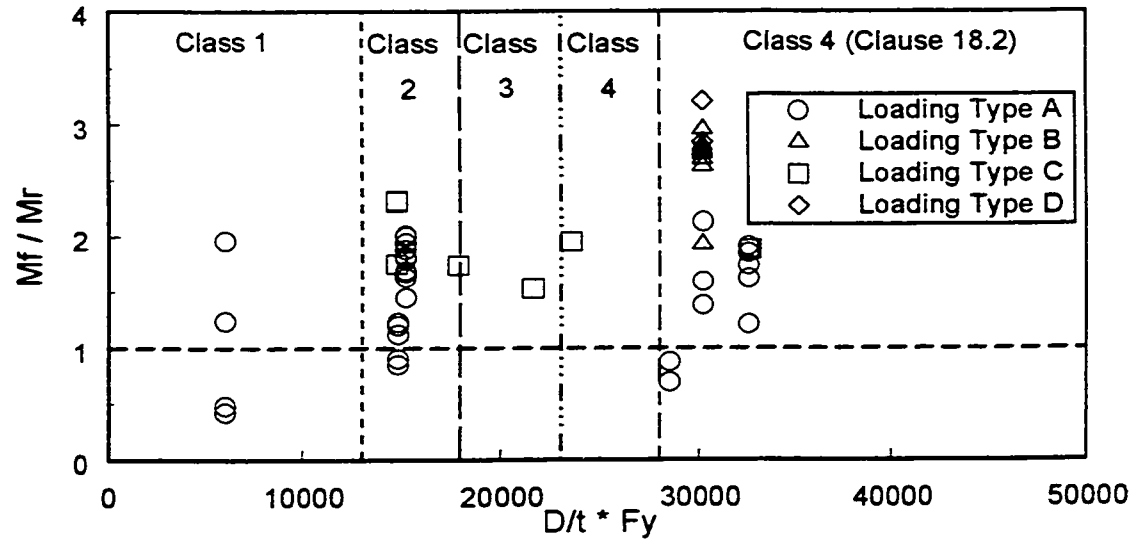

Figure 6.6: Comparison of moment resistance of experimental columns -CAN/CSA-S16.1-M94

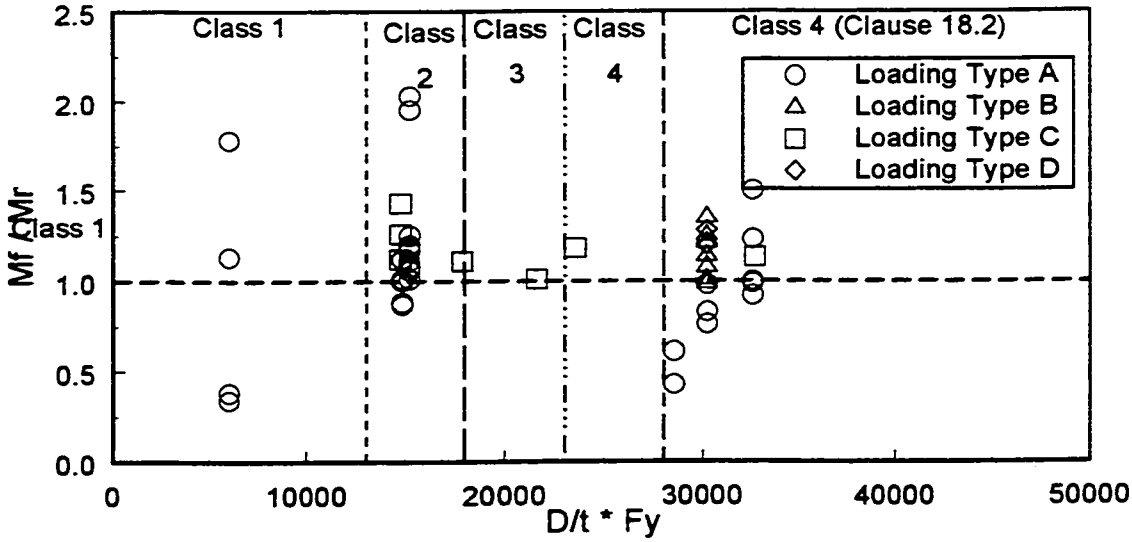

Figure 6.7: Comparison of moment resistance of experimental columns -Eurocode 4 (1994)

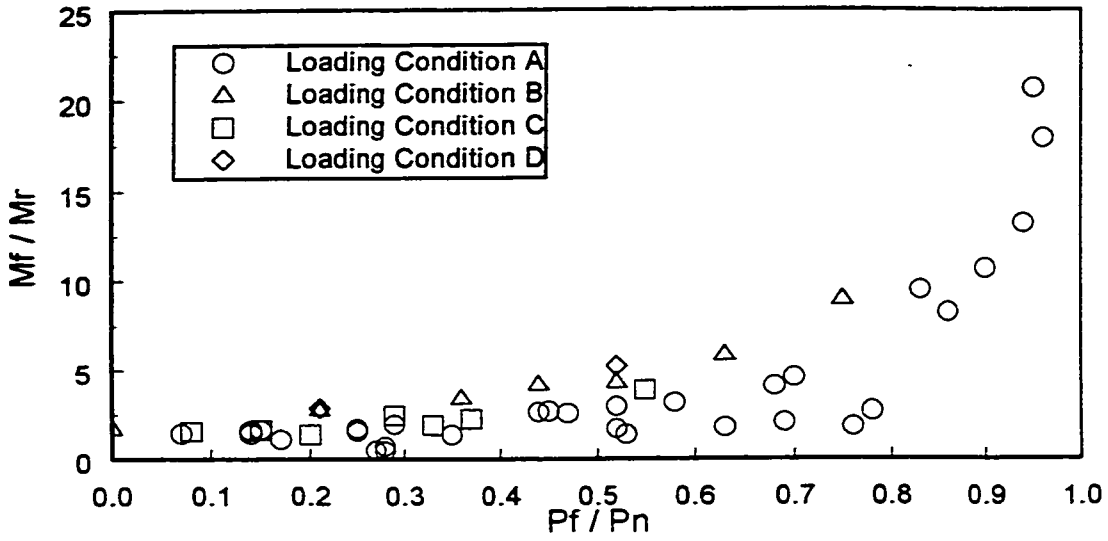

Figure 6.8: Comparison of moment resistance and axial force ratio - AISC LRFD (1994)

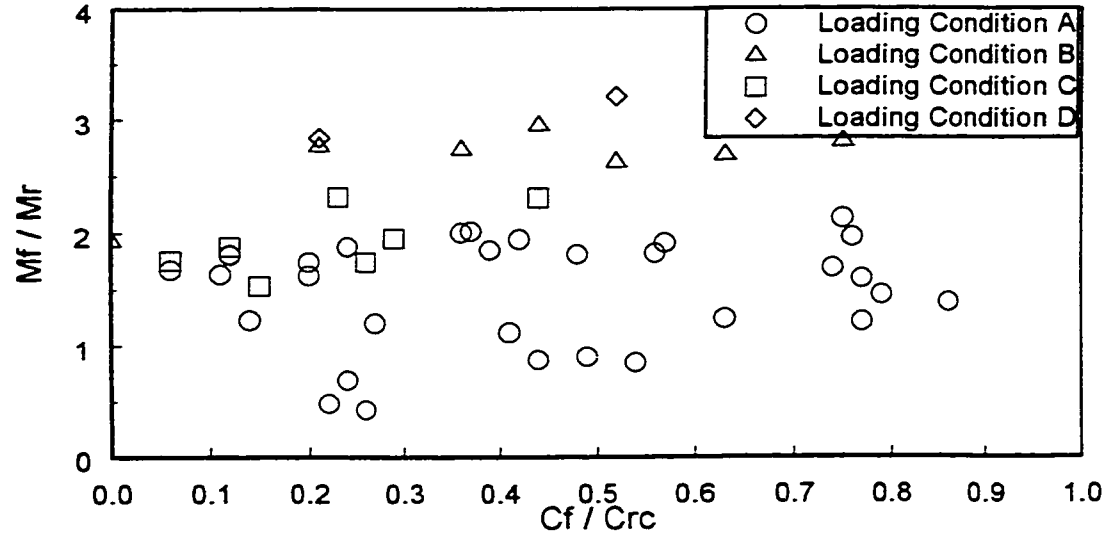

Figure 6.9: Comparison of moment resistance and axial force ratio - CAN/CSA-S16.1-M94

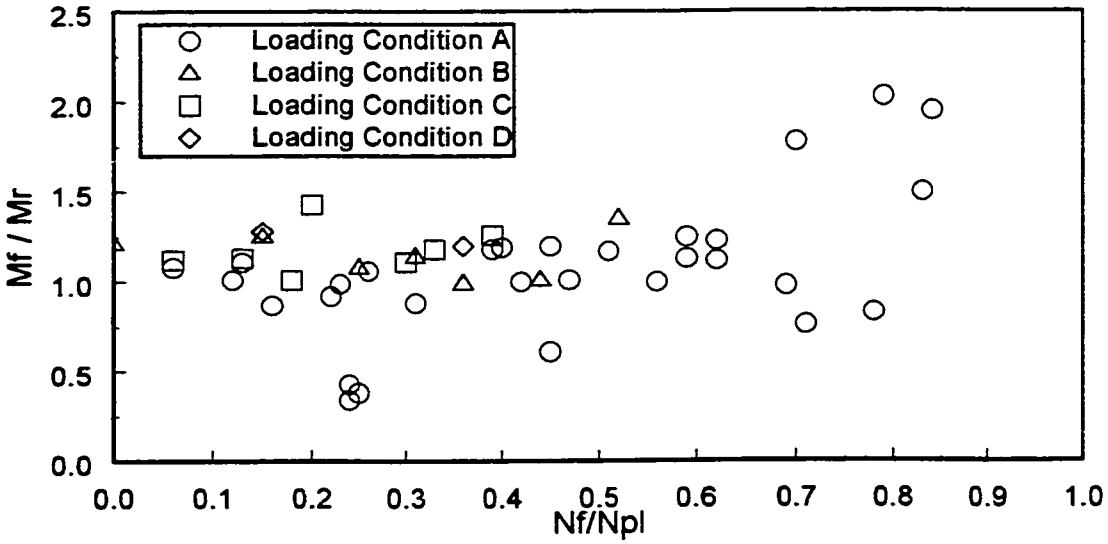

Figure 6.10: Comparison of moment resistance and axial force ratio - Eurocode 4 (1994)

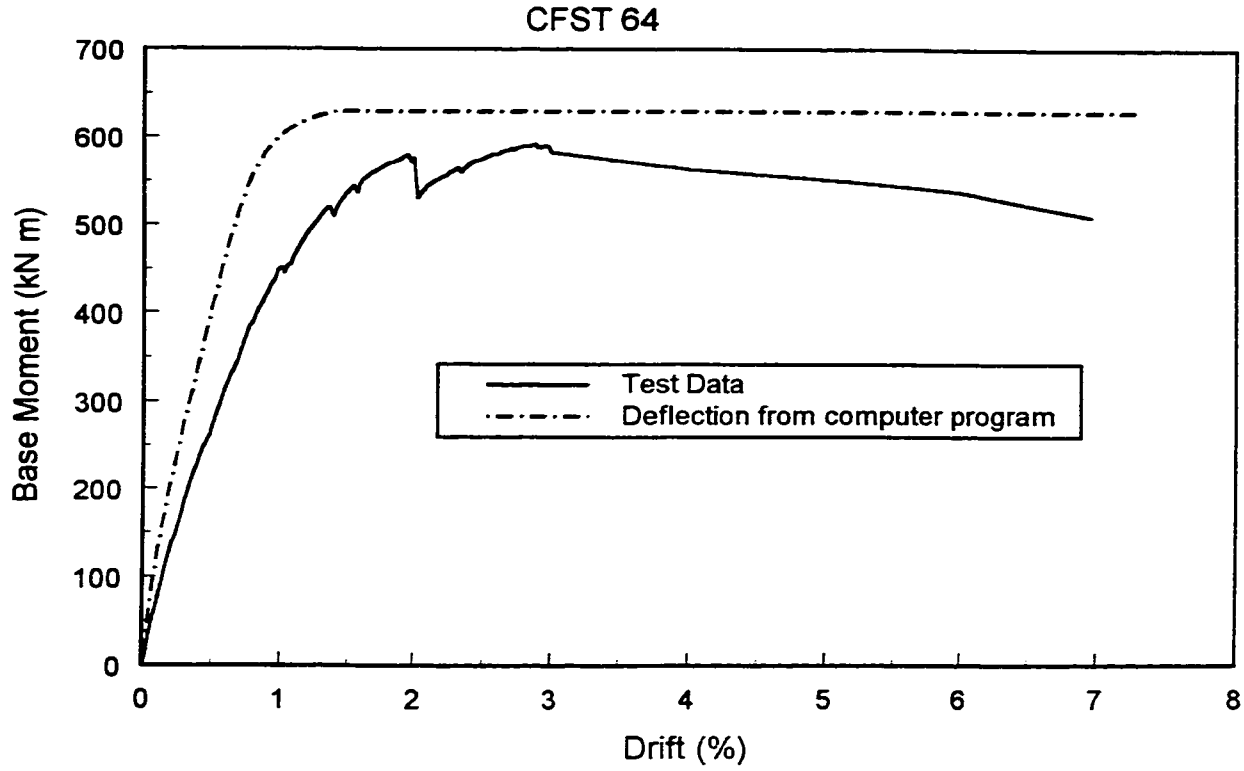

Figure 6.11: Experimental and computer program moment drift envelope for CFST 64

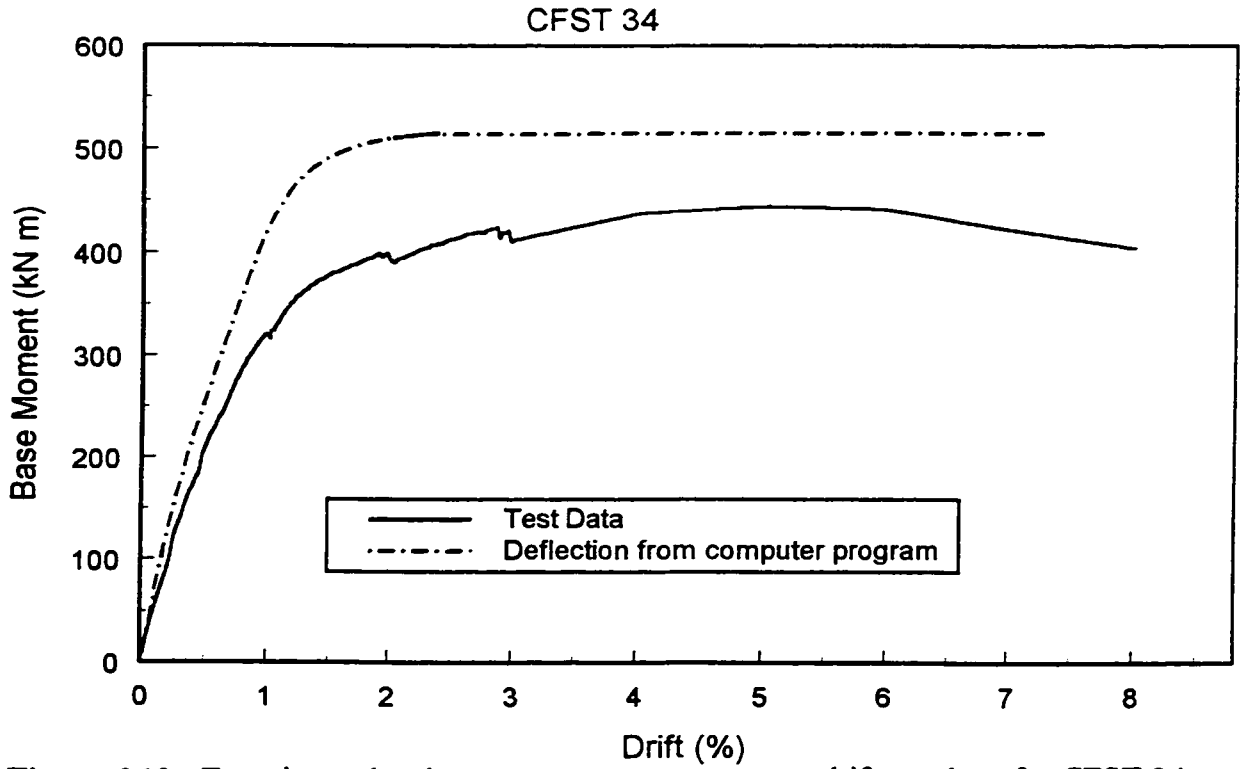

Figure 6.12: Experimental and computer program moment drift envelope for CFST 34

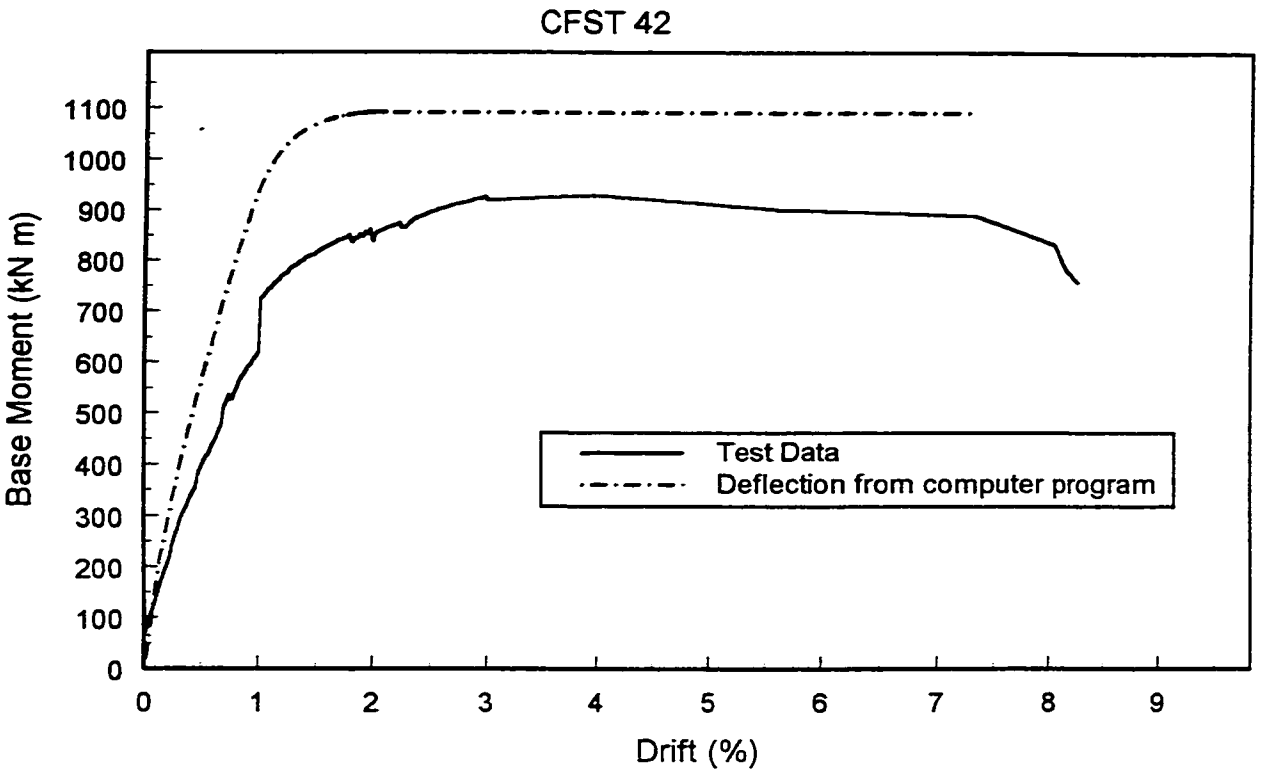

Figure 6.13: Experimental and computer program moment drift envelope for CFST 42

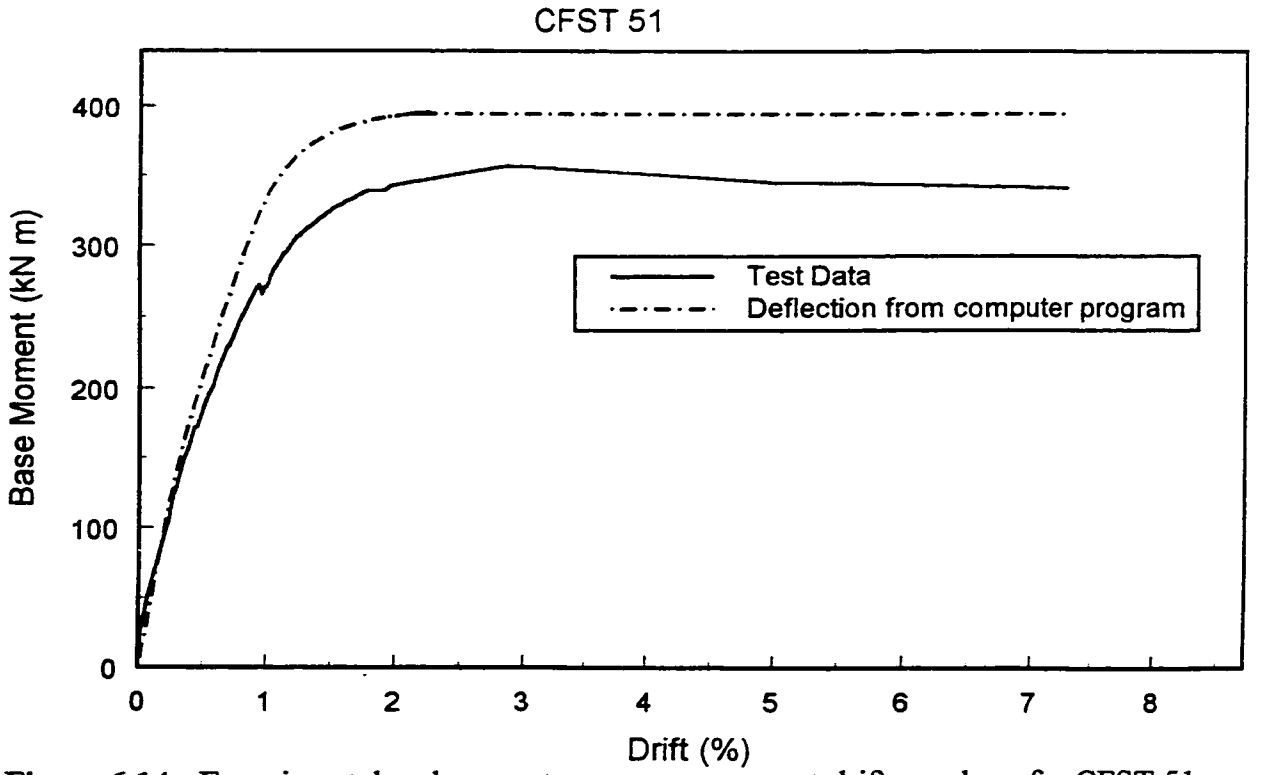

Figure 6.14: Experimental and computer program moment drift envelope for CFST 51

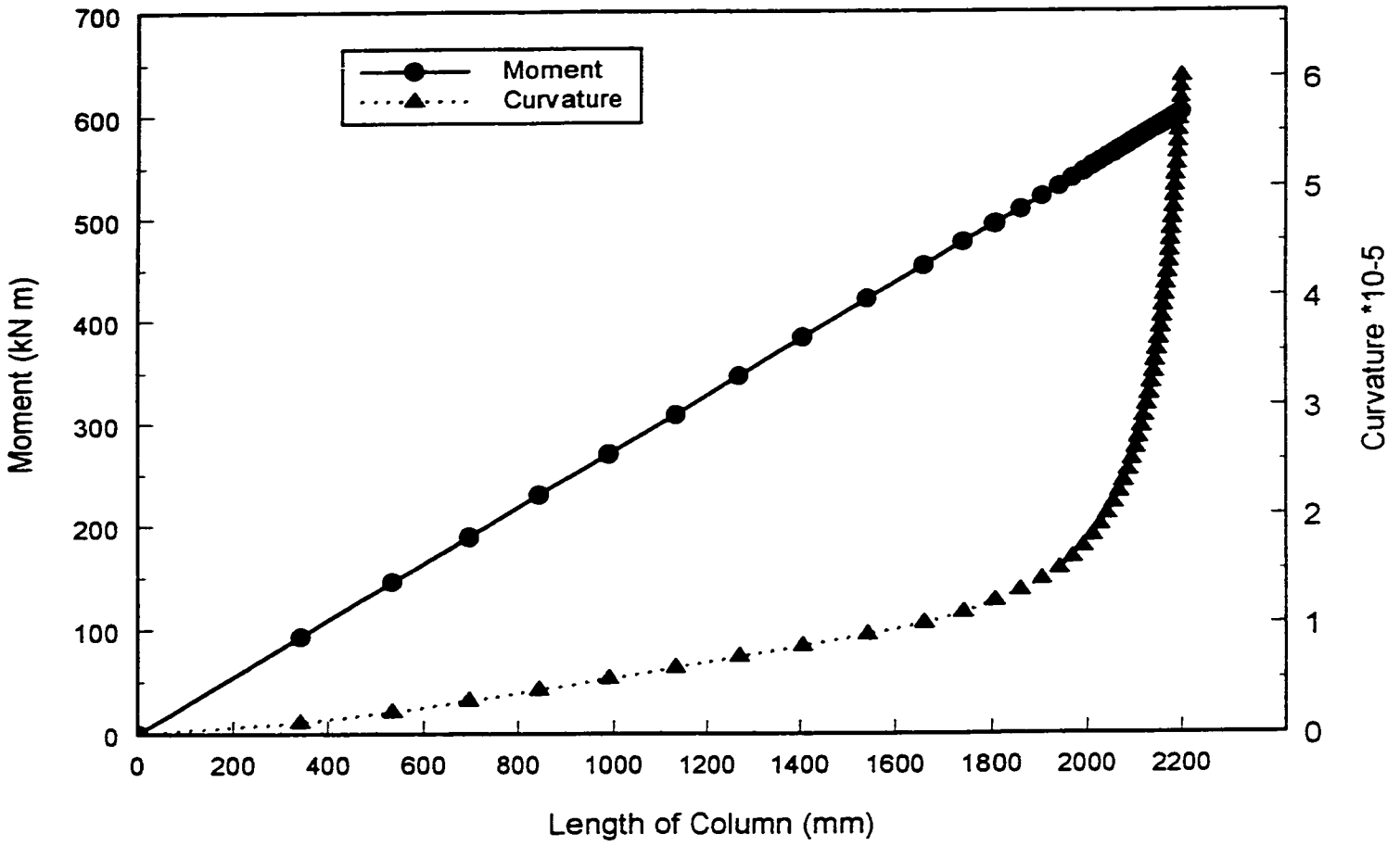

Figure 6.15: Variation of moment and curvature along the length of the column ($\phi = 0.0006$)

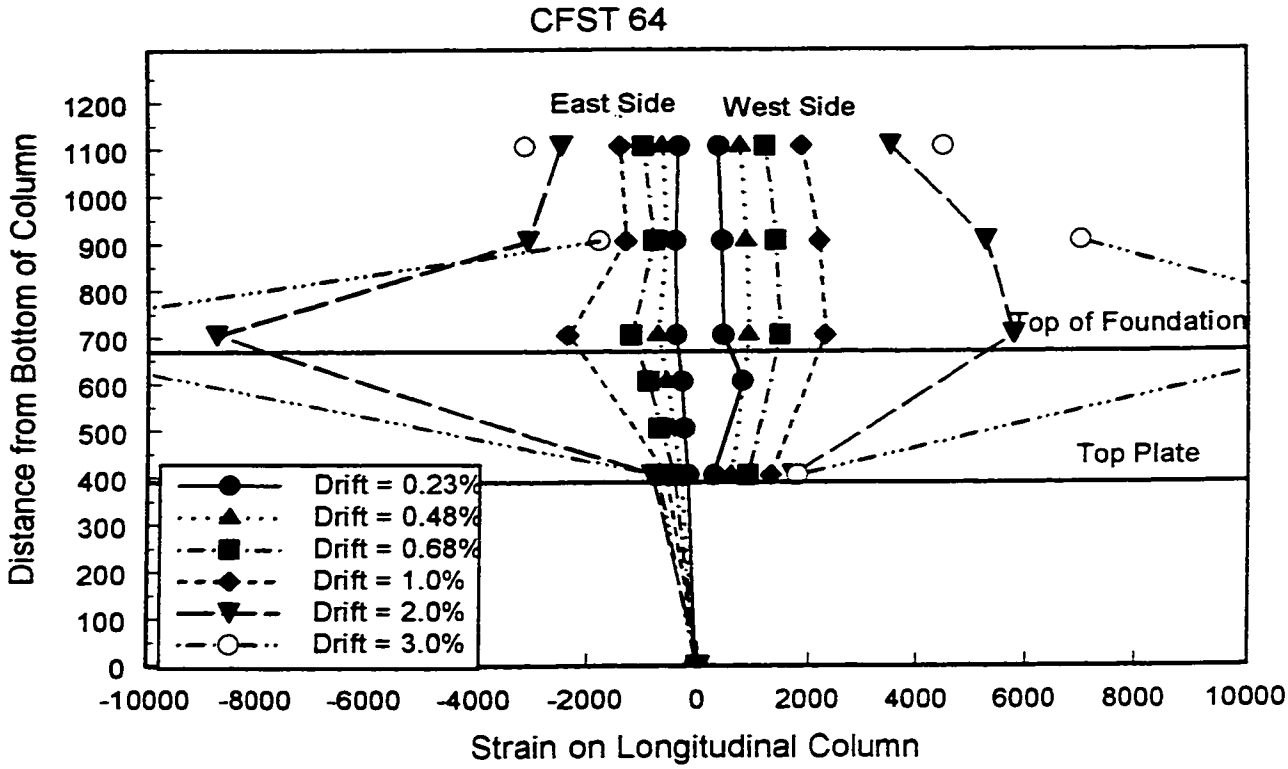

Figure 6.16: Strain distribution along steel tube for positive force for CFST 64

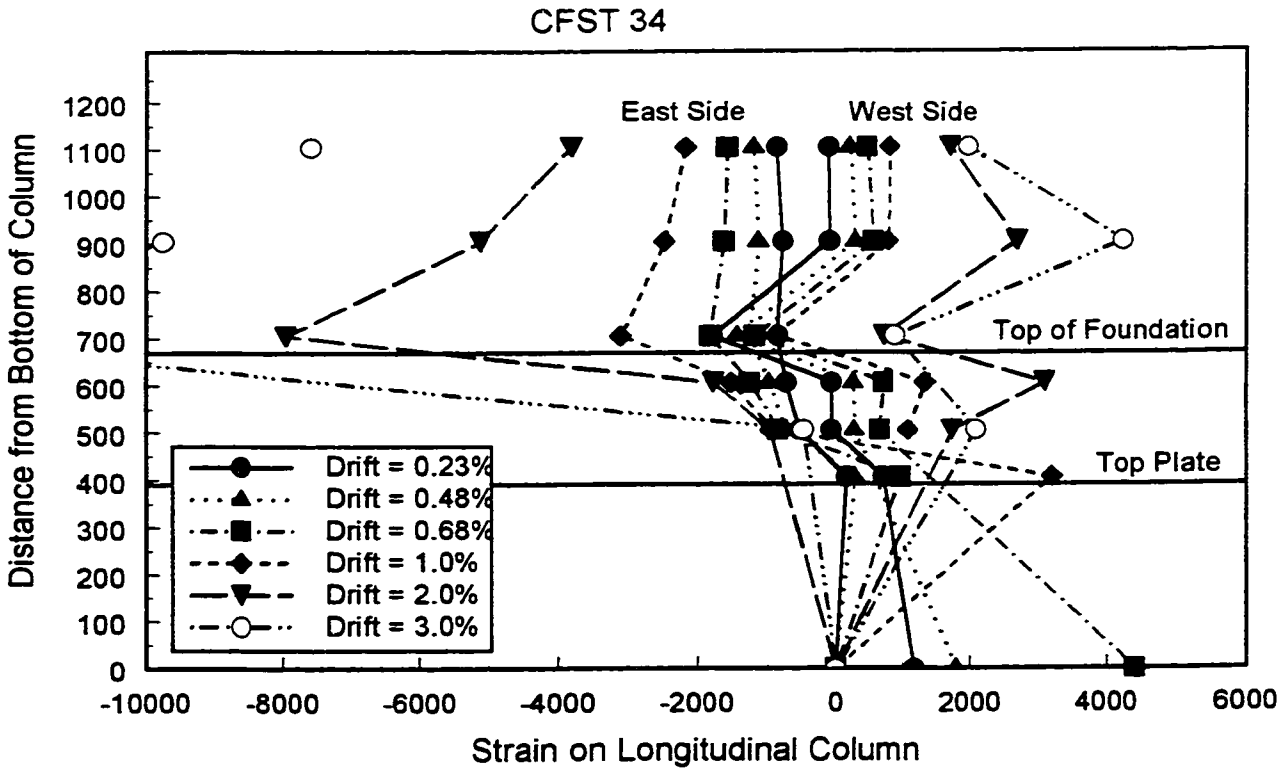

Figure 6.17: Strain distribution along steel tube for positive force for CFST 34

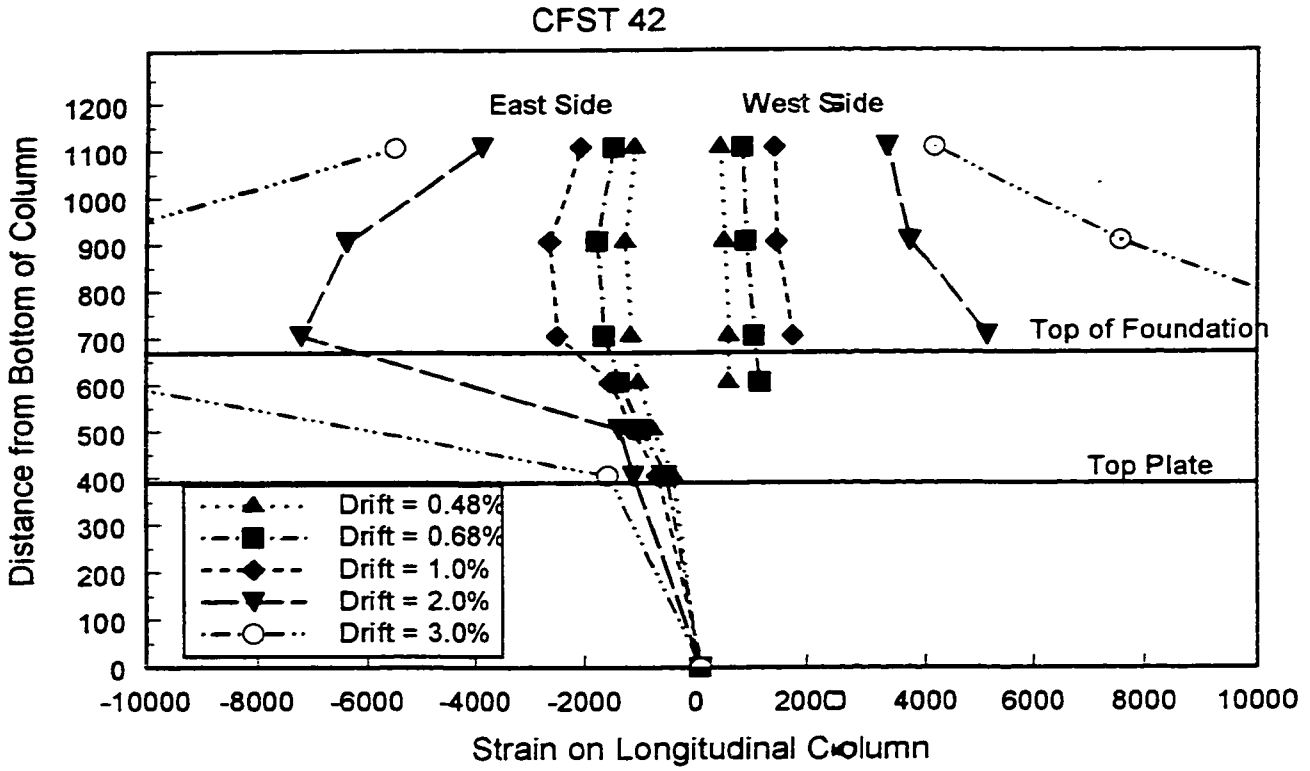

Figure 6.18: Strain distribution along steel tube for positive force for CFST 42

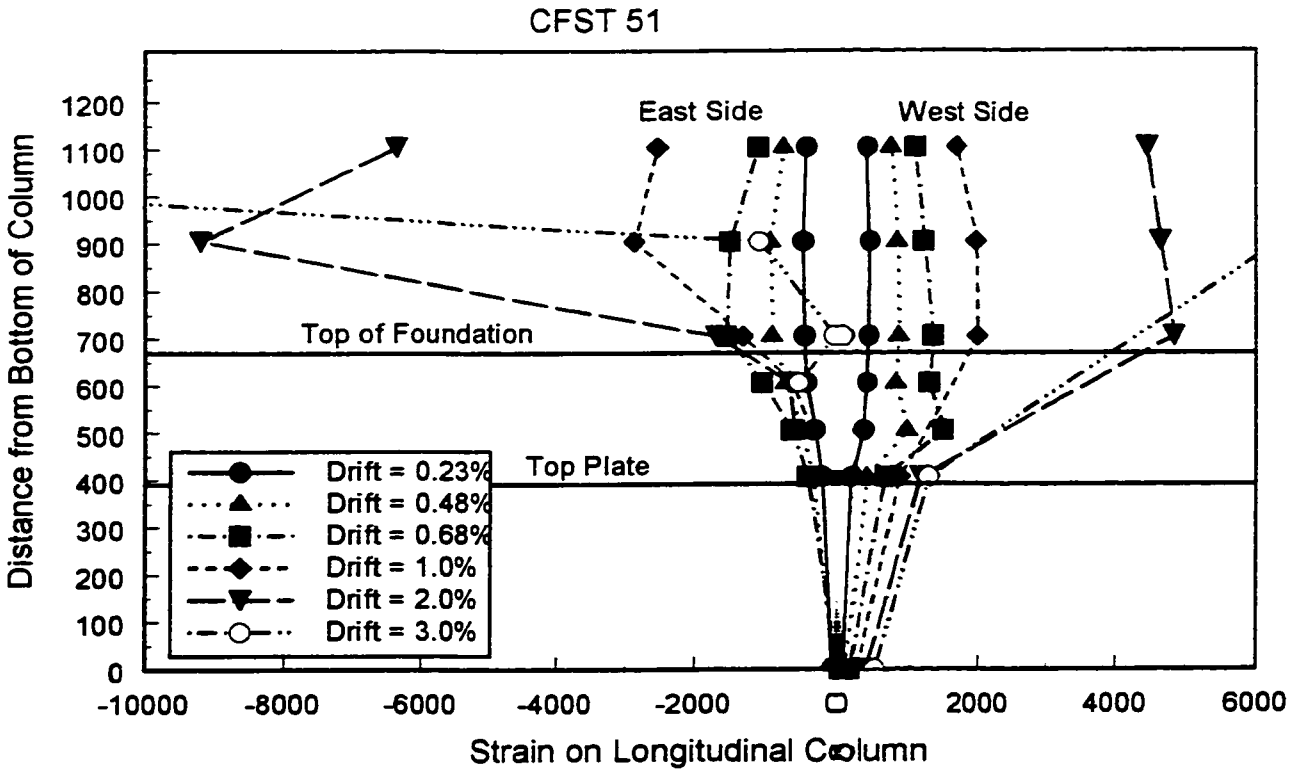

Figure 6.19: Strain distribution along steel tube for positive force for CFST 51

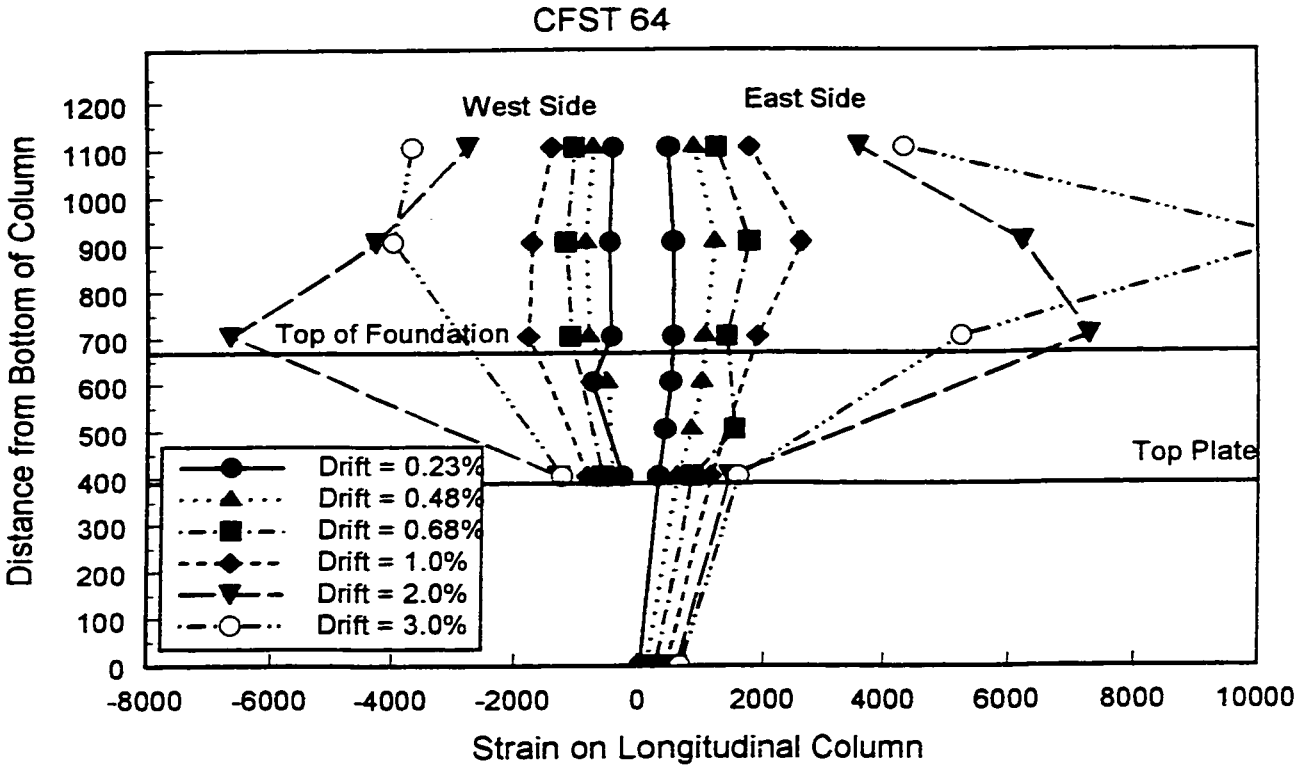

Figure 6.20: Strain distribution along steel tube for negative force for CFST 64

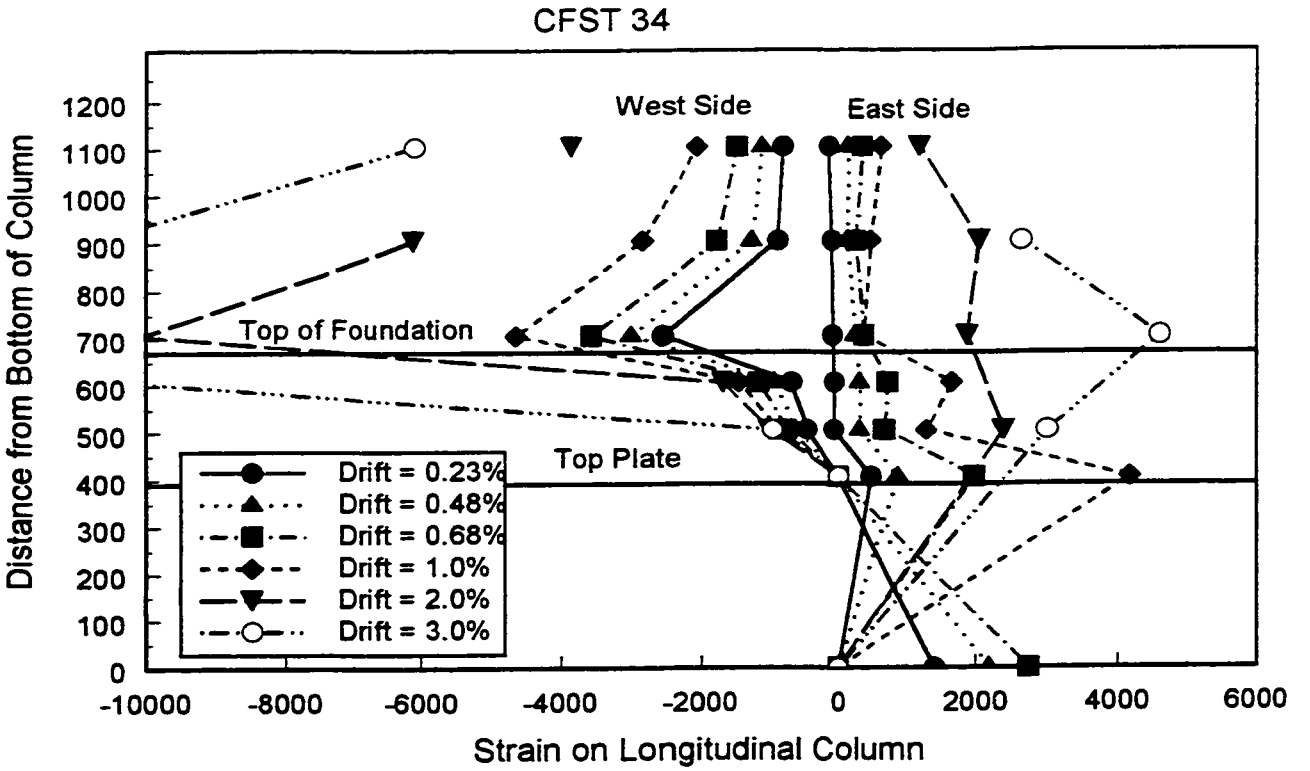

Figure 6.21: Strain distribution along steel tube for negative force for CFST 34

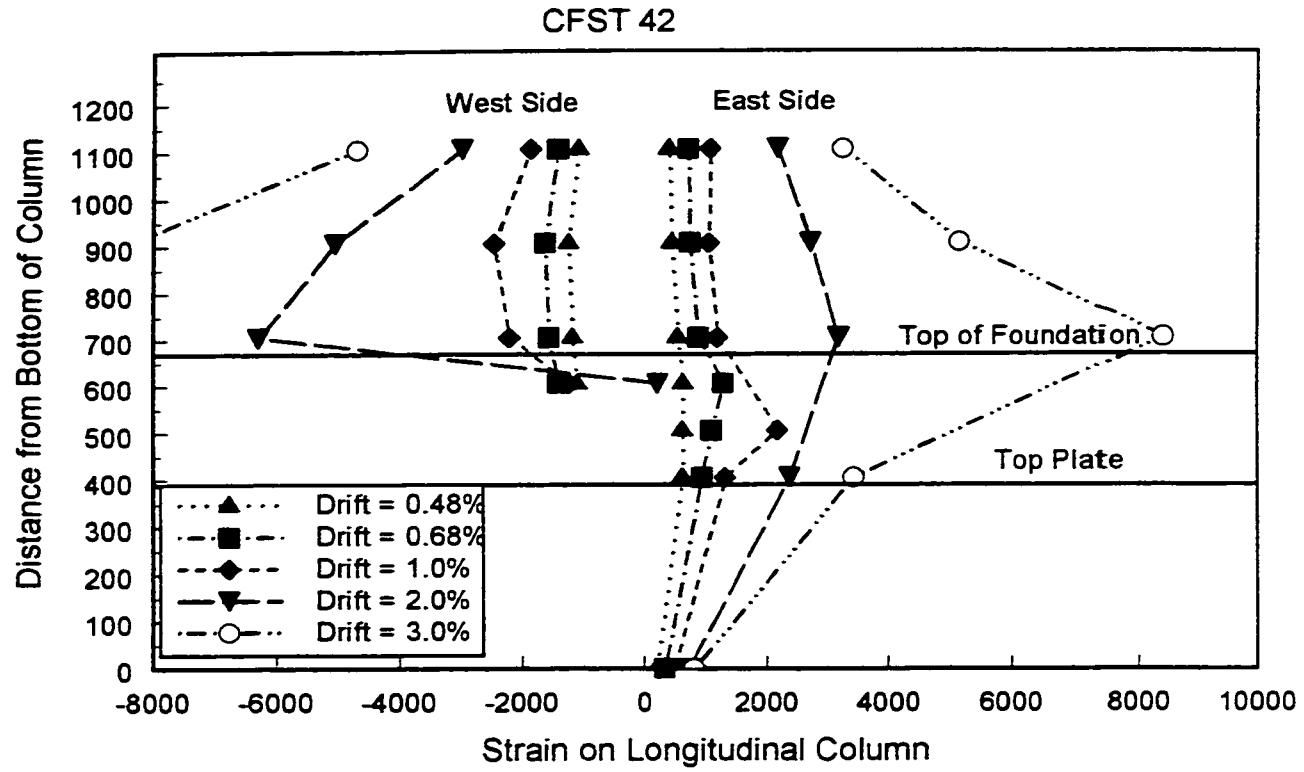

Figure 6.22: Strain distribution along steel tube for negative force for CFST 42

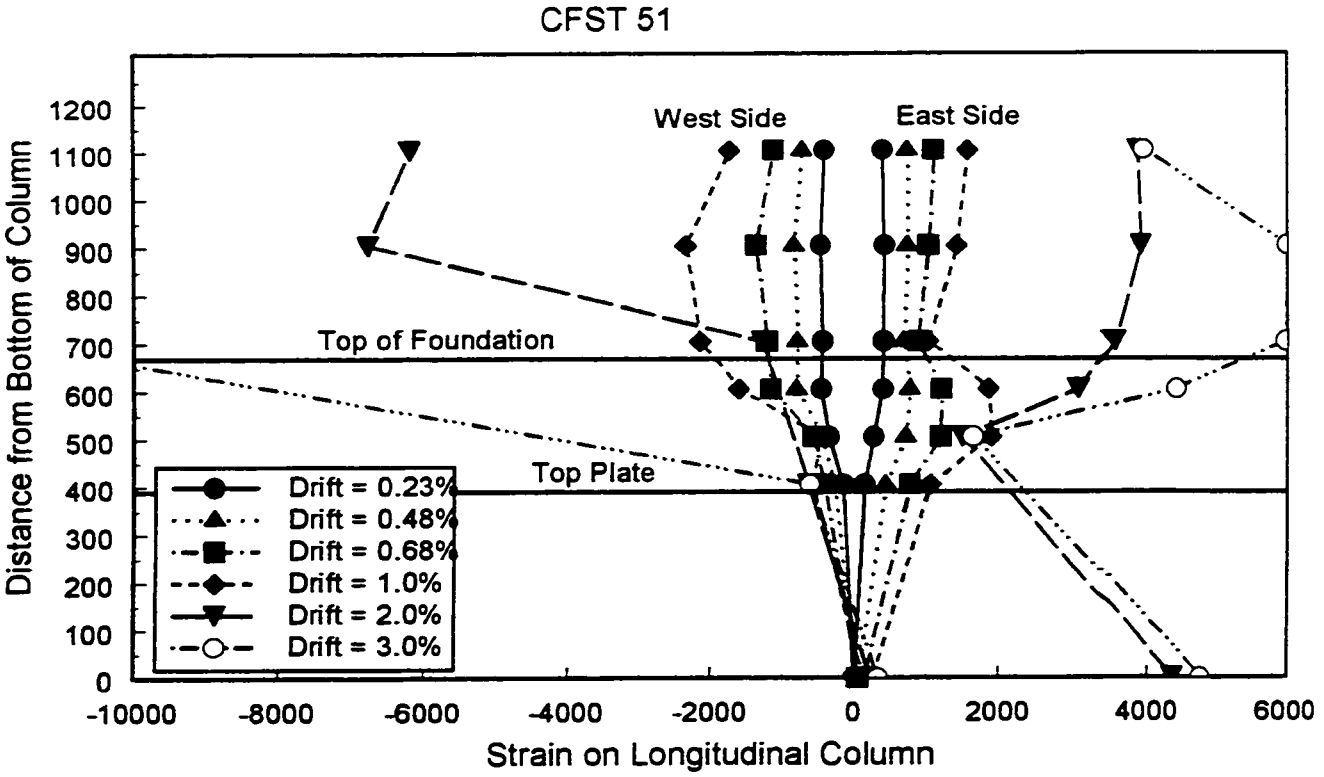

Figure 6.23: Strain distribution along steel tube for negative force for CFST 51

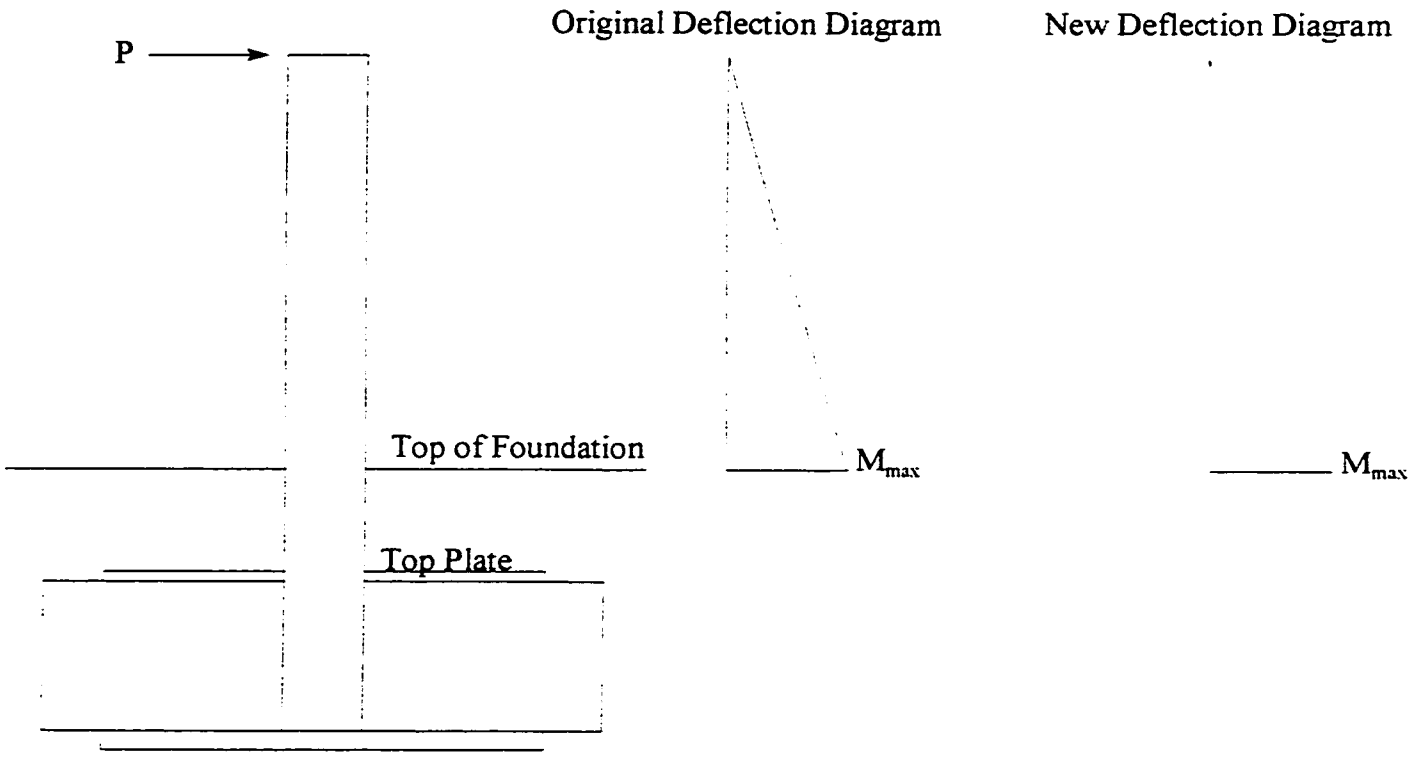

Figure 6.24: Moment distribution assumed for new tip deflection calculation

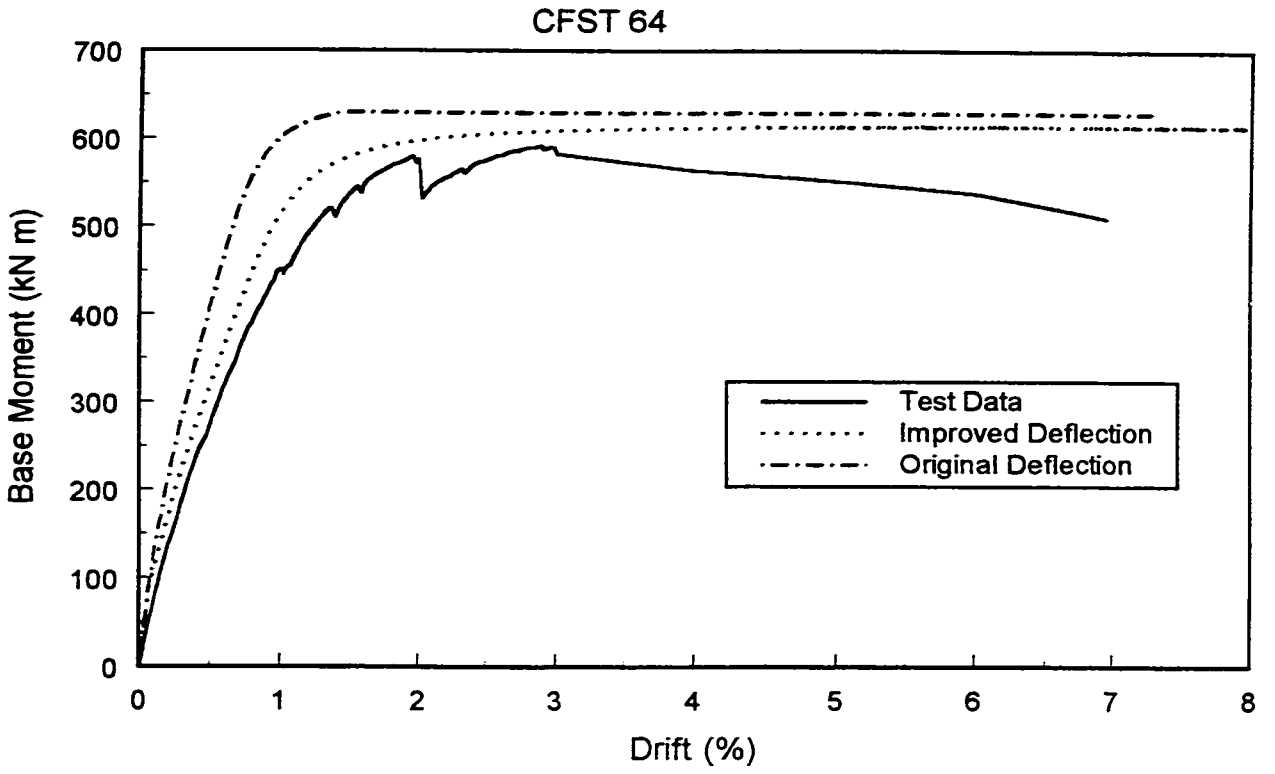

Figure 6.25: Improved drift curves using computer program for CFST 64

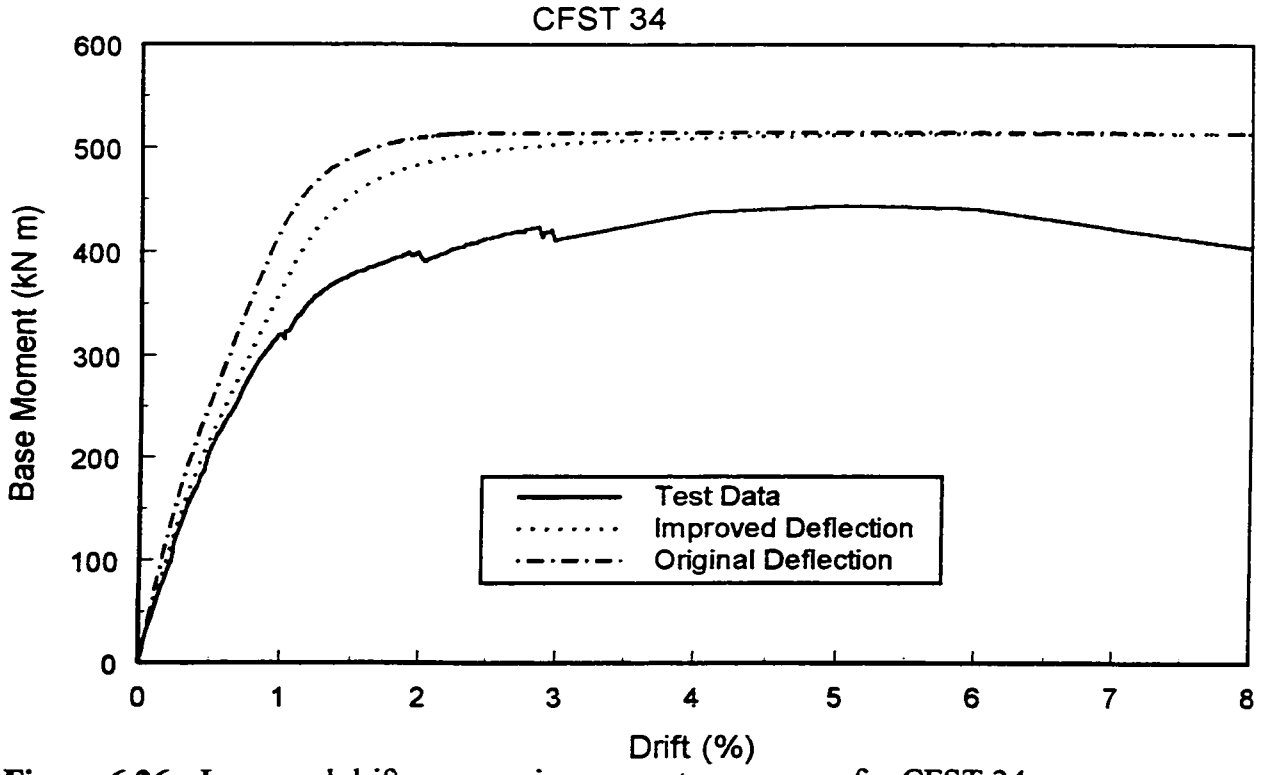

Figure 6.26: Improved drift curves using computer program for CFST 34

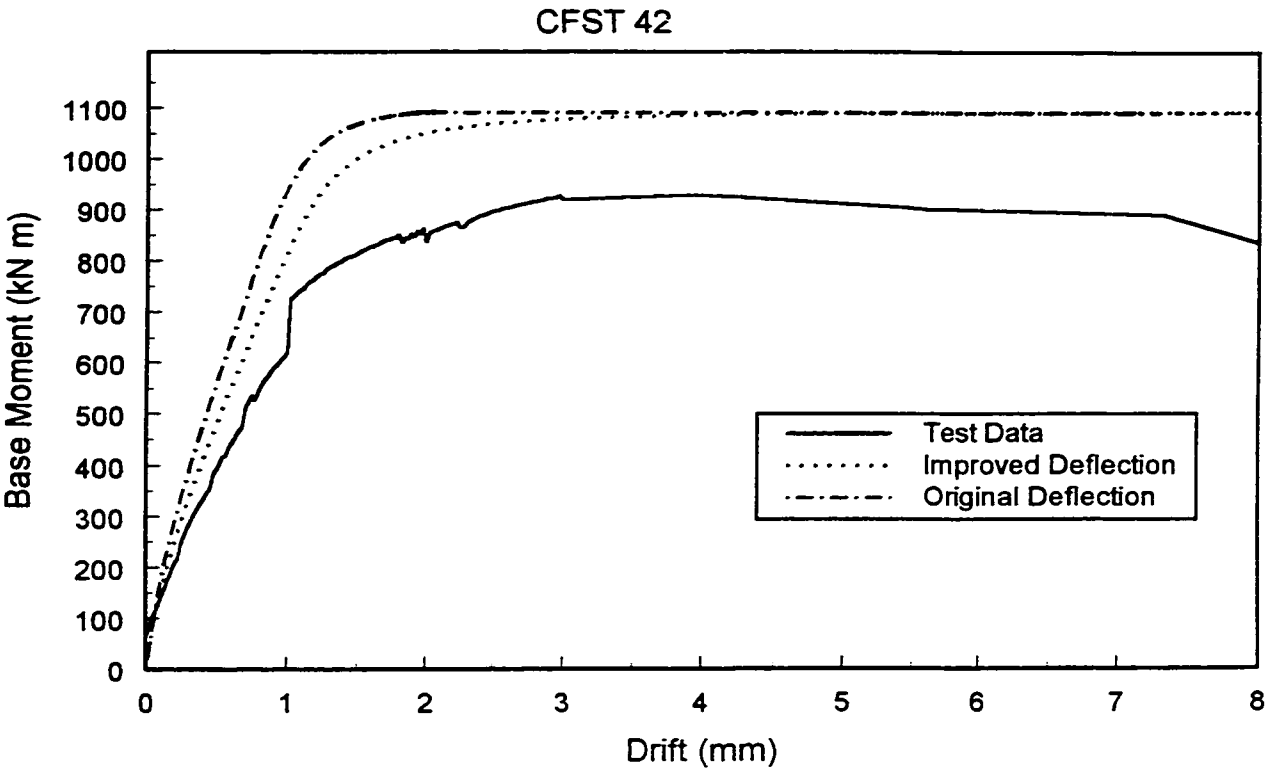

Figure 6.27: Improved drift curves using computer program for CFST 42

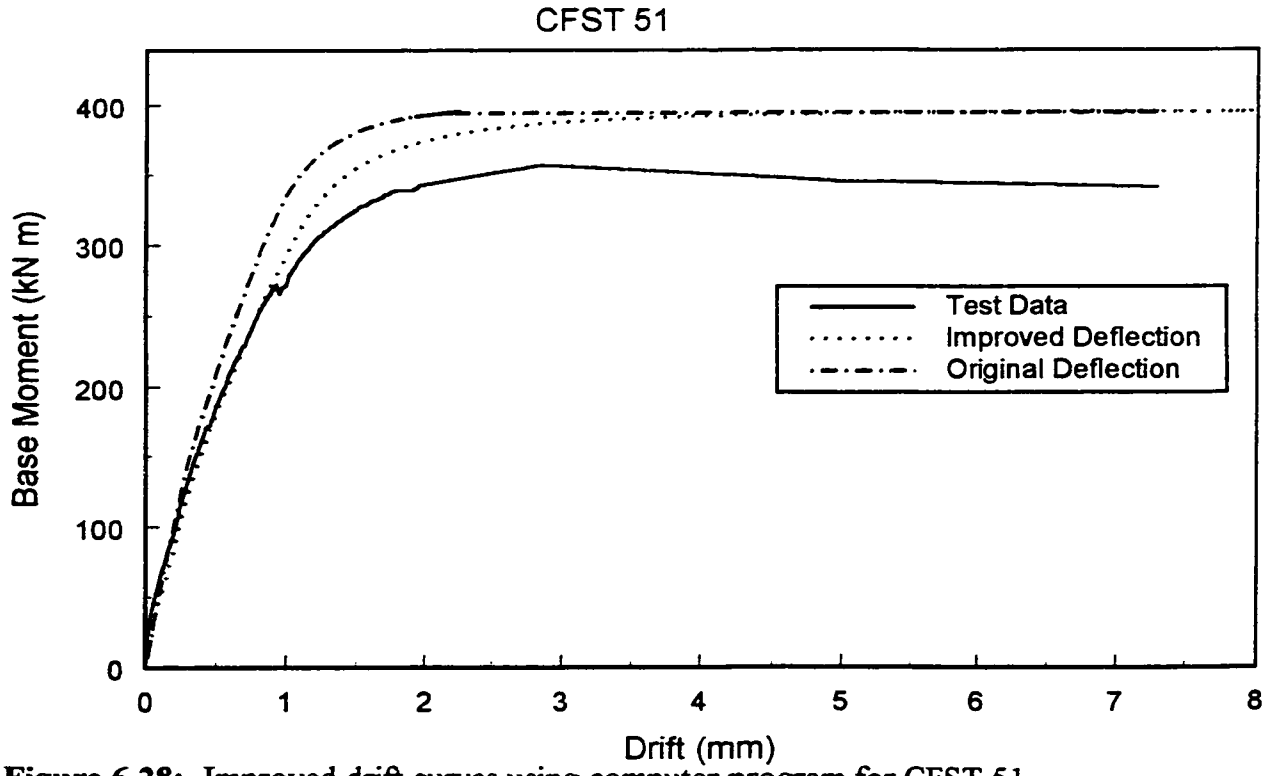

Figure 6.28: Improved drift curves using computer program for CFST 51

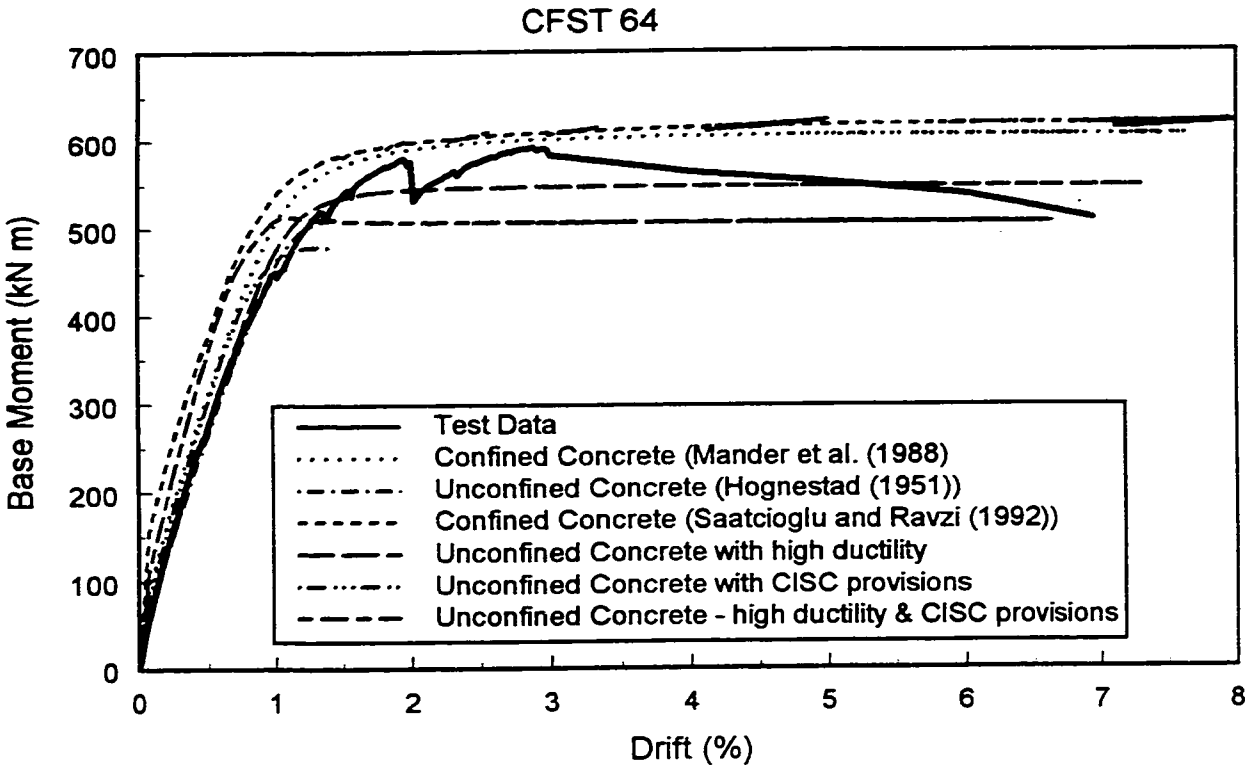

Figure 6.29: Moment curves with different material models for CFST 64

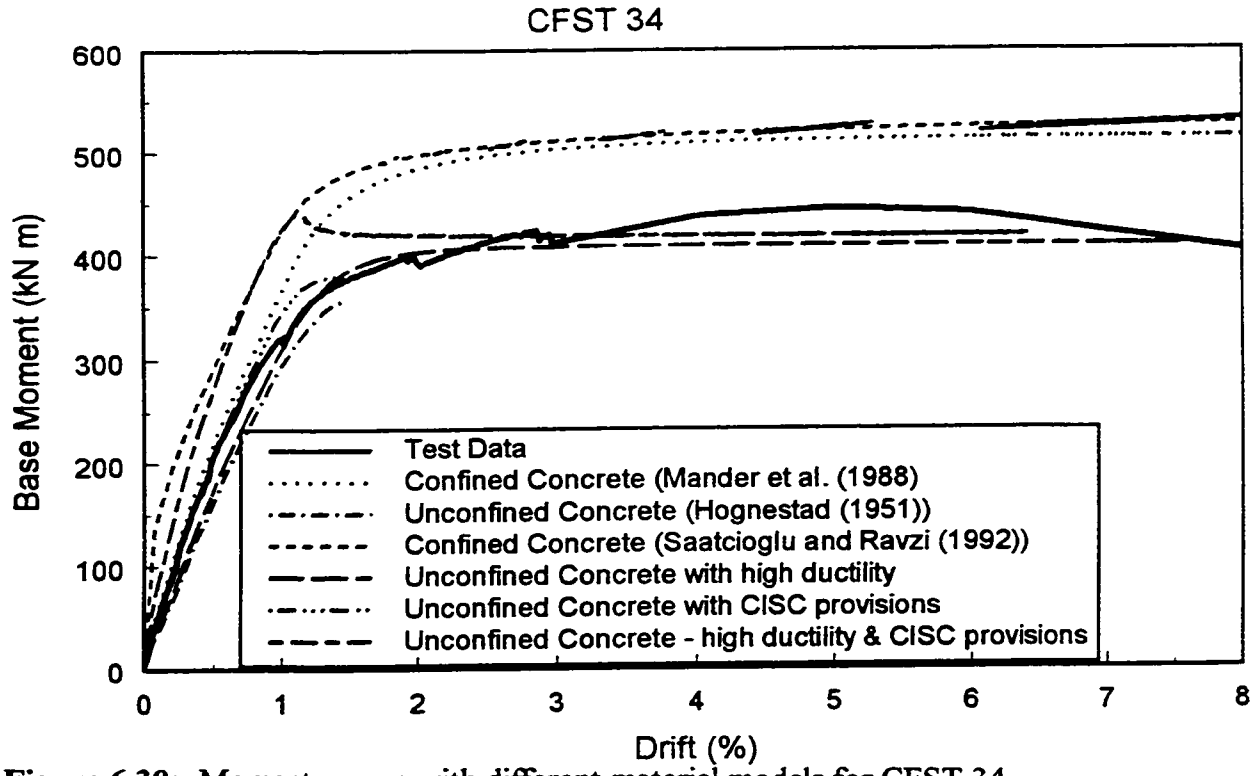

Figure 6.30: Moment curves with different material models for CFST 34

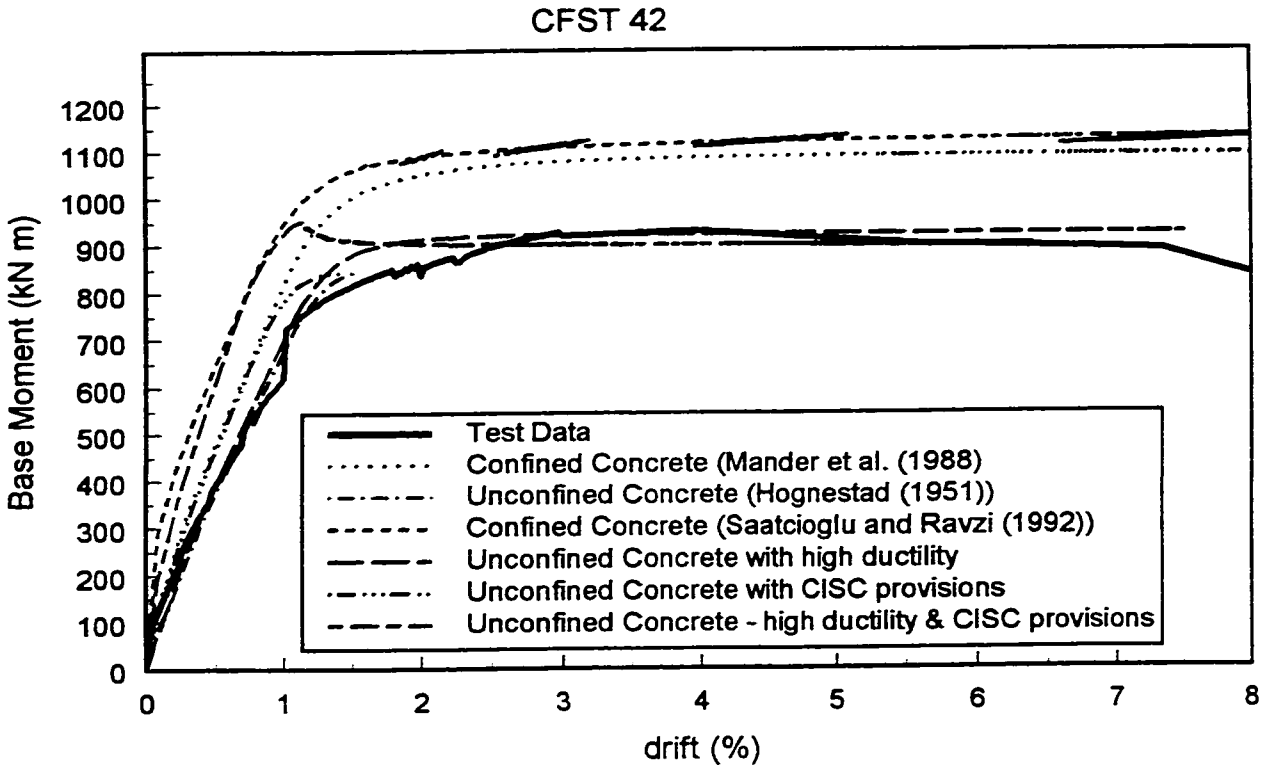

Figure 6.31: Moment curves with different material models for CFST 42

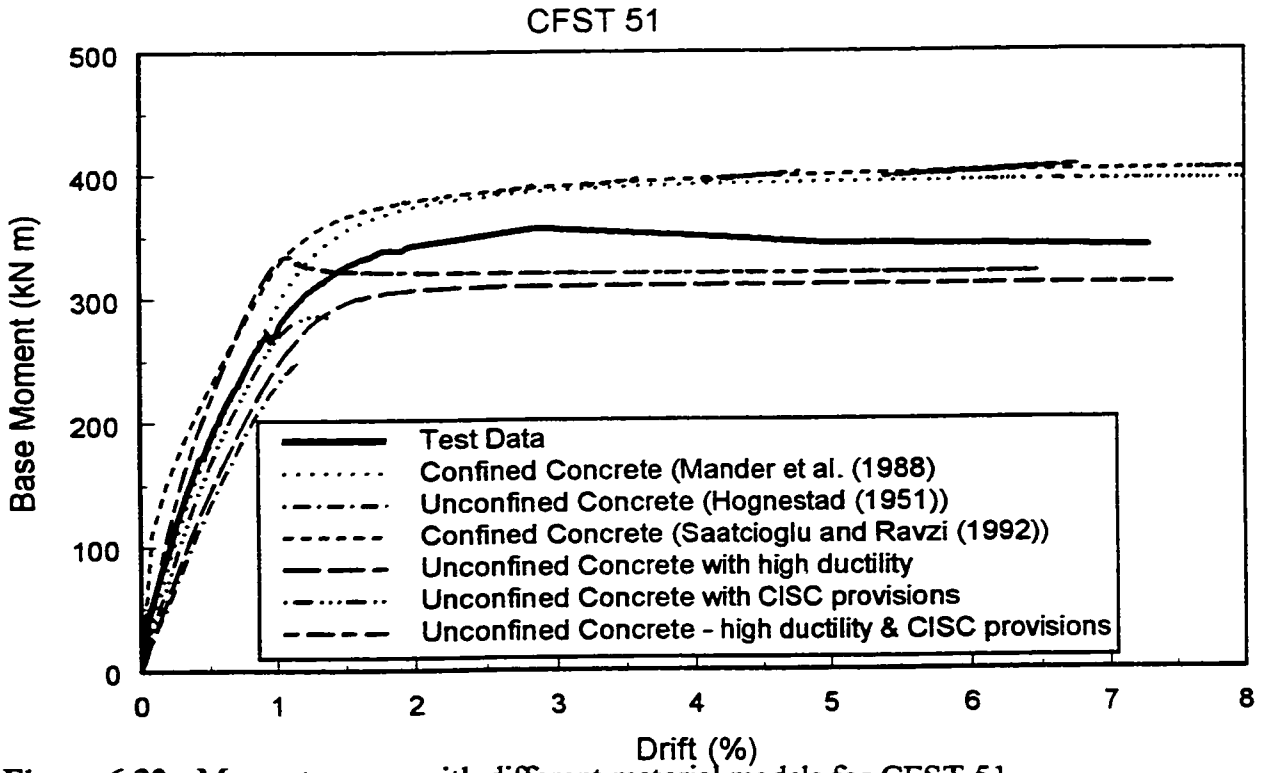

Figure 6.32: Moment curves with different material models for CFST 51

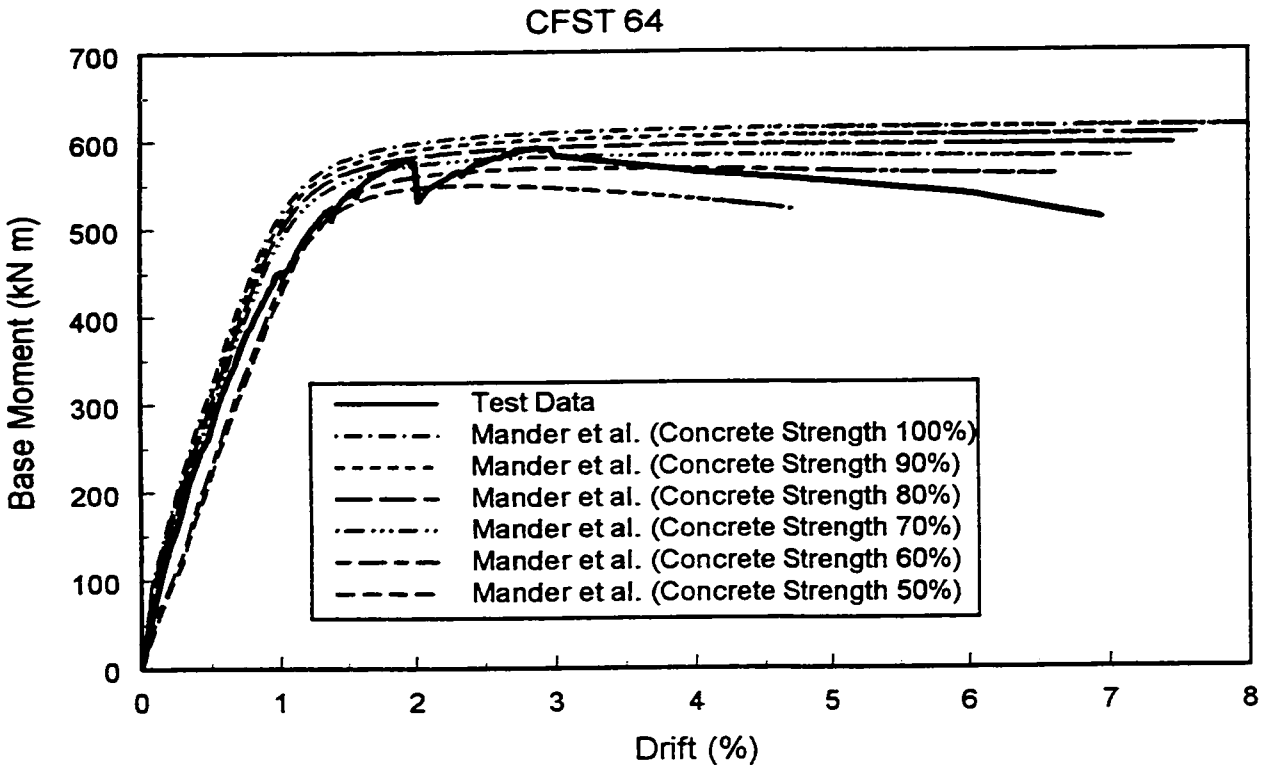

Figure 6.33: Sensitivity analysis using reduced Mander et al. (1988) equations for CFST 64

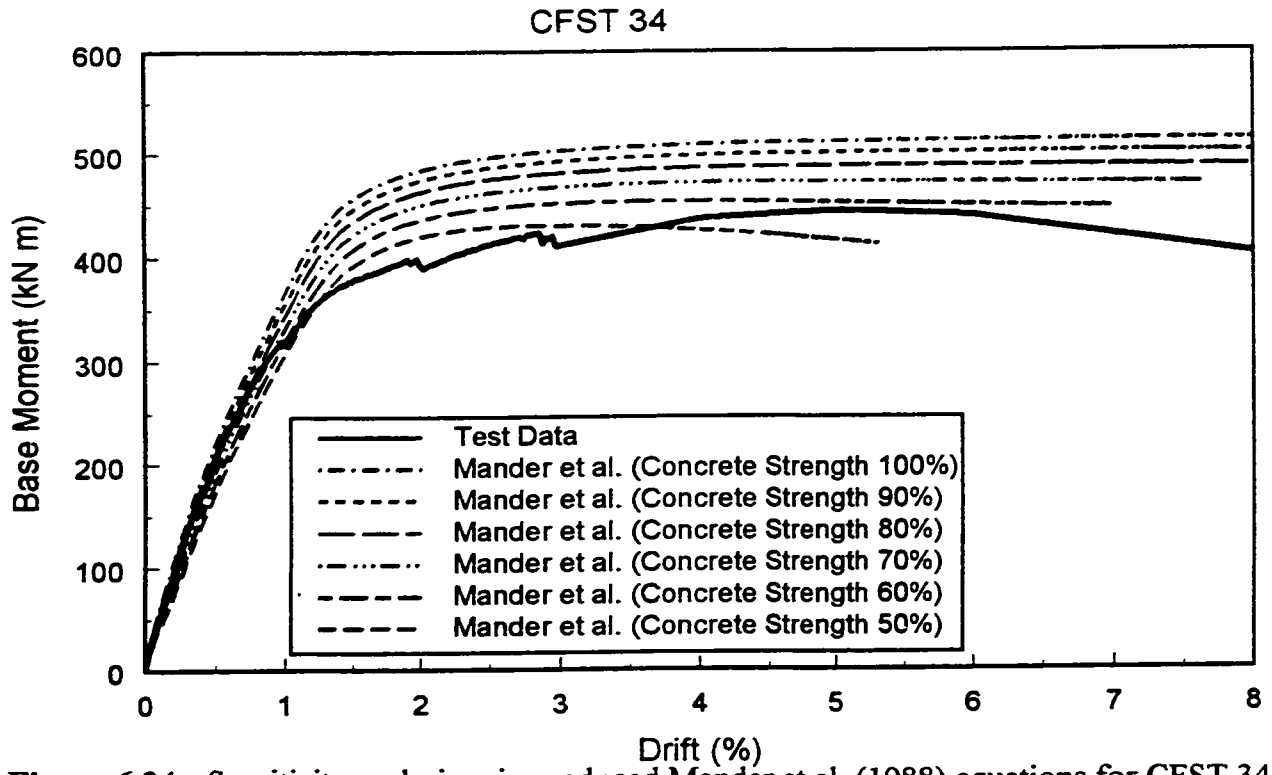

Figure 6.34: Sensitivity analysis using reduced Mander et al. (1988) equations for CFST 34

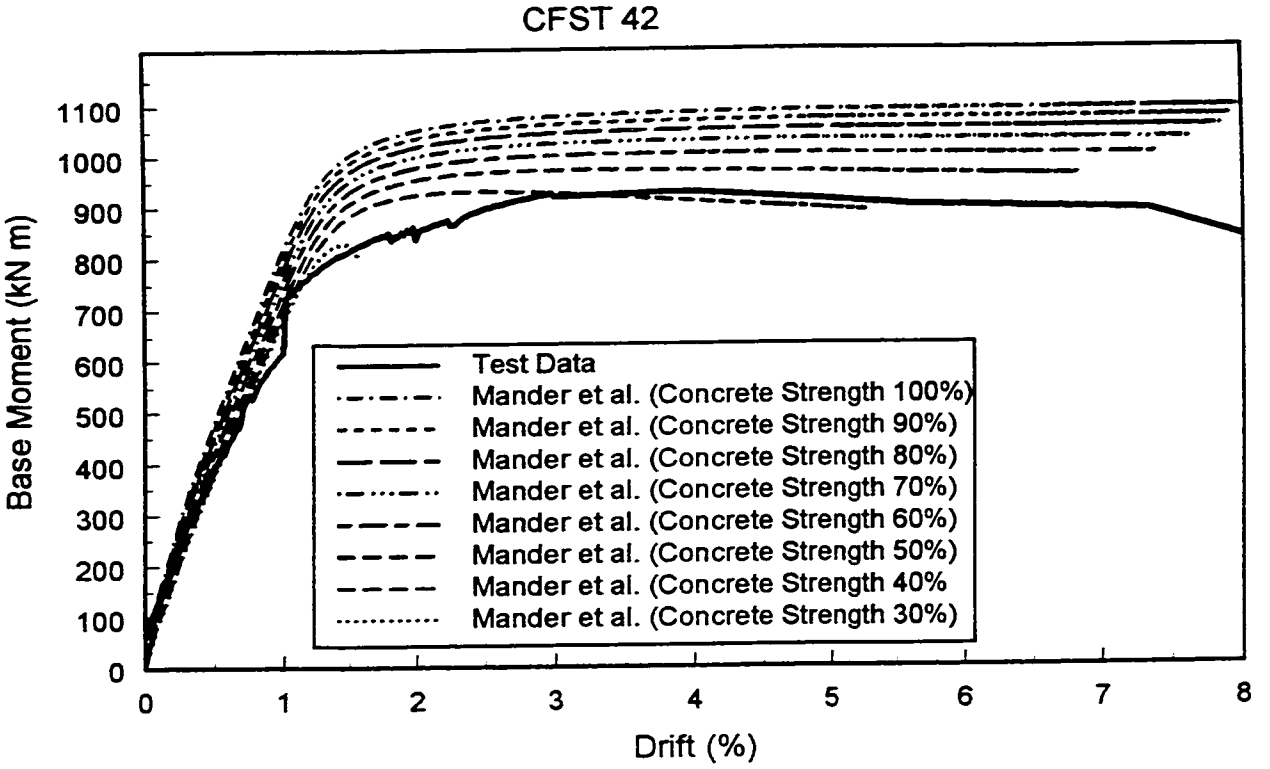

Figure 6.35: Sensitivity analysis using reduced Mander et al. (1988) equations for CFST 42

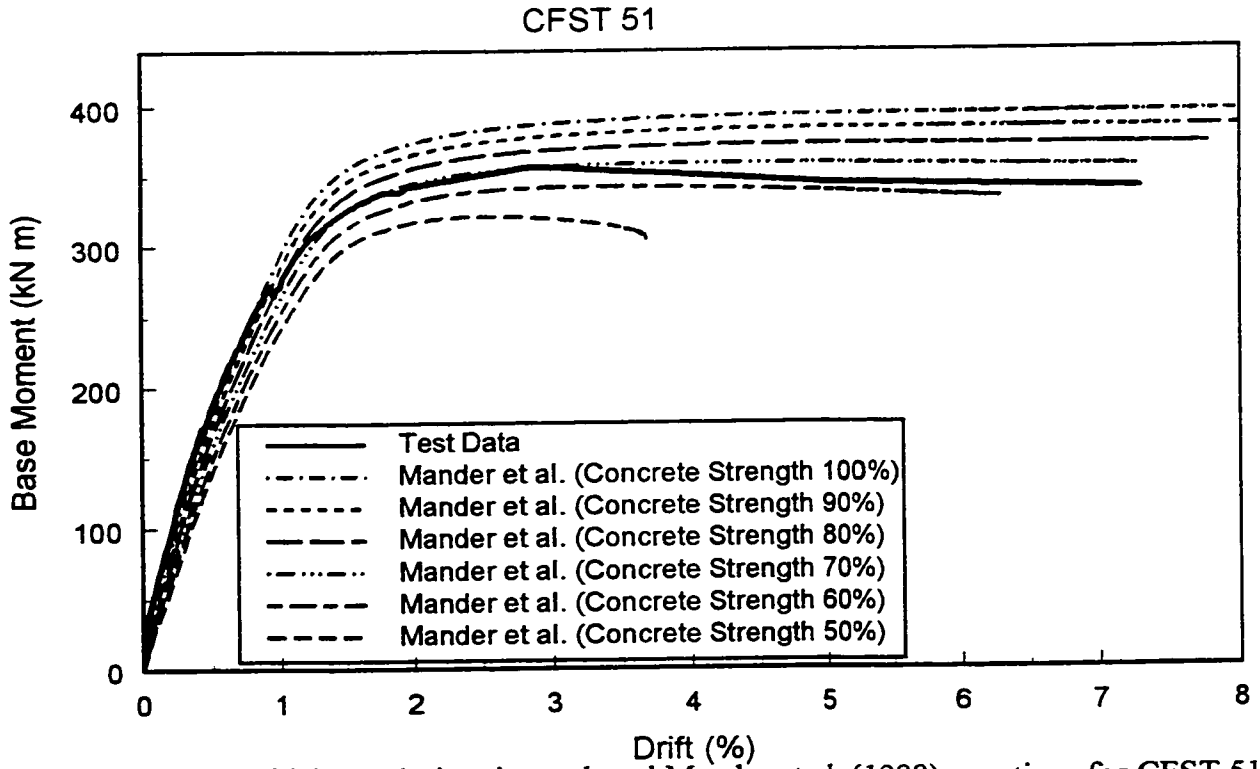

Figure 6.36: Sensitivity analysis using reduced Mander et al. (1988) equations for CFST 51

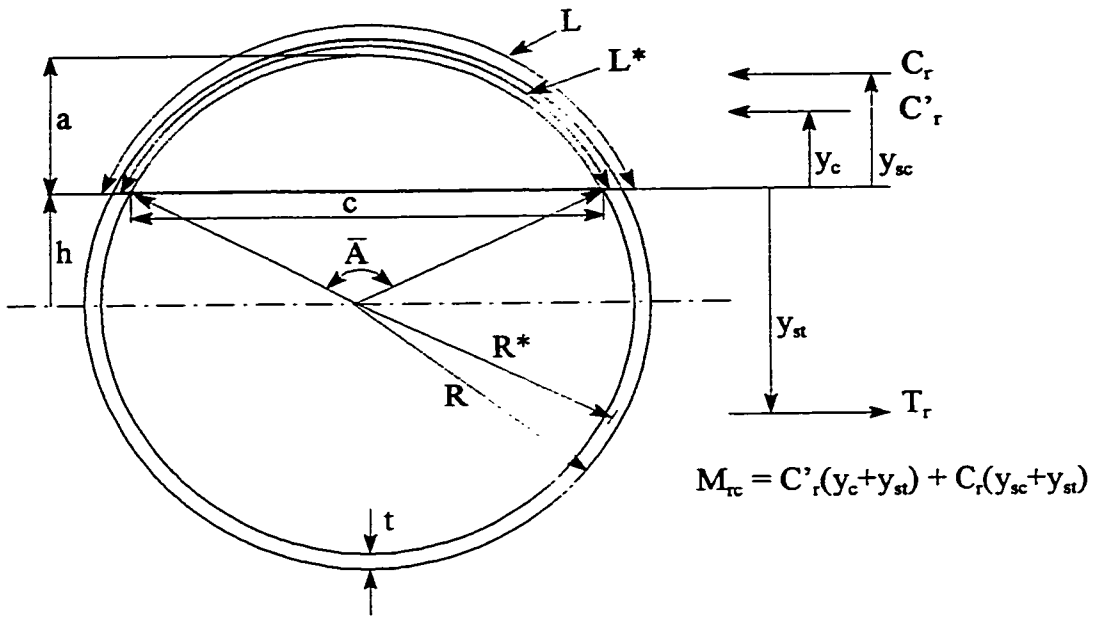

Figure 6.37: Circular cross-section in pure bending

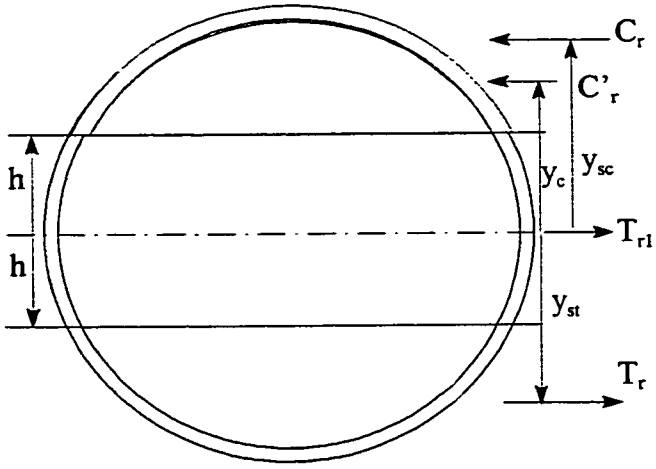

$$C_r = T_r$$
$$\sum F: 0 = C_r + C'_r - T_{r1} - T_r$$
$$T_{r1} = C'_r$$

$$M_{rc} = C_r y_{sc} + C'_r y_c + T_r y_{st}$$

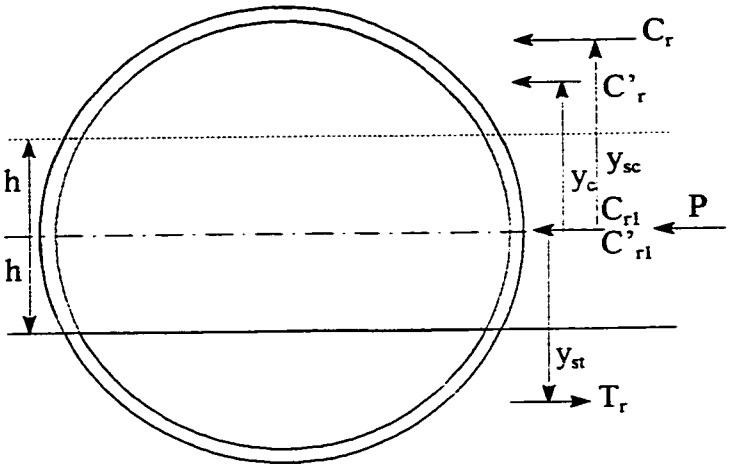

$$C_r = T_r$$
$$C'_r = C_{r1}$$
$$\sum F: P = C_r + C'_r + C_{r1} + C'_{r1} - T_r$$
$$P = C'_r + C'_r + C'_{r1} = C'_c$$

$$\sum M_{\text{at centre}}: M_{rc} = C_r y_{sc} + C'_r y_c + T_r y_{st}$$

Figure 6.38: Moment resistance with two different axial loads

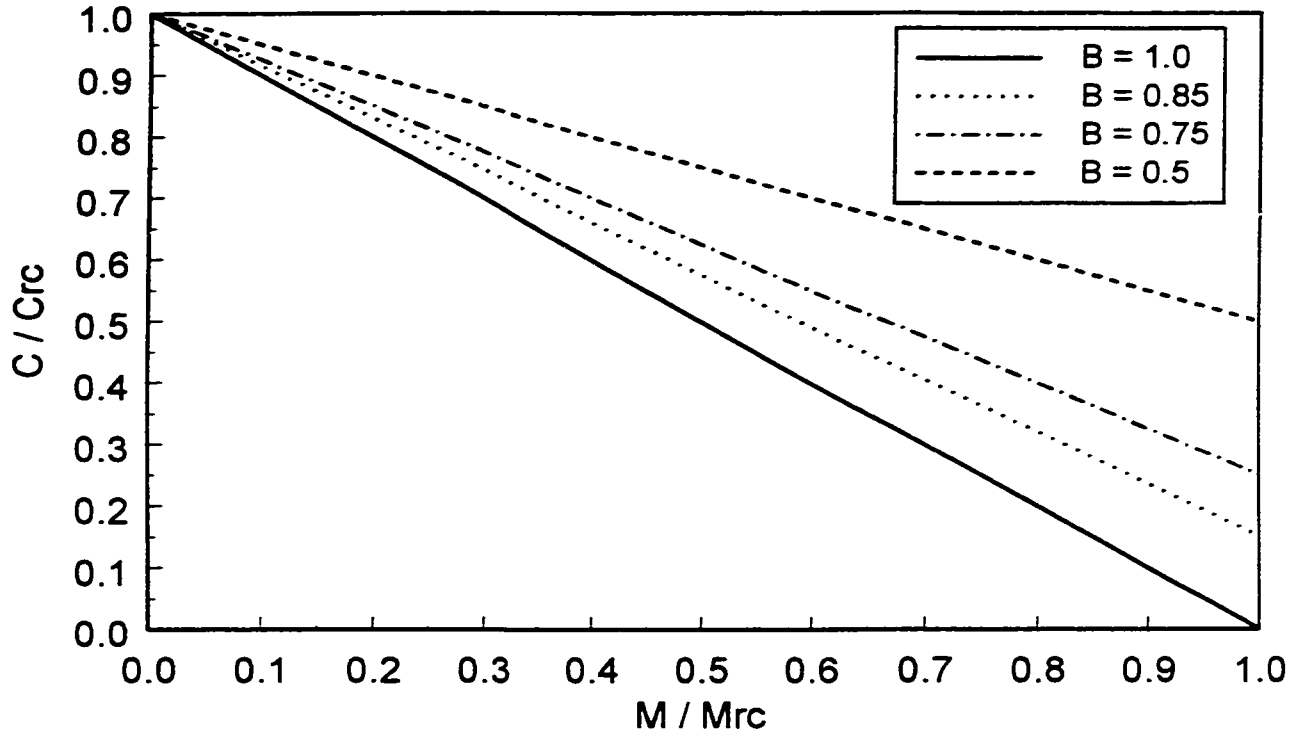

Figure 6.39: Variation of interaction curve for different values of B

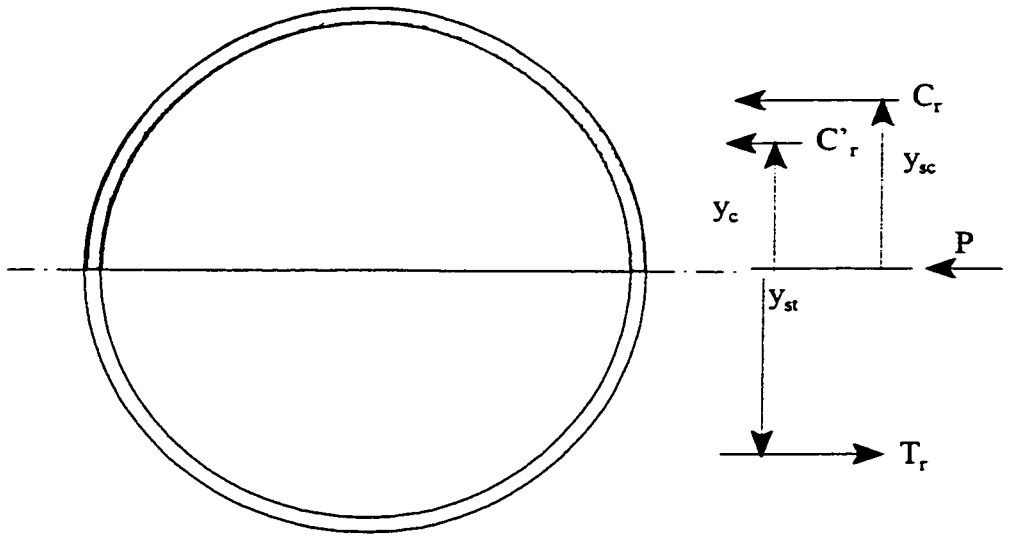

$$T_r = C_r$$
$$\sum F: \; P = C_r + C'_r - T_r$$
$$P = C'_r = 1/2\, C'_c$$

$$M_{max} = C'_r(y_c+y_{st}) + C_r(y_{sc}+y_{st}) = Py_c + 2\, T_r y_{st}$$

Figure 6.40: Maximum moment resistance with neutral axis at centerline

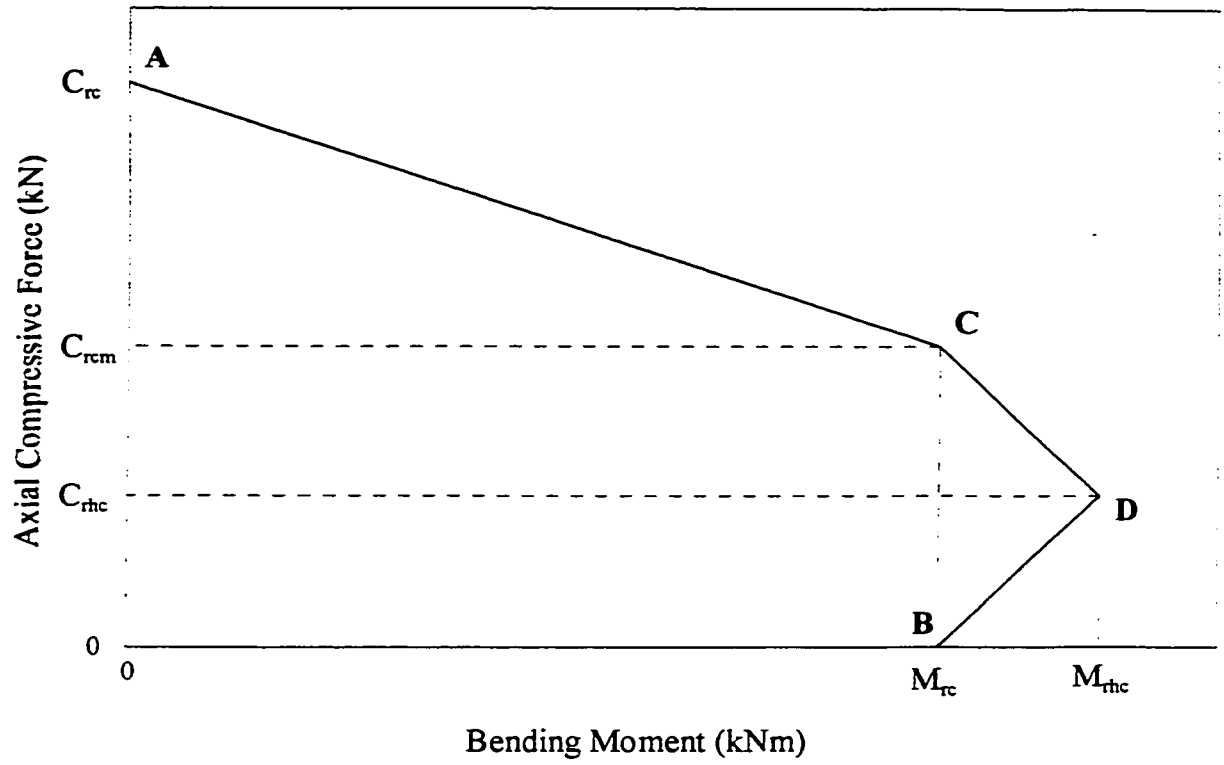

Figure 6.41: Axial compression and bending moment strength interaction curves

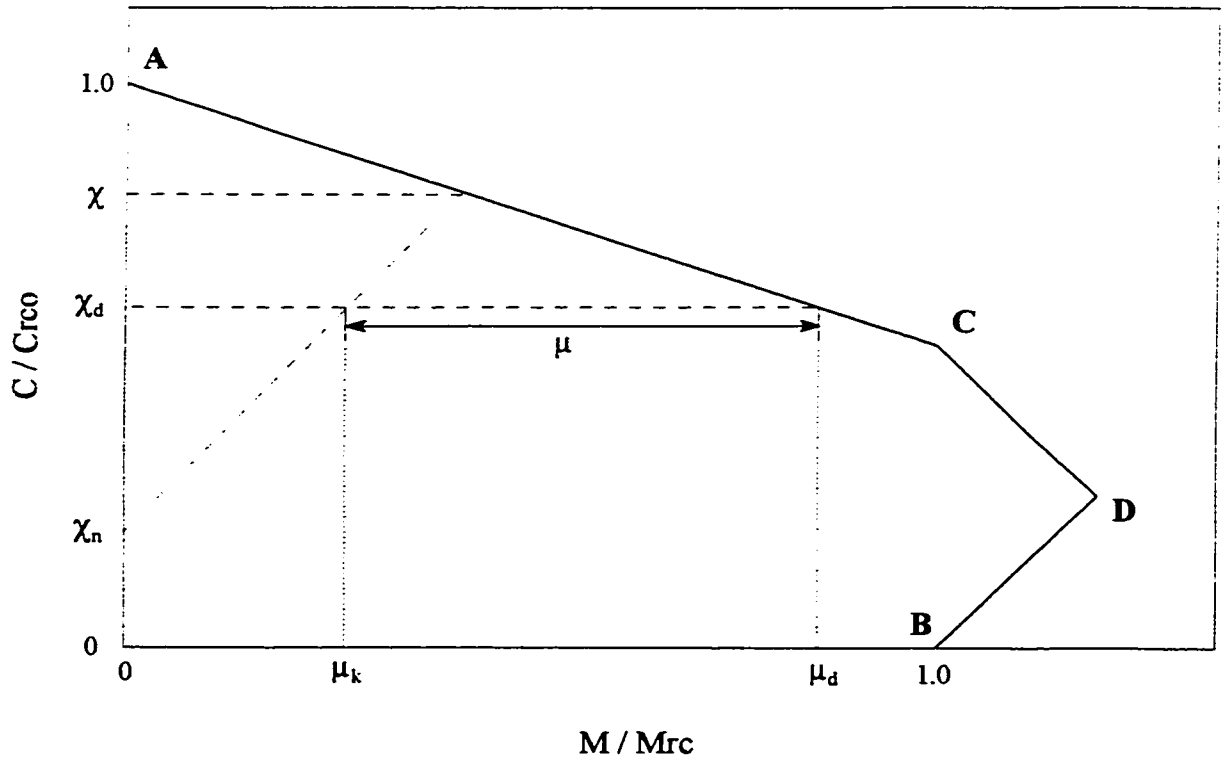

Figure 6.42: Axial compression and bending moment interaction curve [Eurocode 4 (1994)]

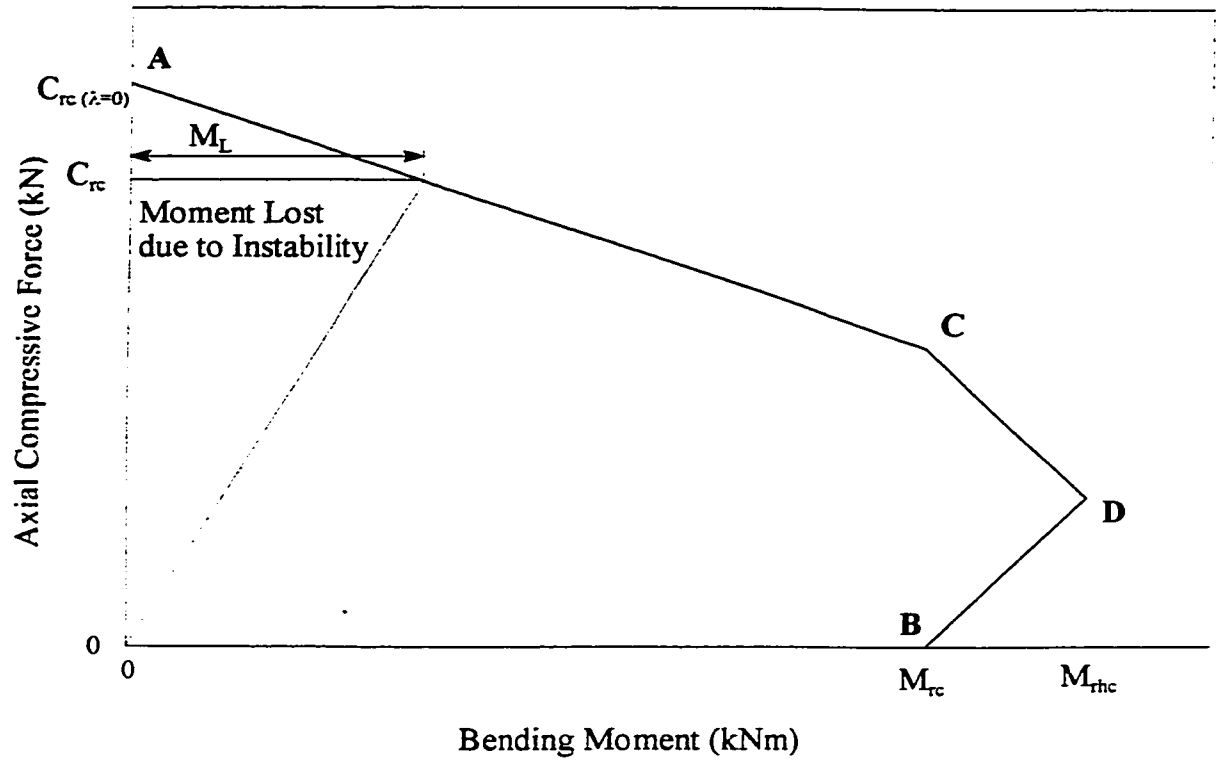

Figure 6.43: Compression and bending strength interaction curves with slenderness effects

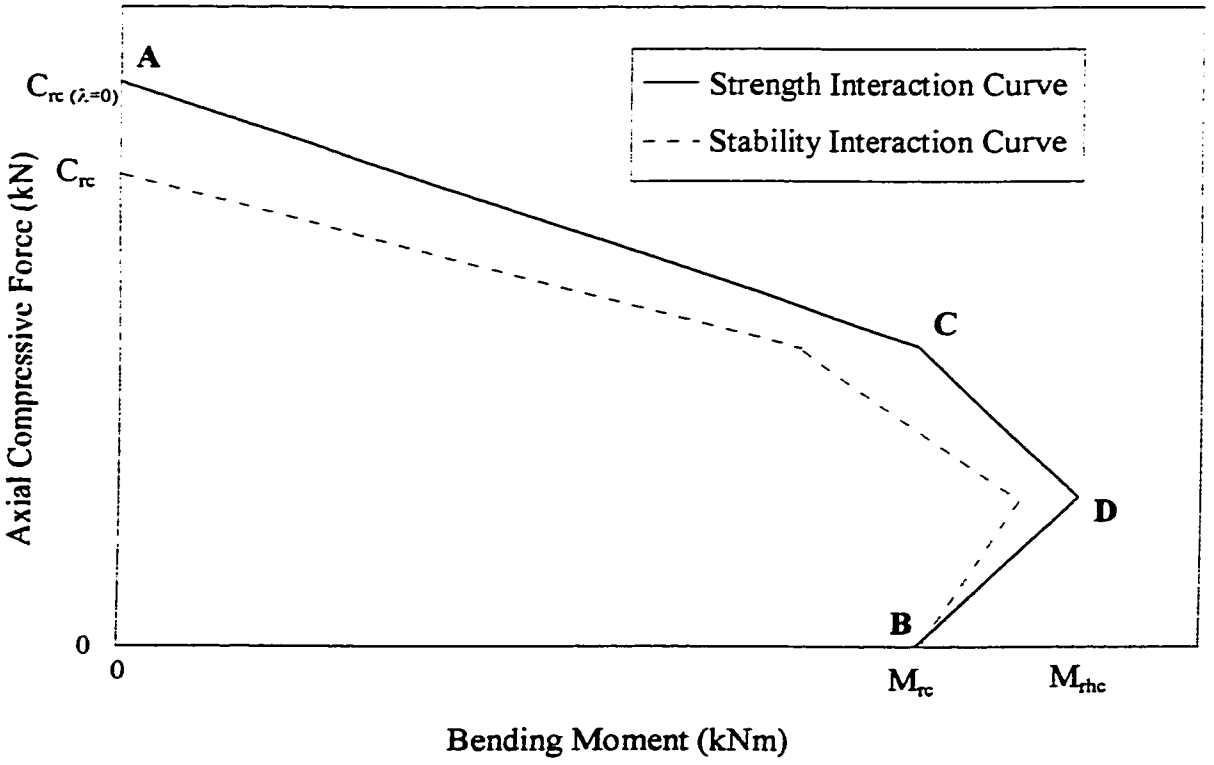

Figure 6.44: Axial compression and bending moment stability interaction curve

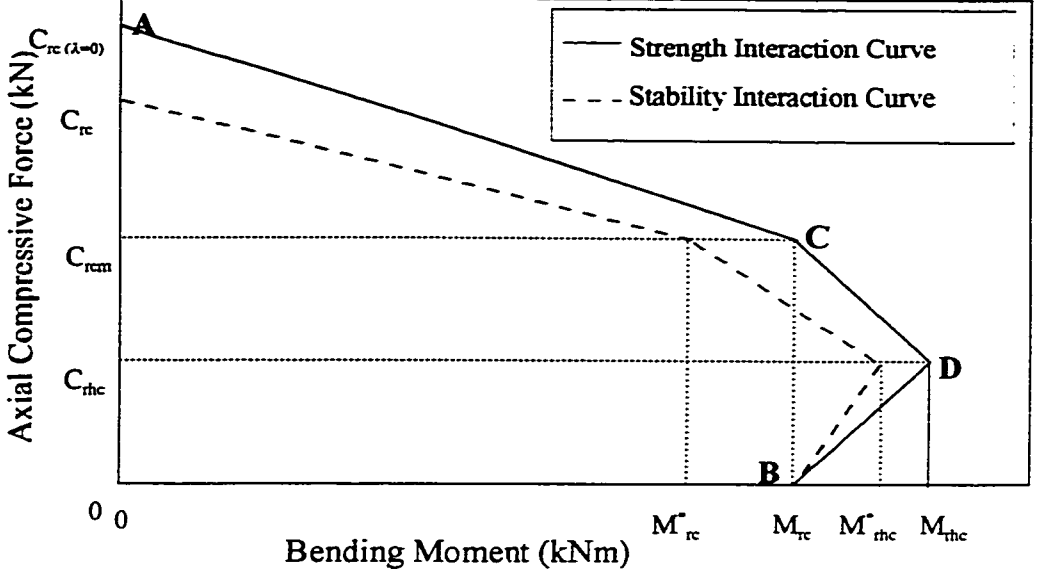

Figure 6.45: Compression and bending stability interaction curve for $C_{rc} \geq C_C$

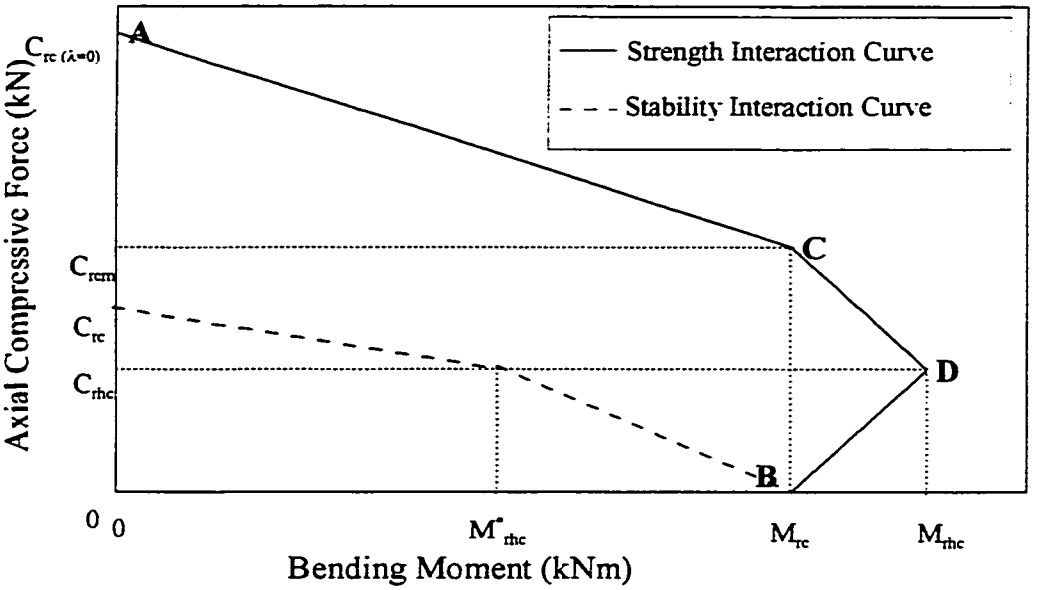

Figure 6.46: Compression and bending stability interaction curve for $C_{rc} \geq C_D$

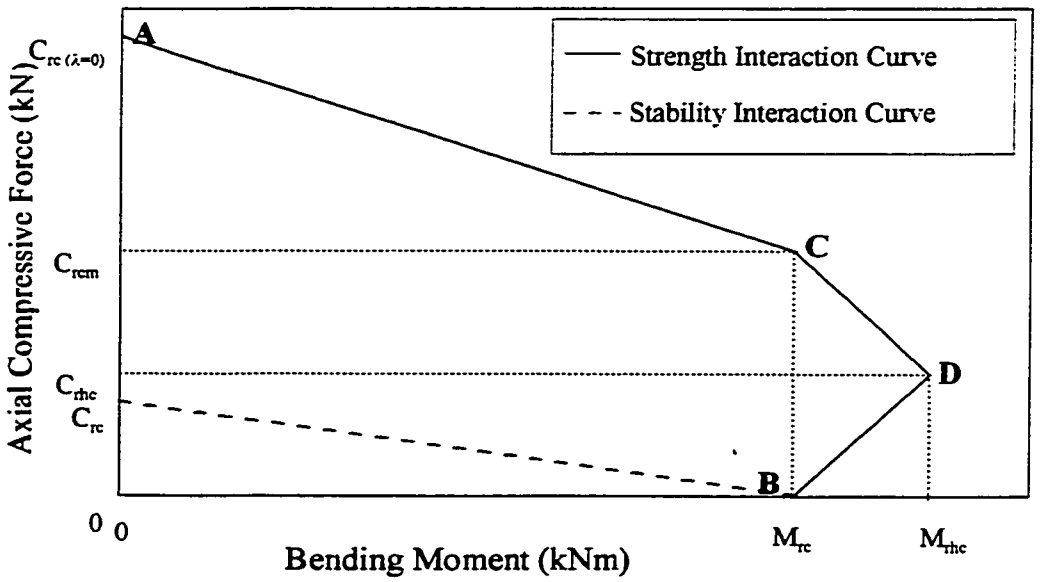

Figure 6.47: Compression and bending stability interaction curve for $C_{rc} \geq C_B$

APPENDIX A

Design of the Computer Program

Design of the Computer Program

A computer program was developed to analyze the relationship of moment curvature for a thin walled hollow steel section filled with concrete. The program was written in subroutines so that each task could be a separate entity. A brief description of the methodology that was used in designing this program follows.

The user will input the values of all variables in either metric, where pressures and lengths are in MPa and millimeters, respectively, or in imperial where the pressures and lengths are in ksi and inches, respectively. The output data, including moments, forces and deflections, is also in the appropriate units. The user also inputs the cyclic loading pattern the section will undergo. This includes the maximum curvature for each incremental loading pattern and the number of times that each loading pattern is repeated. The user can either enter this data from the screen prompts or from data files.

The cross-sectional dimensions are also entered by the user. If a circular section is chosen, the outer diameter and inner diameter of the steel is needed, while if the square section is chosen, the width of the section and the thickness of the steel are needed. The user is also able to control the accuracy of the program by inputting the number of layers which will be used to divide the section. These areas are then used to calculate the center of gravity for each layer measured from the bottom of the composite section.

The user can chose to analyze the steel tube or the concrete core separately. The moment-curvature relationship for the steel tube is an effective analysis to determine the additional strength caused by the composite section as compared to the steel tube alone. However, if the user chooses to just look at the concrete core, the neutral axis remains at the centroid of the section, and the forces are not in equilibrium. The analysis of the concrete core is only to be used to study the concrete behaviour under the prescribed loading condition, and should not be used to calculate the actual strength of the section.

The main program runs all of the subprograms, these subroutines are responsible for incrementing the curvature, calculating the correct neutral axis, and calculating the stresses, forces, and moments in the section. The program is designed to subject the section to cyclic loading. The user inputs the number of cyclic intervals and the maximum curvature at each interval. The loading subroutine is a loop that increments the curvature as long as it is less than the maximum curvature for that loading interval. The unloading subroutine continues to decrease the curvature as long as the total moment acting on the section is not equal to zero. The section is flipped 180° and loaded again. After the maximum curvature is reached and with the section still theoretically flipped, it is unloaded. This sequence is repeated as designated by the user. "total curvature" is also maintained, this curvature is the one used in the moment curvature relationship. The neutral axis is calculated by assuming a location of the neutral axis for a given step, and adjusting the neutral axis location through an iteration loop that is continued until the forces acting on the section equal zero.

The steel behaviour is analyzed using an Elastic Perfectly Plastic model. However, the user has a choice between three concrete models, namely, an unconfined model proposed by Hognestad from his paper entitled, "A Study of Combined Bending and Axial Load in Reinforced Concrete Members", and confined concrete models as proposed by J.B. Mander, M.J.N. Priestley, and R. Park from their paper entitled "Theoretical Stress-Strain Model for Confined Concrete" and Saatcioglu and Ravzi (1992) from their paper entitled "Strength and Ductility of Confined Concrete". Using these models, the stresses are calculated for the steel and concrete at each layer. The stress at each layer is then multiplied by the respective area to calculate the force in both the steel and concrete. The moment is calculated acting about the bottom of the cross section for positive loading, and since the section is effectively turned 180° for reverse loading, acting about the top of the section for reverse loading.

To investigate the use of concrete-filled steel tubes as a column, force and deflection values were calculated. The height of the column from the base to the applied horizontal force is inputted by the user. The applied force at each increment is calculated as the moment divided by

the height of the column. The deflection at each increment is calculated as the integral of the curvature length diagram.

The program outputs the moment and curvature, and the force and deflection at each step along its loading path to a data file. This file can be imported into a graphing program and the moment-curvature relationship can be printed. This data file produces a complete analysis of the cross-sectional resistance of a concrete-filled steel tube subjected to moment and axial force.

APPENDIX B

Computer Code

```
      PROGRAM STEEL

C     THIS PROGRAM WILL CALCULATE THE MOMENTS AND CURVATURES, AND FORCES AND
C     DEFLECTIONS CURVES FOR THE COLUMNS TESTED IN MARSON (1999).
C     THIS PROGRAM WILL NOW CALCULATE THE BIAXIAL STRESS IN STEEL.
C     APRIL 5 1999
C     THIS IS A REVISION TO TEST SENSITIVITY OF MANDER JUNE 4 1999
C
C  THIS PROGRAM HAS THE ABILITY TO EITHER ENTER CONCRETE ENCASED SQUARE
C  OR CIRCULAR HOLLOW TUBE SECTIONS.  IT IS DESIGNED TO DETERMINE THE
C  CYCLIC MOMENT CURVATURE RELATIONSHIP.  THE CYCLIC LOADING PATTERN CAN
C  INPUTTED FROM THE KEYBOARD, AND THE MOMENT CURVATURE RELATIONSHIP IS
C  OUTPUTED.
C
C  THE PROGRAM ALLOWS FOR THE USER TO STUDY THE EFFECT OF THE STEEL ALONE,
C  OR THE CONCRETE ALONE, OR THE COMPOSITE ACTION OF THE STEEL AND CONCRETE.
C  THE USER IS ABLE TO CHOOSE FROM THREE DIFFERENT CONCRETE MODELS,
C  HOGNESTAD'S, SAATCIOGLU & RAZVI, OR MANDER, PRIESTLEY & PARK.  THIS
C  PROGRAM ASSUMES ELASTIC PERFECTLY PLASTIC STEEL BEHAVIOUR.
C
C     E = THE ELASTIC MODULUS OF STEEL
C     FST = THE ULTIMATE STRESS IN THE TENSION OF THE FIBERS IN THE
C         CROSS-SECTION
C     FSC = THE ULTIMATE STRESS IN THE BOTTOM FIBERS OF THE CROSS-
C         SECTION
C     SINIT = THE INITIAL STRESS IN THE CROSS-SECTION
C     E01 = THE STRAIN CORRESPONDING TO PEAK STRESS OF UNCONFINED CONCRETE
C     E085 = THE STRAIN AT 85% STRENGTH LEVEL BEYOND THE PEAK STRESS OF
C         UNCONFINED CONCRETE.
C     ROUT = THE RADIUS OF THE OUTER STEEL IN A CIRCULAR SECTION OR HALF
C         THE OUTSIDE WIDTH OF THE STEEL IN THE SQUARE SECTION
C     RIN = THE RADIUS OF THE INSIDE STEEL IN A CIRCULAR SECTION OR HALF
C         THE INSIDE WIDTH OF THE STEEL IN THE SQUARE SECTION
C     THICK = THE THICKNESS OF THE STEEL ENCASEMENT
C     DLAYER = THE HEIGHT OF EACH LAYER
C     XB(I) = AN ARRAY THAT HOLDS THE TWO BOTTOM X COORDINATES
C         FOR THE SQUARE SECTION
C     XT(I) = AN ARRAY THAT HOLDS THE TWO TOP X COORDINATES FOR
C         THE  SQUARE SECTION
C     YL(I) = AN ARRAY THAT HOLDS THE TWO LEFT Y COORDINATES
C         FOR THE SQUARE SECTION
C     YR(I) = AN ARRAY THAT HOLDS THE TWO RIGHT Y COORDINATES
C         FOR THE SQUARE SECTION
C     HEIGHT = THE TOTAL HEIGHT OF THE CROSS-SECTION
C     AS(I) = AN ARRAY THAT HOLDS OF THE STEEL AREAS FOR EACH LAYER
C     AC(I) = AN ARRAY THAT HOLDS OF THE CONCRETE AREAS FOR EACH LAYER
C     SCG (I) = AN ARRAY OF THE STEEL LAYERS CENTER OF GRAVITIES
C     CCG (I) = AN ARRAY OF THE CONCRETE LAYERS CENTER OF GRAVITIES
C     CURV = THE INCREMENTAL CURVATURE APPLIED AT EACH STEP
C     NA = THE NEUTRAL AXIS OF THE SECTION
C     CSTR(I) = THE VALUE OF CONCRETE STRESS AT THE TOP OF THE PREVIOUS
C         LOADING CYCLE
C     SSTR(I) = THE VALUE OF STEEL STRESS AT THE TOP OF THE PREVIOUS
C         LOADING CYCLE
C     SSP(I) =
C     B = THE CURVATURE REACHED WHEN MTOTAL=0.
C     CU(I) = THE PREVIOUS STRESS IN THE CONCRETE
C     INTC(I) = THE CYCLIC CURVATURES THAT ARE DETERMINED TO BE THE
C         ULTIMATE PER EACH LAYER
C     INTCUR = THE CYCLIC CURVATURE THAT IS THE ULTIMATE FOR A PARTICULAR
C          CYCLIC LOADING.
C     CURVI = THE CURVATURE INCREMENT USED THROUGHOUT THE ANALYSIS
C     CURVL = THE MAXIMUM CURVATURE REACHED AT THE END OF LOADING
C     INC = THE NUMBER OF LAYERS THE CROSS-SECTION IS DIVIDED
C     INT = THE NUMBER OF CYCLIC INTERVALS
C     CYC = THE NUMBER OF CYCLIC LOADING AT A SPECIFIED ULTIMATE CURVATURE
C     STEP = THE ITERATION NUMBER
C     SHAPE = THE SHAPE OF THE SECTION
C     MAT = WHETHER THE USER WANTS STEEL, CONCRETE OR BOTH FOR THE
C         ANALYSIS.
C     DIR = WHETHER THE ANALYSIS IS IN LOADING(L) OR REVERSE LAODING(R)
C     UNIT = THE UNITS OF THE PROBLEM, EITHER METRIC OR IMPERIAL
C     MODEL = WHAT CONCRETE MODEL THE USER WOULD LIKE TO USE.
C     CONFIN = WHAT CONFINEMENT MODEL THE USER WOULD LIKE TO USE.

      REAL E,FST,FSC,SINIT,E01,E085
      REAL ROUT,RIN,THICK,DLAYER
      REAL XB(10),XT(10),YL(10),YR(10)
      REAL HEIGHT
      REAL AS(1000),AC(1000),SCG(1000),CCG(1000)
      REAL CURV,NA,CURVL
      REAL CSTR(1000),SSTR(1000),SSP(1000)
      REAL B,CU(1000),INTC(10),INTCUR,CURVI,P
      REAL ZER,MAN,L,EIS,EIC,EI,PI,DEP
      INTEGER INC,INT,CYC,STEP,FAIL,C
      CHARACTER SHAPE*4,MAT*4,DIR*4,MODEL*4,UNIT*4,COL*4,CONFIN*4
      CHARACTER HARD*4

      COMMON /FIRST/ E,SINIT,FST,FSC,FC,E01,E085,RIN,ROUT,EI
      COMMON /SECOND/ CU,SSTR,CSTR
```

```
COMMON /THIRD/ DIR,MODEL,MAT,UNIT
COMMON /FOURTH/ INC,CURV,INTCUR,CURVI,FAIL
COMMON /FIFTH/ HARD

OPEN(UNIT=6)
OPEN(UNIT=7,FILE='INPUT.DAT')
OPEN(UNIT=4,FILE='MOMEN.DAT')
OPEN(UNIT=3,FILE='CONCR.DAT')
OPEN(UNIT=2,FILE='OUTPUT5.DAT')
OPEN(UNIT=1,FILE='STRESS.DAT')

OPEN(UNIT=5)

PI = 3.14159265359
ZER= 0.0
WRITE (2,'(4F15.8)') ZER, ZER, ZER, ZER
CALL INITS (E,FST,FSC,SINIT,FC,E01,E085,UNIT,P)

 SHAPE = 'CIR'
 MAT = 'B'
 INT = 1
 CYC = 1
   CALL CIRCLE (ROUT,RIN,THICK,UNIT)
   CALL HEIGHC (ROUT,DLAYER,INC)
   CALL AREA (INC,DLAYER,ROUT,RIN,AS,AC,SCG,CCG)
   NA = ROUT

STEP = 0
CALL ZERO(SSP,SSTR,CSTR,CU)

WRITE (6,*) 'WHAT CURVATURE INCREMENT WOULD YOU LIKE TO USE?'
READ (5,*) CURVI

  WRITE (6,*) 'WHAT CURVATURE WOULD YOU LIKE TO STOP AT?'
  READ (5,*) INTC(1)

CURV = 0
B = 0
FAIL = 0
WRITE (6,*) 'What concrete model would you like to use?'
WRITE (6,*) 'Hognestad (1956) (U)'
WRITE (6,*) 'Mander et al (M)'
WRITE (6,*) 'Saatcioglu & Razvi (S)'
READ (6,'(A4)') MODEL
MODEL = 'M'
IF (MODEL.EQ.'M') THEN
   WRITE(6,*) 'WHAT FRACTION OF FCC WOULD YOU LIKE TO TAKE?'
   READ (5,*) MAN
ENDIF
WRITE (6,*) 'What confinement model would you like to use?'
WRITE (6,*) 'Elastic-Plastic Steel? (EP)'
WRITE (6,*) 'Biaxially Stressed Steel? (BA)'
WRITE (6,*) 'Unconfined Concrete with Ductility? (UC)'
READ (6,'(A4)') CONFIN

IF (CONFIN.EQ.'UC') THEN
          MODEL = 'U'

ENDIF
IF (CONFIN.EQ.'EP') THEN
    WRITE (6,*) 'Would you like to consider strain hardening?'
    READ (6,'(A4)') HARD
ENDIF
 HARD = 'N'

   NA = ROUT
CALL ZERO(SSP,SSTR,CSTR,CU)
 CURV = 0
 B = 0
 FAIL = 0

WRITE (6,*) 'Is this for a column? (Y or N)'
READ (5,'(A4)') COL

L = 0

IF (COL.EQ.'Y') THEN
   WRITE (6,*) 'What is the length of the column? (mm)'
   READ(5,*) L
   WRITE (6,*) 'How long is the maximum momoment maintained(mm)'
   READ (5,*) DEP
   EIS = PI/64*E*((2*ROUT)**4-(2*RIN)**4)
   EIC = PI/64*5000*SQRT(FC)*(2*RIN)**4
   EI = EIS + EIC
ENDIF

DO 20 I = 1,6
 IF (I.EQ.1) THEN
      MAN = 1.0
    WRITE (2,*) 'Mander concrete with 100% concrete strength'
```

```
      ELSEIF (I.EQ.2) THEN
         MAN = 0.9
         WRITE (2,*) 'Mander concrete with 90% concrete strength'
      ELSEIF (I.EQ.3) THEN
         MAN = 0.8
         WRITE (2,*) 'Mander concrete with 80% concrete strength'
      ELSEIF (I.EQ.4) THEN
         MAN = 0.7
         WRITE (2,*) 'Mander concrete with 70% concrete strength'
      ELSEIF (I.EQ.5) THEN
         MAN = 0.6
         WRITE (2,*) 'Mander concrete with 60% concrete strength'
      ELSEIF (I.EQ.6) THEN
         MAN = 0.5
         WRITE (2,*) 'Mander concrete with 50% concrete strength'
      ENDIF
      WRITE (2,'(6F15.8)') ZER,ZER,ZER,ZER,ZER,ZER
      CALL ZERO(SSP,SSTR,CSTR,CU)
      CURV = CURVI
        INTCUR = INTC(1)
        DO 30 J = 1,CYC
          DIR = 'L'
          DL = DLAYER
          CALL LOAD(SCG,CCG,AC,AS,STEP,SSP,NA,DL,P,MAN,L,EI,CONFIN,DEP)
          IF (FAIL.EQ.1) THEN
            GOTO 200
          ENDIF
          CURVL = CURV
          CALL UNLOAD(SCG,CCG,AC,AS,STEP,NA,CURVL,DLAYER,B,SSP,P,MAN,L,EI,CONFIN)

30    CONTINUE
20    CONTINUE
40    CONTINUE
200   CONTINUE
      END

C-----------------------------------------------------------------
      SUBROUTINE INITS (E,FST,FSC,SINIT,FC,E01,E085,UNIT,P)

      REAL E,FST,FSC,SINIT,FC,P
      CHARACTER UNIT*4


      WRITE (6,*) 'Will you be using Metric(M) or Imperial(I)?'
      READ (5,'(A4)') UNIT

      IF (UNIT.EQ.'M') THEN
      WRITE (6,*) 'What is the elastic modulus of steel (MPa)?'
      READ (5,*) E
      WRITE (6,*) 'What is the tensile strength of steel (MPa)?'
      READ (5,*) FST
      WRITE (6,*) 'What is the compressive strength (MPa)?'
      READ (5,*) FSC
      WRITE (6,*) 'What is the compressive strength of concrete (MPa)?'
      READ (5,*) FC
      WRITE (6,*) 'What is the applied axial load (N)?'
      READ (5,*) P
         SINIT = 0
         E01 = 0.002
         E085 = 0.0018
      ELSE

      WRITE (6,*) 'What is the elastic modulus of steel (psi)?'
      READ (5,*) E
        E = E*0.006894
      WRITE (6,*) 'What is the tensile strength of steel (psi)?'
      READ (5,*) FST
        FST = FST * 0.006894
      WRITE (6,*) 'What is the compressive strength of steel (psi)?'
      READ (5,*) FSC
        FSC = FSC * 0.006894
      WRITE (6,*)'What is the compressive strength of concrete (psi)?'
      READ (5,*) FC
      WRITE (6,*) 'What is the applied axial force (lb)?'
      READ (5,*) P
        P = P * 4.448

        FC = FC * 0.006894
         SINIT = 0
         E01 = 0.002
         E085 = 0.0018
      ENDIF

      RETURN
      END

C-----------------------------------------------------------------
      SUBROUTINE CIRCLE (ROUT,RIN,THICK,UNIT)
C
C     THIS SUBROUTINE WILL ALLOW THE USER TO INPUT THE CROSS SECTION.
```

```
C
C   OUTERD = THE OUTER DIMENSION OF THE STEEL
C   INNERD = THE INNER DIMENSION OF THE STEEL
C   ROUT = THE OUTER RADIUS OF THE STEEL
C   RIN = THE INNER RADIUS OF THE STEEL

    REAL ROUT,RIN,THICK,OUTERD,INNERD
    CHARACTER UNIT*4

100 WRITE(6,*) 'What is the outer diameter of the steel shell?'
    READ (5,*) OUTERD
    WRITE(6,*) 'What is the inner diameter of the steel shell?'
    READ (5,*) INNERD
    IF (INNERD.GE.OUTERD) THEN
      WRITE(6,*)
      WRITE(6,*)'THE OUTER DIAMETER MUST BE GREATER THAN THE INNER'
      WRITE(6,*)
      GO TO 100
    ENDIF
    ROUT = OUTERD/2
    RIN = INNERD/2
    IF (UNIT.EQ.'I') THEN
       ROUT = 25.4*ROUT
       RIN = 25.4*RIN
    ENDIF
    THICK = ROUT-RIN

    RETURN
    END

C-------------------------------------------------------
    SUBROUTINE HEIGHC (ROUT,DLAYER,INC)


C   THIS SUBROUTINE WILL CALCULATE THE TOTAL HEIGHT OF THE CROSS
C   SECTION, AND CALCULATE THE INCREMENTAL LAYER SIZE.
C
C   ROUT = THE OUTER RADIUS OF THE STEEL CORE
C   DLAYER = THE HEIGHT OF EACH LAYER
C   INC = THE NUMBER OF LAYERS IN THE CROSS-SECTION (USER-DEFINED)


    REAL ROUT, DLAYER
    INTEGER INC

    WRITE (6,*) 'HOW MANY LAYERS FOR THE CROSS-SECTION (100)?'
    READ (5,'(I4)') INC
    DLAYER = 2*ROUT/INC


    RETURN
    END

C-------------------------------------------------------
    SUBROUTINE AREA(INC,DLAYER,ROUT,RIN,AS,AC,SCG,CCG)

C   THIS SUBROUTINE CALCULATES THE AREA AND CENTER OF GRAVITY FOR THE
C   CIRCULAR SECTION AT EACH LAYER OF CONCRETE AND STEEL.
C
C   SSA = AREA OF STEEL
C   SCA = AREA OF CONCRETE
C   DLAYER = THE HEIGHT OF EACH LAYER
C   ROUT = THE OUTER RADIUS OF THE STEEL
C   RIN = THE INNER RAIUS OF THE STEEL
C   AS(I) = THE AREA OF STEEL IN THE iTH LAYER
C   AC(I) = THE AREA OF CONCRETE IN THE iTH LAYER
C   SCG(I) = THE CENTER OF GRAVITY OF STEEL IN THE iTH LAYER
C   CCG(I) = THE CENTER OF GRAVITY OF CONCRETE IN THE iTH LAYER
C   SUMSA = THE TOTAL AREA OF STEEL
C   SUMCA = THE TOTAL AREA OF CONCRETE
C   PI = 3.14159265359
C   CD = CENTER OF GRAVITY OF CONCRETE CALCULATED IN DMOM
C   SD = CENTER OF GRAVITY OF STEEL CALCULATED IN DMOM
C   INC = THE NUMBER OF THE LAYERS THAT THE SECTION IS DIVIDED INTO
C   END = USING SYMMETRY ONLY HALF THE SECTION NEEDS TO BE CALCULATED
C

    REAL SSA,SCA,DLAYER,ROUT,RIN
    REAL AS(1000),AC(1000),SCG(1000),CCG(1000)
    REAL SUMSA,SUMCA,PI,CD,SD
    INTEGER INC,END,I

    PI = 3.14159265359
    END = INC/2
    SSA = 0
    SCA = 0

C   THIS LOOP CALCULATES THE AREA AND CENTER OF GRAVITY OF EACH
C   LAYER. USING SYMMETRY, ONLY HALF OF THE SECTION NEEDS TO BE
C   CALCULATED.
```

```
      DO 10 I=1,END
         CALL DAREA(SSA,SCA,DLAYER,ROUT,RIN,INC,AS,AC,I,SD,CD)
         AS(INC-I+1) = AS(I)
         AC(INC-I+1) = AC(I)
         SCG(I) = -SD+ROUT
         SCG(INC-I+1) = SD + ROUT
         CCG(I) = -CD+ROUT
         CCG(INC-I+1) = CD + ROUT
C        WRITE (6,'(4F10.2)') AC(I),CCG(I),AC(INC-I+1),CCG(INC-I+1)
 10   CONTINUE

      SUMSA = 2*SSA
      SUMCA = 2*SCA

CCCCCCCCCCCCCCCCCCCCCCCCC
      DO 100 J=1,INC
 100     WRITE (3,'(F15.8)') AC(J)
CCCCCCCCCCCCCCCCCCCCCCCCC


C     IF THERE IS AN ODD NUMBER OF LAYERS, THEN LOOP IS ENTERED AND
C     CALCULATES THE AREA AND CENTER OF GRAVITY FOR THE MIDDLE LAYER.
      IF (MOD(INC,2).NE.0) THEN
         A1 = 0.5*PI*(ROUT**2)
         A2 = 0.5*PI*(RIN**2)
         AS(END+1) = 2*(A1-A2-SSA)
         AC(END+1) = 2*(A2-SCA)
         SCG(END+1) = ROUT
         CCG(END+1) = ROUT
         SUMSA = SUMSA + AS(END+1)
         SUMCA = SUMCA + AC(END+1)
      END IF

      RETURN
      END
C-----------------------------------------------------------
      SUBROUTINE DAREA(SSA,SCA,DLAYER,ROUT,RIN,INC,AS,AC,I,SD,CD)

C     THIS SUBROUTINE IS CALLED BY AREA TO CALCULATE A LAYERS AREA AND
C     CENTER OF GRAVITY.
C
C     THETA = THE ANGLE THAT THE LAYER LINE AT OUTER STEEL MAKES WITH
C        THE CENTER OF THE SECTION
C     DLAYER = THE HEIGHT OF EACH LAYER
C     ROUT = THE OUTER RADIUS OF STEEL
C     RIN = THE INNER RADIUS OF STEEL
C     PHI = THE ANGLE THAT THE LAYER LINE AT THE INNER STEEL MAKES WITH
C        THE CENTER OF THE SECTION.
C     A1 = THE TOTAL AREA BELOW THE TOP OF THE LAYER
C     A2 = THE TOTAL AREA OF CONCRETE BELOW THE TOP OF THE LAYER
C     AS(I) = THE AREA OF STEEL IN THE iTH LAYER
C     AC(I) = THE AREA OF CONCRETE IN THE iTH LAYER
C     SSA = TOTAL AREA OF STEEL
C     SCA = TOTAL AREA OF CONCRETE
C     MOM1 = CENTER OF GRAVITY OF A1
C     MOM2 = CENTER OF GRAVITY OF A2
C     MOM3 = CENTER OF GRAVITY AT THE BOTTOM OF THE LAYER
C     MOM4 = CENTER OF GRAVITY AT THE TOP OF THE LAYER
C     AT = TOTAL AREA OF THE LAYER
C     ST = CENTER OF GRAVITY OF THE TOTAL AREA IN THE LAYER
C     SD = CENTER OF GRAVITY OF THE STEEL
C     CD = CENTER OF GRAVITY OF THE CONCRETE
C     INC = THE NUMBER OF LAYERS THAT THE SECTION IS DIVIDED INTO

      REAL THETA,DLAYER,ROUT,PHI,RIN,A1,A2
      REAL AS(1000),AC(1000),AT
      REAL SSA,SCA,MOM1,MOM2,MOM3,MOM4,ST,SD,CD
      INTEGER I,INC
      REAL J

      THETA = ACOS(1-I*DLAYER/ROUT)
      A1 = (ROUT**2)/2*(2*THETA-SIN(2*THETA))

C  THIS LOOP IS ENTERED IF THERE IS SOME CONCRETE IN THE LAYER

      IF ((I*DLAYER).GT.(ROUT-RIN)) THEN
         PHI = ACOS((ROUT-I*DLAYER)/RIN)
         A2 = (RIN**2)/2*(2*PHI-SIN(2*PHI))
         J = -(INC/2-I)
         CALL DMOM (RIN,J,DLAYER,MOM1)
C  THIS LOOP IS ENTERED IF THE BOTTOM OF THE LAYER IS IN THE OUTER CIRCLE
C  OF STEEL.
         IF (((I-1)*DLAYER).LT.(ROUT-RIN)) THEN
            J = -(INC/2-(ROUT-RIN)/DLAYER)
         ELSE
            J = -(INC/2-I+1)
         ENDIF
         CALL DMOM (RIN,J,DLAYER,MOM2)
      ELSE
         A2=0
```

```
      CD=0
    ENDIF
    AS(I) = A1-A2-SSA
    AC(I) = A2 - SCA
    AT = A1-SSA-SCA
    J = -(INC/2-I)
    CALL DMOM (ROUT,J,DLAYER,MOM3)
    J = -(INC/2-I+1)
    CALL DMOM (ROUT,J,DLAYER,MOM4)
    ST = (MOM4-MOM3)/AT
    IF (A2.NE.0) THEN
       CD = (MOM2-MOM1)/AC(I)
    ENDIF


    SD = (AT*ST-AC(I)*CD)/AS(I)
    SCA = SCA + AC(I)
    SSA = SSA + AS(I)

    RETURN
    END
C-------------------------------------------------------
    SUBROUTINE DMOM (RADIUS,I,DLAYER,MOM)

C   THIS SUBROUTINE CALCULATES THE POSITION OF THE CENTER OF GRAVITY
C   IN A GIVEN AREA.
C
C   MOM = CALCULATED CENTER OF GRAVITY OF AN AREA.

    REAL CON,RADIUS,Y,MOM,DLAYER
    REAL I,ZER1

    CON = (RADIUS)**2
    Y = I*DLAYER
    ZER1 = CON-Y**2

    IF (ZER1.LE.0) THEN
       ZER1 = 0
    ENDIF
C   MOM = -2*((CON-Y**2)**1.5)/3
    MOM = -2*(ZER1**1.5)/3

    RETURN
    END

C-------------------------------------------------------
    SUBROUTINE RECT (XB,XT,YL,YR,THICK,UNIT)
C
C   THIS SUBROUTINE WILL ALLOW THE USER TO INPUT THE CROSS SECTION.
C
C   XB(I) = AN ARRAY THAT HOLDS ALL OF THE BOTTOM X COORDINATE FOR
C       ITH RECTANGLE
C   XT(I) = AN ARRAY THAT HOLDS ALL OF THE TOP X COORDINATE FOR
C       ITH RECTANGLE
C   YL(I) = AN ARRAY THAT HOLDS ALL OF THE LEFT Y COORDINATE FOR
C       ITH RECTANGLE
C   YR(I) = AN ARRAY THAT HOLDS ALL OF THE RIGHT Y COORDINATE FOR
C       ITH RECTANGLE
C   THICK = THE THICKNESS OF THE STEEL ENCASEMENT
C   UNIT = THE UNITS OF THE PROBLEM, EITHER METRIC OR IMPERIAL

    REAL XB(2), XT(2), YL(2), YR(2),THICK
    CHARACTER UNIT*4

    WRITE (6,*)
    WRITE (6,*)
    WRITE (6,*) 'WHAT IS THE OUTER WIDTH IN THE X DIR?'
    READ (5,*) YR(1)
    YL(1) = 0
    WRITE (6,*) 'WHAT IS THE OUTER HEIGHT IN THE Y DIR?'
    READ (5,*) XT(1)
    XB(1) = 0
    WRITE (6,*) 'WHAT IS THE THICKNESS?'
    READ (5,*) THICK
    IF (UNIT.EQ.'I') THEN
       XB(1) = 25.4*XB(1)
       XT(1) = 25.4*XT(1)
       YR(1) = 25.4*YR(1)
       YL(1) = 25.4*YL(1)
    ENDIF
    XB(2) = XB(1) + THICK
    XT(2) = XT(1) - THICK
    YL(2) = YL(1) + THICK
    YR(2) = YR(1) - THICK


    RETURN
    END

C-------------------------------------------------------
```

```
      SUBROUTINE HEIGHR (XB,XT,HEIGHT,DLAYER,INC)


C     THIS SUBROUTINE WILL CALCULATE THE TOTAL HEIGHT OF THE CROSS
C     SECTION, AND CALCULATE THE INCREMENTAL LAYER SIZE.
C
C     XB(I) = AN ARRAY THAT HOLDS ALL OF THE BOTTOM X COORDINATE FOR
C         ITH RECTANGLE
C     XT(I) = AN ARRAY THAT HOLDS ALL OF THE TOP X COORDINATE FOR
C         ITH RECTANGLE
C     XLARGE = THE LARGEST X COORDINATE OF THE CROSS-SECTION
C     XSMALL = THE SMALLEST X COORDINATE OF THE CROSS-SECTION
C     HEIGHT = THE HEIGHT OF THE CROSS-SECTION
C     DLAYER = THE HEIGHT OF EACH LAYER
C     NOFR = NUMBER OF RECTANGLES IN THE CROSS-SECTION
C     INC = THE NUMBER OF LAYERS IN THE CROSS-SECTION (USER-DEFINED)
C     I,Y = COUNTERS


      REAL XB(2), XT(2)
      REAL HEIGHT, DLAYER
      INTEGER INC


      HEIGHT = XT(1) - XB(1)

      WRITE (6,*) 'HOW MANY LAYERS FOR THE CROSS-SECTION (100)?'
      READ (5,'(I4)') INC
      DLAYER = HEIGHT/INC


      RETURN
      END


C-----------------------------------------------------------
      SUBROUTINE AREAR (DL,XB,XT,YL,YR,INC,AS,AC,CCG,SCG)


C     THIS SUBROUTINE WILL CALCULATE THE AREA OF EACH LAYER.  IT WILL
C     ALSO TAKE INTO ACCOUNT THAT SOME LAYERS WILL BE PART OF MORE THAN
C     ONE RECTANGLE.
C
C     A(I) = THE AREA OF A LAYER
C     XB(I) = AN ARRAY THAT HOLDS ALL OF THE BOTTOM X COORDINATE FOR
C         ITH RECTANGLE
C     XT(I) = AN ARRAY THAT HOLDS ALL OF THE TOP X COORDINATE FOR
C         ITH RECTANGLE
C     YL(I) = AN ARRAY THAT HOLDS ALL OF THE LEFT Y COORDINATE FOR
C         ITH RECTANGLE
C     YR(I) = AN ARRAY THAT HOLDS ALL OF THE RIGHT Y COORDINATE FOR
C         ITH RECTANGLE
C     DLAYER = THE HEIGHT OF EACH LAYER
C     CG(I,N) = THE CENTER OF GRAVITY OF THE I LAYER OF THE N
C         RECTANGLE.(THIS IS NEEDED TO CALCULATE THE CENTER OF
C         GRAVITY OF LAYERS THAT HAVE RECTANGLES STARTING OR
C         ENDING IN THEM)
C     ACG(I,N) = THE AREA OF THE I LAYER OF THE N RECTANGLE
C     NOFR = NUMBER OF RECTANGLES USED IN THE CROSS SECTION
C     INC = THE NUMBER OF LAYERS THAT THE CROSS-SECTION IS DIVIDED
C     I,N,J = COUNTERS


      REAL AS(1000),AC(1000),XB(10),XT(10),YL(10),YR(10),DL
      REAL SCG(1000),CCG(1000)
      INTEGER I,INC,J
      INTEGER ENTER

C     THE FOLLOWING LOOP WILL SET ALL AREA'S AND CG'S TO ZERO.
      DO 10 I = 1,INC
        AS(I) = 0.0
        AC(I) = 0.0
        SCG(I) = 0.0
        CCG(I) = 0.0
 10   CONTINUE
      ENTER = 0
      DO 40 J = 1,INC
        IF (XB(2).GE.(J*DL)) THEN
          AS(J) = (YR(1)-YL(1))*DL
          SCG(J) = (DL/2)+((J-1)*DL)
        ELSE IF ((XB(2).LE.(J*DL)).AND.(XB(2).GT.((J-1)*DL))) THEN
          AC(J) = (YR(2)-YL(2))*(J*DL-XB(2))
          AS(J) = (YR(1)-YL(1))*(DL) - AC(J)
          CCG(J) = XB(2) + (J*DL-XB(2))/2
          SCG(J) = ((YR(1)-YL(1))*DL*(J*DL-DL/2)-AC(J)*CCG(J))/AS(J)
          ENTER = 1
C       ELSE IF ((XT(2).GE.(J*DL)).AND.(ENTER.EQ.1)) THEN
        ELSE IF (XT(2).GE.(J*DL)) THEN
          AC(J) = (YR(2)-YL(2))*DL
          AS(J) = (YR(1)-YL(1))*DL - AC(J)
```

```
        CCG(J) = J*DL - DL/2
        SCG(J) = J*DL - DL/2
      ELSE IF ((XT(2).LE.(J*DL)).AND.(XT(2).GT.((J-1)*DL))) THEN
        AC(J) = (YR(2)-YL(2))*(XT(2)-(J-1)*DL)
        AS(J) = (YR(1)-YL(1))*(DL) - AC(J)
        CCG(J) = (J-1)*DL + (XT(2)-(J-1)*DL)/2
        SCG(J) = ((YR(1)-YL(1))*DL*(J*DL-DL/2)-AC(J)*CCG(J))/AS(J)
      ELSE
        AS(J) = (YR(1)-YL(1))*DL
        SCG(J) = J*DL-DL/2
      ENDIF
40  CONTINUE
    RETURN
    END
C-----------------------------------------------------------
    SUBROUTINE LOAD(SCG,CCG,AC,AS,ST,SSP,NA,DL,P,MAN,L,EI,CONFIN,DEP)

C   THIS SUBROUTINE LOADS THE STRUCTURE BOTH IN LOADING AND REVERSE
C   LOADING.  THE LIMITS ARE SPECIFIED BY THE USER, THROUGH THE
C   INPUTTED VALUES OF THE ULTIMATE CURVATURE OF EACH LOADING PATTERN
C
C   E = THE ELASTIC MODULUS OF STEEL
C   FST = THE ULTIMATE STRESS IN TENSION OF THE STEEL
C   FSC = THE ULTIMATE STRESS IN COMPRESSION OF THE STEEL
C   SINIT = THE INITIAL STRESS IN THE CROSS-SECTION
C   FC = THE CONCRETE COMPRESSIVE STRENGTH
C   E01 = THE STRAIN CORRESPONDING TO PEAK STRESS OF UNCONFINED CONCRETE
C   E1 = THE STRAIN CORRESPONDING TO PEAK STRESS OF CONFINED CONCRETE
C   E085 = THE STRAIN AT 85% STRENGTH LEVEL BEYOND THE PEAK STRESS OF
C       UNCONFINED CONCRETE.
C   RIN = THE INNER RADIUS OF STEEL
C   ROUT = THE OUTER RADIUS OF STEEL
C   THICK = THE THICKNESS OF THE STEEL
C   CURV = THE INCREMENTAL CURVATURE CALCULATED AT STEP
C   SCG(I) = THE CENTER OF GRAVITY OF STEEL OF THE iTH LAYER
C   CCG(I) = THE CENTER OF GRAVITY OF CONCRETE OF THE iTH LAYER
C   NA = THE NEUTRAL AXIS OF THE SECTION
C   SH(I) = THE DISTANCE FROM THE NEUTRAL AXIS TO THE CENTER OF GRAVITY
C       OF EACH LAYER OF STEEL.
C   CH(I) = THE DISTANCE FROM THE NEUTRAL AXIS TO THE CENTER OF GRAVITY
C       OF EACH LAYER OF CONCRETE.
C   SS(I) = THE STEEL STRESS AT THE iTH LAYER
C   CS(I) = THE CONCRETE STRESS AT THE iTH LAYER
C   SF(I) = THE STEEL FORCE AT THE iTH LAYER
C   CF(I) = THE CONCRETE FORCE AT THE iTH LAYER
C   FTOT = THE TOTAL FORCE ACTING ON THE SECTION
C   AS(I) = THE AREA OF STEEL IN THE iTH LAYER
C   CS(I) = THE AREA OF CONCRETE IN THE iTH LAYER
C   SSTR(I) = THE STEEL STRESS AT THE TOP OF THE LOADING PATTERN
C   CSTR(I) = THE CONCRETE STRESS AT THE TOP OF THE LOADING PATTERN
C   SSP(I) = THE STEEL STRESS AT ZERO MOMENT.
C   CU(I) = THE PREVIOUS CONCRETE STRESS (USED FOR UNLOADING)
C   M(I) = THE MOMENT IN THE iTH LAYER
C   CU(I) = THE PREVIOUS CONCRETE STRESS IN THE iTH LAYER
C   MTOTAL = THE TOTAL MOMENT ACTING ON THE STRUCTURE.
C   INTCUR = THE ULTIMATE CURVATURE FOR THIS PARTICULAR LOADING
C   CSTR(I) = THE VALUE OF CONCRETE STRESS AT THE TOP OF THE PREVIOUS
C       LOADING CYCLE
C   SSTR(I) = THE VALUE OF STEEL STRESS AT THE TOP OF THE PREVIOUS
C       LOADING CYCLE
C   CURVI = THE CURVATURE INCREMENT USED THROUGHOUT THE ANALYSIS
C   NAEQ = TO DETERMINE IF WHEN CALCULATING THE NEUTRAL AXIS IF A
C       SMALLER INTERVAL SHOULD BE USED.
C   STEP,ST = THE NUMBER OF TIMES THE CURVATURE HAS INCREASED FOR A
C       PARTICULAR LOADING CYCLE.
C   COUNT =  INCREMENTED EACH TIME A NEW na IS CALCULATED
C   INC = THE NUMBER OF LAYERS THAT THE SECTION IS DIVIDED INTO
C   DLAYER,DL = THE HEIGHT OF THE LAYER
C   UNIT = THE UNITS OF THE PROBLEM, EITHER METRIC OR IMPERIAL
C   MAT = THE TYPE OF MATERIAL THE ANALYSIS IS ON (STEEL,CONCRETE,OR
C       BOTH)
C   DIR = WHETHER THE LOADING IS POSITIVE LOADING(L) OR REVERSE(R)
C   MODEL = THE TYPE OF CONCRETE MODEL THE USER WOULD LIKE TO USE

    REAL E,SINIT,FST,FSC,FC,E01,E085,RIN,ROUT,THICK,E1
    REAL CURV,SCG(1000),CCG(1000),NA,SH(1000),CH(1000),CS(1000)
    REAL AC(1000),AS(1000),SF(1000),CF(1000),SS(1000),FTOT
    REAL M(1000),CU(1000),MTOT(1000),MTO
    REAL MTOTAL,SSTR(1000),CSTR(1000),SSP(1000)
    REAL DL,DLAYER,INTCUR,CURVI,P,CFTOT
    REAL MAN,L,EI,MOMA(1000),DEP,CT
    INTEGER STEP,COUNT,NAEQ,ST,INC
    INTEGER I,J,K,LL,V,FAIL,A,UNL,Y
    CHARACTER MAT*4,DIR*4,MODEL*4,UNIT*4,CONFIN*4,HARD*4

    COMMON /FIRST/ E,SINIT,FST,FSC,FC,E01,E085,RIN,ROUT,E1
    COMMON /SECOND/ CU,SSTR,CSTR
    COMMON /THIRD/ DIR,MODEL,MAT,UNIT
    COMMON /FOURTH/INC,CURV,INTCUR,CURVI,FAIL
    COMMON /FIFTH/ HARD
```

```
      DIN = RIN*2

      Y = 0
      DLAYER = DL
      CURV1 = CURV
      THICK = ROUT-RIN
      STEP = ST
      STEP = 0

C     THE NEXT TWO LOOPS INITIALIZE THE STRESSES EACH TIME THE SECTION
C     IS LOADED.  TO KEEP TRACK, STEP IS RESET TO ZERO, EACH TIME THE
C     SECTION IS LOADED.
      IF ((MAT.EQ.'C').OR.(MAT.EQ.'B')) THEN
        DO 10 I = 1,INC
           CS(I) = CU(I)
           SS(I) = 0
 10     CONTINUE
      ELSE
        DO 20 I = 1,INC
          CS(I) = 0
 20     CONTINUE
      ENDIF

C     THE LOOP BELOW IS REPEATED UNTIL THE INCREMENTAL CURVATURE REACHES
C     THE ULTIMATE CURVATURE FOR THAT CYCLIC LOADING.

 100  STEP = STEP + 1
      COUNT = 1
      NAEQ = 0
      UNL = 0
      CALL CURVAT (STEP,CURV,CURV1,UNL)
 200  IF (CURV.EQ.0) THEN
        EC = EC
      ELSE
        CALL CALCH(SCG,CCG,NA,INC,SH,CH,DIR)
      ENDIF

C     THE FOLLOWING CALCULATES THE STRESS IN THE STEEL AND CONCRETE
      IF ((MAT.EQ.'S').OR.(MAT.EQ.'B')) THEN
        CALL SSTEEL (INC,CURV,SH,SS,SSP,FAIL,EC,Y,CS,CONFIN,HARD)
C       IF (FAIL.EQ.1) THEN
C          WRITE(6,*) 'HERE IN LOAD'
C          GOTO 222
C       ENDIF
      ENDIF
      IF ((MAT.EQ.'C').OR.(MAT.EQ.'B')) THEN
        IF (MODEL.EQ.'M') THEN
       CALL SCONCM(INC,AC,CH,FC,FST,THICK,RIN,CURV,E01,CS,E1,EC,NA,MAN)
        ELSE IF (MODEL.EQ.'S') THEN
          CALL SCONCA(AC,CURV,CH,THICK,FST,RIN,FC,E01,INC,E085,CS,EM)
        ELSE
          CALL SCONCH(AC,CH,CURV,CS,FC,INC,CU,E01,EC,CONFIN)
        ENDIF
      ENDIF

C     THE FOLLOWING CALCULATES THE FORCE IN THE SECTION
      IF (MAT.EQ.'B') THEN
        Y=0
        CALL FORCE (AS,AC,SS,CS,INC,SF,CF,FTOT,COUNT,NA,NAEQ,P)
      ELSE IF (MAT.EQ.'S') THEN
        FTOT = 0
        DO 30 J = 1,INC
          SF(J) = SS(J) * AS(J)
          FTOT = SF(J) + FTOT
 30     CONTINUE

      ELSE
        FTOT = 0
        DO 40 K = 1,INC
          CF(K) = CS(K)*AC(K)
          FTOT = CF(K) + FTOT
 40     CONTINUE
      ENDIF
      IF (DIR.EQ.'R') THEN
           FTOT=-FTOT
      ENDIF
C     IF THE COMPOSITE ACTION IS DESIRED, THE NEUTRAL AXIS NEEDS TO BE
C     ITERITIVELY FOUND.
C     IF (MAT.EQ.'B') THEN
        IF (FTOT.NE.P) THEN
          CALL NEUT (DLAYER,NA,FTOT,NAEQ,P)
          COUNT = COUNT + 1
          IF (COUNT.GE.5000) THEN
            GO TO 222
          ENDIF
          GO TO 200
C       ENDIF
      ENDIF
```

```
C   THE FOLLOWING CALCULATES THE MOMENTS
    IF (MAT.EQ.'B') THEN
      CALL MOMENT (INC,SF,CF,SCG,CCG,M,MTOTAL,ROUT,DIR,UNIT,P)
    ELSE IF (MAT.EQ.'S') THEN
        MTOTAL = 0
        IF (DIR.EQ.'L') THEN
          DO 50 LL=1,INC
            M(LL) = SF(LL)*SCG(LL)
            MTOTAL = M(LL) + MTOTAL
50        CONTINUE
        ELSE
          DO 60 LL = 1,INC
            M(LL) = SF(LL)*(2*ROUT - SCG(LL))
            MTOTAL = M(LL) + MTOTAL
60        CONTINUE
        ENDIF
        IF (UNIT.EQ.'I') THEN
          MTOTAL = MTOTAL*8.85074E-9
        ELSE
          MTOTAL = MTOTAL/1000000
        ENDIF
    ELSE
        MTOTAL = 0
        IF (DIR.EQ.'L') THEN
          DO 70 V = 1,INC
            M(V) = CF(V) *CCG(V)
            MTOTAL = M(V) + MTOTAL
70        CONTINUE
        ELSE
          DO 80 V = 1,INC
            M(V) = CF(V) *(2*ROUT -CCG(V))
            MTOTAL = M(V) + MTOTAL
80        CONTINUE
        ENDIF
        IF (UNIT.EQ.'I') THEN
          MTOTAL = MTOTAL*8.85074E-9
        ELSE
          MTOTAL = MTOTAL/1000000
        ENDIF
    ENDIF
    IF (DIR.EQ.'R') THEN
        MTOTAL = -MTOTAL
    ENDIF

C   THE CURVATURE RELATING TO THE MOMENT CURVATURE DIAGRAM IS CALCULATED
C   AND THE RESULTANT MOMENT AND CURVATURE ARE SENT TO BE PRINTED
    IF (DIR.EQ.'L') THEN
      CURVT = CURV1+CURV
    ELSE
      CURVT = CURV1-CURV
    ENDIF

     CFTOT = 0
      DO 42 K = 1,INC
        CF(K) = CS(K)*AC(K)
        CFTOT = CF(K) + CFTOT
42    CONTINUE

    MTO = MTOTAL
    CT = CURVT
    CALL PRINT(MTO,CT,UNIT,NA,MTOT,STEP,SS,FST,INC,L,ELMOMA,CS,Y,DEP)



CCCCCCCCCCCCCCCCCCCCCCCCCCCCCC
     CFT =0
     SFT =0

    DO 124 I = 1,INC
     CFT = CF(I)+ CFT
     SFT = SF(I)+ SFT
C   WRITE(3,'(6F16.3,F18.15)')SF(I),SS(I),CF(I),CS(I),NA,CURVT
 124  CONTINUE
C       WRITE (3,'(2F16.3)') CFT,SFT
CCCCCCCCCCCCCCCCCCCCCCCCCCCCCC

C   THE CURVATURE IS CHECKED TO SEE IF IT IS BELOW THE INTCUR VALUE.
C   IF NOT THEN THE LOOP IS REPEATED.
    IF (DIR.EQ.'L') THEN
      IF (CURVT.LT.INTCUR) THEN
        GO TO 100
      ENDIF
    ELSE
      IF (CURVT.GT.-INTCUR) THEN
        GO TO 100
      ENDIF
    ENDIF
```

```
C   THE STEP. TOTAL CURVATURE AND CU VALUES ARE ALL SENT BACK TO THE
C   MAIN PROGRAM.
    ST = STEP
    CURV = CURVT
    IF ((MAT.EQ.'C').OR.(MAT.EQ.'B')) THEN
     DO 90 I=1,INC
        CU(I) = CS(I)
        CSTR(I) = CS(I)
90    CONTINUE
    ENDIF
    IF ((MAT.EQ.'S').OR.(MAT.EQ.'B')) THEN
     DO 110 I = 1,INC
        SSTR(I) = SS(I)
        WRITE (8,*) I,SSTR(I)
110   CONTINUE
    ENDIF


222  CONTINUE

    RETURN
    END
C-----------------------------------------------------------
    SUBROUTINE UNLOAD(SCG,CCG,AC,AS,ST,NA,CURVL,DL,B,SSP,P,L,EI)

C   THIS SUBROUTINE UNLOADS THE STRUCTURE BOTH IN LOADING AND REVERSE
C   LOADING.  UNLOADING STOPS WHEN THE TOTAL MOMENT IS EQUAL TO ZERO.
C
C   E = THE ELASTIC MODULUS OF STEEL
C   FST = THE ULTIMATE STRESS IN TENSION OF THE STEEL
C   FSC = THE ULTIMATE STRESS IN COMPRESSION OF THE STEEL
C   SINIT = THE INITIAL STRESS IN THE CROSS-SECTION
C   FC = THE CONCRETE COMPRESSIVE STRENGTH
C   E01 = THE STRAIN CORRESPONDING TO PEAK STRESS OF UNCONFINED CONCRETE
C   E1 = THE STRAIN CORRESPONDING TO PEAK STRESS OF CONFINED CONCRETE
C   E085 = THE STRAIN AT 85% STRENGTH LEVEL BEYOND THE PEAK STRESS OF
C       UNCONFINED CONCRETE.
C   RIN = THE INNER RADIUS OF STEEL
C   ROUT = THE OUTER RADIUS OF STEEL
C   THICK = THE THICKNESS OF THE STEEL
C   CURV = THE INCREMENTAL CURVATURE CALCULATED AT STEP
C   SCG(I) = THE CENTER OF GRAVITY OF STEEL OF THE iTH LAYER
C   CCG(I) = THE CENTER OF GRAVITY OF CONCRETE OF THE iTH LAYER
C   NA = THE NEUTRAL AXIS OF THE SECTION
C   SH(I) = THE DISTANCE FROM THE NEUTRAL AXIS TO THE CENTER OF GRAVITY
C       OF EACH LAYER OF STEEL.
C   CH(I) = THE DISTANCE FROM THE NEUTRAL AXIS TO THE CENTER OF GRAVITY
C       OF EACH LAYER OF CONCRETE
C   SS(I) = THE STEEL STRESS AT THE iTH LAYER
C   CS(I) = THE CONCRETE STRESS AT THE iTH LAYER
C   SF(I) = THE STEEL FORCE AT THE iTH LAYER
C   CF(I) = THE CONCRETE FORCE AT THE iTH LAYER
C   FTOT = THE TOTAL FORCE ACTING ON THE SECTION
C   AS(I) = THE AREA OF STEEL IN THE iTH LAYER
C   CS(I) = THE AREA OF CONCRETE IN THE iTH LAYER
C   SSTR(I) = THE STEEL STRESS AT THE TOP OF THE LOADING PATTERN
C   CSTR(I) = THE CONCRETE STRESS AT THE TOP OF THE LOADING PATTERN
C   SSP(I) = THE STEEL STRESS AT ZERO MOMENT.
C   CU(I) = THE PREVIOUS CONCRETE STRESS (USED FOR UNLOADING)
C   M(I) = THE MOMENT IN THE iTH LAYER
C   CU(I) = THE PREVIOUS CONCRETE STRESS IN THE iTH LAYER
C   MTOTAL = THE TOTAL MOMENT ACTING ON THE STRUCTURE
C   INTCUR = THE ULTIMATE CURVATURE FOR THIS PARTICULAR LOADING.
C   CSTR(I) = THE VALUE OF CONCRETE STRESS AT THE TOP OF THE PREVIOUS
C       LOADING CYCLE
C   SSTR(I) = THE VALUE OF STEEL STRESS AT THE TOP OF THE PREVIOUS
C       LOADING CYCLE
C   B = THE CURVATURE WHEN TOTAL MOMENT EQUALS ZERO.
C   CUR = THE TOTAL CURVATURE THAT HAS BEEN UNLOADED
C   CURVI = THE CURVATURE INCREMENT USED THROUGHOUT THE ANALYSIS
C   NAEQ = TO DETERMINE IF WHEN CALCULATING THE NEUTRAL AXIS IF A
C       SMALLER INTERVAL SHOULD BE USED.
C   STEP,ST = THE NUMBER OF TIMES THE CURVATURE HAS INCREASED FOR A
C       PARTICULAR LOADING CYCLE.
C   COUNT =  INCREMENTED EACH TIME A NEW na IS CALCULATED
C   INC = THE NUMBER OF LAYERS THAT THE SECTION IS DIVIDED INTO
C   DLAYER,DL = THE HEIGHT OF THE LAYER
C   UNIT = THE UNITS OF THE PROBLEM, EITHER METRIC OR IMPERIAL
C   MAT = THE TYPE OF MATERIAL THE ANALYSIS IS ON (STEEL,CONCRETE,OR
C       BOTH)
C   DIR = WHETHER THE LOADING IS POSITIVE LOADING(L) OR REVERSE(R)
C   MODEL = THE TYPE OF CONCRETE MODEL THE USER WOULD LIKE TO USE

    REAL E,SINIT,FST,FSC,FC,E01,E085,RIN,ROUT,THICK,E1
    REAL SCG(1000),CCG(1000),AC(1000),AS(1000),NA,DLAYER
    REAL SH(1000),CH(1000),SS(1000),CS(1000),SF(1000),CF(1000),FTOT
    REAL M(1000),B,CUR,CURV2,CURVR
    REAL SSTR(1000),CSTR(1000),SSP(1000),DL
    REAL MO(1000),CU(1000),P
```

```
      REAL CURVL,CURV,MTOTAL,CURVI,INTCUR
      REAL L,EI,MOMA,MTO,CT,DEP
      INTEGER STEP,COUNT,NAEQ
      INTEGER J,K,LL,N,ST,FAIL,UNL
      CHARACTER MAT*4,DIR*4,MODEL*4,UNIT*4

      COMMON /FIRST/ E,SINIT,FST,FSC,FC,E01,E085,RIN,ROUT,E1
      COMMON /SECOND/ CU,SSTR,CSTR
      COMMON /THIRD/ DIR,MODEL,MAT,UNIT
      COMMON /FOURTH/INC,CURV,INTCUR,CURVI,FAIL

C     THE FOLLOWING INITIALIZES THE VARIABLES
      STEP = ST
      CURV2 = CURVL
      CURVR = CURV2-B
      DEP = 0
C     NA = ROUT

300   STEP = STEP-1
      DLAYER = DL
      THICK = ROUT-RIN
      COUNT = 1
      NAEQ = 1
      UNL = 0
      CALL CURVAT (STEP,CURV,CURVI,UNL)
      IF (DIR.EQ.'L') THEN
         CURVT= B + CURV
      ELSE
         CURVT = B-CURV
      ENDIF

400   CALL CALCH (SCG,CCG,NA,INC,SH,CH,DIR)
      IF (DIR.EQ.'L') THEN
         CUR = CURVL-(B+CURV)
      ELSE
         CUR = -(CURV2-(B-CURV))
      ENDIF
C     THE FOLLOWING DETERMINES THE STRESSES
      IF ((MAT.EQ.'S').OR.(MAT.EQ.'B')) THEN
        CALL SSTEEU (INC,SS,SSTR,SH,E,SINIT,FST,FSC,CUR)
      ENDIF
      IF ((MAT.EQ.'C').OR.(MAT.EQ.'B')) THEN
        IF (MODEL.EQ.'U') THEN
          CALL SCONUH(INC,AC,CH,CS,FC,CUR,CSTR,CU)
        ELSE
          CALL SCONUM(AC,CH,CSTR,FC,CURV2,CURVT,E1,INC,CS,CU)
        ENDIF
      ENDIF

C     THE FOLLOWING CALCULATES THE FORCE
      IF (MAT.EQ.'B') THEN
        CALL FORCE (AS,AC,SS,CS,INC,SF,CF,FTOT,COUNT,NA,NAEQ,P)
      ELSE IF (MAT.EQ.'S') THEN
          FTOT = 0
          DO 10 J=1,INC
             SF(J) = SS(J)*AS(J)
             FTOT = SF(J) + FTOT
10        CONTINUE
      ELSE
          FTOT = 0
          DO 20 K =1,INC
             CF(K) = CS(K) * AC(K)
             FTOT = CF(K) + FTOT
20        CONTINUE
      ENDIF

C     THE CHANGING OF SIGNS ON FTOT ALLOWS FOR THE NEUT SUBROUTINE
C     TO BE USED IN BOTH DIRECTIONS.
      IF (DIR.EQ.'L') THEN
          FTOT = -FTOT
      ENDIF

C     IF COMPOSITE ACTION IS BEING CONSIDERED, THE NEUTRAL AXIS IS FOUND
C     IN AN ITERATIVE PROCESS
CCCCCCCCCCCCCCCCCCCCCC
      DO 14 I =1,INC
      WRITE (3,*) SF(I),CF(I),FTOT,NA
14    CONTINUE
CCCCCCCCCCCCCCCCCCCCCC
      IF (MAT.EQ.'B') THEN
       IF (FTOT.NE.0) THEN
         CALL NEUT (DLAYER,NA,FTOT,NAEQ,P)
         COUNT = COUNT + 1
         GO TO 400
       ENDIF
      ENDIF

C     THE FOLLOWING CALCULATES THE MOMENTS
      IF (MAT.EQ.'B') THEN
        CALL MOMENT (INC,SF,CF,SCG,CCG,M,MTOTAL,ROUT,DIR,UNIT,P)
```

```
      ELSE IF (MAT.EQ.'S') THEN
         MTOTAL = 0.0
         IF (DIR.EQ.'L') THEN
            DO 30 LL=1,INC
               MO(LL) = SF(LL) * SCG(LL)
               MTOTAL = MO(LL) + MTOTAL
30          CONTINUE
         ELSE
            DO 40 LL=1,INC
               MO(LL) = SF(LL) * (2*ROUT-SCG(LL))
               MTOTAL = MO(LL) + MTOTAL
40          CONTINUE
         ENDIF
         IF (UNIT.EQ.'I') THEN
            MTOTAL = MTOTAL*8.85074E-9
         ELSE
            MTOTAL = MTOTAL/1000000
         ENDIF
      ELSE
         MTOTAL = 0
         IF (DIR.EQ.'L') THEN
            DO 50 N=1,INC
               MO(N) = CF(N) *CCG(N)
               MTOTAL = MO(N) + MTOTAL
50          CONTINUE
         ELSE
            DO 60 N=1,INC
               MO(N) = CF(N) *(2*ROUT-CCG(N))
               MTOTAL = MO(N) + MTOTAL
60          CONTINUE
         ENDIF
         IF (UNIT.EQ.'I') THEN
            MTOTAL = MTOTAL*8.85074E-9
         ELSE
            MTOTAL = MTOTAL/1000000
         ENDIF
      ENDIF
      IF (DIR.EQ.'R') THEN
         MTOTAL=-MTOTAL
      ENDIF

C     THE MOMENT AND CURVATURE ARE SENT TO BE PRINTED
      MTO = MTOTAL
      CT = CURVT
      CALL PRINT(MTO,CT,UNIT,NA,MTOT,STEP,SS,FST,INC,L,EI,MOMA,CS,Y,DEP)

C     THE FOLLOWING LOOPS CHECK IF THE TOTAL MOMENT IS EQUAL TO ZERO.
C     IF IT ISN'T THEN THE LOOP IS REENTERED.
      IF (DIR.EQ.'L') THEN
         IF (MTOTAL.GE.0.0001) THEN
            GO TO 300
         ENDIF
      ELSE
         IF (MTOTAL.LE.-0.0001) THEN
            GO TO 300
         ENDIF
      ENDIF

C     THE STEP,TOTAL CURVATURE  SSP AND CU ARE SENT BACK TO THE MAIN PROGRAM
      ST = STEP
      CURVL = CURVT
      DO 70 NN = 1,INC
         IF ((MAT.EQ.'S').OR.(MAT.EQ.'B')) THEN
            SSP(NN) = SS(NN)
         ENDIF
         IF ((MAT.EQ.'C').OR.(MAT.EQ.'B')) THEN
            CU(NN) = CS(NN)
         ENDIF
70    CONTINUE

      RETURN
      END
C-----------------------------------------------------------------
      SUBROUTINE ZERO(SSP,SSTR,CSTR,CU)

C     THIS SUBROUTINE SETS ALL VALUES EQUAL TO ZERO.
C
C     SSP(I) = THE STEEL STRESS WHEN THE TOTAL MOMENT EQUAL ZERO.
C     SSTR(I) = THE STEEL STRESS AT THE TOP OF THE LOADING CURVE.
C     CSTR(I) = THE CONCRETE STRESS AT THE TOP OF THE LOADING CURVE.
C     CU(I) = THE PREVIOUS CONCRETE STRESS

      REAL SSP(1000),SSTR(1000),CSTR(1000)
      REAL CU(1000)
      INTEGER I

      DO 10 I = 1,1000
         SSP(I) = 0
         SSTR(I) = 0
         CSTR(I) = 0
```

```
      CU(I) = 0
10  CONTINUE

    RETURN
    END
C-----------------------------------------------------------
    SUBROUTINE NEUT (DLAYER,NA,FTOT,NAEQ,P)

C   THIS SUBROUTINE IS ENTERED IF THE FORCES ON THE CROSS-SECTION
C   DO NOT EQUAL ZERO.  IT IS EITHER MOVED UP OR DOWN TO ENSURE
C   EQUILIBRIUM.
C
C   DLAYER = THE HEIGHT OF EACH LAYER
C   C = THE NEUTRAL AXIS LOCATION
C   FTOTAL = THE TOTAL FORCE OF THE CROSS-SECTION AT A PARTICULAR
C        ITERATION

    REAL DLAYER,NA,FTOT,P


    IF (NAEQ.EQ.0) THEN
      IF (FTOT.GT.P) THEN
        NA=NA+1000
      ELSE
        NA=NA-1000
      END IF
    ELSE IF (NAEQ.EQ.1) THEN
      IF (FTOT.GT.P) THEN
        NA=NA+DLAYER
      ELSE
        NA=NA-DLAYER
      END IF
    ELSE
      IF (FTOT.GT.P) THEN
        NA=NA+DLAYER/100
      ELSE
        NA=NA-DLAYER/100
      END IF
    END IF
C   WRITE (6,*) FTOT,P,NA
    RETURN
    END
C-----------------------------------------------------------
    SUBROUTINE STRAIN (ECEQ,FTOT,P,EC)

    REAL FTOT, P , EC
    INTEGER ECEQ

    IF (ECEQ.EQ.0) THEN
        IF (FTOT.GT.P) THEN
            EC = EC + 0.00001
        ELSE
            EC = EC - 0.00001
        ENDIF
    ELSE
        IF (FTOT.GT.P) THEN
            EC = EC + 0.00001/100
        ELSE
            EC = EC - 0.00001/100
        ENDIF
    ENDIF
    RETURN
    END
C-----------------------------------------------------------
    SUBROUTINE CALCH (SCG,CCG,NA,INC,SH,CH,DIR)

C   THIS SUBROUTINE WILL CALCULATE THE DISTANCE FROM THE NEUTRAL
C   AXIS OF THE CROSS SECTION TO THE HEIGHT OF EACH LAYER FROM THE
C   X AXIS.
C
C   NA = THE SECTION'S NEUTRAL AXIS
C   SH(I) = THE DISTANCE FROM THE STEEL LAYER'S CENTER OF GRAVITY TO
C        THE SECTION'S NEUTRAL AXIS
C   CH(I) = THE DISTANCE FROM THE CONCRETE LAYER'S CENTER OF GRAVITY
C        TO THE SECTION'S NEUTRAL AXIS
C   SCG(I) = THE CENTER OF GRAVITY OF THE STEEL IN LAYER i
C   CCG(I) = THE CENTER OF GRAVITY OF THE CONCRETE IN LAYER i
C   INC = THE NUMBER OF LAYERS THE CROSS-SECTION IS DIVIDED INTO
C   DIR = WHETHER THE SECTION IS IN LOADING(L) OR REVERSE LOADING(R)

    REAL NA,SH(1000),CH(1000)
    REAL SCG(1000),CCG(1000)
    INTEGER I, INC
    CHARACTER DIR*4

    IF (DIR.EQ.'L') THEN
    DO 10 I = 1,INC
        SH(I) = (SCG(I)-NA)
        CH(I) = (CCG(I)-NA)
10  CONTINUE
```

```
      ELSE
      DO 20 J=1,INC
         SH(J) = NA-SCG(J)
         CH(J) = NA-CCG(J)
 20   CONTINUE
      ENDIF


      RETURN
      END
C-----------------------------------------------------------------
      SUBROUTINE CURVAT (STEP,CURV,CURVI,UNL)

C     THIS SUBROUTINE WILL CALCULATE THE CURVATURE AT EACH ITERATION.
C
C     CURVI = THE INPUTED VALUE FOR THE CURVATURE INCREMENT
C     CURV = THE CURVATURE AT A PARTICULAR ITERATION
C     STEP = THE ITERATION NUMBER.

      REAL CURV,CURVI
      INTEGER STEP,UNL

      IF (UNL.EQ.0) THEN
        CURVI = CURVI
      ELSE
        CURVI = CURVI/4
      ENDIF
      CURV = STEP * CURVI

      RETURN
      END
C-----------------------------------------------------------------
      SUBROUTINE SSTEEL(INC,CURVI,SH,SS,SSP,FAIL,EC,Y,CS,CONFIN,HARD)
C     SUBROUTINE SSTEEL(INC,CURVI,SH,E,SINIT,FST,FSC,SS,SSP,FAIL,EC,Y)

C     THIS SUBPROGRAM WILL CALCULATE THE STRESS OF EACH LAYER.  IF
C     THIS STRESS IS GREATER THAN THE ULTIMATE VALUE THAN THE ULTIMATE
C     VALUE IS USED FOR THAT LAYER
C
C     CURVI = THE CURVATURE AT A PARTICULAR ITERATION
C     SH(I) = THE DISTANCE FROM THE LAYER'S CENTER OF GRAVITY TO THE
C          SECTION'S NEUTRAL AXIS
C     E = THE ELASTIC MODULUS OF STEEL
C     SINIT = THE INITIAL VALUE OF STRESS IN THE CROSS-SECTION
C     SS(I) = THE STRESS AT ITH LEVEL
C     FST = THE ULTIMATE TENSION STRESS
C     FSC = THE ULTIMATE COMPRESSION STRESS
C     STRAIN = THE STRAIN IN THE ITH LAYER
C     FY = THE ULTIMATE STRESS FOR THE PARTICULAR LAYER
C     INC = THE NUMBER OF LAYERS THAT THE CROSS-SECTION IS DIVIDED

      REAL CURVI,SH(1000),E,SINIT,FST,FSC
      REAL FY,ESH,ESU,R,M,EC,CS(1000)
      REAL SS(1000),SSP(1000),DIN,FC,THICK
C     REAL E,SINIT,FST,FSC,FC,E01,E085,RIN,ROUT,E1
      INTEGER I,INC,FAIL,Y
      CHARACTER CONFIN*4,HARD*4

      COMMON /FIRST/ E,SINIT,FST,FSC,FC,E01,E085,RIN,ROUT,E1

      DIN = 2*RIN
      THICK = ROUT-RIN
      DO 10 I = 1,INC
        IF (CURVI.EQ.0) THEN
           EC = EC
        ELSE
           EC = CURVI * SH(I)
        ENDIF

        IF (EC.LT.0) THEN
           FY = -FST
        ELSE
           FY = FSC
        ENDIF
C     THE STRESS IN THE STEEL MUST BE ADDED TO ANY STRESS THAT WAS THERE
C     AT THE START OF LOADING
        IF ((ABS(EC).LT.(14*ABS(FY)/E)).OR.(HARD.EQ.'N')) THEN
          SS(I) = (EC*E) + SINIT + SSP(I)
          IF ((CONFIN.EQ.'BA').AND.(CS(I).GT.FC)) THEN
C          WRITE (6,*) 'HELLO'
           IF (SS(I).GE.0) THEN
              Z = 1
           ELSE
              Z = -1
           ENDIF
           FL = (ABS(SS(I))-FC)/4.1
           FT = FL*DIN/2/THICK
           SS(I) = (-FT+SQRT(FT*FT-4*(FT-FST)))/2*Z
          ENDIF
```

```
C   IF THE STRESS IS IN THE TOP FIBERS, THIS LOOP IS ENTERED.
        IF (SS(I).LE.(-FST)) THEN
          SS(I) = -FST
        ENDIF

C   IF THE STRESS IS IN THE BOTTOM FIBERS, THIS LOOP IS ENTERED.
        IF (SS(I).GE.FSC) THEN
          SS(I) = FSC
        ENDIF
      ELSE IF (ABS(EC).LT.(0.14+14*ABS(FY)/E)) THEN
C           READ (6,*) YY
        EC = ABS(EC)
        ESH = 14 * ABS(FY)/E
        ESU = 0.14 + ESH
        R = ESU - ESH
        M = ((1.5*FY/FY)*(30*R+1)**2 - 60*R-1)/(15*R**2)
        SS(I) = FY*((M*(EC-ESH)+2)/(60*(EC-ESH)+2)+(EC
     1    -ESH)*(60-M)/(2*(30*R+1)**2))
C     ELSE
C       WRITE(6,*)
C       WRITE(6,*)'THE STRESS HAS BEEN EXCEEDED IN THE STEEL SHELL'
C       WRITE(6,*)'THE COLUMN HAS FAILED'
C       WRITE(6,*) SS(I),SH(I)
C       FAIL = 1
C       GOTO 11
      ENDIF

    IF ((SS(I).GE.FSC).OR.(SS(I).LE.FST)) THEN
      Y = 1
    ENDIF
 10 CONTINUE
 11 CONTINUE


    RETURN
    END

C-------------------------------------------------------
    SUBROUTINE SCONCM(INC,AC,CH,FC,FST,TH,RIN,CUR,E01,CS,ECC,EC,N,MAN)

C   THIS SUBROUTINE CALCULATES THE CONCRETE STRESS ACCORDING TO THE
C   CONFINEMENT MODEL PROPOSED BY MANDER, PRIESTLY, & PARK
C   "THEORETICAL STRESS-STRAIN MODEL FOR CONFINED CONCRETE"
C
C   AC(I) = THE AREA OF CONCRETE IN THE iTH LAYER
C   CH(I) = THE DISTANCE FROM THE LAYER'S SECTION OF GRAVITY TO THE
C       SECTION'S NEUTRAL AXIS
C   FC = THE UNCONFINED CONCRETE STRENGTH
C   FST = THE YIELD STRENGTH OF THE STEEL
C   THICK = THE THICKNESS OF THE STEEL
C   RIN = THE INNER RADIUS OF STEEL
C   R,X = VARIABLES IN THE CALCULATION OF CS
C   CURV = THE CURVATURE AT THAT PARTICULAR INTERATION
C   EC = STRAIN IN THE CONCRETE CORRESPONDING TO CURV
C   E01 = THE STRAIN CORRESPONDING TO PEAK STRESS OF UNCONFINED CONRETE
C   EMC = THE MODULUS OF ELASTICITY OF THE INITIAL CURVE
C   ESEC = SECANT MODULUS OF CONFINED CONCRETE AT PEAK STRESS
C   FCO = COMPRESSIVE STRENGTH OF UNCONFINED CONCRETE IN A COLUMN
C   CS(I) = CONCRETE STRESS IN THE iTH LAYER

    REAL AC(1000),CH(1000),FC,FST,TH,RIN,R,X,CUR,EC
    REAL E01,EMC,ESEC,FCO,N,DIN,THICK
    REAL CS(1000)
    REAL MAN
    INTEGER I,INC


    THICK = TH
    DIN = 2 * RIN
    DO 10 I=1,INC
      IF ((AC(I).GT.0).AND.(CH(I).GT.0))THEN
        IF (CUR.EQ.0) THEN
          EC = EC
        ELSE
          EC = CUR*CH(I)
        ENDIF

        FCO = 0.85*FC

        FL = TH*FST/RIN
      FCC = FCO*(-1.254+2.254*(SQRT(1+7.94*FL/FCO))-2*FL/FCO)*MAN
        ECC = E01*(1+5*(FCC/(0.85*FC)-1))
        EMC = 5000*SQRT(FCO)
        ESEC = FCO/ECC

        X = EC/ECC
        R = EMC/(EMC-ESEC)
        CS(I) = (FCC*X*R)/(R-1+X**R)
C         WRITE (6,'(5F10.2)') CS(I),CH(I),N,X,R
      ELSE
```

```
        CS(I) = 0
      ENDIF
 10  CONTINUE
C     WRITE (6,'(4F10.2)') ECC,EMC,ESEC,R

    RETURN
    END

C-------------------------------------------------------
    SUBROUTINE SCONCA(AC,CURV,CH,THICK,FST,RIN,FC,E01,INC,E085,CS,EM)

    REAL CURV,CH(1000),THICK,FST,RIN,FC,E01,E085
    REAL FL,K1,FCO,K,FCC,E1,ECC,DEN,E85,M,EM
    REAL AC(1000),CS(1000)
C    DOUBLE PRECISION AC(1000),CS(1000)
    INTEGER INC,ST

    DO 10 I = 1,INC
      IF ((AC(I).GT.0).AND.(CH(I).GT.0)) THEN
        FL = THICK*FST/RIN
        K1 = 6.7*FL**(-0.17)
        FCO = 0.85*FC
        K = K1*FL/FCO
        FCC=FCO+K1*FL
        E1=E01*(1+5*K)
        EM = .4*FCC/(1+SQRT(1+0.4**(1+2*K))*E01)
        ECC = CURV*CH(I)
        IF (ECC.GT.E1) THEN
           DEN = THICK/RIN
           E85=260*DEN*E1+E085
           M = (FCC*0.15)/(E1-E85)
           CS(I) = M*ECC+FCC-M*E1
           IF (CS(I).LE.(0.2*FCC)) THEN
              CS(I) = 0.2*FCC
              WRITE (6,*) '0.2*FCC'
           ELSE
              WRITE (6,*) 'DESCENDING'
           ENDIF
        ELSE IF (ECC.LE.E1) THEN
           CS(I) = FCC*(2*(ECC/E1)-(ECC/E1)**2)**(1/(1+2*K))
C       WRITE (8,*) I,CS(I)
        ENDIF
        IF (ECC.GT 0.007) THEN
C             WRITE (6,*) 'STOP'
           ST = 1
        ENDIF
      ELSE
        CS(I) = 0
      ENDIF
 10  CONTINUE
C     WRITE (2,'(3F15.5)') CURV*CH(90),CH(90),CS(90)
    IF (CURV EQ 0.00001) THEN
C     WRITE (6,'(6F15.5)') FL,K1,FCO,K,FCC,E1
    ENDIF

    RETURN
    END




C-------------------------------------------------------
    SUBROUTINE SCONCH(AC,CH,CURV,CS,FC,INC,CU,E01,EC,CONFIN)

C   THIS SUBROUTINE CALCULATES THE CONCRETE STRESS
C   BY USING THE UNCONFINED CONCRETE MODEL PROPOSED BY HOGNESTAD
C
C   AC(I) = THE AREA OF CONCRETE IN A LAYER
C   CH(I) = THE DISTANCE FROM THE LAYER'S CENTER OF GRAVITY TO THE
C        SECTION'S NEUTRAL AXIS
C   CURV = THE CURVATURE AT THAT PARTICULAR INCREMENT
C   CS(I) = STRESS IN CONCRETE AT THE iTH LAYER
C   FC = UNCONFINED COMPRESSIVE STRENGTH
C   EC = STRAIN CORRESPONDING TO THE CURVATURE.
C   CU(I) = THE PREVIOUS STRESS AT THE iTH LAYER
C   INC = THE NUMBER OF LAYERS THAT THE SECTION IS DIVIDED

    REAL AC(1000),CH(1000),CURV,CS(1000),FC
    REAL EC,CU(1000),E01,CCS(1000)
    INTEGER I,INC
    CHARACTER CONFIN*4

    DO 10 I=1,INC

      IF ((AC(I).GT.0).AND.(CH(I).GT.0)) THEN
        IF (CURV.EQ.0) THEN
           EC = EC
        ELSE
```

```
          EC = CURV * CH(I)
        ENDIF

        IF (EC.LE.E01) THEN
          CS(I) = 0.85*FC*(2*(EC/0.002)-(EC/0.002)**2)
          CCS(I) = CS(I)/0.85
        ELSE
          CS(I)=0.85*FC-(EC-0.002)*0.1275*0.85*FC/(0.0035-0.002)
          CCS(I) = FC
        ENDIF
        IF (CONFIN.EQ.'UC') THEN
          CS(I) = CCS(I)
        ENDIF

      ELSE IF (CU(I).GT.0) THEN
        WRITE (6,*) 'HELLO'
        EC = -CURV*CH(I)
        CS(I) = CU(I) - 0.85*FC*(2*(EC/0.002)-(EC/0.002)**2)
        IF (CS(I).LT.0) THEN
          CS(I) = 0
          CU(I) = 0
        ENDIF
      ELSE
        CS(I) = 0
      ENDIF
10  CONTINUE

    RETURN
    END
C-----------------------------------------------------------------
    SUBROUTINE SSTEEU (INC,SS,SSTR,SH,E,SINIT,FST,FSC,CUR)

C   THIS SUBROUTINE CALCULATES THE STRESS IN THE STEEL DURING
C   UNLOADING ASSUMING EEP BEHAVIOUR.

C   CUR = THE CURVATURE AT A PARTICULAR ITERATION
C   SH(I) = THE DISTANCE FROM THE LAYER'S CENTER OF GRAVITY TO THE
C       SECTION'S NEUTRAL AXIS
C   E = THE ELASTIC MODULUS OF STEEL
C   SINIT = THE INITIAL VALUE OF STRESS IN THE CROSS-SECTION
C   SS(I) = THE STRESS AT ITH LEVEL
C   SSTR(I) = THE STEEL STRESS AT THE TOP OF THE LOADING CURVE
C   FST = THE ULTIMATE TENSION STRESS
C   FSC = THE ULTIMATE COMPRESSION STRESS
C   INC = THE NUMBER OF LAYERS THAT THE CROSS-SECTION IS DIVIDED

    REAL SS(1000),SH(1000),E,SINIT,FST,FSC,SSTR(1000),CUR
    INTEGER INC,I


    DO 10 I = 1,INC
      SS(I) = SSTR(I)- CUR*SH(I)*E + SINIT
      IF (SS(I).LE.(-FST)) THEN
        SS(I) = -FST
      ELSE IF (SS(I) GE.(FSC)) THEN
        SS(I) = FSC
      ENDIF
10  CONTINUE

    RETURN
    END
C-----------------------------------------------------------------
    SUBROUTINE SCONUH(INC,AC,CH,CS,FC,CUR,CSTR,CU)

C   THIS SUBROUTINE CALCULATES THE CONCRETE STRESS DURING UNLOADING
C   ACCORDING TO THE UNCONFINED CONCRETE MODEL PROPOSED BY HOGNESTAD
C
C   AC(I) = THE AREA OF CONCRETE IN THE iTH LAYER
C   CH(I) = THE DISTANCE FROM THE LAYER'S SECTION OF GRAVITY TO THE
C       SECTION'S NEUTRAL AXIS
C   FC = THE UNCONFINED CONCRETE STRENGTH
C   CUR = THE CURVATURE AT THAT PARTICULAR INTERATION
C   CS(I) = CONCRETE STRESS IN THE iTH LAYER
C   CSTR(I) = CONCRETE STRESS IN THE iTH LAYER AT THE TOP OF THE LOADING
C       CURVE
C   CU(I) = THE PREVIOUS CONCRETE STRESS IN THE iTH LAYER
C   INC = THE NUMBER OF LAYERS IN THE CROSS SECTION

    REAL AC(1000),CH(1000),CS(1000),FC,CSTR(1000),CUR,CU(1000)
    INTEGER I,INC


    DO 10 I=1,INC
      IF ((AC(I).GT.0).AND.(CH(I).GT.0)) THEN
        IF (CU(I).GT.0) THEN
          CS(I) = CSTR(I)-CUR*CH(I)*4500*SQRT(0.85*FC)
          IF (CS(I).LE.0) THEN
            CS(I) = 0
          ENDIF
        ELSE
```

```
          CS(I) = 0
        ENDIF
      ELSE
        CS(I) = 0
      ENDIF
      CU(I)=CS(I)
10  CONTINUE
    RETURN
    END

C-----------------------------------------------------
    SUBROUTINE SCONUM(AC,CH,CSTR,FC,CURV2,CUR,ECC,INC,CS,CU)

C   THIS SUBROUTINE CALCULATES THE CONCRETE STRESS ACCORDING TO THE
C   CONFINEMENT MODEL PROPOSED BY MANDER, PRIESTLY, & PARK
C   "THEORETICAL STRESS-STRAIN MODEL FOR CONFINED CONCRETE"
C
C   AC(I) = THE AREA OF CONCRETE IN THE iTH LAYER
C   CH(I) = THE DISTANCE FROM THE LAYER'S SECTION OF GRAVITY TO THE
C       SECTION'S NEUTRAL AXIS
C   FC = THE UNCONFINED CONCRETE STRENGTH
C   FST = THE YIELD STRENGTH OF THE STEEL
C   THICK = THE THICKNESS OF THE STEEL
C   RIN = THE INNER RADIUS OF STEEL
C   R,X = VARIABLES IN THE CALCULATION OF CS
C   CURV = THE CURVATURE AT THAT PARTICULAR INTERATION
C   EC = STRAIN IN THE CONCRETE CORRESPONDING TO CURV
C   ECC = THE STRAIN CORRESPONDING TO PEAK STRESS OF CONFINED CONRETE
C   E01 = THE STRAIN CORRESPONDING TO PEAK STRESS OF UNCONFINED CONRETE
C   EMC = THE MODULUS OF ELASTICITY OF THE INITIAL CURVE
C   ESEC = SECANT MODULUS OF CONFINED CONCRETE AT PEAK STRESS
C   FCO = COMPRESSIVE STRENGTH OF UNCONFINED CONCRETE IN A COLUMN
C   CS(I) = CONCRETE STRESS IN THE iTH LAYER
C   CSTR(I) = CONCRETE STRESS IN THE iTH LAYER AT THE TOP OF THE LOADING
C       CURVE

    REAL AC(1000),CH(1000),CSTR(1000),FC,ECC
    REAL CS(1000),CURV2,CUR,CU(1000)
    REAL EU,ESEC,B,C,EPL,A1,A2,A,EUN,EC,EM
    REAL X,R
    INTEGER I,INC

    DO 10 I = 1,INC
      IF ((AC(I).GT.0).AND.(CH(I).GT.0).AND.(CU(I).NE.0)) THEN
        EUN = CURV2 * CH(I)
        IF (EUN.LT.0) THEN
            EUN = - EUN
        ENDIF
        EC = CUR*CH(I)
        IF (EC.LT.0) THEN
            EC = - EC
        ENDIF
              A1 = ECC/(ECC+EUN)
              A2 = 0.08*EUN/ECC
              IF (A1.GT.A2) THEN
                A = A1
              ELSE
                A = A2
              ENDIF
              EA = A*SQRT(EUN*ECC)
              EM = 5000*SQRT(0.85*FC)
            EPL = EUN-(EUN+EA)*CSTR(I)/(CSTR(I)+EM*EA)
          X = (EC-EUN)/(EPL-EUN)
              C = (ECC/EUN)**0.5
              IF (C.GT.1) THEN
                C = 1.0
              ENDIF
              B = CSTR(I)/(0.85*FC)
              IF (B.LT.1) THEN
                B = 1.0
              ENDIF
            EU = B*C*EM
            ESEC = CSTR(I)/(EC-EPL)
          R = EU/(EU-ESEC)
        CS(I)=CSTR(I) - CSTR(I)*X*R/(R-1+X**R)
        IF (CS(I).LT.0) THEN
          CS(I) = 0
        ENDIF
        IF (CU(I).LT.CS(I)) THEN
          CS(I) = 0
        ENDIF
      ELSE
        CS(I) = 0
      ENDIF
      CU(I) = CS(I)
10  CONTINUE


    RETURN
    END
```

```
C-------------------------------------------------
      SUBROUTINE FORCE(AS,AC,SS,CS,INC,SF,CF,FTOT,COUNT,NA,NAEQ,P)

C     THIS SUBROUTINE WILL CALCULATE THE FORCE AT EACH INCREMENTAL
C     STEP.
C
C     C = THE NEUTRAL AXIS
C     A(I) = THE AREA OF THE ITH LAYER
C     S(I) = THE STRESS AT THE ITH LAYER
C     F(I) = THE FORCE AT THE ITH LAYER
C     FTOTAL = THE TOTAL FORCE OF THE CROSS-SECTION.
C     I,COUNT = COUNTERS


      REAL AS(1000),AC(1000),SS(1000),CS(1000)
      REAL SF(1000),CF(1000),CHECK
      REAL NA,C(5000),FTOT,P
      INTEGER I,INC,NAEQ
      INTEGER COUNT

        CFTOT = 0
        SFTOT = 0

      DO 10 I = 1,INC
         SF(I) = SS(I)*AS(I)
         SFTOT = SF(I) + SFTOT
         CF(I) = CS(I)*AC(I)
         CFTOT = CF(I) + CFTOT
10    CONTINUE

      C(COUNT) = NA
      QS = SFTOT
      WC = CFTOT
      FTOT = SFTOT + CFTOT
      IF (COUNT.GT.5) THEN
        IF ((C(COUNT-2).EQ.C(COUNT)).AND.(NAEQ.EQ.0)) THEN
          NAEQ = 1
        ELSE IF ((C(COUNT-2).EQ.C(COUNT)).AND.(NAEQ.EQ.1)) THEN
          NAEQ = 2
        ELSE
          CHECK = C(COUNT-2)-C(COUNT)
          IF ((CHECK.LE.0.001).AND.(CHECK.GE.-0.001)) THEN
           FTOT = P
          ENDIF
        END IF
      END IF
      IF ((FTOT.LE.P+1) AND (FTOT.GE.P-1)) THEN
       FTOT = P
      ENDIF

C     WRITE (6,*) SFTOT,CFTOT,P

      RETURN
      END

C-------------------------------------------------
      SUBROUTINE MOMENT(INC,SF,CF,SCG,CCG,M,MTOTAL,ROUT,DIR,UNIT,P)

C     THIS SUBROUTINE WILL CALCULATE THE MOMENT AT EACH INCREMENTAL STEP.

C     M(I) = THE MOMENT AT THE ITH LAYER
C     CF(I) = CONCRETE FORCE IN ITH LAYER
C     SF(I) = STEEL FORCE IN ITH LAYER
C     SCG(I) = CENTER OF GRAVITY OF STEEL IN ITH LAYER
C     CCG(I) = CENTER OF GRAVITY OF CONCRETE IN ITH LAYER
C     ARMS = THE MOMENT ARM FOR STEEL
C     ARMC = THE MOMENT ARM FOR CONCRETE
C     ROUT = THE OUTER RADIUS OF THE STEEL
C     MTOTAL = THE TOTAL MOMENT ACTING ON THE CROSS-SECTION
C     DIR = WHETHER THE LOADING IS LOADIN(L) OR REVERSE(R)
C     UNIT = THE UNITS OF THE PROBLEM, EITHER METRIC OR IMPERIAL


      REAL M(1000),SF(1000),CF(1000),MTOTAL
      REAL SCG(1000),CCG(1000),ARMS,ARMC,ROUT,P
      INTEGER I,INC
      CHARACTER DIR*4,UNIT*4

      MTOTAL = 0
      M2TOT = 0
      DO 10 I = 1,INC
        IF (DIR.EQ.'L') THEN
          ARMS = SCG(I)
          ARMC = CCG(I)
          ARM = -ROUT
        ELSE
          ARMS = ROUT - SCG(I)
          ARMC = ROUT - CCG(I)
          ARM = ROUT
        ENDIF
```

```
      M(I) = SF(I)*ARMS+CF(I)*ARMC
      MTOTAL = M(I) + MTOTAL
C     WRITE(6,'(F15.2)') MTOTAL
 10  CONTINUE
     MTOTAL = MTOTAL + P*ARM
       IF (UNIT.EQ.'I') THEN
         MTOTAL = MTOTAL*7.37562E-7
       ELSE
         MTOTAL = MTOTAL/1000000
       ENDIF

     RETURN
     END

C-----------------------------------------------------
     SUBROUTINE DEFL(TOT,C,DEF,L,M,MT,DEP,DEPTOT)

C    THIS SUBROUTINE WILL CALCULATE THE DEFLECTION AT EACH INCREMENTAL
C    THE DEFLECTION AT THE TIP OF THE COLUMN IS THE SECOND INTEGRAL OF THE
C    MOMENT DIAGRAM.
C    THE MOMENT DIAGRAM STARTS AT ZERO AT THE TIP OF THE COLUMN AND
C    INCREASES TO A MAXIMUM AT THE BASE
C    FROM THE BASE THE MOMENT REMAINS CONSTANT FOR A LENGTH "DEP"
C    AND THEN DECREASES TO ZERO AT A DISTANCE "DEPTOT"
C
C    C(I) = CURVATURE AT I
C    DEF = DEFLECTION AT THE TIP OF THE COLUMN
C    X(I) = DISTANCE FROM M(I-1) TO M(I) ON THE COLUMN
C    XT(I) = DISTANCE FROM THE TIP OF THE COLUMN TO M(I)
C    TOT = TOTAL NUMBER OF MOMENTS CALCULATED ON THE CURVE
C    L = LENGTH OF THE COLUMN
C    I = CALCULATION STEP
C    M(I) = THE ITH MOMENT
C    MT = TOTAL MOMENT ACTING AT THE GIVEN CURVATURE
C    C(I) = ITH CURVATURE

     REAL C(1000),DEF,L,DEFI,MT,X(1000),M(1000)
     REAL XT(1000),DEPTOT
     INTEGER I, TOT,J

     DEF = 0

     IF (TOT.EQ.1) THEN
        DEF = C(1)/3*L*L
     ELSE
       X(1) = M(1)/MT*L
       XT(1) = X(1)
       XT(2) = M(2)/MT*L
       X(2) = XT(2)-X(1)
       DEF = (X(1)**2)*C(1)/3+C(1)*X(2)*(X(1)+0.5*X(2))
       DEF = DEF + 0.5*(C(2)-C(1))*X(2)*(X(2)*2/3+X(1))

       DO 10 I = 3,TOT
        XT(I) = M(I)/MT*L
        X(I) = XT(I) - XT(I-1)
        DEFI = X(I)*C(I-1)*(XT(I-1)+0.5*X(I))
        DEFI = DEFI + 0.5*X(I)*(C(I)-C(I-1))*(XT(I-1)+X(I)*2/3)
        DEF = DEF + DEFI
 10     CONTINUE

       DEF = DEF + DEP*C(TOT)*(L+DEP/2)
       DEF = DEF+0.5*C(TOT)*(DEPTOT-DEP)*(L+DEP+(1/3*(DEPTOT-DEP)))
     ENDIF

     RETURN
     END

C-----------------------------------------------------
     SUBROUTINE PRINT(MT,CT,U,NA,CURVA,I,SS,FST,INC,L,EI,MOMA,CS,Y,DEP)

C    THIS SUBROUTINE WILL PRINT OUT THE VALUE OF EACH INCREMENTAL STEP.
C
C    MTOTAL = THE TOTAL MOMENT ACTING ON THE CROSS-SECTION
C    CURVT = THE CURVATURE FOR A PARTICULAR INCREMENT
C    INC = THE NUMBER OF LAYERS IN THE SECTION

     INTEGER I,C,GOT,INC,Y
     REAL CURVT,MTOTAL,CUR,NA,CFTOT,DEF,CURVA(1000),SS(1000),FST,MT
     REAL L,EI,MOMA(1000),CS(1000),MP,CT,DEP
     CHARACTER U*4,UNIT*4

     UNIT = U
     CURVT = CT
     MTOTAL = MT
     IF (UNIT.EQ.'I') THEN
        CUR = CURVT * 25.4
     ELSE
        CUR = CURVT
     ENDIF
```

```
      CURVA(I) = CUR
      MOMA(I) = MTOTAL

      GOT = 0
      MP = 0.0
      DO 10 C=1,INC
       IF ((SS(C).GE.FST).OR.(SS(C).LE.-FST)) THEN
          GOT = 1+ GOT
       ENDIF
10    CONTINUE
       IF ((GOT.GT.(0.5*INC)).AND.(Y.EQ.0)) THEN
          MP = MTOTAL
          Y = 1
          WRITE (6,*) MP
       ENDIF


      IF (L.GT.0) THEN
         CALL DEFL(I,CURVA,DEF,L,MOMA,MTOTAL,DEP,DEPTOT)

       WRITE (2,'(6F15.8)') CUR,MTOTAL,MTOTAL/L*1000,DEF,DEFF,DEFFF

       IF (CUR.EQ.(0.00007)) THEN
       DO 50 J = 1,INC
50          WRITE (1,'(F15.8)') CS(J)
       ENDIF

       IF (CUR.EQ.(0.00006)) THEN
       WRITE (6,'(F15.8)') NA
       ENDIF
      ELSE
        WRITE (2,'(3F30.12)') CUR,MTOTAL,NA
        WRITE (6,'(2F30.12)') CUR,MTOTAL
      ENDIF

      RETURN
      END
```

C.1 SAP 90 Analysis

A finite element analysis using SAP 90 (Computers & Structures Inc. 1992) was preformed on the foundation detail to investigate any concentration of high local stresses. It was also preformed to investigate the most efficient thicknesses for the top plate. The steel sections are modeled using four node shell elements that are a combination of membrane and plate bending behaviour. Each element is made up of four predefined joints, and a thickness is given to each shell element. Constraints are used to keep different steel components attached as in the case of welding two components together. Displacement and rotation restraints are assigned at the boundary lines to take advantage of the symmetric design on all steel components.

C.2 Step-up of model

Figure C.1 shows the finite element structure that was designed to replicate the specimen. Using symmetry in both the x and y direction, only one quarter of the specimen needs to be modeled. The origin (0,0,0) is located at the centre of the steel column on top of the bottom plate. The x-axis is located in the transverse direction and the y-axis is located along the longitudinal symmetry line. The height of the steel tube is equivalent to the effective height of the specimen. Since the concrete foundation was not modeled in this analysis, the height of the steel tube starts at the top plate and ends at the top of the steel tube. One quarter of the entire horizontal load applied to the specimen is divided between the nodes at the top of the steel tube.

The top plate is constrained to the channels along both the longitudinal weld and the transverse weld, this ensures that contact remains at these locations. The bottom plate is constrained to the bottom of the steel tube to simulate the weld. The bottom plate is also constrained to the bottom flange of the channel in the transverse direction. The back of the bottom flange is also constrained in the longitudinal direction to the bottom plate even though there is no weld in this location. However, this ensures the channel remains on top of the bottom plate.

The elements along the x-axis of the specimen are restrained from displacing or rotating in the z direction due to the transverse line of symmetry. The elements along the y-axis of the specimen are restrained from movement in the x direction and rotation in either the y or the z directions due to the longitudinal line of symmetry. The end of the channel is restrained from movement in any direction but free to rotate. The concrete core was not simulated in this analysis, however, the ultimate effect of the concrete to the steel tube is to restrain the column from buckling inward. Therefore, all elements were restrained from movement in the x direction.

C.3 Analysis

Analysis was performed on many different configurations for the specimen design but only the chosen design will be addressed in detail in this section. The forces as well as the moments on the specimen components will be examined. A description of the mechanics of why this design works will follow the analysis of the forces and the moments.

C.3.1 Forces

The axial forces on the steel tube are shown in Figure C.2. To effectively show the gradient of forces on the steel tube, the rest of the specimen can not be analyzed in this figure. To produce the actual axial force on the steel tube, the value given in the figure, kN/mm, must be multiplied by the in-plane length of the element, 12.7 mm. The forces increase in the steel tube as the distance from the applied load increases until the top plate, and then the forces decrease until the bottom plate is reached. This figure illustrates the effectiveness of the top plate and the channels at transferring the axial forces from the steel tube. The forces also increase as the distance from the x-axis increases until a maximum occurs along the y-axis. The front of the column, along the y-axis, should experience the highest forces because the stresses are the largest. A significant decrease in force is experienced at the location of the top plate due to a portion of the axial force being taken by the top plate.

The maximum axial force on one element of the steel tube is found on the front of the column just above the top plate with a value of 8.0 kN/mm. At the same horizontal location but

just above the bottom plate, the axial forces have decreased to 1.2 kN/mm. Since the yielding tensile force on the steel tube is 4.7 kN with a steel strength of 350 MPa, the analysis shows that there will be yielding in the steel tube for any colour above the light green in the index. This analysis is only an elastic analysis and plastification is not taken into account. The maximum induced axial force on the steel tube is 1.7 times the capacity of the steel tube. In addition, the minimum steel yield stress was found in coupon testing to be 400 MPa, this corresponds to a

yielding force of 5.3 kN. Even though there will be yielding in the steel tube at the location of the top plate, the steel should remain ductile and resist this force by plastification.

The maximum forces on the top plate are shown in Figure C.3. The scale of the figure has been manipulated to show the greatest variation in the forces on the top plate. The forces on the figure must be multiplied by the in-plane length of the element, 10 mm, to achieve the force on the element. The forces shown in this figure are the greatest forces from the longitudinal forces, the transverse forces, and the shear forces. The shells making up the top plate were circular around the steel tube. Therefore, the longitudinal forces on the individual elements did not line up together. From this figure, it can be seen that the forces are largest around the steel tube and are at a maximum at a 45° angle from the longitudinal centre line of the steel tube. The maximum resistance of the steel plate is 3 kN/mm, and the light blue area corresponds to yielding on the steel plate. The maximum force on the top plate is 4 kN/mm. Therefore, the greatest applied force is 1.33 times the resistance, and there will be yielding in this area on the top plate. However, this area is small and with steel ductility, there should be no failure of the top plate. There are also high localized forces near the weld at the corner of the top plate. These are a result of the constraints applied to the specimen to imitate the weld conditions.

C.3.2 Moments

The internal moments acting on the steel tube are shown in Figure C.4. Two areas of localized moments can be seen, one at the top of the column, and the other at the location of the top plate. The high moments on the top of the column are caused by the applied loading effect

and are due to the simulation of the forces in this analysis. The high moments on the steel tube around the location of the top plate are caused by the fixity of the top plate to the large channels and the steel tube. The steel tube tries to pull the top plate upwards while the weld on the channel restricts this plate movement. The moments shown on this figure must be multiplied by the in-plane length to achieve the moment acting on the element. The moment on the steel tube just above the top plate on the front of the column is 9.3 kN mm/mm. A third of this moment is taken by the top plate and two thirds of this moment is taken by the steel tube below the top plate. The moment capacity of the steel tube is 3.7 kN mm/mm when using 350 MPa steel and 4.2 kN mm/mm when using 400MPa. The yielding of the steel tube due to these moments are shown

as the light blue area on Figure C.4. It can be seen that although the yielding is severe, it is very localized.

The maximum moments on the top plate are illustrated in Figure C.5. The greatest moments are along the longitudinal centre line and have a value of 2.1 kN mm/mm. This moment is caused by the fixity of the top plate to the channel flanges and the steel tube. The moment capacity in the top plate is 5 kN mm/mm, corresponding to the light blue area in the figure. Since there is no light blue are on the top plate, there is no yielding occurring due to the applied moments.

The resultant maximum moments on the bottom plate are shown in Figure C.6. The role of the bottom plate is to resist the axial forces remaining in the bottom of the column by the moment capacity in the plate. As seen in Figure C.6, the maximum moment on the bottom plate occurs around 45° from the longitudinal centre-line. These moments are caused by the tensile forces in the steel tube lifting the bottom plate. The moment capacity of the plate is 45 kN mm/mm for a steel yield strength of 300 MPa. Therefore, all area on the plate that is light blue has yielded. The largest moment found in the figure is 53.5 kN mm/mm, this corresponds to 1.2 times greater than the moment capacity of the plate. Since this area is very localized, it was determined that plasticity in the bottom plate would not fail due to applied moments.

C.4 Mechanics

Figure C.7 is a graph illustrating the internal maximum moment in the elements of the steel tube, directly above the top plate for a number of different mechanisms. 0° degrees correspond to the transverse or x-axis of the steel tube, while 90° corresponds to the longitudinal or y-axis of the steel tube. The steel tube has been loaded for all mechanisms in the same manner as the previously described design, from here after referred to as the "constructed design".

The first mechanism is from a column with a fixed base as in Figure C.8. The length of the column is 2200 mm from the tip of the column to the fixed base, the same effective length as the steel tube in the constructed design. The stresses in this design are similar to the constructed design, however, the stresses flow linearly into the fixed base. Because the base is much stronger than the tube and the top plate, it will remain rigid and not deform. The moments along the circumference of the tube increases from 0° to 90° with a maximum moment reached of 4 kN mm/mm.

The second mechanism consisted of a 30 mm top plate, substituted for the 10 mm plate, in the constructed design. The effective length of the column is 2200 mm from the column tip to the top plate. It can be seen in the graph that the steel tube must resist 3 times as much moment as the fixed base tube. As compared with the 10 mm top plate, the steel tube in this design must resist 50% more moment. To further strengthen the 30 mm top plate to resist the additional loads, two transverse stiffeners were applied to both sides of the top plate, mechanism three. Between 0° and 70°, the addition of the transverse stiffeners appears to reduce the moment in the steel tube. However, near the critical moment location, the stiffeners increase the required moment resistance of the steel tube.

From the analysis of mechanisms two and three with a 30 mm plate, it was concluded that a stiff plate only introduced more stresses into the steel tube instead of reducing them. A flexible plate attached to the steel tube will bend in order to remain attached to the top flange of the channels and therefore, will allow the steel tube to elongate when subjected to large applied

forces. The fourth mechanism studied was the constructed design with a 8 mm top plate. It can be seen on the graph that the moments induced in the steel tube by the 8 mm plate are half as great as the moments induced in the steel tube due to the 30 mm plate. The moments in the steel tube are only slightly higher with the 10 mm plate than with the 8 mm plate. It was decided to use a 10 mm plate for the top plate because the 10 mm thickness was needed in the top plate to resist the stresses. The entire foundation of the constructed design has preformed well in the SAP 90 analysis program as described previously

APPENDIX C

SAP 90 Design

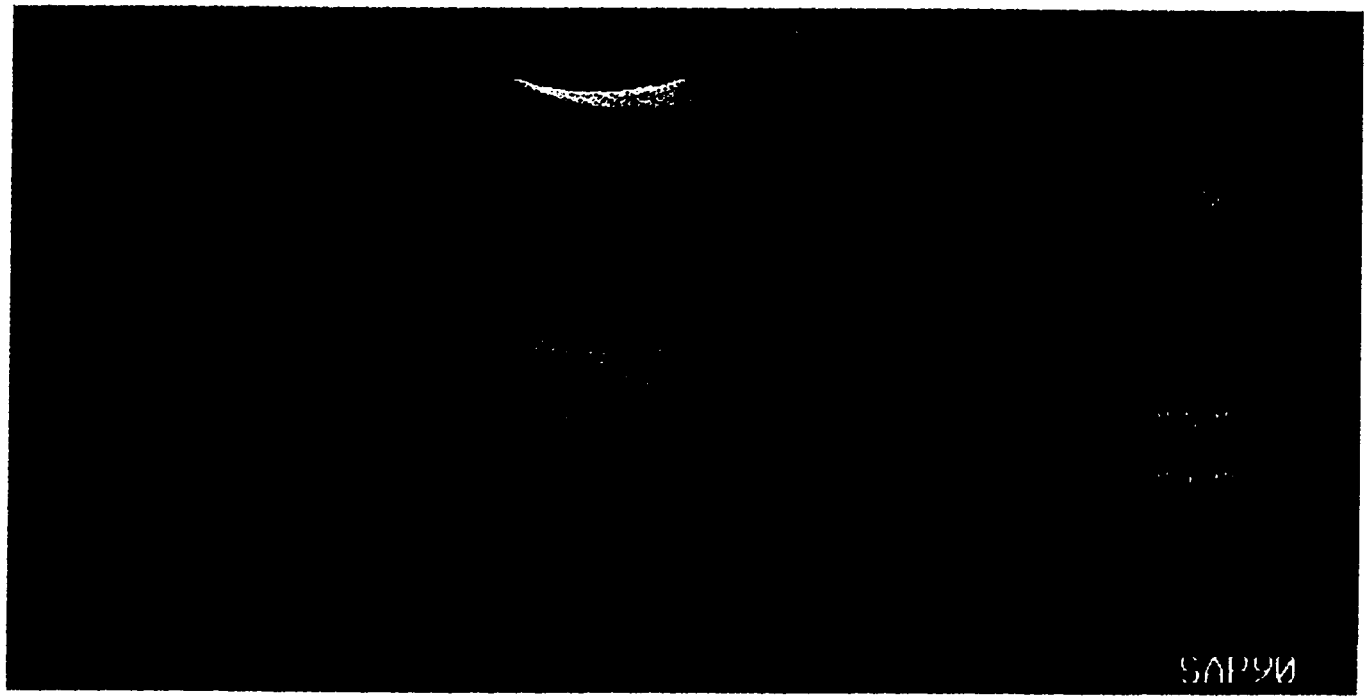

Figure C.1: Finite element structure of designed foundation

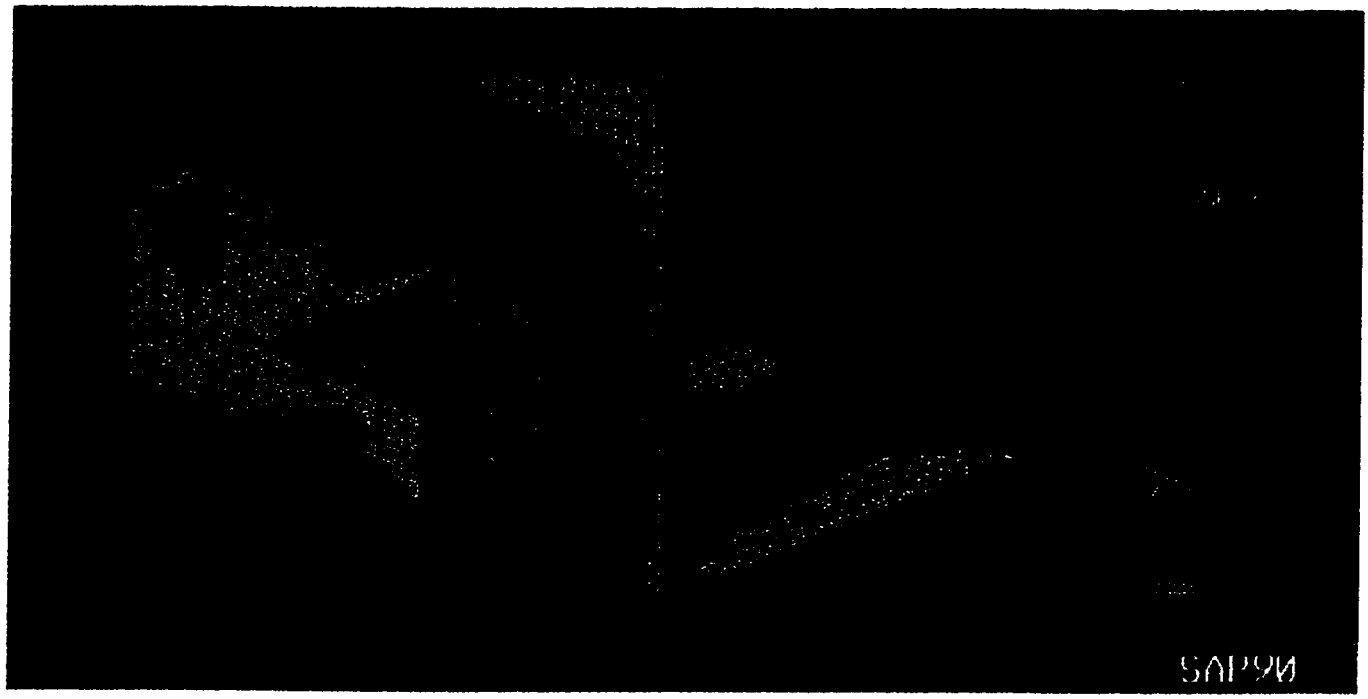

Figure C.2: Axial forces on the steel tube

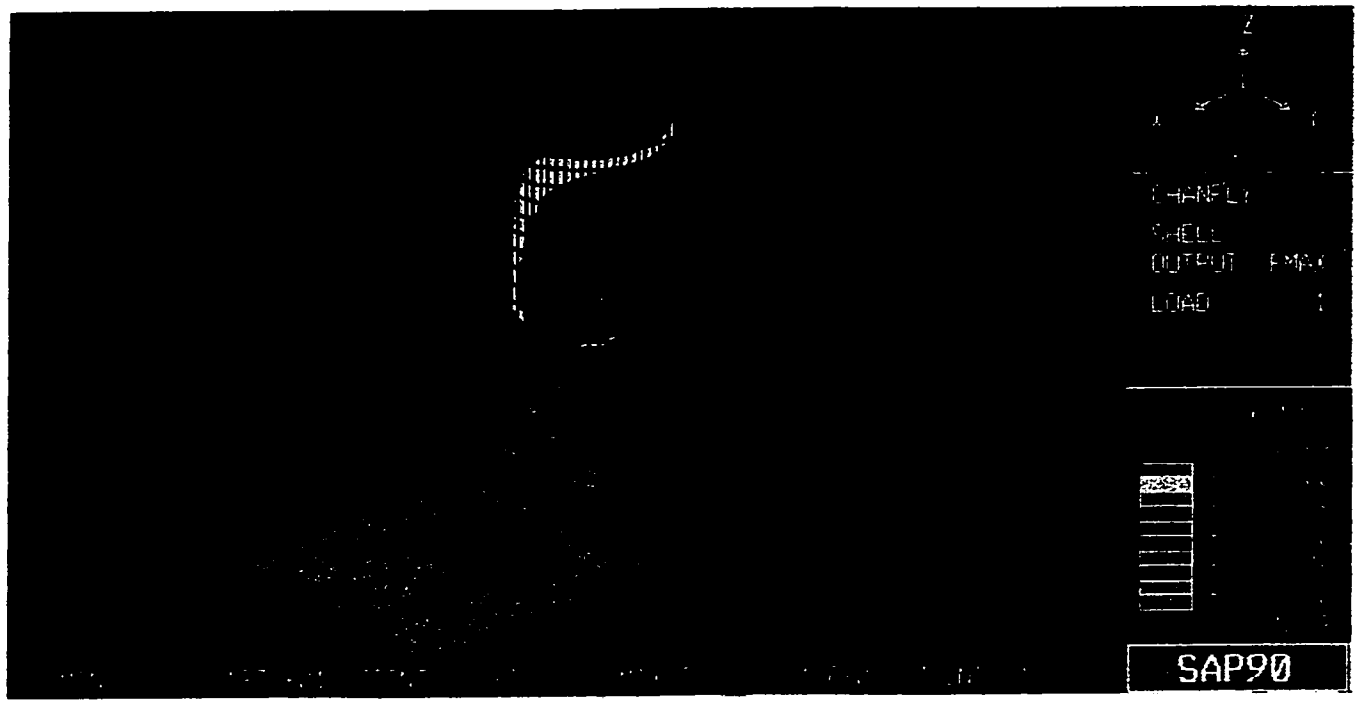

Figure C.3: Maximum forces on the top plate

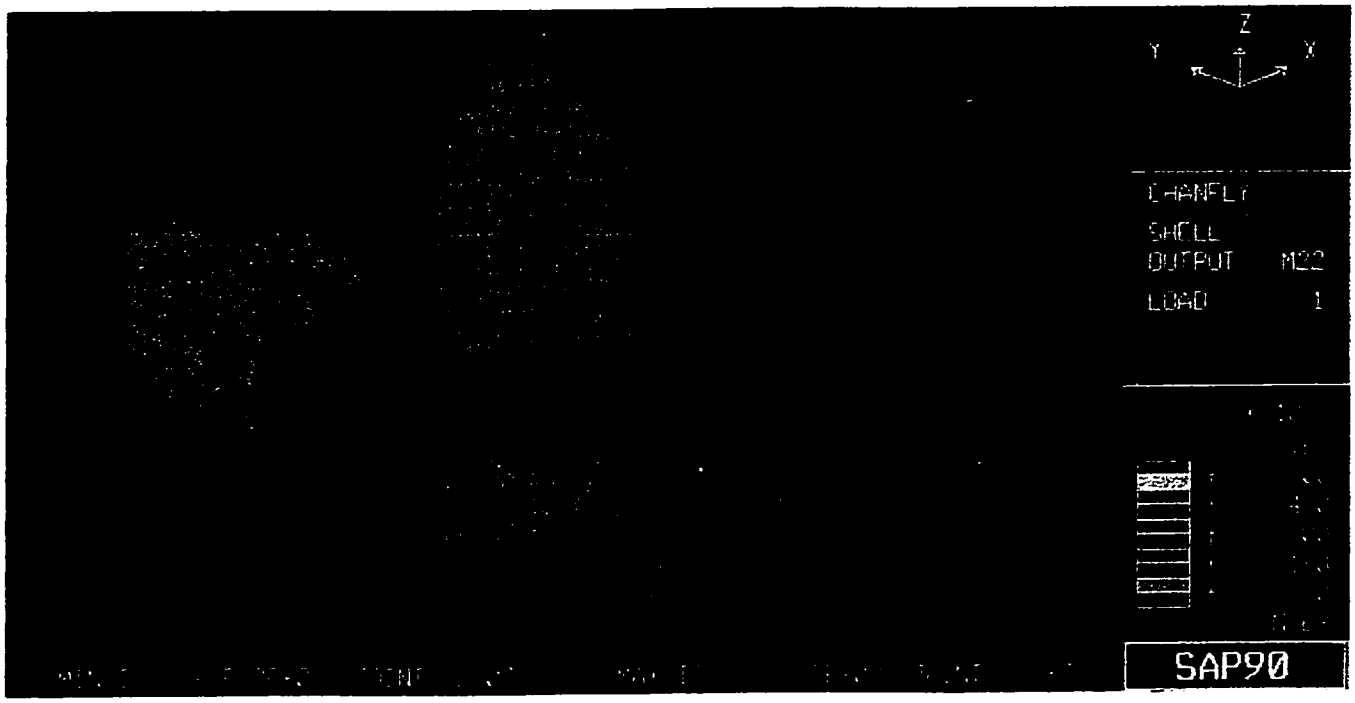

Figure C.4: Maximum moments on the steel tube

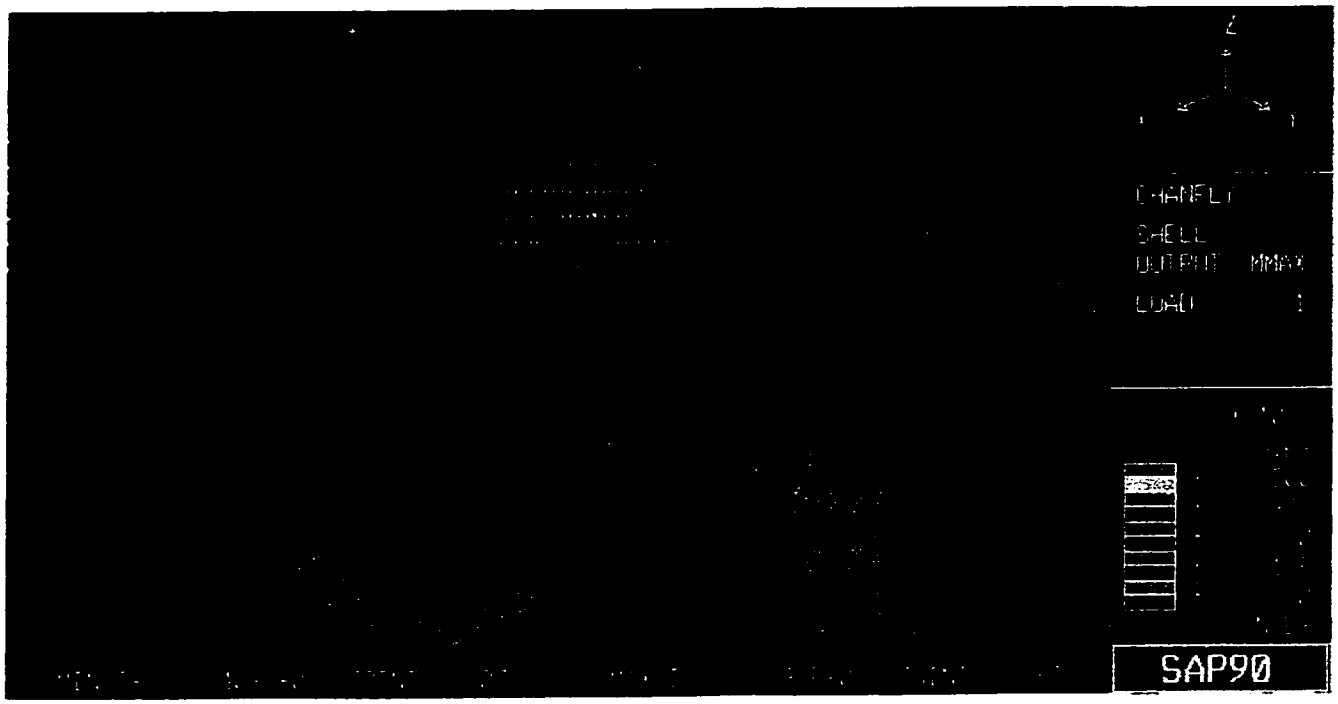

Figure C.5: Maximum moments on the top plate

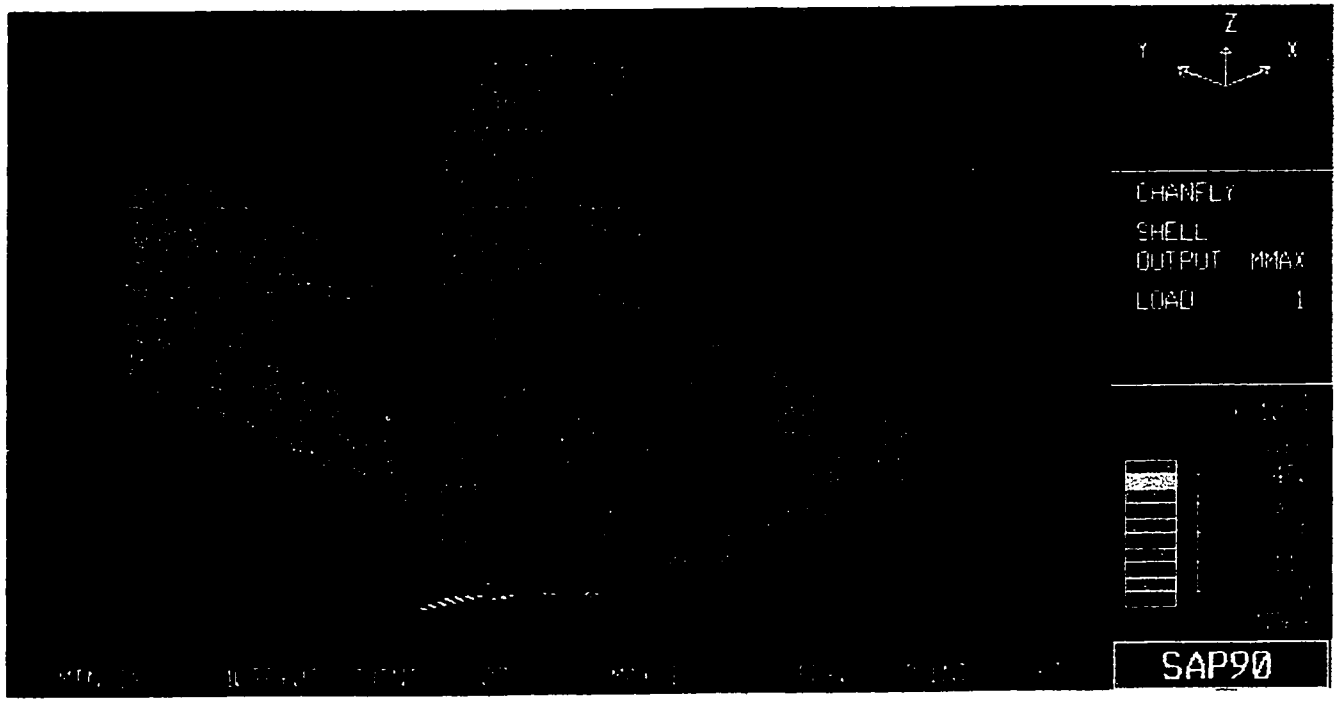

Figure C.6: Maximum moments on the bottom plate

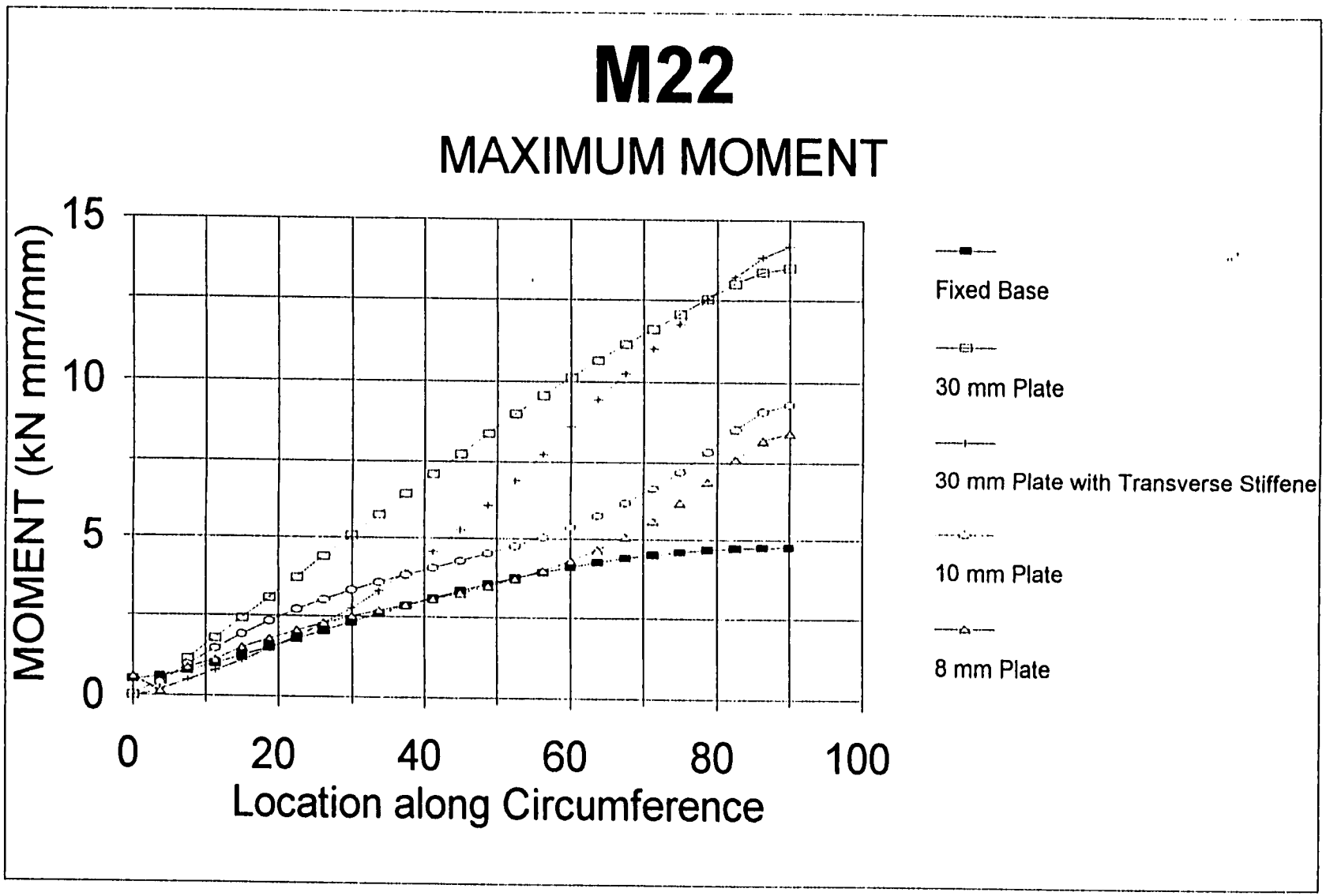

Figure C.7: Maximum moment on steel tube at location of steel tube

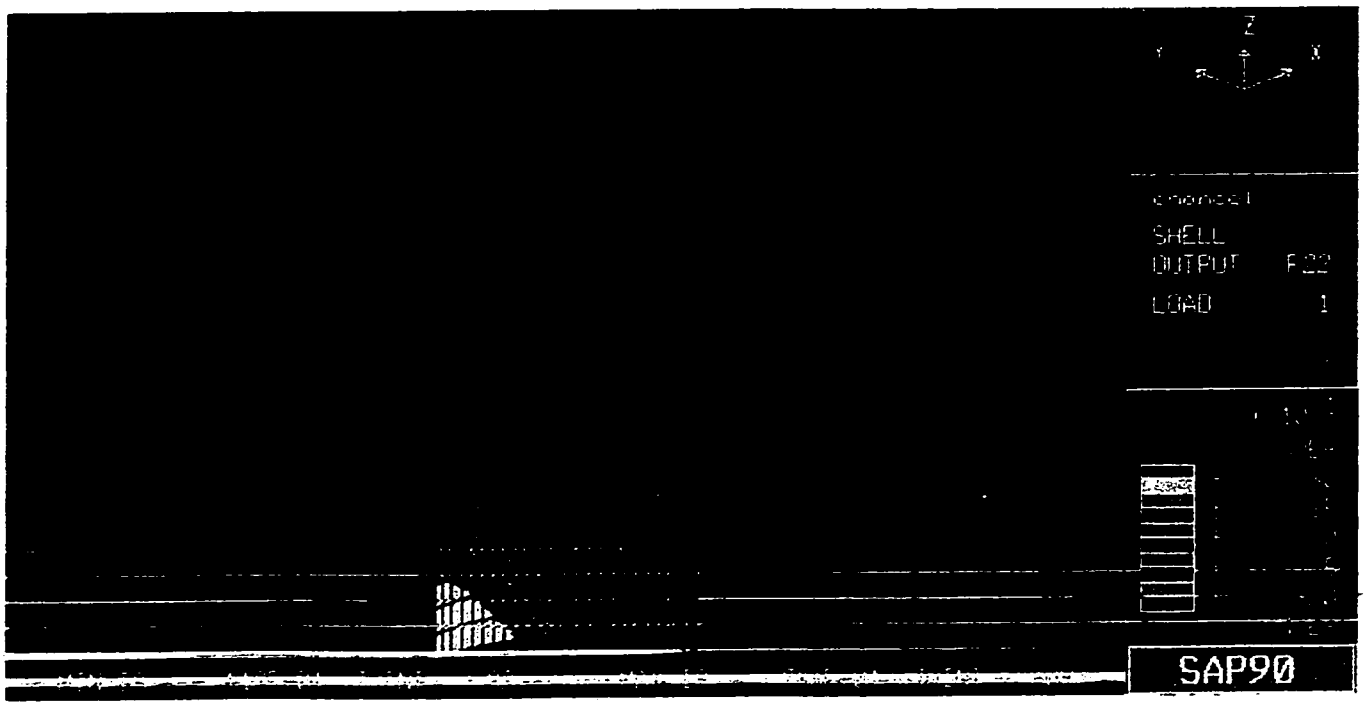

Figure C-8. Maximum moment on a fixed base steel tube

APPENDIX D

Hand Calculations

Beam Column Capacity

CAN/CSA-S16.1-M94

Using CFST 64 from current study

$L = 2200\,mm$
$D = 406.4\,mm$
$t = 5.5\,mm$
$F_y = 442\,MPa$
$f_c' = 37\,MPa$
$P_f = 1000\,kN$

$A_s = 6927\,mm^2$
$A_c = 122790\,mm^2$

$M_f = 592\,kN\,m$

$$\lambda_c = \frac{kL}{r_c}\sqrt{\frac{f_c'}{\pi^2 E_c}} = \frac{2200}{395.4/4}\sqrt{\frac{37}{\pi^2(5000\sqrt{37})}} = 0.25$$

$$C_r' = 0.85 f_c' A_c \lambda_c^{-2}\left(\sqrt{1+0.25\lambda_c^{-4}} - 0.5\lambda_c^{-2}\right)$$
$$= 0.85(37)(122790)(0.25^{-2})\left(\sqrt{1+0.25(0.25^{-4})} - 0.5(0.25^{-2})\right)$$
$$= 3847\,kN$$

$$\lambda_s = \frac{kL}{r_s}\sqrt{\frac{F_y}{\pi^2 E_s}} = \frac{2200}{\frac{1}{4}\sqrt{406.4^2+395.4^2}}\sqrt{\frac{442}{\pi^2(200000)}} = 0.23$$

$$C_r = A_s F_y\left(1+\lambda_s^{2n}\right)^{-1/n}$$
$$= 6927(442)\left(1+0.83^{2(1.34)}\right)^{-1/1.34}$$
$$= 3018\,kN$$

$$\rho_s = 0.02\left(25 - \frac{L}{D}\right) = 0.02\left(25 - \frac{2200}{406.4}\right) = 0.39$$

$$\tau = \frac{1}{\sqrt{1+\rho_s+\rho_s^2}} = \frac{1}{\sqrt{1+0.39+0.39^2}} = 0.81$$

$$\tau' = 1 + \left(\frac{25\rho_s^2\tau}{D/t}\right)\left(\frac{F_y}{0.85 f_c'}\right) = 1 + \left(\frac{25(0.39)^2(0.81)}{406.4/5.5}\right)\left(\frac{442}{0.85(37)}\right) = 1.59$$

$$C_{rc} = \tau C_r + \tau' \cap_r'$$
$$= 0.81(3018) + 1.59(3847) = 8561\,kN$$

$$M_r = Z F_y = \frac{1}{6}\left(406.4^3 - 395.4^3\right)442 = 390.7\,kN\,m$$

$C_f < \tau' C_r'$ so $M_f = \tau M_r$

$$= 0.81(390.7) = 316\,kN\,m$$

$$\frac{M_f}{M_r} = 1.87$$

Beam-Column Capacity

Eurocode 4 (1994)

Using CFST 64 from current study

$L = 2200\,mm$
$D = 406.4\,mm$
$t = 5.5\,mm$
$F_y = 442\,MPa$
$f_c' = 37\,MPa$
$P_f = 1000\,kN$

$A_s = 6927\,mm^2$
$A_c = 122790\,mm^2$
$M_f = 592\,kNm$

$$\lambda = \sqrt{\frac{N_p}{N_{cr}}} = \sqrt{\frac{A_s f_y + A_c f_c'}{\pi^2 EI / L^2}}$$

$$= \sqrt{\frac{6927(442) + 122790(37)}{\pi^2/2200^2\left(210000\left(\frac{\pi}{64}\right)(406.4^4 - 395.4^4) + 0.8 \cdot 5000\sqrt{37}\left(\frac{\pi}{64}\right)(395.4)^4\right)}}$$

$$= 0.25$$

$$\eta_{10} = 4.9 - 18.5\lambda + 17\lambda^2 \geq 0$$
$$= 4.9 - 18.5(0.25) + 17(0.25)^2 = 1.34$$

$$\eta_{20} = 0.25 \cdot (3 + 2\lambda) \leq 1.0$$
$$= 0.25\,(3 + 2(.25)) = 0.875$$

$$e = \frac{M_f}{N_f} = \frac{592}{1000} = 592\,mm > \frac{406.4}{10}$$

so $\eta_1 = 0.0$
$\eta_2 = 1.0$

$$N_p = A_s f_y + A_c f_c$$
$$= 6927(442) + 122790(37) = 7605\,kN = N_A$$

$$N_c = A_c \cdot f_c = 122790(37) = 4543\,kN$$

$$N_D = \tfrac{1}{2} N_c = 2272\,kN$$

$$Z_s = \tfrac{1}{6}(406.3^3 - 395.4^3) = 875764\,mm^3$$

$$Z_c = \tfrac{1}{6}(395.4^3) = 10302882\,mm^3$$

$$h_n = \frac{N_c}{2Df_c' + 4t(2f_y - f_c')}$$
$$= \frac{4543000}{2(406.4)(37) + 4(5.5)(2(442 - 37))} = 95\,mm$$

Beam Column Capacity

Eurocode 4 (1994) con't

$$M_D = Z_s f_y + 0.5 Z_c f_c'$$
$$= 875764(442) + 0.5(1030282)(37)$$
$$= 577.7 \text{ kNm}$$

$$M_B = M_C = M_D - 2(t \cdot h_n^2) f_y - 0.5((D-2t)h_n^2) f_c'$$
$$= 577.7 \times 10^6 - 2(5.5)(95)^2(442) - 0.5(395.4)(95)^2 37$$
$$= 467.8 \text{ kNm}$$

$$f_k = 0.5\lambda^{-2}(1 + 0.21(\lambda - 0.2) + \lambda^2)$$
$$= 0.5(0.25)^{-2}(1 + 0.21(0.25 - 0.2) + 0.25^2) = 8.58$$

$$\chi = f_k - \sqrt{f_k^2 - \lambda^{-2}} \leq 1.0$$
$$= 8.58 - \sqrt{8.58^2 - 0.25^{-2}}$$
$$= 0.99$$

$$\chi_d = \frac{N_f}{N_p} = \frac{1000}{7605} = 0.13$$

$$\chi_n = \chi \cdot 0.25(1-r)$$
$$= 0.99(0.25) = 0.25 \& \chi_d$$
$$= 0.13.$$

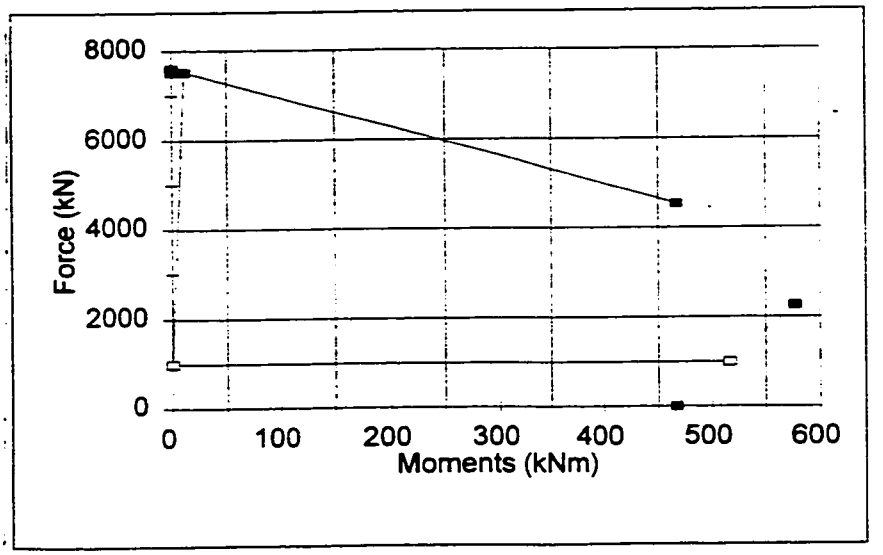

$$M_p = 516 - 0.02 = 516$$

$$\frac{M_f}{M_p} = 1.15$$

Beam Column Capacity

Proposal A.

$L = 2200\,mm$
$D = 406.4\,mm$
$t = 5.5\,mm$
$F_y = 442\,MPa$
$f_c' = 37\,MPa$
$P_f = 1000\,kN$
$M_f = 592\,kN$

$$\frac{2\pi R t F_y + \left(R^2 \sin\frac{\bar{A}}{2} - R^2 \sin^2\frac{\bar{A}}{2} \tan\frac{\bar{A}}{4}\right) f_c'}{\frac{R^2 f_c'}{2} + 2Rt F_y} = \bar{A}$$

substituting and solving for $\bar{A} = 2.14\,rad$

$L = \bar{A}R = 2.14(203.2) = 435\,mm$

$c = 2R\sin\frac{\bar{A}}{2} = 2(203.2)\sin\left(\frac{2.14}{2}\right) = 356\,mm$

$a = \frac{c}{2}\tan\frac{\bar{A}}{2} = 356/2\tan\left(\frac{2.14}{2}\right) = 105\,mm$

$C_r' = f_c'\left(\frac{LR}{2} - c\frac{(R-a)}{2}\right) = \left(\frac{435(203.2)}{2} - 356\frac{(203.2-105)}{2}\right)37 = 988\,kN$

$A_{st} = (2\pi R - L)t = (2\pi(203.2) - 435)5.5 = 4630\,mm^2$

$T_r = A_{st} F_y = 4630(442) = 2046\,kN$

$C_r = T_r - C_r' = 2046 - 988 = 1058\,kN$

$y_{sc} = \frac{R_c}{L} = \frac{203.2(356)}{435} = 166\,mm$

$$y_c = \frac{c^3}{6(RL - c(R-a))} = \frac{356^3}{6[203.2(435) - 356(203.2-105)]} = 141\,mm$$

$$y_{st} = \frac{R_c}{2\pi R - L} = \frac{203.2(356)}{2\pi(203.2) - 435} = 86\,mm$$

Beam Column Capacity

Proposal A (con't)

$M_{rc} = C_{re} + C_r' e'$

$e = y_{st} + y_{sc} = 86 + 166 = 252 \text{ mm}$

$e' = y_{st} + y_c = 86 + 141 = 227 \text{ mm}$

$M_{rc} = 1058(.252) + 988(.227) = 491 \text{ kNm}$

$$\frac{C_f}{C_{rc}} + \frac{\beta_w M_f}{M_{rc}(1 - C_f/C_{ec})} = 1.0$$

$C_{rc} = 8561 \text{ kN}$ (from 1994 code)

$$\beta = 1 - \frac{C_{rcm}}{C_{rco}}$$

$C_{rcm} = f_c' A_c = 37(\pi/4)(395.4)^2 = 4543 \text{ kN}$

with L=0 $\rho_s = .5$

$$\tau = \left(\sqrt{1 + \rho_s + \rho_s^2}\right)^{-1} = 0.76$$

$$\tau' = 1 + \left(\frac{25\rho_s^2\tau}{D/t}\right)\left(\frac{F_y}{0.85 f_c'}\right) = 1 + \left(\frac{25(.5)^2(.76)}{406.4/5.5}\right)\left(\frac{442}{0.85(37)}\right) = 1.90$$

$C_{rco} = 0.76(3018) + 1.90(3847) = 9603 \text{ kN}$

$$\beta = 1 - \frac{4543}{9603} = 0.53$$

$\frac{\omega}{1 - C_f/C_{ec}} = 1.0$ for members in unbraced frames.

$\frac{1000}{8561} + \frac{0.53(M_f)}{491} = 1.0 \qquad M_f = 818 \text{ kNm}.$

but $M_f \leq M_{rc}$ so 491 kNm

$\frac{M_f}{M_r} = 1.21.$

Beam Column Capacity

Proposal B

Using CFST 64

$L = 2200\,mm$
$D = 406.4\,mm$
$t = 5.5\,mm$
$F_y = 442\,MPa$
$f'_c = 37\,MPa$
$P_f = 1000\,kN$
$M_f = 592\,kNm$

$C_A = C_{rco} = 9603\,kN$ (from Proposal A)
$M_A = 0\,kNm$

$C_B = 0$
$M_B = M_{rc} = 491\,kNm$

$C_c = C_{rcm} = 4543\,kN$
$M_c = M_{rc} = 491\,kN$

$C_o = \frac{1}{2}C_c = 2272\,kN$

$M_{rhc} = M_o = \frac{2}{3} f'_c R_c^3 + \frac{4}{3} F_y R_c^2 t = \frac{2}{3}(37)(197.7)^3 + 4(.442)(197.7)^2(5.5) = 571\,kNm$

$C_{rc} = 8561\,kN$

Since $C_{rc} > C_{rcm}$, we have a three line stability curve.

$$M_L = \frac{M_{rc}(C_{rc} - C_{rco})}{(C_{rcm} - C_{rco})} = \frac{491(8561 - 9603)}{(4543 - 9603)} = 101\,kN$$

$$M^*_{rc} = M_{rc} - \frac{M_L C_{rcm}}{C_{rc}} = 491 - \frac{101(4543)}{8561} = 437\,kN$$

$$M^*_{rhc} = M_{rhc} - \frac{M_L C_{rhc}}{C_{rc}} = 571 - \frac{101(2272)}{8561} = 544\,kN$$

$C_f > C_o$ $\quad M_r = M^*_{rhc} - \frac{(M^*_{rhc} - M_{rc})C_f}{C_{rhc}}$

$$= 544 - \frac{(544 - 491)1000}{2272} = 521\,kNm$$

$\frac{M_f}{M_r} = 1.14$